INFORMATION TO USERS

This manuscript has been reproduced from the microfilm master. UMI films the text directly from the original or copy submitted. Thus, some thesis and dissertation copies are in typewriter face, while others may be from any type of computer printer.

The quality of this reproduction is dependent upon the quality of the copy submitted. Broken or indistinct print, colored or poor quality illustrations and photographs, print bleedthrough, substandard margins, and improper alignment can adversely affect reproduction.

In the unlikely event that the author did not send UMI a complete manuscript and there are missing pages, these will be noted. Also, if unauthorized copyright material had to be removed, a note will indicate the deletion.

Oversize materials (e.g., maps, drawings, charts) are reproduced by sectioning the original, beginning at the upper left-hand corner and continuing from left to right in equal sections with small overlaps. Each original is also photographed in one exposure and is included in reduced form at the back of the book.

Photographs included in the original manuscript have been reproduced xerographically in this copy. Higher quality 6" x 9" black and white photographic prints are available for any photographs or illustrations appearing in this copy for an additional charge. Contact UMI directly to order.

UMI®

Bell & Howell Information and Learning
300 North Zeeb Road, Ann Arbor, MI 48106-1346 USA
800-521-0600

BOUNDARY CONDITIONING CONCEPT APPLIED TO THE SYNTHESIS OF MICROSYSTEMS USING FUZZY LOGIC APPROACH

Muthukumaran Packirisamy

A Thesis

in

The Department

of

Mechanical Engineering

Presented in Partial Fulfillment of the Requirements
for the Degree of Doctor of Philosophy at
Concordia University,
Montreal, Quebec , Canada H3G 1M8

March 2000

ABSTRACT

Boundary Conditioning Concept Applied to the Synthesis of Microsystems using Fuzzy Logic Approach

Muthukumaran Packirisamy, Ph.D
Concordia University, 2000

The burgeoning field of MicroSystems Technology (MST) has a tremendous potential for sensing and actuation of industrial systems in almost every field of human interest. This thesis proposes a synthesis of microsystems in order to explore the advantage of miniaturization by developing a technology suitable for fabricating integrated systems that consist of sensing, actuating and computing elements at the micro level. The synthesis involves development of fabrication strategies using industrial CMOS process and design strategies, in order to manipulate the effect of inherent limitations of fabrication and other limitations due to structural configuration and environment on dynamic behavior of microsystems.

Towards the success of fabrication synthesis, micromechanical components are fabricated through an industrial CMOS process, namely, the Mitel 1.5 μm Double-Poly-Double-Metal process, and by post-releasing with gas phase xenon difluoride etching. The etching is described along with the details of the setup, the etching procedure and the effect of etching on end conditions of the fabricated structure. The types of structures fabricated show that they can be adopted for both piezoresistive and capacitive devices.

The different factors that influence the elastic properties of both macro and micro systems include variations in structural geometry, process parameters and operational

environment. A concept of boundary conditioning is proposed in this thesis as a unified approach for the quantification of the influence of structural geometry, support conditions, fabrication process and environmental influence on the dynamic behavior of the system. The influence of all the above parameters is represented by replacing the elastic influence with the equivalent spring stiffnesses.

The modeling of boundary conditioning is carried out using artificial springs and boundary characteristic orthogonal polynomials in the Rayleigh-Ritz method. The eigenvalues are predicted for plate type structures with stiffeners and cutouts using this approach. The concept of boundary conditioning is applied to structural tuning and localization of vibrational response. The results obtained for manipulation of harmonic combinations and vibrational response using artificial springs are useful and interesting. The boundary conditioning conceptualizes micro or macro system into equivalent elastic system.

The equivalent stiffnesses which can be estimated through experiment or other methods may include uncertainties and vagueness. The fuzzy system identification technique is applied for modeling such micro or macro systems with fuzziness on input and output parameters. Automatic fuzzy system identification is carried out using subtractive clustering method. A higher order fuzzy system identification technique is proposed for modeling complicated systems with fewer number of rules. The structural tuning of elastic systems is identified by expert modeling and subtractive clustering.

The influence of structural variations of microsystems on dynamic behavior is modeled using the method of artificial springs. The static and dynamic behavior of free standing microsystems under the influence of electrostatic field and residual stress are also presented. The comparison between predicted and experimental values of snapping voltage for capacitive type systems shows a good agreement. The non-classical end conditions resulting from micromachining processes are modeled using boundary conditioning technique. The application of fuzzy system identification of the boundary conditioning of microsystems shows a potential for direct and indirect design of microsytems for the required dynamic behavior.

Dedicated to

those who attempt

negation of fragmentation of psyche

leading to

psychological globalization

ACKNOWLEDGEMENTS

The author is privileged to submit his sincere thanks and gratitude to the thesis supervisor Dr. R. B. Bhat for his invaluable technical and global guidance, and energetic encouragement. The author was overwhelmed by his support, his rejuvenating " *So, What happened?*" question, his utmost concern and his willingness to discuss even if it was at odd hours. The author is privileged to carry out research under him.

It is the pleasure of the author to thank the co-supervisor Dr.I.Stiharu for his support, sincere concern and efforts through out the study. The author had an enjoyable experience working under him. The author cherishes the discussions with him that were useful for this thesis and the author's career.

The author expresses his sincere thanks to Dr. K. Demirli for his enlightening technical discussions and support during the study.

The author thanks Dr. S. Rakheja for his concern and help shown in the progress of my thesis, and also for examining the thesis proposal.

The author expresses his thanks to Dr.W.Ahmed and Dr.W.Lynch for their effort in examining my thesis proposal.

The author thanks Dr. N.N.Kapoor, Biology Department for his help and time in taking SEM micrographs.

The author would like to thank Concordia University for awarding the Graduate Fellowship and International Tuition Fee Remission Award, Quebec Government for awarding FCAR scholarship and CMC for fabricating the Mitel and MUMPs designs.

It is my pleasure to acknowledge the help offered by Mr. John Elliot, Technical Officer and the technical staff of Mechanical Department workshop and Concave towards the fabrication and installation of experimental setup.

The author appreciates the support of his friends Parthiban, Giri, Ganesh , Matcharajan, Mohan, Narayanan, Sridhar and Ramanamurthy in applying to the Ph.D program, Anand, Krishnan, Prasanna, Sumant, Mahesh, Dinesh, Deiva Venkatesh and others during Ph.D program.

The author wishes to express sincere thanks to Dr. Bhat's family for having extended their support and help whenever needed.

The author wishes to express the gratitude to his parents and relatives for their consistent encouragement.

TABLE OF CONTENTS

LIST OF FIGURES

LIST OF TABLES

NOMENCLATURE

A	Area, deflection coefficient, fuzzy set
a	concave etch distance, side of the plate, deflection coefficient
B	fuzzy set, magnetic field intensity
b	convex etch distance, side of the plate
C	fuzzy set
d	dielectric gap
D	damping coefficient, flexural rigidity
e	stiffener width
E	Young's modulus
F	force, field strength
f	stiffener height
h	plate thickness
I	current, area moment of inertia
K	stiffness coefficient
L	length, lateral etch distance, length of support beam
M	mass, number of mechanical components
N	number of etch pulses, number of plate segments, number of support beams
NSX	number of stiffeners in x direction
NSY	number of stiffeners in y direction
q	eigenratio
R	radius, reaction shear force
T	kinetic energy, number of transistors
U	strain energy
u	total number of points
V	voltage, impulse velocity
w	deflection
W	deflection, width of support beams

x	relative displacement, $= \xi/a$,
X	deflection
α	$= a/b$
δ	association threshold
ε	dielectric constant
ε	permittivity of vacuum
$\bar{\varepsilon}$	acceptance ratio
$\underline{\varepsilon}$	reject ratio
ϕ	polynomial function in x direction
η	coodinate in y direction, squash factor
φ	polynomial function in y direction
Λ	objective fucntion
$\sqrt{\lambda}$	eigenvalue
$\ddot{\bar{\lambda}}$	mean of the entire population
μ	membership function
ν	Poisson's ratio
ρ	density, weighting function
σ	selectivity factor, relative stiffness parameter, residual stress, modeling error, least square error
ω	frequency
ξ	coodinate in x direction
ζ	damping ratio, penalty ratio

Abbreviations:

ASAC	Active Structural Acoustic Control
ASVC	Active Structural Vibration Control
BC	Boundary Conditioning
BCOP	Boundary Characteristic Orthogonal polynomials

BOE	Buffered Oxide Etch solution
COX	Contact oxide
FOX	Field oxide
IMO	Inter-metallic oxide
IPO	Interpoly oxide
M1	Metal1
M2	Metal2
MEMS	MicroElectroMechanicalSystems
MIMO	Multi Input Multi Output
MISO	Multi Input Single Output
MST	MicroSystems Technology
MUMPs	Multi Users MEMS Process
PASS	Passivation layer
PO1	Polysilicon1
PO2	Polysilicon2

Subcripts:

a	cluster radius
b	bending, penalty radius
d	damping, diaphragm, dynamic
e	electrostatic
eq	equivalent
ext	external
f	etch front
h	harmonic
mn	mth polynomial in x direction and nth polynomial in y direction
n	number of data points
out	output
p	plate

P	consequent regression parameter, cluster potential
R	rotational
s	snapping, stiffener, support, static
stru	structural
T	translational
v	vertical
w	window opening

CHAPTER 1

INTRODUCTION

1.1 INTRODUCTION

Scientific and technological advancements have been driven by creativity and innovation of the human genius. New discoveries are made by chipping out the boundaries of knowledge and enlarging the envelope little by little. Simultaneously, the multidisciplinary advancements are made by interlinking the independent discoveries in different directions and creating a fine multidisciplinary subspace which poses new frontiers of knowledge as a challenge to human genius.

Boundary conditioning concept, microsystems and fuzzy logic approach by themselves are independent technological and scientific facets of our knowledge envelope, but by interlinking them an exciting new subspace with unlimited potential for fresh directions are formulated in this thesis. An attempt is made here to chip away the boundary of this subspace with investigations, both analytical and experimental, in order to understand the potential and new possibilities.

The burgeoning field of MicroSystems Technology (MST) or MicroElectroMechanical Systems (MEMS) has elicited a tremendous attention from research community in the recent times in view of its potential for sensing and actuation of industrial systems in

almost every field of interest to the mankind. The applications of this technology spans over not only the conventional engineering systems but more recent applications such as in DNA sequencing, information technology and in communication systems. The application of MST technology is so diverse that it practically links almost every specialized scientific field. The sensors fabricated through MST are used for measuring pressure, acceleration, humidity, temperature and gas flow. MST devices can also be used to pump fluids, reflect or refract radio or fiber optic waves, make memory devices, fabricate control actuators etc. Hence, MEMS (MicroElectroMechanical Systems) or MST (MicroSystems Technology) is not restricted to any specific device, application or fabrication processes. Rather, the aim of MEMS or MST is to develop the technology to merge sensing, actuating and computing in order to realize new microsystems with enhanced level of perception, control and performance. This ability of MEMS to collect and process information, compute the course of action and thereby manipulate the environment or a macrosystem makes the MEMS as the product differentiating technology for the next century.

Sensing and actuation are based on the dynamic behavior of the relevant elements of the sensors and actuators. This is true whether the systems involved are micro or macro in size. As in the case of macro sensors and actuators, microsystems also possess certain elastic and mass properties. They are subjected to vibration excitation from other sources or the external environment during their operation and their performance depends on the dynamic behavior of the sensing or the actuating elements. Hence, the manipulation of

the dynamic behavior is extremely important in order to modify the system properties. The manipulation of dynamic behavior may consist of

1. Control of vibrational response for a given disturbance with the help of external sources.
2. Design of a structural system in order to obtain a required performance. This may be effected through manipulation of natural frequencies and mode shapes by changes in the structural configurations or environment.

Both types of manipulation are applicable to micro and macro systems. Macrosystem structures are of 'mm' to 'm' dimensions while microsystems are of 'μm' dimensions.

The elastic behavior of macro and micro dynamic systems depends on the structural geometry configuration, material property condition determined by the methods of manufacture of the system, and the elastic interaction from the environment. The system consists of both structural and environmental parts. Every system coexists with the environment and reaches an operating position depending on the severity of the influence or interaction of the environment. Whenever the environmental conditions change, system reaches a new operating point. Boundary conditioning is a useful and unified concept for quantifying and manipulating the interactive elastic behavior of the system.

In general, there is no knowledge in the world that is so absolutely certain, especially in the case of understanding of physical systems. Engineering systems suffer from quantification uncertainties, vagueness in the description of the problem, imprecise

objectives, imprecise knowledge about the system, etc. Manipulation of such systems cannot be accomplished by operators that obey strictly by either/or conditions and the law of excluded middle. They need mathematical operators, that can absorb impreciseness of the system, that obey the "either and or" conditions and cover the middle ground also. This requirement is close to the way the human thinks, by attaching *degree* to everything. Understanding of such systems needs multivalued approximate reasoning. *Fuzzy logic approach* comes as a very powerful tool to deal with such systems as it applies approximate reasoning mechanism on appropriately coded knowledge very similar to that of human mind.

1.2 INTRODUCTION TO MICROSYSTEMS

Microsystems Technology is a burgeoning area with applications in diverse engineering and scientific disciplines. Over the past two decades, several microsystems have been designed and fabricated and have been accepted widely. This is confirmed by the projected growth of world wide MEMS market shown in Figure.1.1. As anticipated by Feynman, 1992, [62], the possible areas of MEMS applications include 1) fluid sensing, control and transport, 2) mass data storage, 3) optics and imaging [116, 46], 4) inertial measurements [195], 5) sensor and actuator [56, 59], 6) radio frequency components and communications [109, 125], and 7) biomedicine [110]. The vastness of MEMS applications can also be seen from Figure.1.2 [Fujita, 1998, 65].

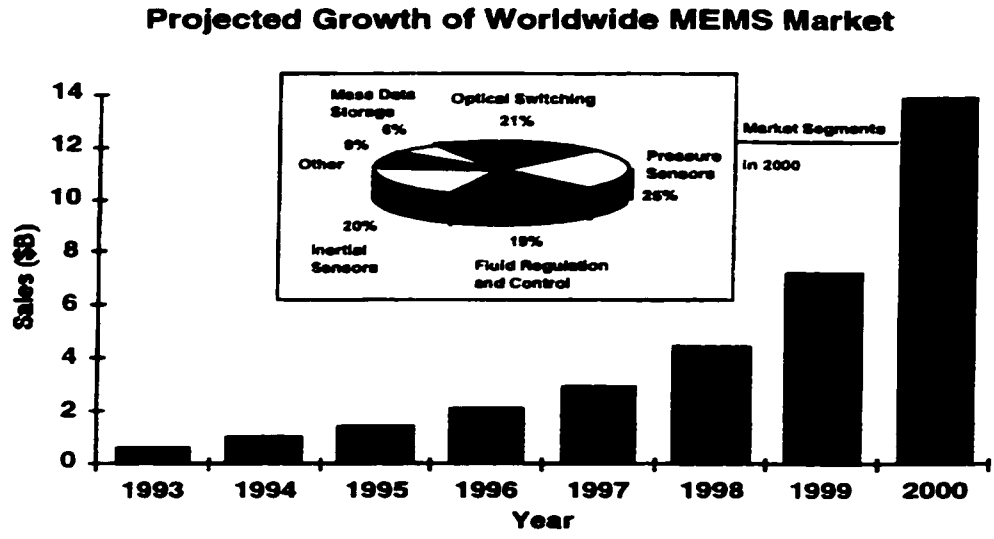

Figure 1.1: Projected wordwide MEMS market. Adopted from [Darpa, 142]

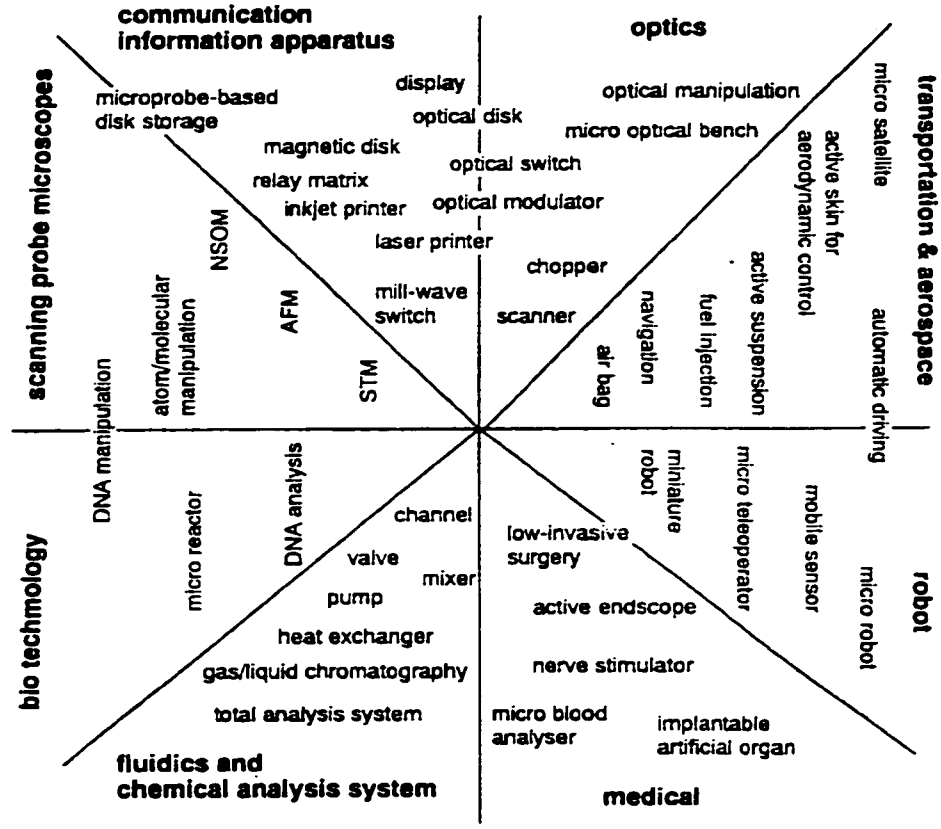

Figure 1.2: Map of MEMS applications [adopted from Fujita, 1998, 65]

The MEMS, to date, have largely evolved from the processes used in semi-conductor industries. However, the MEMS processes also include surface and bulk micromachining, LIGA (lithography and galvo or electroplating), HARMST (high aspect ratio microsystems technology), wafer bonding etc. The overview of MEMS devices and technologies shown in Figure.1.3 [Fujita, 1998, 65] shows the vastness of MEMS potential. The technological capabilities coupled with limitations, the ever growing need for sensing, computing and acting at the device level for effective interaction between the information systems and physical world, drives the development of MEMS [Gabriel, 1998, 69]. On consolidation, MEMS or MST is a collective system of approach to develop microsystems with the advantage of miniaturization, multiplicity and microelectronics and with a tremendous potential for sensing and actuation in almost every field of interest to mankind from DNA sequencing to boundary layer control on aircraft wings.

Although both micromechanical and microelectronics components of MEMS devices are of the order of microns in geometrical domain they are big in property domain [DARPA Report, 142]. In macrosystems the mass related phenomena are comparable with that of energy related phenomena. In the case of *nm* dimensions mass related phenomena are nearly absent and the energy and interaction related phenomenon are very dominant. But in microsystems mass related phenomena can not be ignored and at the same time energy related phenomenon are also dominant. At the micro level of matter both mass related and energy related phenomena coexist making a real application out of micro devices highly demanding.

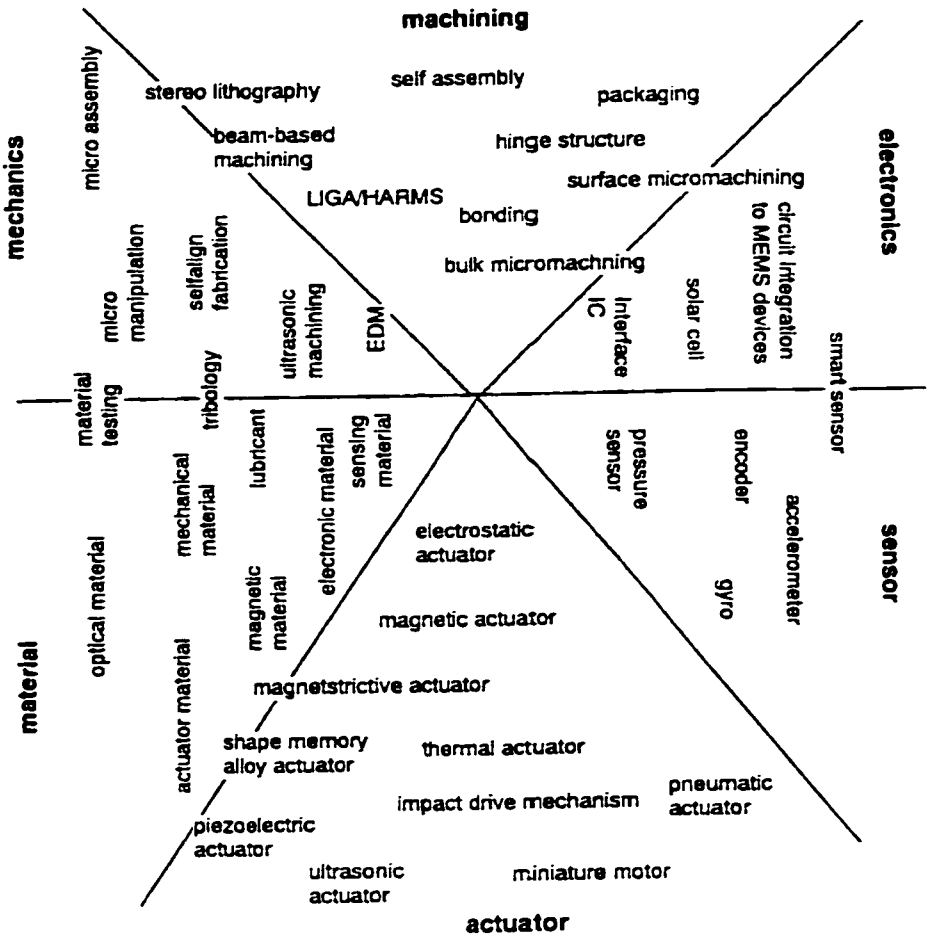

Figure 1.3: Map of MEMS devices and technologies [Fujita, 1998, 65]

The advantages associated with MEMS are miniaturization, multiplicity and microelectronics. The important advantage of miniaturization is the greater accessibility to the vicinity of the physics of the problem. As the fabrication of the MEMS devices evolved from semiconductor process, it inherits multiplicity or batch fabrication property associated mainly with photolithography based MEMS processing leading to the reduced unit cost of the devices. Another important advantage of multiplicity is the possibility of

fabricating massively parallel, interconnected microelectromechanical systems. The real advantage of MEMS is the integration of microelectronics in the microsystems which adds intelligence and control to the microsystems.

1.2.1 Methods of Microsystem Fabrication

Apart from IC fabrication technologies, main fabrication processes available are bulk micromachining, surface micromachining, wafer to wafer bonding, high aspect ratio micromachining such as LIGA, HARMST, etc. A good review of bulk micromachining is available in Kovacs et al. [95].

Bulk micromachining is the general form applied to the selective removal of silicon from the substrates using chemical etchants. This machining includes isotropic etching in which the etch rate is same in all directions and anisotropic etching in which the etch rate is highly dependent on the crystallographic plane of the material. It also includes wet etching in which liquid chemicals such as KOH (potassium hydroxide), EDP (ethylenediamine pyrocatechol) and TMAH (tetramethyl ammonium hydroxide) are used or dry etching in which the gas phase or plasma etchants such as XeF_2 (xenon difluoride), SF_6 (silicon hexafluoride), DRIE (deep reactive ion etchants) are used. Both types of isotropic and anisotropic bulk micromachining are possible through wet and dry etching.

In sacrificial or surface micromachining [31, 83], the sacrificial layers of related materials that were deposited over the structural layers are removed through wet or dry etching. A

wide variety of materials are available for both structural and sacrificial layers depending upon the selectivity of the etchant. Good review of surface micromachining MEMS is available in [31] which could be carried out by the use of both wet and dry etchants.

1.2.2 Trends in MEMS Technology

In the future, the success of the MEMS will depend upon the higher level of functional capability, higher level of integrated electronics and greater number of micromechanical components. This will apply a tremendous pressure on the manufacturers to move from discrete manufacturing of MEMS components to the manufacturing of integrated MEMS devices indicated by a large number of both micromechanical and microelectronics components. In a microsystem, the level of microelectronics or the number of transistors (T) represents information processing ability while the number of micromechanical components (M) represents the ability of perception and control. Hence, the success of MEMS in the future shall depend on the level of integration between the microelectronics and micromechanical components. The demand on MEMS integration is clearly shown in the Figure.1.4 [Gabriel, 1995, 69] indicated by the larger number of components and higher value of T/M ratio.

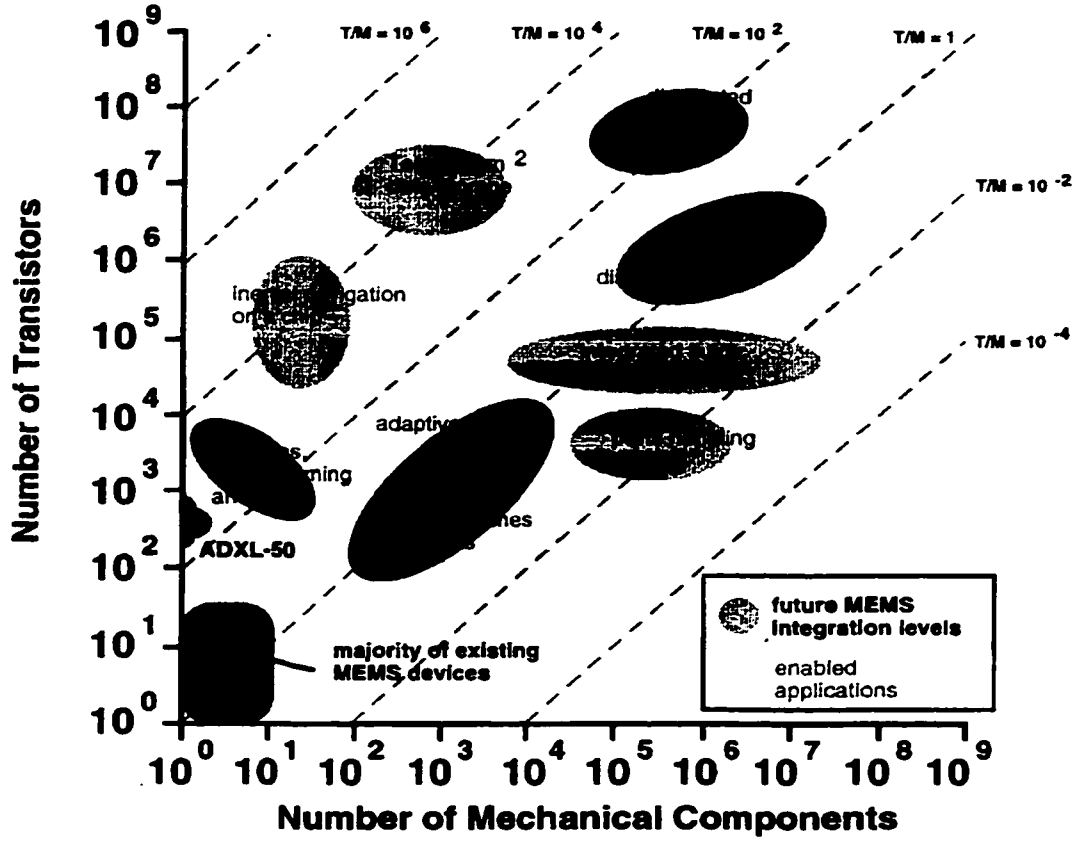

Log-log plot of number of transistors merged with number of mechanical components for MEMS devices and systems. Contours of equal transistors-to-mechanical-components ratios (T/M) are lines of 45° slope. Lines representing T/M ratios ranging from 10^{-4} to 10^{6} are shown for reference. The resulting map represents a quantitative way to measure and track MEMS technology advances across different application areas

Figure 1.4: Number of mechanical components vs. number of transistors in different MEMS applications
[adopted from Gabriel, 1995, 69]

1.2.3 Integration of Micromechanical and Microelectronics Components

The posssible ways of integrating micromechanical and microelectronics components of MEMS devices is schematically shown in Figure.1.5.

In type I method of discrete manufacturing of MEMS devices, micromechanical components are fabricated through dedicated sequence of processes. It may involve all processes including surface or bulk micromachining. Thus a die with micromechanical components will be fabricated along with contact pads and will be connected externally to the electronics circuitry. Silicon accelerometer was fabricated using this approach by Roylance and Angell [152]. The commercialization of this approach for the manufacture of MEMS devices is implemented by MCNC [114] through a process called MUMPs (multiuser MEMS process) in which MEMS devices are fabricated using 3 polysilicon layers, 2 oxide layers and a metal layer by sacrificial etching of oxide layer. Once the arrays of MEMS devices are fabricated they are connected externally with electronic circuitry. The real advantage of miniaturization cannot be fully exploited in this approach as the size of the components are still relatively large. Due to the external integration, the noise to signal ratio can also increase limiting the thresholds on sensing or actuating signals. Hence, the ideal situation would be the integration of micromechanical and microelectronics components at the device level improving the signal to noise ratio and transmitting a reliable signal to the control systems or display.

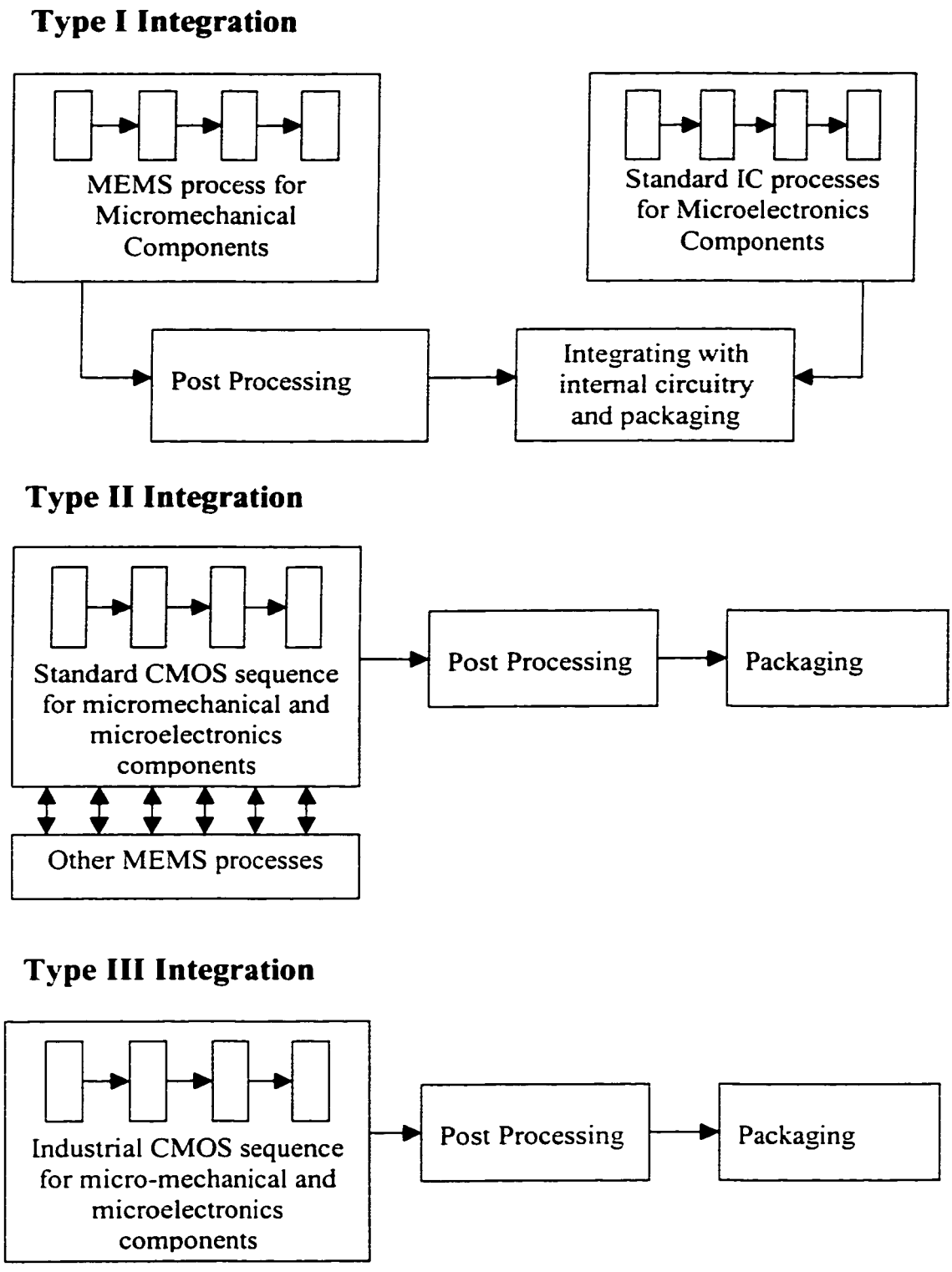

Figure 1.5: Types of integration of micromechanical and microelectronics components

It would be wise to evolve the fabrication of MEMS devices through processes such as standard IC fabrication technology that have high reliability with microelectronics components. Moreover, fabrication through standard industrial VLSI process will also lower the cost. This merging will help in exploiting the full use of microelectronics in the microsystems such that the signals through the micromechanical components could be conditioned and processed on the same device without any external circuitry. However, the actual industrial standard VLSI processes have been optimized for the fabrication of microelectronic components, while mechanical microstructures require, in general, different relevant properties in the various patterned layers.

CMOS has made revolutionary advances [36] in recent years in terms of circuit density, greater yield, reliability, greater multiplicity and greater layout design and analytical supports. It has reached such a level of sophistication in that the design of microelectronics has become just satisfying a set of rules. Hence, it is certainly worthwhile to exploit CMOS technology for manufacturing micromechanical structure [130, 80], even though it will call for violation of some present design rules. This violation forms the motivation for setting new rules for making micromechanical components using standard CMOS technology.

Hence, when an industrial CMOS process enables fabrication of micro-system devices in such a way that both micromechanical and microelectronics components would be fabricated within the same process flow, integration between the micromechanical and microelectronics components will reach the device level. Such a merger could also

benefit the VLSI fabrication industries in view of the vastness of MEMS application areas. However, with the present standard technology, the possible way of building microsystems is to fabricate both micromechanical and microelectronics components through an industrial CMOS process and post-release the structures through selective micromachining outside the fabrication stream. It should also be noted that adoption of an industrial CMOS process restricts the design of micromechanical components due to the type of process, material and geometrical limitations. Moreover, the selected post-releasing method should also be compatible with CMOS layers such that the microelectronics components remain functionally intact.

The direct adoption of CMOS technology to MEMS is limited by the material of the CMOS layers, its process sequence and the type of mechanical structures to be made. Silicon dioxide, silicon nitride, metal, polysilicon and bare silicon substrate doped or undoped are the possible parts of the MEMS devices that could be fabricated through CMOS technology. Some of these materials need to be etched out through post processing in order to make any free standing structures. The post processing could be of the type bulk micromachining, or sacrificial micromachining with wet or dry etchants.

Depending upon the design and CMOS sequences, it may be necessary to add special processes or layers before post-processing and packaging as shown in Figure.1.5. Peterson, et al. [141], fabricated micromechanical accelerometer integrable with MOS circuitry. The beams were made of oxide coated with metal. Final structure was released through anisotropic wet etching with EDP. The etch stop was p^+ doped layer.

Park and Wise, 1983 [133] proposed a method of making pressure sensor with MOS circuitry through anisotropic bulk micromachining.

CMOS technology was applied successfully for the fabrication of polysilicon bridges through sacrificial etching of oxide in BOE (buffered oxide etch solution) with an additional mask by Parameswaran et al. [131, 130]. Later, CMOS integrated capacitive pressure sensor was fabricated by anodic bonding with glass on both sides of the chip after anisotropic bulk etching of the chip by Terable et al. [178].

Even though it is advantageous to use standard CMOS sequence for the fabrication of MEMS devices, the benefit of integration will be maximum only if the commercial CMOS sequence is used for MEMS application.

Riethmuller et al. [145] used a commercial process for the fabrication of accelerometers with introduction of additional processes and 5 masks through bulk anisotropic etching with KOH. Schlichting et al. [158] succeeded in using a 3 μm standard CMOS sequence for making a pressure sensor after the introduction of anodic bonding of pyrex glass along with KOH bulk etching. Condensor microphone was fabricated using standard CMOS sequence with addition of polymide coating and anisotropic etching in Pedersen et al. [138].

Baltes et al. [9] explored the possibility of an industrial CMOS sequence for the fabrication of thermal based sensors after the introduction of 6 steps of post processing including both bulk and surface micromachining along with special masks.

It has been possible to use standard CMOS sequence for the fabrication of MEMS devices only after the introduction of additional processes/layers/masks before post processing with bulk or sacrificial etching. However, the true benefits of integration with microelectronics components at the device level will be available only if the requirement of an additional process, layers and masks is eliminated and the dices containing both micromechanical and microelectronics components fabricated through commercial CMOS process are directly post processed and packaged as shown by Type III integration in Figure.1.5.

Tilmans et al. [181] tried using an industrial single poly double metal 0.7μm CMOS process for MEMS devices through both bulk and sacrificial micromachining. In this attempt spiral inductor was fabricated through anisotropic bulk etching of silicon with EDP and polysilicon bridges through sacrificial etching of oxide without any additional masks. The problem of stiction in the case of sacrificial etching was avoided through deep freeze drying and supercritical carbon drying.

Stiharu et al. [166] succesfully fabricated relative humidity sensors of resistive types by depositing humidity sensitive material on the chips fabricated through Mitel 1.5 μm process, as an example of Type- III integration. Ma et al. [107] and Yu et al. [207]

fabricated cantilever-in-cantilever structure through the Mitel 1.5 μm process followed by bulk etching of silicon substrate, as an example of Type-III integration.

The final success of making mature MEMS devices will depend largely on the finding of completely compatible post-processing methods with a selected commercial CMOS process and the intended design of microsystems. The industrial process being projected in Canada for making the microsystems is Mitel 1.5 μm Double-Poly-Double-Metal process with suitable post-release etching mechanism. It has been an interesting challenge to Canadian MEMS community to find a suitable post-processing technique so that Mitel 1.5 μm process [61] can be used for fabricating fully integrated microsystems. The type of post-processing along with the released structures is discussed in Chapter2.

1.2.4 Development on Free-Standing Microsystems

The importance of the synthesis of microsystems suggested in the thesis is outlined with a few types of devices in this section. The type of devices that could be fabricated is up to the ingenuity of the designer in successfully exploring the limitation of the fabrication and post-processing methods used. In general one could make devices with moving or non-moving parts. The complication increases with devices having moving parts due to limitations from fabrication sequences, mechanism of post releasing, material of the CMOS layers, phenomenon related to micro dimensional domain, type of sensing or actuation required such as capacitive or piezoresistive or piezoelectric,

thermomechanical, etc. In this sense, an overview on the development of some microsystems will be useful.

There are a variety of piezoresistive and capacitive inertial and pressure sensors available. Capacitive sensors are known to have less power consumption, better performance and smaller geometry compared to piezoresistive sensors. Hence, capacitive type of sensing has been applied to both inertial and pressure measurement extensively. In capacitive types of sensors or actuators, two electrodes are needed, namely diaphragm (top plate) and bottom plate (backplate) which are separated by dielectric cavity. In this arrangement the top plate is movable while the backplate is stationary as shown in Figure 1.6.

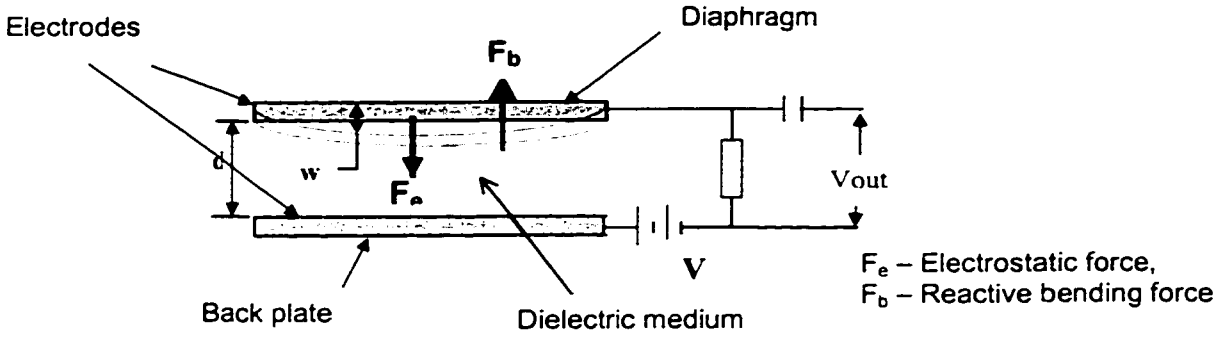

Figure 1.6: Scheme of a capacitive device

The capacitance between the electrodes is dependent on the dielectric gap (d) and the dielectric property while the electrostatic force between the electrodes is dependent on the dielectric gap, dielectric property and bias voltage (V). When one of the electrodes is made movable, the capacitance between the electrodes will vary if the top plate is subjected to deflection as in the case of sensors or the topplate is subjected to deflect

when the electrostatic force is varied by varying bias voltage as in the case of electrostatic actuators.

Initially the micro pressure sensors were fabricated discretely. Diaphragm and the backplate of the capacitive pressure sensor were fabricated separately and bonded together. The dielectric cavity was formed by anisotropic etching.

Clark and Wise [45] fabricated piezoresistive and capacitive thin diaphragm pressure sensors by anodic bonding of structures containing diaphragm and backplate. Dielectric cavity was formed by anisotropic etching. It has been found that the sensitivity of both types of sensors which is a function of diaphragm deflection is dependent on the boundary edge conditions of the diaphragm.

Zahn [213] fabricated a condenser microphone shown in Figure 1.7 and studied the effect of number of holes, dielectric chamber volume, size of the acoustic holes on the acoustic performance of the microphone.

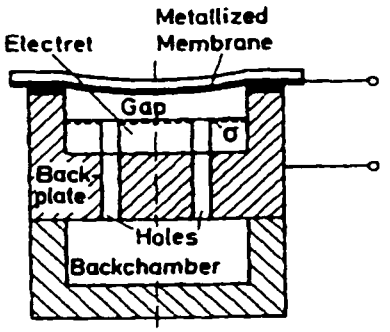

Figure 1.7: Scheme for a electret microphone [213]

Smith et al. [164] succeeded in measuring with integrated circuits connected externally to the sensors, as an example of type-I integration. Improvement was found compared to that of measuring with on-board circuitry because of the reduced effect of parasitic capacitance. This work formed the motivation for further integrating IC fabrication technology at the device level.

Chau and Wise [77] mentioned the influence of electrostatic force on the natural frequency of the diaphragm of capacitive type sensors and presented the effect of diaphragm residual stress on the sensitivity for both piezoresistive and capacitive pressure sensors.

Jornad and Rudolf [89] used CMOS techology for microelectronics part of the microsystem. Pressure sensors and electronics chip were connected externally as an example of type-I integration.

Bergqvist and Rudolf [13] fabricated a condenser microphone with a large number of ventilation holes and low stray capacitance using IC compatible technology in order to achieve further miniaturization. This becomes the motivation for moving to type-II integration of micromechanical and microelectronics components.

All the microphones discussed so far, have the dielectric cavity created by anisotropic etching. But Scheeper et al. [156] fabricated condenser microphone using sacrificial etching of aluminum of 1μm thick. Even though the reduced gap could increase the sensitivity, the electrostatic force between the electrodes also will increase whenever the sensors are made through sacrificial etching. The backplate also contained acoustic holes made by KOH anisotropic etching.

Kuhnel and Hess [97] fabricated a condenser microphone with 0.15μm thick silicon nitride membrane and a backplate with a large number of acoustic holes. These acoustic holes reduce streaming resistance and increase the sensitivity.

In general, for a uniform thick diaphragm, the variation of capacitance is non-linear against pressure as shown in Figure 1.8. This non-linearity was reduced by varying the stiffness distribution at the edges and throughout the structure as shown in Figure 1.9 by Rosengren et al. [150]. Stiffness and notches were introduced onto structure in order to obtain the required elastic property of the structure.

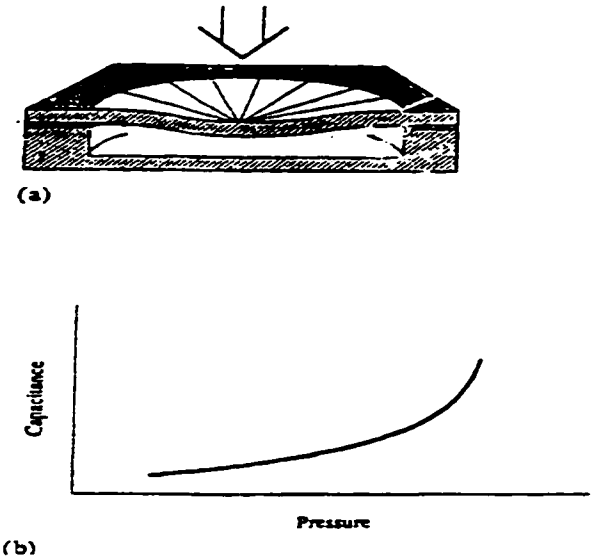

Figure 1.8: Scheme showing a typical non-linear variation of capacitance against pressure [adopted from Rosengren, 150]

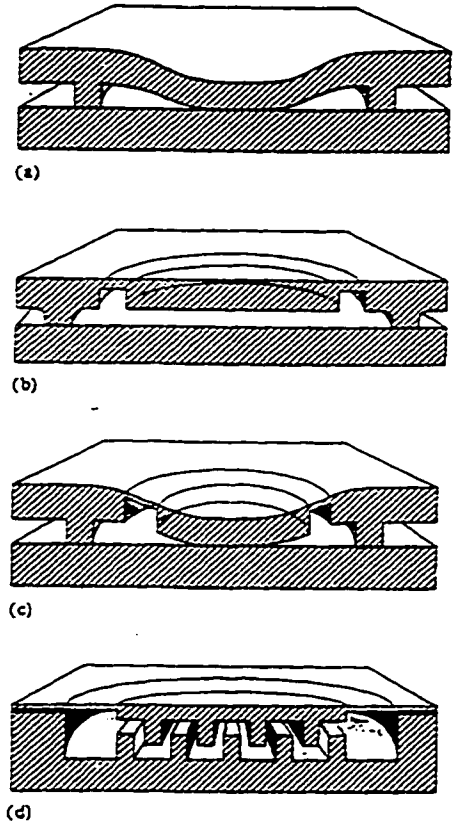

Figure 1.9: Scheme showing geometrical variations introduced to obtain linear variation of capacitance against pressure [adopted from Rosengren, 150]

Bergqvist [12] applied finite element analysis for the estimation of the effect of electrostatic force, thermal stress and acoustic holes on the sensitivity of the microphone.

So far, all the microphones were made by bonding the top and bottom plates. In Thielman and Hess [179] dielectric cavity was formed by sacrificial etching of oxide. Diaphragm and acoustic holes are formed by anisotropic etching with KOH.

Hsu et al. [84] fabricated a condenser microphone in a single wafer process by combining both bulk and sacrificial etching, and measured capacitance variation against bias voltage. Parametric optimization of design variables namely diaphragm width, diaphragm thickness, geometry and number of acoustic holes, and dielectric gap was proposed for improved performance.

Esashi et al. [59] fabricated sensors and sensor arrays with on-chip CMOS circuits as an example of type-II integration. The diaphragm and backplate were vacuum sealed through bonding process.

Another example is the development of micromachined accelerometers. An accelerometer generally consists of a proof mass M suspended by beams with effective stiffness constant K connected to fixed frame as shown in Figure 1.10. C is the damping coefficient affecting the dynamic movement of the mass. The lumped model of the microsystem is also shown in this figure. External acceleration displaces the support frame relative to the proof mass (z-y = -x) changing the stress pattern in the beams. The

relative displacement x, can be used as the measure as in the case of capacitive type accelerometer while the change in the stress can be used as a measure in piezoresistive types of microaccelerometers.

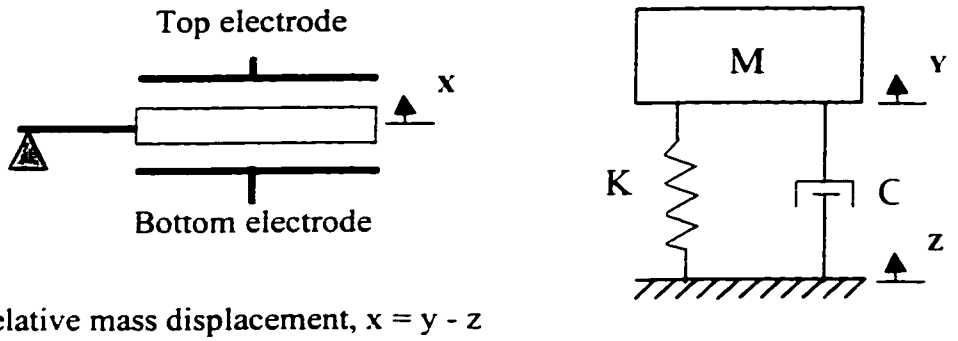

Figure 1.10: Accelerometer scheme and its lumped model [202]

The first micromachined [159] and the most commercialized [10] microaccelerometers were piezoresistive. In piezoresistive devices the silicon piezoresistors are placed at the regions subjected to maximum stress as the case with support ends of suspension beams. The advantage of piezoresistive device is their simplicity in construction and the initial fabrication of sensors were done by bulk micromachining along with wafer bonding technology [159, 10, 143, 5,146,160] as in the case of type-I intergration. Standard CMOS process was used with addition of some process for the fabrication of piezoresistive accelerometers by bulk micromachining in such a way that it was possible to integrate with CMOS circuitry [146, 160], as the case in type-II integration.

The relative motion between the frame and the mass is sensed by the change in capacitance between the electrodes attached to the frame and the moving mass. Mostly

used accelerometers are of the vertical and lateral types. In vertical type [161, 140, 147, 154, 155, 76, 47, 195, 203, 106], the proof mass is separated by a narrow air gap from a fixed plate, forming a parallel plate capacitor as shown in Figure 1.6. In lateral displacement type of accelerometers [162, 27, 35, 188] the moving mass has many fingers that move between parallel vertical walls of fixed electrodes. Fabrication of early micromachined capacitive type of accelerometers [161, 154, 155, 76, 153, 155, 127, 157, 173, 91, 139, 186] used bulk micromachining combined with wafer bonding. In these sensors, the sensing parts are connected externally to the separate sensing circuits, as in the case of type-I integration. As part of the evolution, the use of surface micromachining increased in the fabrication of accelerometers [162, 147, 27, 35, 136, 74] in order to explore the possibility of integrating sensor and integrating circuitry on a single chip, as in the case of type-II integration.

1.2.5 Factors Affecting Dynamic Behavior of Microsystems

Apart from the geometrical/structural constraints that are inherent in the fabrication process, there are some interesting phenomena that are part of the microdomain of matter that affect the dynamic behavior of the microsystems.

1.2.5.1 Squeeze film effect

The dynamics of the oscillating structures such as capacitive type pressure sensors, accelerometers, actuators etc. are strongly affected if the ambient pressure is not zero in the close proximity of other surfaces. The effect of flow of air in the narrow gap between electrodes of the microsystems especially in the case of capacitive type of devices, called squeeze film effect, affect the dynamic behavior in different ways depending upon the operating frequency of the mechanical structure. The dynamic behavior of the system is very much affected by the dissipation of energy especially near the natural frequencies. The dissipation occurs due to structural damping of the moving micromechanical structure and viscous damping due to the friction between the air or a dielectric medium and the surface of the structure. This phenomenon is common for pressure sensors or accelerometers or actuators that have narrow gap between the fixed and moving electrodes. The interaction between the fluid flow and the structural dynamics is dependent on the frequency of oscillations of the structure. At low frequencies, the inertia of the fluid is low leading to higher flow velocities and hence higher frictional forces and damping. This viscous damping is highly dependent on the ambient pressure, size and geometry of the opening in the structure for the movement of the ambient fluid. Besides the damping forces, the movement of the fluid also creates additional spring forces due to the fluid compression and inertial forces due to the mass of the fluid adhering to the surface [7, 115]. At very high oscillation frequencies, velocity of the fluid is very low due to high inertia resulting in low damping and high spring forces. This results in addition of the stiffness to the microsystem due to the movement of

ambient fluid medium at very high oscillation frequencies. The variation of damping constant and spring constant against the operating frequency is schematically shown in Figure 1.11. The damping dominates for frequencies below the critical while spring effect dominates for frequencies above the critical. For such microsystems, the increase in the ambient pressure increases natural frequency due to the increase in squeeze spring constant and reduces the Q-factor due to the reduction in viscous damping [6, 7, 40, 115, 135, 189, 196, 205].

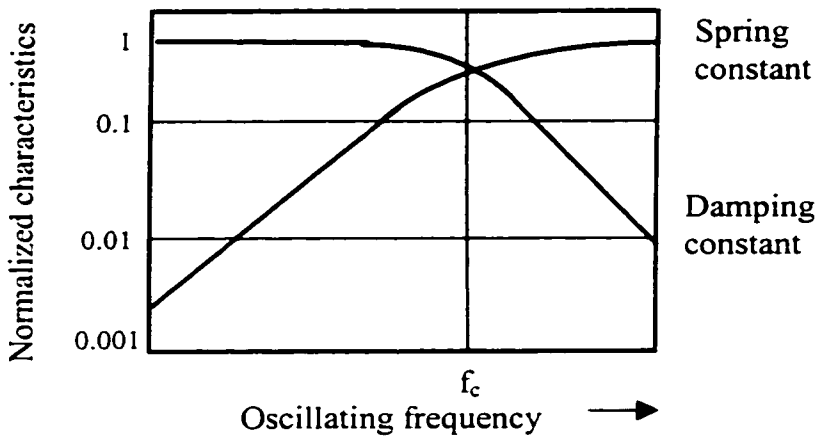

Figure 1.11: Scheme for the variation of damping and spring constant against oscillating frequency due to squeeze film effect [115]

1.2.5.2 Effect of electrostatic force

In capacitive type of sensors and actuators shown schematically in Figure 1.7, the electrostatic force between the electrodes separated by a narrow gap changes the combined elastic properties of the system and hence it affects both static and dynamic

behavior of the structure. The effect of electrostatic force on the static equilibrium of the structure is shown in Figure 1.12.

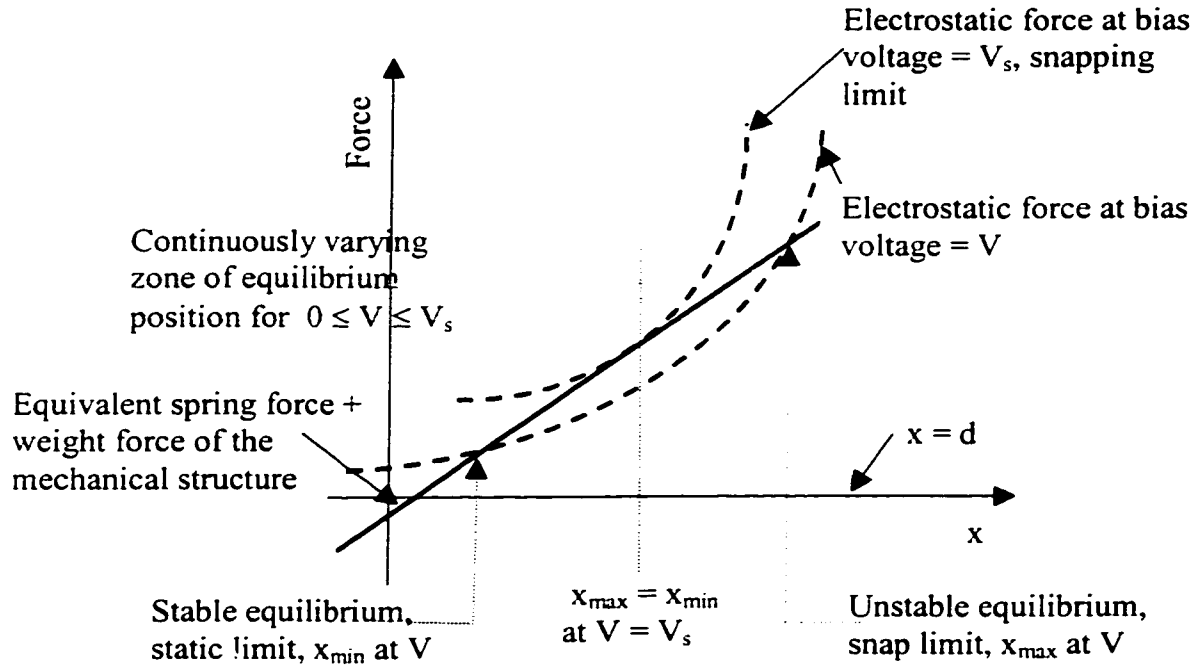

Figure 1.12: Scheme for considering electrostatic force on a elastic structure

When a bias voltage V is applied between the electrodes of a capacitive device, diaphragm deflects due to the electrostatic pull and reaches the stable equilibrium of x_{min} where electrostatic force equals the restoring spring force of the mechanical structure. Any small disturbance close to the equilibrium position is always stable as the available mechanical energy is higher than the electrostatic energy. But the deflection beyond x_{max} results in higher electrostatic energy and hence permanent snapping of the structure towards the backplate. The natural frequency of the structure close to the equilibrium position, becomes amplitude dependent for a given bias voltage. The bias voltage for which $x_{min} = x_{max}$, is called snapping voltage, V_s. The system will always be in unstable

position for bias voltage higher than V_s. Hence, prediction of static and dynamic behavior of the microsystem under the influence of electrostatic field becomes important in manipulating the performance of the capacitive device.

Stiharu and Bhat [165] predicted the effect of electrostatic force on the natural frequency of microplates by applying Rayleigh-Ritz method.

Brugger et al. [29] predicted the static deflection and snapping distance for a capacitive microlever and applied the electrostatic force for gripping with microprobe head. Bobbio et al. [25] applied electrostatic force for making integrated force arrays as in the case of actuators.

Van der Donk et al. [187] predicted the static deflection, sensitivity, snapping limit due to electrostatic force for a capacitive type condenser microphone with and without residual stress in the diaphragm. Classical end conditions were assumed in deriving the deflection equations for the diaphragm.

Kohl et al. [93] studied micromechanical characteristics of electrostatic linear actuators having a driving unit consisting of several arrays of parallel connected capacitor elements. The increase in voltage between the capacitor elements increases the static deflection and decreases eigenfrequency.

Turner and Andrews [184] report the amplitude dependency of the natural frequency of the clamped-clamped oscillators and also possibility of modifying the natural frequency by varying the electrostatic force.

Fan and Crawforth [60] report the spring softening effect through electrostatic force for microstructures.

Park et al. [132] implemented stiffness tuning capability into a surface micromachined silicon accelerometer through a electrostatic comb type capacitive fingers. Through electrostatic tuning, natural frequency was shifted from 5.12kHz to 950Hz. Excitation, sensing and tuning were implemented by capacitive variation. Frequency response of the structure was found by sweeping the input oscillating frequency.

Rangten et al. [144] micromachined a loudspeaker with hermetically sealed cavity and excited electrostatically. The sound pressure level and the natural frequency were found to decrease with biasing voltage. The natural frequency was measured by sweeping the frequency of the electrostatic excitation.

Chu et al. [42] predicted and measured the natural frequency of parallel plate electrostatic actuators fabricated by MCNC [114] after including the squeeze film and electrostatic effect between the electrodes. In measuring the frequency response, the excitation was electrostatic and the detection was by Michaelson interferometer.

Adams et al. [3, 4] implemented the tuning of natural frequency of a micromechanical resonator through a fringing-filed actuator. The positive and negative stiffening can be created by proper positioning of fingers in the actuators. The experimental variation of natural frequency from 7.7% to 146% was achieved by electrostatic tuning. Micromechanical structure was excited electrostatically.

1.2.5.3 Lorentz force

When a conductor of length L carrying a current of $I(\omega)$ is subjected to an external magnetic field of intensity B, Lorentz force of $F(\omega) = I(\omega)L \times B$ is exerted on the conductor as shown in Figure 1.13. The frequency of force can be varied by changing frequency of the current. This force can be used to change the elasticity of the structure and hence to result in different static and dynamic behavior of the structure. The steady electromagnetic force under DC current can also be used to manipulate the static and dynamic behavior of the structure as in the case of electrostatic force. The Lorentz force can also be used for frequency tuning or canceling the effect of electrostatic force through proper designing of the micromechanical structure.

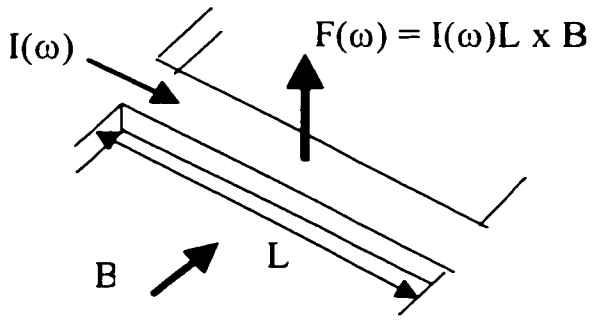

Figure 1.13: Scheme for Lorentz force

Kang et al. [90] used fluctuating Lorentz force in order to excite and measure the natural frequency of a microbeam. Vibration of the structure was detected by optical modulation and a photodiode.

Ma et al. [107] applied fluctuating Lorentz force generated by supplying AC current in measuring the frequency response of a cantilever-in-cantilever type structure. The detection of the vibration was carried out by the change in piezoresitance and by laser deflection measurement. Yu et al. [207] studied the frequency response of the above mentioned cantilever-in-cantilever structure under different steady Lorentz force conditions. The frequency response of the mechanical structure was measured by exciting with 3.6G AC magnetic field under two different conditions of 16G DC and 2G DC magnetic field. It can be inferred from these results that higher DC Lorentz force resulted in lower natural frequencies compared to that of lower Lorentz force with 2G DC magnetic field. Higher electromagnetic force modifies (weakens) the elastic properties of the system leading to reduced natural frequencies.

1.2.6 Synthesis of Microsystems

In general, actuation or sensing will be large if it happens close to the natural frequencies of the micromechanical structures. One could choose or avoid operating closer to natural frequencies of the microsystems based on the structural integrity. This is the case with most of the sensors and actuators when dynamic behavior is important in determining the performance of the microsystem. ***The synthesis of microsystems involves development***

of fabrication strategies using industrial CMOS process and design strategies, in order to manipulate the effect of inherent limitations of fabrication and other limitations due to structural configuration and environment on dynamic behavior of microsystems. The design synthesis of microsystems of sensors, actuators and other devices, includes

1. prediction of dynamic behavior for the given conditions of the microsystem in order to estimate the performance of the microsystem and
2. manipulation of the system elastic properties in order to obtain the required dynamic performance of the system. The manipulation could be effected by proper selection of structural configuration, support conditions, fabrication sequence and by external means such as electrostatic force, squeeze film effect, fringe field effect, etc.

Hence, a unified approach of studying and quantifying the effect of all the above system parameters on elastic property will be of immense help towards the synthesis of microsystems.

1.3 MANIPULATION OF VIBRATION BEHAVIOR OF ELASTIC SYSTEMS

Manipulation of vibration behavior of elastic systems involves manipulation of response with the help of external sources, and manipulation of natural frequencies and mode shapes through change in mass and elastic properties of the system. For any continuous system, the vibration response and depend on modal force distribution, excitation

frequency, relative position of excitation frequency in relation to natural frequencies and mode shapes of the elastic system. As the principle of superposition holds for vibrational response, the distribution of modal forces due to different types of external loads could be manipulated such that net response from both primary and secondary sources is minimized. Sound radiated from structures are due to the structural vibration and hence the sound radiated from continuous systems also can be understood from the vibrational response.

As the natural frequencies (eigenvalues) and normal modes (eigenvectors) of a given structure are constant in many cases, minimization of deflection by producing anti-modal forces in proportion to disturbance force is called Active Structural Vibration Control (ASVC). Similarly, minimization of radiated sound through optimization of the load distribution, is called Active Structural Acoustic Control (ASAC). Thus it can be seen that the vibration or the radiated sound depends upon the eigenvalues, normal modes and the external load. In the types of controls mentioned so far, only the distribution of external load is manipulated such that vibration or sound is minimized.

In general, the active control of sound and vibration will be useful in the audible range of 20Hz-20kHz. The passive damping technique which absorbs vibrational energy is effective at higher frequencies and is used for excitation frequencies more than 1000Hz. At low excitation frequencies both active and semi-active methods of control are useful. In structural applications such as in aircraft fuselages, automobile cabins, the excitations are relatively steady and they are produced by rotating type mechanisms such as the gas

turbine engine, propeller, engine mechanism or rotating tires interacting with road. As the transients associated with audio range vibrations decay very fast, only the steady state disturbances which are multiple tones are important for active and adaptive type controls [67]. In Active type control, the generated sound and vibration due to the primary disturbance is suppressed or canceled by producing sound or vibration equal in magnitude and exactly out of phase by secondary sources, such that the resultant sound or vibration is minimized. Anti-sound source could be a speaker while anti-vibration source could be electro-dynamic shakers, piezo-ceramics actuators, electro-hydraulic and magnetostrictive devices.

Active control of sound/vibration can be effected with speakers or actuators as secondary sources. Active control can be implemented by feedforward or feedback control methods. Leng [104] was the first to implement active control of sound in a duct with a feedforward controlled speaker. Later Olson and May [128] demonstrated local reduction in noise using feedback controlled speaker arrangement. The general representation for both feedback (F/B) and adaptive feedforward (F/F) active controls is shown in Figure 1.14.

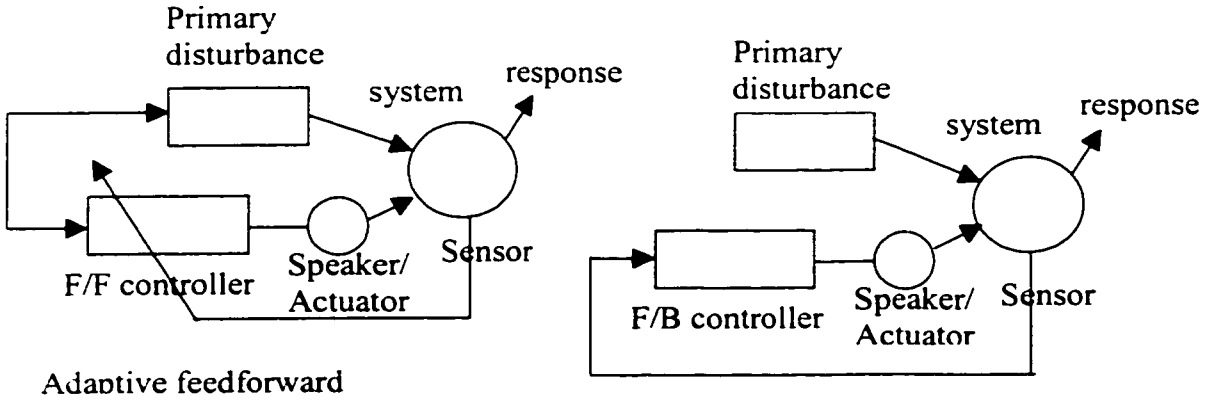

Figure 1.14: Types of control by manipulation of external load

Feedback controller which results in fast convergence and high steady state error compared to feedforward controller, makes it suitable for random noise cancellation [11, 53]. Feedback control is useful when no reference signal partly correlated to input excitation is available. Feedforward control is preferred whenever reference signal is available because of its simplicity and easy implementation. Adaptive feedback control is not widely available for application to structures. The available feedback control works are of pole-zero placement types in a general sense [53].

Adaptive feedback control was applied based on minimization of volume velocity [88]. Actuator was designed to be reciprocal of volume velocity sensor such that transfer function between actuator and sensor was of minimum phase with performance as good as that of feedforward one.

Baumann [11] recommends feedback controller only in cases where reference signal is not available.

The adaptive feedforward method is simple and effective for noise and vibration control as the primary disturbance is harmonic in nature and it is a simple task to have a reference signal. Feedforward speaker control has been implemented for reducing noise inside aircraft fuselage successfully in many practical applications like Emborg [58] in Saab 340 propeller aircraft and Koers [92] in Dornier 228 aircraft. In many cases, reduction of radiated noise through speaker control resulted in the increase of structural

vibration. It also resulted in only local reduction of noise with the application of large number of speakers.

As against these limitations in using speaker based control, structure based actuator control results in noise and vibration reduction with minimum number of actuators. The published results [43, 44, 52, 68, 70, 94, 172] recommend the structural actuated adaptive feedforward control for both structural vibration control and control of radiated noise.

In semi-active type of control, passive elements are controlled actively such that dissipation or absorption of energy becomes effective at the new operating condition. Semi-active actuators are generally constructed from electro or magneto rheological fluids, shape memory alloys (SMA) or fluid filled varying orifice devices.

From a comparison of active, passive and semi-active controls for reducing aircraft cabin noise. Flotow et al. [64] found that the use of semi-active control in tuning the passive vibration absorbers to resonate at the excitation frequencies was comparable to Active Structural Acoustic control, in terms of added mass per seat, cost and power consumption.

From the above discussion on the control of sound and vibration, it is clear that all methods are not suitable for specific applications. Hence, evaluation of the methods against each application is necessary before a choice can be made. This calls for a clear understanding between the vibration behavior of the structure and all the design

parameters of the structure such as geometry including method of manufacturing and external forces. Moreover, whether it is ASAC, ASVC or semi-active control, manipulation of vibration response is carried out through external means.

It is possible to control the vibrational behavior of a system by staggering the natural frequencies in a required fashion in relation to the excitation frequencies [118]. It is also possible to control the radiated sound pressure by modifying the acoustic coupling coefficients through the change in mode shapes [117, 120].

Whenever the excitation has single or multiple tones, the relative location of eigenfrequencies as shown in Figure 1.15 is important in order to manipulate the vibration behavior.

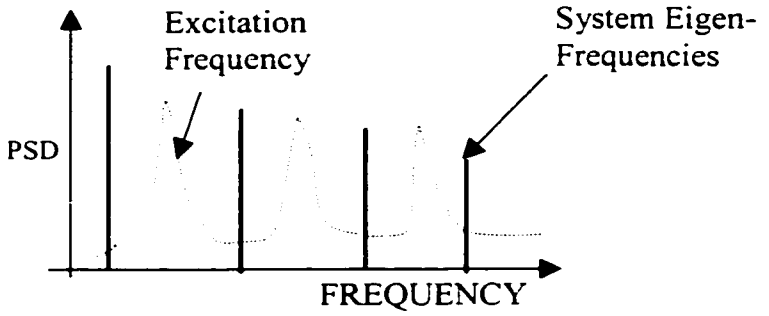

Figure 1.15: Scheme for structural tuning

Minimization of vibration is possible by moving the eigenfrequencies of the system away from the excitation frequencies and maximization of the efficiency in the case of semi-active vibration absorbers is possible by moving the eigenfrequencies of the absorbers close to excitation frequencies. The arrangement of the natural frequencies in a certain order gives an inherent quality to the sound, and this quality is responsible for the richness of the sound in musical instruments. This process of staggering the natural frequencies in a required order in relation to excitation frequencies in order to minimize or maximize the response or simply to enrich the sound quality of musical instruments, is called structural tuning [118].

The concept of structural tuning is applicable to microsystems also where higher natural frequencies are also important in determining the performance of the sytem. In An et al. [6], the performance of gyroscope is dependent on the natural frequencies. In this report, the modification of the arrangement of natural frequencies for gyroscopes achieved through bias voltage is also an example of structural tuning.

Another important aspect of the manipulation of vibration behavior is modification of mode shapes of macro or micro structures. The acoustic radiation which depends on the mode shapes can be altered by modifying the mode shapes or changing the elastic and inertial properties of systems [105]. It is also possible to localize the vibrational response to a certain part of the system through modification of mode shapes, which will be useful for better/easier control of the response [117, 120]. If the localization of the response is effected close to the source of disturbances, then the control will be easier with a few

additional sources and moreover the fatigue life of the other parts of the system will improve.

Thus, the manipulation of the vibrational behavior of the system, especially natural frequencies and mode shapes, has tremendous potential for control, design, enhancement of structural systems of micro and macro dimensions. This kind of manipulation of vibrational behavior of a system by changing elastic properties of the structure or the environment [117-123, 129] can be effected in many ways as mentioned below:

1. *Changes to the elastic property by modification of structural geometry*: Examples includes addition of stiffness, notches, slots, slits corrugation etc. Stiffened plates of different geometries find various application in engineering. The positive stiffeners [23, 75, 99, 124, 199] are used to increase the strength of the structure. The other methods like notches, slots, corrugations work as negative stiffeners and may find applications where it becomes necessary to attenuate or control the transmission of vibrations through the joints.

2. *Changes to the elastic property by using different support conditions*: The different support conditions could be end supports or supports anywhere within the structure. Examples include clamping, riveted joints, strap joints or any other supports. It is well known that vibration behavior of structures is strongly influenced by boundary conditions such as clamped, simply supported and free. Changing the boundary conditions from simply supported to clamped conditions in beams and plates can

more than double their respective natural frequencies [102, 103]. The boundary conditions of real structures are not always homogeneous such as clamped or simply supported. The boundary conditions may be flexible either in translation or rotation [99, 100, 206]. Furthermore, even along a single edge of a two-dimensional structure such as a plate, the boundary conditions may not be uniform and may change along the edge [163]. In structures which is supported at several points or lines within the domain of the structures such as in periodically supported beams or plates, such supports may be considered as providing boundary conditions for the structure. Addition of supports [206] also changes the vibration behavior. James and Fahy [86] studied the coupling effect of number of straps between two plates and found the dependencies of transmissibility between structures. Thus, the elastic property of the entire system can be altered by modifying the support conditions between structural and environmental parts of the elastic system.

3. *Changes to elastic property through the fabrication process*: It is also possible to alter the distribution of elastic property of the system through fabrication techniques such as heat treatment, hammering, work hardening, peening etc. An example for this type of change is the steel pan musical instrument. The vibration behavior of the pan is modified through only such processes [1, 2, 185]. Sometimes the change of elastic property of the structure is due to the inherent nature of the process. For example, structural properties may change due to residual stress introduced in the structure because of different temperature cycles involved in the manufacturing processes.

Hence, it is possible to modify the vibration behavior of elastic systems through structural modification, support conditions and manufacturing process.

1.3.1 Concept of Boundary Conditioning

As seen in previous sections, good performance of the elstic systems depends on its dynamic behavior characterized by natural frequencies and mode shapes and is relevant to inertial sensors, pressure sensors, micro-resonators and free standing structures in the case of microsystems and many structures in the case of macrosystems. The dynamic behavior in turn is dependent on the mass and stiffness properties of the systems. It is clear from the previous sections that the stiffness of the elastic system is strongly dependent on the fabrication process, structural geometry, support conditions and the operational environment.

Any structural modification such as stiffening, notching etc. affects the dynamic behavior of the micro and macro systems. The micromechanical components that are fabricated either through a standard CMOS process or a dedicated MEMS process, are subjected to different support conditions that are inherent to the fabrication process. The different support conditions result in different rotational elasticity at the supports which make end conditions non-classical and intermediate between the free and the clamped conditions. These conditions are common for macrosystems and can also be created by clamping, riveting etc. Hence it is not possible to exactly create the end conditions known from

classical mechanics at the micro level even though the clamped condition is assumed in literature for all supports. Many environmental phenomena were also seen to affect the dynamic performance of the microsystem in the previous Section 1.2.5.

Hence, a unified quantification of the influence of fabrication process, geometry, support conditions and environmental influence on the dynamic behavior of the system will be very useful during the design process and also for modeling the dynamic performance of the system. The concept of modification of elastic property of the system through structural modification, support conditions, manufacturing process and other environmental influences, is introduced as *boundary conditioning.*

1.4 APPLICATION OF BOUNDARY CONDITIONING TO SYNTHESIS OF MICROSYSTEMS

The principle of applying boundary conditioning applied to the synthesis of microsystems is outlined in this section:

1.4.1 Boundary Conditioning by Structural Variations

The general scheme for adding stiffeners and notches to a mechanical diaphragm is given in Figure 1.16. Rosengren et al. [150] improved the performance of the condenser microphone with addition of stiffeners and notches as shown in Figure 1.11 in order to modify the system elastic property. Rangsten et al. [144] added notches as shown in

Figure 1.17 at the end supports of diaphragm of an electrostatically excited loudspeaker in order to weaken the stiffness of the diaphragm and to have larger deflections. These kinds of notched ends or structural joints result in weakened regions compared to that of clamped condition. A diaphragm of Metal1 with stiffeners of Metal2, fabricated out of the Mitel 1.5 μm process using isotropic etching is shown in Figure 1.18 as an example of a device that will be fabricated using type-III integration. In piezoresistive devices, piezoresistor elements that are added at the locations of high stresses as shown in Figure 1.16c make the mechanical structure rotationally stiffer resulting in the end conditions different from classical ones. Figure 1.19 [122] shows such a microsystem with piezoresistor elements of polysilicon2 fabricated through Mitel 1.5 μm process.

Corrugating the structure closer to the support or anywhere in the structure alters the distribution of system elastic property and the dynamic performance. The corrugations weaken the structure rotationally and make the end conditions intermediate between the clamped and simply supported. Figures 1.20 and 1.21 show microsysystems with corrugations that were fabricated through type-II integration method.

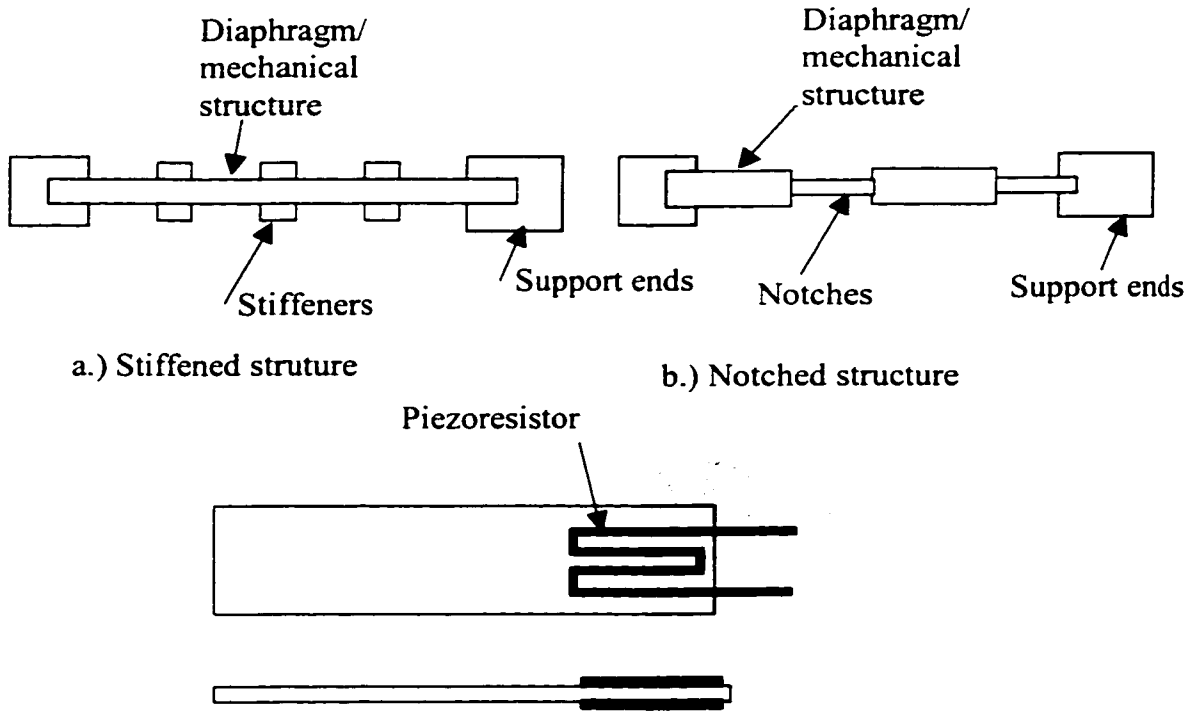

a.) Stiffened struture

b.) Notched structure

c.) Stiffened end condition due to piezoresistor element

Figure 1.16 Scheme for adding stiffeners and notches to a microsystem

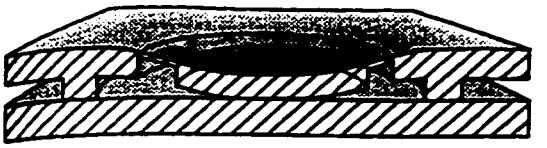

a) unexcited

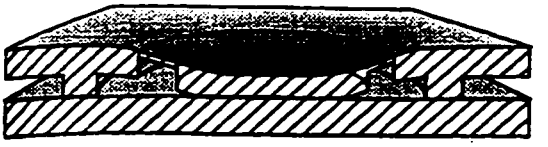

b) excited

Figure 1.17: Rotationally weakened end supported diaphragm of a electrostatic loudspeaker [adopted from [144]]

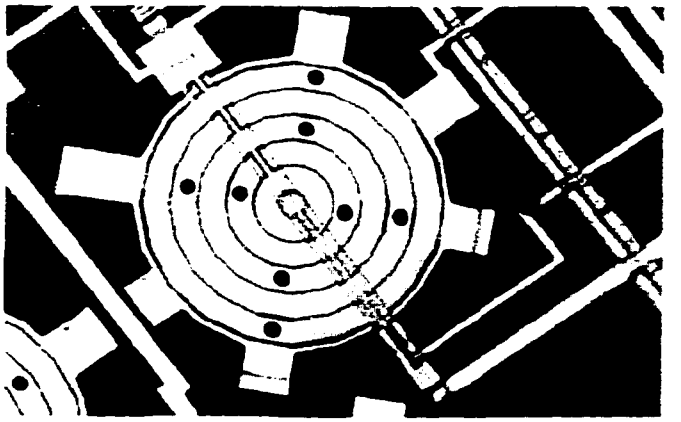

Figure 1.18: A circular diaphragm of Metal1 with Metal2 stiffeners, fabricated by Mitel 1.5 mm process combined with isotropic post-processing. (Diameter is 650μm)

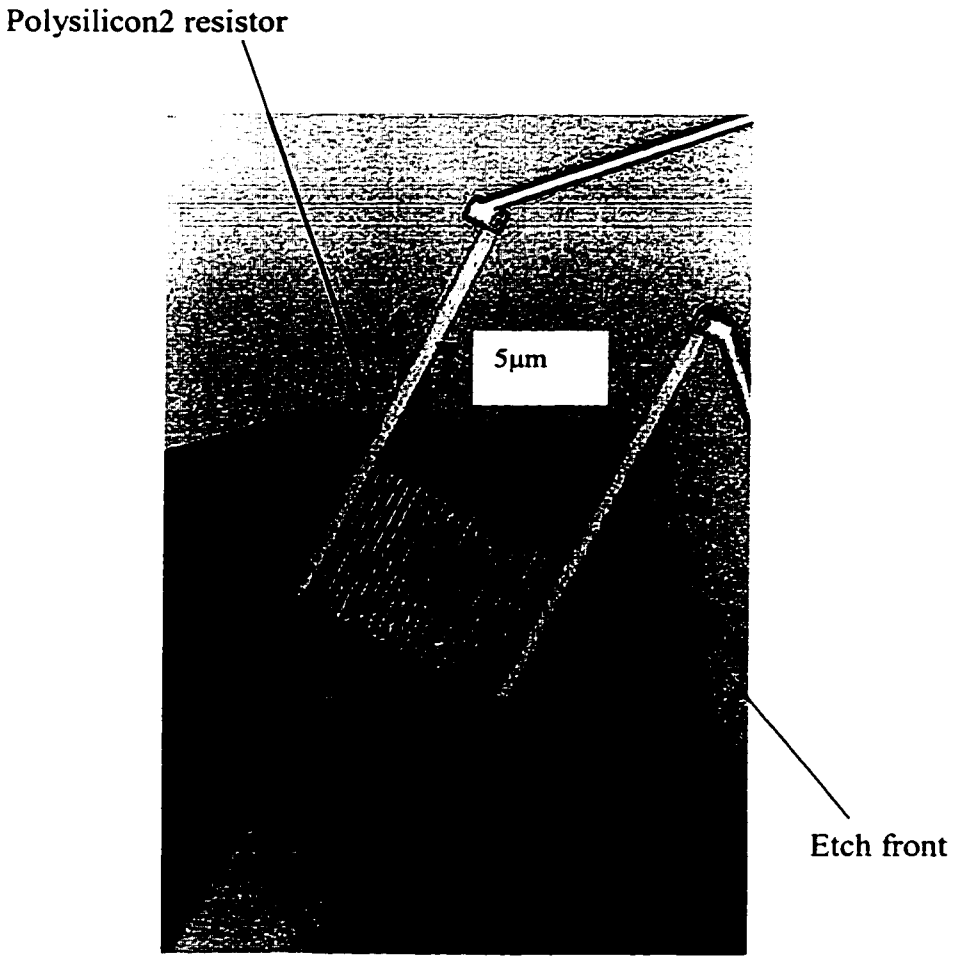

Figure 1.19: Stiffened at support end by piezoresistive elements [122]

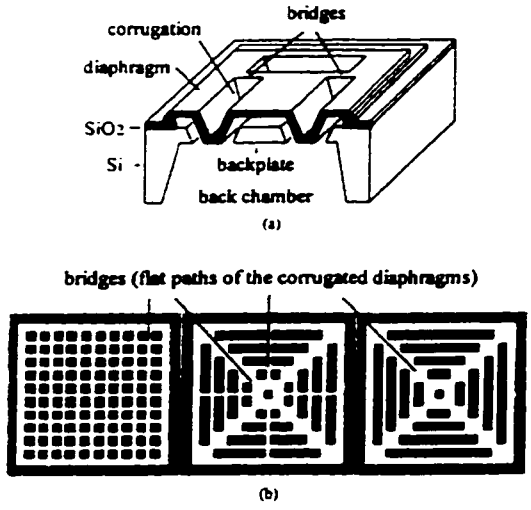

Fig. 1. Schematic description of (a) the microphone and (b) three corrugation placements.

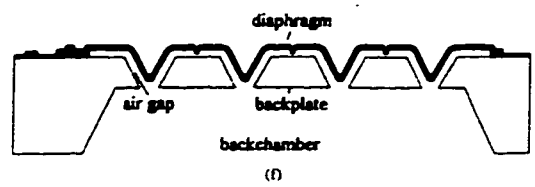

Fig. 3. Fabrication process for the microphones.

Figure 1.20: Schematic representation of microphone with different arrangements of corrugations [adopted from [214]]

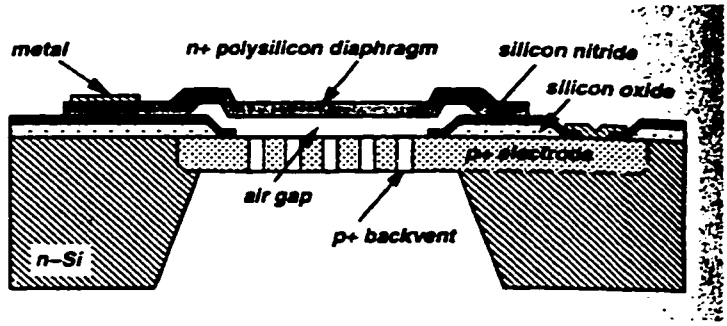

Figure 1.21: Scheme for a polysilicon diaphragm condenser microphone with a corrugation resulting from sacrificial etching [adopted from [84]]

It is also possible to fabricate corrugated structures through type-III integration as proposed in this thesis. The diaphragms with corrugated beam extensions fabricated out

of Mitel 1.5 μm process and post-released by isotropic etching are given in Figures 1.22 and 1.23. The corrugation in transverse direction in Figure 1.22 was fabricated by stacking different layers of Mitel 1.5 μm process in order to weaken the structure rotationally at the supports and obtain larger deflection. The increased rotational flexibility at the supports make them different from the classical clamped conditions. Corrugations present in the structure introduce both translational and rotational freedoms between the adjacent structural parts. Modeling such microsystems should be able to accommodate such conditions which are different from the classical ones, and also the sudden changes in elastic properties between the adjacent parts of the structure.

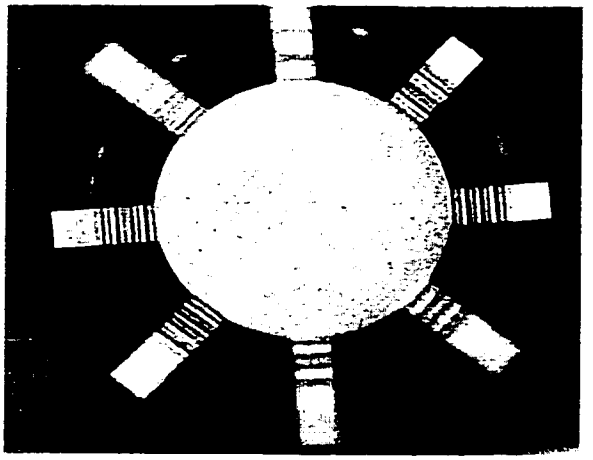

Figure 1.22: Corrugated diaphragm of Metal1 obtained by stacking of different layers in the Mitel 1.5 μm process (Type-III integration). Diameter of the diaphragm is 250μm

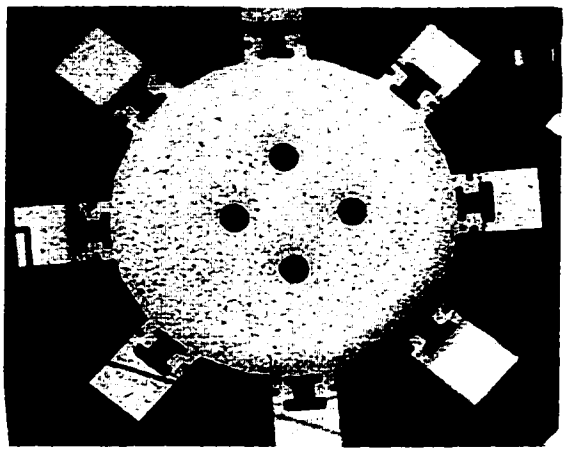

Figure 1.23: Corrugated diaphragm of Metal1 obtained in the Mitel 1.5 μm process (Type-III integration). Diameter of the structure is 650μm

1.4.2 Boundary Conditioning through Fabrication Methods

1.4.2.1 Effect of support conditions

In general, free-standing structure in a microsystem can have support at the ends or anywhere in the structure and the supports can be of point or line types. The support conditions that exist in microsystems fabricated through all types of integration methods, are very much dependent on the fabrication process and are always intermediate to classical conditions. It was seen in the previous paragraphs that it is possible to create different support conditions by modifying the structural geometry. The fabrication process selected for microsystems determine the end support conditions due to inherent limitations of the process.

Whenever free-standing structures are fabricated through aniostropic etching [45, 164] as shown in Figure 1.24 etch is stopped at <111> plane resulting in support structures as shown in Figure 1.24.

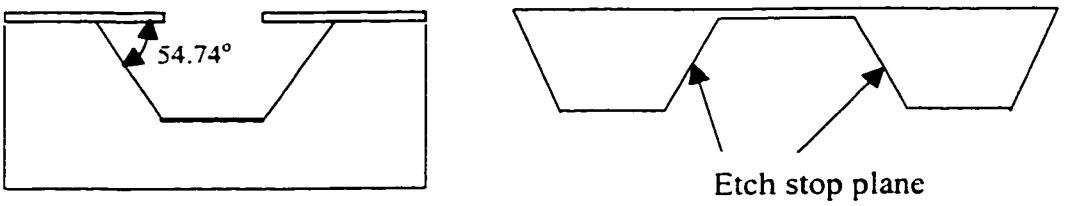

Figure 1.24: Scheme for anisotropic etching of free standing structures

Whenever the MEMS devices are fabricated using CMOS process, they have laminated layers of structural and sacrificial layers. Surface micromachining of sacrificial layers

can result in complex, noncrystalline and integrated microelectromechanical free standing structures that are not fabricated in bulk or bonded process. Surface micromachining will be the heart of the scientific and commercial activity in MEMS [142] in future for post-releasing the structures fabricated through type-III integration. In sacrificial etching methods, free-standing structures formed by etching out the sacrificial layers can result in step-up or corrugated structures as shown in Figures 1.21 and 1.25. The adhesion of the mechanical structure to the substrate at the support areas is dependent on the type of fabrication process such as deposition, growth of the substrate etc. as shown in Figure 1.25. Such support conditions can exist at the end of the mechanical structures as shown in Figure 1.25 or at the center of the structure as shown in Figure 1.26 or anywhere else in the structure resembling point or line supports. Whenever microsystems are fabricated through surface micromachining, the supports introduce additional rotational freedom and make the support conditions away from classical clamped conditions. The point support at the center of the diaphragm in Figure 1.26 can completely arrest the translational motion and can introduce some rotational freedom to the structure. In literature, all the support conditions resulting from sacrificial etching are generally treated as clamped, neglecting the rotational flexibility introduced by the real supports. Hence, in modeling the dynamic performance of such microsystems, support conditions different from the classical ones need to be accomodated.

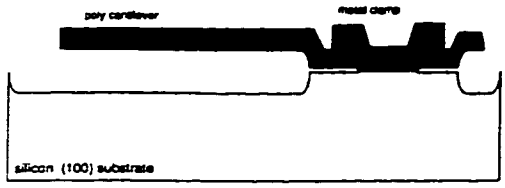

a) Free standing resonator from standard CMOS (type - III). [adopted from [152]]

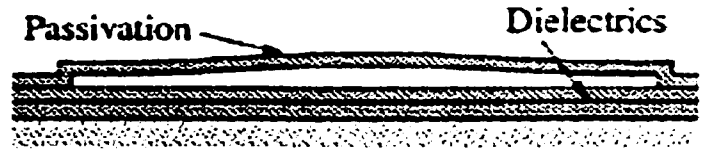

b) clamped-clamped beam of a 2μm CMOS process [Adopted from Paul [135]]

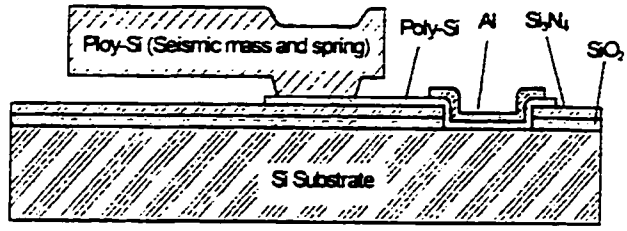

c) Scheme of a gyroscope [adopted from Park et al [132]]

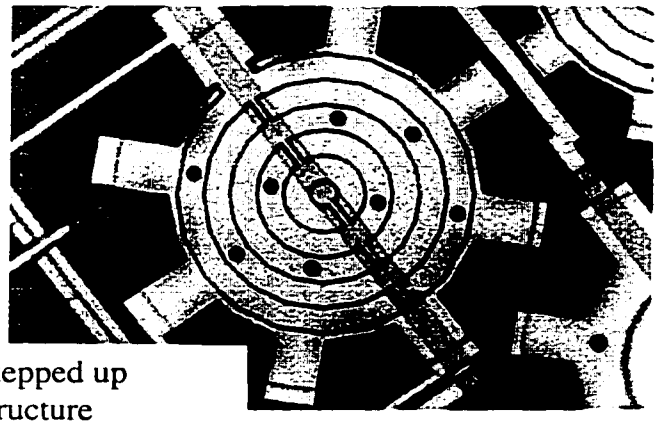

Stepped up structure

d) A diaphragm with stepped up end beams fabricated out of the Mitel1.5 μm process at Concordia (type III) Diaphragm diameter is 650μm

e) Stepped up plate type polysilicon structures fabricated through the MUMPS process

Figure 1.25: Different stepped up end conditions inherent to sacrificial machining

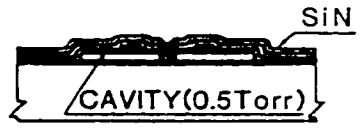

Figure 1.26 A diaphragm with a point support at the center [adopted from Sugiyama et al [171]]

1.4.2.2 Boundary conditioning through fabrication processing parameters

Even though MEMS fabrication tries to adopt the standard microelectronics fabrication process and materials to its full advantage, it also suffers from the same limitations of the microelectronics fabrication process and materials which are not optimized for MEMS applications. Hence, fabrication process and the materials are at their extremes when applied to fabrication of microsystems. The process layers of different materials that are generally made by deposition at different temperatures are subjected to different residual stresses. The greatest difficulty occurs when moving structures are released in a post-release etch since the entire microelectronics processing parameters are optimized for the static microelectronics components. One of the important considerations in the selection of processing parameters is the residual stress in released structures which make the structures to bow and bend, and change the distribution of elastic property. In future, the processing parameters need to be revised in order to fabricate matured microsystems. The microresonators fabricated out of the Mitel1.5 μm process [122 , 123] shown in Figure 1.27, indicates the deflected shape of beams due to residual stresses. The curved up diaphragm of a condenser microphone fabricated through MUMPs process [121]

given in Figure 1.28 shows the change in elastic property of the diaphragm due to residual stress. Hence, in modeling the dynamics of such microsystems, the change in the elastic property of the system due to the effect of processing parameters like residual stress has to be incorporated.

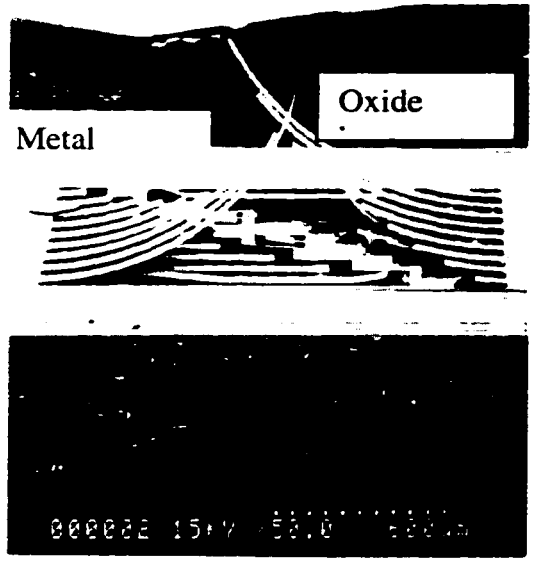

Figure 1.27: Beams under residual stress fabricated through the Mitel 1.5μm process [122,123]

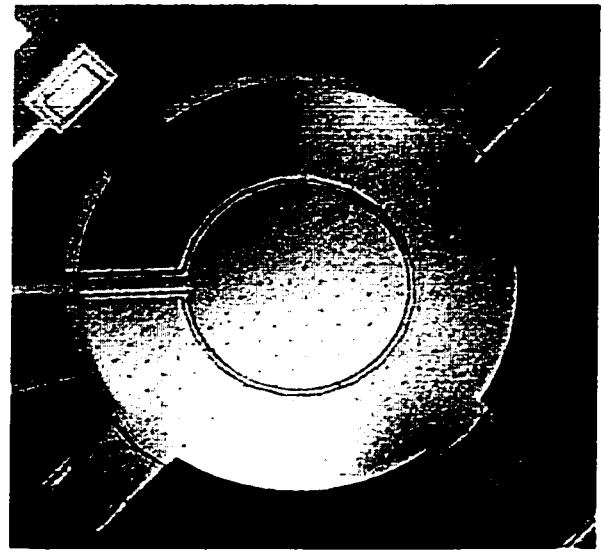

Figure 1.28 A capacitive microphone diaphragm under residual stress fabricated through the MUMPs process [121]

1.4.3 Boundary Conditioning through Environmental Influence

Apart from the structural geometry and process influence on the system elastic property, there are phenomenological influences due to the presence of environment on the system elastic property in microdomain of matter. As seen in Section 1.6, the dynamic behavior of a microsystem with an oscillating structure in a fluid environment is changed due to the stiffening effect of the squeeze film under the structure. The stiffness

of the microsystem is increased by the environmental contribution (squeeze film effect). The microsystem of condenser microphones having electrodes separated by a narrow gap and connected to a bias voltage, is subjected to electrostatic force in the presence of the dielectric environment. The stiffness of the microsystem is weakened by the negative stiffening effect of the electrostatic environment. But in the case of fringe-field electrostatic environment, both strengthening and weakening of the microsystem is possible depending upon the direction of the electrode movement. The environmental part of microsystems play a significant role in determining the system elastic property and hence the dynamic behavior, due to phenomena present in microdomain of matter. Even though geometry and process related effect on the system elastic property is common to macrosystems, the effect of environment on system elastic property is relevant only to microsystems. A common strategy for capturing the effect of both structural and environmental influence on the system elastic property will be very useful.

The concept of boundary conditioning and its implementation is common to both micro and macro elastic systems. This concept can be applied for the control of dynamic behavior of the systems and their efficient design. The modeling and its application to both micro and macro systems will be discussed in detail in Chapter 3.

1.5 INTRODUCTION TO FUZZY SYSTEM IDENTIFICATION

Identification of systems through their behavior has tremendous applications in almost every field of human interest. In general, system identification could represent any

complicated input/output function approximation, output classification or input-output mapping. System could be of multi-input-multi-output (MIMO) type (with many antecedents and many consequents according to fuzzy logic terminology) or multi-input-single-output (MISO) type with many antecedents and single consequent. In many situations, the conventional quantitative modeling of systems is subjected to limitations due to assumptions and lack of information, uncertainties and ambiguities in the system, vast number of parameters influencing the system behavior, unpredictable interactions between the influencing parameters, exceptional computational requirement, presence of noise, etc. As a result, they could even fail to represent completely the behavior of the systems. Quantitative modeling could become more difficult for some applications even when perfect mathematical modeling is possible especially when modeling is required frequently in the case of problems with many dimensions. In such cases, it could be useful to use the approximate human reasoning being implemented with appropriately coded knowledge. Identification of such systems with inherent fuzziness may be called as fuzzy system identification which has to be done with mathematical operators and logic that are multivalued and not based on *law of excluded middle* (everything must either be or not be), thereby attaching *degree* to everything.

Charles Sanders Peirce was the first to assert that vagueness is an ubiquitous presence and important to logic as important as friction to mechanics [113]. Bertrand Russell went further and said "Vagueness, is clearly, a matter of degree". But Jan Lukasiewicz [113] tried formal modeling of vagueness and invented the substructure of fuzzy sets, an early logic based on more than just the two strict outcomes of true and false. Later Lofti

Zadeh correctly addressed vagueness and set forth the mechanics of fuzzy set theory through the definition of graded memberships. Hence, the theory of fuzzy sets proposed by Zadeh [210] comes as a relief to deal with such a problem since it can model the fuzziness associated with the mechanism of approximate reasoning, system definition and its behavior, through qualitatively defined system variables. The fuzzy set theory finds its application in a variety of engineering problems due to its capacity to model the fuzziness associated with observations and system definition, and to manipulate the required outputs for the engineering world. The proposal of linguistic approach by Zadeh [210, 211] has the capability to model any complex system behavior in such a qualitative way that the model will be more effective and versatile in capturing the behavior of any ill-defined systems with fuzziness or fully defined systems with realistic approximations. The main idea behind fuzzy systems is the fuzzy partitioning of information. Zadeh's [211] proposal of modeling the human thinking helped to introduce fuzziness into systems theory and develop a class of systems called *fuzzy systems*. Zadeh's approach was later developed for modeling fuzzy systems by Tong [182], Pedrycz [137], Trojan et al. [183], Sugeno and Kang [168], Takagi and Sugeno [175], Sugeno and Yasukawa [168], Yager and Filev [200, 201], Mamdani and Assilian [108], Bezdek [15], Bezdek et al. [16], Emami et al. [57] and Chiu [38, 39].

It is possible to identify the fuzzy system using the knowledge of an expert about the system behavior expressed in terms of linguistic values or through *a priori* knowledge about the system. The *a priori* knowledge can be obtained through the mathematical understanding about the system behavior or experimental input-output data of the system.

Fuzzy system identification technique can solve both types of problems with ease. Fuzzy system modeling provides an approximate and yet effective means of describing the behavior of systems that are complex and ill-defined and consists of the following:

1. Identification and use of linguistic variables in place of, or in addition to, numerical variables
2. Representation of the behavior between the variables through conditional fuzzy statements
3. Characterization of the behavior of the entire system through fuzzy algorithms.

Modeling of fuzzy systems consists of two types, namely linguistic models (LMs) and fuzzy-non fuzzy models. Linguistic models are fully fuzzy in nature, described by a collection of IF-THEN rules with vague predicates that use fuzzy reasoning [137, 182]. In this modeling, both antecedents and consequents are defined in terms of fuzzy quantities that can be associated with linguistic labels. Linguistic models can express the system behavior in a qualitative way using natural language [168]. Fully fuzzy linguistic modeling can be used for modeling the system from expert knowledge as well as *a priori* knowledge. When Mamdani [108] type of reasoning is used, the models are called Mamdani fuzzy models.

The second category of fuzzy modeling is based on the Takagi-Sugeno-Kang (TSK) method of reasoning [168, 170, 174, 175]. These TSK models have a set of rules that consist of fuzzy antecedents and functional consequent and they are a combination of fuzzy and nonfuzzy models. This method of reasoning has the ability to integrate both

qualitative and quantitative knowledge representations, and to learn adaptively. Fuzzy models using the TSK reasoning will be called TSK fuzzy models and suitable for identification of system from *a priori* knowledge about the system.

In general, the system identification has two phases, namely, *structure identification* and *parameter identification* [38, 57, 175, 201]. The structure identification involves identification of input and output variables, partitioning of input and output universes into fuzzy sets, identification of number of fuzzy rules and selection of suitable reasoning mechanism for duplicating the system behavior. The parameter identification involves tuning of the parameters defining the fuzzy sets and the consequents. Both parameter and structure identification are common for both LM and TSK models.

The structure identification is the most difficult phase and can be carried out by duplicating the expert knowledge or by auto generation technique using *a priori* knowledge about the system behavior. Modeling using the expert knowledge involves the incorporation of intuition of the expert about the system behavior. One of the techniques for the auto generation of rules from the *a priori* knowledge is *clustering* of input-output data. Each cluster represents a bundle of data representing similar behavior of the system. There are different types of clustering, namely, Fuzzy C-Means (FCM) [15, 16, 54, 57], mountain clustering [200, 201] and subtractive clustering [38, 39, 48, 51]. In short, fuzzy system identification can be implemented from the expert knowledge or clustering of *a priori* knowledge with reasoning of LM models or TSK models.

1.6 FUZZY SYSTEM IDENTIFICATION OF BOUNDARY CONDITIONING

It is clear from the earlier discussions that many parameters such as fabrication processing parameters, structural geometric parameters and environmental parameters affect the elasticity of the system. All the above parameters that affect the elastic property of the system are referred as boundary conditioning (BC) parameters. In general, this is similar to the case of a main system with many inter-connected sub-systems or main system with many number of boundary conditioning parameters. These parameters can have uncertainty in their quantification and also be interactive in nature

Consider an elastic system shown in Figure 1.29 whose elastic properties are influenced by the input variables $x_1,\ldots, x_m$ that are boundary conditioning parameters. The different outputs from the system are denoted by $y_1,\ldots, y_r$ which represent the different measures of dynamic behavior.

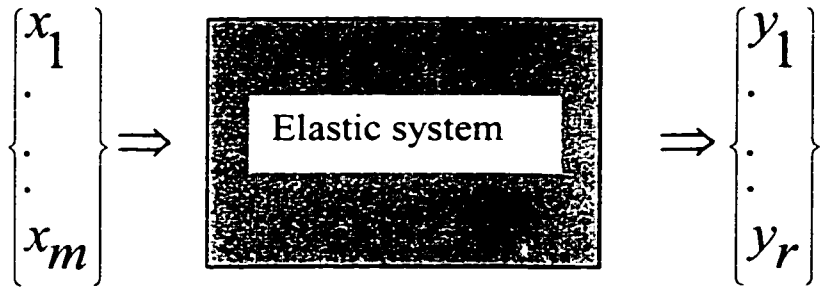

input BC parameters

output dynamic performance measures

Figure 1.29: Scheme of a elastic system with variables representing dynamic behavior

If the number of boundary conditioning variables of a elastic system is large, identification of relevant variables for a particular required output function becomes difficult. Presence of too many conditioning variables as in the case of a real working system, will make the manipulation of a required vibration performance difficult. Hence, it becomes important to identify only the relevant conditioning parameters corresponding to required vibration performance measures such as natural frequencies, eigenratios, mode shapes etc. and hence make the manipulation of required vibration performance possible, leading to the better control of vibration performance or enhancement of the system behavior. These requirements also call for the prediction of relationship between the required output dynamic behavior and the related conditioning parameters which is generally non-linear in nature. Hence a global system identification technique with the following capabilities will be useful for modeling the boundary conditioning of elastic systems:

- Ability to absorb the limitations due to assumptions and unavailability of information, uncertainties and ambiguities about the system.
- Handling a vast number of parameters influencing the system behavior with unpredictable interactions between them
- Automatic generation of the model, capability to learn and to be adaptive.
- Automatic identification of only relevant input variables influencing a required output function, such that noise disturbances could be eliminated.

It is also possible to model qualitatively the elastic system behavior using the experts' knowledge of the system. The qualitative model is the one that describes the system behavior through linguistic explanations. Even though the model developed by an expert is able to represent the complete behavior of the system (which is not possible in all the cases,) it will become expensive to develop another model when the requirements are changed. Hence, even the model by an expert, which may not be available in all cases, loses its versatility and fails to accommodate new situations. Alternatively, in such situations, it will be more appropriate to evolve the system that has the automatic generation capability.

The fuzzy system identification is capable of modeling boundary conditioning response through linguistic values representing human intuitive judgment through output classification and function approximation types of modeling. Fuzzy system identification of boundary conditioning will be useful in the following cases:

1. When the boundary conditioned system is very complicated and is made of many subsystems that are interactive in nature
2. When there is a large number of conditioning variables affecting the system behavior.
3. When specific value of output (such as particular eigenvalues, eigenratios, modal response, localization or behavior of a particular sub system etc.) is required for both macro and micro boundary conditioned systems from the large bank of system conditioning variables
4. When the system is ill-defined and is in need of adapting to the new situation

5. When qualitative definitions of vibrational response and conditioning parameters are needed
6. When classification or grouping of output performance into different categories based on some objective measures are possible [119]. Examples include structural tuning with qualitative requirement of harmonic ratios
7. When function approximation or input-output mapping of vibration behavior is possible with conditioning parameters. Examples include : Variation of particular eigenvalue in terms of boundary conditioning parameters

The quantification of the influence of boundary conditioning parameters on the elastic property of the system needs estimation of equivalent stiffness values which could be done through experimental or some other methods. In order to absorb the uncertainty in the influencing parameters, and vagueness associated with their definition, it would be advantageous if the quantification of the stiffness has qualitative values. When a system is subjected to many inputs, it may result in many outputs depending upon the requirement. The output requirement need not be single valued and could be approximate with blend of intuitive judgement evolved through experience. Example for this is the tuning of musical instrument by professional artist.

The fuzzy system identification of boundary conditioning could be done through expert modeling [119] and auto generation modeling techniques [15, 16, 38, 39, 48, 51, 57]. For example, it is not possible to define the boundary conditions like clamped, simply supported or free by a single value of the boundary stiffness. Definition of these

boundary conditions is fuzzy in nature depending upon the output requirement. Hence a fuzzy range of stiffness values need to be assigned to represent any boundary condition including the extreme classical boundary conditions. This could be represented by fuzzy sets and a rule base of IF-AND-THEN form in terms of linguistic values as schematically shown in Figure 1.30.

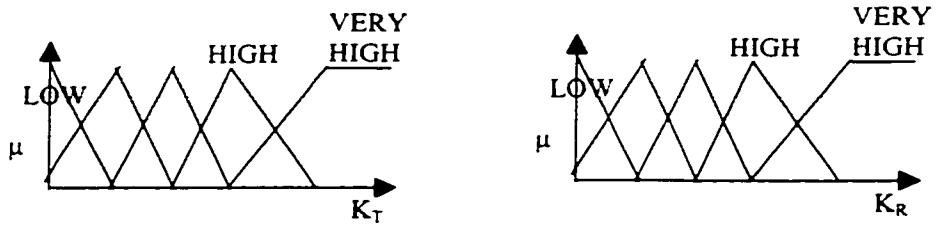

Figure 1.30: Fuzzy representation of boundary stiffness

RULE BASE ***for extreme boundary conditions*** is

IF K_T is *VERY HIGH* **AND** K_R is *VERY HIGH* **THEN** boundary is *CLAMPED.*

IF K_T is *VERY HIGH* **AND** K_R is *LOW* **THEN** boundary is *SIMPLY SUPPORTED.*

IF K_T is *LOW* **AND** K_R is *LOW* **THEN** boundary is *FREE.*

In the same way, rule could be formed for any type of boundary conditions. The quantification of such fuzzy sets is dependent on experience and requirement.

The identified system of boundary conditioning in terms of such simple fuzzy rule base shall be useful for easy implementation of boundary conditioning and further development of control logic for manipulating the structural dynamic behavior of a complicated set of systems. The expert modeling could be useful only for a system with small number of inputs. The expert modeling might also become obsolete if the system

behavior changes. In a system with many input conditioning variables, (or in large input-output data base of boundary conditioning), it is almost impossible to identify by an expert only those conditioning input stiffnesses affecting a particular dynamic behavior of interest. Hence the identification of system should be able to automatically select/identify only those significant inputs for a given output. Hence, the automatic generation of fuzzy rule base will be very useful for identifying boundary conditioning with large number of variables. Both expert and automatically generated modeling of vibrational behavior are possible and are given in Chapter 4 along with examples.

1.6 OBJECTIVES AND LAYOUT OF THE THESIS

It is obvious from the earlier discussion that the success of the MEMS depends on the successful implementation of Type III integration of microsystems and microelectronics. The post processing technique that releases the MEMS structure influences the boundary conditions for the released structures and influences significantly the dynamic behavior of micromechanical components in the microsystems. It is also explained how the vagueness in quantifying the structural parameters can be accommodated through fuzzy logic modeling.

The main objective in this thesis is to develop a successful synthesis procedure to implement microsystems through the application of boundary conditioning concept along with a fuzzy logic modeling of the phenomenon.

Towards the achievement of the above objective, the following sub objectives are charted out:

1 *Development of fabrication synthesis in order to implement the Type-III integration on Mitel 1.5 μm process:* In order to achieve this synthesis, a fabrication strategy of post releasing the free standing structures using XeF_2 gas phase iostropic etching is proposed in Chapter 2. The basic etching characteristics of XeF_2 on the Mitel 1.5 μm designs along with released structures are also given in Chapter 2.

2 *Development of a unified concept to model the influence of the parameters of fabrication synthesis on performance, and the design synthesis of elastic systems:* The modeling of boundary conditioning of elastic systems along with various applications are outlined in Chapter 3.

3 *Development of a system identification technique in order to evolve any complicated system like boundary conditioning using a priori knowledge:* Towards this, the concept and various types of fuzzy system identification methods are explained in Chapter 4. The application of fuzzy system identification to boundary conditioning is also presented in Chapter 4 along with examples.

4 *Systemic understanding of dynamic performance of MEMS structures:* The concept of boundary conditioning is applied to both fabrication and design synthesis of microsystems in Chapter 5 along with examples. The concept of fuzzy boundary conditioning is also applied to the synthesis of microsystems.

5 The Chapter 6 presents the conclusions and possible future extensions of the present work.

CHAPTER 2

GAS PHASE XENON DIFLUORIDE ETCHING OF MEMS DEVICES FABRICATED THROUGH THE MITEL1.5 μm CMOS PROCESS.

2.1 INTRODUCTION

A brief introduction to the micromachined silicon technology along with its revolutionary role in the fabrication of sensors and actuators was discussed in Chapter 1. The influence of the fabrication techniques on the properties of finished microstructure, and how the microstructure can be synthesized by properly incorporating these influences in the design stage itself was also described. A survey of the literature was also provided in support of the arguments presented. The motivation of the present thesis project was put forth based on the presented state of the art of the field. The objectives of the thesis were set out at the end of the Chapter 1. In this chapter, a detailed description of the gas phase etching as a post processing method for the Mitel 1.5 μm process is given. Characteristics of microcomponents etched using XeF_2 etching is also provided.

The success of MEMS technology is dictated by the maximum number of microelectronic components (Transistors, T) and micro-mechanical components (M), in the device depending upon the application. This is possible only if Type-III integration

with industrial CMOS process is used for the fabrication of microsystems. When an industrial CMOS process enables fabrication of micro-system devices, both micromechanical and microelectronics components would be fabricated within the same process flow and integration between the micromechanical and microelectronics components will reach the device level resulting in low noise to signal ratio. The possible way of building microsystems through Type-III integration is to fabricate both micromechanical and microelectronics components through an industrial CMOS process, post-release the structures through selective micromachining outside the fabrication stream and package the chips. Such a technology could also benefit the VLSI fabrication industries in view of the potential and vastness of MEMS applications. However, the direct adoption of an industrial CMOS process would invariably restrict the design and type of micromechanical components to be made due to the limitations associated with the sequence of process, material and geometry of different layers.

In general, the materials available in the standard CMOS technology are silicon dioxide, silicon nitride, metal (aluminum), polysilicon and bare silicon substrate, doped or undoped, and hence the parts of the MEMS devices that could be fabricated are necessarily made out of these materials.

The industrial CMOS process that is being promoted in Canada for the development of microsystems is the Mitel 1.5 μm Double-Poly-Double-Metal process [61]. It has been an interesting challenge to Canadian MEMS community to adopt Mitel 1.5 μm process for fabricating fully integrated microsystems by overcoming the limitations during the

development and to propose design methodologies for fabricating various MEMS devices.

2.2 INTEGRATION OF THE MITEL 1.5 μm TECHNOLOGY FOR MICROSYSTEMS

The Mitel 1.5 μm [61] process is a reliable industrial Double Polysilicon Double Metal CMOS process, which yields the minimum feature size of 1.5μm. This process offers nine layers for MEMS fabrication: two polycrystalline silicon layers, two metal (aluminum) layers, four insulating layers and a passivation layer (which is a combination of silicon nitride and silicon dioxide). The layers are shown schematically in Figure 2.1. The material, the sequence, the thickness and the shape of these layers determine the type of mechanical devices that can be fabricated through the adoption of The Mitel 1.5 μm process. The thickness of the layers are given in Table 2.1. The patterned layers could be used either as sacrificial or structural elements depending upon the adopted releasing process.

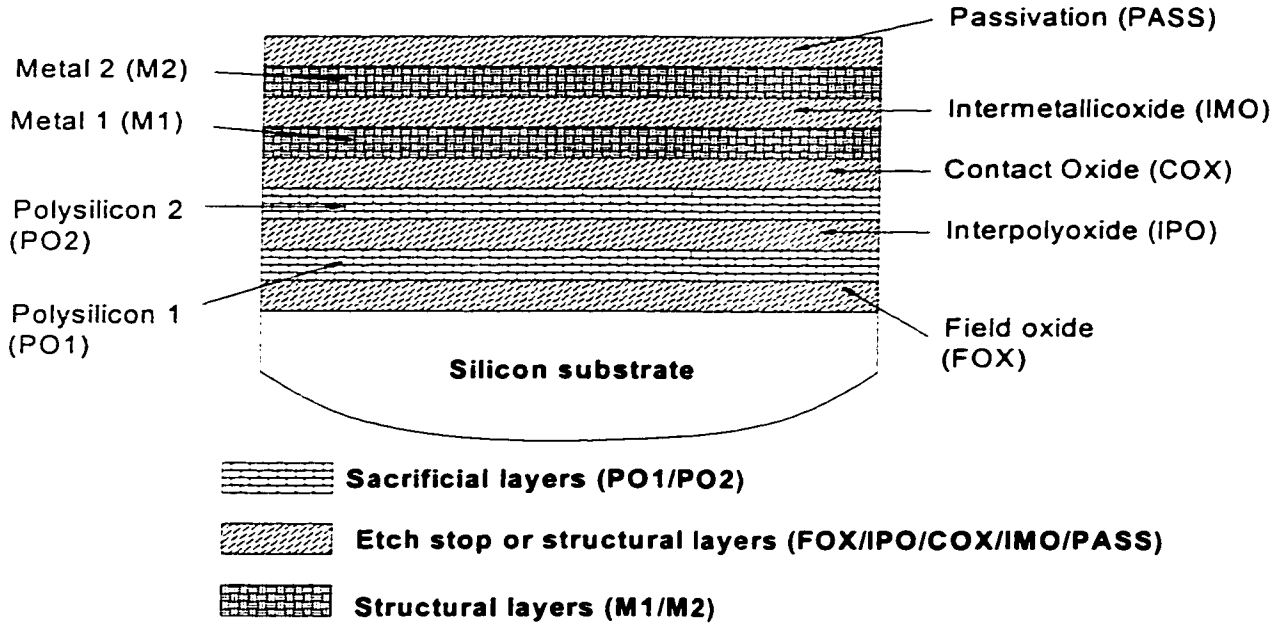

Figure 2.1: Scheme indicating the sequence, material and the possible grouping of layers of the Mitel 1.5 μm Double Poly Double Metal Process.

Table 2.1: Thickness of process layers of the Mitel 1.5 μm technology [61]

Layer Code	Layer Name	Material	Thickness, $\mathring{A}$
FOX	Field Oxide	Silicon dioxide	9000±500
PO1	Polysilicon 1	Polycrystalline silicon	3225±300
IPO	Inter-poly oxide	Silicon dioxide	480
PO2	Polysilicon 2	Polycrystalline silicon	2500±250
COX	Contact Oxide	SG/PSG/SOG	8100
M1	Metal 1	Aluminum	8000±800
IMO	Inter-met allic oxide	SG/PSG/SOG	3000±300
M2	Metal 2	Aluminum	8000±800
PASS	Passivation	Silicon dioxide + Silicon Nitride	10000

The scheme of type III integration of the Mitel 1.5 μm process is shown in Figure 2.2 for making complete MEMS devices.

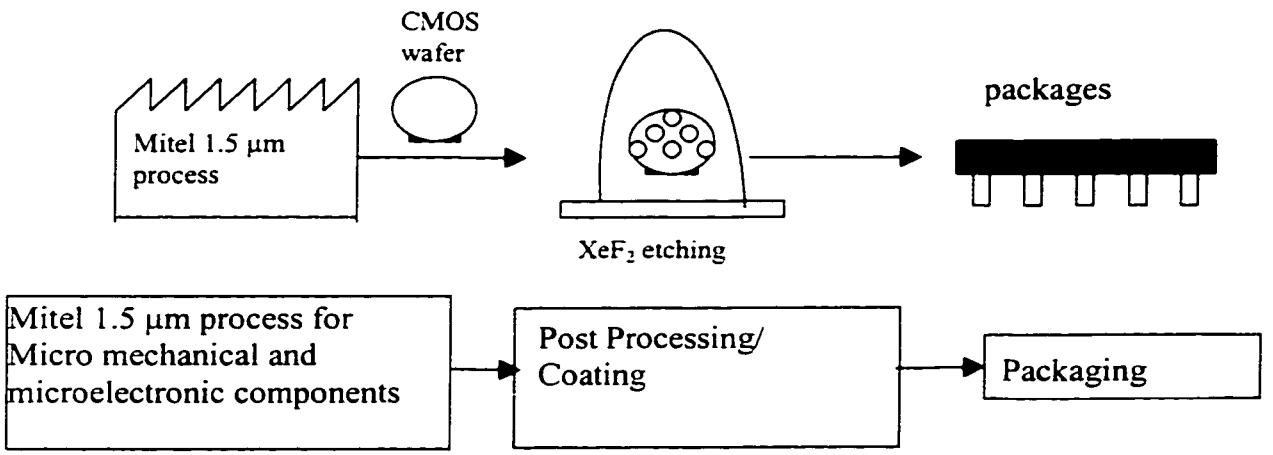

Figure 2.2: Type-III integration of the Mitel 1.5 μm technology

The devices that could be fabricated can have some free standing structures. The development of MEMS devices involves the following steps:

1. *Design and Layout of micromechanical and microelectronic components*: This involves design of both micromechanical and microelectronic components meeting the design requirements and layout of both components using suitable application packages such as CADENCE supporting the Mitel 1.5 μm technology. All the modules of a micro system such as sensors, signal conditioning circuitry, memory, controller and actuators could be laid out using this package. Microelectronics has matured so much that the design of microelectronic components is merely satisfying a set of design rules. When the micromechanical components are designed using the same layout editor, they are subjected to both

design and process violations that are to be overlooked if they are not serious in order to fabricate MEMS devices. The possible process and design violations, that could happen during the design of micromechanical components and not affect the CMOS process seriously, need to be established initially as part of adopting the Mitel 1.5 μm technology for MEMS development.

The process sequence of CMOS process strongly dictates the possible design rule violation for making the mechanical components and the need for the development of new design strategies to be adopted in order to fabricate any fully operating MEMS device. This thesis attempts to develop design methodologies for making different types of MEMS devices which are very much dependent on the processing sequence parameters and post releasing parameters. Hence, the design strategies for the development of MEMS devices through Type-III integration need to be developed in concurrence with the Mitel 1.5 μm technology and post-processing methods. The purpose of MEMS design methodologies for the Mitel 1.5 μm technology will be an important breakthrough towards Type–III integration of microsystems. As fabrication of microelectronic components has matured enough through industrial CMOS process, the bottleneck in the development of MEMS devices through commercial CMOS process is the development of micromechanical components. Once this bottleneck is understood and cleared, further integration with microelectronics will be an easier task. Hence, the present study concentrates on the development of micromechanical components through the Mitel 1.5 μm technology,

understanding the limitations imposed by the process sequence, proposal of design strategies in concurrence with post releasing technologies, and fabrication of micromechanical and microelectronic components through the Mitel 1.5 μm technology following the same stream of process flow.

2. *Post processing of MEMS devices*: Once the dies with both micromechanical and microelectronics are ready from the Mitel 1.5 μm technology, they have to undergo suitable post processing such that MEMS devices are obtained. The post processing can include special coating or some other operations for devices without free standing structures, or micromachining for releasing the free standing structures.

   Stiharu et al. [166] introduced a post processing technique of deposition of humidity sensitive material on the Mitel 1.5 μm chips and fabricated resistive as well as capacitive type humidity sensors. Cantilever–in–Cantilever structure [28, 167] was fabricated through the Mitel 1.5 μm technology using post-releasing methods.

Thus, the final success of making mature MEMS devices depends upon finding completely compatible post-processing methods with a selected commercial CMOS process. The suitable micromachining methods that could be used as post releasing process for fabricating freestanding structures are bulk or surface micromachining depending upon the application and etch material.

2.3 LIMITATIONS ASSOCIATED WITH THE SELECTION OF POST RELEASING METHODS

An important aspect in the post processing of microsystems is the integrity of the contact pads after etching. Most wet etching processes (e.g. NaOH, KOH, TMAH) attack the metal contact pads, which makes the electrical connections impossible. Hence, whether it is sacrificial or bulk micromachining, the scope of wet etchants becomes limited. The wet etchant TMAH will be the main anisotropic etchant of the future because of its improved safety standard compared to other etchants. But, TMAH is also known for its selectivity with aluminum contact pads. In general, the structures are subjected to the problem of stiction [101, 111, 112] when wet etchants are used in case of sacrificial etching. Hence, the use of wet etchants for sacrificial etching also requires additional anti-stiction drying methods.

Besides, the post releasing mechanism for micromechanical structures could also affect the overall performance of the microsystem. It would be desirable if the mechanical components only are released through a chemical etching process in such a way that the microelectronics components are protected without additional process or layers and also the stiction problem encountered in the case of wet sacrificial etching is avoided. Moreover, it would be advantageous if the same post-release process could be used for both sacrificial and bulk micromachining of MEMS devices.

Depending upon the selection of etch and etch stop layers, one could fabricate microstructures through both bulk micromachining and surface micromachining. For

both types of micromachining, the etch stop could be any of the oxide, metal or passivation layers. The etch layer could be polysilicon in the case of sacrificial micromachining or the silicon substrate in the case of bulk micromachining. The structural layers of MEMS devices could be bare metal layers or metal layers sandwiched in oxide layers. The microelectronic components fabricated using the Mitel 1.5 μm process could be protected by the top passivation layer from post-release etching.

Due to the above mentioned limitations of the industrial CMOS process, the conventional liquid etchants such as EDP, KOH, TMAH and HNA or high-energy plasma etchants have restricted scope in post processing MEMS devices following an industrial CMOS process. In order to overcome all these constraints explained above and to fabricate useful MEMS devices, the gas phase xenon difluoride isotropic etching is proposed [122, 123] as a post-releasing process for microsystems fabricated using the Mitel 1.5 μm technology, which is discussed below.

2.4 GAS PHASE XeF_2 ETCHING OF SILICON

Earlier attempts on etching silicon with XeF_2 sublimate are reported in [198,81]. Later XeF_2 etching was used for releasing the free structures in MEMS devices fabricated through CMOS process [79, 177, 73, 72, 96, 33]. XeF_2 was first synthesized in and then used for etching of silicon by Winters and Coburn [198] in 1979 followed by Ibotsan [85] in 1984. Winter and Coburn [198] are the first to use XeF_2 in gas phase for etching silicon. They studied the effect of vacuum pressure at a temperature of 300°K and

amount of incident flux of XeF_2 (gas) on etch rate and found that XeF_2 has extreme selectivity to SiO_2, Si_3N_4 and SiC and etches isotropically. XeF_2 is suggested as environmentally attractive since larger fractions of the reaction products with silicon are SiF_4 and Xe. Ibbotson et al. [85] studied the etching of silicon by XeF_2 at temperatures ranging from –17°C to 360°C and pressures from 0.05 to 2Torr. Houle [81] proposed that the major product of silicon etching is SiF_4 and minor products are Si_2F_6, SiF_2 and SiF. Houle [81] studied the effect of pressure and XeF_2 flux on the etching of silicon. The silicon etch rate was linear in XeF_2 over a large range of pressures.

After the above studies, etching of silicon was not taken up seriously until Hoffman et al. [79] applied it for micromachining of silicon in 1995. Hoffman et al. [79] studied the aperture effect on the etch rate of silicon using pulse etching techniques, and found that the etch rate with smaller openings are slower than with larger openings, and fabricated 0.04 μm thick SiO_2 beam and 0.05 μm thick aluminum beams.

Chang et al. [34] and Chu, et al. [41] established basic etching characteristics of gas phase pulse XeF_2 etching for silicon wafers. Chang et al. [34] reports extreme selectivity of XeF_2 to aluminum, photoresist, several polyamides, copper, gold, titanium-nickel alloy, acrylic, stainless steel, SiO_2 and etch rates depend upon the size of the window opening, etching time and number of pulses. Pulse etching is proposed in [34] compared to constant pressure etch for better uniformity of the etched surface. Due to the exothermic nature of reactions between silicon and XeF_2 the substrate temperature increases by tens to hundreds of degrees [34]. Chu et al. [41] reports extreme selectivity

of XeF_2 to Cr, TNi, W, Ti, Mo and possible etch stop by even 50°A thermal oxide. Effect of window size and pulse time is also reported in [41]. Lin et al. [72] fabricated CMOS piezorestitive sensor using XeF_2 etching. Vugts et al. [190] studied the temperature dependence of XeF_2 etching and repeated increased etch rates when the temperature is different from 400°K.

Recently, the application of XeF_2 etching for Microsystems has increased substantially [33, 40, 63, 72, 73, 96, 177]. Lin et al. [72] fabricated CMOS piezorestitive sensor using XeF_2 etching. Piezorestitive accelerometers with poly1 resistors were released by XeF_2 etching from CMOS 0.5 μm process in [96]. XeF_2 etching along with TMAH was used for the fabrication of capacitive type angular response gyroscopes in [40]. Tea Nim et al. [177] fabricated microstructures by CMOS process using hybrid-etching techniques, which combines both XeF_2 and TMAH etching and membranes (≅ 400°A thick) of gate oxides using XeF_2 etching.

From the above study it can be understood that XeF_2 has extreme selectivity to silicon dioxide, silicon nitride, photo resist, aluminum, gold, copper, chromium, titanium-nickel alloy, tungsten, acrylic, molybdenum and polyamides and high selectivity for silicon in the range of 1-10 μm/min, depending upon the geometry conditions.

The selectivity of the etchants thus suits the materials used in the Mitel 1.5 μm technology. The passivation layer of the Mitel 1.5μm technology made of both silicon dioxide and silicon nitride can act as an etch stop for XeF_2 and protect the components

below from etching. Due to extreme selectivity to aluminum and gold, the contact pads and bonding wires of the Mitel 1.5 μm processed chips will not be affected by XeF_2 etching while they are affected by wet etching. As the etching is carried out with gas phase XeF_2, free standing structures are not subjected to the problem of stiction as in the case of wet etching and thus the need for special drying methods do not arise. XeF_2 etching of the Mitel 1.5 μm chips does not need any mask as passivation layer itself can be used as a mask. Another advantage is that XeF_2 is suitable for both bulk and surface micromachining. These properties of XeF_2 isotropic etching makes it ideal for post-releasing the micromechanical components fabricated through the Mitel 1.5 μm process for both sacrificial and bulk micromachining. Hence, XeF_2 etching is proposed for the post release of free standing structures fabricated through the Mitel 1.5μm technology in this thesis. Two types of etching methods are possible as follows:

1. Gas phase pulse etching.
2. Gas phase constant pressure etching.

Gas phase pulse etching is used in this study and is recommended since the constant pressure etching results in high non-uniformity of etching [34, 41, 79].

XeF_2 is a white solid crystal at room temperature and pressure and it sublimates at around 4 Torr at 25°C. The etching has to be carried out with gas phase xenon difluoride. The gas phase XeF_2 etching has high affinity for polysilicon as well as silicon substrate and extreme selectivity to aluminum, gold, silicon dioxide, PSG, photoresist and silicon nitride. The primary reaction during the etching of silicon can be given as:

$$2XeF_2 + Si \rightarrow 2Xe + SiF_4 \qquad (2.1)$$

The etching mechanism involves the following steps [198]: (1) non-dissociative adsorption of the XeF_2 gas phase species at the solid surface; (2) dissociation of the adsorbed gas (dissociative chemisorptions); (3) reaction between adsorbed atoms and the solid surface to form adsorbed product molecule e.g., SiF_4; (4) desorption of the product molecule into the gas phase and (5) the removal of non-reactive residue from the surface.

2.4.1 Designing XeF_2 Etching Setup

Even though XeF_2 vapor has characteristics ideal for silicon etching, the formation of HF acid when XeF_2 is in contact with water vapor is a safety hazard. Hence, XeF_2 crystals should never be exposed to atmosphere or humid atmosphere and the entire handling and etching with XeF_2 should be done in a totally inert atmosphere like a dry nitrogen box and also under a fume hood. In the present study, the entire XeF_2 etching setup was designed, fabricated and installed in-house, using materials/components that are not attacked by XeF_2 vapor.

Gas phase pulse etching was used for the fabrication of MEMS devices in this thesis. The scheme of the pulse etching setup is shown in Figure 2.3. The setup consists of an etch chamber connected to a vacuum pump through a liquid nitrogen trap and an on-off valve. The chamber is also connected to the stainless steel container of XeF_2 crystals through a supply valve, and to a nitrogen gas supply through a purge valve. A capacitance manometer and a pressure gauge are also connected to the etch chamber.

The chamber has a feed-through for loading the specimen chips into the chamber. The materials used for building the etching system include stainless steel (AISI 304 or 316), aluminum, Viton elastomer O-rings, glass, Inconel alloy and a standard mechanical high vacuum pump.

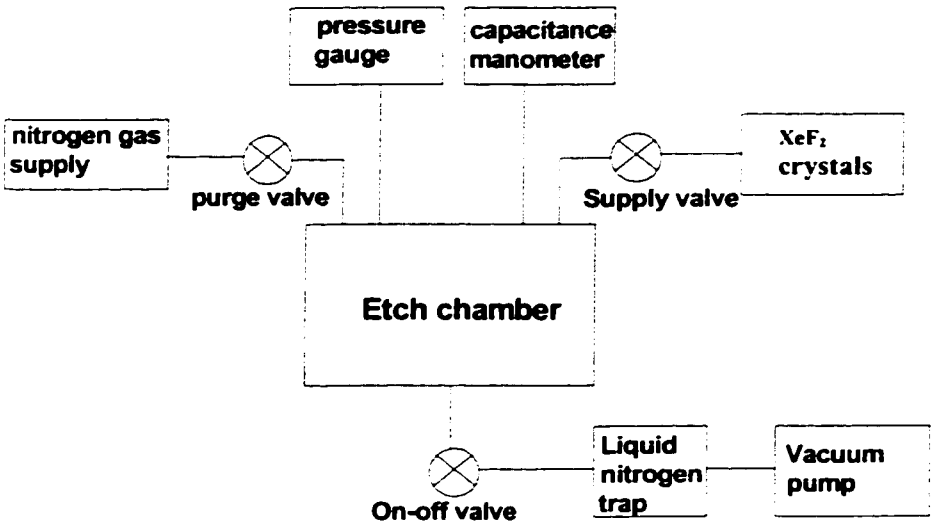

Figure 2.3: Scheme for XeF_2 pulse etching setup.

XeF_2 gas is toxic, corrosive oxidant, odorless and stable at room temperature and in dry nitrogen atmosphere. The reaction product SiF_4 is also toxic, corrosive and it hydrolyzes rapidly in the atmosphere to form hydrofluoric acid [55, p185]. The pump used is a high vacuum mechanical pump with ordinary pump oil. The pump is connected to the etch chamber through a liquid nitrogen trap which condenses corrosive vapor from the chamber as well as back streaming oil vapor from the pump [30, 55, 126]. Purging of reactants with dry nitrogen will avoid the corrosion of pump and hydrolyzing of XeF_2 and SiF_4. The capacitance meter selected has a sealed stainless steel diaphragm and its sensitivity is independent of the gas medium. The photograph of the XeF_2 pulse etching system is as shown in Fig. 2.4 and 2.5. Loading and unloading of XeF_2 crystals must be carried out under the fume hood. The safety precautions include particulate respirator, nitrile gloves, full shields etc. The etch chamber is isolated from vibration of the mechanical pump by using bellow joints between the setup and pump as shown in Figures 2.4 and 2.5.

Figure 2.4: Photograph of the XeF_2 pulse etching setup

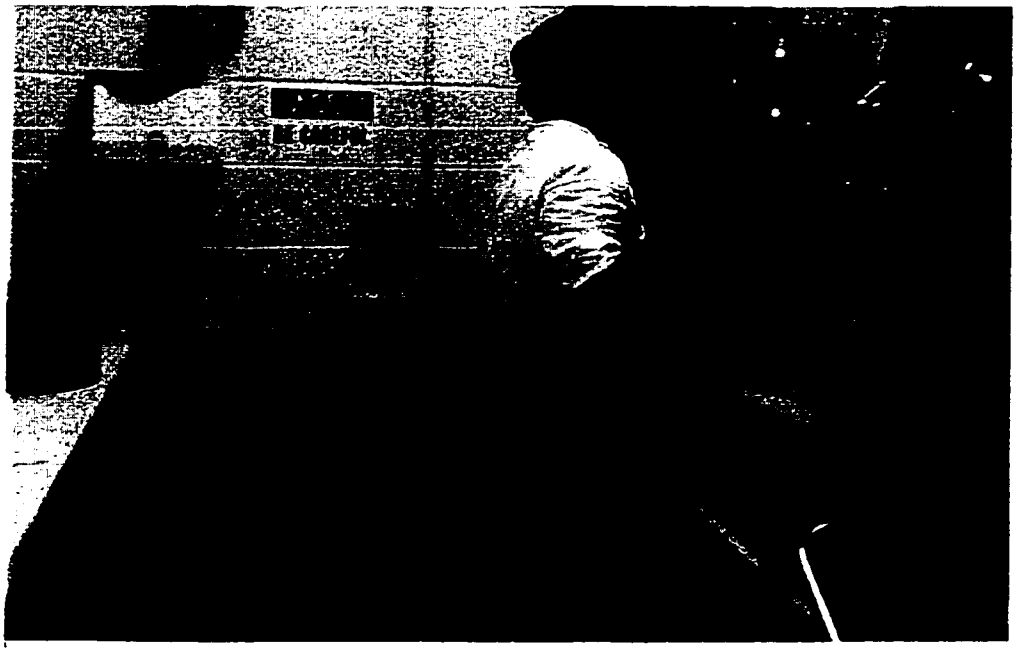

Figure 2.5: Photograph of the XeF_2 pulse etching setup in fumehood during operation

2.4.2 XeF_2 Gas Phase Pulse Etching

Preparation of the samples is very important in order to micromachine the sample in XeF_2 pulse etching. The back and edges of the sample are coated with photoresist and hard-baked at 120°C for 15 minutes. The samples are etched in BOE (Buffered Oxide Etch solution) containing HF and ammonium fluoride in the ratio of 1:4, for 10 seconds. BOE dip removes the native oxide formed on the exposed silicon areas. Even though the native oxide does not prevent etching, it slows down the onset of etching. Presence of moisture on the chip can form HF in exposure to XeF_2 vapor which will etch the oxide layers. Water vapor can also form a tough white layer of silicon fluorine polymer [41] on the silicon surface which can slow or stop the etching process. In order to avoid the problem, the sample is subjected to a dehydration bake just before the start of the etching. In the dehydration bake the samples are heated to 120°C and this temperature is maintained for 5 minutes. The prepared samples are immediately transferred to the etch chamber in nitrogen environment.

The procedure for each pulse of pulse etching includes the following steps:

1. After loading the specimens (the Mitel 1.5μm processed chips) into the etch chamber and closing both supply and purge valves, the chamber is pumped down to a vacuum pressure of approximately 1 mTorr.
2. The supply valve is slowly opened such that XeF_2 sublimates and its vapor fills the chamber. The supply valve is closed once the chamber pressure reaches around 2

Torr. It takes approximately 20 seconds to fill the chamber, and then the timing for pulse duration starts.

3. The XeF_2 vapor stays in the chamber until the pulse duration of 1 min is reached. During this time, main etching of silicon or polysilicon takes place.
4. Once pulse duration of one minute is reached, purge valve is opened for some time such that enough nitrogen gas fills the chamber until the pressure reaches around 5 psig.
5. The gas mixture in the chamber is pumped back down to approximately 1 mTorr vacuum and the next pulse begins.

The procedure is repeated until desired etching is completed. After many trials pulse duration of one minute was decided for the entire study reported in this thesis . The surface roughness was high when the pulse duration was high. The etch rate and the amount of silicon etched are found to be dependent on the number of pulses (N), etch window opening and etching pressure [34, 41, 81]. For the entire etching study, the pressure was kept at around 2 Torr. The etching results mentioned in the following sections correspond to designs fabricated through the Mitel 1.5 μm process. In order to release any useful MEMS devices through the Mitel 1.5 μm process, the etching characteristics of XeF_2 with the Mitel 1.5 μm process layers must be well understood.

2.5 POSSIBLE MICROMACHINING STRATEGIES

Both bulk and surface micromachining are possible by post processing the Mitel 1.5 μm design using XeF_2 gas phase etching. The scheme for surface micromachining of sacrificial layers of polysilicon 1 and polysilicon 2 is shown in Figure 2.6. The etching of bare silicon is prevented by the mask layers of IPO or FOX oxide layers. For sacrificial micromachining of PO1, FOX layer will be the mask layer for silicon substrate. For sacrificial micromachining of polysilicon2, IPO or FOX layers can protect the substrate. Any of oxide, metal and passivation layers on top of PO1or PO2 can be used for the definition of the etch window opening depending upon the design requirement and also as etch masks. The dimension 'L' shown in Figure 2.6 indicates the lateral surface etch distance.

Similarly, the scheme for bulk micromachining of silicon substrate of the Mitel 1.5 μm designs is shown in Figure 2.7. Etch window openings can be defined by individual or by combination of any metal, oxide or passivation layers. Etching progresses in both lateral and vertical dimensions. Lateral etch distance is denoted by 'L' when 'D' represents the etch depth as shown in Figure 2.7. Thus, it becomes possible to fabricate MEMS devices through bulk and surface micro machining of the Mitel 1.5 μm designs. The type of MEMS devices that could be fabricated using the Mitel 1.5 μm technology depends upon the ingenuity of the designer in combining the process sequence and post releasing methods.

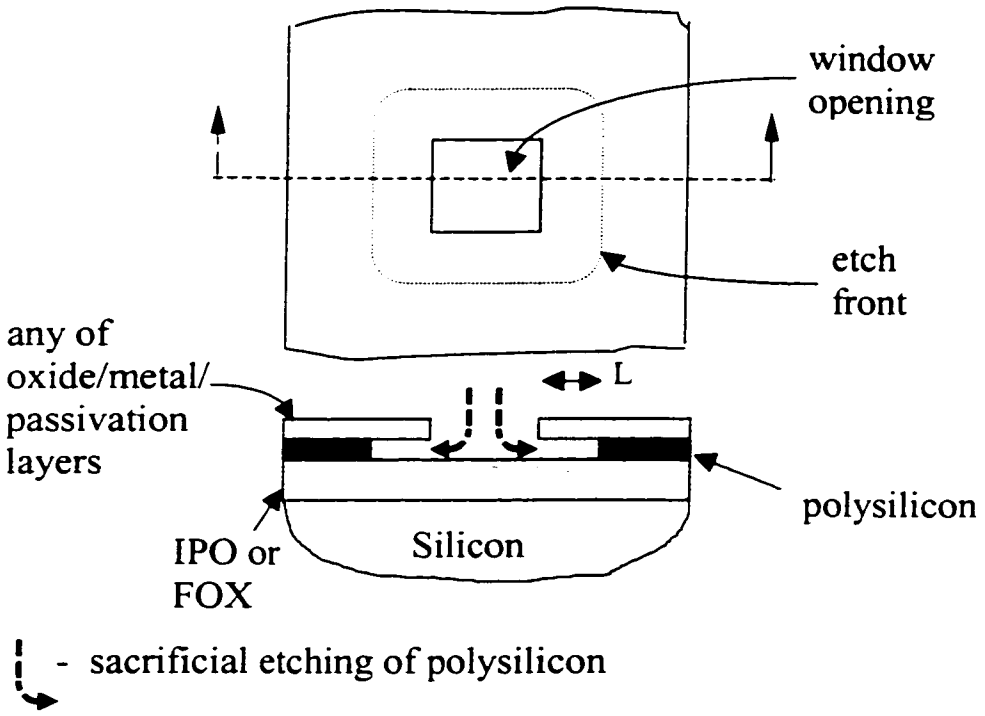

Figure 2.6: Scheme for sacrificial etching of polysilicon

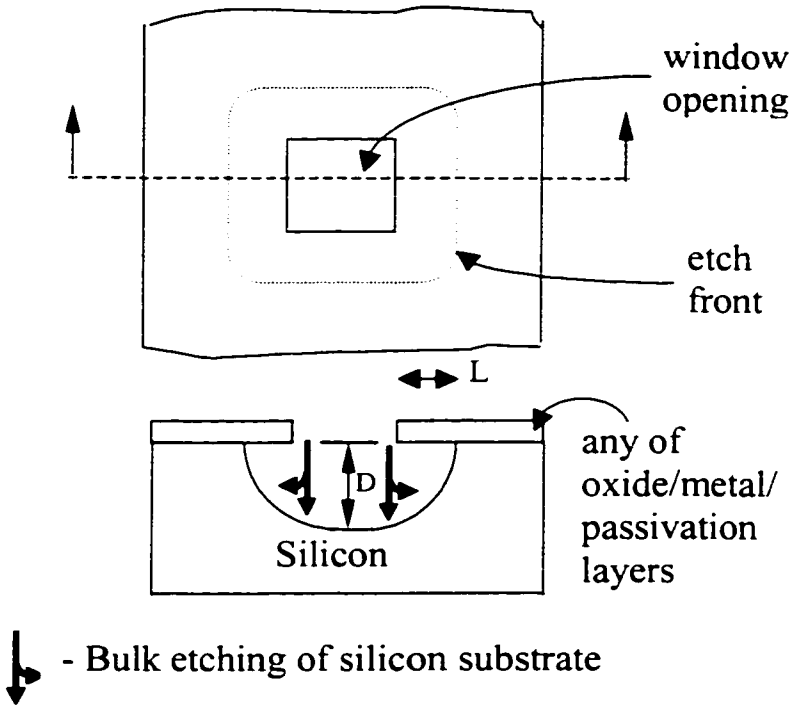

Figure 2.7: Scheme for bulk etching of silicon substrate

The etch results mentioned in the following sections correspond to the designs fabricated through the Mitel 1.5 μm process. In order to release any useful MEMS devices through the Mitel 1.5 μm process, the engineering quantification of basic etching behavior of XeF_2 with the Mitel 1.5 μm process layers need to be established as given in the following section.

2.6. GAS PHASE XeF_2 ETCH RESULTS OF THE MITEL 1.5 μm CHIPS

The post-processing release of useful devices through XeF_2 etching depends mainly on the size of the window opening. This study will help in the optimum positioning and dimensioning of etch holes such that nearby microelectronics are not affected.

2.6.1. Effect of Etch Opening Size on Bulk and Sacrificial Post-Releasing

The fabrication of MEMS involves the XeF_2 etching of silicon substrate in the case of bulk post-processing or polysilicon in the case of sacrificial post-processing through some etch opening as shown in Figures 2.6 and 2.7. The post-process release of structures using the Mitel 1.5 μm process strongly depends upon the limitations imposed by the etching characteristics of gaseous XeF_2 on both types of micromachining. Hence, it is very important to study the dependence of the size of the etch opening on etch rate, surface roughness and etch pattern. In order to study the influence of the size of etch window, three square windows of 10μm × 10μm, 25μm × 25μm and 50μm × 50μm sizes

as shown in Figure 2.8 (schematic) were used for both bulk and sacrificial post-processing.

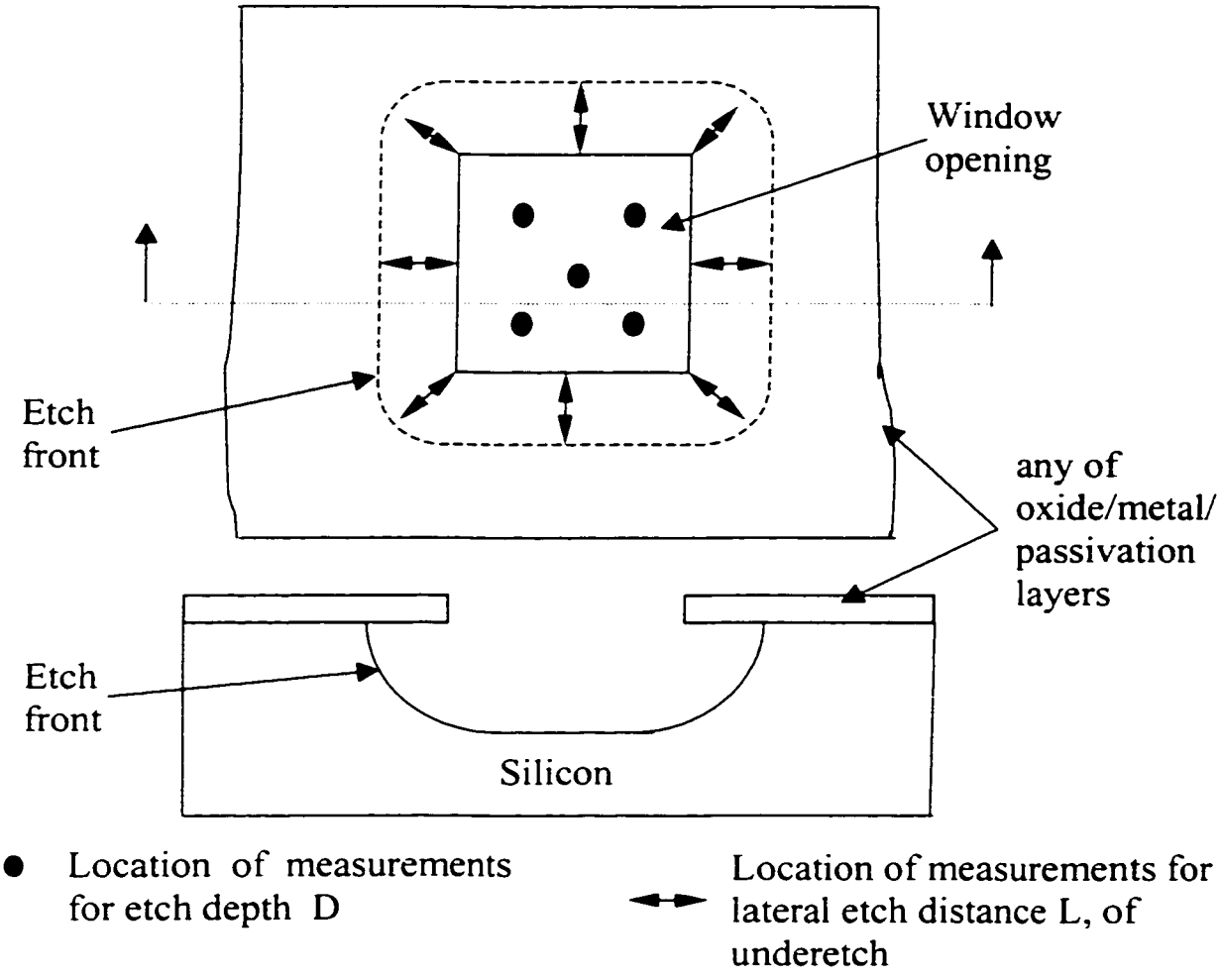

Figure 2.8: Measurement locations used for etch study

Consider the scheme of the window opening as shown in Figure 2.8 for the locations of the measurements for lateral etch distance L and etch depth D. The etched front of surface micromachining of polysilicon2 for a window opening of 50μm × 50μm after 15 pulses is shown in Figure 2.9. The etch front pattern was similar for different number of pulses. The etch pattern of bulk micromachining of silicon substrate after 15 pulses is shown in Figure 2.10. The isotropic nature of XeF_2 etching is seen by the emerging rounded features for both surface micromachining and bulk micromachining. The average of the lateral etch distance measured at those locations after different number of pulses is given in Figure 2.11 in order to understand the bulk etching characteristics. This figure shows that the lateral etch rate decreases as the number of pulses increases. This may be due to the increased surface area faced by the etch front.

The average etch depth measured at the locations shown in Figure 2.8 is shown in Figure 2.12 for windows of various sizes. The vertical error bars represent ± 1 standard deviation. This figure also shows a similar trend of reduced etch depth rate at higher number of pulses. It has also been found that the etched surface becomes very rough at higher number of pulses as indicated by the increased standard deviation. The surface roughness increases with window size as seen from Figure 2.12. Figures 2.11 and 2.12 also illustrate that both lateral and depth etch rates reduce as the window size is reduced. The variation of lateral etch distance against number of pulses is shown in Figure 2.13 for sacrificial micromachining of the polysilicon2 layer.

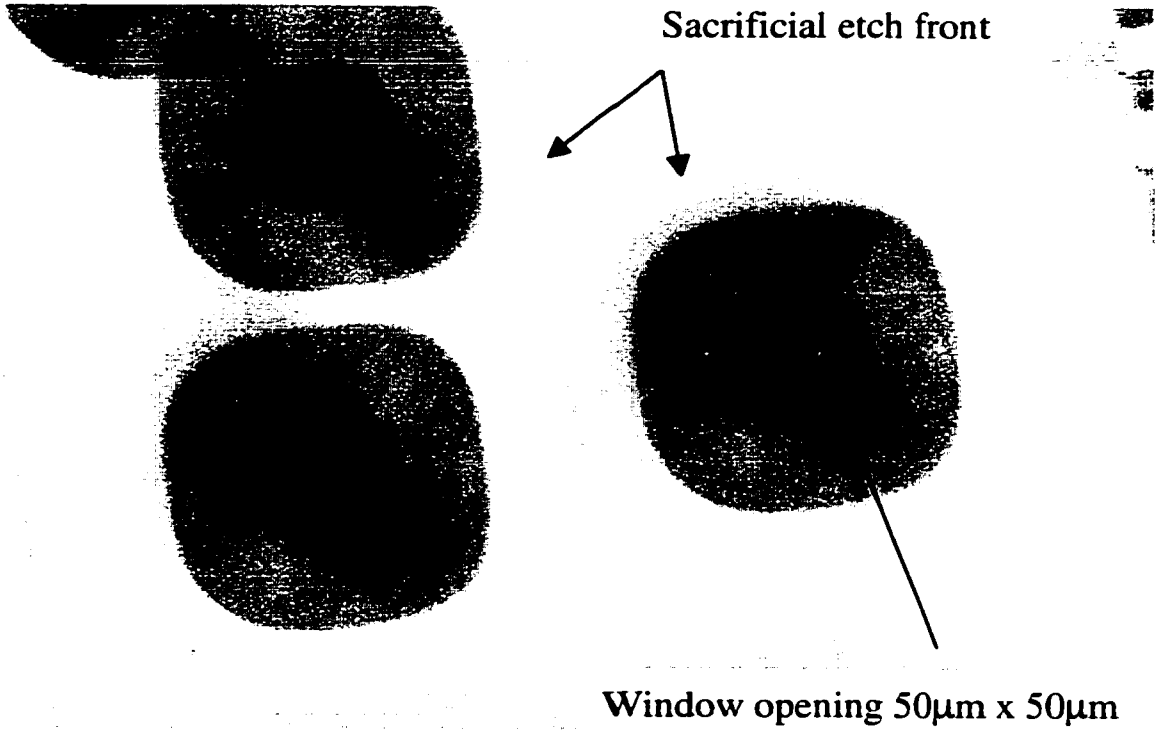

Figure 2.9: Observed sacrificial etch pattern of polysilicon2 after 15 number of XeF_2 pulses for 50μm X 50μm window opening

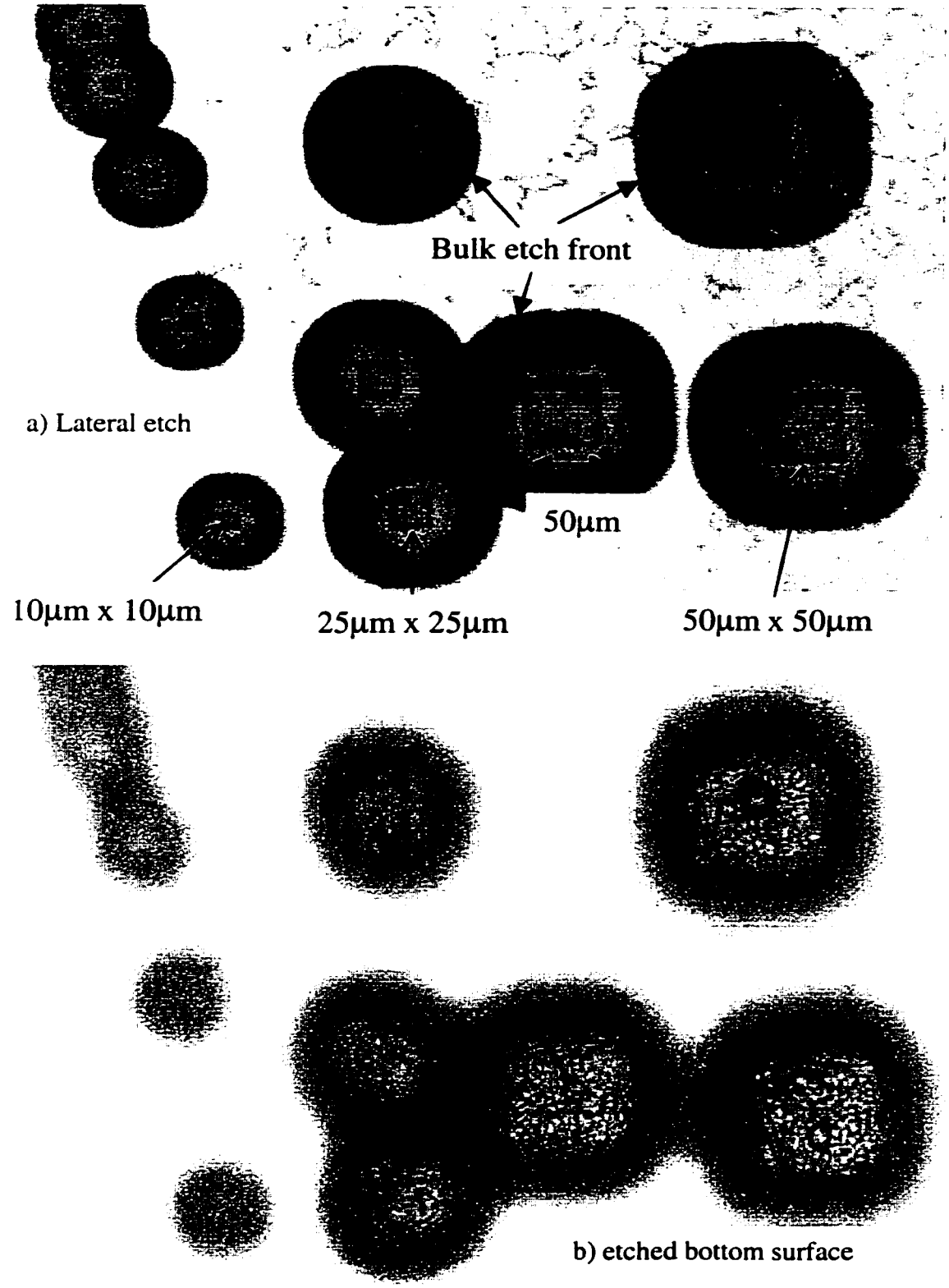

Figure 2.10: Observed etch front and bottom surface for square windows for bulk etching of silicon substrate after 15 number of XeF_2 pulses.

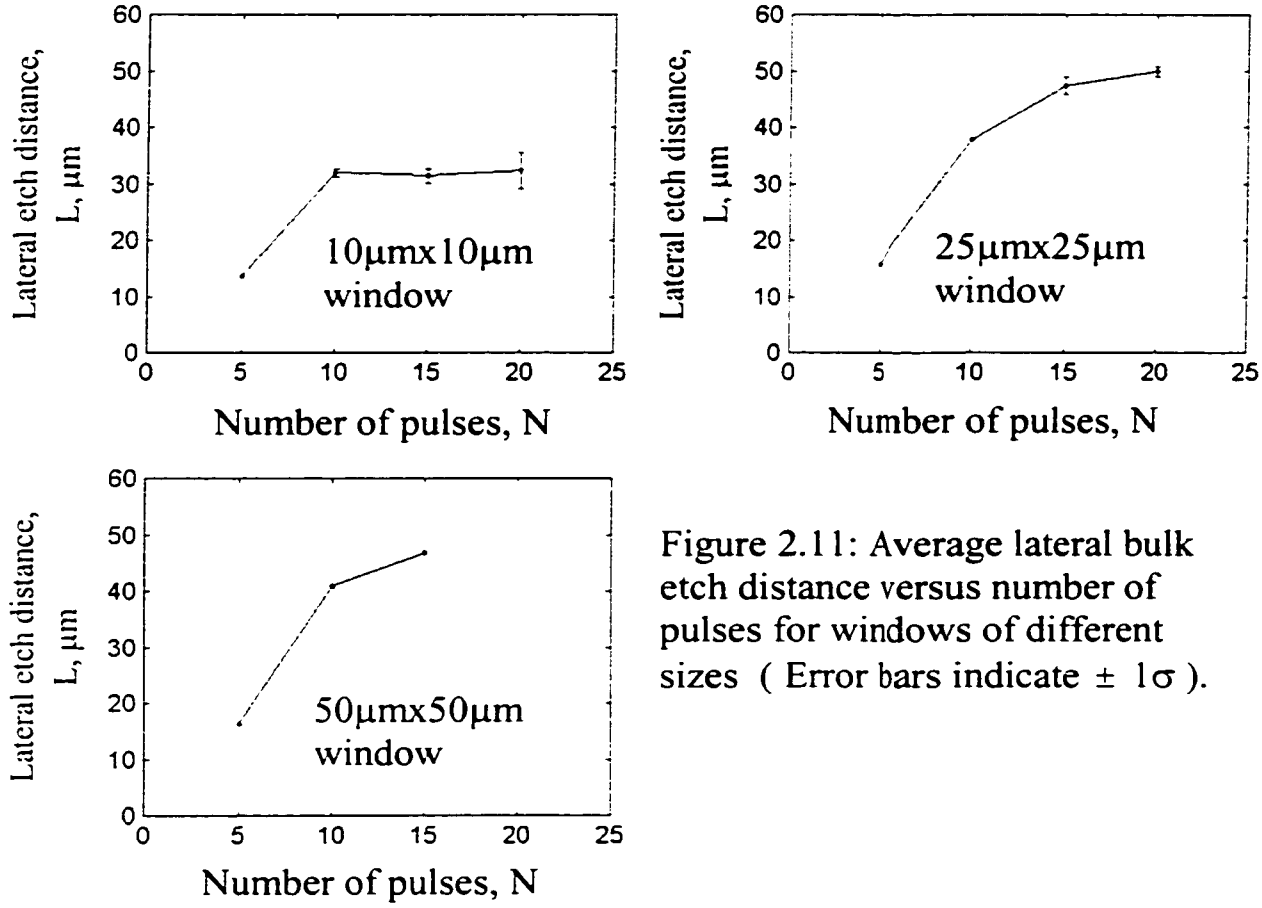

Figure 2.11: Average lateral bulk etch distance versus number of pulses for windows of different sizes (Error bars indicate ± 1σ).

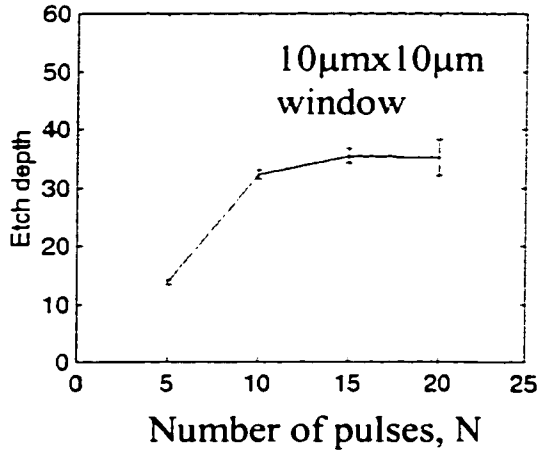

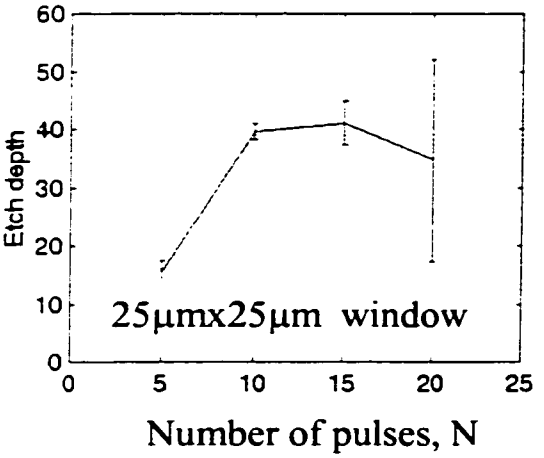

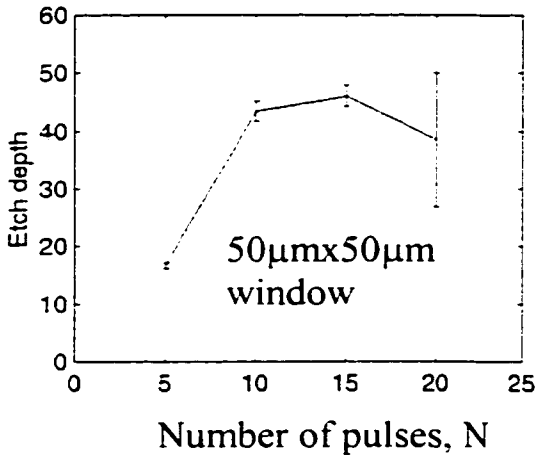

Figure 2.12: Average etch depth versus number of pulses for windows of different sizes (Etch depth in μm . Error bars indicate ± 1σ).

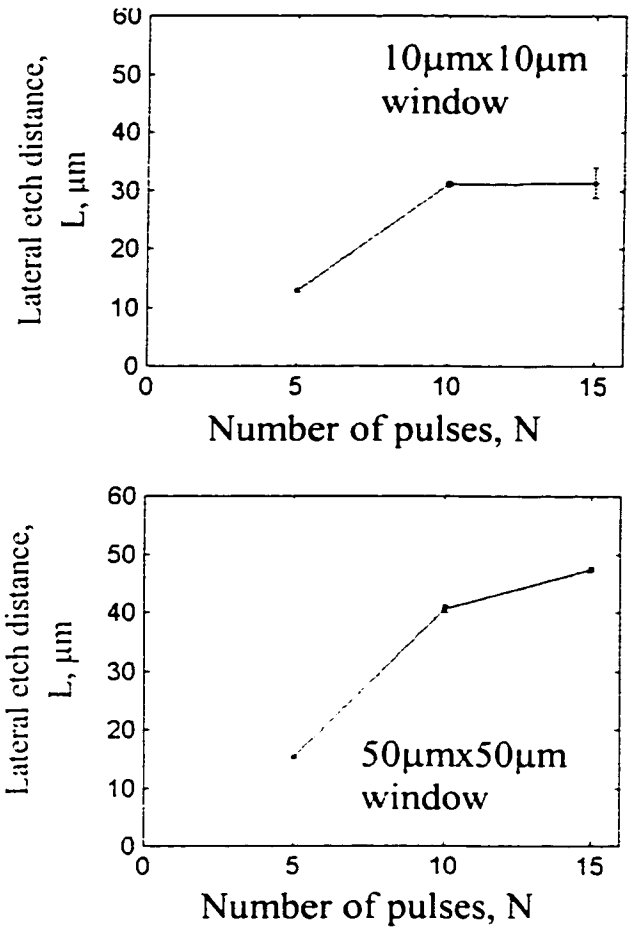

Figure 2.13: Average lateral surface etch distance versus number of pulses for windows of different sizes for polysilicon (Error bars indicate ± 1σ).

For bulk and surface micromachining, the reduction in etch rate at higher number of pulses limits the maximum number of effective etching pulses and hence the spacing between the etch windows for the release of structures depending upon the etch time. This also dictates the minimum distance between the nearby microelectronic components and the micromechanical components.

It can also be seen from Figure 2.13 that smaller etch windows result in reduced etch rates. Smaller etch windows also result in smaller etch fronts. The average etch rate is in the order of 2.5μm/min for bulk post-processing and 3μm/min for the polysilicon2 sacrificial layers. Thus, this study will help in deciding the number of pulses, window sizes and number of windows required for post releasing of MEMS devices. The minimum spacing to protect the microelectronics components is dependent on the number of pulses required for the release of structures and the size of the etch window.

Bulk micromachined silicon pit resulting from XeF_2 etching is shown in Figure 2.14. The etched cavities show the isotropic nature of xenon diflouride etching. The different etch patterns formed under the beams of the field oxide are shown in Figure 2.14. The etching pattern and the resulting planes can be seen from Figure 2.15. Figure 2.15a shows the etch pattern through the opening around the main plate structure. The plate structure at the center is released through concave etching while the end supports and surroundings are released through convex type of bulk etching. The emerging etch planes seen in Figure 2.15(b) follow the etch opening isotropically.

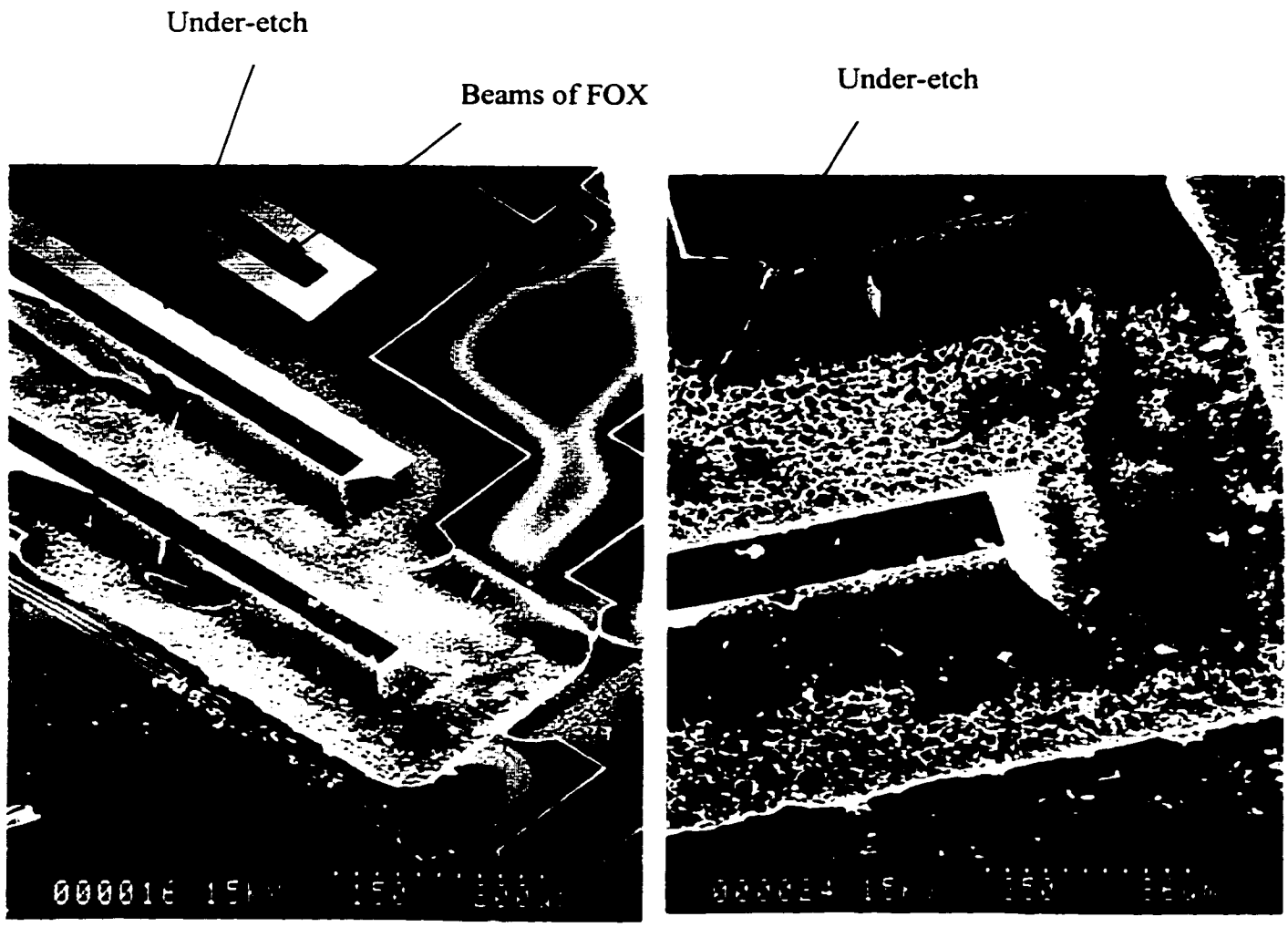

Figure 2.14: Pit formed by bulk isotropic postprocessing of silicon substrate

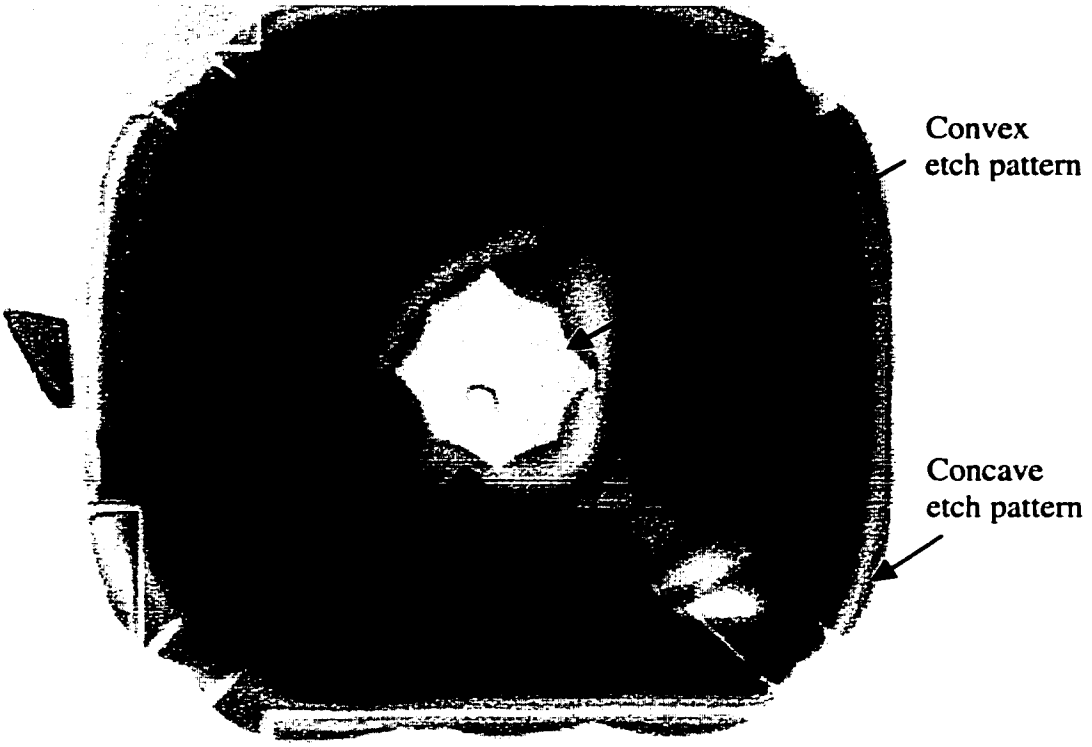

Figure 2.15a: Etch pattern for a piezoresistive plate structure of silicon dioxide and silicon nitride

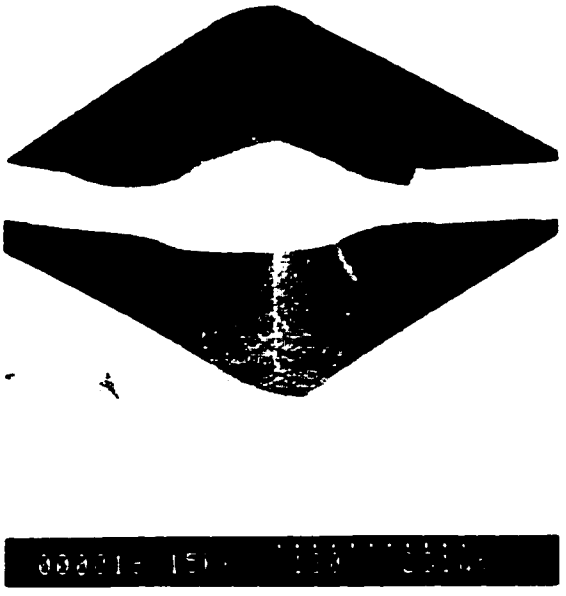

Figure 2.15b: SEM micrograph of bulk etched surfaces of silicon substrate

2.6.2 Corner Selectivity of XeF_2 Etching

A cantilever type structure, which was subjected to both sacrificial and bulk post-processing is shown in Figure 2.16. The concave etch rate is measured through the dimension 'a' while convex etch rate is measured through the distance 'b' (as indicated in Figure 2.16a). The measured average etch distance for concave and convex zones are given in Figure 2.17. Etch rate is found to be higher for convex zones compared to that of concave zones as shown in Figures 2.16 and 2.17.

This study shows another important characteristic of corner selectivity of XeF_2 etching. Considering the isotropic nature of XeF_2 etching, the etch rate is geometry dependent. As an initial approximation, at any instant of time, the energy required for etching can be related to the area of the etch front (A_f) while the maximum energy supply for etching could be dependent upon the area of the window opening (A_w). Then the selectivity factor, σ, is defined as

$$\sigma = \frac{A_f}{A_w}. \tag{2.2}$$

The selectivity factor represents the proportion of required energy for etching in terms of available etching energy and distinguishes distinctly the effect of concave and convex zones on XeF_2 etching. The maximum energy supply is limited by the size of the opening (A_w) and will be more for larger windows. Because of the lower available energy, the lateral etch distance L for smaller windows stabilizes at a lower number of pulses compared to that of larger windows. Even though the σ has the same value at the

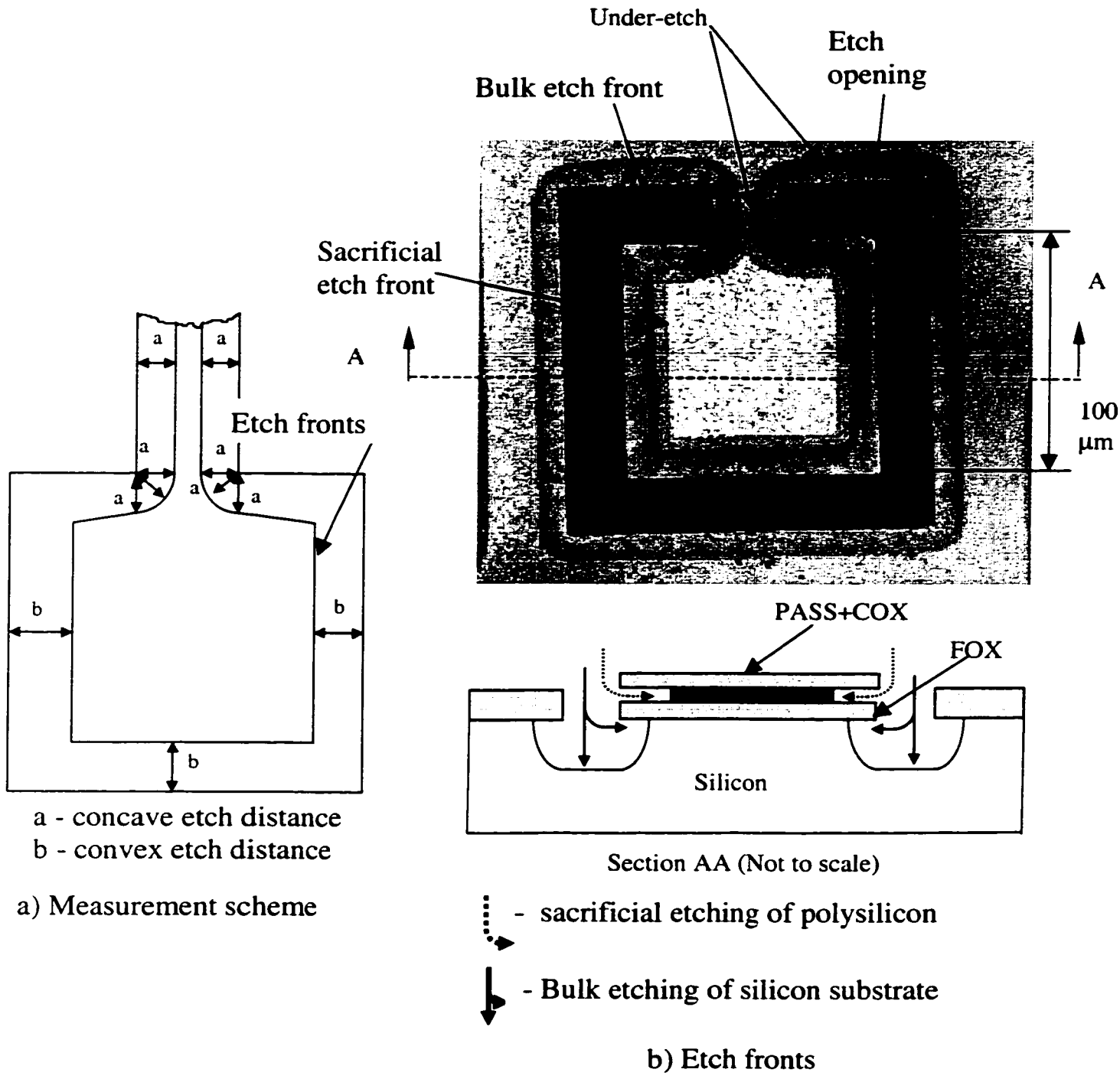

Figure 2.16: Bulk and surface post-processing etch fronts for a square type cantilever structure showing corner selectivity.

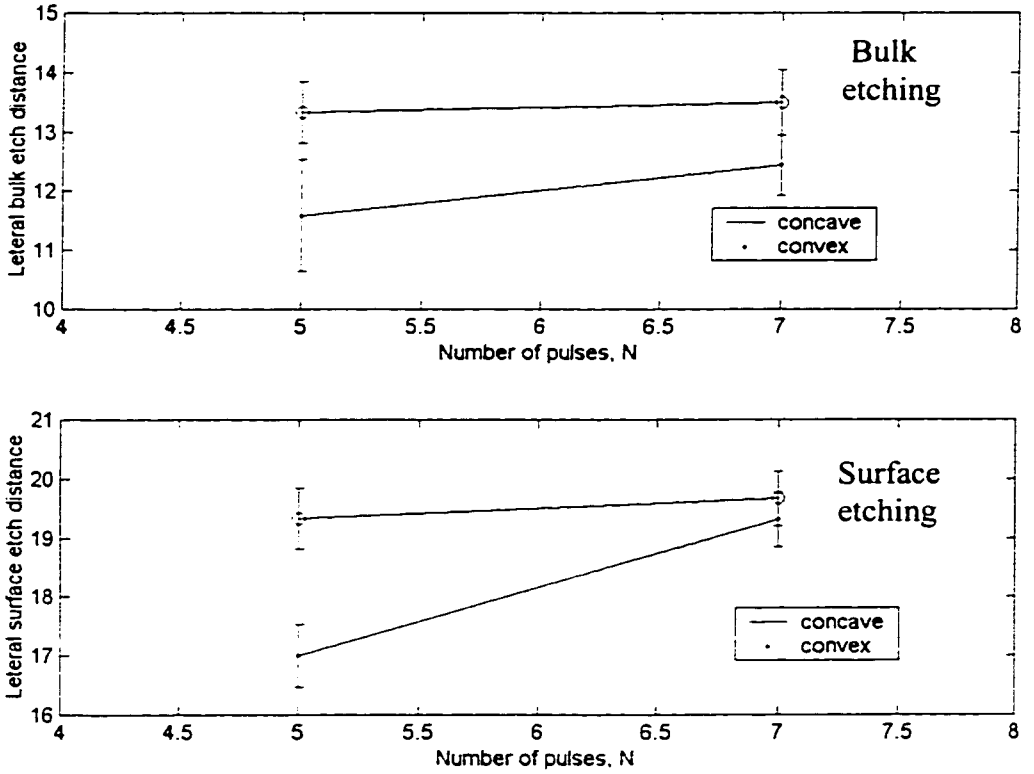

Figure 2.17: Lateral etch distance versus number of pulses showing corner selectivity of XeF_2 etching (Etch distance in μm, Error bars indicate $\pm 1\sigma$)

start of the etch for both corners, the σ value keeps increasing as the etch proceeds for concave corners while it reduces for convex corners. This is due to the increase in the area of the etch front (A_f) for the concave zone and the decrease in the etch front for the convex zone during etching. Thus, the higher value of σ indicating the relatively higher demand on the etching energy could be a reason for reduced etch rates for concave corners.

2.7 CAPACITIVE AND PIEZORESISTIVE TYPES OF MEMS DEVICES

It is possible to fabricate both capacitive and piezoresistive MEMS devices through the Mitel 1.5 μm process using gas phase XeF_2 post-process etching by proper selection of structural layers. A scheme for fabricating a piezoresistive sensor is shown in Figure 2.18 in which the piezoresistor shaped out of polysilicon2 layer is sandwiched between structural and etch mask layers to protect the polysilicon during post-process etching. The structural layer along with polysilicon2 could be released by bulk post-processing of the silicon substrate as shown in Figure 2.19. The bulk etching of the silicon substrate without affecting the polysilicon (PO2) layer is seen in Figure 2.19.

Similarly, it is possible to make capacitive type sensors as shown schematically in Figure 2.20 by selecting the layers such that PO2 is sacrificial, PO1 is backplate, and any metal layer sandwiched in oxide layers is the top plate. IPO (inter-polysilicon oxide) is the etch stop for backplate. The sacrificial etching of the polysilicon (PO2) forms the dielectric

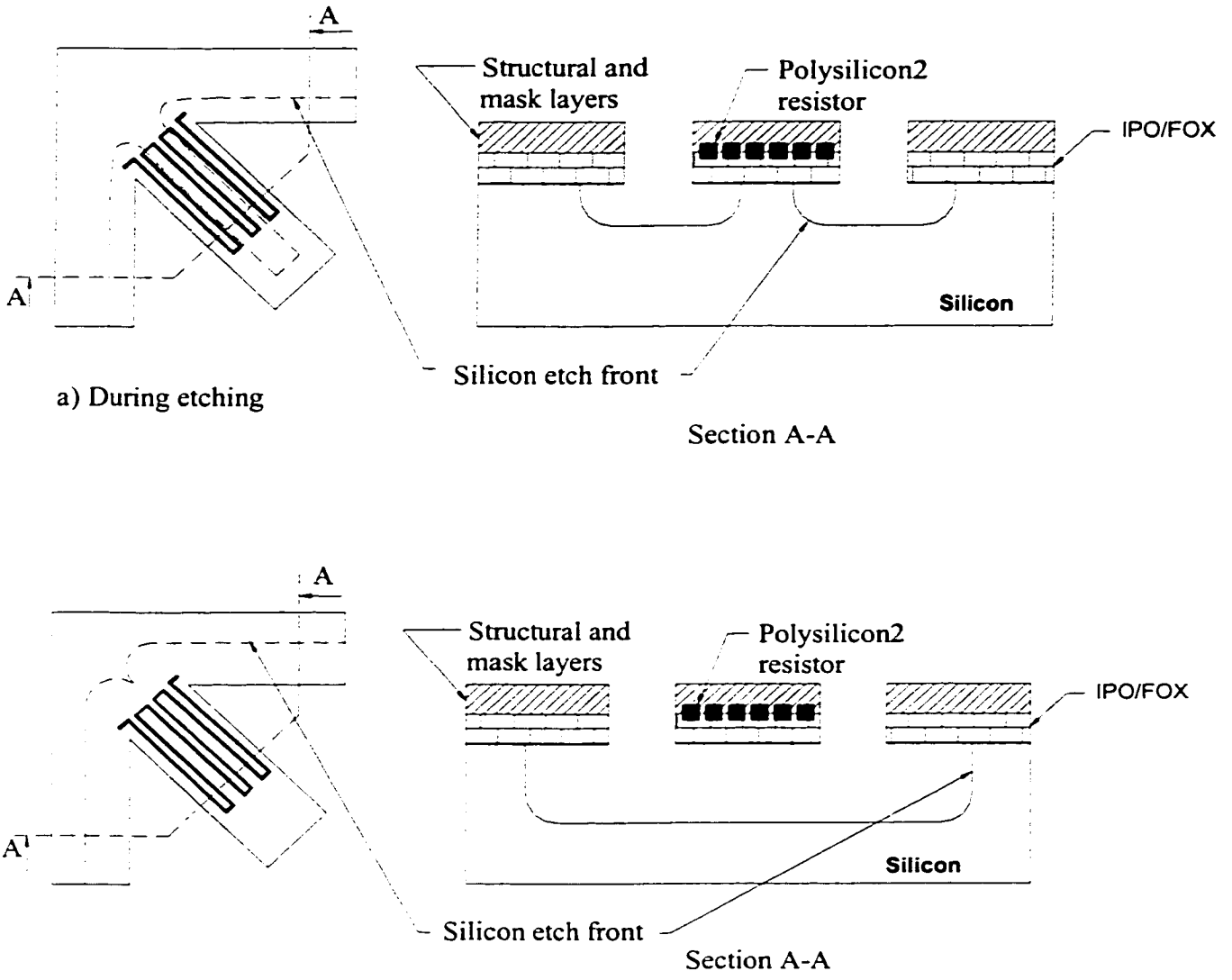

Figure 2.18: Scheme for bulk micromachining of piezoresistive sensors

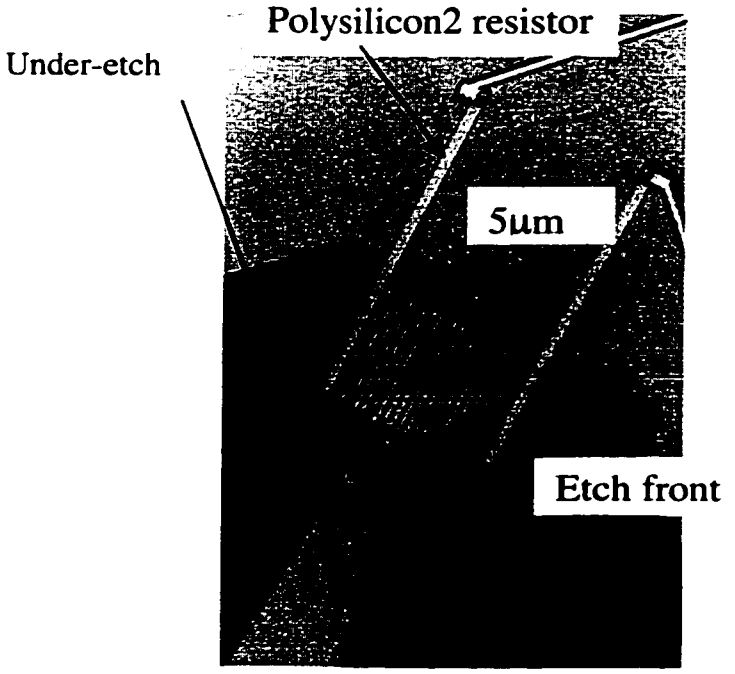

Figure 2.19: Bulk micromachining of piezoresistive structures made of PASS, IMO, COX and FOX layers

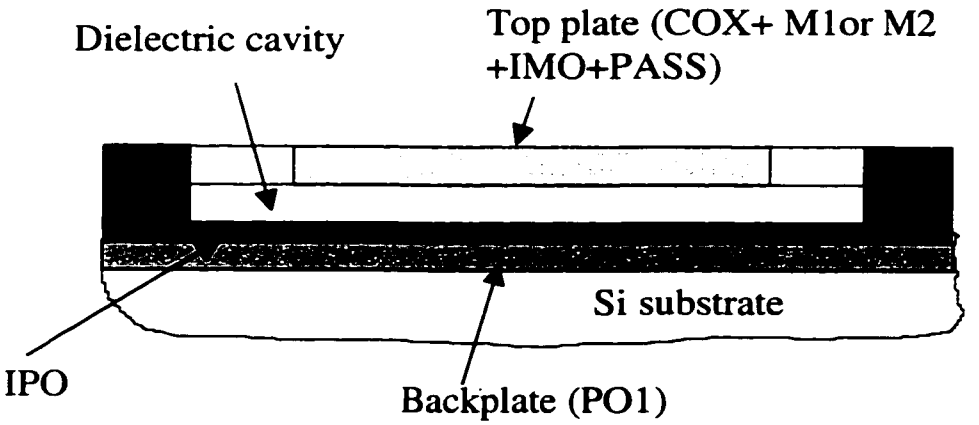

Figure 2.20: Scheme for sacrificial post-processing of polysilicon2 for the fabrication of capacitive sensors

cavity. However, the successful release of these sensors depends on the optimum selection of etch window size and number of XeF_2 pulses.

These capacitive devices will have a dielectric cavity of height 0.3 μm and hence they are subjected to an electrostatic force as discussed in Section 1.2.5.2, when bias voltage is applied across the electrodes. It has been seen that the dynamic behavior of such capacitive devices depends upon electrostatic force. Hence, the development of capacitive devices using the Mitel 1.5μm technology is restricted by the boundary conditioning effect due to the electrostatic field effect.

2.8. DIFFERENT TYPES OF POST-ETCH RELEASED MEMS STRUCTURES

Several types of microstructures with different end conditions fabricated with the Mitel 1.5 μm process were released using XeF_2 etching. The released cantilever type of structures formed with both silicon dioxide and metal layers are shown in Figures 2.21 and 2.22. The clamped - clamped beam type structures made of both aluminum and IPO are shown in Figure 2.22. The released plate type structures, shown in Figures 2.23 and 2.24, in fact, consists of three layers, a metal layer sandwiched by oxide layers. The free standing structures released can be adapted for piezoresistive and capacitive types of sensing devices. The curl of free standing structures due to residual stresses can be seen in Figures 2.21-2.24 and 2.29-2.30. The designer must consider the effect of curling on the device performance during the design stage.

Even though the end conditions of the micromechanical structures are generally considered as clamped, they never correspond to the actual classical clamped conditions due to the limitations that are inherent to the micromachining process. One of the limitations is the under etch due to bulk micromachining that extends well beyond beam/structure supports as seen from Figures 2.14, 2.16(b), 2.19, 2.26, 2.27, 2.28 and 2.30. The scheme of the support condition that results from the under etch of silicon is shown in Figure 2.25a. The other limitation of stepped up end conditions due to surface micromachining of the sacrificial layer PO2 is shown schematically in Figure 2.25b. Prediction of the dynamic behavior for such systems with end conditions which differ from the classical clamped conditions need to be done through proper modeling of the boundary conditions in order to explore the Mitel 1.5 μm technology for the development of MEMS devices. The stepped-up and under etched support conditions introduce an increased rotational freedom and make the boundary conditions different from the classical clamped conditions. In applications where the dynamic behavior of free-standing structures is important in determining the performance of MEMS devices, the modeling of the influence of non-classical boundary conditions formed from fabrication processes will be helpful.

Circular plate type structures of Metal1 sandwiched in oxide layers with Metal2 stiffener are shown in Figure 2.26. These stiffeners that change the elastic property of the system can also be used as Lorentz conductors. The corrugated end supports that were released are shown in Figures 2.27 and 2.28. Corrugations introduce both translational and rotational flexibility to the structure and also change the end support conditions to be

different from the classical conditions. The stepped end conditions and the under etched supports introduce rotational flexibility to the supports and make it different from classical end conditions. The stepped up end conditions of the structures can be seen from the Figure 2.26.

Different temperatures involved in the fabrication process introduce residual stress in the structure, which changes the elastic property of the system. The structures shown in Figures 2.21, 2.22, 2.23, 2.24, 2.29 and 2.30 are curled up due to the residual stress. One has to take into account the residual stress during designing of the MEMS devices. It can be seen that different types of MEMS could be fabricated using the Mitel 1.5μm technology from Figures 2.29 and 2.30.

As discussed in Section 1.4, the elastic property of MEMS structures from the Mitel technology can be influenced by variations in stiffener configurations, corrugations, stepped up end conditions, under-etched end supports, electrostatic force, residual stress etc. Modeling the vibration behavior of microsystems fabricated through the Mitel 1.5μm technology, should be capable of including the variations in elastic property due to limitations imposed above from structural geometry (stiffness, corrugations etc.) and fabrication processes (stepped up, under etch at the supports, residual stress etc.).

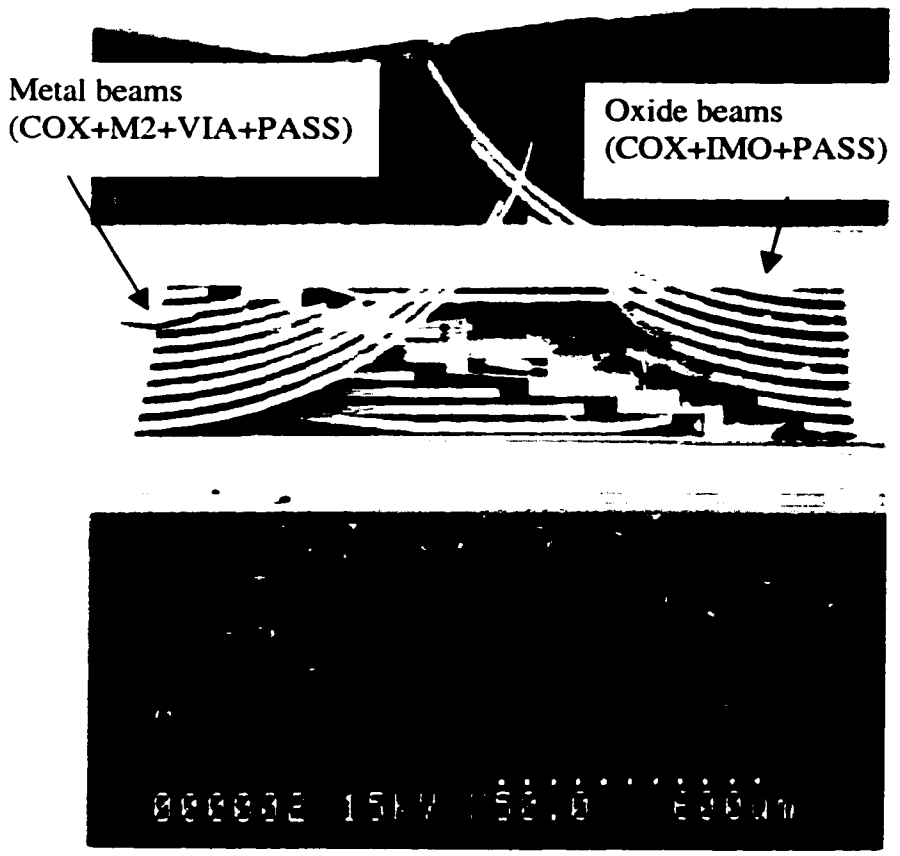

Figure 2.21: SEM of cantilevered beams, showing curl of beams due to residual stress. Beams of free-nearly clamped end conditions post released though surface micromachining of polysilicon2 after 20 pulses.

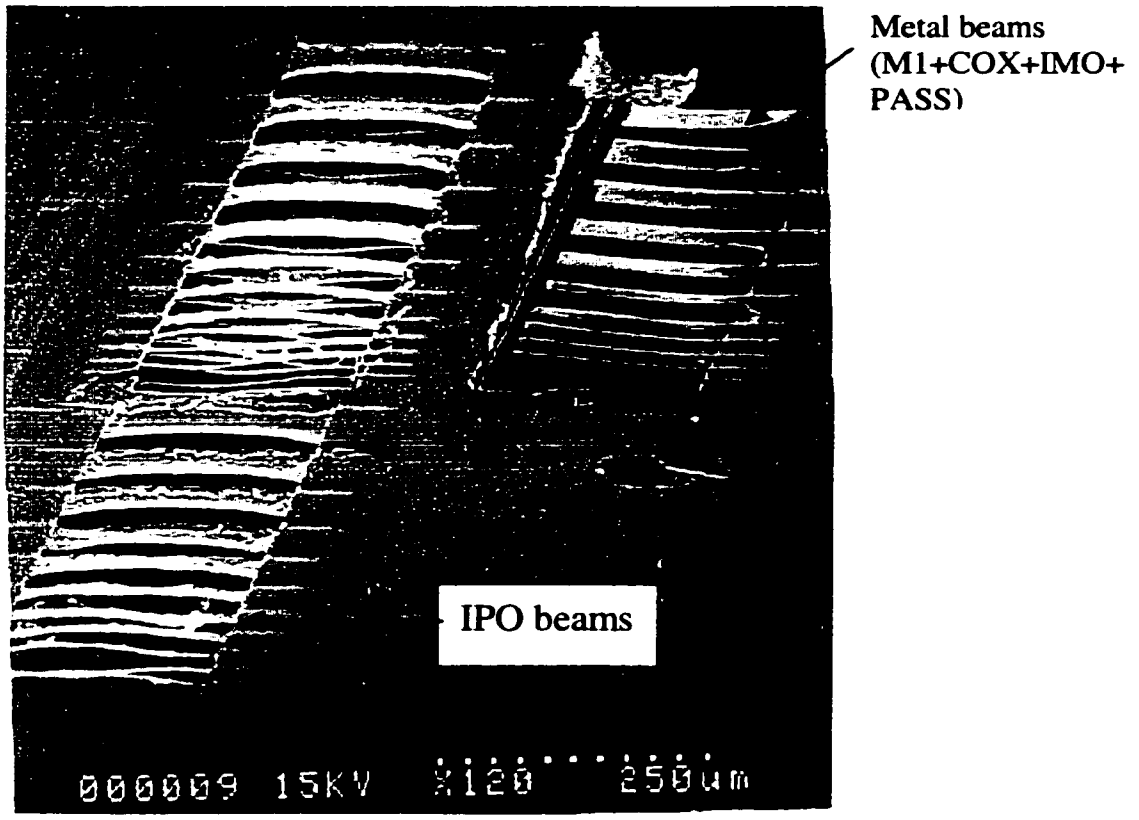

Figure 2.22: SEM of beams of clamped-clamped and cantilevered end conditions. Curl of beams due to residual stress is noticed.

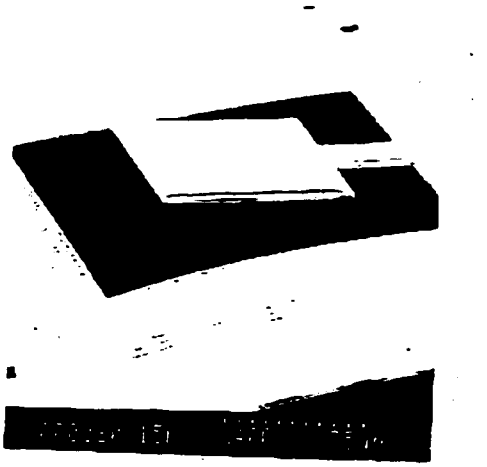

Figure 2.23: SEM of a cantilevered plate type structure of Metal2 with polysilicon2 as piezoresistor at the root of cantilever.

Figure 2.24: Piezoresistive microresonators under residual stress

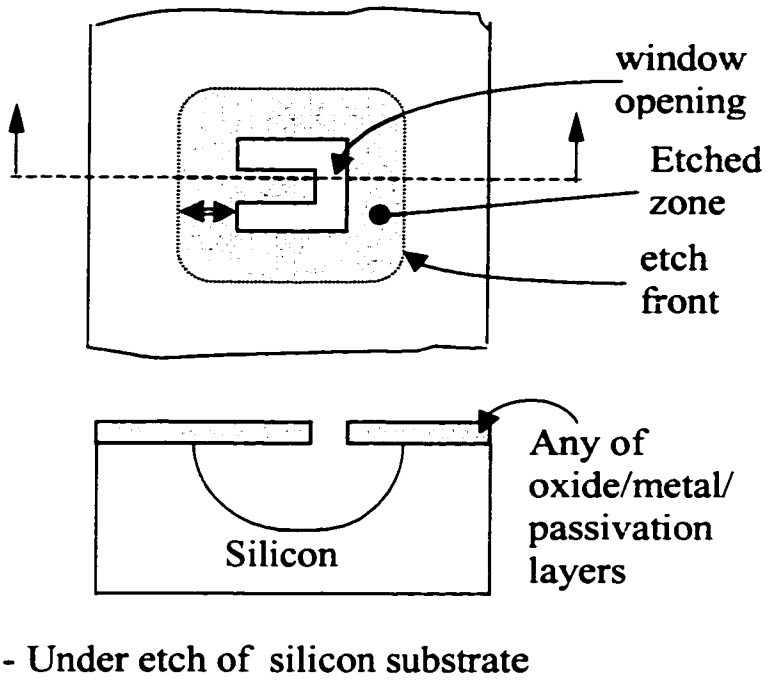

Figure 2.25a: Scheme for under etching of silicon substrate due to bulk micromachining

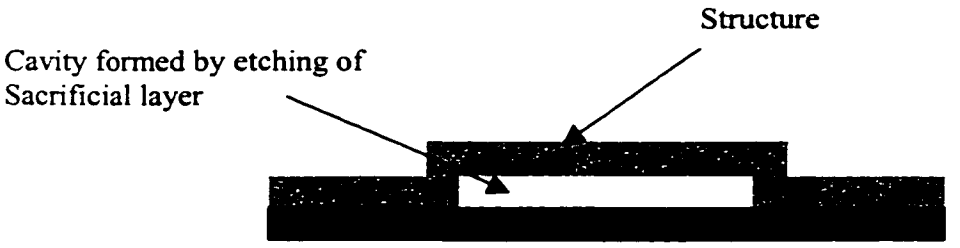

Figure 2.25b: Scheme of stepped-up boundary conditions inherent to surface micromachining

Figure 2.25: Scheme showing limitations on support conditions that are inherent to micromachining processes

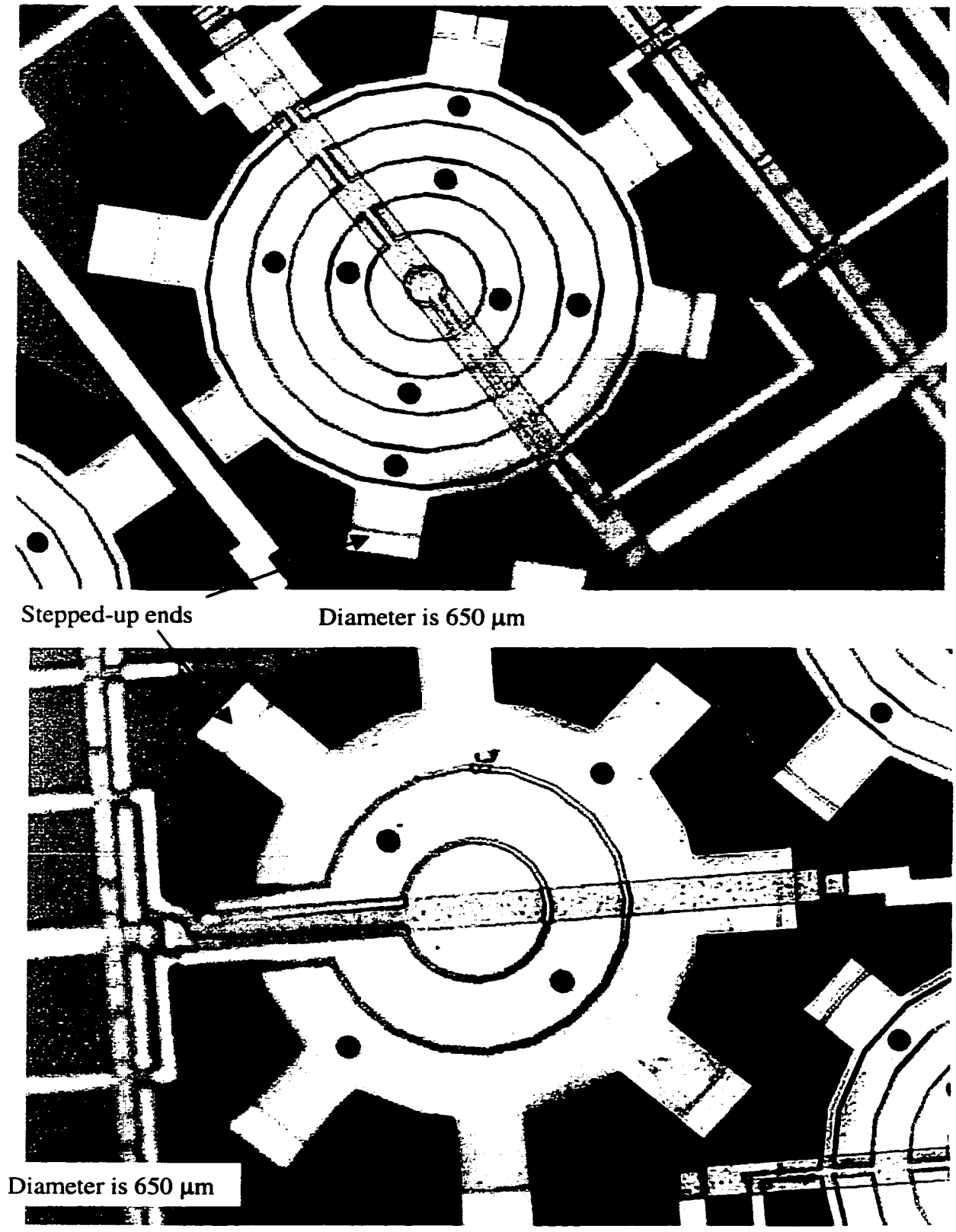

Figure 2.26: Circular plate type structure of Metal1 with Metal2 stiffeners with stepped up end supports

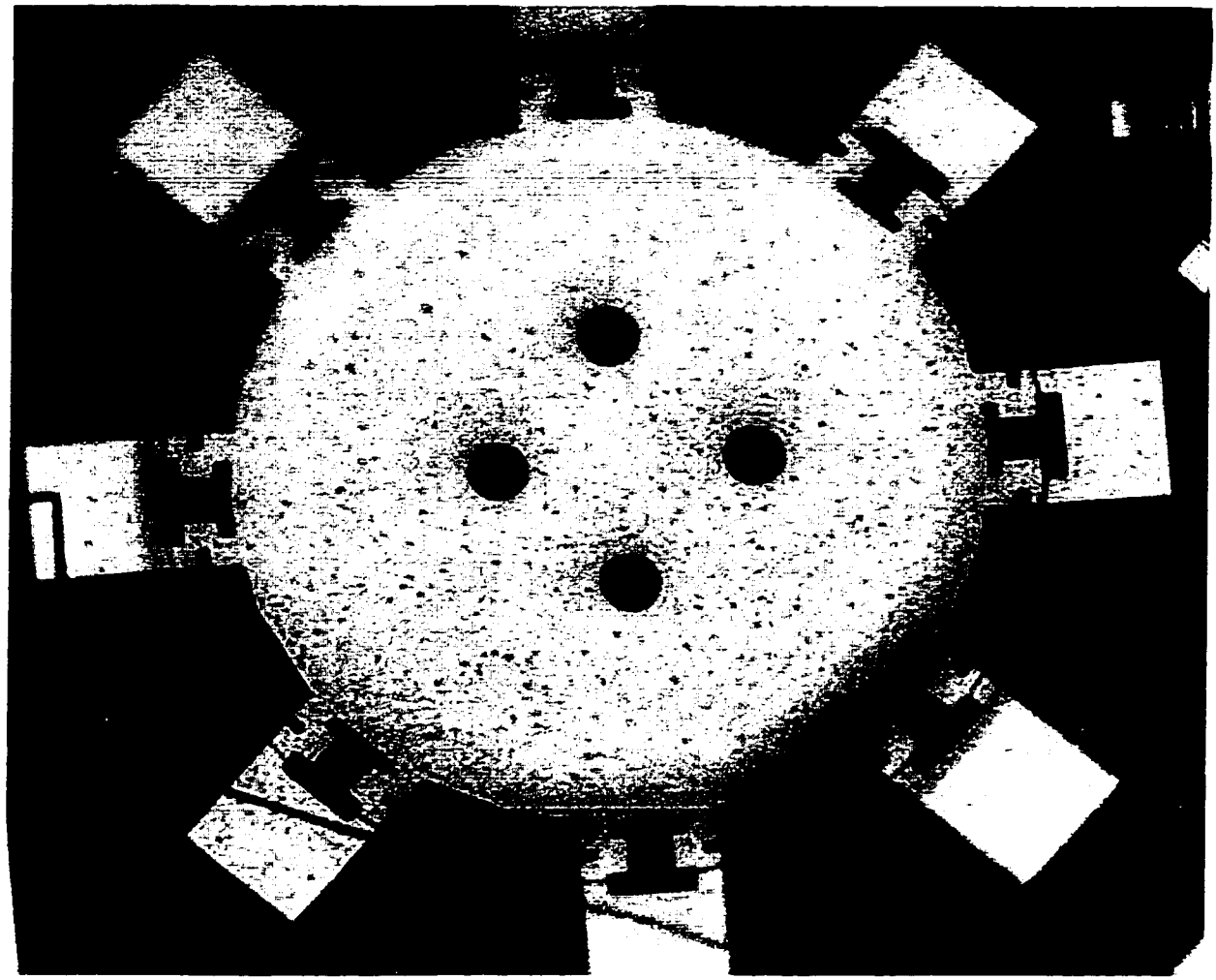

Figure 2.27: Circular plate type structure suitable for pressure sensors with corrugated and stepped up ends. (Diameter is 650 μm.)

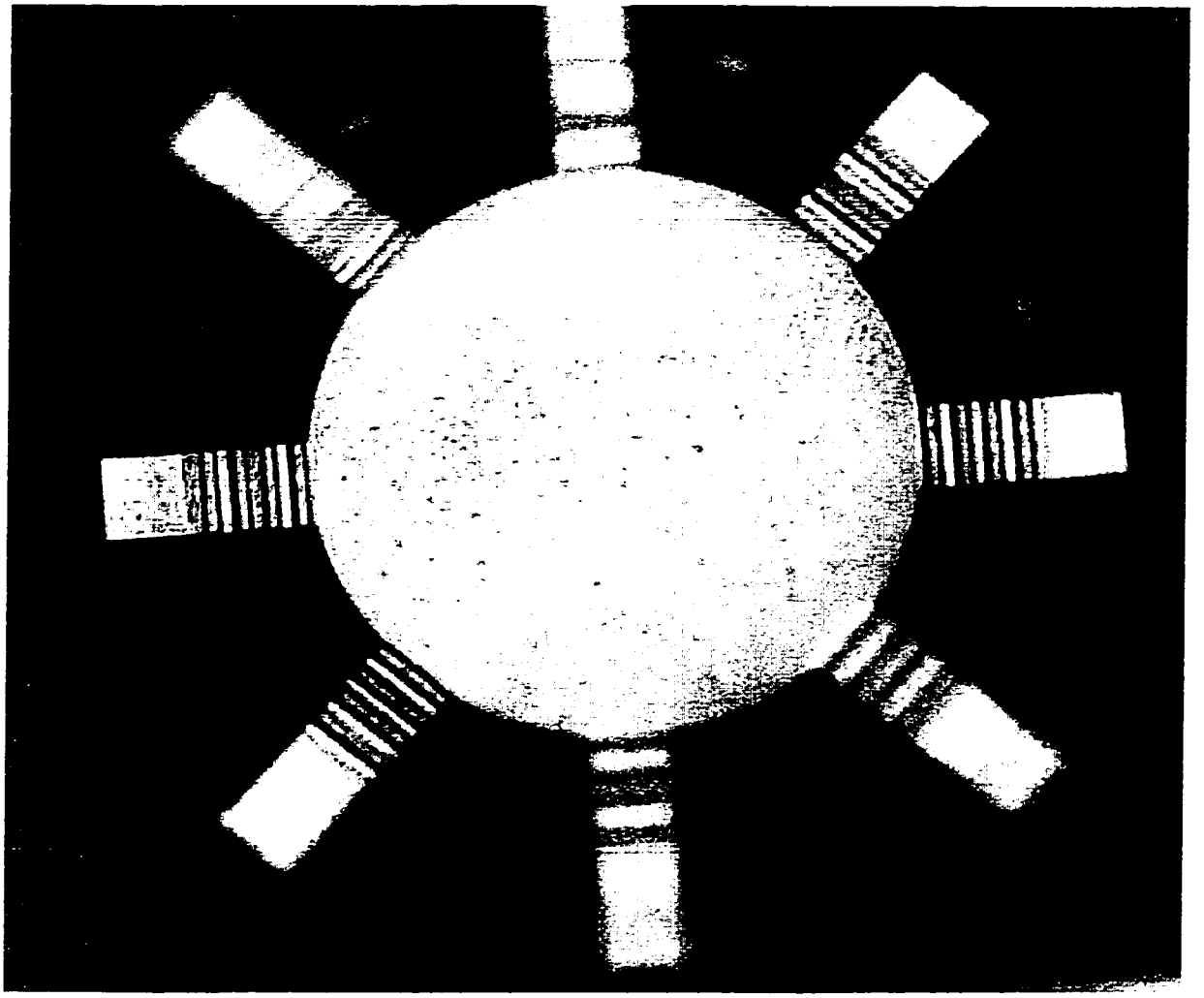

Figure 2.28: Circular plate type structure with transverse corrugated support ends. (Diameter is 250 μm.)

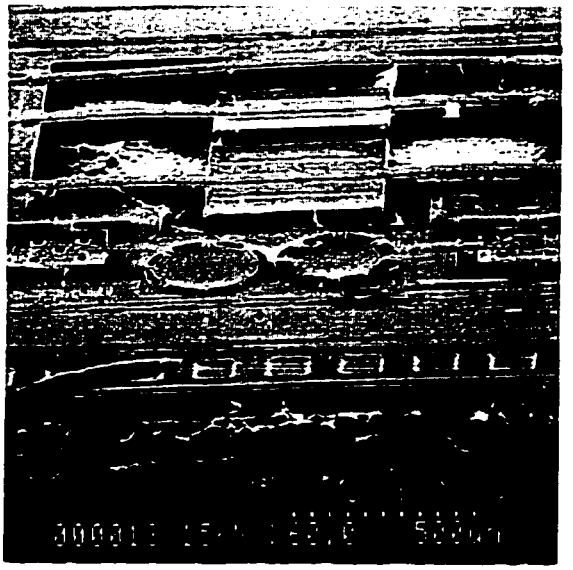

Figure 2.29: SEM of plate type structures with partially supported ends. Structures are made of PASS, IMO, M2, M1 and COX layers. Curl due to residual stress is seen.

Figure 2.30: Photograph of plate type structures with stepped up ends and residual stress suitable for piezoresistive devices

In Chapter 2, the gas phase etching has been described with details of the setup, the etching procedure and also the effect of etching on the end conditions of the finished structure. Further, it was shown in Chapter 1 that a common methodology for modelling microelastic systems is possible through the concept of boundary conditioning. In the next chapter, the influence of the specific boundary conditions on the dynamic behavior of the structure is discussed.

CHAPTER 3

BOUNDARY CONDITIONING OF ELASTIC SYSTEMS

In the previous chapter, the fabrication synthesis of MEMS devices using the Mitel 1.5 μm process and XeF_2 post-release etching have been studied along with examples. The strategies for fabricating piezoresistive, capacitive and other elastic devices have also been proposed. The proposed fabrication synthesis resulted in certain limitations such as stepped-up end conditions, under-etch conditions, electrostatic force etc. which are very important in determining the performance of elastic systems. In this chapter, a concept of boundary conditioning is developed in order to quantify and model the influence of fabrication limitations, operational constraints and structural variations on the performance of elastic systems that could be macro or micro order in dimension. The modeling of boundary conditioning is presented in this chapter along with various applications and case studies.

The Manipulation of vibration behavior through the modification of structural and effective environmental stiffness properties has tremendous applications for both micro and macro elastic systems. The vibration behavior which is dependent on the mass and stiffness properties of the systems, is influenced by the structural geometry, support conditions, manufacturing sequence and the operational environment. A unified approach for the quantification of the influence of structural geometry, support conditions, fabrication process and environmental influence on the dynamic behavior of the system is attempted here for the influence of the above parameters and modeling the dynamic

performance of the system. The influence of all the above parameters is represented by replacing the elastic influence with the equivalent spring stiffnesses as explained for lumped elastic system below:

Consider a lumped model of a system with distributed mass and elastic properties as shown in Figure 3.1. Neglecting damping, the equation of motion of the system can be written as:

$$M\ddot{X} + (K_{stru} + K_{ext}(X))X = 0$$

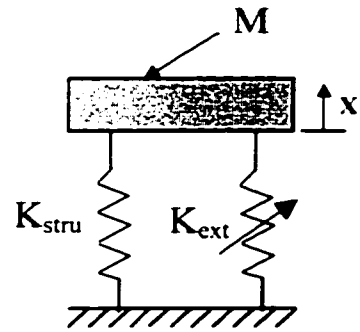

Figure 3.1: Lumped Model of an Elastic System

where

K_{stru} - stiffness representing the elastic property of the structural part of the system

K_{ext} - stiffness representing the external influence (support conditions, environmental influence, process influence such as residual stress, manufacturing processes such as heat treatment, peening etc.) on the elastic property of the system.

The stiffness K_{stru} indicates the stiffness due to geometry of the mechanical structure and it can be modified by changing the geometry of the structure and by adding features such as stiffeners, notches, slots, corrugations. K_{ext} represents the external influence that modifies the elastic property of the system and hence the dynamic behavior. The external

influence includes different end conditions like free, clamped and any intermediate condition, and also electrostatic force, Lorentz force, squeeze film effect, capillary force, work hardening, structural weakening etc. The external stiffness can be dependent on the displacement also. It is thus possible to modify the dynamic behavior of a system by altering the structural and/or external elastic property. This process is called boundary conditioning [117-122, 129]. Hence, *Boundary Conditioning may be defined as the manipulation of the dynamic behavior (eg. eigenvalue, mode shapes, eigenratios, acoustic radiation properties, localization of response, manipulating harmonic combinations etc.) of a system by modifying the structural or environmentally influenced part of elastic property of the system.*

3.1 BOUNDARY CONDITIONING BY STRUCTURAL MODIFICATION

The simplest way of increasing the stiffness of the system is by means of adding stiffeners. Stiffened plates of different geometries find various applications in engineering. The positive stiffeners are used to increase the strength of the structure. The negative stiffening methods such as notches, slots, corrugations may find applications where it is required to attenuate or control the transmission of vibrations through the joints, and to limit the vibrations to local areas. The prediction of natural frequencies of plates with positive stiffeners will be useful to understand the effect of stiffeners on the structural dynamic behavior. It is possible to extend this approach to negatively stiffened structures also. In this thesis a rectangular plate is considered to study the effect of stiffeners on fundamental frequencies. Study on various

configurations of stiffeners also will be very helpful in understanding the effect of stiffeners. Nair and Rao [124] used finite element method to investigate the effect of length of stiffeners on natural frequencies of a rectangular plate. Ritz method was used by [75, 99, 124] for the study of stiffened plates. The Rayleigh-Ritz method is widely used in the study of vibration of plates. The accuracy of the method is dependent on the deflection expressions assumed for the continuous plate domain. Beam characteristic functions and degenerate beam functions were used in the past to study plate vibration using Rayleigh Ritz method (Leissa [102, 103]). The boundary characteristic orthogonal polynomials (BCOP) proposed by Bhat [17-22] in the Rayleigh-Ritz method are used in this report. These functions were used by many other authors [32, 17, 199, 208] and found to yield excellent results for plates.

3.1.1. Natural Frequencies of Stiffened Plates

3.1.1.1 Boundary characteristic orthogonal polynomials

It is necessary to use the deflection functions satisfying at least the geometrical boundary conditions of the structure for the application of the Rayleigh-Ritz method. The boundary characteristic orthogonal polynomials used in this study are generated by using Gram-Schmidt process as proposed by Bhat [17, 21] in both x and y directions.

Given the polynomial of the lowest order satisfying at least the geometrical boundary conditions of the plate, $\Phi_0(x)$, an orthogonal set of polynomials in the interval $0 \leq x \leq 1$ can be generated using the Gram-Schmidt process as follows

$$\Phi_1(x) = (x - B_1)\,\Phi_0(x) \tag{3.1}$$

$$\Phi_k(x) = (x - B_k)\,\Phi_{k-1}(x) - C_k\Phi_{k-2}(x) \tag{3.2}$$

where

$$B_k = \frac{\int_0^1 x\rho(x)\phi_{k-1}^2(x)dx}{\int_0^1 \rho(x)\phi_{k-1}^2(x)dx} \tag{3.3}$$

$$C_k = \frac{\int_0^1 x\rho(x)\phi_{k-1}(x)\phi_{k-2}(x)dx}{\int_0^1 \rho(x)\phi_{k-2}^2(x)dx} \tag{3.4}$$

where $\rho(x)$ is a weighting function and is taken as unity for a uniform plate. The interval is from 0 to 1 and the coefficients are chosen in such a way as to make the polynomials orthonormal,

$$\int_0^1 \phi_k(x)\phi_l(x)dx = \begin{cases} 0 & \text{if } k \neq l \\ 1 & \text{if } k = l \end{cases} \tag{3.5}$$

The starting function $\Phi_0(x)$ is chosen as the simplest polynomial that satisfies all the boundary conditions if possible or at least the geometrical boundary conditions of the plate. Even though $\Phi_0(x)$ satisfies all the boundary conditions, the other members of the

orthogonal set satisfy only the geometrical boundary conditions, which can be seen from Equations (3.1) and (3.2).

A rectangular plate of sides a and b is considered for analysis with all edges clamped. The actual co-ordinates ξ and η are non-dimensionalized as $x=\xi/a$ and $y=\eta/b$, and consequently, the boundary conditions at a clamped edge are

$$W(0) = W(1) = W'(0) = W'(1) = 0 \tag{3.6}$$

along both x and y directions. Hence, the first member of the polynomial set, $\Phi_0(x)$, must satisfy the above boundary conditions. Assuming the beam deflection function as the simplest polynomial

$$W(x) = a_0 + a_1 x + a_2 x^2 + a_3 x^3 + a_4 x^4 \tag{3.7}$$

and applying the boundary condition of Equation (3.6) gives the deflection shape as

$$W(x) = a_4 (x^2 - 2x^3 + x^4) \tag{3.8}$$

where a_4 is an arbitrary constant. The normalized mode function is obtained as

$$\Phi_0(x) = \frac{(x^2 - 2x^3 + x^4)}{(\int_0^1 (x^2 - 2x^3 + x^4)^2 dx)^{1/2}} \tag{3.9}$$

Similarly polynomial functions along x and y directions $\Phi_i(x)$ and $\psi_j(y)$, respectively, were generated using Equations (3.3, 3.4, 3.5) for the analysis of a square plate.

3.1.1.2 Elastic system of rectangular plate with positive stiffeners

Consider a rectangular plate with stiffeners as shown in Figure 3.2.

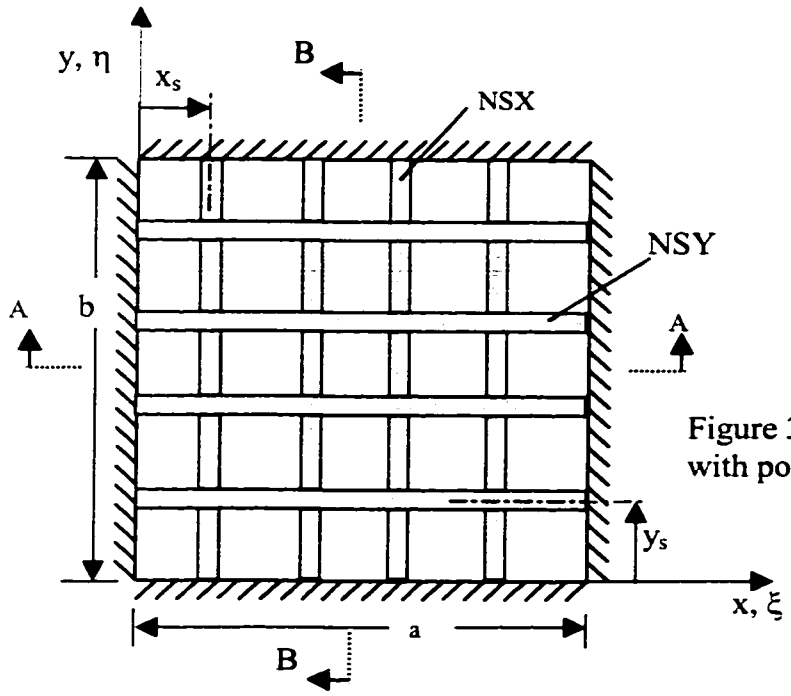

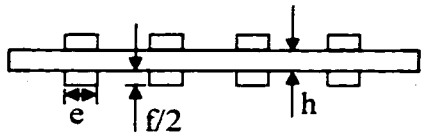

Section AA, BB

Figure 3.2: Clamped rectangular plate with positive stiffeners

where a and b are side dimensions of the plate, h is the thickness of the plate, NSX is number of stiffeners in x direction, NSY is number of stiffeners in y direction, e is width of the stiffener and f is the height of the stiffener. Torsion of the stiffeners is neglected in the present analysis.

The deflection equation of the rectangular plate shown in Figure 3.2 assuming flexural vibration, is expressed in separable form as [17, 21]

$$W(x, y) = \sum_{m}\sum_{n} A_{mn}\, \phi_m(x)\, \varphi_n(y) \qquad (3.10)$$

where $\phi_m(x)$ and $\varphi_n(y)$ are boundary characteristic orthogonal polynomials in x and y directions, respectively, and A_{mn} are the arbitrary deflection coefficients.

3.1.1.3 Kinetic energy of the elastic system

The total kinetic and potential energies of the stiffened plate is the sum of the respective energies for the rectangular plate and all the stiffeners in both x and y directions. The maximum kinetic energy [17,21] of the plate is given by

$$T_{max,p} = \frac{1}{2}\rho hab\omega^2 \int_0^1 \int_0^1 W^2(x,y)\,dx\,dy \qquad (3.11)$$

and maximum kinetic energy of all stiffeners on both directions is given by

$$T_{max,s} = \frac{1}{2}\rho efa\omega^2 \sum_{i=1}^{NSY} \int_0^1 W^2(x,y_i)\,dx + \frac{1}{2}\rho efb\omega^2 \sum_{j=i}^{NSX} \int_0^1 W^2(x_j,y)\,dy \qquad (3.12)$$

Then the total maximum kinetic energy is obtained by adding Equations (3.11) and (3.12) as

$$T_{max} = \frac{1}{2}\rho hab\omega^2 \int_0^1 \int_0^1 W^2(x,y)\,dx\,dy + \frac{1}{2}\rho efa\omega^2 \sum_{i=1}^{NSY} \int_0^1 W^2(x,y_i)\,dx + \frac{1}{2}\rho efb\omega^2 \sum_{j=i}^{NSX} \int_0^1 W^2(x_j,y)\,dy \qquad (3.13)$$

where ρ is the density of the plate, i and j refer to the position of the stiffeners in y and x directions, respectively, and ω is the frequency.

3.1.1.4 Potential energy or strain energy of elastic system

The strain energy of the rectangular plate can be written as

$$U_{max,p} = \frac{1}{2a^4} Dab \int_0^1 \int_0^1 \left[W_{xx}^2 + \alpha^4 W_{yy}^2 + 2\gamma\alpha^2 W_{xx} W_{yy} + 2(1-\gamma)\alpha^2 W_{xy}^2 \right] dx\, dy \qquad (3.14)$$

where α=(a/b) and γ is the Poisson's ratio. The strain energy of all the stiffeners can be written as

$$U_{max,s} = \frac{E}{2a^3} \sum_{i=1}^{NSY} I_i \int_0^1 W_{xx}^2(x, y_i)\, dx \quad + \frac{E}{2b^3} \sum_{j=1}^{NSX} I_j \int_0^1 W_{yy}^2(x_j, y)\, dy \qquad (3.15)$$

where i, j refer to the stiffener position and subscripts x and y refer to differentiation with respect to normalized x and y coordinates, respectively.

The total maximum strain energy of the stiffened plate will be the sum of the strain energies of the plate and thickness given by Equations (3.14) and (3.15), respectively, and expressed as

$$\begin{aligned} U_{max} = {} & \frac{1}{2a^3} Db \int_0^1 \int_0^1 \left[W_{xx}^2 + \alpha^4 W_{yy}^2 + 2\gamma\alpha^2 W_{xx} W_{yy} + 2(1-\gamma)\alpha^2 W_{xy}^2 \right] dx\, dy \\ & + \frac{E}{2a^3} \sum_{i=1}^{NSY} I_i \int_0^1 W_{xx}^2(x, y_i)\, dx \quad + \frac{E}{2b^3} \sum_{j=i}^{NSX} I_j \int_0^1 W_{yy}^2(x_j, y)\, dy \end{aligned} \qquad (3.16)$$

From Rayleigh's condition of the plate which is $T_{max} = U_{max}$, the Rayleigh's quotient can be obtained as

$$\omega^2 = \frac{U_{max}}{T^{\bullet}_{max}} \tag{3.17}$$

where

$$\omega^2 T^{\bullet}_{max} = T_{max} \tag{3.18}$$

The substitution of deflection Equation (3.10) in (3.13) and (3.16), and optimization of the Rayleigh's quotient of Equation (3.17) with respect to arbitrary constants A_{mn}, i.e. $\frac{\partial W^2}{\partial A_{mn}} = 0$, yield the following eigenvalue equation:

$$\sum_m \sum_n \left[C_{mnij} - \lambda \left(E^{00}_{mi} F^{00}_{nj} + J \right) \right] A_{mn} = 0 \tag{3.19}$$

where

$$\begin{aligned} C_{mnij} = {} & E^{22}_{mi} F^{00}_{nj} + \alpha^4 E^{00}_{mi} F^{22}_{nj} + \gamma\alpha^2 \left(E^{02}_{mi} F^{20}_{nj} + E^{20}_{mi} F^{02}_{nj} \right) + 2(1-\gamma)\alpha^2 E^{11}_{mi} F^{11}_{nj} \\ & + \sum_{i=1}^{NSY} 4\left(1-\gamma^2\right) \frac{e}{b} \left[\left(\frac{f}{h}\right)^3 + 1.5\left(\frac{f}{h}\right)^2 + 0.75\left(\frac{f}{h}\right) \right] E^{22}_{mi} . \varphi_n(y_i) . \varphi_j(y_i) \\ & + \sum_{j=1}^{NSX} 4\left(1-\gamma^2\right) \frac{e}{a} \alpha^4 \left[\left(\frac{f}{h}\right)^3 + 1.5\left(\frac{f}{h}\right)^2 + 0.75\left(\frac{f}{h}\right) \right] F^{22}_{nj} . \phi_m(x_j) . \phi_i(x_j) \end{aligned} \tag{3.20}$$

$$J = \sum_{i=1}^{NSY} \frac{f}{h} \frac{e}{b} E^{00}_{mi} . \varphi_n(y_i) . \varphi_j(y_i) + \sum_{j=1}^{NSX} \frac{f}{h} \frac{e}{a} F^{00}_{nj} \phi_m(x_j) \phi_i(x_j) \tag{3.21}$$

$$E^{rs}_{mi} = \int_0^1 \left(\frac{d^r \phi_m}{dx^r} \right) \times \left(\frac{d^s \phi_i}{dx^s} \right) dx \tag{3.22}$$

$$F_{nj}^{rs} = \int_0^b \left(\frac{d^r \varphi_n}{d y^r}\right) \times \left(\frac{d^s \varphi_j}{d y^s}\right) dy \qquad (3.23)$$

$$\alpha = a/b \,, \quad \lambda = \frac{\rho h \omega^2 a^4}{D}$$

The solution of the eigenvalue Equation (3.19) will yield 'm times n' number of natural frequency coefficients (λ) and mode shapes (A_{mn}) of the stiffened plate corresponding to 'm times n' number of modes.

Six number of polynomials were used in both x and y directions which resulted in the prediction of eigenvalues corresponding to first 36 modes. These eigenvalues were predicted for different geometries of rectangular plate and also for different numbers and geometries of stiffeners. The results of this prediction are discussed and compared with already published results below.

3.1.2 Results on a rectangular plate with positive stiffeners

Fundamental natural frequencies for the stiffened plate have been computed for various values of side ratios a/b, number of stiffeners (NSX and NSY) and geometries of stiffeners by solving the eigenvalue Equation (3.19). The predicted fundamental eigenvalues ($\sqrt{\lambda}$) are compared with those reported by Wu and Liu [199]. Wu and Liu [199] employed the Rayleigh-Ritz method using the boundary characteristic orthogonal polynomial functions, however, with different number of polynomial functions.

3.1.2.1 Plate with one central stiffener

The plate with one central stiffener is shown in Figure 3.3. Natural frequencies for three values of a/b (1,0.75 and 0.5) and stiffener height ratio f/h (0.2,1.5 and 2) are computed.

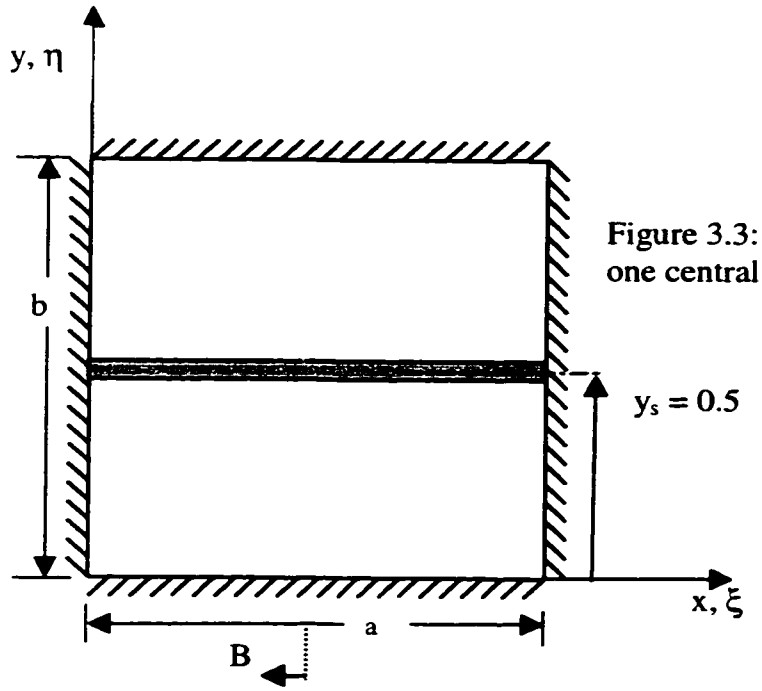

Figure 3.3: Clamped rectangular plate with one central stiffener at y = 1/2

The predicted values for the fundamental eigenfrequency is compared with the results of Wu and Liu [199] in Table 3.1. The comparison shows good agreement. Wu and Liu [199] used 4x4 number of polynomials while the present results use 6x6 number of polynomial functions and hence an improvement in upper bound values of the eigenvalues is noticed. It can be seen from the results that increase of f/h increases the fundamental eigenfrequency for constant side ratio a/b (1 or 0.5) proving the positive stiffening.

Table 3.1: Predicted eigenvalues of a rectangular plate with one stiffener

Sl. No	a/b	e/a	e/b	f/h	Nsy	ys	Nsx	xs	fn	Present	Wu & Liu [199]
1	1	0.01	-	1.5	1	0.5	-	-	1	39.64	39.83
2			-	2.0			-	-		43.14	43.34
3	0.75	0.01	-	1.5			-	-		32.21	32.36
4	0.5	0.01	-	0.2			-	-		24.62	24.64
5			-	1.5			-	-		27.16	27.24
6			-	2			-	-		29.12	29.11

The lowest four predicted eigenvalues are presented in Table 3.2 along with the results of [199] showing a good agreement of natural frequencies of the higher modes. Wu and Liu [199] used 10x10 terms in their computation and deflection functions satisfying simply supported conditions along with elastic rotational restraints. Present results have been computed with the double precision, while the precision of results in [199] is not known, which would explain the small discrepancies between the present results and those in [199] in Tables 3.2-3.6.

Table 3.2 Predicted higher eigenvalues of a rectangular plate with one stiffener

Sl. No	a/b	e/a	e/b	f/h	Nsy	ys	Nsx	xs	fn	Present	Wu & Liu [199]
1	1	-	0.01	1.5	1	0.5	-	-	1	39.639	39.829
									2	73.395	73.394
									3	85.907	86.285
									4	108.218	108.22

3.1.2.2 Plate with two stiffeners

A square plate with two stiffeners at distances of b/3 and 2b/3 as shown in Figure 3.4 is analyzed.

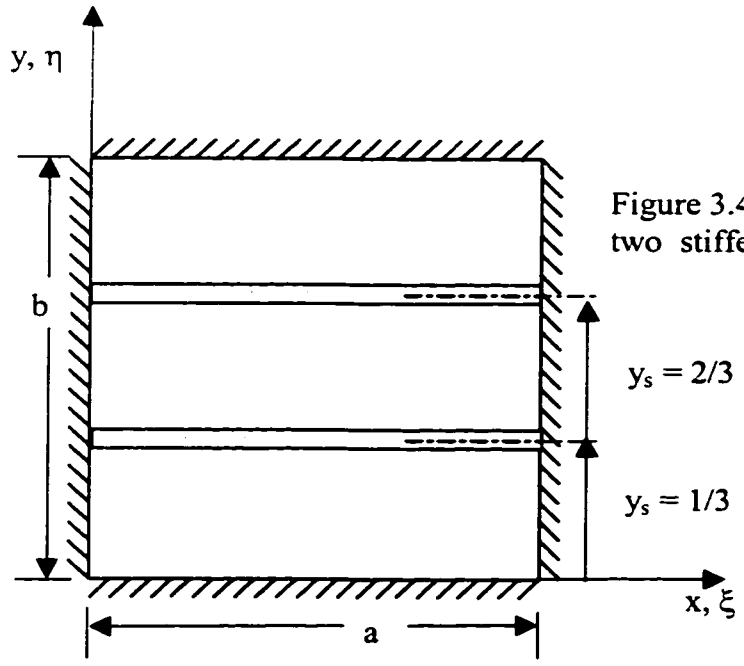

Figure 3.4: Clamped rectangular plate with two stiffeners at y = 1/3, 2/3

The geometry details and results are provided in Table 3.3 along with the results of [199]. The comparison shows close agreement for all the four modes.

Table 3.3: Predicted eigenvalues of a rectangular plate with two stiffeners

a/b	e/a	e/b	f/h	Nsy	ys	Nsx	xs	fn	Prediction	Wu & Liu [199]
1	-	0.01	1.5	2	0.33,0.66	-	-	1	40.488	40.715
								2	74.954	75.129
								3	90.327	90.752
								4	121.713	122.44

Eigenvalues are higher when compared to the results of plates with single stiffener, showing the positive increase in stiffness.

3.1.2.3 Plate with three stiffeners

Predicted eigenvalues for a square plate with three stiffeners as shown in Figure 3.5, are presented in Table 3.4, and are compared with the results of [299] showing good agreement.

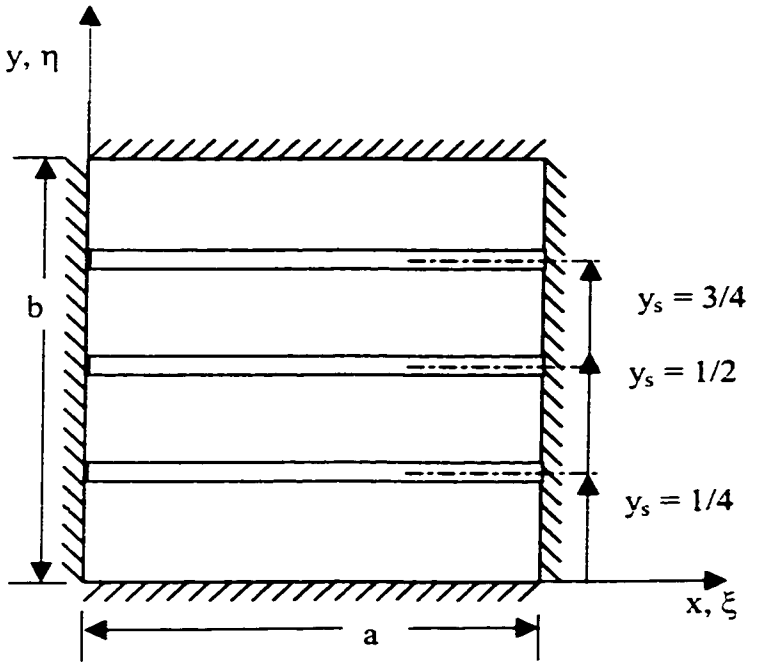

Figure 3.5: Clamped rectangular plate with three stiffeners at y = 1/4, 1/2, 3/4

Table 3.4: Predicted eigenvalues of a rectangular plate with three stiffeners

a/b	e/a	e/b	f/h	Ns y	ys	Nsx	xs	fn	Present	Wu & Liu [199]
1	-	0.01	1.5	3	0.25, 0.5, 0.75	-	-	1	41.725	42.025
								2	74.991	75.167
								3	95.01	95.814
								4	122.947	123.62

It can be seen from the results that the eigenvalue for the second mode is closer to that of second eigenvalue of plate with 2 stiffeners (see Table 3.3), indicating that the second mode shape is symmetric about y=b/2. The small difference is due to change in the position of stiffeners.

3.1.2.4 Plate with one stiffener in both directions

The geometric details and predicted results of first four eigenvalues are provided in Table 3.5 along with the results of [199] for a plate with one stiffener in each direction as shown in Figure 3.6.

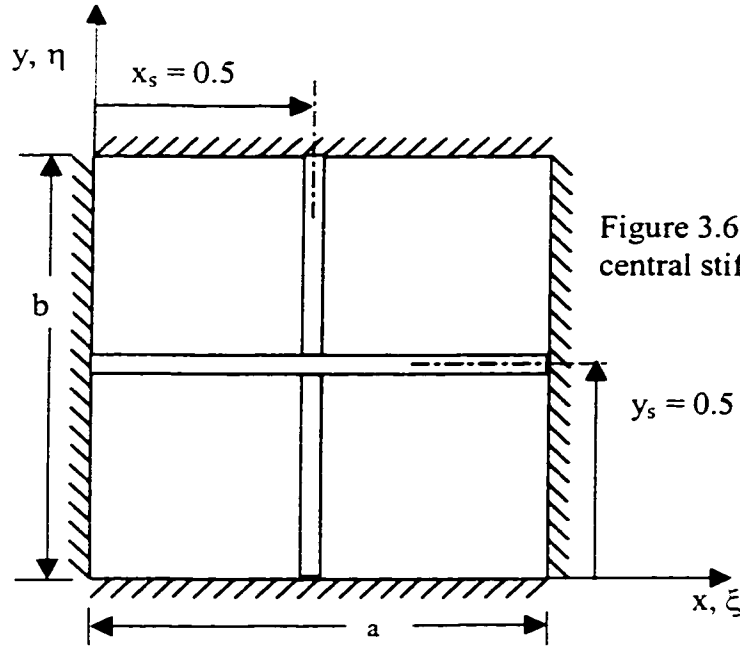

Figure 3.6: Clamped rectangular plate with central stiffeners in both directions

Table 3.5: Predicted eigenvalues of a rectangular plate with one stiffener in both directions

a/b	e/a	e/b	f/h	Nsy	ys	Nsx	xs	fn	Present	Wu & Liu [199]
1	-	0.01	1.5	1	0.5	1	0.5	1	42.839	43.186
								2	85.907	86.285
								3	85.907	86.285
								4	108.218	108.22

The crossed arrangement of two stiffeners gives higher value of first and second eigenvalues when compared to that of plate having two stiffeners in the same direction (Section 3.1.2) while third and fourth eigenvalues are lower. Crossed stiffener at the center will always result in identical second and third eigenvalues while stiffeners in the same direction will yield a lower second mode and a higher third mode. The second mode which is symmetric with respect to y=b/2, has a lower value than that for plate with parallel stiffeners in x direction, while the third mode which is symmetric with respect to x=a/2 yields higher eigenvalue for the case of two parallel stiffeners due to the presence of two effective stiffeners. This analogy is useful in selecting the proper configuration of stiffeners for the required operating range.

3.1.2.5 Plates with 2 or 3 stiffeners in both directions

Predicted eigenvalues for plates with 2 or 3 stiffeners in both x and y directions as shown in Figure 3.7 are given in Table 3.6 with comparison of results from that of [199]. Results once again show good agreement and also show an increase of eigenvalue as the number of stiffeners is increased. It also shows symmetrical mode shape along both x and y directions as the second and third eigenvalues are identical due to the symmetric nature of stiffener arrangement in both directions.

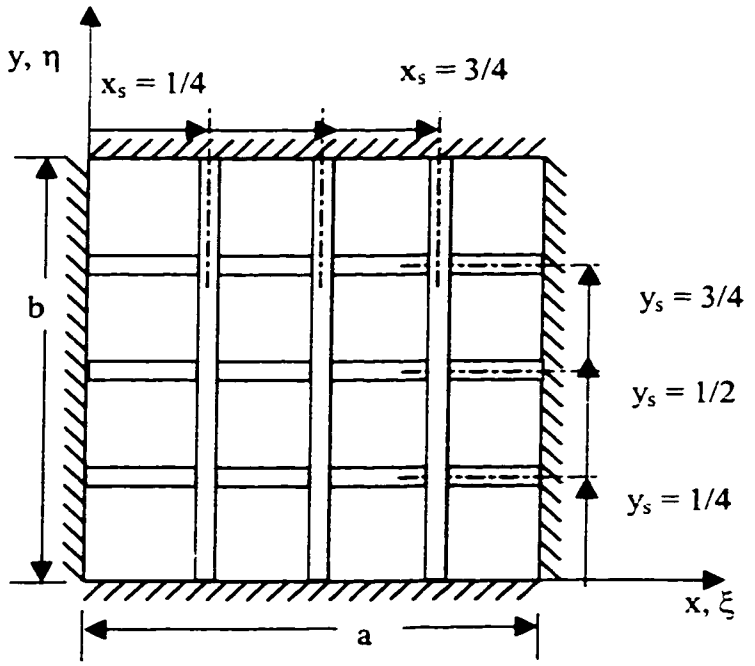

Figure 3.7a: Clamped rectangular plate with three stiffeners in both directions at y,x = 1/4, 1/2, 3/4

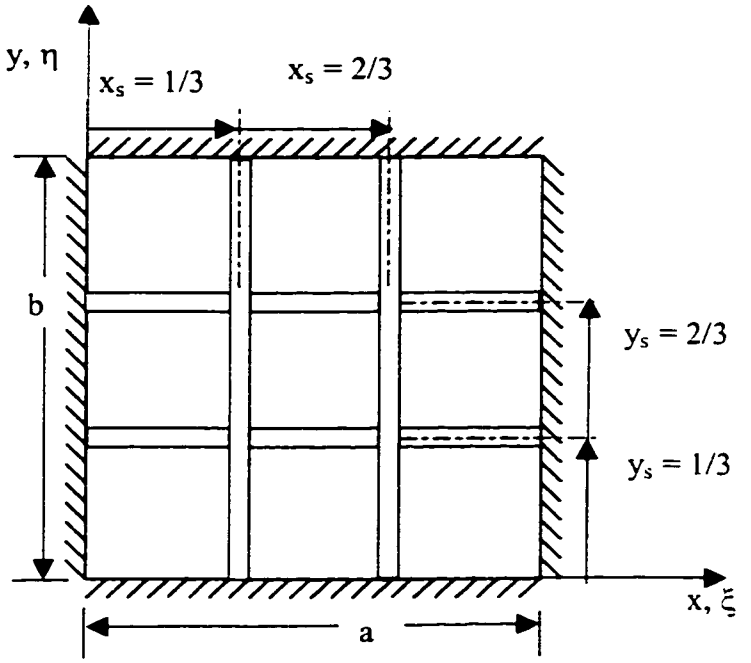

Figure 3.7b: Clamped rectangular plate with two stiffeners in both directions at y,x = 1/3, 2/3

Figure 3.7

Table 3.6: Predicted eigenvalues of a rectangular plate with two and three stiffeners in both directions

a/b	e/a	e/b	f/h	Nsy	ys	Nsx	xs	fn	Present	Wu & Liu [199]
1	-	0.01	1.5	2	0.33, 0.66	2	0.33, 0.66	1	44.206	44.614
								2	90.773	91.46
								3	90.773	91.46
								4	133.398	134.74
1	-	0.01	1.5	3	0.25, 0.5, 0.75	3	0.25, 0.5, 0.75	1	46.245	46.763
								2	95.089	96.067
								3	95.089	96.067
								4	134.731	136.00

3.1.2.6 Effect of stiffener geometry on elastic behavior

Boundary conditioning by structural modification includes modification of stiffener arrangement and stiffener geometrical parameters such as thickness and width. In order to investigate the sensitivity of the stiffener geometry on the elastic behavior, the eigenvalues were predicted for a clamped plate with one stiffener in each direction as shown in Figure 3.8 for the stiffener widths of e/b=0 to 0.1 in steps of 0.01 and the stiffener heights of f/h=0 to 4 in steps of 0.4. The predicted variation of the first five

eigenvalues given in Figure 3.8 shows the strong influence of stiffening on elastic behavior. This study will be useful during the design stage in selecting the appropriate stiffener geometry for the required eigenvalues.

Apart from the eigenvalues $\sqrt{\lambda}$, the eigenratios $q_i = \frac{\sqrt{\lambda_i}}{\sqrt{\lambda_1}}$ (ratio of higher eigenvalues to the first eigenvalue) are also important in some applications since it will influence the response of the structures as well as its sound radiation behavior. In order to determine the influence of stiffener geometry on the resultant harmonic combination when compared to that of a clamped plate without stiffeners, an objective function (Λ_{CCCC}) is defined as follows:

$$\Lambda_{CCCC} = \sum_{n=2}^{5} \left(\frac{\sqrt{\lambda_n} - q_n \sqrt{\lambda_1}}{q_n \sqrt{\lambda_1}} \right)^2 \tag{3.24}$$

where

$\sqrt{\lambda_n}$ - n^{th} eigenvalue of the stiffened system

q_n – required 2^{nd} to 5th eigenratios with reference to a clamped plate without stiffeners such as, {2.04, 2.04, 3.01, 3.69}

The minimum value of this objective function indicates that the combinations are close to that of a fully clamped plate without stiffeners. The predicted variation of higher eigenratios and Λ_{CCCC} against the stiffener thickness and height are given in Figure 3.9. The Figures 3.8 and 3.9 show the possibility of modifying the elastic behavior of the system though structural modifications.

In this way of stiffening, the mass properties are also changed in addition to the stiffness properties. The modeling of the change in elastic properties by adding stiffeners can not be applied in general to all boundary conditioning methods. Hence, a method of artificial springs is proposed in order to represent the influence of stiffening through equivalent artificial springs. The stiffeners can be modeled by a combination of lumped mass and artificial springs at the locations of the stiffeners.

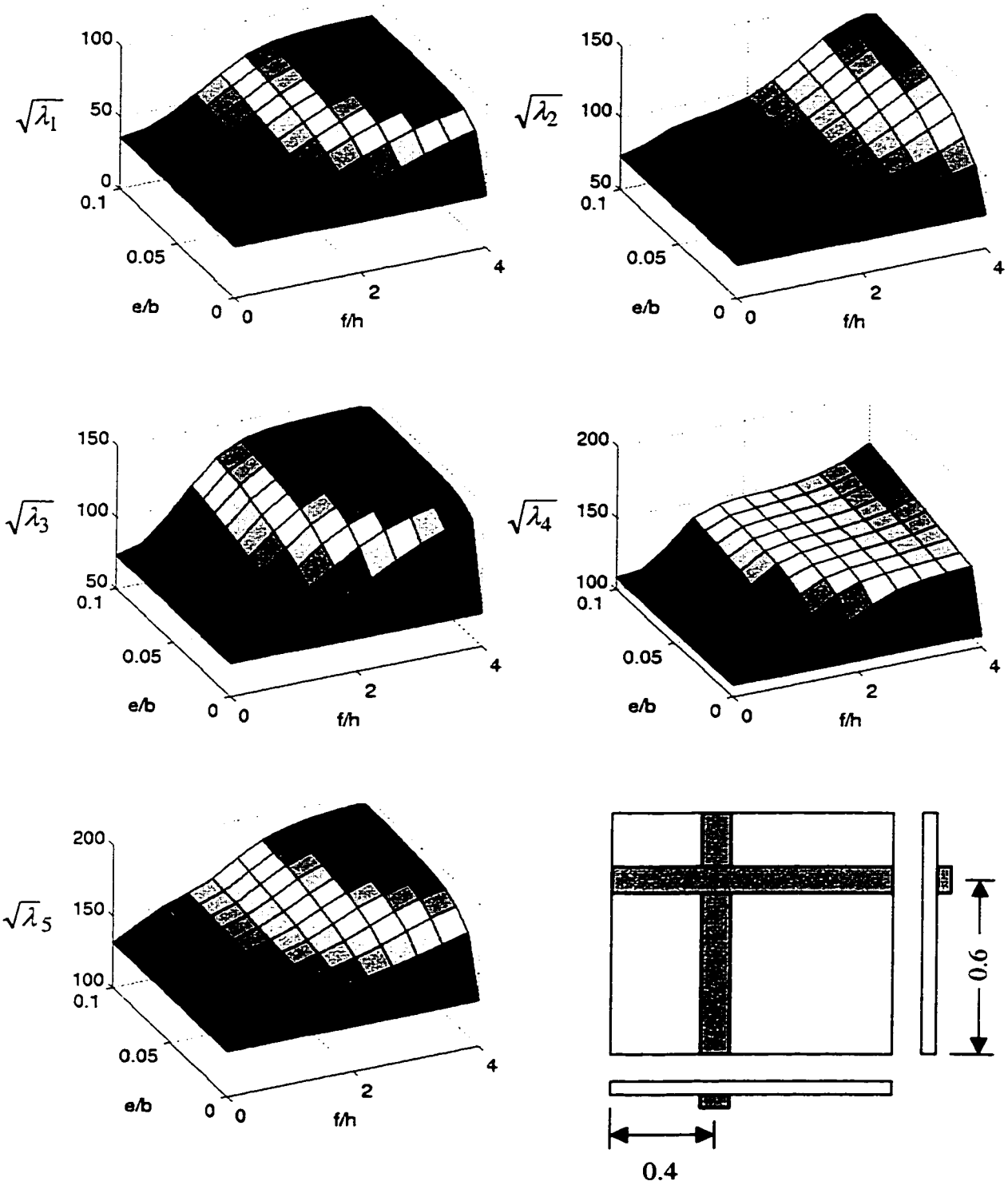

Figure 3.8: Variation of the first five eigenvalues against stiffener geometry

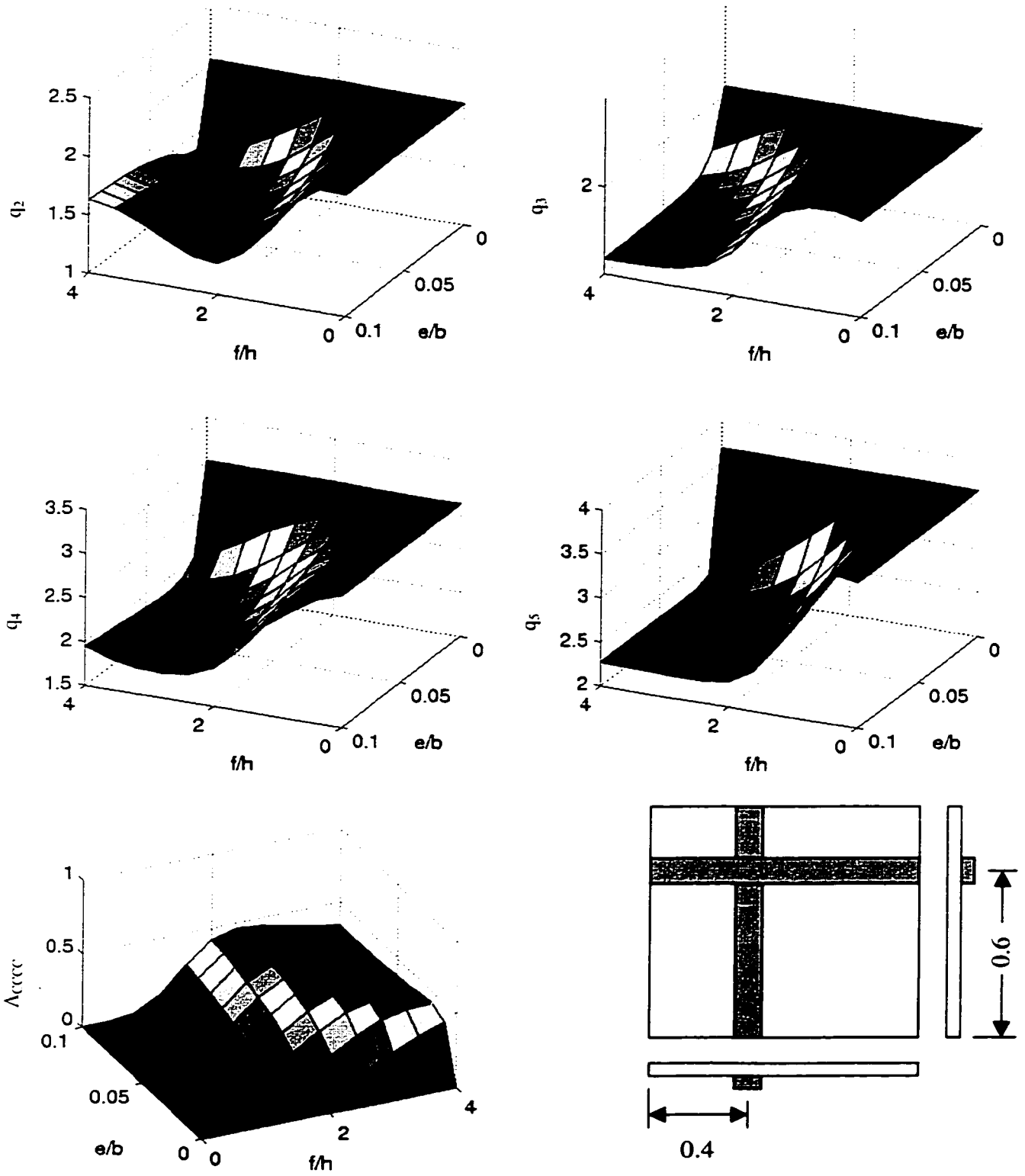

Figure 3.9: Variation of first five eigenratios and objective function Λ_{CCCC} against stiffener geometry

3.2 BOUNDARY CONDITIONING BY SUPPORT CONDITIONS

Boundary conditioning due to the change in the structural configuration has been modeled for the clamped boundary conditions. It is possible to model the other classical boundary conditions such as free and pinned by properly selecting the boundary characteristic polynomials described in Section 3.1.1.1 that satisfy at least the geometrical boundary conditions. In the place of classical boundary conditions such as the clamped, simply supported or free conditions, it will be advantageous if the boundary conditions are modeled by quantifiable attributes. The quantifiable property selected to represent boundary conditioning should also be able to capture the influence of end support conditions, supports anywhere within the structure, effect of the manufacturing process, etc. on elastic properties of the systems in a unified way.

The support conditions may include end supports and supports anywhere within the structure, arising due to clamping, riveted joints, strap joints or any other form of joining methods. The support conditions could be classical ones such as clamped, simply supported and free or non-classical ones that are intermediate between the classical ones. Support conditions strongly influence the vibration behavior of structures and changing the boundary conditions from simply supported to clamped conditions in beams and plates can more than double their respective natural frequencies [102, 103]. The boundary conditions of real structures are not always homogeneous and hence the modeling of real boundary conditions has to accommodate the flexibility of the joints and supports in translation or rotation [99, 100, 206]. The boundary conditions available

along an edge may not be uniform also [163]. The point or line supports that exist within the domain of the structures also change the dynamic behavior [206], and such supports may be considered as providing boundary conditions for the structure, as in the case of periodically supported beams or plates. In a structure made through joining of many sub structures, the vibration behavior is influenced by the method of coupling between the sub structures that affect the flow of vibrational energy in the structure. James and Fahy [86] studied the coupling effect of number of straps between two plates and found the dependencies of transmissibility between the structures. The elastic property of the entire system can be affected by modifying the support conditions between structural and environmental parts of the elastic system and the joint conditions between the sub structures of the systems. The boundary conditioning through varying the support elastic conditions, can be used for the manipulation of the dynamic behavior if the stiffness of the support conditions are quantifiable, suitable for implementation and able to represent both classical and non-classical support conditions. Hence, the supports are represented with artificial springs of translational and rotational types. The stiffness value of these artificial springs can be used to represent different support conditions. In this study, the boundary conditioning is illustrated by changing support conditions through artificial springs for a rectangular type plate structure in the following section. The boundary conditioned plate element can be used to model other complicated plate type structures by assembling them with proper boundary or end support conditions.

3.2.1 Modeling of Boundary Conditioning of a Rectangular Plate Element by Artificial Springs

Consider a rectangular plate shown in Figure 3.10 divided into nine rectangular segments (shown by dotted lines) in order to demonstrate the concept of boundary conditioning. The plate segments are connected together and also to the environment by inter-translational (K_T) and inter-rotational springs (K_R) [208, 209]. K_T is the stiffness value of the translational springs per unit length in N/m^2, and K_R is the rotational stiffness value per unit length in Nm/m-rad.

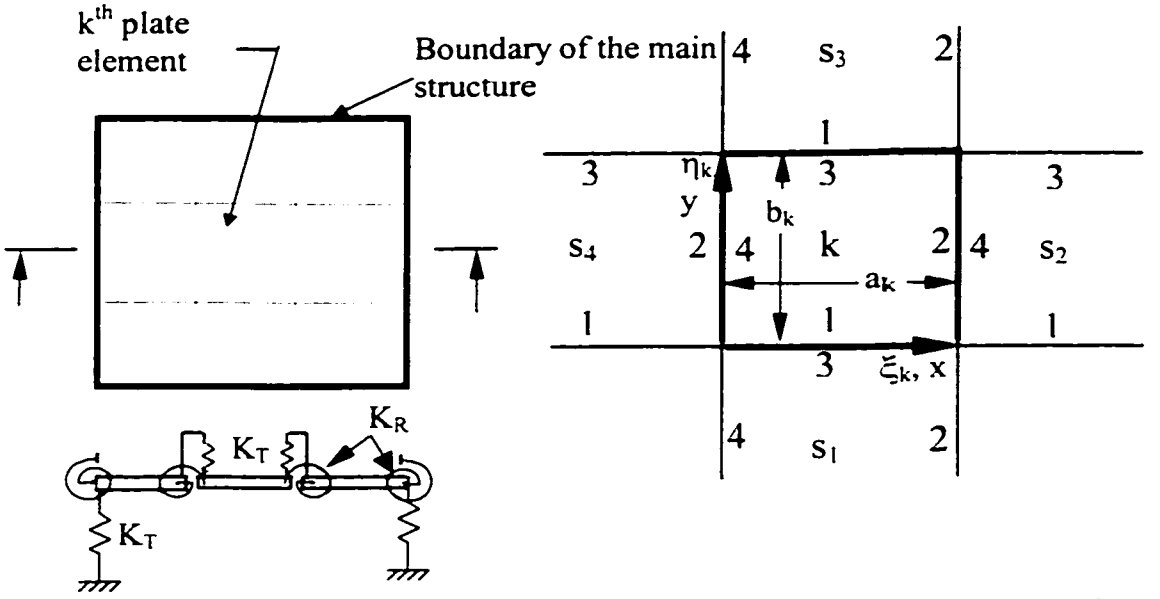

Figure 3.10: Scheme of the plate structure represented by joining many rectangular segments with artificial springs

The boundaries that connect segments of the main structure, are represented by very high values of inter-rotational and inter-translational spring stiffnesses. The plate vibration is analyzed using normal modes obtained using boundary characteristic orthogonal polynomials in the Rayleigh-Ritz method [17,19]. The orthogonal polynomials are generated using Gram-Schmidt process [37] for each segment satisfying free edge conditions on all boundaries of the segments. The first polynomial is given by $\phi_0 = 1$, satisfying the geometrical boundary conditions of the free edges and the remaining polynomials are generated as described in Section 3.1.1.1.

The flexural deflection equation for k[th] segment is defined as

$$W_k(x,y) = \sum_m \sum_n A_{mn.k}\phi_m(x)\varphi_n(y) \tag{3.25}$$

where $x = \frac{\xi_k}{a_k}$, $y = \frac{\eta_k}{b_k}$

ξ_k and η_k are coordinates of k[th] plate

a_k and b_k are dimensions of the k[th] plate with $\alpha_k = \frac{a_k}{b_k}$

$A_{mn.k}$ is the deflection coefficient of the k[th] plate

$\phi_m(x)$ and $\varphi_n(y)$ are orthogonal polynomials generated through Gram-Schmidt process.

The maximum total strain energy U_{max} and the maximum kinetic energy T_{max} of the structure are,

$$U_{\max} = \sum_{k=1}^{N} U_{\max,k} + \sum_{k=1}^{N}\sum_{s=1}^{4} U_{T,k,s} + \sum_{k=1}^{N}\sum_{s=1}^{4} U_{R,k,s} \tag{3.26}$$

and

$$T_{\max} = \sum_{k=1}^{N} \frac{1}{2}\rho_k h_k a_k b_k \omega^2 \int_0^1\int_0^1 W_k^2(x,y)dxdy \tag{3.27}$$

where

$U_{\max,k}$ - strain energy of the k[th] plate

$U_{T,k,s}$ - potential energy of s[th] side translational spring of k[th] plate

$U_{R,k,s}$ - potential energy of s[th] side rotational spring of k[th] plate and

are estimated using the following equations:

$$U_{\max,k} = \frac{D_k a_k b_k}{2a_k^4} \int_0^1\int_0^1 \left[W_{xx,k}^2 + \alpha_k^4\, W_{yy,k}^2 + 2\upsilon\alpha_k^2\, W_{xx,k}W_{yy,k} + 2(1-\upsilon)\alpha_k^2\, W_{xy,k}^2\right]dxdy \tag{3.28}$$

$$U_{T,k,s} = \frac{1}{2} K_{T,k,s} \int_0^{l_s} (\Delta W_s)^2 dl_s \tag{3.29}$$

$$U_{R,k,s} = \frac{1}{2} K_{R,k,s} \int_0^{l_s} (\Delta W_s^1)^2 dl_s \tag{3.30}$$

where

D_k - flexural rigidity of the k[th] plate

l_s - length of the side, s

ΔW_s - difference in deflection along the s[th] side of the k[th] plate

ΔW_s^1 - difference in slope along the s[th] side of the k[th] plate

$W_{k,s}$ - deflection of k[th] plate along side s

ρ_K - mass density of the k[th] plate

h_k - thickness of the k^{th} plate

ω - natural frequency of entire structure

ν - Poisson's ratio

N - total number of segments and

subscripts x,y refer to differentiation with respect to respective coordinates.

Substitution of deflection Equation (3.25) in strain energy and kinetic energy Equations (3.26) and (3.27), and optimization of the Rayleigh quotient with respect to $A_{ij,k}$ result in the following eigenvalue equation:

$$\sum_m \sum_n \left[C_{mnij,k} + C^I_{mnij,k} - \lambda \Pi_k E^{00}_{mi} F^{00}_{nj} \right] A_{mn,k} - \sum_m \sum_n D_{mnij,s} A_{mn,s} = 0 \qquad (3.31)$$

$$\forall \cdot k = 1,2,\ldots,N$$

where

$$C_{mnij,k} = E^{22}_{mi} F^{00}_{nj} + \alpha_k^4 E^{00}_{mi} F^{22}_{nj} + \upsilon \alpha_k^2 \left(E^{02}_{mi} F^{20}_{nj} + E^{20}_{mi} F^{02}_{nj} \right) + 2 \cdot (1-\upsilon) \alpha_k^2 E^{11}_{mi} F^{11}_{nj}$$

$$C^I_{mnij,k} = K^{\bullet}_{T,k,1} \alpha_k E^{00}_{mi} \varphi_n(0) \varphi_j(0) + K^{\bullet}_{T,k,2} \phi_m(1) \phi_i(1) F^{00}_{nj} + K^{\bullet}_{T,k,3} \alpha_k E^{00}_{mi} \varphi_n(1) \varphi_j(1)$$

$$+ K^{\bullet}_{T,k,4} \phi_m(0) \phi_i(0) F^{00}_{nj} + K^{\bullet}_{R,k,1} \alpha_k^3 E^{00}_{mi} \varphi^1_n(0) \varphi^1_j(0) + K^{\bullet}_{R,k,2} \phi^1_m(1) \phi^1_i(1) F^{00}_{nj}$$

$$+ K^{\bullet}_{R,k,3} \alpha_k^3 E^{00}_{mi} \varphi^1_n(1) \varphi^1_j(1) + K^{\bullet}_{R,k,4} \phi^1_m(0) \phi^1_i(0) F^{00}_{nj}$$

$$D_{mnij,s} A_{mn,s} = [K^{\bullet}_{T,k,1} \alpha_k E^{00}_{mi} \varphi_n(1) \varphi_j(0) + K^{\bullet}_{R,k,1} \alpha_k^2 \alpha_{s1} E^{00}_{mi} \varphi^1_n(1) \varphi^1_j(0)] A_{mn,s1} +$$

$$[K^{\bullet}_{T,k,2} \phi_m(0) \phi_i(1) F^{00}_{nj} + K^{\bullet}_{R,k,2} \frac{\alpha_k}{\alpha_{s2}} \phi^1_m(0) \phi^1_i(1) F^{00}_{nj}] A_{mn,s2} +$$

$$[K^{\bullet}_{T,k,3} \alpha_k E^{00}_{mi} \varphi_n(0) \varphi_j(1) + K^{\bullet}_{R,k,3} \alpha_k^2 \alpha_{s3} E^{00}_{mi} \varphi^1_n(0) \varphi^1_j(1)] A_{mn,s3} +$$

$$[K^{\bullet}_{T,k,4} \phi_m(1) \phi_i(0) F^{00}_{nj} + K^{\bullet}_{R,k,4} \frac{\alpha_k}{\alpha_{s4}} \phi^1_m(1) \phi^1_i(0) F^{00}_{nj}] A_{mn,s4}$$

and

$$K^{\bullet}_{T,k,j} = \frac{K_{T,k,j} a_k^3}{D_k}, K^{\bullet}_{R,k,j} = \frac{K_{R,k,j} a_k}{D_k}, \quad \Pi_k = \frac{\rho_{r,k} a_{r,k}^4}{E_{r,k} h_{r,k}^2}, \quad \lambda = \frac{\rho_1 h_1 a_1^4 \omega^2}{D_1},$$

$$E_{mi}^{rs} = \int_0^1 \left(\frac{d^r \phi_m}{dx^r}\right)\left(\frac{d^s \phi_i}{dx^s}\right) \cdot dx, \quad F_{nj}^{rs} = \int_0^1 \left(\frac{d^r \varphi_n}{dy^r}\right)\left(\frac{d^s \varphi_j}{dy^s}\right) \cdot dy, \quad \phi_i^1 = \frac{d\phi_i}{dx}, \quad \varphi_j^1 = \frac{d\varphi_j}{dy}$$

Subscript (r,k) refers to ratio of parameter of k^{th} segment to that of first segment.

The solution of Equation (3.31) yields both eigenvalues and mode shapes of the system. Segments that have edge on the boundary of the main structure on 's' side have, $A_{mn,s} = 0$. Required edge conditions for any segment can be generated by suitable choice of the values of K_T and K_R. The accuracy of the results are dependent on the number of orthogonal polynomials considered, number of segments, and the stiffness value of artificial springs. Hence a parametric study of the results will be useful in determining optimum parameters.

3.2.2 Parametric Study on Analysis Using Artificial Springs

In order to identify the stiffness values of the artificial springs, the number of polynomials and the number of segments required to represent the classical boundary conditions such as clamped, pinned and free for a plate structure, a parametric study on the eigenvalues was carried out and the results are given in Tables 3.7-3.9. The Figure 3.11 shows the numbering scheme used to represent boundary conditions. For example, CSCS

correspond to clamped conditions on sides 1 and 3 while simple supported condition on sides 2 and 4.

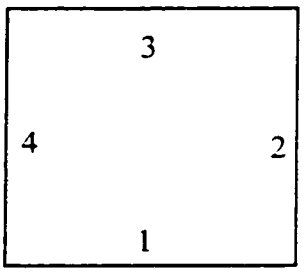

Figure 3.11 Numbering scheme of boundary conditions

3.2.2.1 Plate modeled by one segment

The eigenvalues were predicted for a plate represented with one segment. The stiffness values of the springs on four sides of the plate and number of polynomials were varied in order to find the optimum values and the results are given in the Table 3.7. The predicted values are compared with those obtained by the *direct method* where the classical boundary conditions are incorporated in the boundary characteristic orthogonal polynomials that were generated so as to satisfy the geometrical boundary conditions as explained in Bhat, 1985 [17]. The results from the *direct method* corresponds to the number of polynomials m,n=6.

Table 3.7: Effect of number of polynomials and stiffnesses for different classical conditions: Model with one segment

	m,n	$K_T^*=K_R^*$	$\sqrt{\lambda_1}$	$\sqrt{\lambda_2}$	$\sqrt{\lambda_3}$	$\sqrt{\lambda_4}$	$\sqrt{\lambda_5}$	$\sqrt{\lambda_6}$
CCCC	Analytical		35.988	73.406	73.406	108.250	131.620	132.230
$K_{T,i}^* = K_T^*$	Direct Method		35.988	73.395	73.395	108.218	131.779	132.410
$\forall i = 1,2,3,4$	6	$1x10^2$	17.388	25.268	25.268	33.873	47.892	48.551
		$1x10^3$	30.869	54.702	54.702	72.643	91.330	95.742
$K_{R,i}^* = K_R^*$		$1x10^4$	35.348	71.542	71.542	102.385	261.082*	263.538*
$\forall i = 1,2,3,4$		$1x10^5$	35.933	74.011	74.011	107.928	816.282*	817.101*
		$1x10^6$	35.933	74.268	74.268	108.524	2578.34*	2578.60*
		$1x10^8$	35.999	74.296	74.296	108.590	25780.1*	25780.1*
		$1x10^{10}$	36.000	74.296	74.296	108.590	257801*	257801*
	8	$1x10^8$	35.985	73.420	73.420	108.257	137.293	138.069
		$1x10^{10}$	35.990	73.421	73.421	108.256	137.303	138.061
	9	$1x10^6$	35.979	73.385	73.385	108.192	131.696	132.331
		$1x10^8$	35.985	73.412	73.412	108.257	131.778	132.409
		$1x10^{10}$	35.985	73.413	73.415	108.257	131.780	132.410
	10	$1x10^8$	35.985	73.394	73.394	108.217	131.778	132.409
		$1x10^{10}$	35.981	73.395	73.397	108.220	131.777	132.409
SSSS	Analytical		19.739	49.348	49.348	78.957	98.696	98.696
$K_{T,i}^* = K_T^*$	Direct Method		19.739	49.348	49.348	78.957	99.304	99.304
$\forall i = 1,2,3,4$	7	$1x10^6$	19.736	49.480	49.480	79.136	100.080	100.080
		$1x10^8$	19.739	49.491	49.491	79.166	100.116	100.116
$K_{R,i}^* = 0$		$1x10^{10}$	19.739	49.491	49.491	79.167	100.117	100.117
$\forall i = 1,2,3,4$	8	$1x10^6$	19.736	49.337	49.337	78.924	100.080	100.080
		$1x10^8$	19.739	49.349	49.349	78.957	100.116	100.116
	9	$1x10^6$	19.734	49.337	49.337	78.924	98.680	98.691
		$1x10^8$	19.739	49.348	49.348	78.957	98.716	98.716
		$1x10^{10}$	19.739	49.349	49.349	78.958	98.716	98.716
	10	$1x10^6$	19.734	49.335	49.335	78.919	98.680	98.680
		$1x10^8$	19.739	49.348	49.348	78.956	98.716	98.716
		$1x10^{10}$	19.739	49.348	49.348	78.957	98.716	98.716
		$1x10^{12}$	19.739	49.348	49.348	78.957	98.716	98.716

* The values are high due to numerical problems associated with high stiffness values and fewer number of polynomials. These values became close to clamped condition when the number of polynomials is increased.

	m,n	K_T^*	$\sqrt{\lambda_1}$	$\sqrt{\lambda_2}$	$\sqrt{\lambda_3}$	$\sqrt{\lambda_4}$	$\sqrt{\lambda_5}$	$\sqrt{\lambda_6}$
CSSC	Analytical							
$K_{T,i}^* = K_T^*$ $\forall i = 1,2,3,4$ $K_{R,i}^* = K_T^*$ $\forall i = 1,4$ $K_{R,i}^* = 0$ $\forall i = 2,3$	Direct Method		27.054	60.539	60.787	92.837	114.846	114.846
	9	$1x10^8$	27.054	60.542	60.790	92.844	114.694	114.843
		$1x10^{10}$	27.054	60.541	60.790	92.843	114.694	114.843
	10	$1x10^8$	27.054	60.538	60.786	92.836	114.615	114.764
		$1x10^{10}$	27.054	60.542	60.789	92.837	114.612	114.762
SCCS	Analytical							
$K_{T,i}^* = K_T^*$ $\forall i = 1,2,3,4$ $K_{R,i}^* = K_T^*$ $\forall i = 2,3$ $K_{R,i}^* = 0$ $\forall i = 1,4$	Direct Method		27.054	60.539	60.787	92.837	114.846	114.846
	9	$1x10^8$	27.054	60.542	60.790	92.844	114.694	114.843
		$1x10^{10}$	27.055	60.541	60.790	92.844	114.694	114.844
	10	$1x10^8$	27.054	60.538	60.786	92.836	114.615	114.764
		$1x10^{10}$	27.053	60.542	60.789	92.837	114.612	114.762
CFFC	Analytical							
$K_{T,i}^* = K_{R,i}^* = K_T^*$ $\forall i = 1,4$ $K_{T,i}^* = K_{R,i}^* = 0$ $\forall i = 2,3$	Direct Method		27.054	60.539	60.787	92.837	114.846	114.846
	9	$1x10^8$	27.054	60.542	60.790	92.844	114.694	114.843
		$1x10^{10}$	27.055	60.541	60.790	92.844	114.694	114.844
	10	$1x10^8$	27.054	60.538	60.786	92.836	114.615	114.764
		$1x10^{10}$	27.053	60.542	60.789	92.837	114.612	114.762
SFFS	Analytical							
$K_{T,i}^* = K_T^*$ $\forall i = 1,4$ $K_{T,i}^* = 0$ $\forall i = 2,3$ $K_{R,i}^* = 0$ $\forall i = 1,2,3,4$	Direct Method		27.054	60.539	60.787	92.837	114.846	114.846
	9	$1x10^8$	27.054	60.542	60.790	92.844	114.694	114.843
		$1x10^{10}$	27.055	60.541	60.790	92.844	114.694	114.844
	10	$1x10^8$	27.054	60.538	60.786	92.836	114.615	114.764
		$1x10^{10}$	27.053	60.542	60.789	92.837	114.612	114.762

It can be seen from the results of a plate with single segment that the increase in the number of polynomials and stiffness values result in natural frequencies that are close to classical conditions. Higher number of polynomials is required for clamped condition when compared to simply supported condition. For single segment, the number of

polynomials $m, n \geq 9$ and a stiffness value of $K_T^* \geq 1x10^9$ can yield results that are close to that of classical conditions.

3.2.2.2 Plate modeled by many segments

The consolidated results of the effect of number of segments and stiffness values on the first six eigenvalues are given in Table 3.8. RxC segments in the table indicates that the plate is modeled by segments formed by R number of rows and C number of columns.

Table 3.8: Minimum number of polynomials required for SSSS condition: Model with RxC segments with $K_T^* = 10^8$ at the boundaries

		$\sqrt{\lambda_1}$	$\sqrt{\lambda_2}$	$\sqrt{\lambda_3}$	$\sqrt{\lambda_4}$	$\sqrt{\lambda_5}$	$\sqrt{\lambda_6}$
Analytical		19.739	49.348	49.348	78.957	98.696	98.696
Direct		19.739	49.348	49.348	78.957	99.304	99.304
RxC	m,n						
1x1	10	19.739	49.348	49.348	78.956	98.716	98.716
2x2	8	19.739	49.348	49.348	78.956	98.696	98.696
3x3	7	19.739	49.348	49.348	78.956	98.695	98.695
4x4	6	19.739	49.348	49.348	78.956	98.697	98.697

The above table validates the use of many segments to represent the plate structure. It has been seen that larger number of polynomials are required if the plate is modeled with only one segment since each polynomial needs to satisfy the deflection equation throughout the plate domain. Instead, it can be noticed from the Table 3.8 that if the plate is modeled with many segments, the number of polynomials required will be reduced. Thus, it is

possible to model a plate with cut outs, slots, slits, partial supports etc. In the following section, modeling is applied to a plate with cutouts.

3.2.2.3 Plate with a cutout of 0.333x0.333

The predicted values of eigenvalues for a plate with a cutout as shown in Figure 3.12 are given in the Table 3.9. The plate is simply supported at all the four edges. The stiffness value is kept at $K^* = \frac{K_{T,}a^3}{D} = \frac{K_{R,}a}{D} = 1x10^8$. The rotational stiffness at the boundaries are kept at zero.

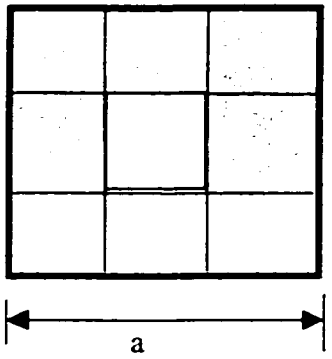

Figure 3.12: Model of a plate with cutout using 8 segments

Table 3.9: Eigenvalues for a plate with cutout, SSSS boundary conditions and $K_T^* = 10^8$ at the boundaries

m,n	$\sqrt{\lambda_1}$	$\sqrt{\lambda_2}$	$\sqrt{\lambda_3}$	$\sqrt{\lambda_4}$	$\sqrt{\lambda_5}$	$\sqrt{\lambda_6}$
6	19.780	43.285	43.285	72.911	89.813	121.749
7	19.768	43.190	43.190	72.874	89.292	121.440
8	19.763	43.103	43.103	72.848	89.280	121.431

3.2.2.4 Fully clamped plate with a cutout of 0.5x0.5

The predicted eigenvalues for a fully clamped plate (CCCC) with cutout as shown in Figure 3.13 are given in the Table 3.10. The stiffnesses are kept at $K^* = \frac{K_T a^3}{D} = \frac{K_R a}{D} = 1x10^8$. The predicted values are compared with the results of Patel [134] and FEM package ANSYS. In Patel [134], boundary characteristic orthogonal polynomials are generated in order to satisfy the classical boundary conditions. The comparison shows a good agreement with ANSYS results and that of Patel [134].

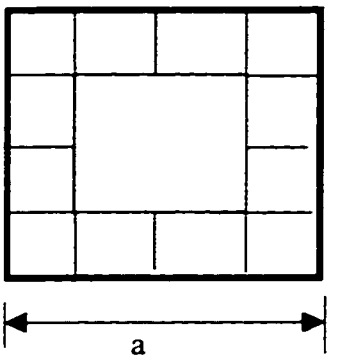

Figure 3.13: Model of a plate with cutout using 12 segments

Table 3.10: Eigenvalues for a plate with cutout, CCCC boundary conditions and $K^* = 10^8$ at the boundaries

m,n	$\sqrt{\lambda_1}$	$\sqrt{\lambda_2}$	$\sqrt{\lambda_3}$	$\sqrt{\lambda_4}$	$\sqrt{\lambda_5}$	$\sqrt{\lambda_6}$
Patel [134], *Direct method*	65.715	81.680	81.680	110.857	135.879	166.360
ANSYS	65.003	75.622	75.622	101.225	105.731	143.223
6	65.384	76.503	76.503	103.621	106.685	145.402
7	65.378	76.424	76.424	103.251	106.641	145.109
8	65.372	76.369	76.371	103.010	106.614	144.926
9	65.370	76.339	76.340	102.874	106.600	144.824

Thus the above parametric study validates the modeling of support conditions through artificial springs and shows that classical conditions such as clamped, simply supported and free conditions can be modeled with proper stiffness values of the springs. Clamped conditions correspond to very high translational and rotational stiffnesses and simply supported conditions correspond to very high translational stiffness and zero rotational stiffness, while both rotational and translational stiffnesses are zero for free condition. Any condition intermediate to the classical ones can also be modeled with stiffness values that are in between the above extremes. This study validates the use of artificial stiffnesses as a measure to quantify the boundary or support conditions. Thus, the manipulation of dynamic behavior of the elastic systems by boundary conditioning is possible by modifying the support conditions and the same can be quantified through artificial springs. Structural tuning is an example of boundary conditioning through support conditions, in which structural dynamic behavior is altered by tuning the boundary conditions, as will be discussed in the following section.

3.3 APPLICATION OF BOUNDARY CONDITIONING FOR STRUCTURAL TUNING

The dynamic performance of linear elastic systems, whether it is macro or micro, is dependent upon its natural frequencies, and the mode shapes. The relative positioning of eigen frequencies has potential for the manipulation of dynamic behavior. Such manipulation includes appropriate design of the structures in order to get the required dynamic performance or required vibration response. This involves staggering the natural frequencies in a required fashion, which could be in relation to the excitation frequencies [118] or as per the design requirement. It is also possible to control the radiated sound pressure by modifying the acoustic coupling coefficients through the change in mode shapes [117, 120]. Structural tuning has many applications such as noise control in aircraft fuselage using passive control. An interesting non-engineering application is in the tuning of musical instruments.

In the case of aircraft subjected to excitations from the rotating machinery, the disturbances are multiple tones in nature [26, 58, 92]. Hence, whenever excitation is of single or multiple tones, the relative location of eigenfrequencies of the structure as shown in Figure 3.14 is important in order to manipulate the vibration behavior [118].

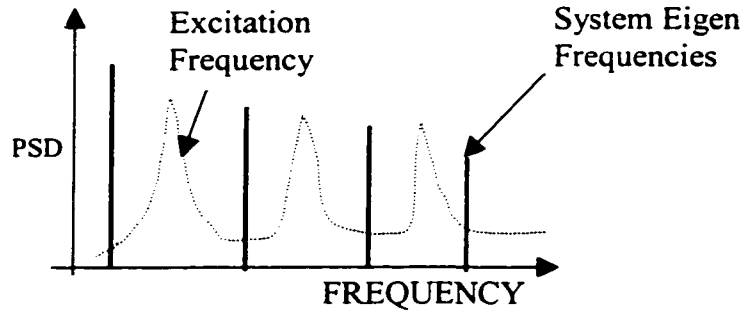

Figure 3.14: Scheme for structural tuning

Minimization of vibration response is possible by staggering the eigenfrequencies of the system away from the excitation frequencies. Sometimes, the response of the main structure can be minimized by maximization of the response of semi-active vibration absorbers [64] by moving the eigenfrequencies of the absorbers close to excitation frequencies. If the excitation frequencies are known and nearly fixed, structure can be designed in such a way that the natural frequencies are staggered farther away from the excitation frequencies. Whenever the excitation frequencies or the required pattern of frequencies changes, the natural frequencies of the system have also to be adaptively changed as in the case of semi-active type of control.

Higher natural frequencies are also important in determining the performance of some microsystems. For a surface micromachined microgyroscope [6], the performance is dependent on the three natural frequencies as shown in Figure 3.15. The arrangement of these natural frequencies can be modified by changing the structural geometry, structural support conditions and capacitive bias voltage. The modification of the arrangement of natural frequencies for gyroscopes through bias voltage or support conditions is also an example of boundary conditioning.

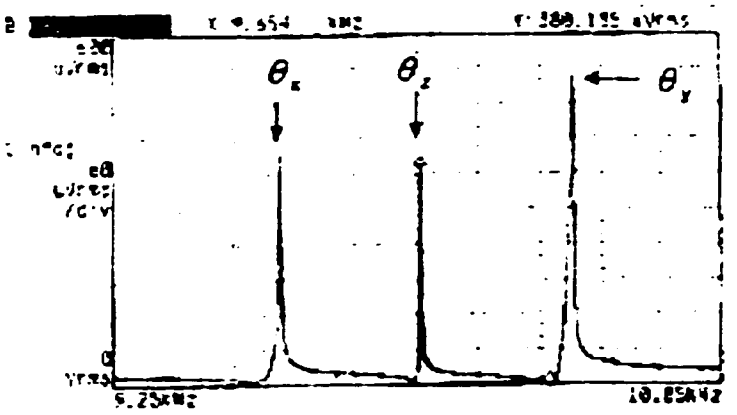

Figure 3.15: Eigenfrequencies of a microgyroscope.
Adapted from An et al. [6]

During the tuning of a musical instrument the pattern of natural frequencies is varied in order to obtain the required harmonic combinations of eigenfrequencies by changing the support condition of the vibrating structure. The arrangement of the natural frequencies in a certain order adds a rich quality to the sound of musical instruments.

The staggering of natural frequencies finds applications in semi-active control of vibration behavior, design of structures with required pattern of eigenfrequencies or tuning of a musical instrument. This process of staggering the natural frequencies in a required order, which could be in relation to excitation frequencies in order to minimize or maximize the response or simply to generate musical harmonics or required pattern of natural frequencies, is possible through the modification of structural elastic property and is called structural tuning [118]. Thus, the understanding of the influence of structural tuning on natural frequencies becomes very important for further implementation of this technique. The modeling of structural tuning is carried out by the application of boundary conditioning through the modification of support conditions and is presented in

this section. The modeling of structural tuning is explained using a simple plate structure even though this technique can be extended to any complicated structures.

In structures which are supported at several points or lines within their domain such as in periodically supported beams or plates, such supports may be considered as providing boundary conditions for the structure. Addition of supports [206] also changes the vibration behavior and hence the designer has a lot of flexibility in positioning the supports in a structure in order to obtain specific natural frequencies for the structure. Such control of the frequency characteristics of a structure has many applications in the control of the noise transmission properties of structures such as in aircraft fuselages [58, 64, 92]. The support conditions can be created by clamping, riveting etc. In the present study, the concept of boundary conditioning is investigated on a plate type structure, supported on four translational and rotational type springs distributed along the four edges.

3.3.1 Modeling of Structural Tuning

Consider a rectangular plate as shown in Figure 3.16. The plate is assumed to be supported at all the four edges with both translational and rotational springs [208] with stiffness per unit length of K_T and K_R, respectively.

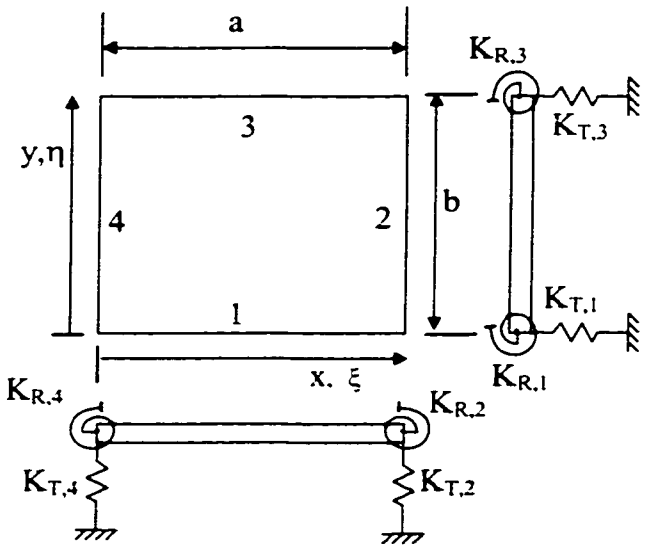

Figure 3.16 Structural scheme for boundary conditioning

The plate eigenvalues are estimated using boundary characteristic orthogonal polynomials in the Rayleigh-Ritz method [17]. These orthogonal polynomials are generated so as to satisfy the free edge conditions on all its boundaries.

The flexural deflection of the plate with one segment becomes

$$W(x,y) = \sum_m \sum_n A_{mn} \phi_m(x) \varphi_n(y) \tag{3.32}$$

where $x = \frac{\xi}{a}$, $y = \frac{\eta}{b}$

ξ and η are coordinates of the plate,

a and b are dimensions of the plate with $\alpha = \frac{a}{b}$,

A_{mn} is the deflection coefficient of each term describing the plate deflection in Equation (3.32) and $\phi_m(x)$ and $\varphi_n(y)$ are boundary characteristic orthogonal polynomials.

Hence, the maximum total strain energy U_{max} and the maximum kinetic energy T_{max} of the structure with one segment become,

$$U_{max} = U_{max.p} + \sum_{s=1}^{4} U_{T.s} + \sum_{s=1}^{4} U_{R.s} \qquad \text{and} \tag{3.33}$$

$$T_{max} = \frac{1}{2}\rho\, h\, a\, b\, \omega^2 \int_0^1 \int_0^1 W^2(x,y)dxdy \tag{3.34}$$

where

$$U_{max.p} = \frac{D\, a\, b}{2a^4} \int_0^1 \int_0^1 \left[W''^2 + \alpha^4\, \ddot{W}^2 + 2\upsilon \cdot \alpha^2 \cdot W''\ddot{W} + 2(1-\upsilon)\alpha^2\, \dot{W}'^2 \right] dxdy \tag{3.35}$$

$$U_{T.s} = \frac{1}{2} K_{T.s} \int_0^{l_s} W_s^2 dl_s \tag{3.36}$$

$$U_{R.s} = \frac{1}{2} K_{R.s} \int_0^{l_s} W_s'^2 dl_s \tag{3.37}$$

Substitution of deflection Equation (3.32) in strain energy and kinetic energy expressions (3.33) and (3.34), and optimization of Rayleigh quotient with respect to A_{ij} result in the following eigenvalue equation:

$$\sum_m \sum_n \left[C_{mnij} + C^I_{mnij} - \lambda \cdot E^{00}_{mi} F^{00}_{nj} \right] A_{mn} = 0 \tag{3.38}$$

where

$$C_{mnij} = E^{22}_{mi} F^{00}_{nj} + \alpha^4 E^{00}_{mi} F^{22}_{nj} + \upsilon \cdot \alpha^2 \left(E^{02}_{mi} F^{20}_{nj} + E^{20}_{mi} F^{02}_{nj} \right) + 2 \cdot (1-\upsilon)\alpha^2 E^{11}_{mi} F^{11}_{nj}$$

$$C^I_{mnij} = K^*_{T.1}\alpha\, E^{00}_{mi}\varphi_n(0)\varphi_j(0) + K^*_{T.2}\phi_m(1)\phi_i(1)F^{00}_{nj} + K^*_{T.3}\alpha\, E^{00}_{mi}\varphi_n(1)\varphi_j(1) +$$

$$K^*_{T.4}\phi_m(0)\phi_i(0)F^{00}_{nj} + K^*_{R.1}\alpha^3 E^{00}_{mi}\varphi^1_n(0)\varphi^1_j(0) + K^*_{R.2}\phi^1_m(1)\phi^1_i(1)F^{00}_{nj} +$$

$$K^*_{R.3}\alpha^3 E^{00}_{mi}\varphi^1_n(1)\varphi^1_j(1) + K^*_{R.4}\phi^1_m(0)\phi^1_i(0)F^{00}_{nj}$$

and

$$E_{mi}^{rs} = \int_0^1 \left(\frac{d^r \phi_m}{dx^r}\right)\left(\frac{d^s \phi_i}{dx^s}\right) \cdot dx,\ F_{nj}^{rs} = \int_0^1 \left(\frac{d^r \varphi_n}{dy^r}\right)\left(\frac{d^s \varphi_j}{dy^s}\right) \cdot dy,\ \phi_i^1 = \frac{d\phi_i}{dx}, \varphi_j^1 = \frac{d\varphi_j}{dy}$$

The solution of Equation (3.38) yields both eigenvalues and mode shapes of the system. The different boundary conditions can be represented by different values of K_T and K_R. The eigenvalues of the system depends upon both translational and rotational stiffnesses at the boundaries for a given plate. The conditioning of the boundary by altering both the rotational stiffness and translational stiffness affects the flow of distribution of vibrational energy in the structure and hence the eigenvalues and natural frequencies.

The condition of $K_{T,i}^* = 0$ and $K_{R,i}^* = 0$ corresponds to free edge condition, $K_{R,i}^* = 0$ and very high values of $K_{T,i}^*$ corresponds to simply supported condition while very high values of both $K_{T,i}^*$ and $K_{R,i}^*$ corresponds to clamped condition. The tuning of a structure by boundary conditioning thus means ensuring proper distribution of stiffness on the boundary such that the structure exhibits prescribed patterns of natural frequencies. In engineering applications, the natural frequencies may need to be prescribed in order to be away from exciting frequencies. In order to illustrate the use of the boundary-conditioning concept to manipulate the natural frequencies, the prescribed natural frequencies pattern is chosen as a harmonic combination of natural frequencies in this study. The possible harmonic combinations for a square plate through boundary conditioning are found out by solving the Equation (3.38) for eigenfrequencies at different discrete values of four rotational stiffnesses ($K_{R,i}^*$ where i=1,2,3,4) and four

translational stiffnesses ($K^{*}_{T,i}$ where i=1,2,3,4) placed at the edges. It is found that the range of rotational stiffness between 0 and 10^3 and translational stiffness between 0 and 10^5 only have significant effect on the vibration behavior of the plate and hence the boundary conditioning is demonstrated in these ranges of stiffenesses.

The harmonic combination is represented by '*h=1ijk*' where i,j,k are integers and are the ratios of the first three dominating eigenfrequencies with respect to the fundamental eigenfrequency. It was felt that requiring i, j and k to be 2,3 and 4, respectively, would be too stringent a requirement for compliance. Hence, in the present study, i, j and k were considered to be an acceptable combination if they fall close to any integers. In an actual engineering structure these ratios could be prescribed real numbers indicating the desired natural frequency patterns.

At each boundary condition defined by different values of boundary stiffnesses, the closest available harmonic combination of '*h=1ijk*' is the one which gives minimum error function (Λ_h), given by

$$\Lambda_h = \sum_{n=2}^{N_f} Min\left[\left(\frac{\sqrt{\lambda_n} - q\sqrt{\lambda_1}}{q\sqrt{\lambda_1}}\right)^2 \forall q = i, j, k\right] \tag{3.39}$$

where

N_f - number of eigenfrequencies considered in the combination= 4

$\sqrt{\lambda_n}$ - n^{th} eigenvalue

In this study, the integers i,j and k that could give a minimum value for Λ_h were checked upto a value of 25.

The value of Λ_h indicates the relative closeness of the arrangement of eigenfrequencies to a harmonic combination of '$h=1ijk$'. A value of Λ_h closer to zero shows the availability of perfect harmonic combination of h. In the present investigation, a value of 0.02 for Λ_h, is considered accurate enough to consider the natural frequencies as a harmonic combination. Thus, it becomes possible to manipulate the natural frequencies into a required harmonic combination by minimizing Λ_h through boundary conditioning as explained in the next section.

3.3.2 Results and Discussion

In order to illustrate the boundary conditioning technique, the boundary stiffness distribution of a square plate is arranged in such a way as to have harmonic relation among the plate natural frequencies. Denoting the harmonic order of the natural frequencies with respect to the fundamental natural frequency by their corresponding numbers, the different sets of harmonic combination obtained for a square plate by boundary conditioning of the four edges are 1234, 1235, 1236, 1346, 1356, 1357, 1358 and 1368 for $\Lambda_h \leq 0.02$. A value of $\Lambda_h \leq 0.02$, which is considered to indicate the presence of a harmonic combination, is possible to be obtained over a range of boundary conditions. But the optimum or reference boundary condition for a set of harmonic combination results in the least value of Λ_h, ideally close to zero. The increase of

Λ_h from 0.02 as boundary conditions (stiffnesses) are changed, indicates either the destruction of the present harmonic combination or the presence of other harmonic combinations.

The following results present the effect of boundary conditioning on achieving a particular set of harmonic combination. The results are presented for a few combinations of harmonics taken four at a time. In order to study the effect of boundary conditioning on the objective function of a particular combination of harmonics, a relative stiffness parameter is defined with respect to the boundary stiffness values corresponding to the optimum conditioning called reference values, as follows:

$$\sigma_h = \sqrt{\frac{\left[\sum_{i=1}^{4}\left(K^{\bullet}_{T.i} - K^{\bullet}_{T.i.ref}\right)^2 + \sum_{i=1}^{4}\left(K^{\bullet}_{R.i} - K^{\bullet}_{R.i.ref}\right)^2\right]}{\sum_{i=1}^{4} K^{\bullet}_{T.i.ref}{}^2 + \sum_{i=1}^{4} K^{\bullet}_{R.i.ref}{}^2}} \qquad (3.40)$$

where

$K^{\bullet}_{..ref}$ - reference value corresponding to optimum boundary conditioning

The reference stiffness values for three sets of combination of harmonics corresponding to the minimum objective function Λ_{1ijk} for a given combination of harmonics $h=1ijk$ in order to demonstrate the effect of boundary conditioning, are given in Table 3.11. A value of 10^5 in the table indicates an infinitely stiff condition.

Table 3.11 Reference stiffness values for optimum conditioning

	Reference values							
Harmonics	$K^{\bullet}_{T,1,ref}$	$K^{\bullet}_{T,2,ref}$	$K^{\bullet}_{T,3,ref}$	$K^{\bullet}_{T,4,ref}$	$K^{\bullet}_{R,1,ref}$	$K^{\bullet}_{R,2,ref}$	$K^{\bullet}_{R,3,ref}$	$K^{\bullet}_{R,4,ref}$
1234	10^5	10	10^5	10^3	0	10	10	0
1236	10	10	10	10	10	10	10^2	10^2
1357	10	10	10^3	10^3	10	10	0	0

At the optimum boundary stiffness distribution, it can be seen that the relative stiffness parameter σ_h is equal to 0. The effect of changing the individual boundary stiffness values on the natural frequencies are presented in Figures 3.17 to 3.25. In these figures, the parameter Λ_{1ijk} showing the deviation from the desired harmonic combination is plotted against the relative stiffness parameter σ_h, which is affected by changing individual boundary stiffness values. In all these figures, while the boundary stiffness value under study is varied from 0 to the optimum value and beyond, the other stiffnesses are held at their optimum values. In all the figures, the solid arrows indicate the direction of relative stiffening of the boundary with respect to the optimum, while the broken arrows indicate a relative weakening of the boundary.

3.3.2.1 Harmonic combination 1234

The variation of error function corresponding to 1234 harmonics (Λ_{1234}) in relation to relative boundary stiffness parameter σ_h are given in Figures 3.17 to 3.25.

3.3.2.1.1 Effect of translational stiffness

The influence of translational stiffnesses on sides 1 and 3 are shown in Figure 3.17. When $K_{T,1}$ is varied from 0 to 10^5, the deviation parameter Λ_{1234} reduces from 1.86 towards zero. When $\sigma_h = 0$, all the stiffnesses including $K_{T,1}$ are at their reference values. The behavior is identical when $K_{T,3}$ is varied from 0 to 10^5 while keeping the other stiffness values at the optimum. The influence of translational stiffnesses on sides 2 and 4 are shown in Figure 3.18. The relative weakening of $K_{T,2}$ from the optimum stiffness value of 10 has insignificant effect on the quality of harmonic combination 1234, and a similar trend is seen for relative strengthening of $K_{T,4}$. A relative weakening of $K_{T,4}$ from the optimum value of 10^3 destroys the harmonic combination 1234 as shown in Figure 3.18. A relative strengthening of $K_{T,2}$ also destroys the harmonic combination.

3.3.2.1.2 Effect of rotational stiffness

The effect of varying the rotational stiffnesses on sides 1 and 3 are shown in Figure 3.19. The relative stiffening of $K_{R,1}$ from the reference value of zero aggravates the harmonics while the relative stiffening of $K_{R,3}$ is ineffective. The relative weakening of $K_{R,3}$ from

the reference value affects the harmonics drastically. But Figure 3.20 indicates that this harmonic combination is insensitive to relative changes in stiffnesses $K_{R,2}$ and $K_{R,4}$.

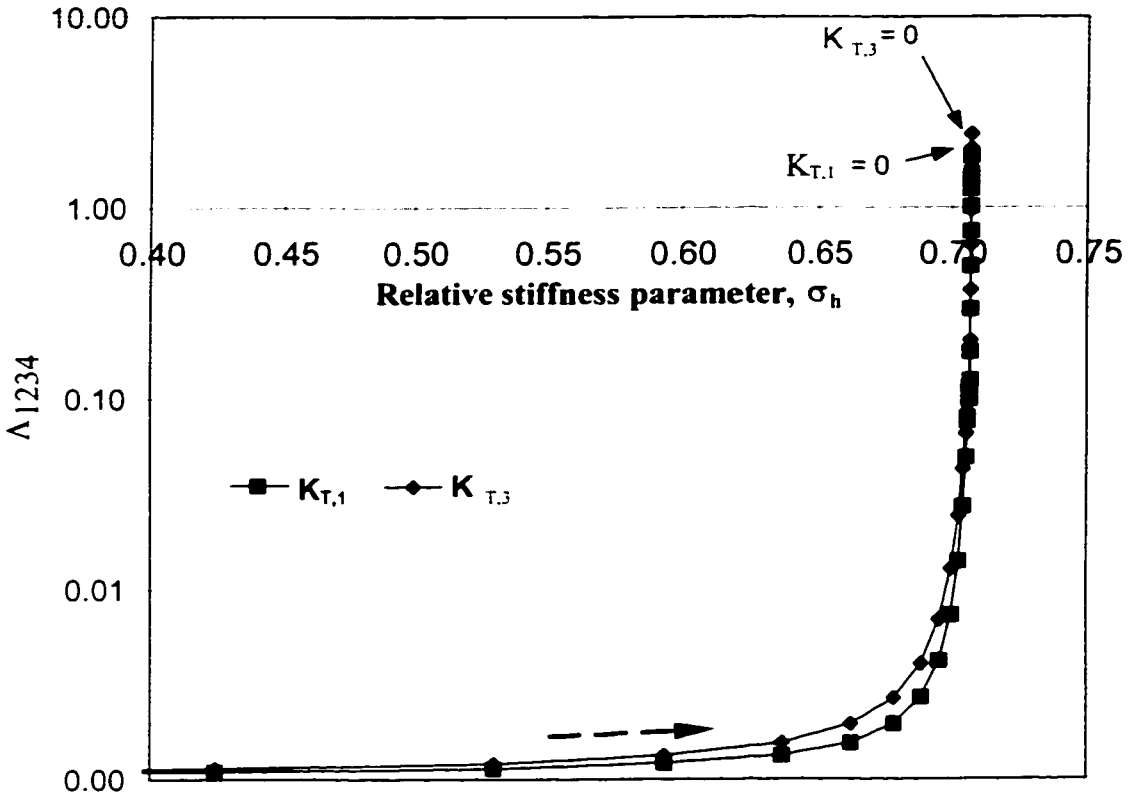

Figure 3.17 Effect of $K_{T,1}$ and $K_{T,2}$ on Λ_{1234}.

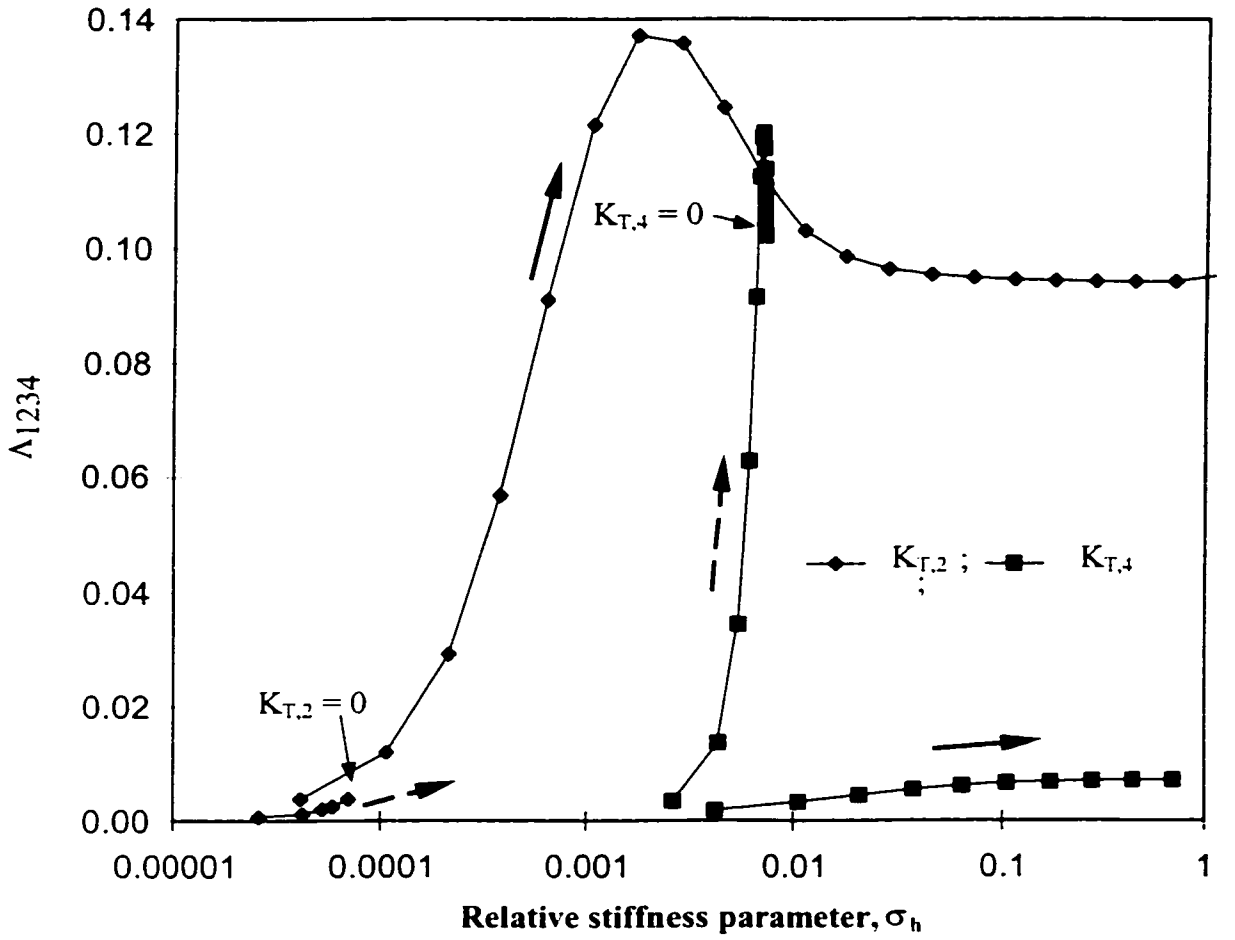

Figure 3.18 Effect of $K_{T,2}$ and $K_{T,4}$ on Λ_{1234}

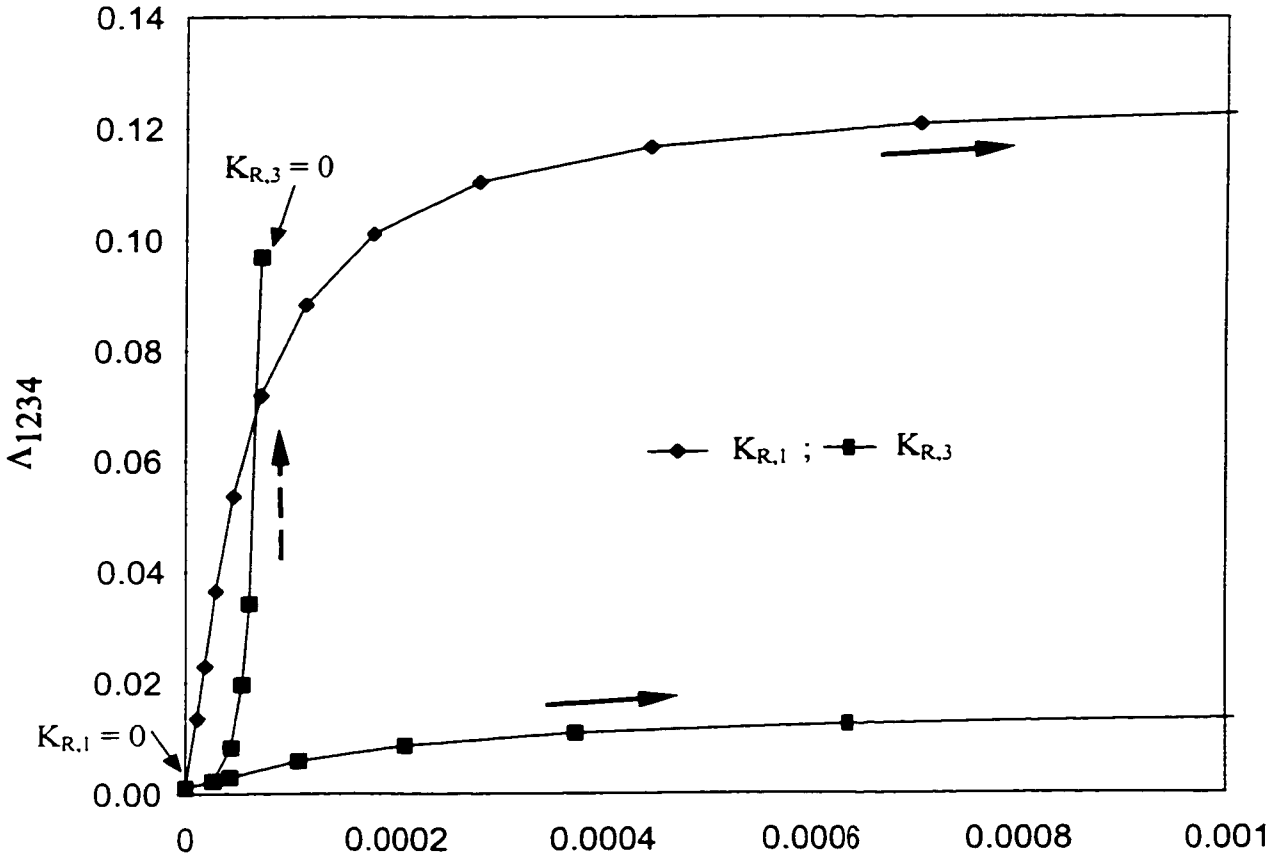

Figure 3.19 Effect of $K_{R,1}$ and $K_{R,3}$ on Λ_{1234}

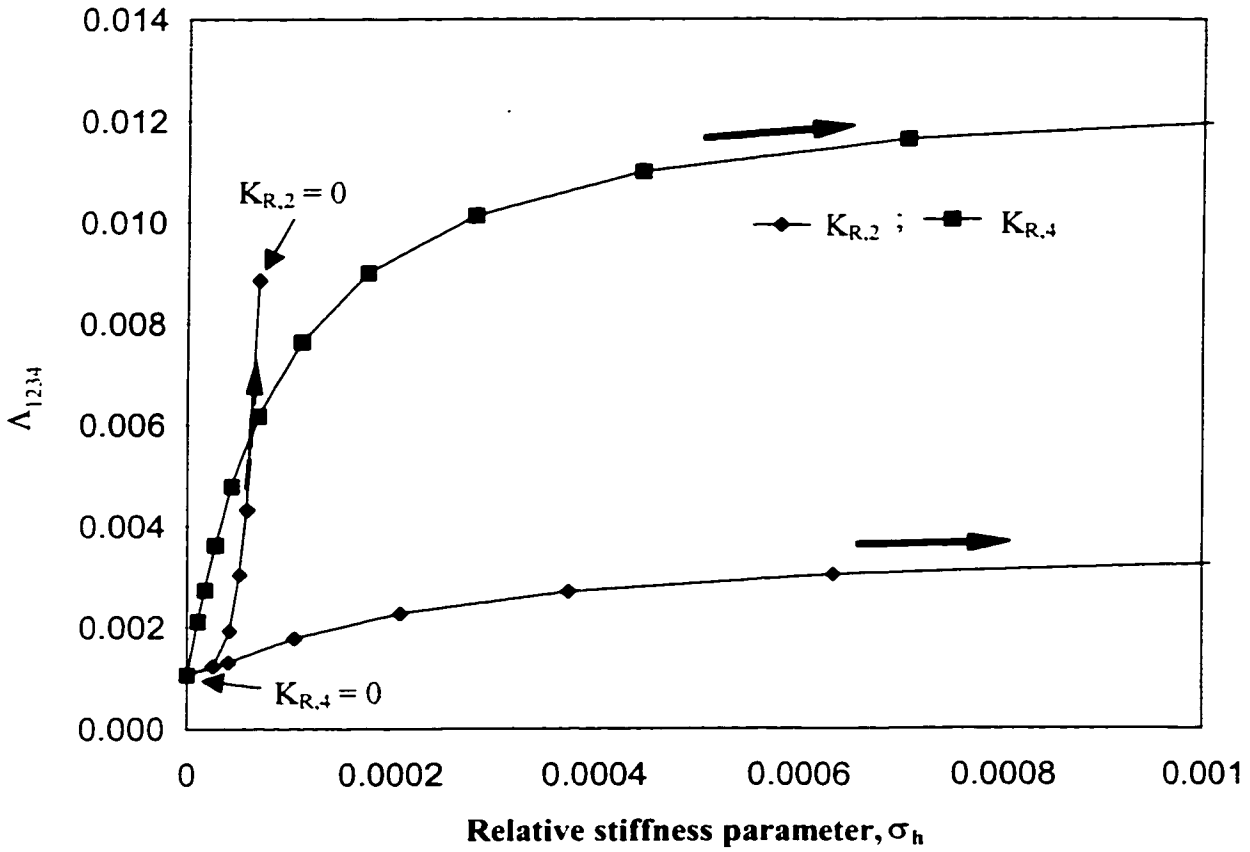

Figure 3.20 Effect of $K_{R,2}$ and $K_{R,4}$ on Λ_{1234}

3.3.2.2 Harmonic combination 1236

The effect of boundary conditioning by changing the translational stiffnesses at edges is shown in Figure 3.21. This figure shows that the harmonic combination 1236 is quite sensitive to translational stiffness on any edge. Translational strengthening and weakening on any side in relation to reference values destroys the harmonics 1236 rapidly as shown in Figure 3.21.

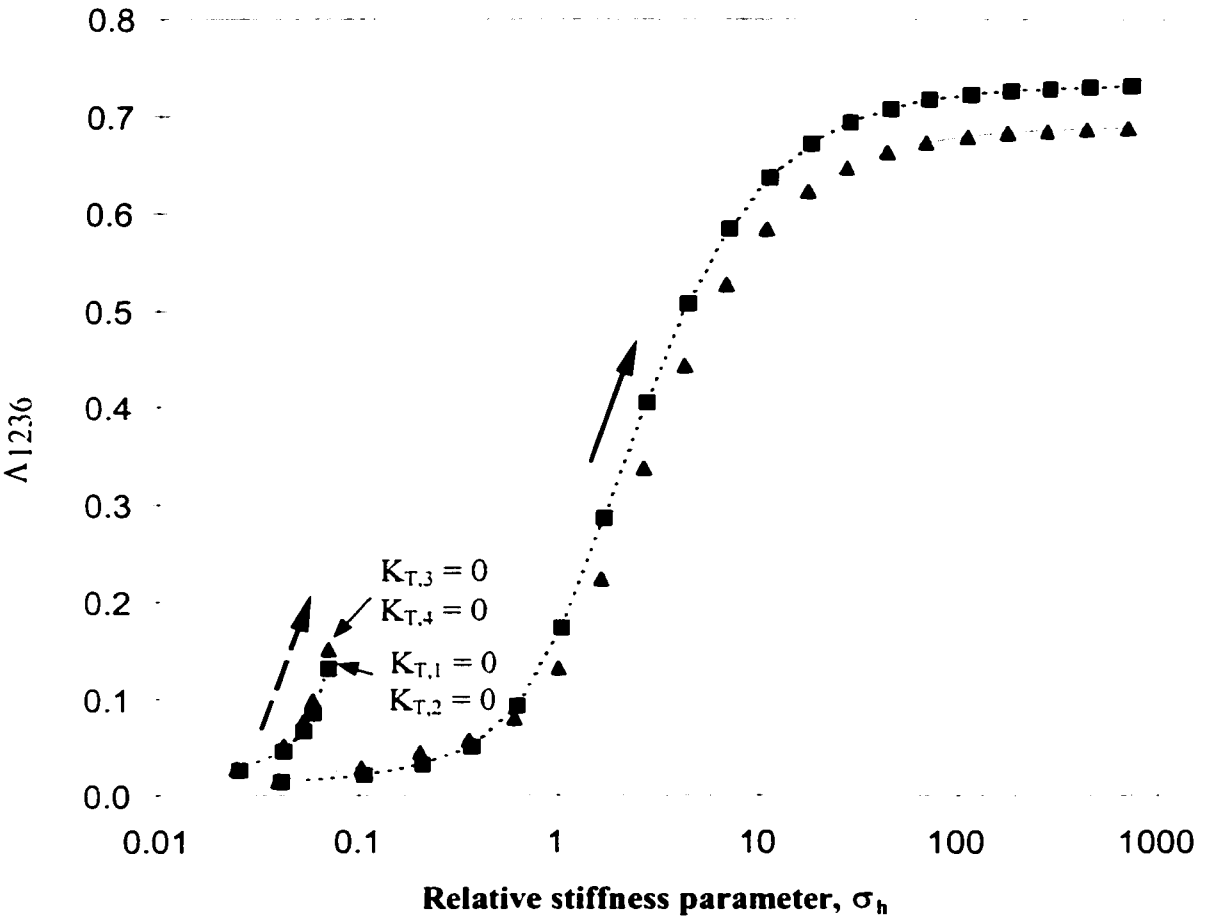

Fig. 3.21 Effect of $K_{T,1}$, $K_{T,2}$, $K_{T,3}$ and $K_{T,4}$ on Λ_{1236}, ■ $K_{T,1}$ ····· $K_{T,2}$; ▲ $K_{T,3}$; – $K_{T,4}$

The effect of boundary conditioning by changing the rotational stiffnesses is shown in Figure 3.22. It is seen that the harmonics 1236 is less sensitive to changes in rotational stiffnesses than translational stiffnesses. Further, rotational weakening affects the harmonics rapidly than the rotational strengthening.

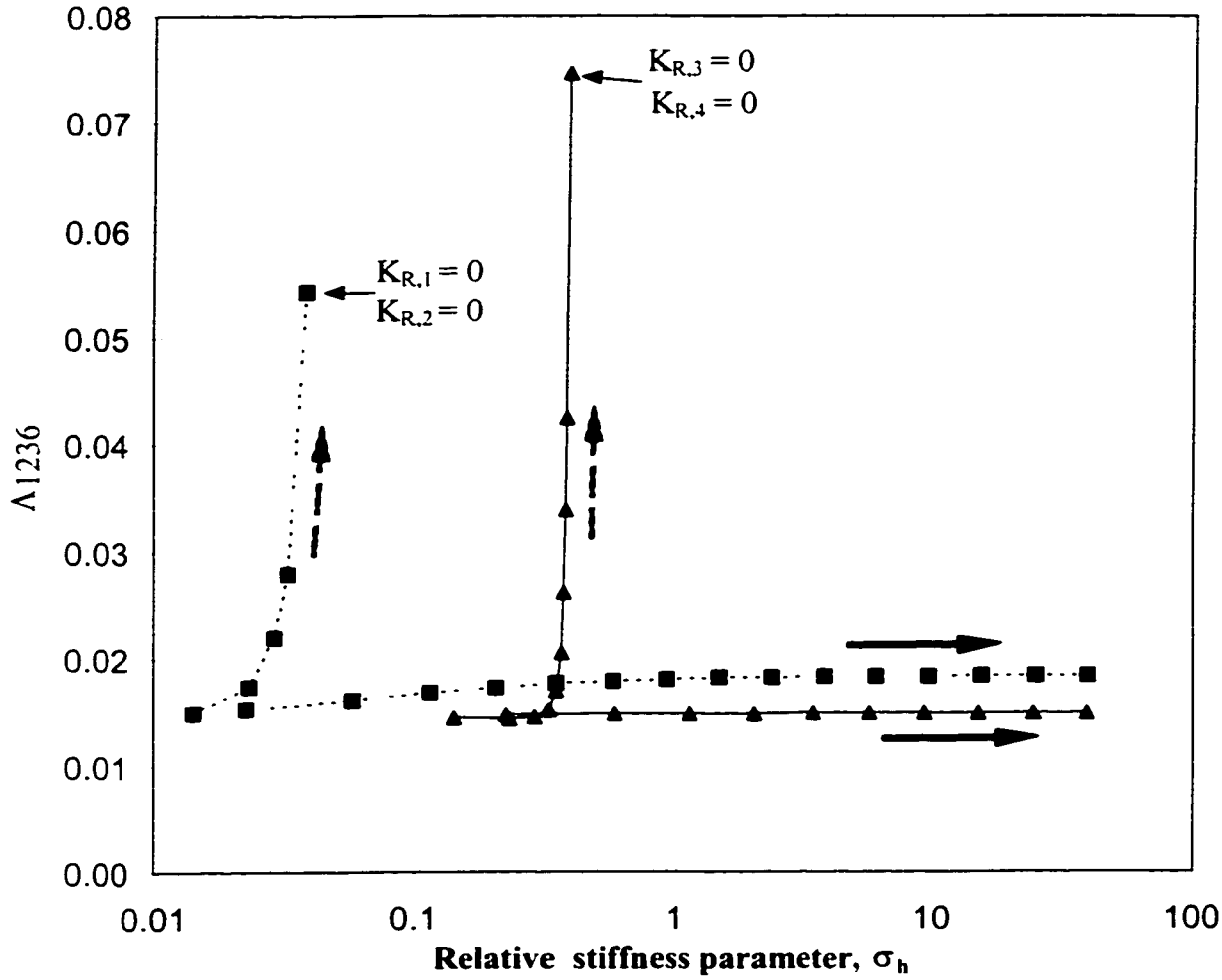

Fig. 3.22 Effect of $K_{R,1}$, $K_{R,2}$, $K_{R,3}$ and $K_{R,4}$ on Λ_{1236} ■ $K_{R,1}$; ····· $K_{R,2}$; ▲ $K_{R,3}$; —— $K_{R,4}$

3.3.2.3 Harmonic combination 1357

The effect of boundary conditioning on harmonic combination 1357 is shown in Figures 3.23 to 3.25. The effect of change in rotational stiffnesses is less significant than that due to change in translational stiffnesses. Rotational stiffness on sides 3 and 4 have similar effect on harmonics and rotational strengthening on these sides deteriorates the harmonics 1357 while the variation of rotational stiffnesses on sides 1 and 2 have negligible effect on the desired harmonic combination.

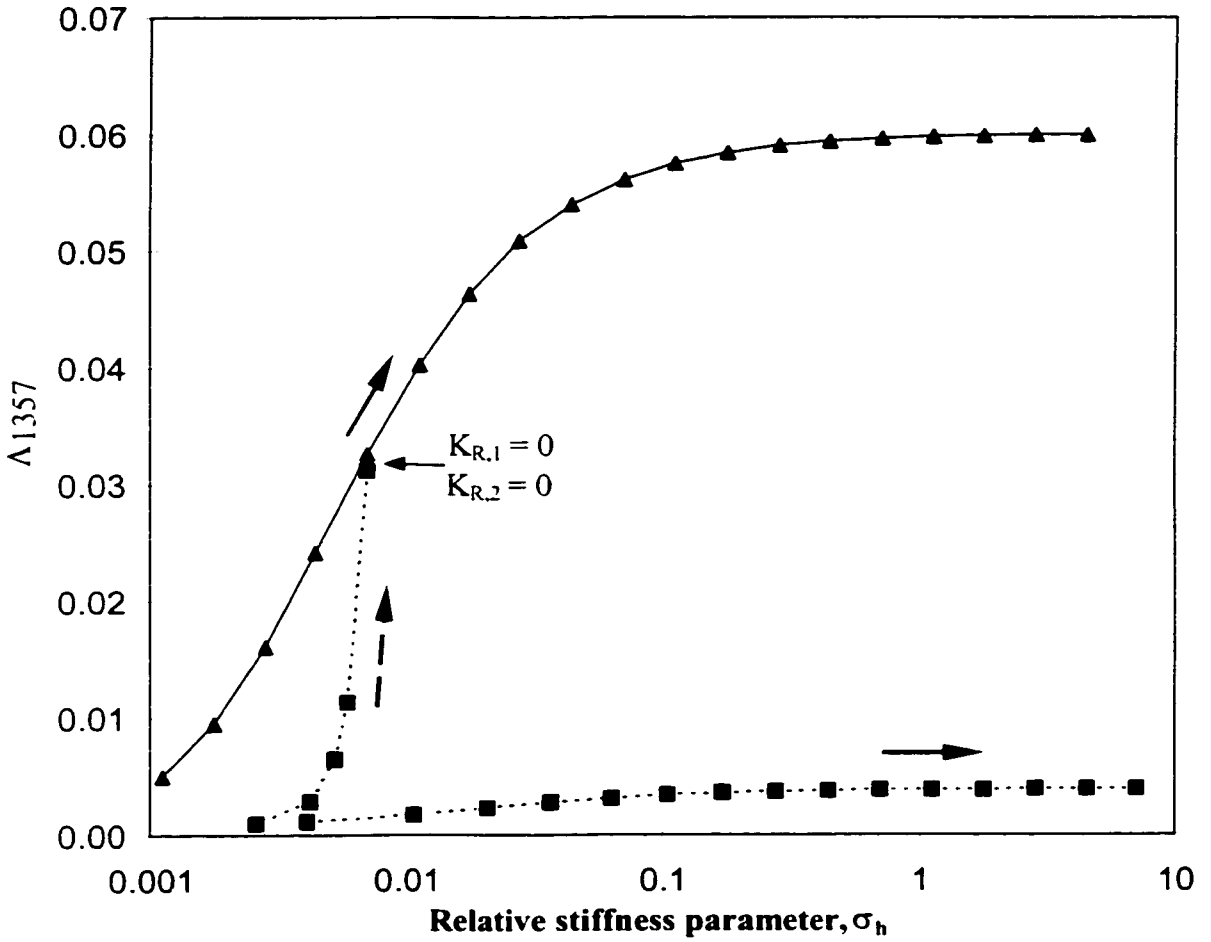

Fig. 3.23 Effect of $K_{R.1}$, $K_{R.2}$, $K_{R.3}$ and $K_{R.4}$ on Λ_{1357}, ■ $K_{R.1}$; ····· $K_{R.2}$; ▲ $K_{R.3}$: —— $K_{R.4}$

The relative change in translational stiffnesses from their reference values has a significant effect on harmonic combination 1357 as seen from the Figures 3.24 and 3.25.

The above results confirm that the method of obtaining a combination of harmonics for a given structure through boundary conditioning is quite feasible. These results also show the complexity and uniqueness associated with each harmonic combination in terms of distribution of boundary stiffness.

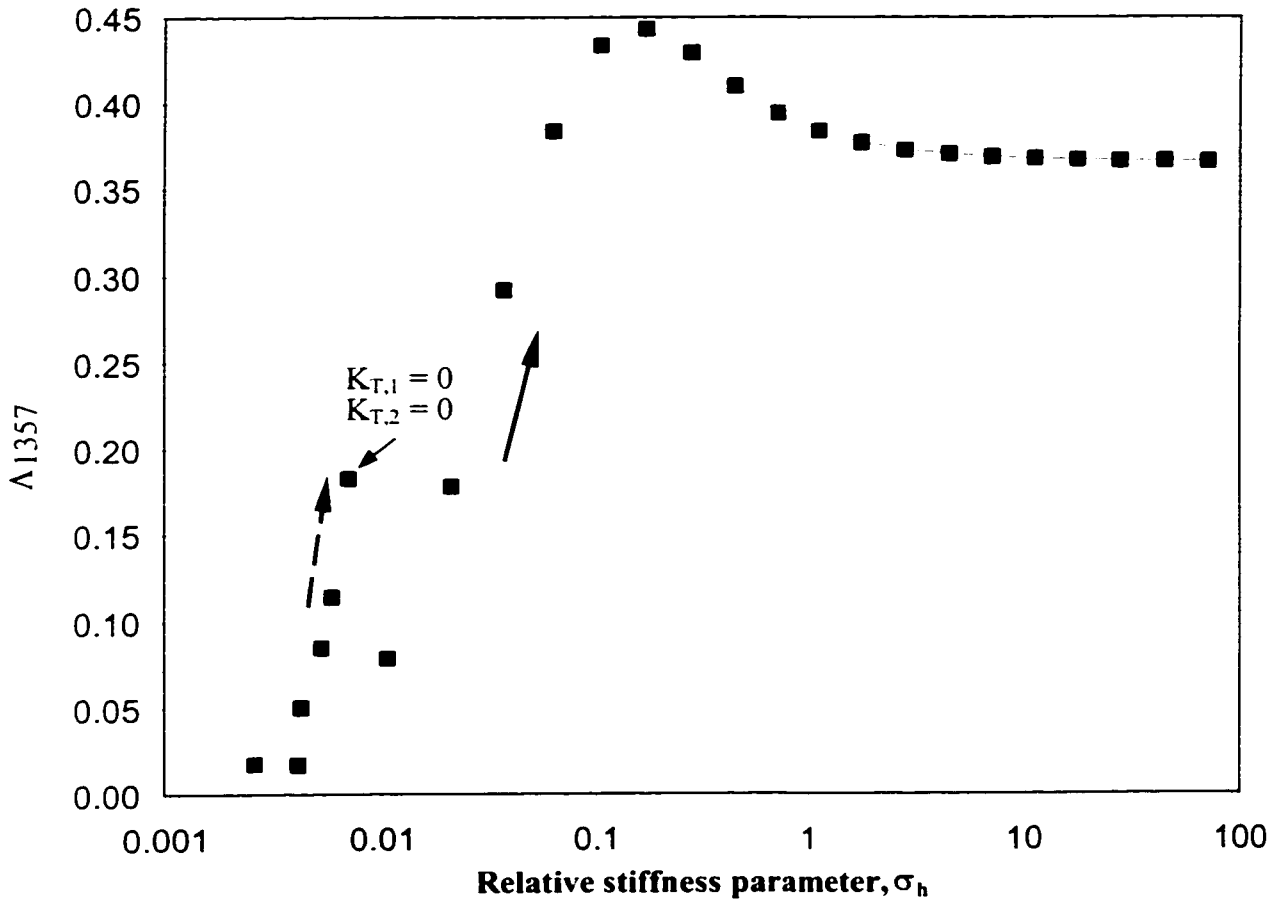

Fig. 3.24 Effect of $K_{T,1}$ and $K_{T,2}$ on Λ_{1357}, ■ $K_{T,1}$; - - - $K_{T,2}$

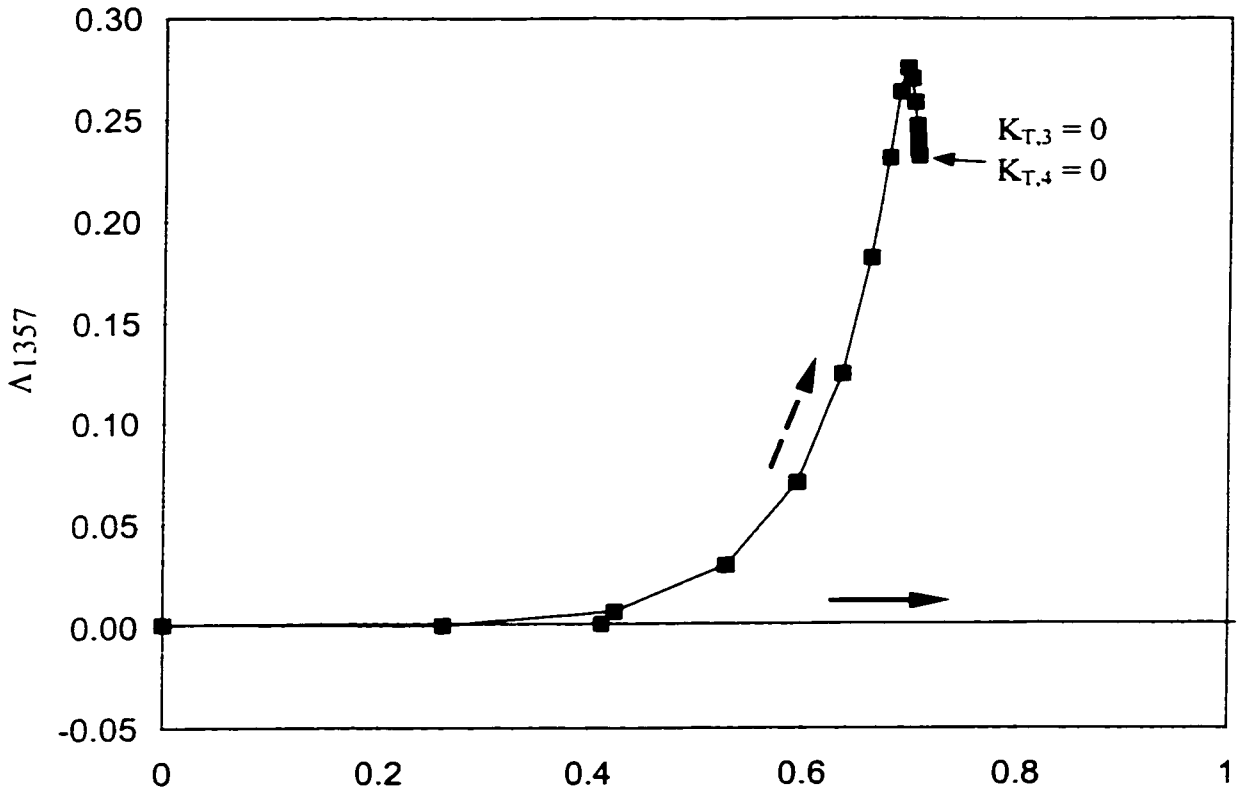

Fig. 3.25 Effect of $K_{T,3}$ and $K_{T,4}$ on Λ_{1357}, ■ $K_{T,3}$; —— $K_{T,4}$

3.3.3 Role of Boundary Conditioning in Tuning of Steel Pans

The boundary conditioning technique discussed above can be seen as a general technique to manipulate the natural frequencies of a structure by changing the boundary conditions of the existing or newly created boundaries. Since the vibration behavior of the structure is dependent on the distribution of material properties, structural geometry and boundary conditions, the required pattern of natural frequencies can be achieved by conditioning any of the above mentioned parameters in isolation or in combination. Part of the tuning process of a steel pan instrument, a musical instrument prevalent in West Indies in the shape of a hemispherical vessel with its surface containing demarcated areas as musical notes and played using two sticks, employs this boundary conditioning technique. The

steel pan is essentially a hemispherical shell type structure, made by hammering the flat end of a tar drum. Circular, elliptical or trapezoidal areas called notes are marked on the hemispherical surface by indenting the periphery of these regions using dot punches resulting in the creation of boundaries of the notes which are rotationally weak. During the process of steel pan making, the areas in between these notes are hardened by heat treatment representing translationally stiff boundaries. The localization of note vibration and the coarse tuning are achieved by grooving, punching, hammering, peening, stretching, heat treatment etc [185]. Hence, the individual note regions that act as individual vibrator elements are capable of producing distinct tones by tuning each note to generate a distinct fundamental natural frequency and a combination of harmonics in isolation or in pair with adjacent notes. Modeling the individual note as a shell-like structure and replacing its surrounding areas with equivalent springs, for analysis purposes, have been suggested by Achong [1]. The model of a rectangular plate with rotational and translational stiffnesses at the edges may be considered as a very simplistic example of an individual localized vibrator, of the steel pan, and varying the stiffness values at the edges in order to achieve a certain relation among natural frequencies resembles the boundary conditioning part of the tuning operation in steel pans. The final tuning process of the steel pan includes the manipulation of several other non-linear parameters, particularly in view of the curvature of the shell note area, residual stresses etc., as suggested by Achong [1, 2]. It can be seen from the above results and discussion that the boundary conditioning becomes one of the techniques, like modifying geometry and material properties, responsible for structural tuning a particular note in order to obtain a desired harmonic relation among its natural frequencies.

It was mentioned earlier that it is also possible to alter the elastic property of the system through fabrication techniques such as heat treatment, hammering, work hardening, peening etc. Examples for this is the steel pan musical instrument. The vibration behavior of the pan is modified through such processes. In order to study the effect of local variation of conditioning parameters within the structure and also to study the coupling between many sub structures, the above approach is extended below. The modeling used to analyze the influence of boundary conditioning can be applied to study the localization of [8, 78, 204] vibration or modification of acoustic radiation [14, 71, 88, 105, 148, 149, 176, 191] from the vibrating structure.

3.4 LOCALIZATION OF STRUCTURAL VIBRATION THROUGH BOUNDARY CONDITIONING DUE TO PROCESS INFLUENCE

As vibration of structures in a compressible medium results in sound radiation, control of structural vibration can result in global reduction of sound radiated and also the sound transmitted through the structure. Consider a plate structure as shown in Figure 3.26. When the structure is excited at point A, the entire structure vibrates and radiates sound. The radiation of sound depends on mode shapes of the structure and distribution of external load on the structure.

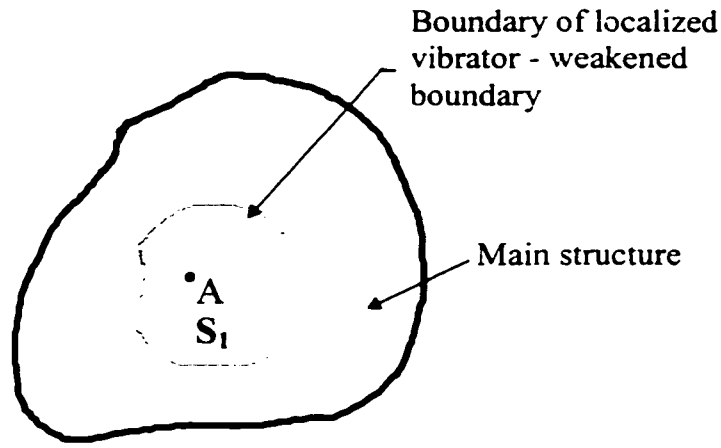

Figure 3.26: Layout for localized vibrator

The conventional control of vibration level through manipulation of external excitation needs distribution of control sources throughout the structure. Controlling will become easier and more effective if the vibration could be localized around the excitation source, say, to the zone represented by S_1. If it is possible to localize the vibration to the area S_1, the localization will result in less number of control sources for effective control of structural vibration. In the case of acoustic radiation, the radiated sound can be controlled either by modifying acoustically coupled mode shapes or by vibration control or by isolating vibrating area from the location of interest by the method of localization.

Control of structural vibrations through boundary conditioning involves modification of boundary parameters, where the boundary surrounding any region of the structure characterized by a sudden change in structural properties. This paper examines applications of boundary conditioning method to localize the structural vibrations by modifying the boundary conditions around the zone to which response is to be contained. The localization of vibration facilitates easy control of structural vibrations and hence the

radiated sound. The principle of localization of vibration through boundary conditioning is very effectively used in the West Indian Steel Pan instruments as discussed earlier. [1, 2, 151, 185]. Vibration behavior of the complete structure has been analyzed by using boundary characteristic orthogonal polynomials in the Rayleigh - Ritz method as explained in the previous section. A square plate having square localized area at the center is considered to study the effect of boundary conditioning and localization of vibration response achieved through fabrication processes. The boundary conditions of the interior square segment could be varied by varying the stiffness of translational and rotational springs introduced on the segment boundary. These springs can also represent the elastic condition of the structure obtained due the fabrication processes.

3.4.1 Analysis

Consider a rectangular plate as shown in Figure 3.27 with a central zone S_1 to which the vibration is to be localized. The plate is divided into nine rectangular segments (shown by dotted lines) connected by inter-translational (K_T) and inter-rotational springs (K_R) [208, 209].

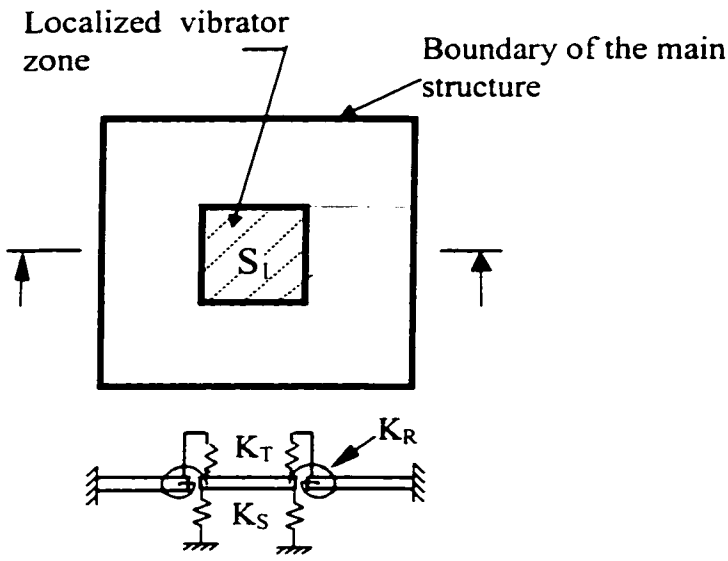

Figure 3.27: Plate structure with one localized area

As explained in the Section 3.2.1, the boundaries that connect segments of the main structure, are represented by very high values of inter-rotational and inter-translational spring stiffnesses. The interior segment is connected to adjacent segments through translational and rotational springs with stiffness per unit length of K_T and K_R, respectively. In addition, the interior segment is also supported around its boundary with support translational springs of stiffness K_S per unit length in order to effect the transmission of vibrational energy to the adjacent segments. These support translational springs represent the change in condition of the elastic property due to the manufacturing process. In the present study the support translational springs represent the highly stiff environment outside the boundary.

The plate vibration under the process influence is analyzed with additional support springs using normal modes obtained using boundary characteristic orthogonal polynomials in the Rayleigh-Ritz method [17, 19]. These orthogonal polynomials are again generated using Gram-Schmidt process [37] for each segment so as to satisfy the free edge conditions on all boundaries of all segments.

The flexural deflection equation for k^{th} segment is defined as per Equation (3.25) as

$$W_k(x,y) = \sum_m \sum_n A_{mn.k}\phi_m(x)\varphi_n(y)$$

The maximum total strain energy U_{max} becomes

$$U_{max} = \sum_{k=1}^{N} U_{max.k} + \sum_{k=1}^{N}\sum_{s=1}^{4} U_{T.k.s} + \sum_{k=1}^{N}\sum_{s=1}^{4} U_{R.k.s} + \sum_{k=1}^{N}\sum_{s=1}^{4} U_{S.k.s} \qquad (3.40)$$

and the maximum kinetic energy T_{max} of the structure remains same as given by Equation (3.27) as

$$T_{max} = \sum_{k=1}^{N} \frac{1}{2}\rho_k h_k a_k b_k \omega^2 \int_0^1\int_0^1 W_k^2(x,y)dxdy$$

where

$U_{max.k}$ - strain energy of the k^{th} plate

$U_{T.k.s}$ - potential energy of s^{th} side translational spring of k^{th} plate

$U_{R.k.s}$ - potential energy of s^{th} side rotational spring of k^{th} plate

$U_{S.k.s}$ - potential energy of s^{th} side support spring of k^{th} plate and are estimated using the following equations:

$$U_{\max,k} = \frac{D_k a_k b_k}{2a_k^4} \int_0^1 \int_0^1 \left[W_{xx,k}^2 + \alpha_k^4 W_{yy,k}^2 + 2\upsilon\alpha_k^2 W_{xx,k} W_{yy,k} + 2(1-\upsilon)\alpha_k^2 W_{xy,k}^2 \right] dxdy$$

$$U_{T,k,s} = \frac{1}{2} K_{T,k,s} \int_0^{l_s} (\Delta W_s)^2 dl_s$$

$$U_{R,k,s} = \frac{1}{2} K_{R,k,s} \int_0^{l_s} \left(\Delta W_s^1\right)^2 dl_s$$

$$U_{S,k,s} = \frac{1}{2} K_{S,k,s} \int_0^{l_s} (W_{k,s})^2 dl_s$$

Substitution of deflection Equation (3.25) in strain energy and kinetic energy Equations (3.40) and (3.27), and optimization of the Rayleigh quotient with respect to $A_{ij,k}$ result in the following eigenvalue equation:

$$\sum_m \sum_n \left[C_{mnij,k} + C_{mnij,k}^I + C_{mnij,k}^S - \lambda \Pi_k E_{mi}^{00} F_{nj}^{00} \right] A_{mn,k} - \sum_m \sum_n D_{mnij,s} A_{mn,s} = 0 \qquad (3.41)$$

$$\forall \cdot k = 1,2,\ldots,N$$

where

$$C_{mnij,k} = E_{mi}^{22} F_{nj}^{00} + \alpha_k^4 E_{mi}^{00} F_{nj}^{22} + \upsilon\alpha_k^2 \left(E_{mi}^{02} F_{nj}^{20} + E_{mi}^{20} F_{nj}^{02} \right) + 2 \cdot (1-\upsilon)\alpha_k^2 E_{mi}^{11} F_{nj}^{11}$$

$$C_{mnij,k}^I = K_{T,k,1}^{\bullet} \alpha_k E_{mi}^{00} \varphi_n(0)\varphi_j(0) + K_{T,k,2}^{\bullet} \phi_m(1)\phi_i(1) F_{nj}^{00} + K_{T,k,3}^{\bullet} \alpha_k E_{mi}^{00} \varphi_n(1)\varphi_j(1)$$
$$+ K_{T,k,4}^{\bullet} \phi_m(0)\phi_i(0) F_{nj}^{00} + K_{R,k,1}^{\bullet} \alpha_k^3 E_{mi}^{00} \varphi_n^1(0)\varphi_j^1(0) + K_{R,k,2}^{\bullet} \phi_m^1(1)\phi_i^1(1) F_{nj}^{00}$$
$$+ K_{R,k,3}^{\bullet} \alpha_k^3 E_{mi}^{00} \varphi_n^1(1)\varphi_j^1(1) + K_{R,k,4}^{\bullet} \phi_m^1(0)\phi_i^1(0) F_{nj}^{00}$$

$$C^{S}_{mnij,k} = K^{\bullet}_{S.k.1}\alpha_k E^{00}_{mi}\varphi_n(0)\varphi_j(0) + K^{\bullet}_{S.k.2}\phi_m(1)\phi_i(1)F^{00}_{nj} + K^{\bullet}_{S.k.3}\alpha_k E^{00}_{mi}\varphi_n(1)\varphi_j(1)$$

$$+ K^{\bullet}_{S.k.4}\phi_m(0)\phi_i(0)F^{00}_{nj}$$

$$D_{mnij,s}A_{mn,s} = [K^{\bullet}_{T.k.1}\alpha_k E^{00}_{mi}\varphi_n(1)\varphi_j(0) + K^{\bullet}_{R.k.1}\alpha_k^2\alpha_{s1}E^{00}_{mi}\varphi^1_n(1)\varphi^1_j(0)]A_{mn.s1} +$$

$$[K^{\bullet}_{T.k.2}\phi_m(0)\phi_i(1)F^{00}_{nj} + K^{\bullet}_{R.k.2}\frac{\alpha_k}{\alpha_{s2}}\phi^1_m(0)\phi^1_i(1)F^{00}_{nj}]A_{mn.s2} +$$

$$[K^{\bullet}_{T.k.3}\alpha_k E^{00}_{mi}\varphi_n(0)\varphi_j(1) + K^{\bullet}_{R.k.3}\alpha_k^2\alpha_{s3}E^{00}_{mi}\varphi^1_n(0)\varphi^1_j(1)]A_{mn.s3} +$$

$$[K^{\bullet}_{T.k.4}\phi_m(1)\phi_i(0)F^{00}_{nj} + K^{\bullet}_{R.k.4}\frac{\alpha_k}{\alpha_{s4}}\phi^1_m(1)\phi^1_i(0)F^{00}_{nj}]A_{mn.s4}$$

and

$$K^{\bullet}_{T.k.i} = \frac{K_{T.k.i}a_k^3}{D_k},\ K^{\bullet}_{R.k.i} = \frac{K_{R.k.i}a_k}{D_k},\ K^{\bullet}_{S.k.i} = \frac{K_{S.k.i}a_k^3}{D_k},\ \Pi_k = \frac{\rho_{r.k}a^4_{r.k}}{E_{r.k}h^2_{r.k}},\ \lambda = \frac{\rho_1 h_1 a_1^4\omega^2}{D_1},$$

$$E^{rs}_{mi} = \int_0^1\left(\frac{d^r\phi_m}{dx^r}\right)\left(\frac{d^s\phi_i}{dx^s}\right)\cdot dx,\quad F^{rs}_{nj} = \int_0^1\left(\frac{d^r\varphi_n}{dy^r}\right)\left(\frac{d^s\varphi_j}{dy^s}\right)\cdot dy,\quad \phi^1_i = \frac{d\phi_i}{dx},\quad \varphi^1_j = \frac{d\varphi_j}{dy}$$

In the above, subscript (r,k) refers to ratio of parameter of k^{th} segment to that of first segment.

The solution of Equation (3.41) yields both eigenvalues and mode shapes of the system. Segments that have edge on the boundary of the main structure on 's' side have, $A_{mn,s} = 0$. Required edge conditions for any segment can be generated by suitable choice of the values of K_T and K_R.

Response of a plate depends upon translational, rotational and support stiffnesses, and the boundary conditions of the main structure. Hence, the vibrational behavior of the

structure, mode shapes, modal frequencies and the response can be effected by modifying the stiffness values of the artificial springs. In practice, the reduction of the rotational stiffness K_R can be effected by weakening the boundary by methods such as peening, drilling of a series of holes or slots, notching etc. along the boundaries of any segment while the increase of rotational stiffness can be achieved by strengthening the joints with additional rotational stiffeners. By the use of proper techniques of heat treatment, work hardening, surface hardening etc., areas of interest like areas other than localized zone in a structure can be made stiff in comparison with the rest of the structure. This is analogous to the increase of support stiffness at the boundaries of localized zone. For analysis, these stiff zones are represented by high values of support stiffnesses. The boundary conditioning by changing both rotational and support stiffnesses affect the flow of vibrational energy across boundaries to the adjacent areas. This type of boundary conditioning is used in this paper in order to manipulate the vibrational behavior of the structure. Value of K_T is kept always very high for all joints such that the continuity of deflection is maintained.

3.4.2 Results and Discussion

As this chapter focuses on localization of vibration and modification of mode shapes, the corresponding boundary conditioning is achieved by reducing the rotational stiffness and by increasing the support stiffness at the boundaries around the interior segment. This type of boundary conditioning restricts the flow of vibrational energy through boundaries to the adjacent areas of the structure resulting in accumulated response at the localized

area. The exact stiffness values of the rotational and support springs required for localization and modification of mode shapes depend on the strength of vibration source, geometry of the structure and material properties. For further demonstration on localization and modification of mode shapes, the boundary conditioning is applied only to the boundaries of a square segment S_1 shown in Figure 3.27 and the results are presented in the following section. The support springs are distributed only along the four edges of the localized zone. It is assumed that the boundaries of localized zone are weakened rotationally by plastic indentations or by a series of holes, slots or by notching etc. along the edges such that the rotational stiffness is very small. It is also assumed that non-localized areas are hardened and stiffened by suitable heat treatment such that it is stiff in comparison to the inner segment.

3.4.2.1 Effect of boundary conditioning on mode shapes

The eigenvalue Equation (3.41) is solved for the selected plate structure for different stiffness values of both rotational and support springs at the four boundaries of the central zone in order to obtain both eigenvalues and eigenvectors of the complete structure. The effect of stiffening the non-central zone on the first, second and fourth mode shapes, which is analogous to the increase of support stiffness value K_S, is presented in Figures 3.28, 3.29 and 3.30, respectively. The translational stiffness value of $K_T = 1x10^{10}$ N/m^2 and rotational stiffness value of $K_R = 2.5x10^9$ N are selected for all boundaries in order to study the effect of only support stiffness. Figures 3.28.a, 3.29.a and 3.30.a correspond to nearly homogeneous plate condition with small value of $K_S = 1$ N/m^2 while Figures

3.28.b, 3.29b and 3.30.b correspond to stiffened non-central zone represented by very high values of $K_S = 1x10^{10}$ N/m^2. Even though a smooth variation of mode shapes was found while varying support stiffness, results at only these two extreme values of support stiffness are presented here for clarity. It can be seen from these figures that deflection at the boundaries of the central segment are nearly zero for all the mode shapes at $K_S = 1x10^{10}$ N/m^2. The variation in mode shape is more for fundamental mode than higher modes when the support stiffness is increased. The dependency between the mode shape and boundary conditioning is strongly dependent on the location selected for boundary conditioning. Depending upon the acoustic coupling of the mode shapes under different boundary conditions, the acoustic radiation will change. As nonvolumetric modes correspond to poor sound radiation efficiency [105], the modification of volumetric modes will be helpful in reducing sound radiation. Figure 3.28 shows such a possibility of altering volumetric mode to nonvolumetric mode through boundary conditioning.

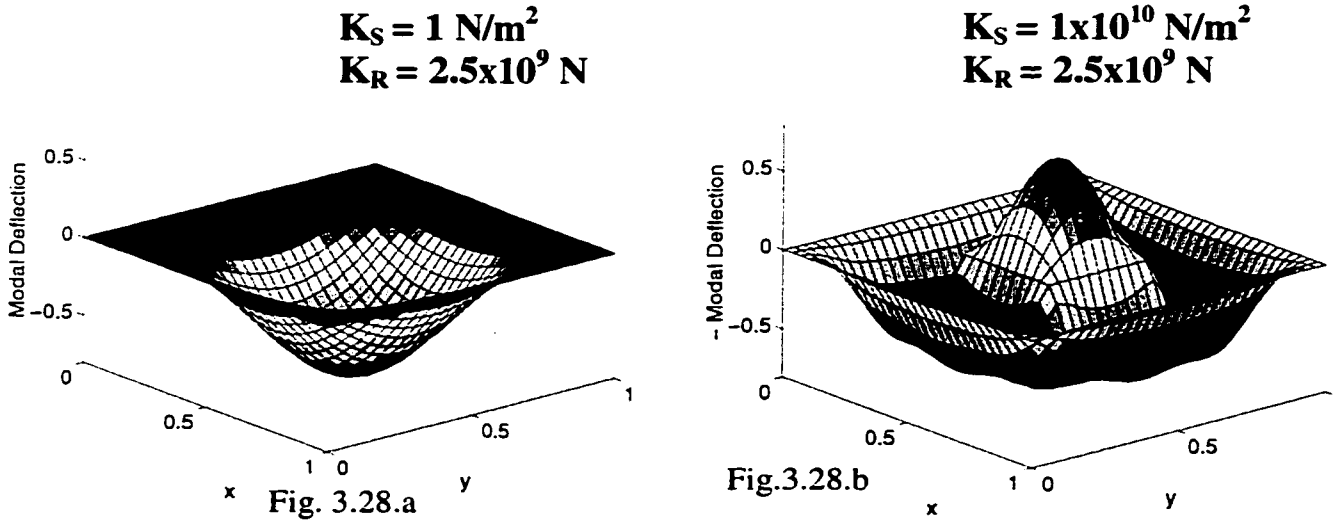

Figure 3.28: Effect of support stiffness on the first mode shape

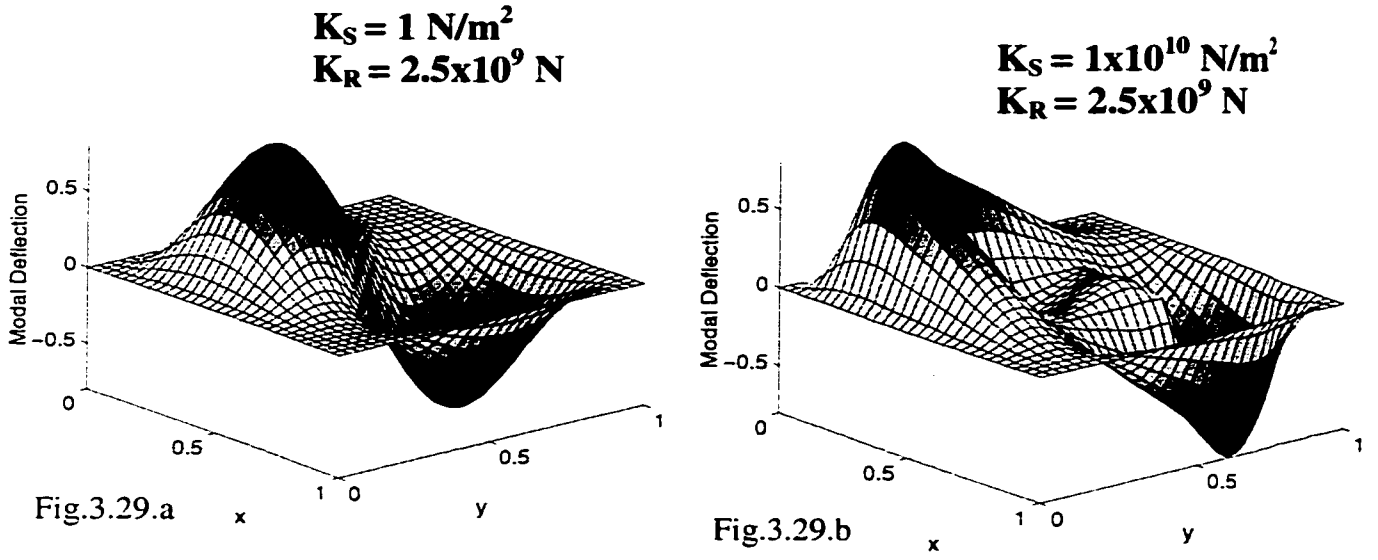

Figure 3.29: Effect of support stiffness on the second mode shape

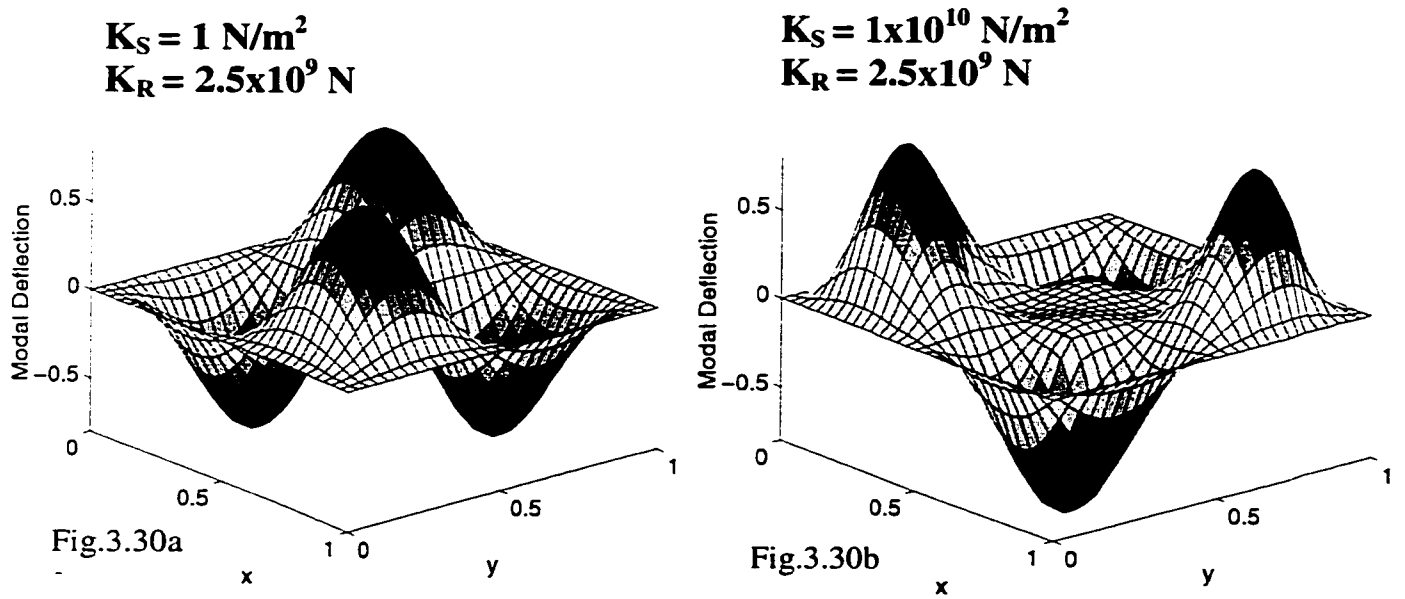

Figure 3.30: Effect of support stiffness on fourth mode shape

In addition to the support stiffening, effect of rotational weakening at the boundaries of the central segment on the first, second and third mode shapes is presented in Figures 3.31, 3.32 and 3.33, respectively. The translational stiffness value is kept at the same value of $K_T = 1x10^{10}$ N/m^2 for all segment boundaries and stiffness value for the support springs at central segment boundaries are kept at the value of $K_S = 1x10^{10}$ N/m^2 for this study of rotational weakening part of boundary conditioning. Figures 3.31.a, 3.32.a and 3.33.a correspond to a rotational stiffness of $K_R = 1x10^3$N while Figures 3.31.b, 3.32.b and 3.33.b correspond to weakened rotational stiffness of $K_R = 1$N. The reduction of rotational stiffness further restricted the flow of vibrational energy across the boundaries of central segment leading to additional change in the mode shapes. The mode shapes show the confinement of vibrational response to either the central segment or the rest of the plate such that excitation in any one of these zones does not affect the other. Hence, the above process of boundary conditioning resulting in such favorable mode shapes can be conveniently exploited for localization of structural response. These mode shapes also confirm the use of boundary conditioning technique for the possible manipulation of the flow of vibrational energy in the structure in order to obtain required vibrational behavior. Boundary conditioning can be effected by various means such as discrete or uniform distribution of boundary parameters, strengthening or weakening of the surrounding environment external to the structure, different forms of supports.

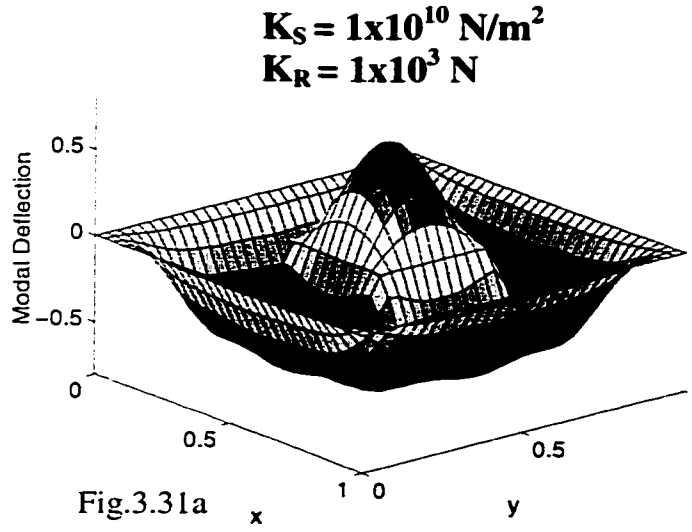

Fig.3.31a

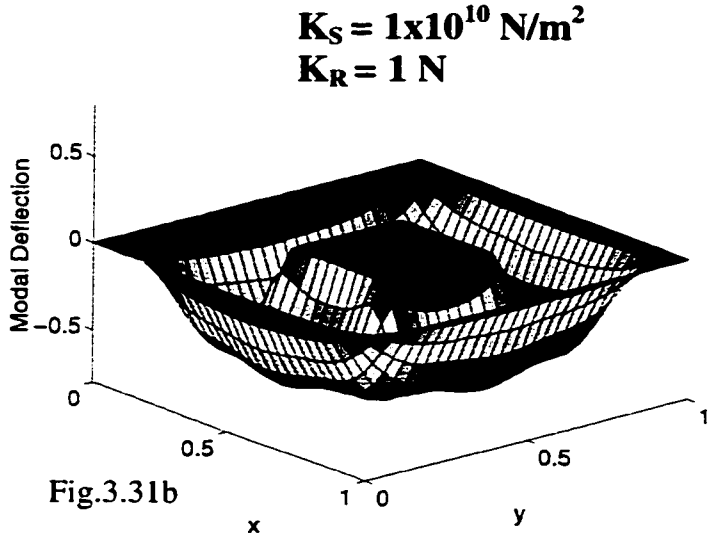

Fig.3.31b

Figure 3.31: Effect of rotational stiffness on the first mode shape

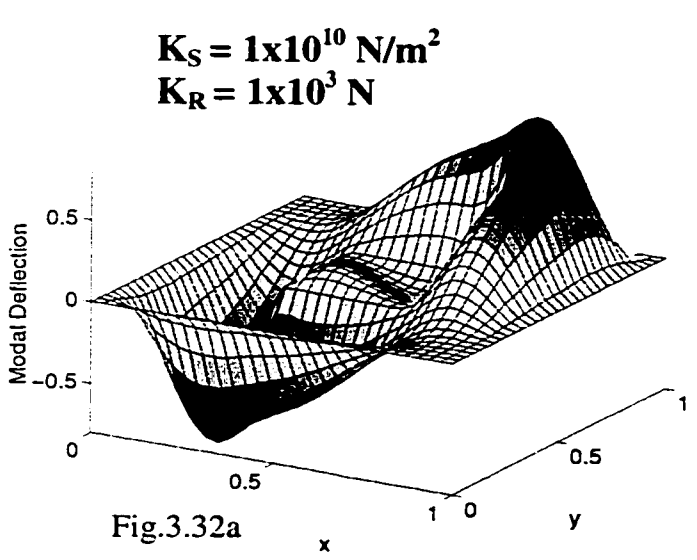

Fig.3.32a

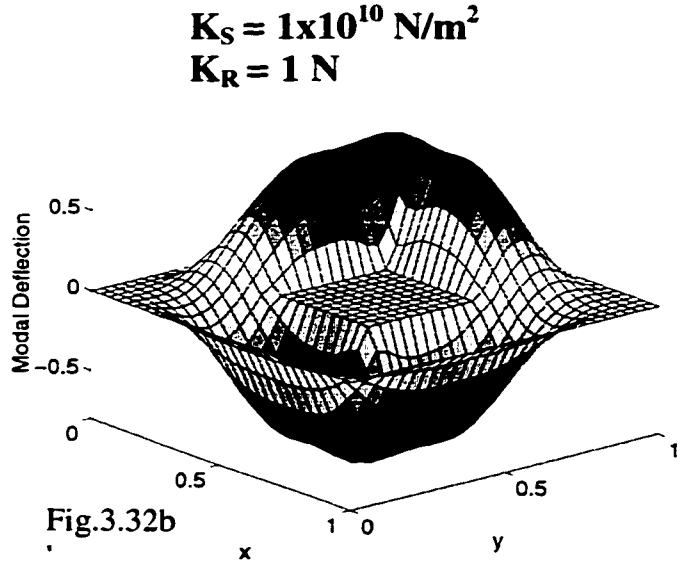

Fig.3.32b

Figure 3.32: Effect of rotational stiffness on the second mode shape

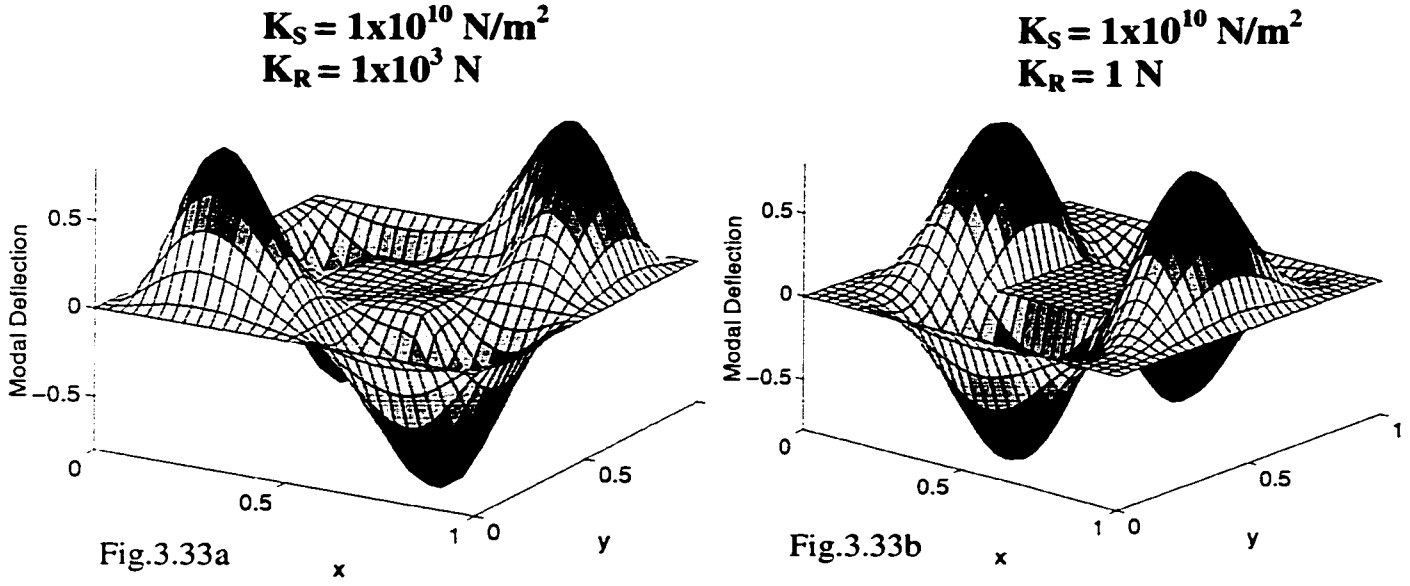

Figure 3.33: Effect of rotational stiffness on the fourth mode shape

3.4.2.2. Response localization through boundary conditioning

The localization of vibration can be visualized by the response of a plate to an impulse acting at the center of inner segment S_I. A square steel plate selected for analysis is of size 0.5x0.5m with thickness of 1mm. It is fully clamped on all edges. The area to be localized is of the size 0.17x0.17m at the center of the plate as shown in Figure 3.27. An impulse that induces a velocity of 0.1m/s is supplied at the center of the plate which is also the center of localized area. The same boundary conditioning of high support stiffness and very low rotational stiffness mentioned in the previous section is again selected for the demonstration of localizing impulse response.

When the impulse is applied, the system responds in all the modes. The contribution of each mode is determined by the strength of the impulse and also the location (x_0, y_0) where impulse is applied. For a lightly damped system, the response due to an impulse can be written as

$$W(x,y,t) = \sum_m e^{-\zeta\omega_m t} A_m \Phi_m \sin\omega_{dm} t \qquad (3.42)$$

where

$A_m = V_0 \Phi_m(x_0, y_0) / \omega_{dm}$

Φ_m - undamped modal vector corresponding to m^{th} mode obtained using the Equation (3.41)

ω_{dm} - damped modal frequency

ω_m - modal frequency

V_0 - initial impulse velocity = 0.1m/s

ζ - damping ratio (0.01 assumed for all modes)

The response estimated using the Equation (3.42) for different stiffness values of rotational and support springs along the boundaries of the localized area is presented below.

In general, the vibrational energy transfer across the boundaries can be viewed as a manifestation of the effort to maintain deflection and slope continuities at the boundaries. Hence, the change of support stiffness and rotational stiffness modify the transfer of vibrational energy across the boundaries as can be seen from Figures 3.34, 3.35 and 3.36.

The damped response patterns at different times of t = 1 and 5 ms for three sets of values of support stiffness and rotational stiffness are shown in Figures 3.34, 3.35 and 3.36. Figure 3.34 shows the impulse response for $K_S = 1x10^3$ N/m^2 and $K_R = 2.5x10^9$ N which are close to the condition of homogeneous plate itself. Further increase of only support stiffness to a value $K_S = 1x10^{10}$ N/m^2 shows improvement in the localization of response to the inner segment as seen from Figure 3.35. Even though the deflection at the boundaries of inner segment is minimized at higher support stiffness of $K_S = 1x10^{10}$ N/m^2 the transfer of vibrational energy can still be seen as a consequence of high values of rotational stiffness along the boundaries. As seen from the previous section, any further localization could be achieved by reducing rotational stiffness along the boundaries, which is equivalent to negative stiffening. The damped response at different times of t = 1 and 5 ms for a reduced rotational stiffness of K_R = 10N at a constant high value of $K_S = 1x10^{10}$ N/m^2 shown in Figure 3.36, demonstrates the use of boundary conditioning technique for localization of vibrational response.

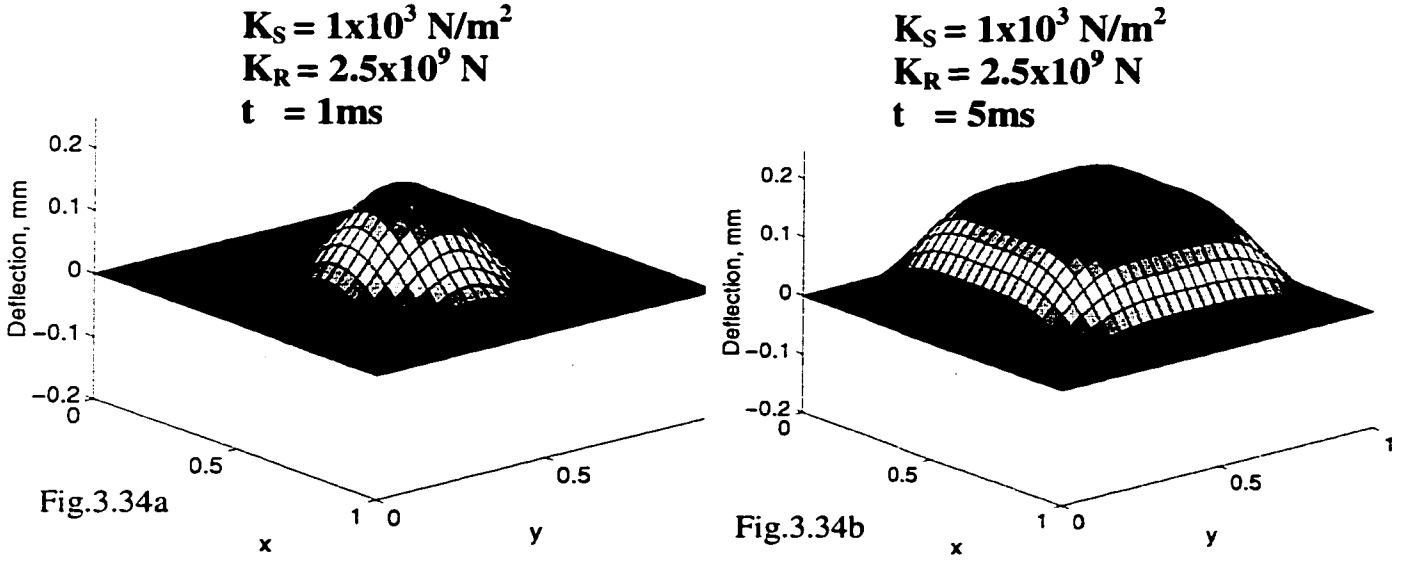

Figure 3.34: Impulse response at low support stiffness and high rotational stiffness

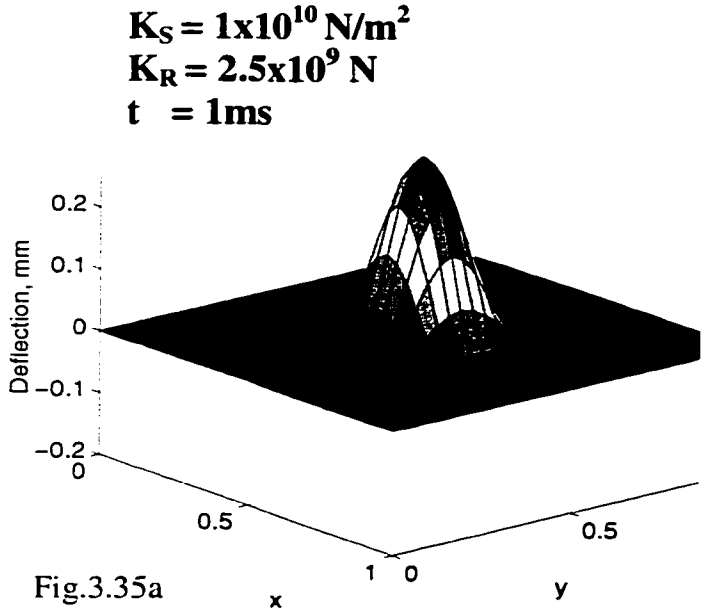

Fig.3.35a

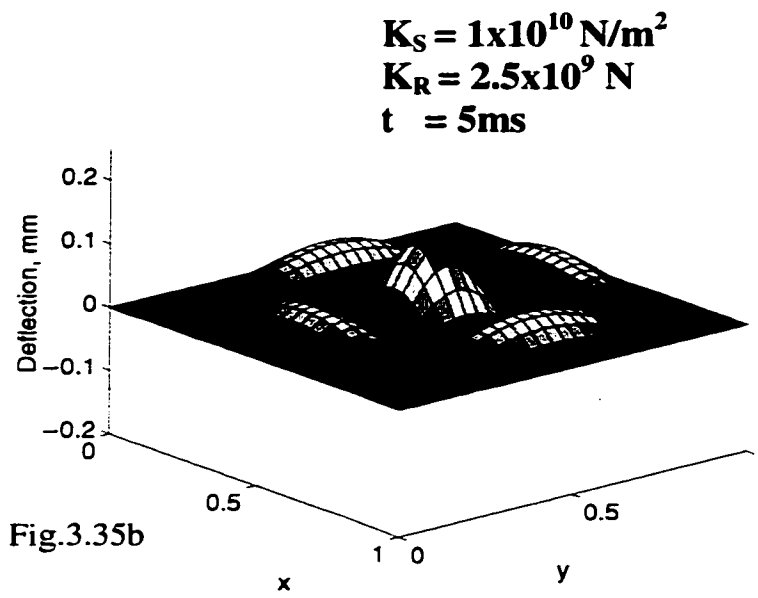

Fig.3.35b

Figure 3.35: Impulse response at high support stiffness and high rotational stiffness

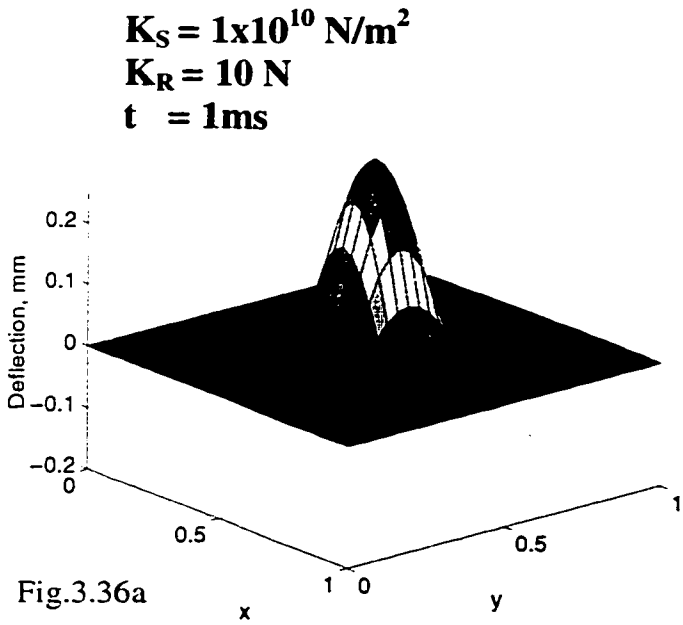

Fig.3.36a

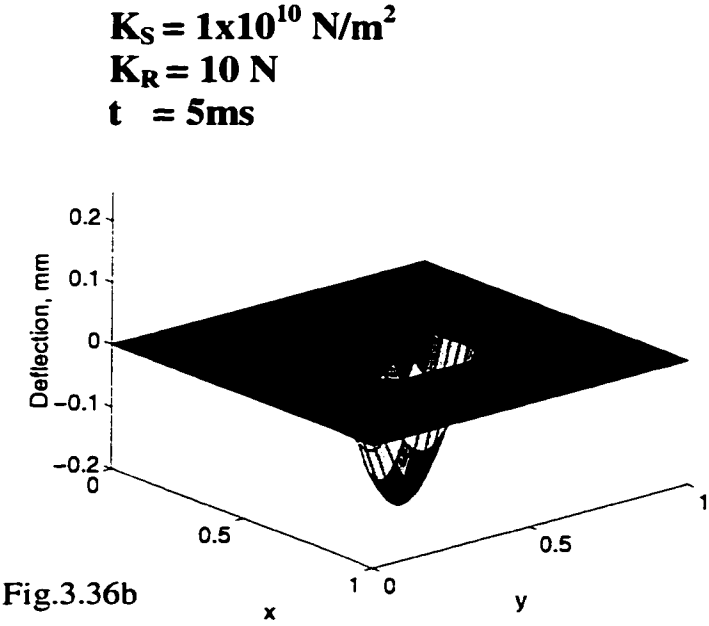

Fig.3.36b

Figure 3.36: Impulse response at high support stiffness and low rotational stiffness

Even though the application of boundary conditioning for modifying vibration behavior of a simple structure is demonstrated conceptually in this thesis, the interesting challenge still remains for structural engineers in obtaining exact boundary conditioning parameters in real structures.

3.5 CONCLUSIONS

The concept of boundary conditioning was modeled with artificial springs. The stiffness value of the artificial springs quantifies the effect of boundary conditioning on the dynamic behavior of elastic systems. The modeling of boundary conditioning by structural modification, support conditions and fabrication process has been successfully modeled by the method of artificial springs with application of boundary characteristic orthogonal polynomials in the Rayleigh-Ritz method. The influence of structural modification such as stiffeners has been successfully modeled. Effect of boundary conditioning through support conditions on vibration behavior such as harmonic combinations has been modeled and applied to a rectangular plate. The boundary conditioning procedure implies the modification of translational and rotational stiffness distribution on the edges in order to achieve the required results. The boundary conditioning technique by structural tuning can be applied to different problems of interest such as the manipulation of noise transmission into aircraft fuselage interior, structural tuning in order to get required combination of eigenfrequencies and tuning of musical instruments. The results of the present study confirm that the natural frequencies are strongly influenced by boundary conditioning. The analytical model has been extended to accommodate the boundary conditioning technique due to fabrication

process. The application of boundary conditioning technique to modify the structural mode shapes and to localize the vibration has been examined analytically for a plate type structure. Different mode shapes obtained by changing segmental boundary stiffness values show the potential of boundary conditioning technique in manipulating the mode shapes, the response and the resulting acoustic radiation, localization of response and quantification of the influence due to fabrication process on dynamic behavior. Impulse response of the structure has been obtained for different boundary stiffnesses in order to study the effect of boundary conditioning due to fabrication process on localization of vibrational response. This study suggests a type of boundary conditioning which involves rotational weakening of the boundaries of the localized area and stiffening the area outside this region, in order to achieve the localization of vibrational energy. The degree of localization depends on geometry, strength of vibration source in relation to support and rotational stiffnesses. Thus, the modeling of boundary conditioning has been successfully developed for an elastic system in order to accommodate and quantify the effect of support conditions, structural geometry and fabrication processes on the dynamic behavior. The next chapter discusses the formulation of a fuzzy system modeling of boundary conditioning in order to synthesize structures that exhibit required dynamic chracteristics.

CHAPTER 4

FUZZY SYSTEM IDENTIFICATION OF BOUNDARY CONDITIONING

System identification is a general technique useful for the identification of any system by modeling the behavior of the system. In general, system identification could represent any complicated input/output function approximation, output classification or input-output mapping for systems subjected to boundary conditioning. It was seen in the previous chapters that the boundary conditioning of elastic systems is influenced by many parameters such as fabrication processing parameters, structural geometric parameters and environmental parameters that affect the elasticity of the system, as schematically shown in Figure 4.1. We have also studied a method of quantifying the influence of conditioning parameters such as structural geometry, support conditions, manufacturing process parameters such as heat treatment temperature, bias voltage, Lorentz current though stiffness values. For modeling, the boundary conditioning (BC) parameters $x_1,\ldots,$ x_m as shown in Figure 4.1 can be in their respective units or equivalent stiffness values. The outputs denoted by $y_1,\ldots,y_r$ represent different required dynamic behaviors such as eigenfrequencies, eigenratios and mode shapes.

The equivalent stiffnesses can be estimated through experiment or other methods such as FEM. When the main elastic system has many subsystems interconnected, the number of BC parameters becomes large.

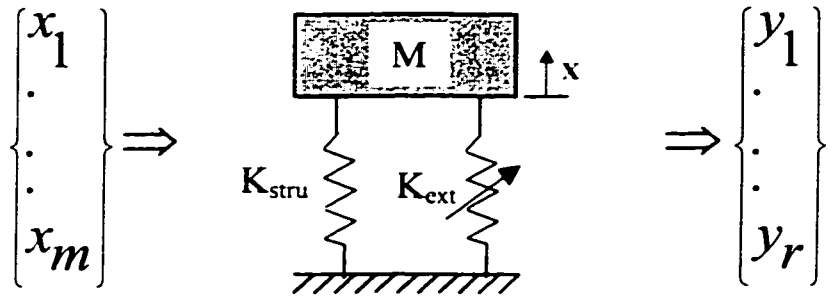

Figure 4.1: Scheme of an elastic system subjected to boundary conditioning

The estimation of the stiffnesses may include statistical uncertainties and vagueness due to imprecise output quantification. In order to absorb the uncertainty, with influencing parameters and vagueness associated with definition, it would be advantageous if the quantification of the stiffness has qualitative values. The qualitative quantification also provides the scope for further learning of the system behavior. In many situations, the output requirement may be approximate with blend of intuitive judgement of the human mind evolved through experience. Example for this is the tuning of musical instruments by a professional artist. In such situations the conventional models fail to represent the behavior of the system.

The qualitative model is the one that describes the system behavior through linguistic explanations. Zadeh's proposal of fuzzy sets [210] comes as a relief to deal with such a problem since it can model the fuzziness associated with the system definition and its behavior, through qualitatively defined system variables and with the mechanism of approximate reasoning. The fuzzy set theory finds its application in a variety of

engineering problems due to its capacity to model the impreciseness associated with observations and system definition, and to manipulate the required outputs for the engineering world.

It is also possible to model qualitatively the system behavior using the experts' knowledge of the system. Even though the model developed by an expert is able to represent the complete behavior of the system this is not possible in all the cases, and it will become expensive to develop another model when the requirements are changed. Hence, even the model by an expert, which may not be available in all cases, also loses its versatility and fails to accommodate new situations. Alternatively, in such situations, it will be more appropriate to evolve the system that has the automatic generation capability.

Zadeh's [210, 211] proposal of linguistic approach has the capability to model any complex system behavior in such a qualitative way that the model will be more effective and versatile in capturing the behavior of any ill-defined systems with fuzziness or fully defined systems with realistic approximations. Zadeh's approach was later developed for modeling fuzzy systems by Tong [182], Pedrycz [137], Trojan *et al.* [183], Sugeno and Kang [168], Takagi and Sugeno [175], Sugeno and Yasukawa [169], Yager and Filev [200, 201], Mamdani and Assilian [108], Bezdek [15], Bezdek *et al.* [16], Emami *et al.* [57] and Chiu [38, 39].

It is possible to identify the fuzzy system using the expert's knowledge of the system behavior expressed in terms of linguistic values or through *a priori* knowledge of the system. The *a priori* knowledge can be obtained through the mathematical understanding of the system behavior or through experimental input-output data of the system. Fuzzy system identification technique can solve both types of problems with ease. Fuzzy system modeling provides an approximate and yet effective means of describing the behavior of systems that are complex and ill-defined and consists of the following:

1. Identification and use of linguistic variables in place of or in addition to numerical variables
2. Representation of the behavior between the variables through conditional fuzzy statements
3. Characterization of the behavior of the entire system through fuzzy algorithms.

Modeling of fuzzy systems consists of two types, namely linguistic models (LMs) and fuzzy-non fuzzy models. Linguistic models are fully fuzzy in nature, having a collection of IF-THEN rules with vague predicates that use fuzzy reasoning [137, 182]. In this modeling, both antecedents and consequents are defined in terms of fuzzy quantities that can be associated with linguistic labels. Linguistic models can express the system behavior in a qualitative way using natural language [168]. Fully fuzzy linguistic modeling can be used for modeling the system from expert knowledge as well as *a priori* knowledge. When Mamdani [108] type of reasoning is used, the models are called Mamdani fuzzy models.

The second category of fuzzy modeling is based on the Takagi-Sugeno-Kang (TSK) method of reasoning [106, 143, 146, 203]. These TSK models have a set of rules that consist of fuzzy antecedents and functional consequent and they are a combination of fuzzy and nonfuzzy models. This method of reasoning has the ability to integrate both qualitative and quantitative knowledge representations, and to learn adaptively. Fuzzy models using the TSK reasoning will be called TSK fuzzy models and suitable for identification of system from *a priori* knowledge of the system.

In general, the system identification has two phases, namely, *structure identification* and *parameter identification* [38, 39, 57, 175, 201]. The structure identification involves identification of input and output variables, partitioning of input and output universes into fuzzy sets, number of fuzzy rules and selection of suitable reasoning mechanism for duplicating the system behavior. The parameter identification involves tuning of the parameters defining the fuzzy sets and the consequents. Both parameter and structure identification are common for both LM and TSK models.

Both types of fuzzy system identification is applied to boundary conditioning in this chapter. The fuzzy system identification is capable of modeling boundary conditioning response through linguistic values representing human intuitive judgement or through output classification and function approximation types of modeling.

A system subjected to boundary conditioning is a fuzzy system. The process of structural tuning is taken as an example of boundary conditioning concept and fuzzy logic is applied to identify the system of structural tuning through expert system modeling and auotogeneration fuzzy modeling.

4.1 EXPERT FUZZY MODELING OF STRUCTURAL TUNING

It was discussed in Chapter 3.3 that structural tuning through boundary conditioning is a general process in which the structural boundaries are suitably adjusted in order to get a desired vibratory or acoustic response [102, 103]. This technique has wide engineering applications in many areas dealing with structural control for various purposes. One such application is the manipulation of structural natural frequencies so as to stagger them away from excitation frequencies or to arrange them have specific ratios among themselves, through the tuning by boundary conditioning [103]. Most often the structural tuning operation is imprecise in nature due to both probabilistic uncertainty associated with the BC parameters describing the problem and fuzziness or vagueness associated with the problem definition itself. Modeling this problem needs a blend of intuitive judgement evolved through experience and engineering quantification.

As an example, a plate structure as shown in Figure 3.16 with edge supports represented by equivalent springs of both translational and rotational types [99], is studied in order to demonstrate fuzzy expert modeling of boundary conditioning. Quantification of the boundary conditions of actual structures is difficult by itself and hence the manipulation

of boundary conditions for the control of output is extremely fuzzy. In order to demonstrate the control of the structural behavior through the tuning procedure, a fuzzy model of the structural tuning of a square plate can be constructed from the analytical results that are obtained by the Rayleigh-Ritz analysis explained in Chapter 3. The output functions of harmonic objective functions can be estimated using the eigenvalues obtained from solving Equation 3.38. Different boundary conditions leading to structural tuning can be generated by different stiffness values of artificial springs on boundaries. The structural tuning by boundary conditioning thus means ensuring proper distribution of stiffness on the boundary so as to manipulate the natural frequencies of the structure and obtain the required frequency response.

4.1.1 Fuzzy Modeling Approach

The generalized fuzzy model consists of qualitative description of the system behavior using linguistic values such as *small, medium* or *high* which group the behavior into different categories. The linguistic description is given in the form of fuzzy algorithm representing the *knowledge base* characterizing the complete behavior of the system. Such a *knowledge base* consists of conditional statements called *rules* characterizing the input-output relationship of the system through linguistic values or fuzzy sets.

The fuzzy model of a system, developed on the basis of results of an analysis carried out using a mathematical model of the system and the expert's knowledge of the system behavior, is expressed in terms of *rules*. Consider a fuzzy system as shown in Figure 4.2

where the parametric domain is partitioned in order to formulate the rules. X_1 and X_2 are the input variables called antecedents, and A_i and B_i are fuzzy sets of X_1 and X_2. Y is the output or the consequent, and C_i could be a crisp value of output called a singleton, or a fuzzy set of the output. The relationship between the input space $(X_1 \times X_2)$ and the output space (Y) is given by many rules 'R_i' in IF-AND-THEN structure as shown in Figure 4.3.

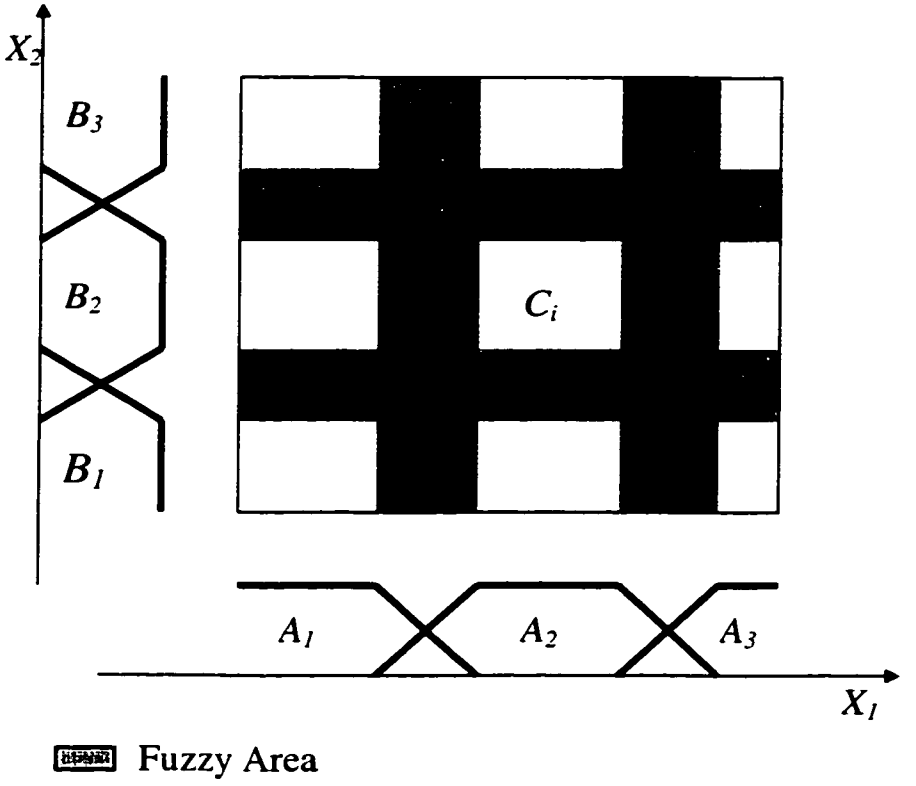

Figure 4.2: Scheme for fuzzy partitioning of input space

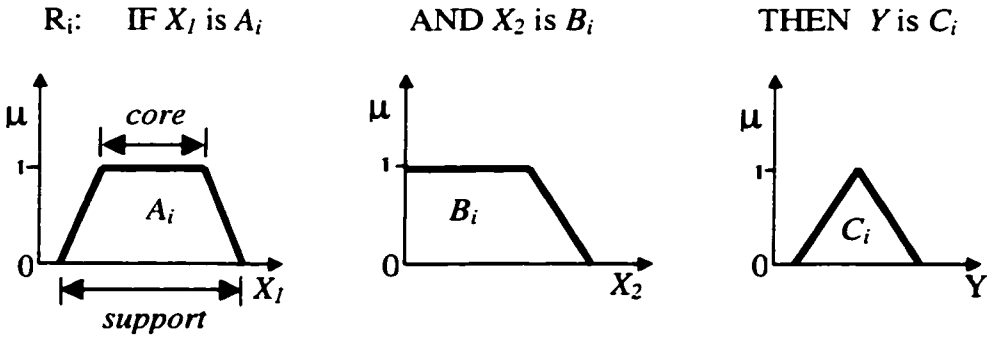

Figure 4.3: Scheme for a fuzzy rule

The complete system behavior could be represented by many such *rules* made of fuzzy sets. Intuitive judgement is needed in finding the *core* and *support* of the fuzzy sets, which are shown in Figure 4.3. *Core* is the range of an antecedent in which the possibility of obtaining the required output is certain and is represented with unit value of membership function or possibility distribution (μ). *Support* is the region of the antecedent outside of which there is no possibility of obtaining the required output. The *support* of a fuzzy set is represented by the range of an antecedent having a non-zero membership function. A fuzzy set with non-empty core, having a region of fuzzy set with unit membership function, is called normalized fuzzy set. In general, the development of a fuzzy model includes system parameter identification of the input and output, estimation of universes of input and output space, partitioning of these variables into fuzzy sets of linguistic values, formulation of *rule base* containing enough *rules*, and selection of suitable *inference* and *defuzzification* mechanisms representing the system behavior.

In the case of structural tuning, the input variables to represent the boundary conditioning of the structure and the output variable to represent the quality of the output must be defined. The output definition should also be used as criteria for fuzzy set definition. The understanding of the whole process of structural tuning involves a systematic generation of *rule base* or *knowledge base* in terms of input and output, and also the modeling of tuning of the input variable within the purview of the acquired *knowledge base* until the required harmonic combinations are obtained.

4.1.2 Selection of Input and Output Variables

In order to demonstrate the application of fuzzy logic, the objective for the structural tuning procedure in this study is chosen as the arrangement of the plate natural frequencies in a prescribed fashion, into a harmonic order. The desired harmonic combination is denoted by $h=1ijkl$ where i,j,k and l are eigenratios, which are the normalized 2^{nd}, 3^{rd}, 4^{th} and 5^{th} eigenfrequencies with respect to the fundamental eigenfrequency. When all these normalized eigenratios are integers they form harmonic combinations. The output objective function (Λ_h) for a harmonic combination $h=1ijkl$ is defined as,

$$\Lambda_h = \sum_{q=1}^{5}\left[\left(\frac{\sqrt{\lambda_q} - n_q\sqrt{\lambda_1}}{n_q\sqrt{\lambda_1}}\right)^2\right] \tag{4.1}$$

where

λ_q - q^{th} eigenvalue of the structure

$n = \{1, i, j, k, l\}$, set of harmonic combination.

A minimum value of the objective function for set 'n', represents a perfect harmonic combination h of the set 'n'. The value of Λ_h is a qualitative measure of the desired harmonic combination and it indicates the relative closeness of the arrangement of eigenfrequencies to a harmonic combination of $h=1ijkl$. A value of Λ_h close to zero indicates the availability of a desired harmonic combination while higher values indicate either the absence of the desired harmonic combination or the presence of other harmonic combinations.

Thus the input and output variables have been identified to represent the process of structural tuning. This example has some resemblance to the process of tuning a West Indian steel pan instrument where the tuning procedure is intuitive in nature and depends heavily on the expertise of the tuner. The fuzzy modeling of tuning a rectangular plate is explained in this paper as a general case of such structural tuning in terms of boundary stiffnesses and comprehensive harmonic function.

4.1.3 Estimation of the Universes of Input and Output Space

For various combinations of rotational stiffness $K_{R.i}^{\bullet}$ between 0 and 10^3 and translational stiffness $K_{T.i}^{\bullet}$ between 0 and 10^5, the possibility of obtaining the natural frequencies in different harmonic combinations to a reasonable accuracy was studied for a square plate using the already defined output function (Λ_h), given by the Equation (4.1). The variation of stiffnesses beyond these limits have insignificant effect on the response.

By minimizing Λ_h, it is possible to bring the natural frequencies close to a required harmonic combination '*h*'. The minimum value of Λ_h represents the limit of the acceptance quality to distinguish between harmonic combinations and hence the quality of the output itself. In an eight dimensional input space of four rotational stiffnesses ($K_{R.i}^{\bullet}$ where i=1,2,3,4) and four translational stiffnesses ($K_{T.i}^{\bullet}$ where i=1,2,3,4), and in the range of $K_{R.i}^{\bullet}$ between 0 and 10^3 and $K_{T.i}^{\bullet}$ between 0 and 10^5, all possible optimal

harmonic combinations were estimated using the approach explained in Section 3.3 through a parametric study at discrete stiffness values of $K_{T,i}^{*}$ and $K_{R,i}^{*}$ of the springs at the four edges. The different sets of optimal harmonic combinations for the square plate by boundary conditioning of the four edges with $\Lambda_h \leq 0.02$ are 12345, 12356, 12236, 13346, 13356, 13357, 13358 and 13368.

The minimum value of Λ_h for a set of harmonic combinations obtained by input parametric search corresponds to the optimum boundary condition for that set of harmonic combination. These stiffness values of the springs at the edges could be called the reference values for the desired harmonic combination. The deviation from this minimum Λ_h as boundary conditions (stiffness) are changed from the reference values, indicates either the destruction of the present harmonic combination or the presence of other harmonic combinations leading to the movement of harmonic patterns in the output space, which is what exactly happens during the process of structural tuning. The fuzzy model of the structural tuning process should be able to capture the movement of harmonic patterns through the input space. The modeling is focused on 1335X series of harmonic combinations with only two antecedents $K_{R,1}^{*}$ and $K_{R,2}^{*}$ for simplicity while the other antecedents are kept at the reference values that are same for all the selected harmonic combinations. In order to capture the influence of simultaneously varying the antecedents and to capture the movement of harmonics pattern over the antecedent space, it was decided to study only two antecedents at a time on 1335X harmonic series for the design of fuzzy system. This, however, limited the available harmonic combinations to 13358 and 13357, while 13356 was impossible to achieve. Hence in the present study

13356 is substituted by the eigenratio combinations 13356.6 where l=6.6. Even though the 2nd and the 3rd normalized eigenratios correspond to the 3rd harmonic ratio, they are considered separately in the harmonic definition. In order to study only the influence of $K^*_{R.1}$ and $K^*_{R.2}$ on the above harmonic functions, all boundary stiffnesses other than $K^*_{R.1}$ and $K^*_{R.2}$ are kept at the following reference values established through parametric search:

$K^*_{T.1} = 10^5, K^*_{T.2} = 10^5, K^*_{T.3} = 10$, $K^*_{T.4} = 10$, $K^*_{R.3} = 10$ and $K^*_{R.4} = 10$.

This condition yielded the minimum objective function for all the three harmonic patterns. The two antecedents $K^*_{R.1}$ and $K^*_{R.2}$ are varied simultaneously over the entire input space and the corresponding harmonic objective functions are predicted using the mathematical model explained in the previous chapter. The subjective generation of a *rule base* representing the behavior of a system involves the intuitive judgement of an expert and hence it becomes complicated apart from the increase in size of the *rule base* when the number of antecedents becomes more and especially when the antecedents are interactive in nature. A method for automatic generation of *rule base* will be required when the number of antecedents is large. As the present study aims at modeling only the mechanism behind structural tuning through parametric quantification, two antecedents approach is selected for fuzzy modeling.

4.1.4 Fuzzification and Design of *Rule Base* for a Two Antecedent System

The harmonic sets of different combinations 13358, 13357 and 13356.6 selected for the present study can be represented by linguistic values namely $\#T_1$, $\#T_2$ and $\#T_3$,

respectively. The axonometric plots of comprehensive objective functions Λ_{13358}, Λ_{13357} and $\Lambda_{13356.6}$ are given in Figures 4.4a, 4.5a and 4.6a respectively. The contour plots of comprehensive objective functions Λ_{13358}, Λ_{13357} and $\Lambda_{13356.6}$ are shown in Figures 4.4b, 4.5b and 4.6b, respectively. The variation of the minimum of these three objective functions over the antecedent space is shown in Figure 4.7. This figure also shows a smooth movement between the tones and also the regions of domination of distinct harmonic combinations over the input space. It is now up to the judgement of the expert to form fuzzy linguistic sets from the analytical results, which would invariably represent the physical system. The expert's intuition involves judging the thresholds of the objective function and also the structure of the membership function.

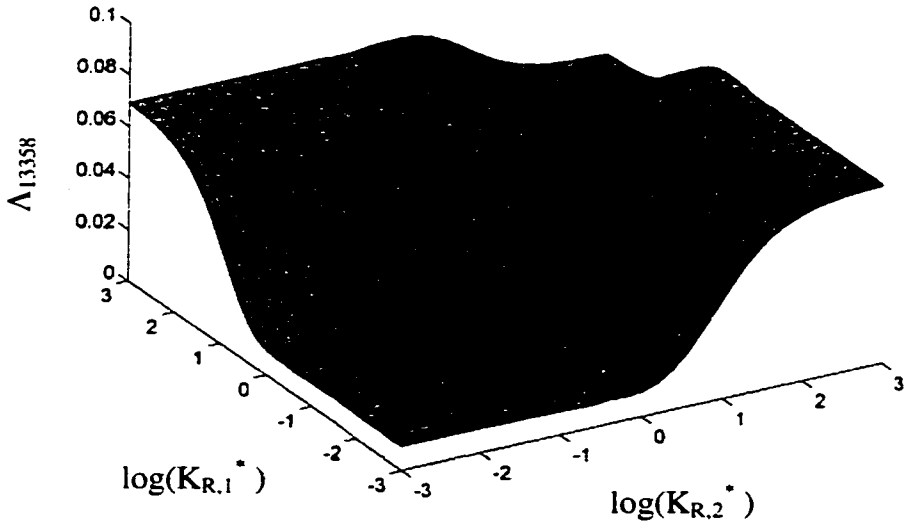

Figure 4.4a: Axonometric plot of objective function Λ_{13358}

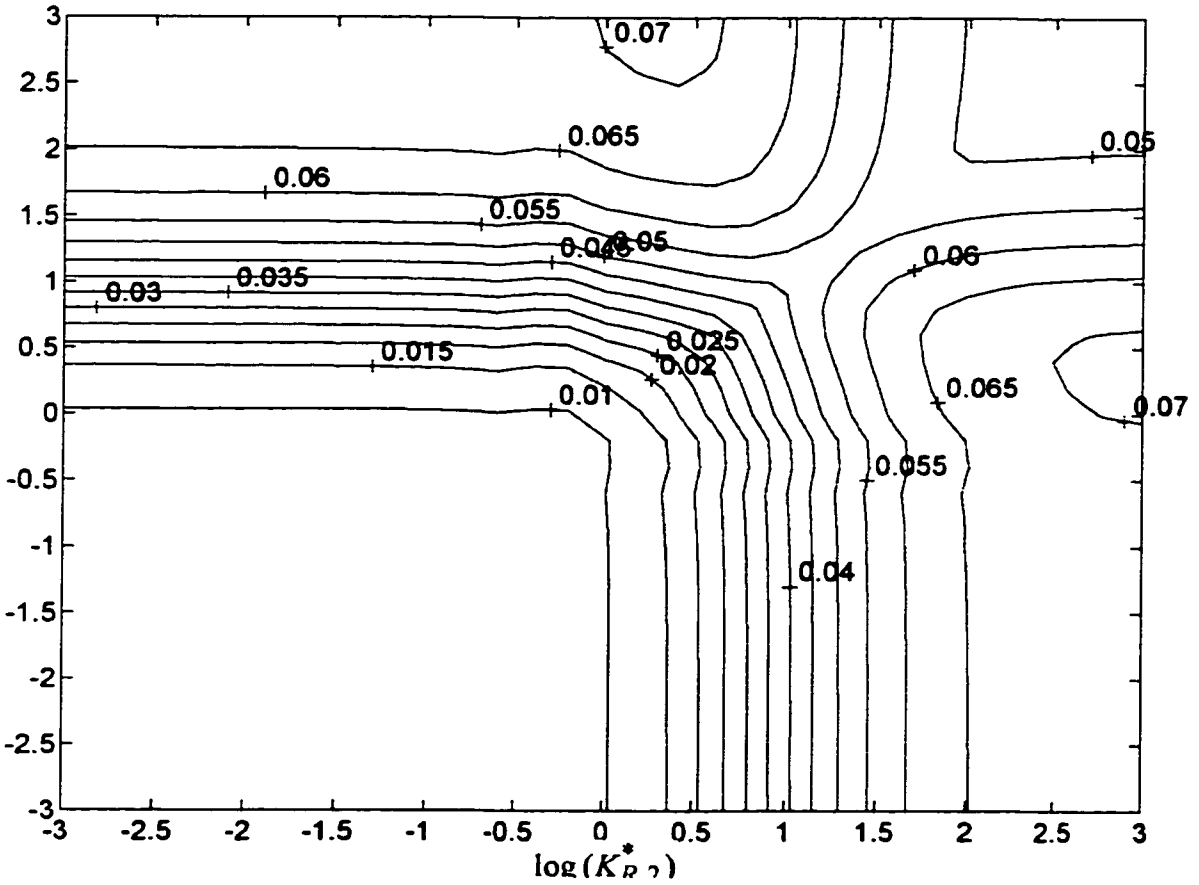

Figure 4.4b: Contour plots of objective function Λ_{13358}

Figure 4.4

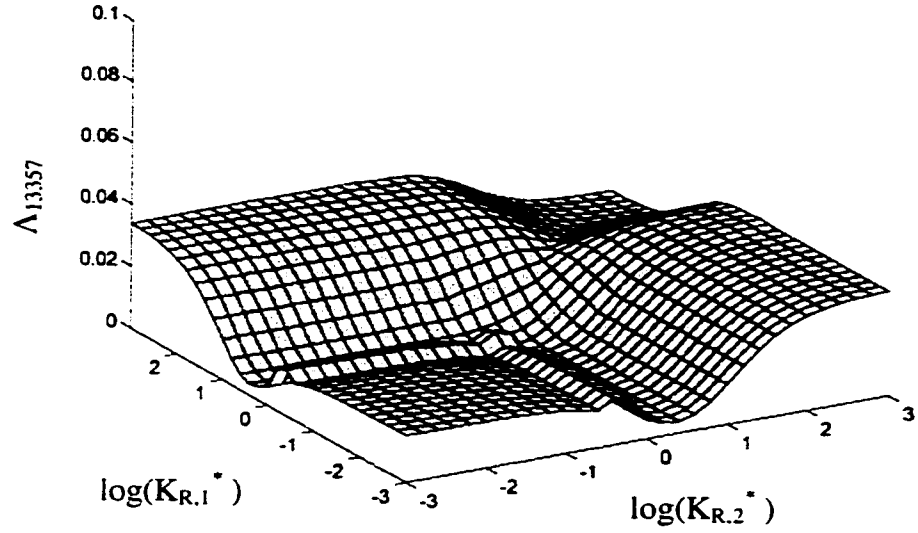

Figure 4.5a: Axonometric plot of objective function Λ_{13357}

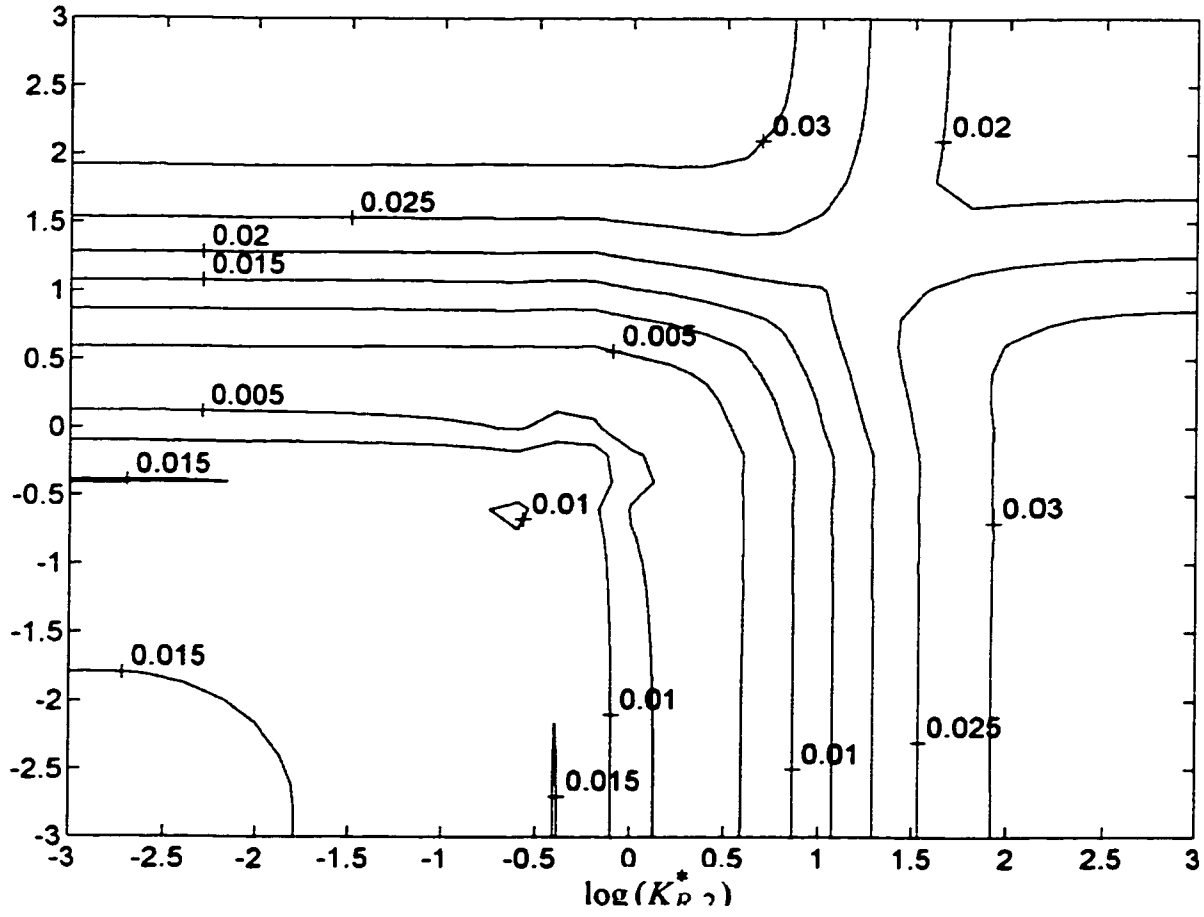

Figure 4.5b: Contour plots of objective function Λ_{13357}

Figure 4.5

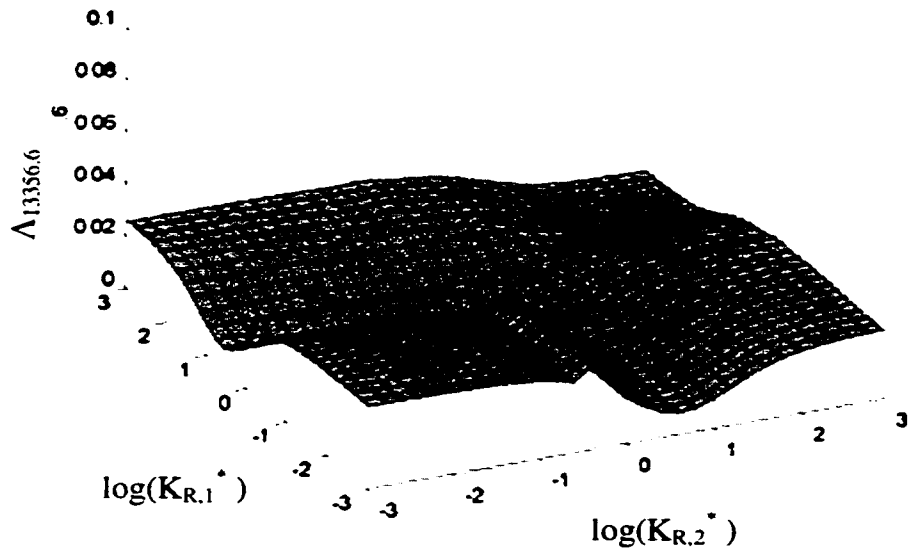

Figure 4.6a: Axonometric plot of objective function $\Lambda_{13356.6}$

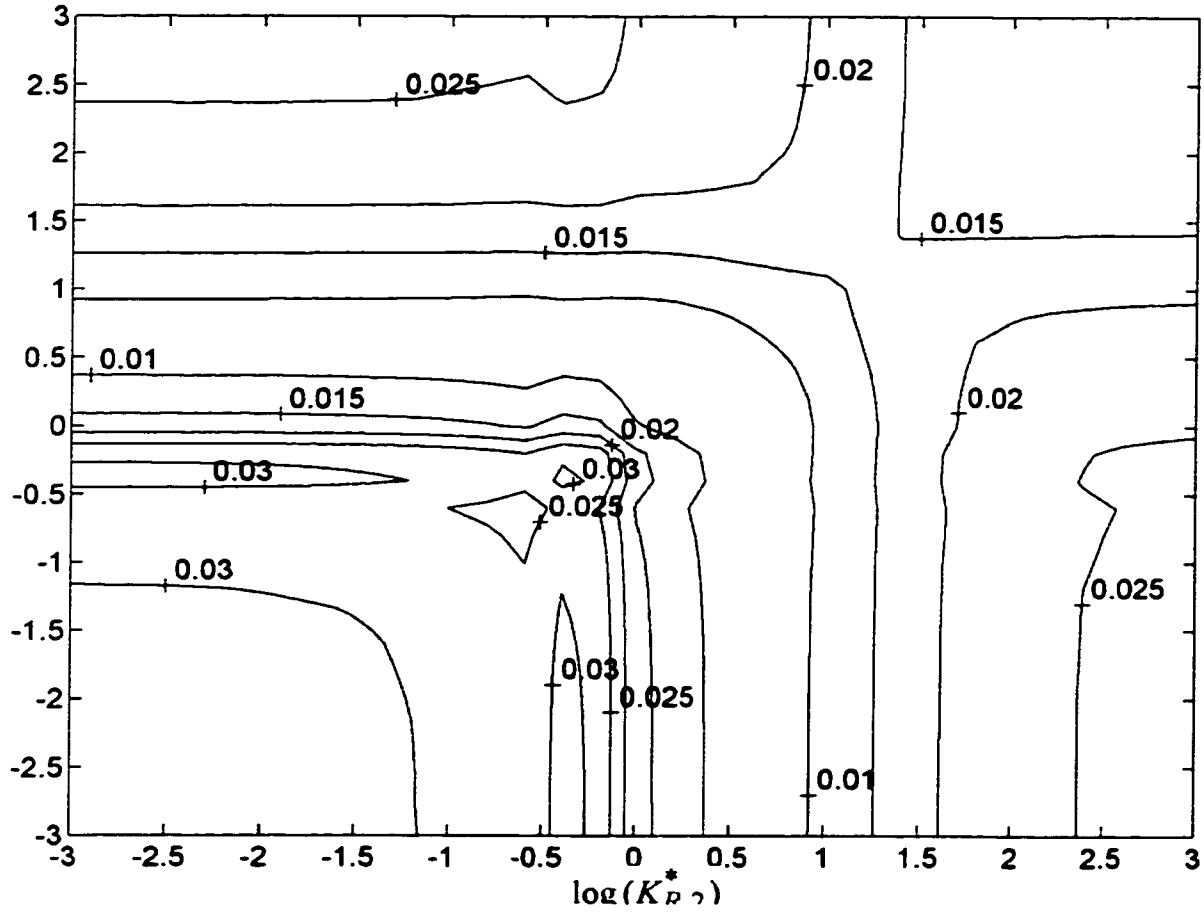

Figure 4.6b: Contour plots of objective function $\Lambda_{13356.6}$

Figure 4.6

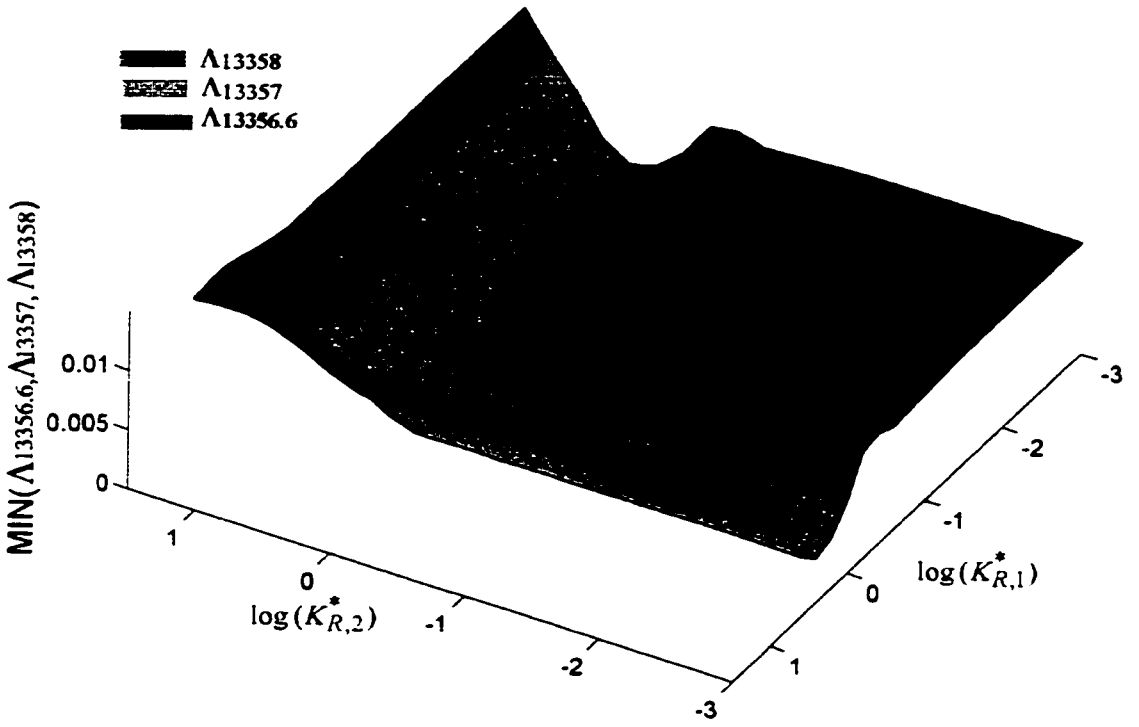

Figure 4.7: Axonometric plot of minimum of objective functions Λ_{13358}, Λ_{13357} and$\Lambda_{13356.6}$

The thresholds of objective functions defining *core* and *support* are equivalent to the intuitive capability of the expert in fixing the quality of the tones. Hence, there is a flexibility in selecting the thresholds in fuzzy modeling of structural tuning. During the parametric study of the influence of $K^{\bullet}_{R.1}$ and $K^{\bullet}_{R.2}$ on objective functions, a maximum variation of 8% was found in normalized eigenratios with reference to perfect harmonic eigenratios for $\Lambda_h \leq 0.009$ while the maximum variation was 11% for $\Lambda_h \leq 0.015$. Different thresholds of objective functions depending upon the expert's requirement will result in different fuzzy models. Hence a value of $\Lambda_h = 0.009$ was used for the definition of *core* representing the intuitive upper limit in order to indicate the presence of a perfect combination of harmonics *h=1ijkl*. The objective function of $\Lambda_h \leq 0.009$ indicates the full possibility of getting this harmonic combination and it is represented by a unit value of membership function or possibility distribution. The range of input antecedents $K^{\bullet}_{R.1}$ or $K^{\bullet}_{R.2}$ resulting in $\Lambda_h \leq 0.009$ forms the *core* of the fuzzy set representing a linguistic value. For the *support*, a value of $\Lambda_h = 0.015$ is selected to indicate the beginning of the absence of a given set of harmonic combination. The objective function of $\Lambda_h \geq 0.015$ represents the impossibility of achieving the given set of harmonic combination and the range of antecedents $K^{\bullet}_{R.1}$ or $K^{\bullet}_{R.2}$ resulting in this objective function of $\Lambda_h \geq 0.015$ is represented by zero value of membership function. The range of input antecedents resulting in the harmonic function of a value between 0.009 and 0.015 indicates the partial possibility or fuzziness in obtaining the required set of harmonic combination. There are different types of variations of membership function

in the possible range. A linear variation of possibility function forming trapezoidal or triangular fuzzy set is selected in this study to define the linguistic values.

The values of objective function selected for the definition of the *core* and *support* of fuzzy sets are 0.009 and 0.015 as represented below:

$$\begin{aligned} Core(A) &= \left\{ x_i \in X_i \mid \quad \Lambda_{1ijkl} \le 0.009 \right\} \\ &= \alpha \quad cut \ of \quad \Lambda_{1ijkl} \\ &= \Lambda_{1ijkl}^{0.009} \end{aligned} \tag{4.2}$$

and

$$\begin{aligned} Supp(A) &= \left\{ x_i \in X_i \mid \quad \Lambda_{1ijkl} < 0.015 \right\} \\ &= \alpha \quad cut \ of \quad \Lambda_{1ijkl} \\ &= \Lambda_{1ijkl}^{0.015} \end{aligned} \tag{4.3}$$

where A can be any fuzzy set of input variable $K_{R.1}^{\bullet}$ and $K_{R.2}^{\bullet}$ and X_i is the input space of $K_{R.1}^{\bullet}$ and $K_{R.2}^{\bullet}$.

The fully normalized fuzzy sets representing the linguistic values of LOW, MEDIUM and HIGH of the input antecedents $K_{R.1}^{\bullet}$ and $K_{R.2}^{\bullet}$, obtained from the analytical results using the above definition of *core* and *support* are shown in Figure 4.8. As the harmonic combinations 13358, 13357 and 13356.6 differ mainly in the 5th eigenratio, the fuzzy sets of output objective functions are represented around the dominating ratio of the 5th eigenvalue as shown in Figure 4.9. Due to the comprehensive nature of the output

objective function, its fuzzy sets can represent linguistic values of different tones like $\#T_1$, $\#T_2$ and $\#T_3$.

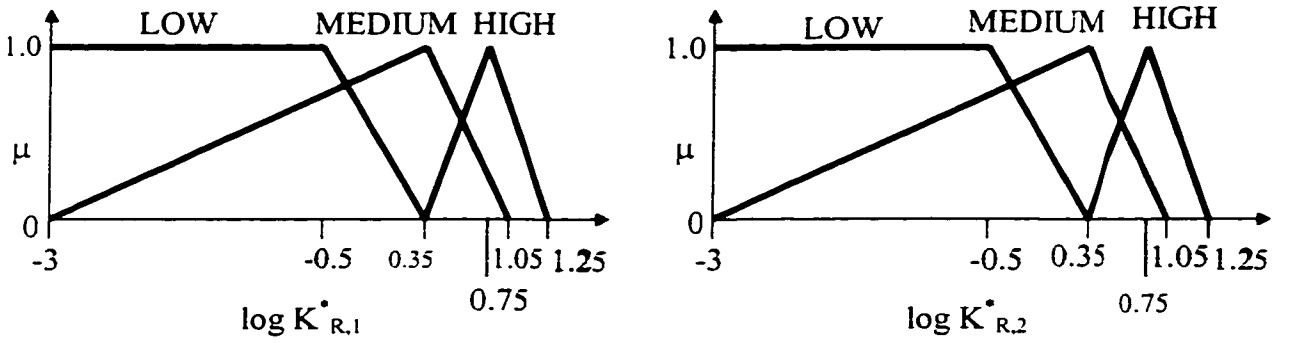

Figure 4.8: Fuzzy sets of input

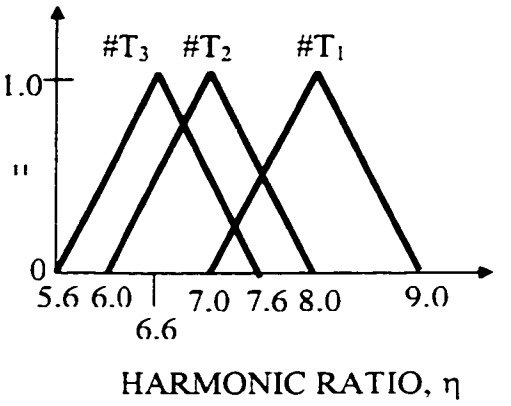

Figure 4.9: Fuzzy sets of output harmonic ratios

The following *rule base* was obtained subjectively from the analytical results to represent the relationship between the input and output space in terms of linguistic values:

RULE 1: **IF** $K^{\bullet}_{R.1}$ *is LOW* **AND** $K^{\bullet}_{R.2}$ *is LOW* **THEN** *HARMONICS is* *13358* ($\#T_1$)

RULE 2: **IF** $K^{\bullet}_{R.1}$ *is LOW* **AND** $K^{\bullet}_{R.2}$ *is MEDIUM* **THEN** *HARMONICS is* *13357* ($\#T_2$)

RULE 3: **IF** $K^{\bullet}_{R.1}$ *is MEDIUM* **AND** $K^{\bullet}_{R.2}$ *is LOW* **THEN** *HARMONICS is* *13357* ($\#T_2$)

RULE 4: **IF** $K^{\bullet}_{R.1}$ *is MEDIUM* **AND** $K^{\bullet}_{R.2}$ *is MEDIUM* **THEN** *HARMONICS is* *13357* ($\#T_2$)

RULE 5: **IF** $K^{\bullet}_{R.1}$ *is LOW* **AND** $K^{\bullet}_{R.2}$ *is HIGH* **THEN** *HARMONICS is* *13356.6* ($\#T_3$)

RULE 6: **IF** $K^{\bullet}_{R.1}$ *is MEDIUM* **AND** $K^{\bullet}_{R.2}$ *is HIGH* **THEN** *HARMONICS is* *13356.6* ($\#T_3$)

RULE 7: **IF** $K^{\bullet}_{R.1}$ *is HIGH* **AND** $K^{\bullet}_{R.2}$ *is HIGH* **THEN** *HARMONICS is* *13356.6* ($\#T_3$)

RULE 8: **IF** $K^{\bullet}_{R.1}$ *is HIGH* **AND** $K^{\bullet}_{R.2}$ *is MEDIUM* **THEN** *HARMONICS is* *13356.6* ($\#T_3$)

RULE 9: **IF** $K^{\bullet}_{R.1}$ *is HIGH* **AND** $K^{\bullet}_{R.2}$ *is LOW* **THEN** *HARMONICS is* *13356.6* ($\#T_3$)

The *rule base* for various harmonic combinations could be different based on the intuitive capability quantified by the values of objective function defining the *core* and the

support. The *rule base* is able to exhibit the symmetric influence of rotational stiffnesses $K^{\bullet}_{R.1}$ and $K^{\bullet}_{R.2}$ on the harmonic combinations. Due to symmetric nature of the behavior, the swapping of fuzzy sets between two antecedents results in the same harmonic combinations. For example, LOW - LOW for 13358, LOW -MEDIUM and MEDIUM - MEDIUM for 13357, and LOW - HIGH, MEDIUM - HIGH and HIGH - HIGH for 13356.6.

4.1.5 Design of *Mamdani Inference* Mechanism

In general, for a system of two antecedents and one consequent, the i[th] rule R_i in the form

IF $K^{\bullet}_{R.1}$ is A_i ***AND*** $K^{\bullet}_{R.2}$ is B_i ***THEN*** harmonics is C_i

can be written as

$$R_i: \qquad (A_i \cap B_i) \Rightarrow C_i \tag{4.4}$$

where A_i and B_i are fuzzy sets of linguistic values of input variables $K^{\bullet}_{R.1}$ and $K^{\bullet}_{R.2}$, respectively. AND is represented by a conjunction operator $\cap$ at the computational level. The consequent C_i is the fuzzy set of linguistic value C_i (#T_i) for the i[th] rule. When the boundary conditions dealing with two antecedents $K^{\bullet}_{R.1}$ and $K^{\bullet}_{R.2}$ are changed, one can intuitively predict the resultant response of the system. The *inference* mechanism of approximate reasoning used for the prediction of a new conclusion from the rule base for a given set of new facts in antecedent space, includes inference of conclusion from each rule and combination of inferred conclusions from all rules. The basic rule of *inference* in fuzzy logic is Generalized Modus Ponens (GMP) [212]. Application of GMP

inference representing the mechanism of approximate reasoning in the structural tuning for a given fact of A' and B' will result in a conclusion C_i^* from the i^{th} rule as,

$$C_i^* = \left(A' \cap B'\right) \bullet \left[\left(A_i \cap B_i\right) \Rightarrow C_i \right] \tag{4.5}$$

where A' is a value of $K_{R.1}^*$, B' is a value of $K_{R.2}^*$, $\bullet$ denotes composition, $\cap$ denotes conjunction and $\Rightarrow$ denotes an implication.

The combination of conclusion C_i^* from all the available rules will result in a final conclusion, representing the complete system response. Combination of conclusions selected in this paper to get the final conclusion from all rules is,

$$C^* = \text{Combination}\left(C_i^*\right) = \oplus C_i^* \tag{4.6}$$

where $\oplus$ is a combination operator of conjunction or disjunction type.

Even though, a generalized framework [49, 50] is available for the selection of fuzzy operators, Mamdani type inference [108] is used in this study due to singleton inputs for representing the process of structural tuning with the following operators:

$$\bigcup_i = MAX\,,\ \cap = MIN \ \ and \ \ \Rightarrow = MIN$$

The *inference* mechanism using Mamdani type approximate reasoning is illustrated in Figure 4.10 with only two rules for clarity. a' and b' are the singleton inputs of rotational stiffnesses $K_{R.1}^*$ and $K_{R.2}^*$, respectively. The singleton inputs fire all the relevant rules in the *rule base.* Firing of only two rules is shown in Figure 4.10 as an example. The firing strength, f_i, of each rule is the minimum of the membership function of fuzzy sets A_i and B_i at a' and b' , respectively, given by

$$f_i = MIN\left(\mu_{A_i}(a'), \mu_{B_i}(b')\right) \tag{4.7}$$

The conclusion obtained from each rule C_i^* is shown by the shaded area in the corresponding fuzzy output C_i for Mamdani type *inference* where

$$C_i^* = MIN(f_i, C_i) \tag{4.8}$$

The *conclusions* obtained using only two *rules* are shown in Figure 4.10. Similarly, *conclusions* are generated from all the nine *rules* of the *rule base.* The combined conclusion for two *rules* is shown as the addition of shaded regions obtained by MAX operation as per the Equation (4.6) in Figure 4.10.

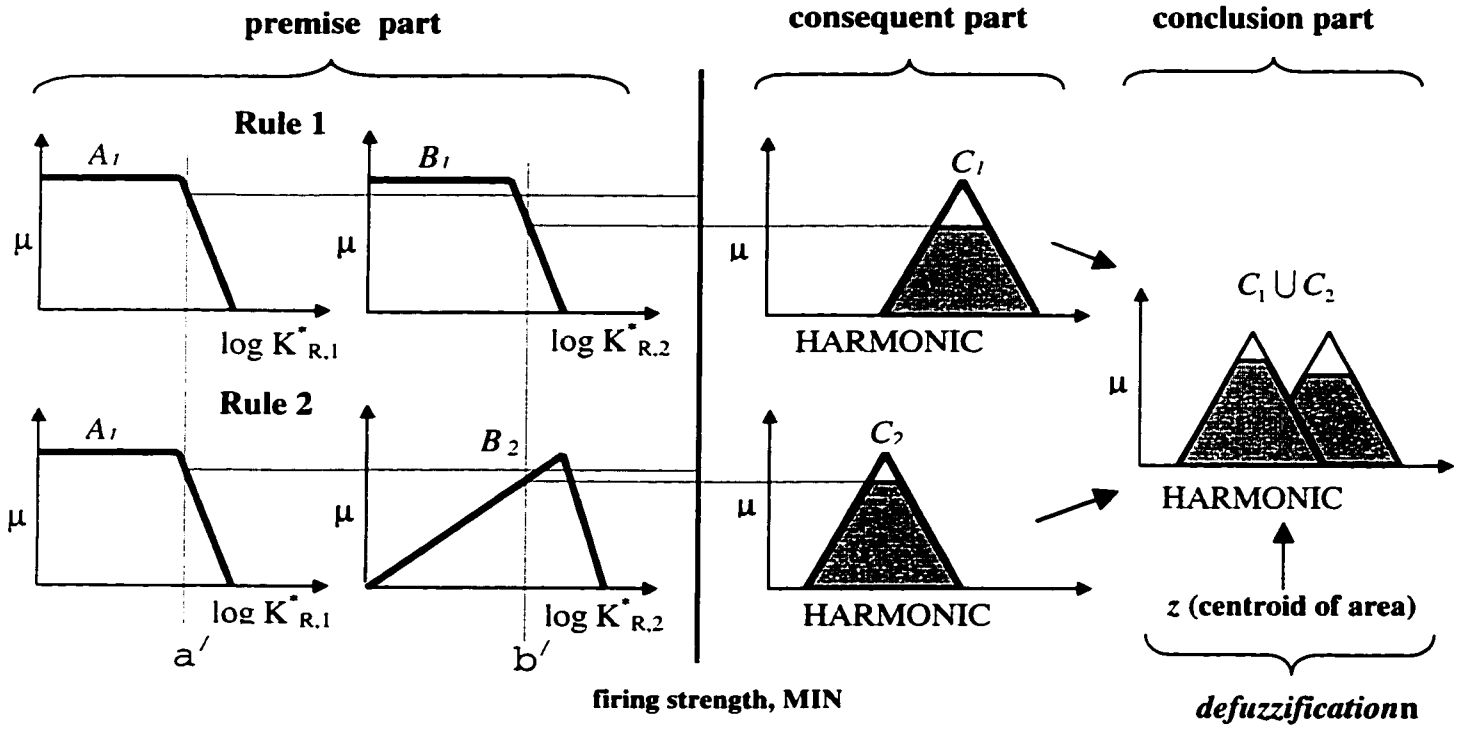

Figure 4.10: Mamdani type approximate reasoning

Once the aggregation of conclusions from all the rules is obtained, it is defuzzified using *center of gravity* method which outputs the centroid of fuzzy area corresponding to the

final conclusion. The *defuzzified* crisp output z, in terms of the output harmonic ratio η, is obtained by the equation

$$z(\eta) = \frac{\int_{-\infty}^{\infty} \mu_{C^*}(\eta) \cdot \eta \cdot d\eta}{\int_{-\infty}^{\infty} \mu_{C^*}(\eta) \cdot d\eta} \tag{4.9}$$

Integration is replaced by summation for discrete values of η.

4.1.6 Verification of the Expert Fuzzy Model

The verification of the fuzzy model is presented in this section in order to check whether the model outputs the harmonic ratio close to analytical value or not. *Inference* followed by *defuzzification* is carried out to generate a control surface of defuzzified value of fifth eigenvalue ratio by providing the singleton facts for both antecedents covering the entire input space. The comparison between the analytical results and the defuzzified values of the dominating harmonic ratio of the 5^{th} eigenvalue η, given in Table 4.1, at a few input values shows good agreement.

Table 4.1 Comparison of defuzzified dominating harmonic ratio, η

$K^{*}_{R.1}$	$K^{*}_{R.2}$	ANALYTICAL	FUZZY MODEL
10^{-3}	10^{-3}	7.626	8
10^{-2}	10^{-2}	7.621	7.690
10^{-1}	10^{-1}	7.572	7.551
1	1	7.203	7.380
10	10	6.480	6.642

As the output variable of the analytical method is the comprehensive objective function, objective function is calculated from the defuzzified values of the harmonic ratio as given below;

$$\Lambda_{13358} = \left[\frac{\eta - 8}{8}\right]^2$$

$$\Lambda_{13357} = \left[\frac{\eta - 7}{7}\right]^2 \text{ and} \qquad (4.10)$$

$$\Lambda_{13356.6} = \left[\frac{\eta - 6.6}{6.6}\right]^2.$$

The variation of the least value of the three defuzzified objective harmonic functions is shown in Figure 4.11 indicating the movement of harmonics pattern and also the dominating regions of respective harmonics. This inference is in close agreement with analytically predicted variation as shown in Figure 4.7 over larger area of the stiffness space. The slight mismatch in the input range of $\log(K^{*}_{R.1})$ or $\log(K^{*}_{R.2})$ between 1.05 and 1.25 is due to the non-availability of competing fuzzy sets of nearby harmonic ratios indicating the absence of 1335X series as a dominating harmonic combination or the presence of a new dominating harmonic series in that range of input stiffnesses. This limitation may be due to the modeling of only parts of output domain of harmonic series

and input domain of boundary stiffnesses. It is considered acceptable since this chapter attempts only to demonstrate the application of fuzzy logic to capture the fuzziness of boundary conditioning used in structural tuning. Thus the fuzzy model developed based on Mamdani type *inference* is able to capture the movement of harmonics pattern by structural boundary conditioning. The fuzzy model is shown to be good for establishing the relationship between boundary stiffnesses and required harmonics including the symmetric effects of stiffnesses as shown in this study. The prediction of minimum objective function by the fuzzy model could also be used as a control surface for achieving the required harmonic combination through controlling the boundary stiffnesses.

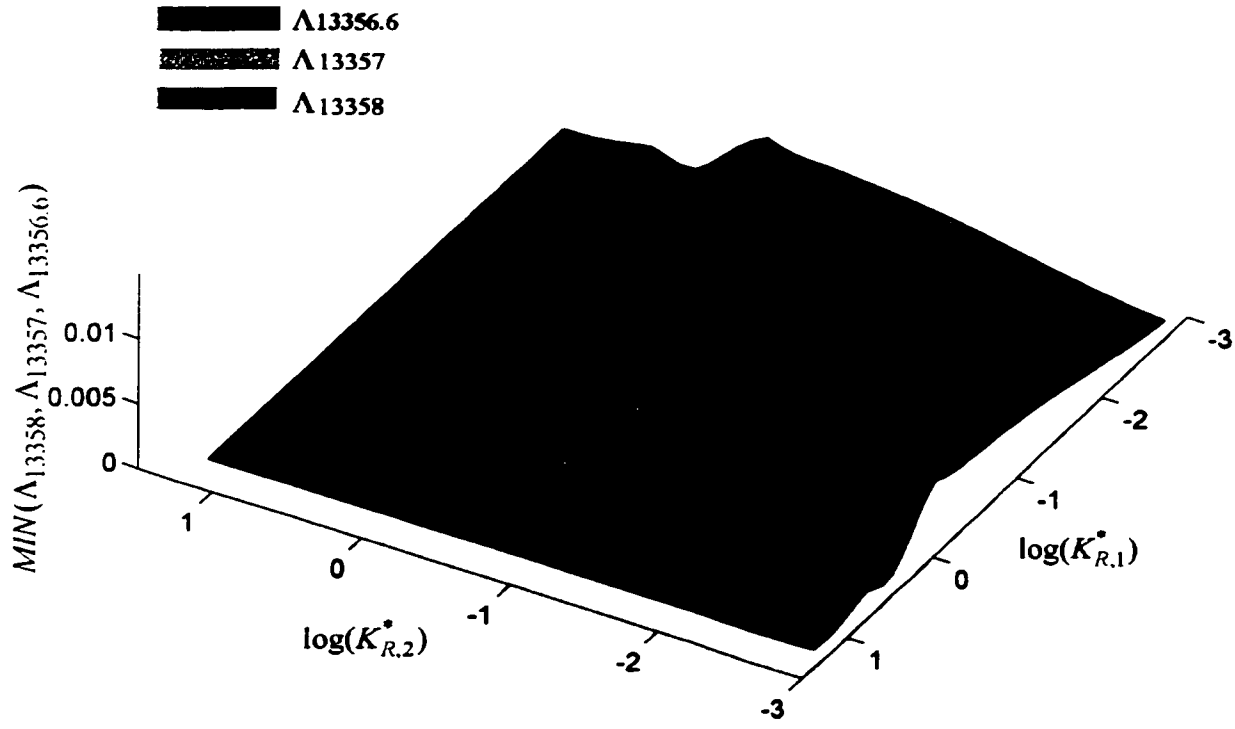

Figure 4.11: Defuzzified variation of minimum of objective functions Λ_{13358}, Λ_{13357} and $\Lambda_{13356.6}$

An expert fuzzy *rule base* has been successfully developed in terms of fuzzy linguistic values to represent structural tuning. The fuzzy rule base can be used for classification and function approximation. Even though the model developed by an expert is able to represent the complete behavior of the system, it will become expensive to develop another model when the requirements are changed. Hence, even the model by an expert, which may not be available in all cases, loses its versatility and fails to accommodate new situations. The expert modeling lacks the auto generation capability and hence the application is limited whenever the number of antecedents and consequents are large, and the antecedents are mixed with noisy variables or insignificant antecedent, resulting in system behavior changes in due course of time.

Presence of too many conditioning variables as could be the case of a real working system will make the manipulation of a required vibration performance difficult. Hence, it becomes important to identify only the relevant conditioning parameters corresponding to required vibration performance measures such as natural frequencies, eigenratios, mode shapes etc. and hence the manipulation of required vibration performance is possible leading better control of vibration performance or enhancement of the system behavior. These requirements also call for prediction of relationship, between the required output dynamic behavior and the related conditioning parameters, which is generally non-linear in nature.

Alternatively, in such situations, it will be more appropriate to evolve the system model from *a priori* knowledge of the system using a technique that has the automatic

generation capability. The *a priori* knowledge can be obtained through the mathematical understanding of the system behavior or experimental input-output data for the system. The data could be obtained using perfect mathematical modeling or from expert's knowledge or from experimental measurements on the system. In such situations, the system identification can be done by a clustering technique which involves grouping of data into clusters of similar behavior and evaluating system behavior from these clusters. As these data can also contain uncertainties and vagueness, a suitable approach is essential in order not to miss any information about the system.

4.2 HIGHER ORDER FUZZY SYSTEM IDENTIFICATION USING SUBTRACTIVE CLUSTERING

In general, system identification could represent any complicated input/output function approximation, output classification or input-output mapping. In any case, the system identification has to be automatic in order to make it more versatile and amenable for further learning. The clustering technique is used in this thesis for automatic generation of rules, in which each cluster represents a group of associated data in a data space and also a rule in the knowledge base of the system. Fuzzy identification of systems invariably uses fuzzy partitioning or fuzzy grouping in data space based on certain measures. It is assumed that each data point in a data space has equal contribution towards system identification and hence the grouping of data into clusters is determined by density of the data based on a search criterion. The relative positioning of a data into different clusters depends on the measure it scored with reference to different cluster centers. A data point that scored the extreme search measure represents a cluster center.

The identification of the system becomes easier when the number of data is large such that the system is represented enough over the entire data space and data is also reliable without noise and insignificant variables. The accuracy of the model in relation to system behavior depends on the relative availability [48] of the data points in relation to the complexity of the system behavior. Hence, the minimum number of data required in order to capture the complete behavior of the system becomes problem dependent. When the data space is densely populated, the system behavior at any part of the input domain could be easily predicted using the system behavior at nearby points. But, this is not the case when the scarcity of the data increases where the system behavior at any point has to be modeled using the system response at farther data points. This demands the clustering technique to be capable of evolving a reasonable model with available partial number of data without losing the global behavior of the system.

A cluster of data in input-output data space represents a grouping of data points with related behavior and hence each cluster represents a part of the system behavior in a phenomenological domain, which is the behavior of the cluster center itself. As each cluster is responsible for capturing a particular aspect of the system behavior, in general, higher number of clusters may represent the system in a better way. The data space can include many inputs and outputs. The fuzzy system could be of multi-input-multi-output (MIMO) type with many antecedents and many consequents or multi-input-single-output (MISO) type with many antecedents and single consequent.

4.2.1 System Identification

In general, the identification of the system involves structure identification and parameter identification. The structure identification consists of initial rule generation after elimination of insignificant variables [169, 57], in the form of IF-THEN-ALSO rules in terms of fuzzy sets of data dimensions which would approximate the final rule base. Parameter identification may include tuning of membership function of variables or parameters responsible for the reasoning process based on certain objective criterion. When input-output data are available *a priori*, clustering is a technique that can be used for structure identification due to its automatic generation capability. Fuzzy clustering is applied in this thesis for identification of the system. Clustering is basically fuzzy partitioning of the data space, which could be of the type either MIMO or MISO.

The fuzzy model of MIMO systems of m inputs and r outputs defined with N rules can be written as

$$R^1 : IF\ x_1 \text{ is } A_1^1 \text{ AND } x_2 \text{ is } A_2^1 \text{ AND} \ldots \text{AND } x_m \text{ is } A_m^1 \text{ THEN } y_1 \text{ is } B_1^1 \text{ AND } y_2 \text{ is } B_2^1 \text{ AND} \ldots \text{AND } y_r \text{ is } B_r^1$$

$$ALSO$$

$$\vdots$$

$$ALSO$$

$$R^N : IF\ x_1 \text{ is } A_1^N \text{ AND } x_2 \text{ is } A_2^N \text{ AND} \ldots \text{AND } x_m \text{ is } A_m^N \text{ THEN } y_1 \text{ is } B_1^N \text{ AND } y_2 \text{ is } B_2^N \text{ AND} \ldots \text{AND } y_r \text{ is } B_r^N \tag{4.10}$$

while for the case of MISO systems, fuzzy rule base is the same with $r = 1$,

where $x_1, x_2, \ldots, x_m$ are m antecedents and $y_1, y_2, \ldots, y_r$ are r consequents. R^i represents the i'th rule, A_i^j *for* $(i = 1,2,\ldots,m)$ and $(j = 1,2,\ldots,N)$ are linguistic fuzzy sets of input variables and B_i^j *for* $(i = 1,2,\ldots,r)$ *and* $(j = 1,2,\ldots,N)$ are linguistic fuzzy sets of consequents.

In these models, both antecedent and consequent parts of the IF-THEN-ALSO rules consist only of fuzzy sets. In the other type of model which is the combination of fuzzy and nonfuzzy modeling proposed by Takagi and Sugeno [175] which is called TSK [201] fuzzy model, the consequent part is expressed as a linear combination of antecedents as given below for both MIMO and MISO systems.

In TSK modeling, a MIMO system with N rules, m antecedents and r consequents can be expressed as

$$\begin{aligned} R^1 : IF\ x_1 \text{ is } A_1^1 \text{ AND } x_2 \text{ is } A_2^1 \text{ AND} \ldots \text{AND } x_m \text{ is } A_m^1 \text{ THEN } y_1 &= P_{10}^1 + P_{11}^1 x_1 + \ldots + P_{1m}^1 x_m \\ \text{AND} \ldots \text{AND } y_r &= P_{r0}^1 + P_{r1}^1 x_1 + \ldots + P_{rm}^1 x_m \\ ALSO & \\ \vdots & \\ ALSO & \end{aligned}$$

$$R^N : IF\ x_1 \text{ is } A_1^N \text{ AND } x_2 \text{ is } A_2^N \text{ AND} \ldots \text{AND } x_m \text{ is } A_m^N \text{ THEN } y_1 = P_{10}^N + P_{11}^N x_1 + \ldots + P_{1m}^N x_m$$

$$\text{AND} \ldots \text{AND } y_r = P_{r0}^N + P_{r1}^N x_1 + \ldots + P_{rm}^N x_m \qquad (4.11)$$

When $r = 1$, this rule base represents a MISO system.

where P_{ij}^{k} $for (i = 1,2,....,r; j = 0,1,....,m; k = 1,2,....,N)$ are consequent regression parameters that are optimized by least square estimation (LSE) given by Takagi and Sugeno [175]. Even though both fuzzy and TSK modeling are possible through clustering technique, TSK model is used in this thesis.

4.2.2 System Identification using Fuzzy Clustering

The identification of the system using fuzzy clustering involves formation of clusters in the data space and translation of these clusters into fuzzy or TSK rules such that the model obtained is close to the system to be identified. The fuzzy clustering involves both structure identification and parameter identification. The optimization of regression parameters P_{ij}^{k} for minimum output error in TSK modeling is in a way similar to tuning of output membership functions. The clusters of data points are formed based on certain measure scored by the data points. Every cluster is represented by a cluster center, which is a data point with extreme measure. The measure is generally a distance or sequential norms like Euclidean, Diagonal, Mahalanobis, Hamming, etc. The degree of association of any data point to a cluster is a strong function of the measure it scored against the measure of the cluster center. The membership value obtained based on the measure could also indicate the degree of representation by that data point of the behavior of the cluster center. Depending on the requirement, clustering of data could be done in only output space or in combined input-output space as explained below.

In the approach of clustering only in output space, clusters are formed in the output space of r dimensions. Once clusters in the output space are formed, they are projected onto the input space of m dimensions as shown in Figure 4.12. The membership function of a data point is maintained in all its projections onto input space dimensions. The output-to-input projection of a cluster could result in the formation of non-convex fuzzy sets in the input domain. As the input space is not involved during the cluster formation, this method would be very useful in evolving a model from data space with insignificant variables or with a large number of variables, even though the reasoning using this method shall be less accurate. Due to these limitations, the fuzzy sets obtained using this method may require more tuning in parameter identification part.

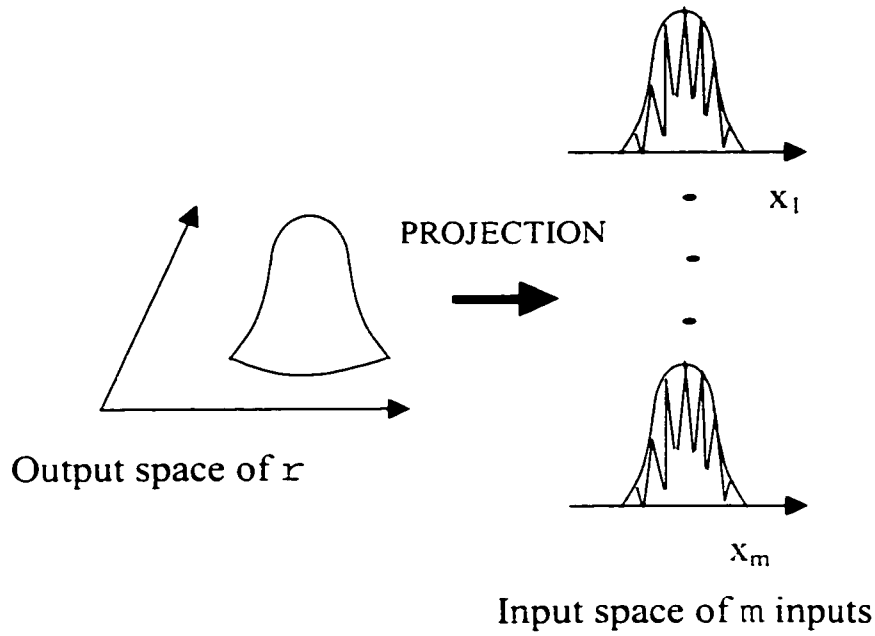

Figure 4.12: Scheme for clustering in output space and projecting onto input space

In the other approach, clusters are formed in the combined input-output space of $m+r$ dimensions. The distance measure used for clustering is a combined distance in input-output space. Once the clusters are formed in the input-output space, they could be

projected in two ways. In one way, the clusters are projected onto the input space of m dimensions and each output dimension as shown in Figure 4.13. While in the other way the clusters are projected into each dimension as shown in Figure 4.14. Unlike the earlier approach, these two methods of projection of clusters result in convex fuzzy sets in every projection as seen from Figures 4.13 and 4.14. This avoids the approximation of the input fuzzy sets and hence avoids the requirement of excessive tuning of fuzzy sets in the parameter identification step. This approach may result in more accurate system identification than that of the earlier approach requiring less tuning of fuzzy sets as inputs also participate in the cluster formation. During the comparison study of the modeling performance, the above two ways of projecting for combined input-output space clustering approach have been found to result in similar performance even though they had different zones of optimum clustering parameters. The approach of clustering in the combined data space and projecting the cluster onto each dimension is selected for study in this thesis.

In other clustering methods, the tuning of fuzzy sets after initial structure identification is done in parameter identification step. As part of structure identification, in Emami *et al.* [57], reasoning mechanism is optimized in order to get the closest model. The tuning of fuzzy sets after structure identification is done as part of a parameter identification step using Sugeno and Yasukawa's [169] method. In contrast, this thesis performs a parametric search [51] on the clustering parameters to identify the closest model while using the same inference mechanism and the membership functions provided by the clustering method.

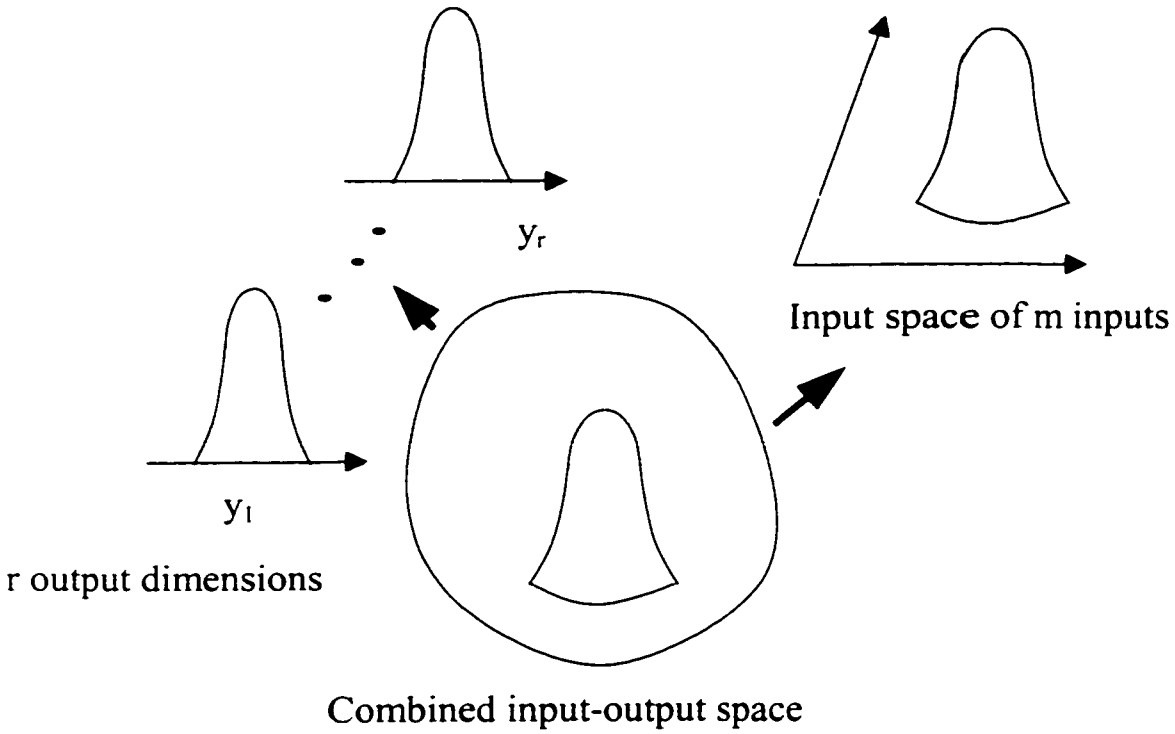

Figure 4.13 Scheme for clustering in input-output space and projecting onto input space and each output dimension

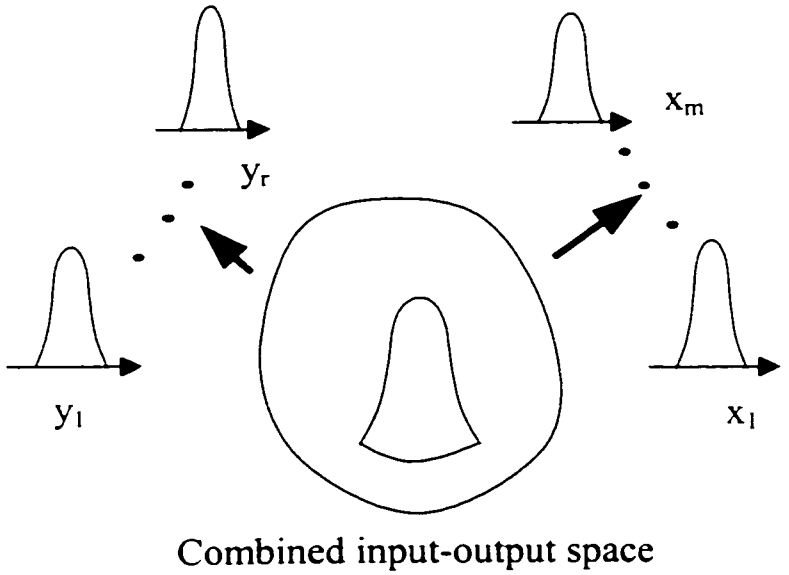

Figure 4.14 Scheme for clustering in input-output space and projecting onto each input and output dimension

The fuzzy C-means (FCM) clustering algorithm of Bezdek [15], Bezdek *et al.* [16] and Dunn [54] which has been widely studied and applied, needs *a priori* knowledge of the number of clusters. Whenever FCM requires a desired number of clusters and initial guess positions for each cluster center, the output rules depend strongly on the choice of initial values as the FCM algorithm forms iteratively a suitable cluster pattern in order to minimize an objective function dependent on cluster locations. The initial selection of cluster details has been made automatic by Emami *et al.* [57].

The auto-generation capability for determining the number and initial location of cluster centers through search techniques was introduced [156, 17] in the mountain clustering method. This method can provide approximate estimation of cluster centers based on a search measure called the *mountain function* by Yager and Filev [200]. A data point with highest mountain function represents a cluster center. In order to find cluster centers, the data space is discretized into grid points and each grid point is assumed to be a potential candidate for cluster centers. Grid points could be evenly or unevenly spaced. The potential value for each grid point based on its distance measure to the actual data points is estimated in order to select those with high potential values as cluster centers. Once a cluster center with highest mountain function is selected, all the grid points are penalized in proportion to the distance from the cluster center. Hence, the grid points that are close to cluster center are penalized more than the farther ones. This penalizing process can control the formation of other clusters in terms of its closeness to the previous one. The subtraction process can help in the creation of new cluster centers away from the previous center such that entire data space is represented with minimum clusters. The grid point

with new maximum mountain function is selected as a new cluster center and all the grid points are penalized in proportion to the distance from the new cluster center. This procedure of identifying cluster centers and penalizing all grid points continue as long as the mountain function falls below a threshold potential value. Even though this method is simple and effective, its application becomes limited due to a large amount of computation involved when the dimensions of the data space are large.

Chiu [38, 39] proposes a *subtractive clustering* method with improved computational effort, in which the data points themselves are considered as candidates for cluster centers instead of grid points. By using this method, the computation is simply proportional to the number of data points and independent of the dimension of the problem. In this method also, a data point with the highest potential, which is a function of the distance measure, is considered as a cluster center and data points close to new cluster center are penalized in order to control the emergence of new cluster centers. In Chiu's subtractive method, the potential P_i of the i'th data point is estimated by the following equation:

$$P_i = \sum_{j=1}^{n} e^{-\alpha \|x_i - x_j\|^2} \tag{4.12}$$

where $\alpha = \frac{\gamma}{r_a^2}$ (4.13)

r_a is a positive constant defining the neighborhood range of the cluster or simply the *radius* of hypersphere cluster in data space (also represents the support of fuzzy sets representing the cluster), n is the total number of data points, γ is a positive constant and is selected as 4, x_i and x_j are vectors in combined data space of input and output

dimensions. The potential of a data point is a function of its distances to all data points including itself. The more the neighborhood data points the higher the potential values.

After calculating the potential of each data point, the data point with the highest potential is selected as the first cluster center. The identification of other cluster centers is carried out through the subtraction process. In this process the potential of all data points is revised each time a new cluster center is obtained, by using the following equation:

$$P_i \Leftarrow P_i - P_k^* \zeta \tag{4.14}$$

where

$$\zeta = e^{-\beta \|x_i - x_k^*\|^2} \tag{4.15}$$

$$\beta = \frac{4}{r_b^2} \tag{4.16}$$

$$r_b = \eta * r_a \tag{4.17}$$

where

x_k^* and P_k^* are position and potential of k'th cluster center, respectively, r_b is a positive constant representing the radius of penalizing zone for a given cluster center, η is called *squash factor* and is also a positive constant. Chiu [38, 39] proposes r_b to be somewhat greater than r_a in order to avoid obtaining closely spaced cluster centers.

After revising the potential of all the clusters following subtraction, the cluster center is selected based on its new potential value in relation to an upper acceptance threshold $\bar{\varepsilon}$ called *accept ratio*, lower rejection threshold $\underline{\varepsilon}$ called *reject ratio*, and a relative distance

criterion. The acceptance of a data point with the potential between the upper and the lower thresholds depends on the shortest of the distances between that point and all other previously found cluster centers as given by the following equation:

$$\frac{d_{min}}{r_a} + \frac{P_k^*}{P_1^*} \geq 1 \tag{4.18}$$

where d_{min} is the shortest of the distances between x_k^* and all previously found cluster centers. This will avoid the emerging of new clusters close to the existing ones even though they have potential higher than the lower threshold, enhancing the uniform representation of system in entire data space.

Once all the cluster centers are found through the subtraction process, the membership functions of all data points are assigned exponentially as proposed by Chiu [38, 39] with respect to all cluster centers as follows:

$$\mu_{ij} = e^{-\alpha \|x_i - x_j\|^2} \tag{4.20}$$

where α is given by the Equation (4.13). $\|x_i - x_j\|$ is the distance measure between the i'th data point and j'th cluster center. γ in Equation (4.13) is a positive constant determining fuzziness in the cluster. This value is important in order to generate meaningful fuzzy sets. A value of around 4 proposed by Chiu [38, 39] will give fuzzy sets closer to a triangular shape and this value is maintained throughout this thesis. This parameter can also be used to tune the fuzzy sets in order to absorb small variations in the system after it is identified. The closeness of the model to the system depends upon the optimum selection of the clustering parameters such as cluster radius, squash factor,

accept ratio and reject ratio. Chiu [38, 39] proposes the optimum default values of 1.5, 0.5 and 0.15 for η, $\bar{\varepsilon}$ and $\underline{\varepsilon}$, respectively. Each of these clustering parameters has specific influence on the clustering performance and hence the model.

The values of accept ratio and reject ratio have influence on selecting the cluster centers and hence the rule base. These parameters affect the modeling depending upon the potential distribution in data space in relation to system behavior.

The cluster radius r_a in Equation (4.13) basically indicates the zone of influence or zone of association of a cluster center in data space. It also indicates the zone in which the influence of the behavior of the cluster center could be felt to a certain degree. The penalty radius r_b indicates the zone of penalty for enhancing the emergence of new clusters outside the zone of r_b. It also indicates the zone of penalty for being influenced by the cluster center. There is a contradiction in the requirements of r_a and r_b which is the very essence of getting a better distribution of clusters such that the system behavior is represented over the entire data space. The compromise in the requirement of r_a and r_b is met by the squash factor.

Consider the simple case of 9 data points as shown in Figure 4.15 showing the projection of potentials on a dimension x_i. As per the definition, the data point 4 with the highest potential will be selected as the first cluster center. The fuzzy set representing the cluster with the fourth point as the cluster center is shown in Figure 4.16. The support of fuzzy

set indicates the zone of influence of the cluster center. In order to facilitate the emergence of new cluster centers representing the different aspects of system behavior, penalizing of potential of all data points is carried out in proportion to a closeness measure scored by a data point with respect to the cluster center. The penalty ratio ζ proposed by Chiu [38, 39] as per the Equation (4.15) is shown in Figure 4.16, indicating the extent of penalizing zone decided by the squash ratio. The relative value of r_b in relation to r_a will determine the revised potential distribution and hence the position and number of new cluster centers.

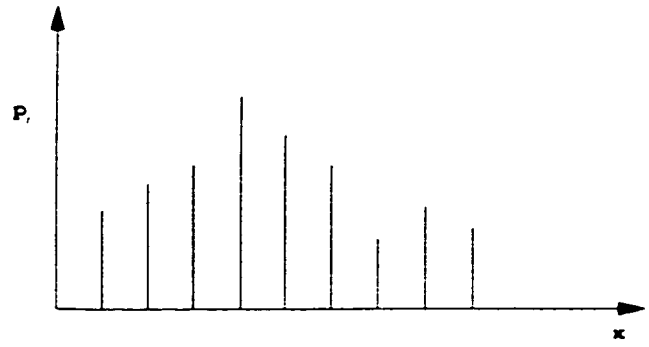

Figure 4.15 Scheme for potential measure for 9 data points

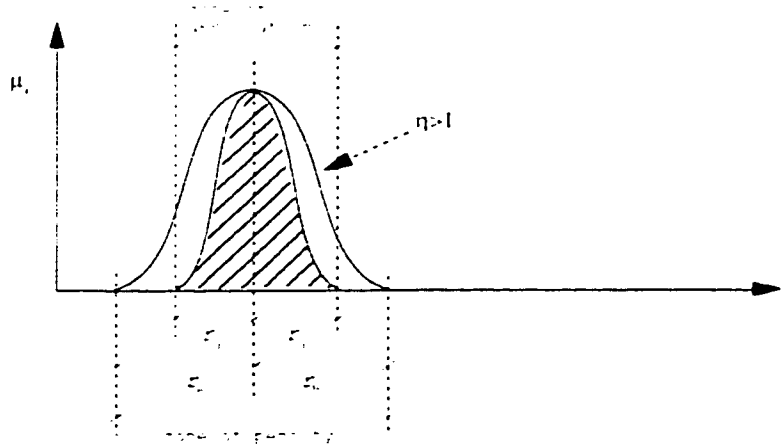

Figure 4.16 Scheme for potential based subtraction

Higher values of squash factor will help in identifying new cluster centers farther apart from the previous ones. As the potential calculation during penalty is stronger than association due to squash factor, there are chances of reduced possibility for creation of new clusters in the neighborhood of the existing clusters. This situation will be beneficial when available data is large enough to represent the system behavior. The optimum range of the squash factor or the penalty radius could be dependent on the relative availability of data points in order to represent the system behavior [48] and also to the complexity of the system behavior. Each set of clustering parameters will result in different system model and hence finding of optimum set of values for these clustering parameters is similar to structure and parameter identification of the model.

A cluster center represents completely the entire cluster. The association or closeness of a data point with this cluster center could be represented by its membership degree scored with reference to that cluster center. The membership function μ_{ik}, scored by the i'th data point with reference to the k'th cluster center, is limited by a value called *association threshold* δ_k [48] as a closeness measure in order to quantify the strength of the closeness of the i'th data point to the k'th cluster center. The data point with μ_{ik} equal to or greater than δ_k, are identified as the *strong members* of the k'th cluster while the rest of the data points are the *weak members* of that cluster. When the available data is relatively scarce, the weak members of the clusters, i.e., the data points farther from the center need to be given a chance to form clusters of their own and also all the cluster centers should be allowed to influence over the vast region [48]. This could be effected by penalizing only

the strong members as shown in Figure 4.17 through membership based penalty by defining penalty ratio as

$$\varsigma = e^{-4\left|\frac{1-\mu_{ik}}{1-\delta_k}\right|^2} \tag{4.20}$$

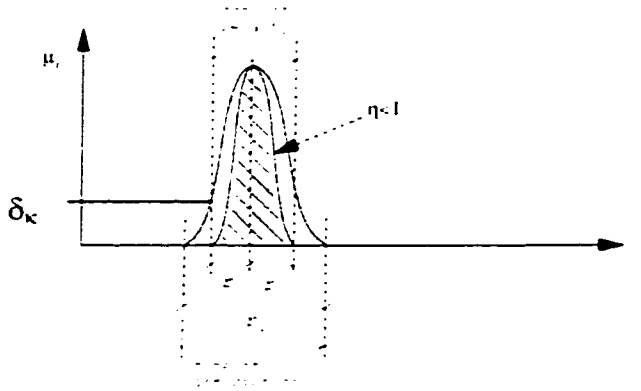

Figure 4.17 Scheme for membership based subtraction

The *membership based subtraction* with higher cluster radius, lower penalty radius and thus fractional squash factors, is similar to penalizing with squash factor less than one. Hence, in the cases of evolving a model from weakly represented data space, the contribution from each point towards the system modeling will be made stronger by the introduction of squash factor less than 1.0 [48] in addition to greater than one as proposed by Chiu [38, 39]. When the relative availability of the data points in order to represent the system is not clear, the optimum models could be found out by searching the entire space of clustering parameters. As this thesis presents the effect of clustering and optimizing the regression parameters on system identification, it was decided to apply parametric search for accept ratio, reject ratio, squash factor and cluster radius on subtractive clustering method.

4.2.3 Higher Order System Identification

Even though this technique could be applied to MIMO system, only MISO modeling is presented here for simplicity. Consider the MISO system for fuzzy-nonfuzzy modeling in which the output function could be represented in general as a higher order hypersurface of input variables with even interactive terms of inputs, as follows:

$$R^1 : IF\ x_1 \text{ is } A_1^1 \text{ AND } x_2 \text{ is } A_2^1 \text{ AND. . . AND } x_m \text{ is } A_m^1 \text{ THEN } y^1 = \sum_{i=0}^{q}\sum_{j=0}^{q}\cdots\sum_{k=0}^{q} P_{ij\cdots k}^1 x_1^i x_2^j \cdots x_m^k$$

$$ALSO$$

$$\vdots$$

$$ALSO$$

$$R^N : IF\ x_1 \text{ is } A_1^N \text{ AND } x_2 \text{ is } A_2^N \text{ AND} \ldots \text{AND } x_m \text{ is } A_m^N \text{ THEN } y^N = \sum_{i=0}^{q}\sum_{j=0}^{q}\cdots\sum_{k=0}^{q} P_{ij\cdots k}^N x_1^i x_2^j \cdots x_m^k \tag{4.21}$$

where $P_{ij\ldots k}^s$ $for\ (i, j, \ldots, k = 0, 1, \ldots, q; s = 1, 2, \ldots, N)$ are consequent regression parameters that are to be optimized such that the model is close to the given system. y^s is the output from the s'th rule.

In applying TSK [175] modeling the regression function for the output of the given inputs $(x_1, x_2, \ldots, x_m)$ is written as

$$
\begin{aligned}
y &= \frac{\sum_{s=1}^{N}(A_1^s(x_1)\wedge A_2^s(x_2)\wedge\cdots\wedge A_m^s(x_m))\cdot\ y^s}{\sum_{s=1}^{N}(A_1^s(x_1)\wedge A_2^s(x_2)\wedge\cdots\wedge A_m^s(x_m))} \\
&= \frac{\sum_{s=1}^{N}\sum_{i=0}^{q}\sum_{j=0}^{q}\cdots\sum_{k=0}^{q}\ (A_1^s(x_1)\wedge A_2^s(x_2)\wedge\cdots\wedge A_m^s(x_m))\cdot P_{ij\cdots k}^s x_1^i x_2^j\cdots x_m^k}{\sum_{s=1}^{N}(A_1^s(x_1)\wedge A_2^s(x_2)\wedge\cdots\wedge A_m^s(x_m))} \\
&= \sum_{s=1}^{N}\sum_{i=0}^{q}\sum_{j=0}^{q}\cdots\sum_{k=0}^{q}\beta_s P_{ij\cdots k}^s x_1^i x_2^j\cdots x_m^k
\end{aligned}
\tag{4.22}
$$

where

$$
\beta_s = \frac{A_1^s(x_1)\wedge A_2^s(x_2)\wedge\cdots\wedge A_m^s(x_m)}{\sum_{s=1}^{N}(A_1^s(x_1)\wedge A_2^s(x_2)\wedge\cdots\wedge A_m^s(x_m))} \tag{4.23}
$$

The system has to be identified with the training set of data points $(x_{1t}, x_{2t}, \ldots, x_{mt}) \Rightarrow y_t$ for t=1,2,...,u where u is the total number of training data pairs. The final system equation can be written in matrix form using the entire set of training pairs as

$$
[Y] = [X][P] \tag{4.24}
$$

where

the known output matrix $[Y]^T = [y_1, y_2, \ldots, y_t, \ldots, y_u]$ of dimension $1 \times u$

the known input matrix $[X]^T = [X_1^T, X_2^T, \ldots, X_t^T, \ldots, X_u^T]$ of dimension $N(q+1)^m \times u$.

The value of the output y_t for the given set of input $(x_{1t}, x_{2t}, \ldots, x_{mt})$ from the system model is given by Equation (4.11) as

$$y_t = \sum_{s=1}^{N}\sum_{i=0}^{q}\sum_{j=0}^{q}\cdots\sum_{k=0}^{q} P^s_{ij\cdots k}\beta_{st}x^i_{1t}x^j_{2t}\cdots x^k_{mt}$$
$$= [X_t][P] \qquad \forall\, t = 1,2,\ldots,u \tag{4.25}$$

where

$$\beta_{st} = \frac{A^s_1(x_{1t}) \wedge A^s_2(x_{2t}) \wedge \cdots \wedge A^s_m(x_{mt})}{\sum_{s=1}^{N}(A^s_1(x_{1t}) \wedge A^s_2(x_{2t}) \wedge \cdots \wedge A^s_m(x_{mt}))} \tag{4.26}$$

$$[X_t] = [\beta_{11},\ldots,\beta_{N1},\beta_{11}x_{1t},\ldots,\beta_{N1}x_{1t},\ldots,\beta_{11}x_{mt},\ldots,\beta_{N1}x_{mt},$$
$$\beta_{11}x^2_{1t},\ldots,\beta_{N1}x^2_{1t},\ldots,\beta_{11}x^2_{mt},\ldots,\beta_{N1}x^2_{mt},\ldots, \quad \text{of dimension}$$
$$\beta_{11}x^q_{1t}\cdots x^q_{mt},\ldots,\beta_{N1}x^q_{1t}\cdots x^q_{mt}\,]$$

$$1 \times N(q+1)^m \tag{4.27}$$

The unknown regressor matrix

$$[P]^T = [P^1_{00\cdots0},\ldots,P^N_{00\cdots0},P^1_{10\cdots0},\ldots,P^N_{10\cdots0},\ldots,P^1_{00\cdots1},\ldots,P^N_{00\cdots1},$$
$$P^1_{20\cdots0},\ldots,P^N_{20\cdots0},\ldots,P^1_{00\cdots2},\ldots,P^N_{00\cdots2},\ldots, \quad \text{of dimension } 1 \times N(q+1)^m$$
$$P^1_{qq\cdots q},\ldots,P^N_{qq\cdots q}\,]$$

(4.28)

in Equation (4.24) could be estimated by least square estimation (LSE) methods like pseudo-inverse solution [175] of the form

$$P = (X^T X)^{-1} X^T Y \tag{4.29}$$

or recursive least squares methods [3,4]. This thesis uses the recursive least square methods given by Chiu [3,4] due to their computational efficiency. Once all the data points are clustered, the fuzzy rule base which is a collection of all the clusters and also is

the basic model of the system, is identified through the TSK model proposed by Takagi and Sugeno [175] and is given by the Equation (4.24).

Each cluster is projected onto all input dimensions as seen in Figure (4.14) and the membership function for fuzzy sets of these input dimensions are assigned as per Equation (4.19). The number of rules in a model will be equal to the number of clusters. In TSK modeling, as explained in Section 5.2.1, the variation of output sequence in each cluster is approximated by hyperplanes of input dimensions.

Once all the clusters of data are identified, the collection of clusters forming the fuzzy rule base becomes the basic model of the system. The input fuzzy sets are formed by the projection of these clusters onto the respective input dimension and the membership function for fuzzy sets of these input dimensions are assigned as per Equation (4.19). The input matrix X of Equation (4.24) can be estimated using the input training data and the fuzzy sets obtained from clusters. The output matrix Y is formed using output training data. The unique solution for regressor matrix P is possible whenever $u \geq N(q+1)^m$. Even though it is possible to estimate the regressor matrix P for the cases with $u < N(q+1)^m$ based on the recursive least squares method, this thesis presents models only when $u \geq N(q+1)^m$ due to the following reasons:

1. Uniqueness of the solution is maintained and
2. Size of the rule base is already large and the error is lower than the acceptable value.

Thus, the number of rules in a model which is same as that of the number of clusters, is restricted by the available number of data points in relation to the order of the hyper

surface. When more than one output is available as in the case of MIMO the regression coefficients have to be found out for all the outputs in a similar way.

Even though this method is general, it will not be practical to have a very high order for regression surfaces. The output function in a cluster is approximated by a hyper-plane in TSK modeling [38, 39, 175] with $q=1$ and without any interactive terms of input variables. Despite the fact that the first order method is simple and elegant to apply to many problems, the higher order regression equation can have advantages in some occasions.

These occasions can be identified as follows:

1. The maximum number of rules is very critical for some applications for the acceptable amount of error in system identification.
2. The global variation of the system is highly non-linear and it has to be identified with a minimum number of rules. In such cases, modeling with hyperplanes may result in a large number of rules and hence higher order regression becomes inevitable.

Even though the direct selection of the highest order for capturing the system behavior is not available in this thesis, the development of this technique for automatic selection of the order of the model for the specified amount of error could be very useful for the compact identification of the system.

For demonstrating the effect of higher order subtractive clustering on identification of MISO system with two inputs, the simple case of second order regression equation

without interactive terms is selected. The regression equation of y^s for the s'th rule is defined as

$$y^s = P_{00}^s + P_{10}^s x_1 + P_{01}^s x_2 + P_{20}^s x_1^2 + P_{02}^s x_2^2 \tag{4.30}$$

with five regression coefficients. This can be called second order Sugeno model while the first order Sugeno model is

$$y^s = P_{00}^s + P_{10}^s x_1 + P_{01}^s x_2 . \tag{4.31}$$

The maximum number of rules limited for the study in this thesis is $u/5$ for the second order model and $u/3$ for the first order model where u is the number of training pairs. In a nutshell, the fuzzy system identification involves generation of clusters using the training data set for the given values of clustering parameters such as squash factor, cluster radius, accept ratio and reject ratio, and estimation of regression coefficients by least-square estimation. Subtractive clustering with these two above regression models given by Equations (4.30) and (4.31) are applied to three systems of varying complexity and the results are compared in this thesis. So, this study will help in understanding the behavior of the clustering mechanism on system modeling in relation to accept ratio, reject ratio, squash factor and cluster radius.

4.2.4 Structure Optimization

Finding optimal models is an essential requirement for all system identification problems, which involves both structure identification and parameter identification. It is difficult to separate these parts in the case of subtractive clustering. The least square estimation part of subtractive clustering ensures the overall optimization of the regression parameters for

the given set of clusters. Hence, the optimization of the system identification depends mainly on finding the optimal clustering parameters such as squash factor, cluster radius, accept ratio and reject ratio such that set of clusters obtained result in a minimum modeling error. The influence of all the clustering parameters are highly interactive in nature and are also dependent on the system behavior and nature of available data to identify the system. The simplest way of finding optimum range of clustering parameters will be parametric search on all the variables affecting the clustering mechanism. Hence, an enumerative search is carried out on the clustering parameters and the resulting models are compared based on the modeling least square error, σ, defined as

$$\sigma = \sum_{i=1}^{u} \left(y_i - \hat{y}_i \right)^2 \tag{4.32}$$

where y_i is the actual training output used for modeling, $\hat{y}_i$ is the predicted output from the identified model and u is the total number data used for training.

The range of the clustering parameters such as accept ratio, reject ratio, squash factor and cluster radius selected for enumerative search are 0-1.0, 0-0.9, 0.05-2.0 and 0.15-1.0, respectively, that cover entirely the possible range. The step sizes for accept ratio, reject ratio, squash factor and cluster radius are selected as 0.1, 0.1, 0.05 and 0.002, respectively, in order not to miss any model. It has been found during the parametric search that cluster radius and squash factor have strong influence on performance of the modeling when compared to accept ratio and reject ratio. Hence smaller step sizes were selected for squash factor and cluster radius compared to that of accept ratio and reject ratio. The optimum values of these parameters may depend upon the complexity of the

system behavior and the relative availability of the number of data points in order to represent such behavior. The performance measures used for comparison are least square error σ, and number of rules N. The better models shall always result in minimum error and less number of rules. Three systems of different complexity are selected for demonstrating the performance of higher order subtractive clustering technique and the results obtained through enumerative search of clustering parameters are given in the next section.

4.2.5 Case Studies of System Identification

Three systems are selected for further demonstration of higher order system identification technique. The systems selected vary in complexity from simple plane to highly non-linear function of Sugeno and Yasukawa [169], and the PEAKS function of Matlab [87]. Both the first order (Equation (4.31)) and the second order (Equation (4.30)) system identification techniques have been applied to the set of input-output training data representing the above mentioned systems over the entire selected range of clustering parameters and the results are given in the following sections. The results include the minimal models, influence of clustering parameters on the optimality of the modeling and comparison between first and second order subtractive clustering models. As these models are obtained through enumerative search without any distinct parameter identification process, these models could further be improved through parameter optimization of input fuzzy sets as done in [57, 169].

CASE 1: Non-linear system of Sugeno and Yasukawa [169]

The nonlinear system of two inputs and one output defined by the equation

$$y = (1 + x_1^{-2} + x_2^{-1.5})^2, \qquad 1 \le x_1, x_2 \le 5 \tag{4.33}$$

is identified with the training set of 50 data points given in Sugeno and Yasukawa [169]. The results are compared with those of Sugeno and Yasukawa [169] and Emami *et al.* [57]. The system identification of Sugeno and Yasukawa [169] involves structure identification based on fuzzy c- means method and parameter optimization by tuning the positions of input fuzzy sets while Emami et.al. [57] applies fuzzy line clustering with unified parameterized reasoning formulation for structure identification and the same tuning formulation for parameter identification. The error measure used in [57,169] is the average error defined as $PI = \frac{\sigma}{u}$, where $u = 50$.

Numerous models were identified through parametric search of first and second order identification using 50 data points and the resulting least square error σ is calculated for all the models. The models are compared based on σ and number of rules N, and the results of this study are presented in Figures 4.18 - 4.27. A point in these figures indicates a model obtained with certain values of clustering parameters. All the possible models with $\sigma \le 2.315$ or $PI \le 0.0463$ are shown in Figures 4.18 - 4.27. The compilation of modeling performance in terms of σ and N is shown in Figures 4.18 and 4.19 for first and higher order models, respectively. There is a rapid decrease in the minimum error when N increases. Both types of models show similar trend except reduction in maximum

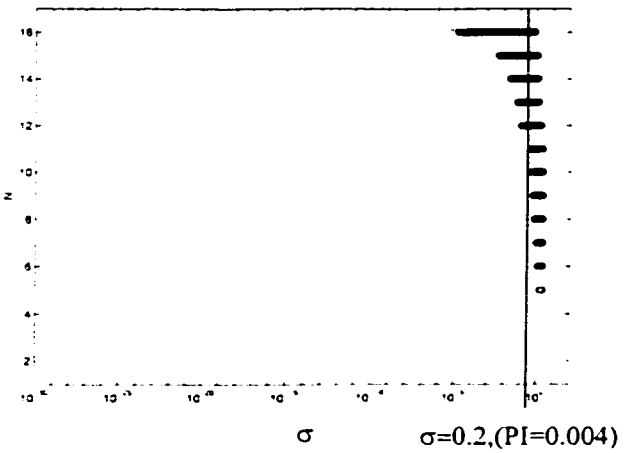

Figure 4.18 Variation of σ against N from collection of first order models with $\sigma \leq 2.315$ for a nonlinear system [169]

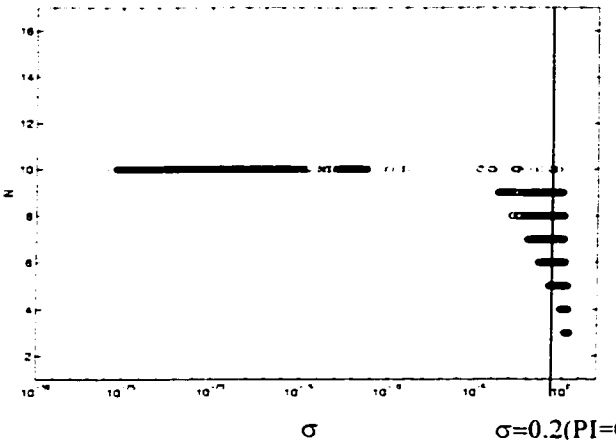

Figure 4.19 Variation of σ against N from collection of higher order models with $\sigma \leq 2.315$ for a nonlinear system [169]

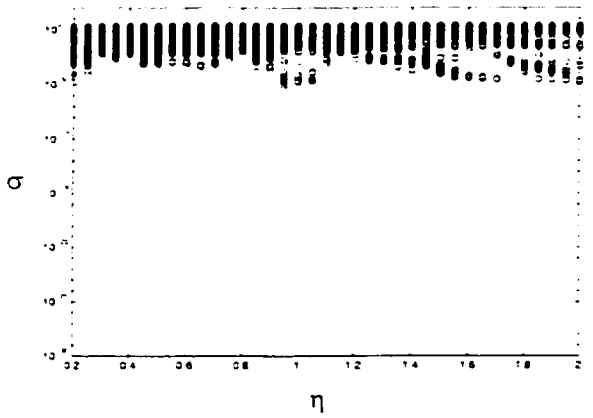

Figure 4.20 Collection of first order models with $\sigma \leq 2.315$ for a nonlinear system [169] in the domain of squash factor and least square error.

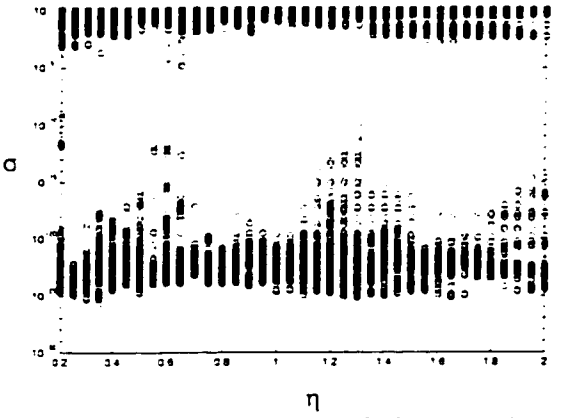

Figure 4.21 Collection of higher order models with $\sigma \leq 2.315$ for a nonlinear system [1169] in the domain of squash factor and least square error.

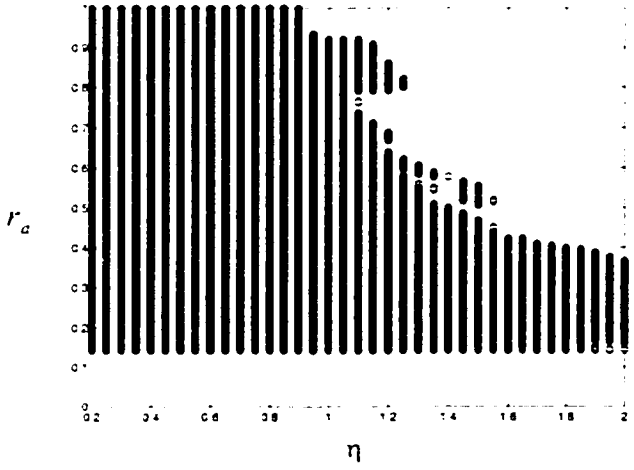

Figure 4.22 Collection of first order models with $\sigma \leq 2.315$ for a nonlinear system [169] in the domain of squash factor and cluster radius.

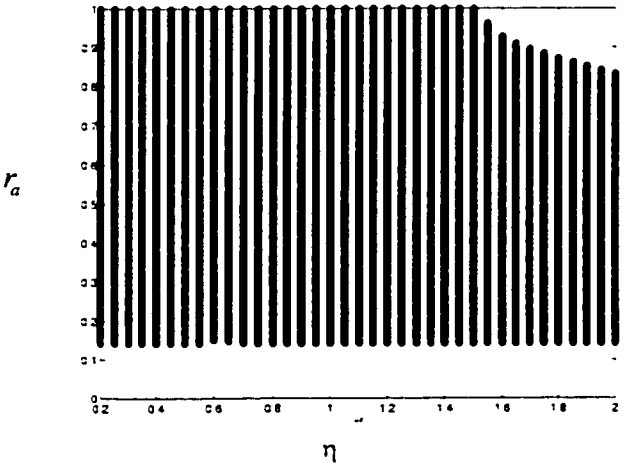

Figure 4.23 Collection of higher order models with $\sigma \leq 2.315$ for a nonlinear system [169] in the domain of squash factor and cluster radius.

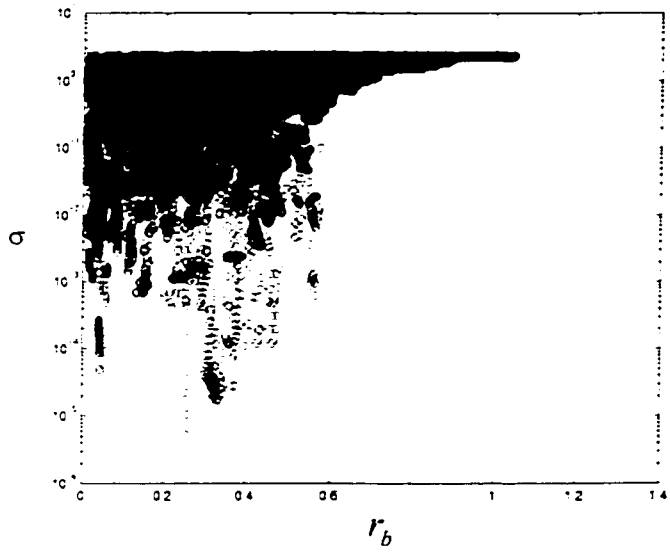

Figure 4.24 Collection of first order models with $\sigma \leq 2.315$ for a nonlinear system [169] in the domain of penalty radius and least square error.

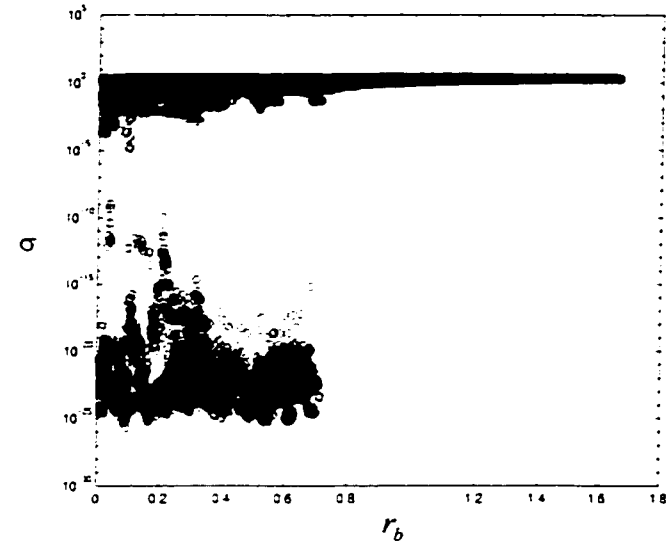

Figure 4.25 Collection of higher order models with $\sigma \leq 2.315$ for a nonlinear system [169] in the domain of penalty radius and least square error.

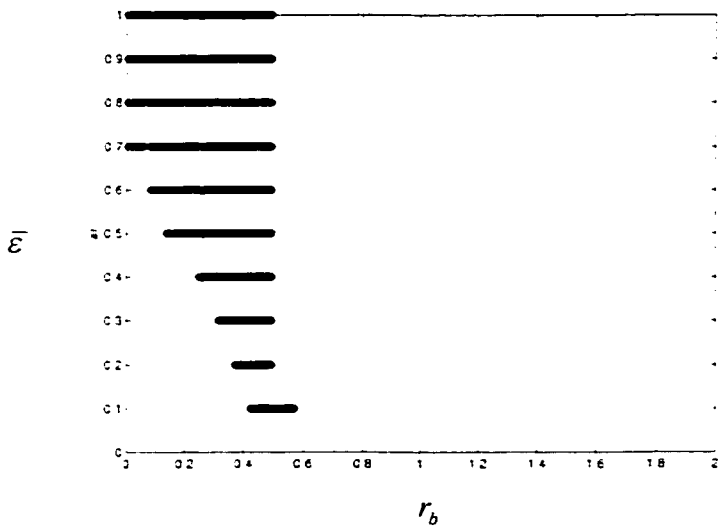

Figure 4.26 Collection of first order models with $\sigma \leq 0.2315$ for a nonlinear system [169] in the domain of penalty radius and accept ratio.

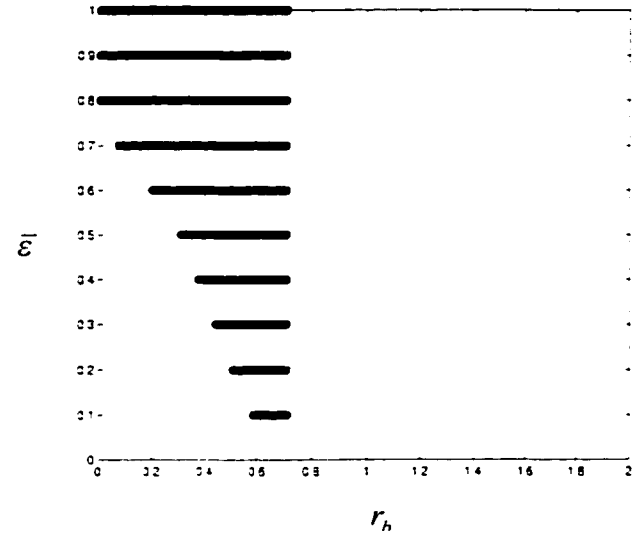

Figure 4.27 Collection of higher order models with $\sigma \leq 0.2315$ for a nonlinear system [169] in the domain of penalty radius and accept ratio.

number of rules and error for the higher order model. The minimum error obtained is σ = 0.0000052 with 16 rules for the first order model while minimum error obtained is σ = 2.11×10^{-26} with 10 rules for the second order case. Figures 4.20 and 4.21 show the general trend between squash factor and least square error for the first order and the second order models, respectively. They show that it is possible to get models with reasonable error over the entire range of squash factor, suggesting both potential based and membership based subtraction processes. In membership based subtraction, squash factor is reduced to fractional values with penalty radius less than cluster radius. Figures 4.22 and 4.23 show the possible range of cluster radius and squash factor with $\sigma \leq 2.315$ for both types of models. Even though it is possible to get models over the entire range of cluster radius at lower squash factor, a higher squash factor results in a lower cluster radius indicating clearly the preference over the penalty radius as given by Equation (4.17) for reduced error. The range of cluster radius and squash factor is larger for higher order modeling. This preference over the penalty radius is shown in Figures 4.24 and 4.25 for both types of models. These figures show that the range of penalty radius becomes narrower as the error is minimized indicating the need for a fractional squash factor whenever the cluster radius is high. Apart from penalty radius, accept and reject ratios are also important in deciding the formation of clusters. The inverse relation between penalty radius and accept ratio is given in Figures 4.26 and 4.27 for finer models with $\sigma \leq 0.2315$ of first and second order models, respectively. Whenever the penalty zone of a cluster center is large, potential of the neighborhood data points are penalized severely. This lowers the potential values of other data points low and so the chance of forming new clusters is also reduced unless the accept ratio is low. The contradictory

requirement, between penalty radius and accept ratio for facilitating the formation of more number of clusters in order to identify models with minimum error, is seen in Figures 4.26 and 4.27.

The comparison of the performance of first and higher order models with the results of Sugeno and Yasukawa [169] and Emami *et al.* [57] is given in Table 4.2. When the models after structure identification are compared, the first order identification method results in many models for $\sigma \leq 0.53$ with $N \geq 10$ while the clustering technique of Emami *et al.* [57] results in a model with $N = 8$. It is possible to reduce the error substantially such that it becomes close to zero by increasing the number of rules. The first order models with even $N = 5$ show substantial improvement over the results of $\sigma \leq 3.95$ of Sugeno and Yasukawa [169] with parameter identification. On comparing the models after structure identification, the models obtained using higher order regression do better even with less number of rules. Higher order identification method results in models with $N \geq 7$ for $\sigma \leq 0.53$. The higher order models with $N \geq 5$ obtained after structure identification result in $\sigma \leq 0.18$ which is less than the error of 0.2 obtained after parameter identification by Emami *et al.* [57]. If N is allowed to be 10, then error further reduces substantially. This comparison validates the use of higher order modeling as an improvement over Chiu's [38, 39] subtractive clustering and also as a simple technique even without parameter identification to achieve good modeling performance. The higher order as well as the first order models could be improved further if parameter identification is incorporated.

Table 4.2 Comparison of results with other models [57, 169]

	N	σ					
		Structure identification	Parameter identification				
Sugeno and Yasukawa [169]	6	15.90	3.95				
Emami *et al.*[57]	8	0.53	0.20	Subtractive Clustering Parameters			
				r_a	η	$\bar{\varepsilon}$	$\underline{\varepsilon}$
First order subtractive clustering	16	5.22×10^{-6}		0.268	0.95	0.5-1.0	0.3
	15	4.65×10^{-3}		0.416	0.50	0.60	0.50
	14	2.23×10^{-2}		0.294	1.05	0.4-1.0	0.3
	13	6.05×10^{-2}		0.280	0.05	0.9-1.0	0.70
	12	0.11		0.284	0.85	0.6-1.0	0.5
	11	0.45		0.252	0.15	0.80	0.70
	11	0.45		0.252	0.10-0.15	0.9-1.0	0.70
	10	0.49		0.334	0.05	0.9-1.0	0.8
	9	0.60		0.160	0.05-0.15	0.8-1.0	0.7
	8	0.73		0.206	0.05-0.10	0.9-1.0	0.8
	7	0.99		0.310	0.25	0.9-1.0	0.8
	6	1.17		0.266	0.35	0.9-1.0	0.8
	5	1.56		0.312	0.35	1.0	0.8
Higher order subtractive clustering	10	2.11×10^{-26}		0.266	0.35	0.8-1.0	0.7
	9	2.04×10^{-4}		0.168	0.05-0.15	0.8-1.0	0.7
	8	1.30×10^{-3}		0.168	0.20-0.30	0.8-1.0	0.7
	7	1.04×10^{-2}		0.198	0.40	0.8-1.0	0.7
	6	4.23×10^{-2}		0.206	0.25-0.35	0.9-1.0	0.80
	5	0.18		0.166	0.20-0.25	0.9-1.0	0.80
	4	0.82		0.206	0.05-0.10	1.0	0.9
	3	1.39		0.150	0.2-0.25	0.9-1.0	0.8

As an example, the rule bases for the first and higher order models with approximately equal error are shown in the Figures 4.28 and 4.29. These models show minimum error at the corresponding number of rules as seen from the Table 4.2. The first order rule base for r_a=0.284, η=0.85, $\bar{\varepsilon}$ =1.0 and $\underline{\varepsilon}$ = 0.5 which is shown in Figure 4.28 result in $\sigma = 0.11$ with 12 rules. The higher order rule base with r_a=0.166, η=0.20, $\bar{\varepsilon}$ =1.0 and $\underline{\varepsilon}$ = 0.8 which is shown in Figure 4.29 result in $\sigma = 0.18$ with only 5 rules when compared to 8 rules of Emami *et al.* [57] as seen in Table 4.2.

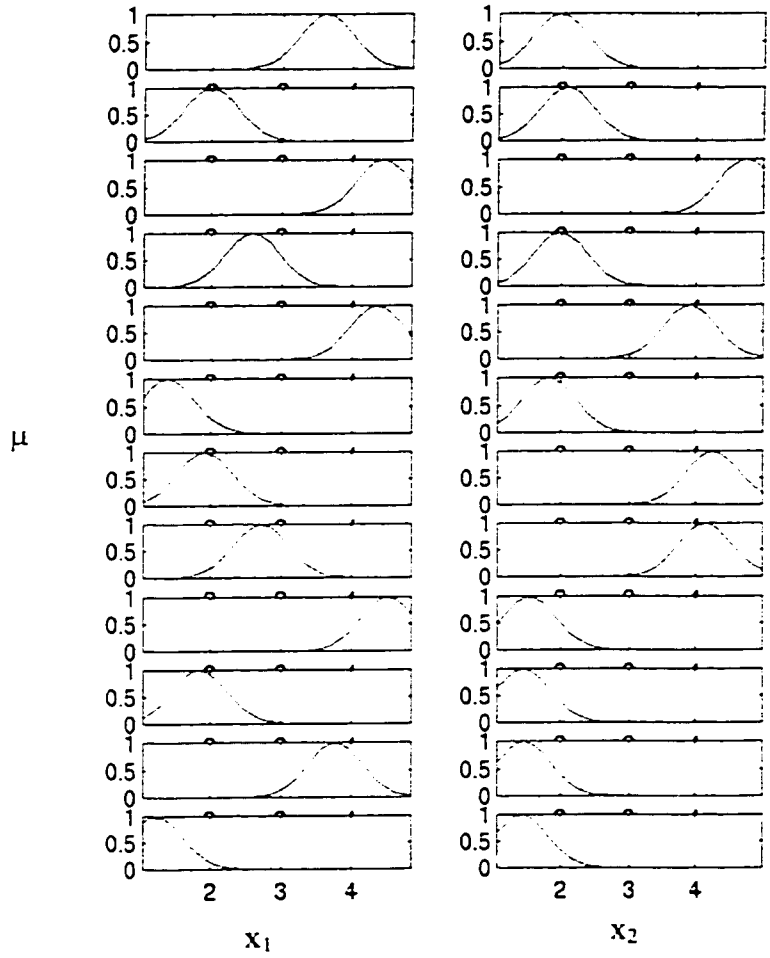

$$y^1 = -2.989 + 4.278x_1 - 4.663x_2$$

$$y^2 = 46.69 + 0.8639x_1 - 17.46x_2$$

$$y^3 = 2.385 - 0.04835x_1 - 0.1754x_2$$

$$y^4 = -51.39 + 8.587x_1 - 16.55x_2$$

$$y^5 = 2.627 - 0.077838x_1 - 0.2322x_2$$

$$y^6 = -50.07 + 3.080x_1 + 18.38x_2$$

$$y^7 = 10.34 - 1.94x_1 - 1.107x_2$$

$$y^8 = 1.946 - 0.2933x_1 + 0.143x_2$$

$$y^9 = 22.69 - 4.119x_1 - 0.788x_2$$

$$y^{10} = 145.8 - 38.89x_1 - 36.73x_2$$

$$y^{11} = 24.62 - 3.933x_1 - 6.368x_2$$

$$y^{12} = 47.94 - 65.47x_1 + 28.38x_2$$

Figure 4.28 A first order model for a nonlinear system [169] with r_a=0.284, η=0.85, $\bar{\varepsilon}$ =1.0 and $\underline{\varepsilon}$ = 0.5

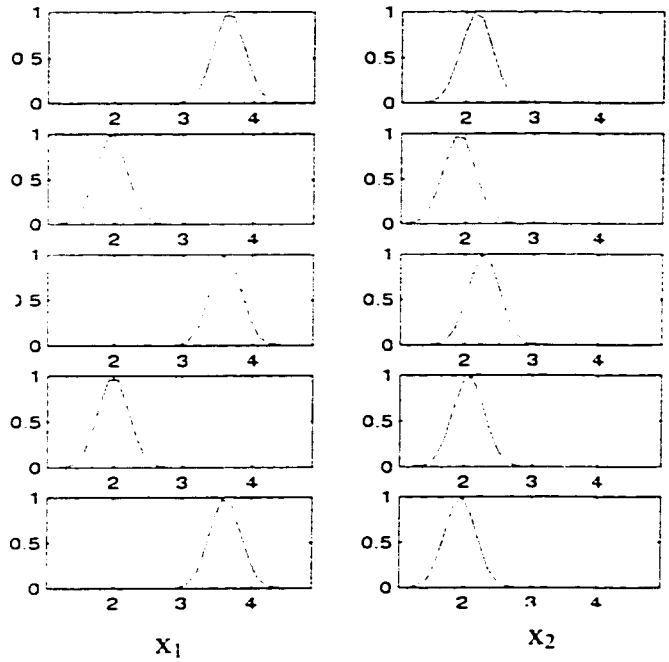

$$y^1 = -83.86 + 42.92x_1 - 1.617x_2 - 5.364x_1^2 + 0.1901x_2^2$$

$$y^2 = 24.08 - 11.62x_1 - 8.866x_2 + 2.692x_1^2 + 2.062x_2^2$$

$$y^3 = 16.74 - 1.778x_1 - 5.351x_2 + 0.2202x_1^2 + 0.5981x_2^2$$

$$y^4 = 7.912 + 2.533x_1 - 4.783x_2 - 8.798x_1^2 + 7.701x_2^2$$

$$y^5 = 47.10 - 22.21x_1 - 4.069x_2 + 3.006x_1^2 + 1.321x_2^2$$

Figure 4.29 A higher order model for a nonlinear system [169] with r_a=0.166, η=0.20, $\bar{\varepsilon}$ =1.0 and $\underline{\varepsilon}$ = 0.8

CASE 2: Nonlinear system of PEAKS function

The PEAKS function (MATLAB file: peaks.m) [87] in terms of two inputs x_1 and x_2 is defined as

$$y = 3\left(1-x_1\right)^2 e^{-x_1^2-\left(x_2+1\right)^2} - 10\left(\frac{x_1}{5} - x_1^3 - x_2^5\right)e^{-x_1^2-x_2^2} - \frac{1}{3}e^{-\left(x_1+1\right)^2-x_2^2}$$

$$\text{for} \quad -3 \le x_1 \le 3; -3 \le x_2 \le 3 \tag{4.34}$$

and the surface of this function is shown in Figure 4.30. The number of data points selected randomly for identifying the above function is 216 and they are given in Table 4.3.

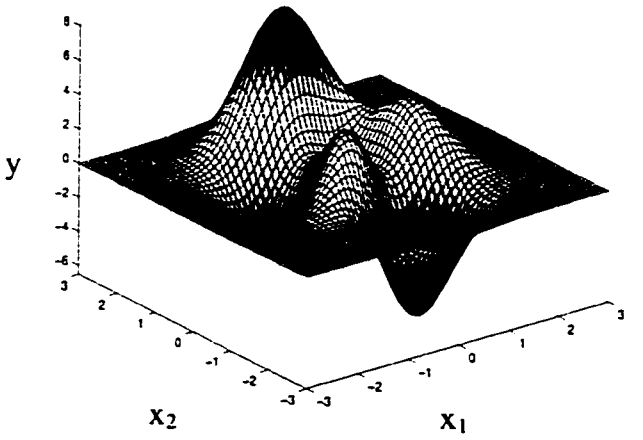

Figure 4.30 Surface plot of PEAKS function

Table 4.3: Input-output data for PEAKS function

x_1	x_2	y	x_1	x_2	y	x_1	x_2	y
-3	-3	0	-1	-2.2	-0.476	0.6	2.6	0.962
-3	-2.6	0	-1	-1.8	-0.51	1	-3	-0.11
-3	-2.2	0.001	-1	-1.4	0.56	1	-2.6	-0.503
-3	-1.8	0.001	-1	-1	1.979	1	-2.2	-1.476
-3	-1.4	0	-1	-0.6	1.509	1	-1.8	-2.607
-3	-1	-0.007	-1	-0.2	-0.501	1	-1.4	-2.372
-3	-0.6	-0.018	-1	0.2	-1.781	1	-1	-0.271
-3	-0.2	-0.028	-1	0.6	-1.512	1	-0.6	1.854
-3	0.2	-0.03	-1	1	0.352	1	-0.2	2.827
-3	0.6	-0.022	-1	1.4	2.386	1	0.2	2.829
-3	1	-0.011	-1	1.8	2.609	1	0.6	2.253
-3	1.4	-0.004	-1	2.2	1.476	1	1	2.436
-3	1.8	0	-1	2.6	0.503	1	1.4	3.201
-3	2.2	0	-0.6	-3	-0.111	1	1.8	2.838
-3	2.6	0	-0.6	-2.6	-0.547	1	2.2	1.522
-2.6	-3	0	-0.6	-2.2	-1.579	1	2.6	0.51
-2.6	-2.6	0.002	-0.6	-1.8	-2.364	1.4	-3	-0.041
-2.6	-2.2	0.004	-0.6	-1.4	-0.814	1.4	-2.6	-0.185
-2.6	-1.8	0.007	-0.6	-1	2.545	1.4	-2.2	-0.531
-2.6	-1.4	0.002	-0.6	-0.6	3.72	1.4	-1.8	-0.871
-2.6	-1	-0.032	-0.6	-0.2	2.18	1.4	-1.4	-0.521
-2.6	-0.2	-0.166	-0.6	0.2	0.628	1.4	-1	0.826
-2.6	0.2	-0.179	-0.6	0.6	0.325	1.4	-0.6	2.403
-2.6	1	-0.068	-0.6	1	2.418	1.4	0.2	3.351
-2.6	1.4	-0.019	-0.6	1.4	5.208	1.4	0.6	2.503
-2.6	1.8	0.001	-0.6	1.8	5.139	1.4	1	1.796
-2.6	2.2	0.003	-0.6	2.2	2.838	1.4	1.4	1.556
-2.6	2.6	0.001	-0.6	2.6	0.96	1.4	1.8	1.178
-2.2	-3	0.002	-0.2	-3	-0.212	1.4	2.2	0.601
-2.2	-2.6	0.007	-0.2	-2.6	-1.002	1.4	2.6	0.198
-2.2	-2.2	0.019	-0.2	-2.2	-2.929	1.8	-3	-0.01
-2.2	-1.8	0.038	-0.2	-1.8	-4.909	1.8	-2.6	-0.046
-2.2	-1.4	0.033	-0.2	-1.4	-3.698	1.8	-1.8	-0.166
-2.2	-1	-0.083	-0.2	-1	0.729	1.8	-1.4	0.069
-2.2	-0.6	-0.36	-0.2	-0.6	3.23	1.8	-1	0.72
-2.2	0.2	-0.718	-0.2	-0.2	2.481	1.8	-0.6	1.538
-2.2	0.6	-0.54	-0.2	0.2	1.282	1.8	-0.2	2.099
-2.2	1	-0.263	-0.2	0.6	1.057	1.8	0.2	2.077
-2.2	1.4	-0.053	-0.2	1	3.724	1.8	0.6	1.522
-2.2	1.8	0.027	-0.2	1.4	7.335	1.8	1	0.934
-2.2	2.2	0.026	-0.2	1.8	7.124	1.8	1.4	0.599
-2.2	2.6	0.01	-0.2	2.2	3.918	1.8	1.8	0.374
-1.8	-3	0.005	-0.2	2.6	1.324	1.8	2.2	0.177
-1.8	-2.6	0.015	0.2	-3	-0.254	1.8	2.6	0.056
-1.8	-2.2	0.042	0.2	-2.6	-1.181	2.2	-3	-0.002
-1.8	-1.4	0.186	0.2	-2.2	-3.481	2.2	-2.6	-0.007
-1.8	-1	-0.011	0.2	-1.8	-6.149	2.2	-2.2	-0.018
-1.8	-0.6	-0.731	0.2	-1.4	-5.75	2.2	-1.8	-0.009
-1.8	-0.2	-1.573	0.2	-1	-1.803	2.2	-1.4	0.083

-1.8	0.2	-1.841	0.2	-0.6	0.836	2.2	-1	0.302
-1.8	0.6	-1.403	0.2	-0.2	0.674	2.2	-0.6	0.588
-1.8	1	-0.627	0.2	0.2	0.145	2.2	-0.2	0.793
-1.8	1.4	-0.002	0.2	0.6	0.449	2.2	0.2	0.784
-1.8	1.8	0.206	0.2	1	3.455	2.2	0.6	0.57
-1.8	2.6	0.051	0.2	1.4	7.241	2.2	1	0.327
-1.4	-3	0.002	0.2	1.8	7.099	2.2	1.4	0.174
-1.4	-2.6	-0.01	0.2	2.2	3.913	2.2	1.8	0.09
-1.4	-2.2	-0.025	0.2	2.6	1.323	2.2	2.2	0.039
-1.4	-1.8	0.105	0.6	-3	-0.203	2.2	2.6	0.012
-1.4	-1.4	0.518	0.6	-2.6	-0.934	2.6	-3	0
-1.4	-1	0.639	0.6	-2.2	-2.758	2.6	-2.6	-0.001
-1.4	-0.6	-0.424	0.6	-1.8	-4.96	2.6	-2.2	-0.001
-1.4	-0.2	-2.052	0.6	-1.4	-4.906	2.6	-1.8	0.004
-1.4	0.2	-2.758	0.6	-1	-1.985	2.6	-1.4	0.027
-1.4	0.6	-2.157	0.6	-0.6	0.374	2.6	-1	0.077
-1.4	1	-0.714	0.6	-0.2	0.818	2.6	-0.2	0.195
-1.4	1.4	0.586	0.6	0.2	0.725	2.6	0.2	0.192
-1.4	1.8	0.907	0.6	0.6	0.872	2.6	1	0.077
-1.4	2.2	0.547	0.6	1	2.819	2.6	1.4	0.037
-1.4	2.6	0.19	0.6	1.4	5.381	2.6	1.8	0.016
-1	-3	-0.03	0.6	1.8	5.189	2.6	2.2	0.006
-1	-2.6	-0.169	0.6	2.2	2.848	2.6	2.6	0.002

Using these data, models were identified through first order and higher order identification methods over the entire parametric range. In order to be in line with previous case, models of $\sigma \leq 10$ ($PI \leq 0.0463$) and $\sigma \leq 1$ ($PI \leq 0.00463$) are used for analysis. All the possible models with $\sigma \leq 10$ that were obtained by parametric study are shown in Figures 4.31-4.32. These figures present the performance behavior of first and higher order subtractive clustering models. Both types of modeling result in low error as the number of clusters is increased. The minimum error that is obtained with the second order model is higher than that of the first order model. This is due to the restriction imposed on the maximum number of rules as explained in Section 4.2.3 for the second order model which prevents it from further reduction in error. Alternatively, the higher order models will result in lower error than that of the first order model for the given number of rules, or the higher order models can result in less number of rules for the

acceptable range of error which is the important criterion for making the rule base compact. One could expect a similar trend of increase in the minimum error with decrease in the number of rules to follow as the order of regression is further increased.

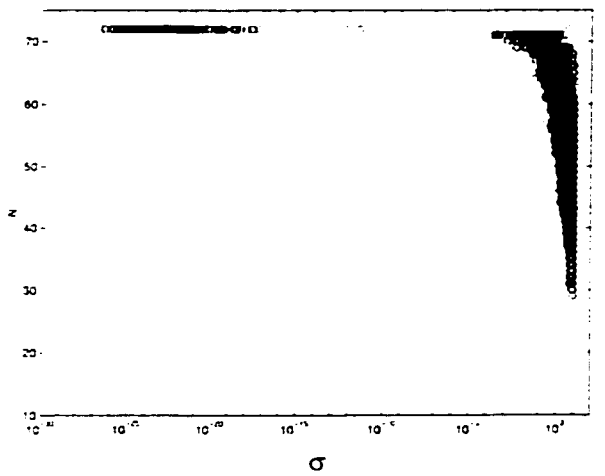

Figure 4.31 Variation of σ against *N* from collection of first order PEAKS models.

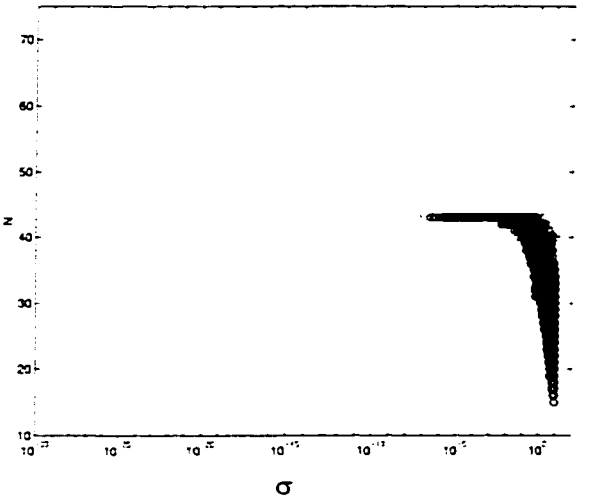

Figure 4.32 Variation of σ against *N* from collection of higher order PEAKS models.

Results given in Figures 4.33-4.40 present the effect of clustering parameters on performance of both types of model. Figures 4.33 and 4.34 present again the possibility of obtaining minimum error models over the entire range of squash factor. The variation of squash factor against cluster radius as given in Figures 4.35 and 4.36 for the first and the second order models show a similar trend of requiring lower cluster radius at high values of squash factor. This results in a preferred range of penalty radius as error is minimized as shown in Figures 4.37 and 4.38. In general it can be inferred that the possibility of obtaining models with lower error is high with lower penalty radius. The requirement of high cluster radius with smaller penalty radius could increase the zone of influence of cluster centers over the data space and also increase the possibility of forming new clusters in the neighborhood of cluster centers so that data space is

represented enough by the clusters [48]. The preferred range of accept ratio and penalty radius shown in Figures 4.39 and 4.40 for both types of model with $\sigma \leq 1$ ($PI \leq 0.00463$) indicate the similarity with previous nonlinear model.

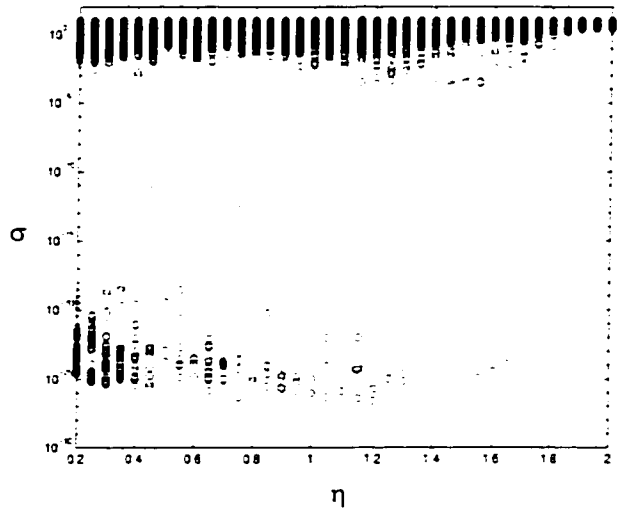

Figure 4.33 Collection of first order PEAKS models with $\sigma \leq 10$ in the domain of squash factor and least square error

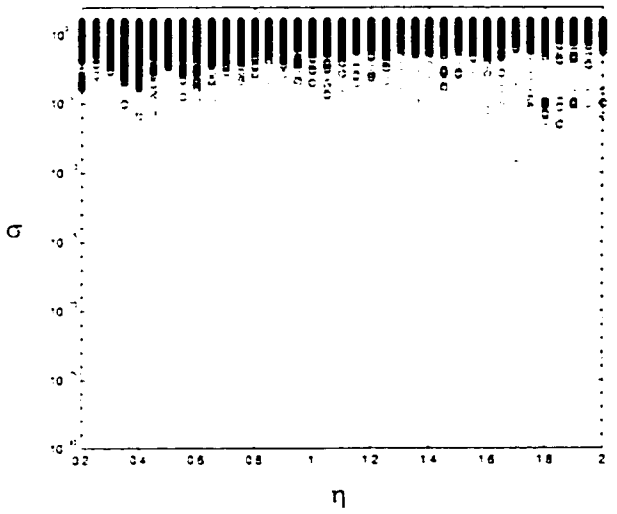

Figure 4.34 Collection of higher order PEAKS models with $\sigma \leq 10$ in the domain of squash factor and least square error

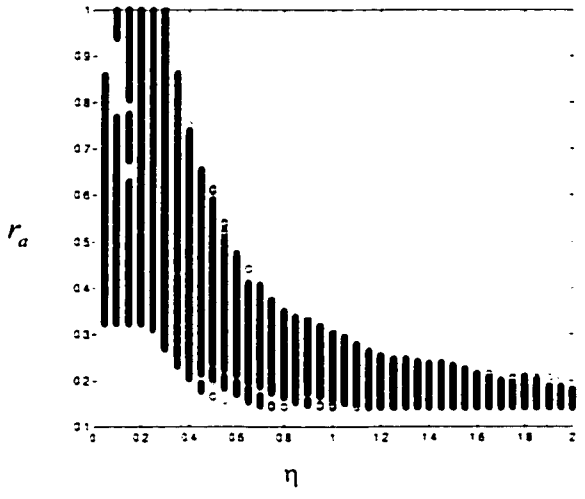

Figure 4.35 Collection of first order PEAKS models with $\sigma \leq 10$ in the domain of squash factor and cluster radius

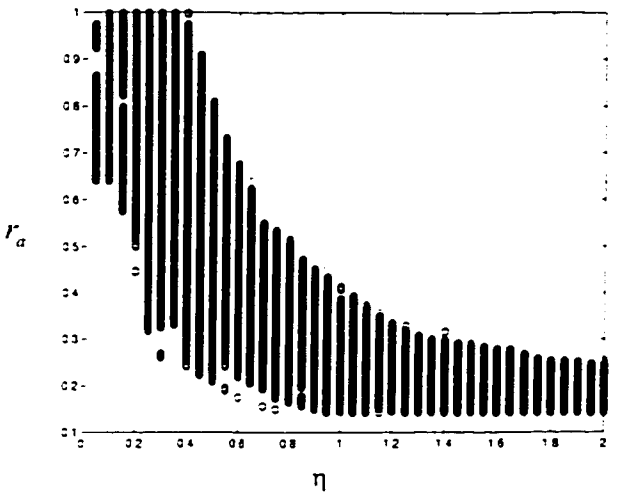

Figure 4.36 Collection of higher order PEAKS models with $\sigma \leq 10$ in the domain of squash factor and cluster radius

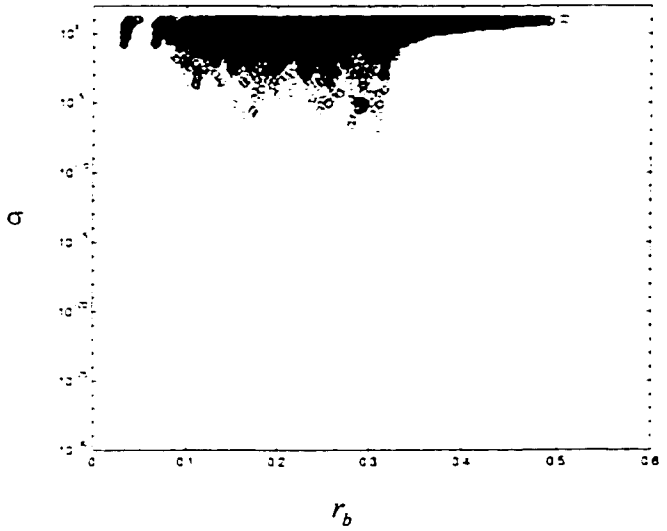

Figure 4.38 Collection of higher order PEAKS models in the domain of penalty radius and least square error

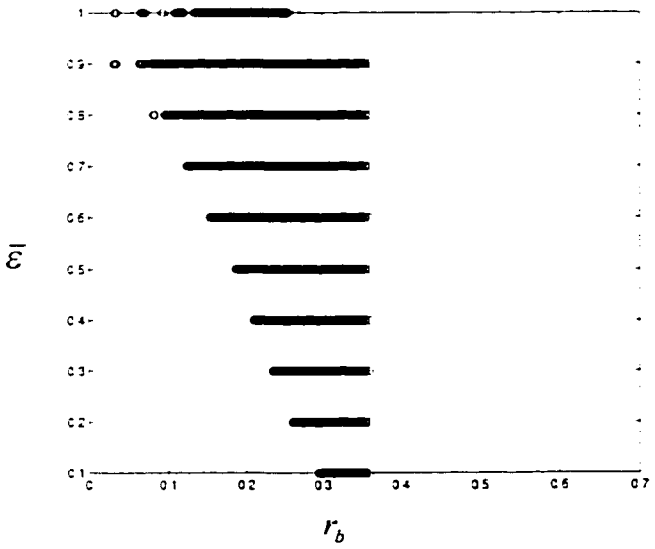

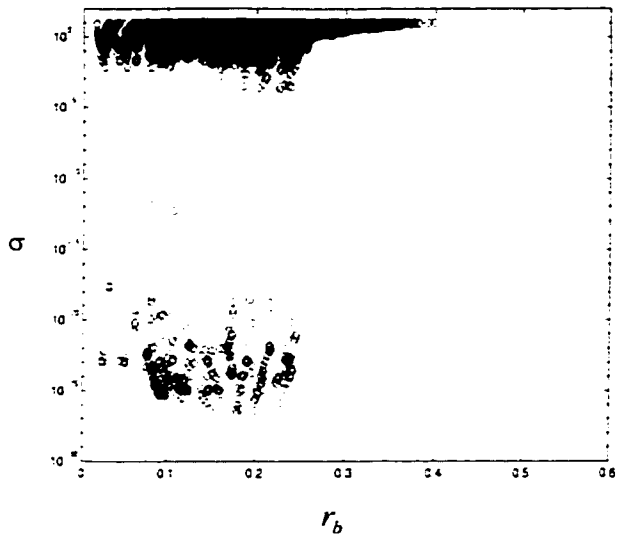

Figure 4.37 Collection of first order PEAKS models in the domain of penalty radius and least square error

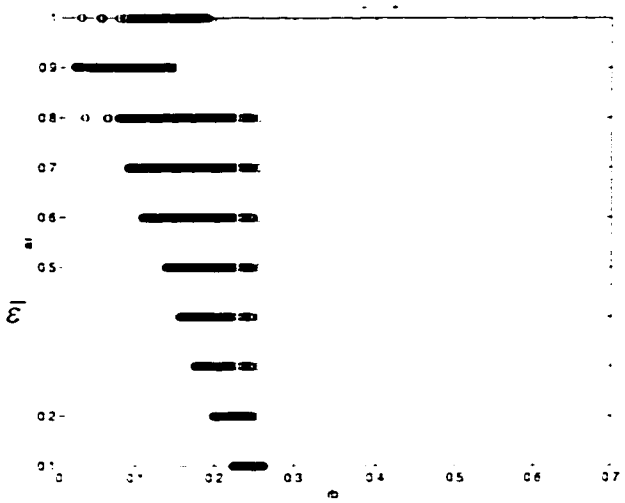

Figure 4.39 Collection of first order PEAKS models with $\sigma \leq 1$ in the domain of penalty radius and accept ratio

Figure 4.40 Collection of higher order PEAKS models with $\sigma \leq 1$ in the domain of penalty radius and accept ratio

The comparison of performance of first and higher order minimum error models for the PEAKS system is given in Table 4.4. These models are the ones without parameter identification. The models given in the table correspond to those with minimum error obtained through parametric search for different number of rules, and were selected only as examples. The drastic reduction of errors is found for the same number of rules with higher order system identification compared to that of first order system identification. The number of rules in higher order modeling is reduced to almost half of first order modeling and thus improves the performance of the system identification.

Table 4.4: Comparison of modeling performance for PEAKS system

N	σ		Clustering parameters for minimal model							
	First order clustering	Second order clustering	First order				Second Order			
			r_a	η	$\bar{\varepsilon}$	$\underline{\varepsilon}$	r_a	η	$\bar{\varepsilon}$	$\underline{\varepsilon}$
72	2.55×10^{-27}		0.150	1.20	0.4-0.9	0.3				
70	1.25×10^{-3}		0.168	1.25	0.20	0.0-0.1				
60	3.86×10^{-1}		0.164	1.20	0.4-0.9	0.30				
50	1.16		0.142	1.75	0.3-0.9	0.10				
43	1.86	3.55×10^{-10}	0.216	1.10	0.4-0.9	0.0-0.2	0.148	1.70	0.3-0.9	0.2
			0.216	1.10	1.0	0.0				
40	3.86	4.92×10^{-2}	0.176	1.65	0.2-0.9	0.00	0.190	1.60	0.10	0.0
30	7.87	1.16	0.208	1.50	0.3-0.9	0.0-0.1	0.208	1.50	0.3-0.9	0.-0.1
20		4.36					0.242	1.85	0.1	0.0

The identification results of the above two nonlinear systems (Cases 1 and 2) suggest performance improvement with higher order modeling even without parameter identification. The exact order of modeling depends upon the actual order of the system and hence it becomes problem dependent. The second order models without any input interactive terms are used as a simple case of higher order clustering in this thesis. The performance of a second order model on a first order system is investigated next.

CASE 3: Linear system with plane function

In order to demonstrate the generality of the modeling performance of the higher order subtractive clustering technique in capturing lower order systems, it is tested for a linear system of two inputs. The linear system considered is given by the equation

$$y = x_1 + x_2 : \quad -3 \le x_1 \le 3; -3 \le x_2 \le 3 \tag{4.35}$$

Randomly selected 72 input-output data points used for modeling above system are given in Table 4.5. Many models with zero error (i.e. in the order of $1x10^{-28}$) are obtained using both types of identification methods through a parametric search of clustering parameters. These zero error models are obtained over the entire range of clustering parameters for both the first order and the second order methods. The number of rules for these zero error models vary from 1 to 24 and 1 to 14 for the first order and the second order methods, respectively, which are limited by the number of regression coefficients. As expected, it is found from the results that the performance of higher order modeling is similar to that of first order modeling for this case of linear system. As an example, the rule bases with two rules of first order model with $\sigma = 1.74x10^{-29}$ and of

higher order model with $\sigma = 2.97x10^{-30}$ are given in Figures 4.41 and 4.42. The first order model in Figure 4.41 corresponds to the set of clustering parameters with r_a=0.9, η=1.85, $\bar{\varepsilon}$=1.0 and $\underline{\varepsilon}$=0.8 while the higher order model in Figure 4.42 corresponds to clustering parameter values of r_a=0.878, η=1.1, $\bar{\varepsilon}$=1.0 and $\underline{\varepsilon}$=0.4. As it can be observed from the rule base of the higher order model in Figure 4.42, the coefficients of the higher order terms are correctly identified as negligible. Thus, in the case of systems of unknown order, the higher order modeling will still be useful even when the system is over represented as in the case of the linear system except the computation effort would become large.

Table 4.5: Input-output data for plane function

x_1	x_2	y	x_1	x_2	y	x_1	x_2	y
-3	-3	-6	-1	-1	-2	1.5	-2	-0.5
-3	-2.5	-5.5	-1	0.5	-0.5	1.5	-1.5	0
-3	-0.5	-3.5	-1	1.5	0.5	1.5	-1	0.5
-3	0	-3	-1	2.5	1.5	1.5	-0.5	1
-3	0.5	-2.5	-0.5	-3	-3.5	1.5	0	1.5
-3	1	-2	-0.5	-1.5	-2	1.5	0.5	2
-3	2	-1	-0.5	-0.5	-1	1.5	1.5	3
-3	2.5	-0.5	-0.5	2	1.5	1.5	2	3.5
-2.5	-2.5	-5	0	-3	-3	1.5	2.5	4
-2.5	-1	-3.5	0	-2.5	-2.5	2	-3	-1
-2.5	0	-2.5	0	-1.5	-1.5	2	-2.5	-0.5
-2.5	0.5	-2	0	1	1	2	-1	1
-2.5	1	-1.5	0	2	2	2	0	2
-2.5	2	-0.5	0	2.5	2.5	2	0.5	2.5
-2	-2	-4	0.5	-3	-2.5	2	1	3
-2	-1	-3	0.5	-1.5	-1	2	2	4
-2	0.5	-1.5	0.5	0	0.5	2	2.5	4.5
-2	2.5	0.5	0.5	1	1.5	2.5	-3	-0.5
-1.5	-1.5	-3	0.5	1.5	2	2.5	-2	0.5
-1.5	-0.5	-2	0.5	2.5	3	2.5	-1	1.5
-1.5	0.5	-1	1	-1.5	-0.5	2.5	-0.5	2
-1.5	1	-0.5	1	-1	0	2.5	0.5	3
-1	-2.5	-3.5	1	0	1	2.5	1.5	4
-1	-2	-3	1.5	-3	-1.5	2.5	2.5	5

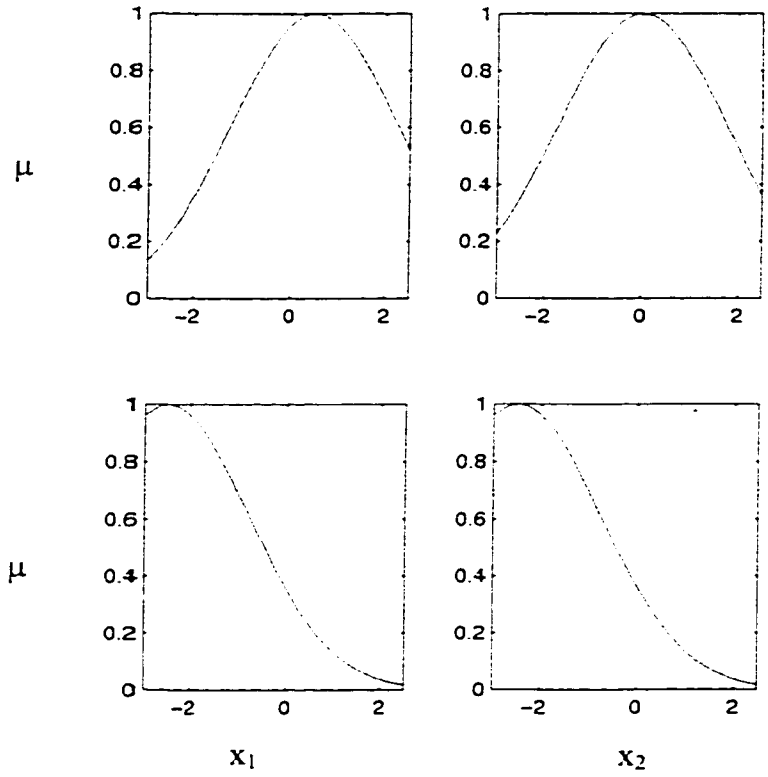

$$y^1 = -4.205 \times 10^{-17} + 1.0x_1 + 1.0x_2$$

$$y^2 = 8.704 \times 10^{-16} + 1.0x_1 + 1.0x_2$$

Figure 4.41 A first order model for a linear system with r_a=0.9, η=1.85, $\bar{\varepsilon}$ =1.0 and $\underline{\varepsilon}$ = 0.1

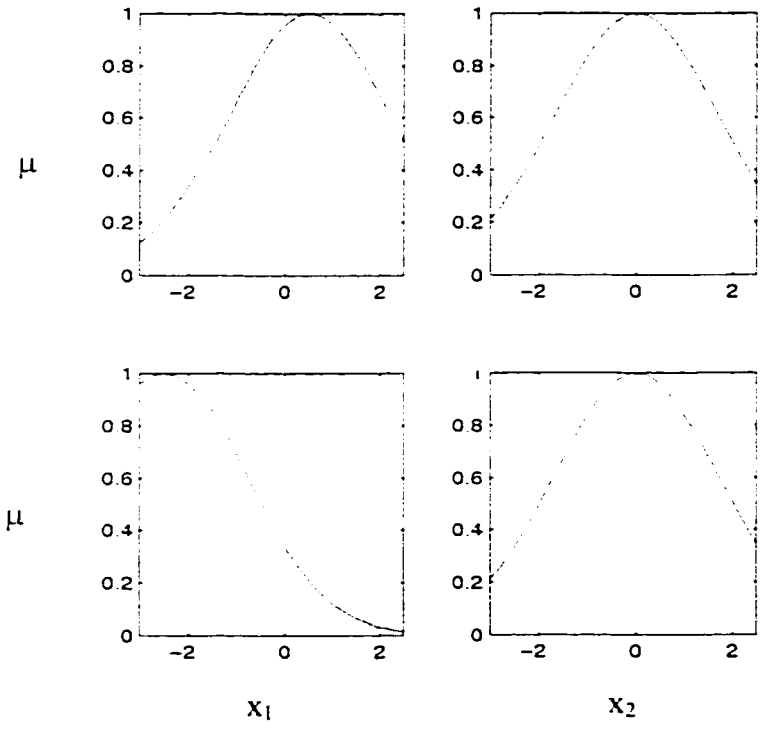

$$y^1 = -6.062 \times 10^{-17} + 1.0x_1 + 1.0x_2 + 1.383 \times 10^{-16} x_1^2 - 1.803 \times 10^{-17} x_2^2$$

$$y^2 = 5.528 \times 10^{-16} + 1.0x_1 + 1.0x_2 - 2.546 \times 10^{-18} x_1^2 + 5.369 \times 10^{-18} x_2^2$$

Figure 4.42 A higher order model for a linear system with r_a=0.878, η=1.1, $\bar{\varepsilon}$ =1.0 and $\underline{\varepsilon}$ = 0.5

4.3 FUZZY SYSTEM IDENTIFICATION OF STRUCTURAL TUNING USING SUBTRACTIVE CLUSTERING

The modeling with fuzzy subtractive clustering has been validated for complex and simple cases in the previous section as an example of auto generation of models from the input-output data. The higher order system identification has been developed as a tool for identifying very complex systems such as structural tuning with minimum number of rules. The higher order system identification will be very useful when the number BC parameters is large and the output dynamic performance is complicated with reference to input BC parameters.

An automatic fuzzy system identification of structural tuning is demonstrated in this section as an example to boundary conditioning. In many real applications, it may be possible to measure the input BC parameters and output performance measures experimentally. When the number of input parameters are large, the insignificant variables can be eliminated as given in [48]. Once the relevant BC parameters are identified for the required output, the input-output relationship can be identified through subtractive clustering.

In this section, the system identification of structural tuning is performed using subtractive clustering technique combined with Mamdani, TSK first order and second order types of regression as seen in the Section 4.2. The function approximation of three harmonic functions Λ_{13358}, Λ_{13357} and $\Lambda_{13356.6}$ given in Figures 4.4a, 4.5a and 4.6a are

performed through input-output data representing these surfaces. Only the data pairs having the $\Lambda_h \leq 0.016$ are considered for system identification. The corresponding input-output data are selected for system identification. The number of data pairs selected for Λ_{13358}, Λ_{13357} and $\Lambda_{13356.6}$ are 310, 434 and 320 and are given in Tables A.1, A.2 and A.3 respectively.

4.3.1 Identification of Objective Functions using Mamdani Reasoning

The system of three objective harmonic functions Λ_{13358}, Λ_{13357} and $\Lambda_{13356.6}$ are identified in terms of fully MISO fuzzy models with fuzzy subtractive clustering. The fuzzy rule base will be of the from:

$$R^1 : IF \log K^*_{R.1} \text{ is } A^1_1 \text{ AND } \log K^*_{R.2} \text{ is } A^1_2 \text{ THEN } \Lambda_h \text{ is } B^1$$

$$ALSO$$

$$\vdots$$

$$ALSO$$

$$R^N : IF \log K^*_{R.1} \text{ is } A^N_1 \text{ AND } \log K^*_{R.2} \text{ is } A^N_2 \text{ THEN } \Lambda_h \text{ is } B^N \tag{4.37}$$

where $K^*_{R.1}$ and $K^*_{R.2}$ are two antecedents Λ_h is the consequent which can be any of one of the harmonic functions. A^j_i *for (i = 1 and 2)* and *(j = 1,2,...., N)* are linguistic fuzzy sets of input rotational stiffnesses and B^j *for (j = 1,2,...., N)* are linguistic fuzzy sets of the consequent. These fuzzy sets need to be generated through subtractive clustering technique.

The clusters are formed using the data given in the Tables A.1 - A.3 in the combined input-output space of rotational stiffnesses and objective functions and they are projected onto each dimension as shown in Figure 4.14. Each cluster forms a rule and projections of these clusters are the fuzzy sets of antecedents and consequent. The output from the model can be estimated for Mamdani type of inferencing as given in the Section 4.1.4. The modeling least square σ is estimated using the Equation 4.32. It is known that the performance of the model is very much dependent on the clustering parameters and the pattern of input-output data. The models with minimum error are obtained through enumerative search of clustering parameters. The range of the clustering parameters such as accept ratio, reject ratio, squash factor and cluster radius selected for enumerative search are 0-1.0, 0-0.8, 0.2-2.0 and 0.05-1.0, respectively, that cover entirely the possible range. The step sizes for accept ratio, reject ratio, squash factor and cluster radius are selected as 0.2, 0.2, 0.1 and 0.05, respectively. It has been found during the parametric search that cluster radius and squash factor have strong influence on performance of the modeling when compared to accept ratio and reject ratio. For example, the variation of number of rules, N and the error σ shown in Figures 4.43 to 4.48 for the fixed vales of accept ratio and reject ratio indicate the strong influence of cluster radius on the performance for Mamdani reasoning. The possible models that were obtained for Λ_{13358} with $\sigma \leq 0.0014$ through enumerative search and are shown in Figures 4.49, 4.50 and 4.51. The other models for $\Lambda_{13357}(\sigma \leq 0.003)$ and $\Lambda_{13356.6}$ $(\sigma \leq 0.0019)$are shown in Figures 4.52 to 4.57. These figures that suggest the decrease in cluster radius and penalty radius improve the error which in turn result in increase of the number of rules. Hence, optimum values of clustering parameters need to be obtained based on the acceptable

error. The average error of α=0.002 is used as the limit of acceptance for the models and it is defined as

$$\alpha = \frac{\sqrt{\sigma}}{u \cdot \dddot{\lambda}} \tag{4.38}$$

where σ is the least square error, u is the number of data points used for modeling and $\dddot{\lambda}$ is mean of the entire output population.

The variation of model and predicted Λ_{13358} is shown in Figure 4.58 for at $\bar{\varepsilon}$ =1.0, $\underline{\varepsilon}$=0.2, η=1.8, r_a=0.05, N=125 and σ = 5.111e-5 which corresponds to α=0.002. The upper limit of the least square error used for selecting the model for Λ_{13358}, Λ_{13357} and $\Lambda_{13356.6}$ are 5.111e-5, 8.468e-5 and 8.67e-5, respectively. The identified system Λ_{13358} for the clustering parameters of $\bar{\varepsilon}$ =1.0, $\underline{\varepsilon}$=0.2, η=1.8 and r_a=0.05, with σ=5.1116e-5 and N=125 is given in Figures 4.59. In similar way, the identified system for Λ_{13357} for the clustering parameters of $\bar{\varepsilon}$ =0.4, $\underline{\varepsilon}$=0.2, η=1.4 and r_a=0.05, with σ=8.4686e-5 and N=222 is given in Figure 4.60 and the rule base identifying $\Lambda_{13356.6}$ for the clustering parameters of $\bar{\varepsilon}$ =0.4, $\underline{\varepsilon}$=0.2, η=0.8 and r_a=0.05, with σ=8.671e-5 and N=294 is given in Figure 4.61. The identified systems in Figures 4.59-4.61 can be used for function approximation or for classification of the harmonics functions.

The number of rules is extremely large because the model is not subjected to any parameter identification process. The number of rules will increase if the number of BC parameters increase further.

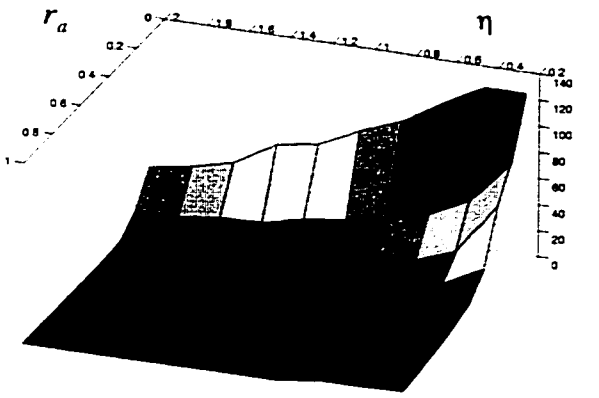

Figure 4.43 Variation of number of rules against squash factor and cluster radius for Λ_{13358} at $\bar{\varepsilon}$ = 0.8 and $\underline{\varepsilon}$ = 0.2

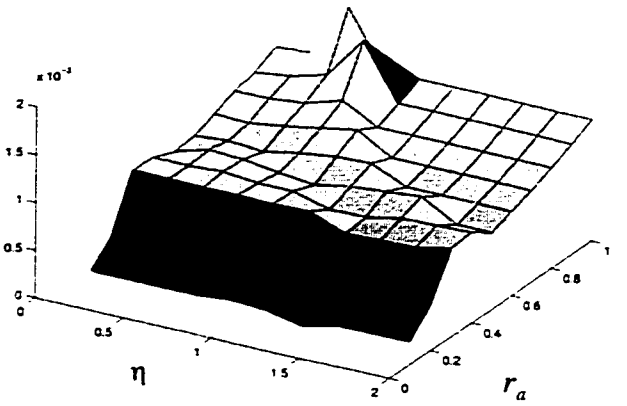

Figure 4.44 Variation of σ against squash factor and cluster radius for Λ_{13358} at $\bar{\varepsilon}$ = 0.8 and $\underline{\varepsilon}$ = 0.2

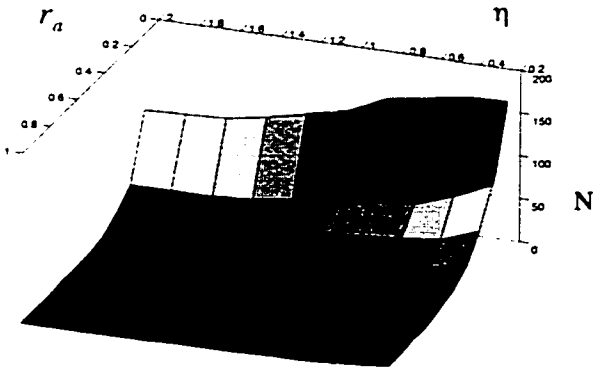

Figure 4.45 Variation of number of rules against squash factor and cluster radius for Λ_{13357} at $\bar{\varepsilon}$ = 1.0 and $\underline{\varepsilon}$ = 0.0

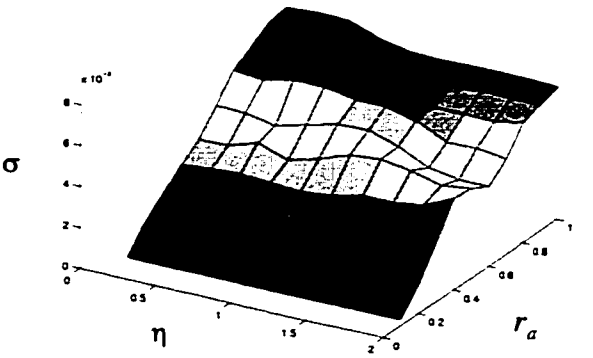

Figure 4.46 Variation of σ against squash factor and cluster radius for Λ_{13357} at $\bar{\varepsilon}$ = 1.0 and ε = 0.0

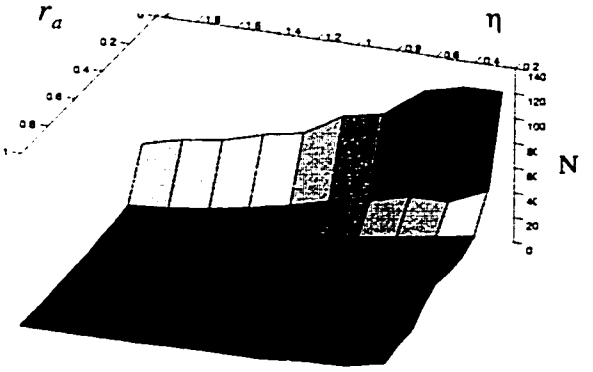

Figure 4.47 Variation of number of rules against squash factor and cluster radius for Λ_{133566} at $\bar{\varepsilon}$ = 1.0 and $\underline{\varepsilon}$ = 0.8

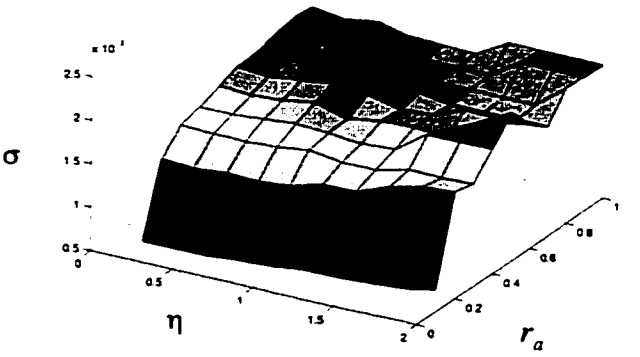

Figure 4.48 Variation of σ against squash factor and cluster radius for Λ_{133566} at $\bar{\varepsilon}$ = 1.0 and $\underline{\varepsilon}$ = 0.8

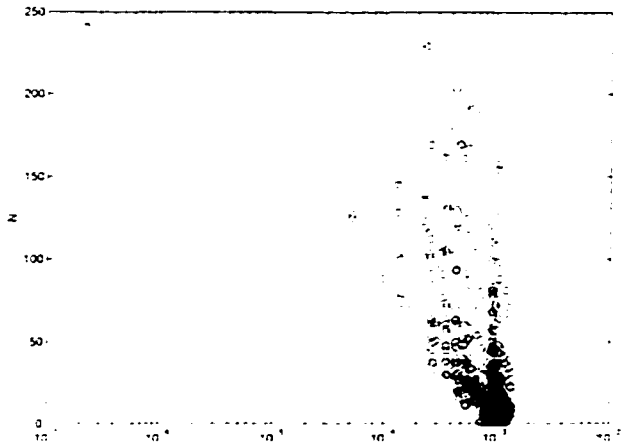

Figure 4.49 Variation of σ against N for Λ_{13358} models for $\sigma \leq 0.0014$

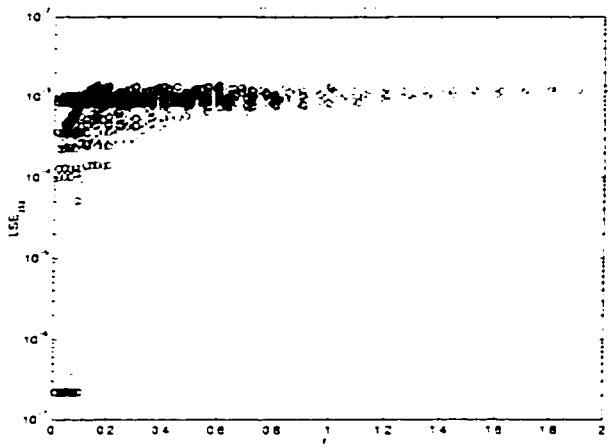

Figure 4.50 Collection of Λ_{13358} models in the domain of penalty radius and least square error for $\sigma \leq 0.0014$

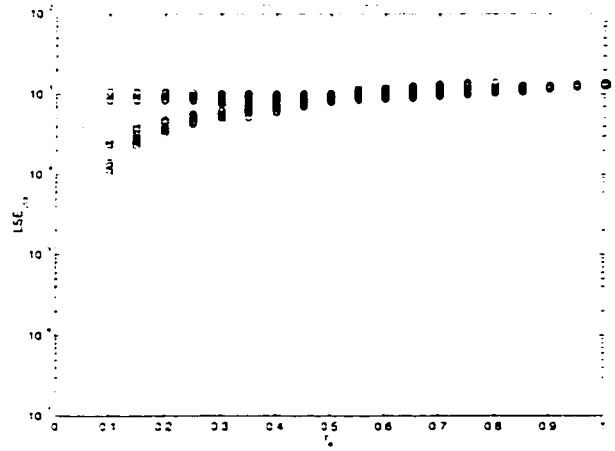

Figure 4.51 Collection of Λ_{13358} models with $\sigma \leq 0.0014$ in the domain of least square error and cluster radius

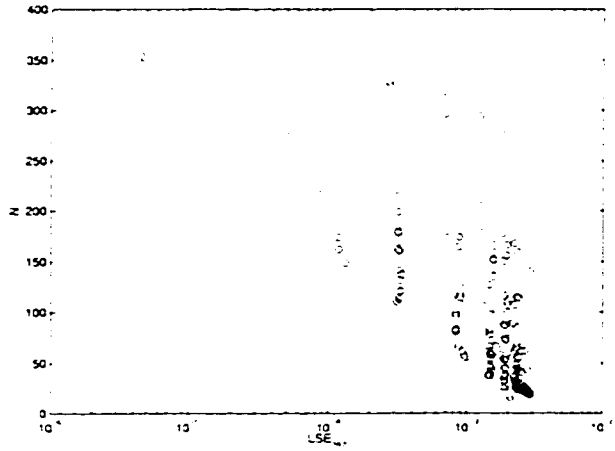

Figure 4.52 Variation of σ against N for Λ_{13357} models for $\sigma \leq 0.003$

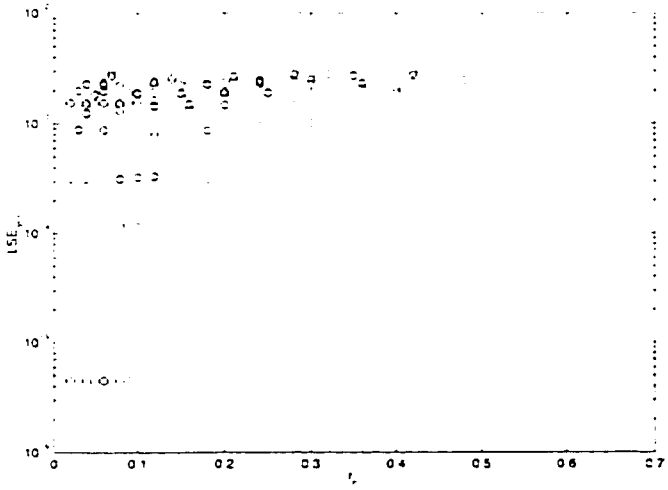

Figure 4.53 Collection of Λ_{13357} models in the domain of penalty radius and least square error for $\sigma \leq 0.003$

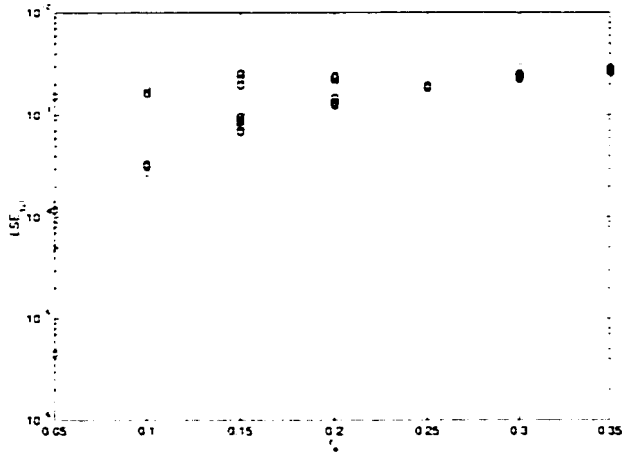

Figure 4.54 Collection of Λ_{13357} models with $\sigma \leq 0.003$ in the domain of least square error and cluster radius

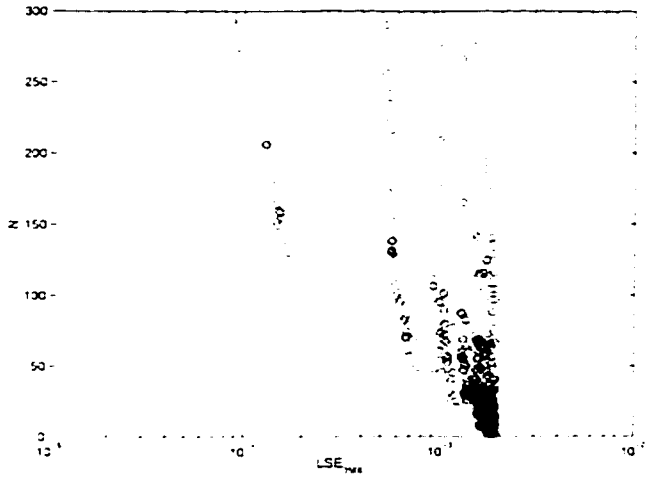

Figure 4.55 Variation of σ against N for Λ_{13358} models for $\sigma \leq 0.0019$

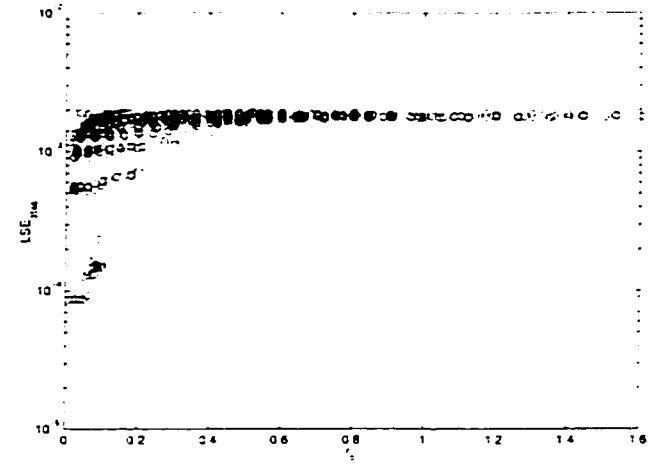

Figure 4.56 Collection of $\Lambda_{13356.6}$ models in the domain of penalty radius and least square error for $\sigma \leq 0.0019$

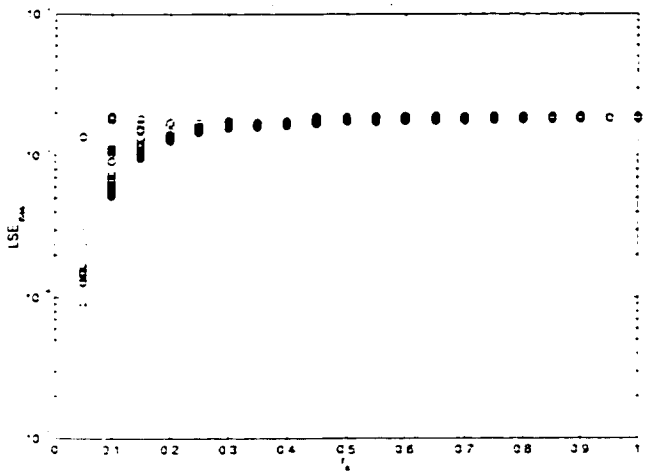

Figure 4.57 Collection of $\Lambda_{13356.6}$ models with $\sigma \leq 0.0019$ in the domain of least square error and cluster radius

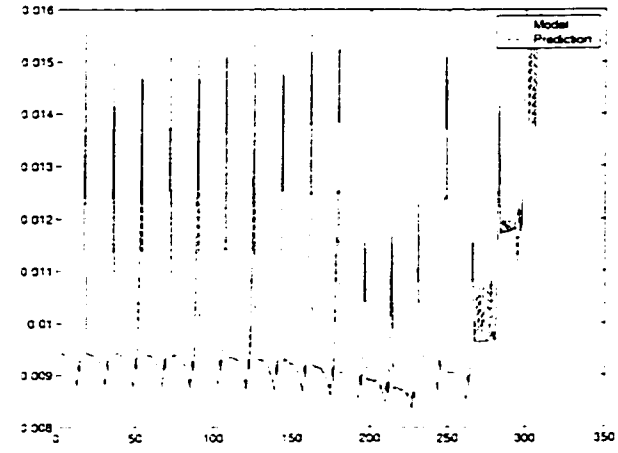

Figure 4.58 Model and predicted variation of Λ_{13358} at $\bar{\varepsilon}$ =1.0, $\underline{\varepsilon}$=0.2, η=1.8, r_a=0.05, N=125 and α = 0.002

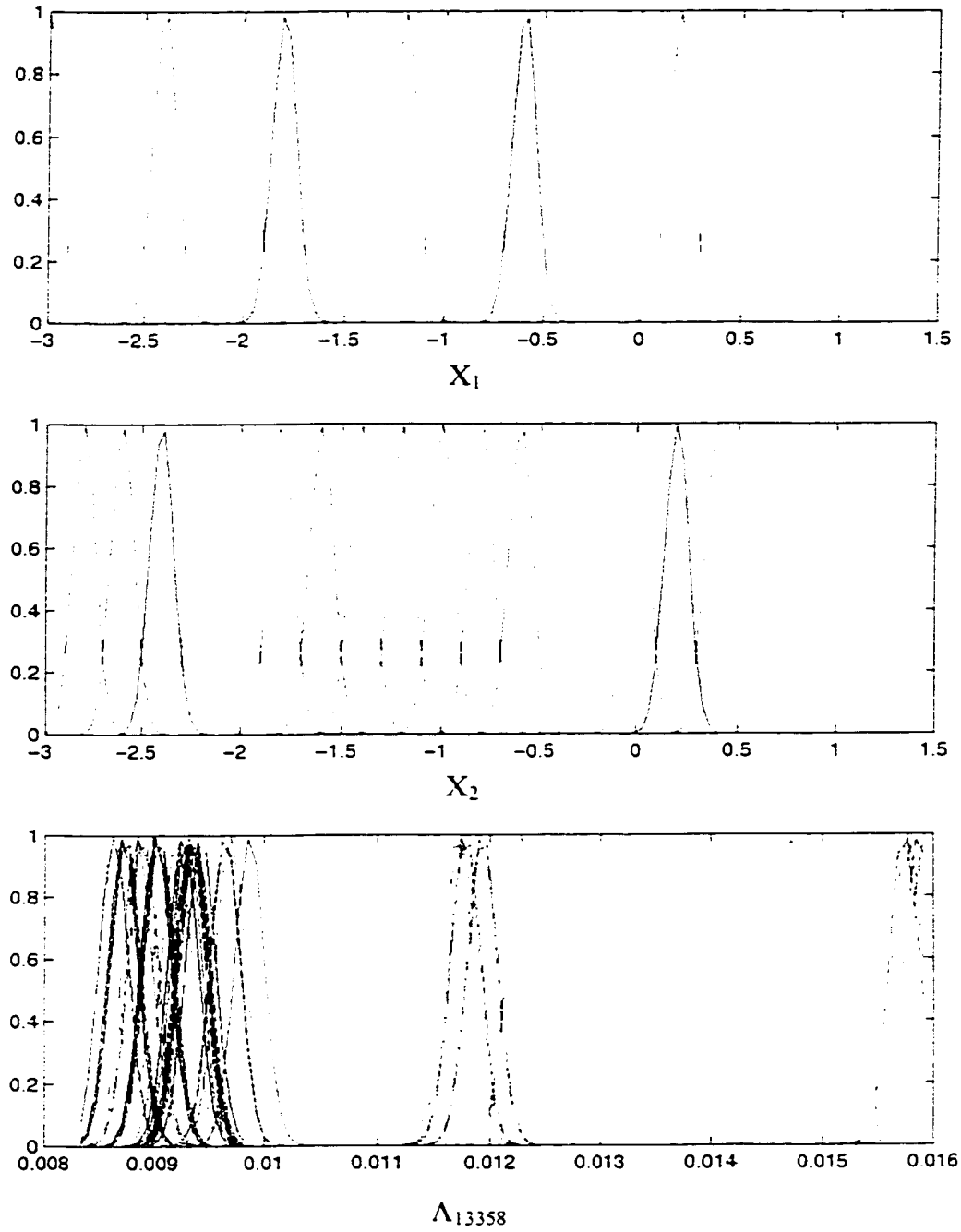

Figure 4.59 Mamdani rule base for Λ_{13358} $\bar{\varepsilon}$ =1.0, $\underline{\varepsilon}$=0.2, η=1.8, r_a=0.05, N=125 and σ=5.1116e-5

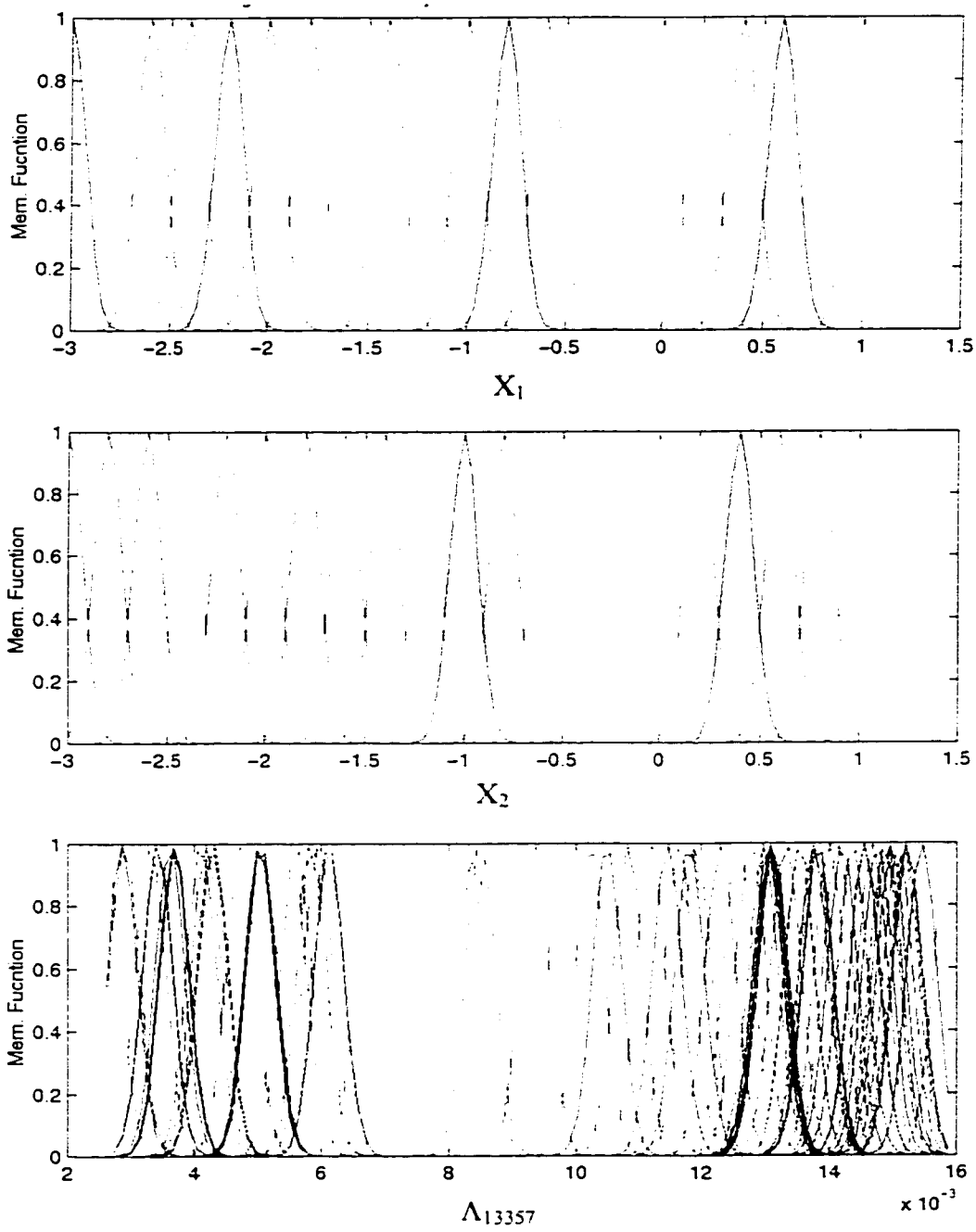

Figure 4.60 Mamdani rule base for Λ_{13357} $\bar{\varepsilon}$ =0.4, $\underline{\varepsilon}$=0.2, η=1.4, r_a=0.05, N=222 and σ=8.468e-5

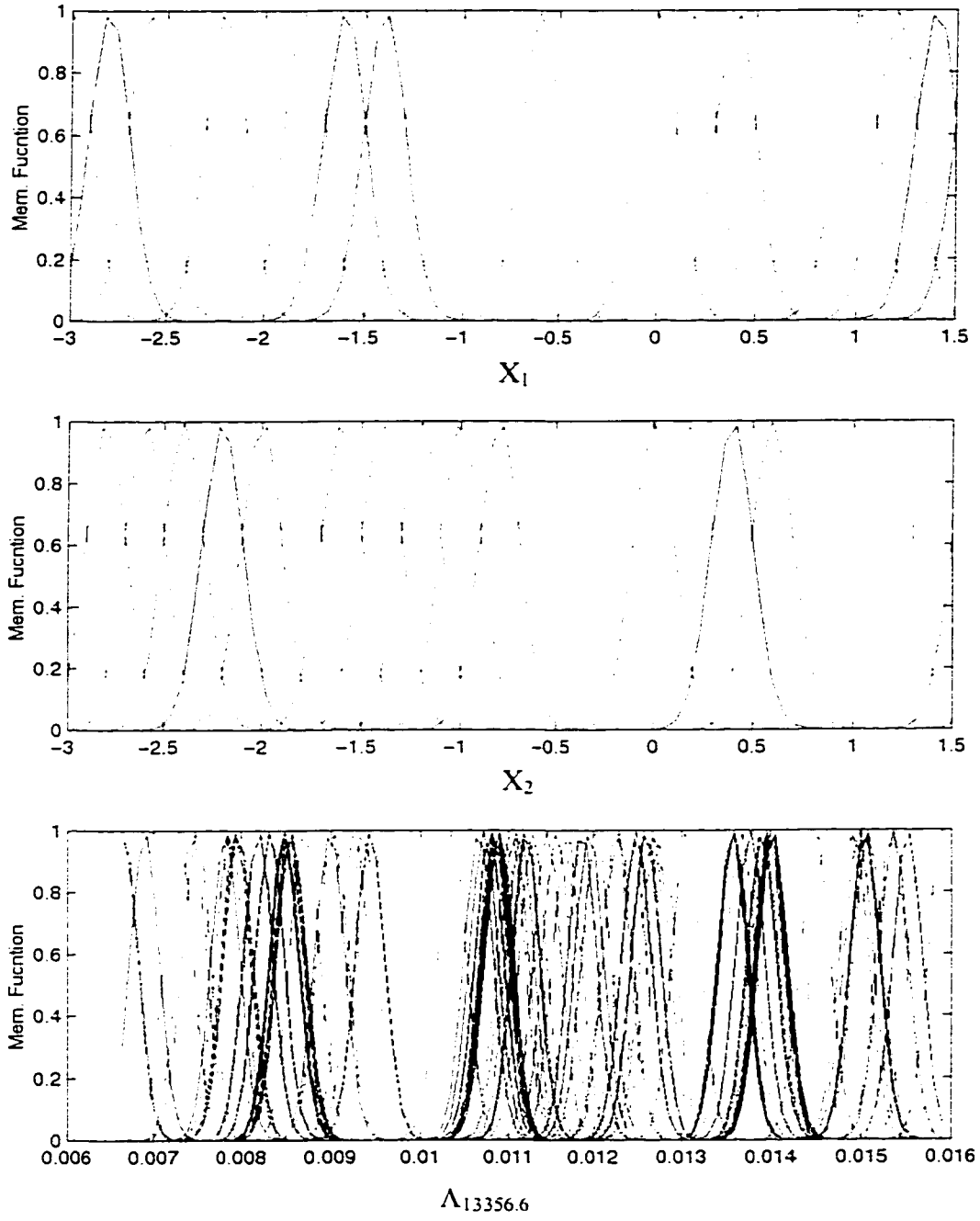

Figure 4.61 Mamdani rule base for $\Lambda_{13356.6}$ $\bar{\varepsilon}$ =0.4, $\underline{\varepsilon}$=0.2, η=0.8, r_a=0.05, N=294 and σ=8.6716e-5

4.3.2 Identification of Objective Functions using Sugeno Reasoning

We have seen that the Sugeno reasoning involves parameter optimization in obtaining regression parameters which will result in lower number of rules compared to that of Mamdani reasoning. The identification of objective functions are carried out in this section by applying the first order and higher order system identification technique in line with case studies.

The system identified will be of the form

$$R^1 : IF\ x_1\ is\ A_1^1\ AND\ x_2\ is\ A_2^1\ \ THEN\ \ \Lambda_h = P_{00}^1 + P_{10}^I\ x_1 + P_{01}^I\ x_2$$

$$ALSO$$

$$\vdots$$

$$ALSO$$

$$R^N : IF\ x_1\ is\ A_1^N\ AND\ x_2\ is\ A_2^N\ \ \ THEN\ \ \Lambda_h = P_{00}^N + P_{10}^N\ x_1 + P_{01}^N\ x_2 \tag{4.39}$$

for the first order modeling and

$$R^1 : IF\ x_1\ is\ A_1^1\ AND\ x_2\ is\ A_2^1\ \ THEN\ \ \Lambda_h = P_{00}^1 + P_{10}^I\ x_1 + P_{01}^I\ x_2 + P_{20}^I\ x_1^2 + P_{02}^I\ x_2^2$$

$$ALSO$$

$$\vdots$$

$$ALSO$$

$$R^N : IF\ x_1\ is\ A_1^N\ AND\ x_2\ is\ A_2^N\ \ \ THEN\ \ \Lambda_h = P_{00}^N + P_{10}^N\ x_1 + P_{01}^N\ x_2 + P_{20}^I\ x_1^N + P_{02}^I\ x_2^N \tag{4.40}$$

for the second order modeling.

where P_{ij}^{k} *for* $(i, j = 0,1,2; k = 1,2,\ldots,N)$ are consequent regression parameters that are optimized by least square estimation (LSE) given by Takagi and Sugeno [175], antecedents x_1 and x_2 are $\log K_{R,1}^{*}$ and $\log K_{R,2}^{*}$ and Λ_h is the consequent which can be any one of the harmonic functions. A_i^j *for* $(i = 1 \text{ and } 2)$ and $(j = 1,2,\ldots,N)$ are linguistic fuzzy sets of input rotational stiffnesses to be obtained through subtractive clustering.

The models of the objective functions were obtained through the parametric search of first and second order regression using the data points in the Tables A.1 - A.3. The range of the clustering parameters such as accept ratio, reject ratio, squash factor and cluster radius selected for enumerative search are 0-1.0, 0-0.8, 0.1-2.0 and 0.12-1.0, respectively, that cover entirely the possible range. The step sizes for accept ratio, reject ratio, squash factor and cluster radius are selected as 0.2, 0.2, 0.1 and 0.02, respectively. The variation of least square error with penalty and cluster radii was similar with that of other cases. Hence, only the performance of the models are discussed in this section.

The first and second order models of the objective function Λ_{13358} for $\sigma \leq 0.0014$ $(\alpha \leq 0.012)$ that were obtained by parametric study are shown in Figures 4.62 and 4.63, respectively. Similarly, the first and second order models of Λ_{13357} for $\sigma \leq 0.003$ $(\alpha \leq 0.012)$ and of $\Lambda_{13356.6}$ for $\sigma \leq 0.0019$ $(\alpha \leq 0.012)$ are given in Figures 4.64-4.65 and 4.66-4.67, respectively. These figures present the effect of first and higher order modeling methods on the performance behavior of models which is similar to that of previous examples. It is very interesting to note the great reduction in number of rules

for the higher order system identification when compared to that of first order method. Thus, the development of higher order methods becomes very useful for identifying the complex systems such as structural tuning or boundary conditioning. The identified models of first and second order with minimum number of rules and error within the acceptable limits, are given in Figures 4.68-4.69, 4.70-4.71 and 4.72-4.73 for objective functions Λ_{13358}, Λ_{13357} and $\Lambda_{13356.6}$, respectively. The final comparison of the performance of Mamdani models, and first and higher order sugeno clustering models are given in the Table 4.6 and this comparison explains the necessity for the development of higher order system identification methods for identifying complicated systems like boundary conditioning.

Table 4.6 Comparison of performance results of clustering

				Subtractive Clustering Parameters			
		N	σ	$\bar{\varepsilon}$	$\underline{\varepsilon}$	η	r_a
Λ_{13358}	Mamdani	125	5.11×10^{-5}	1.0	0.2	1.8	0.05
	I order	7	3.68×10^{-5}	0.2	0.0	2.0	0.44
	II order	4	2.26×10^{-5}	0.2	0.0	2.0	0.48
Λ_{13357}	Mamdani	222	8.46×10^{-5}	0.4	0.2	1.4	0.05
	I order	20	4.66×10^{-5}	0.2	0.0	2.0	0.30
	II order	6	4.74×10^{-5}	0.2	0.0	1.4	0.58
$\Lambda_{13356.6}$	Mamdani	294	8.67×10^{-5}	0.4	0.2	0.8	0.05
	I order	20	6.03×10^{-5}	0.2	0.0	1.0	0.22
	II order	5	6.68×10^{-5}	0.6	0.4	1.6	0.26

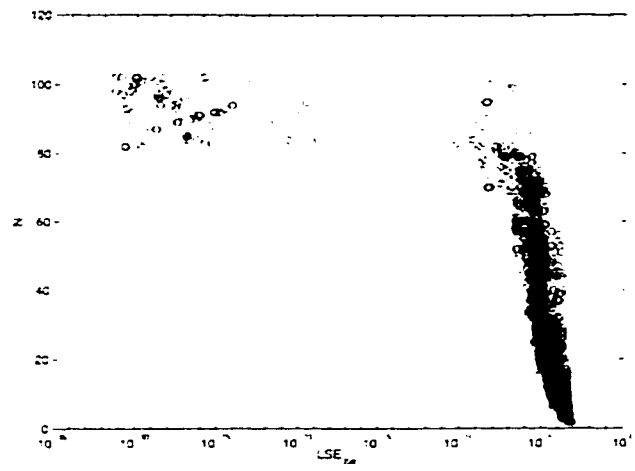

Figure 4.62 Variation of σ against N for the first order models of Λ_{13358} for $\sigma \leq 0.0014$

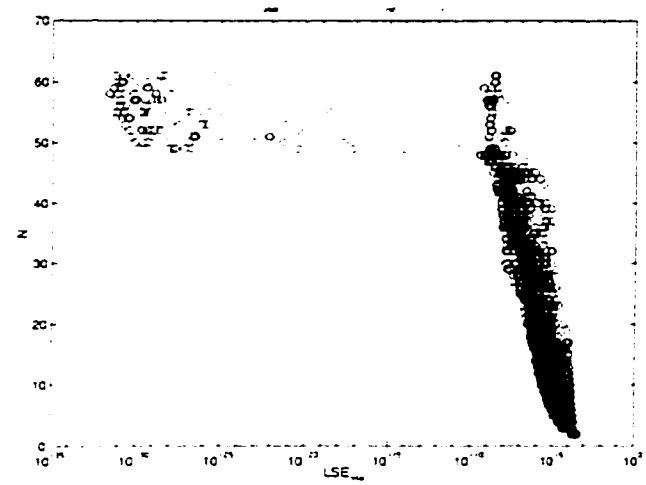

Figure 4.63 Variation of σ against N for the second order models of Λ_{13358} for $\sigma \leq 0.0014$

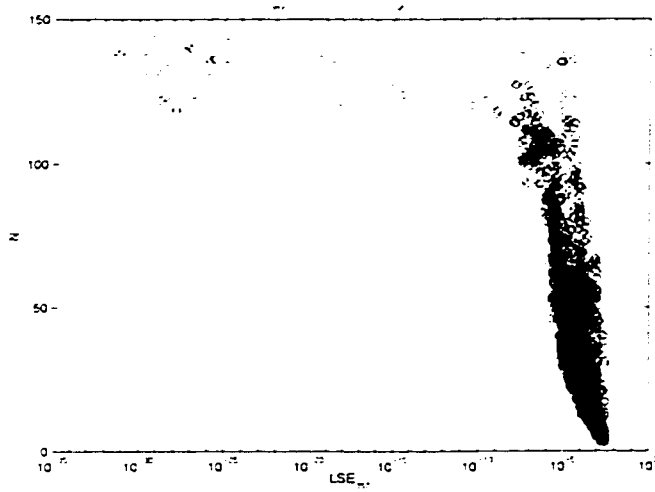

Figure 4.64 Variation of σ against N for the first order models of Λ_{13357} for $\sigma \leq 0.003$

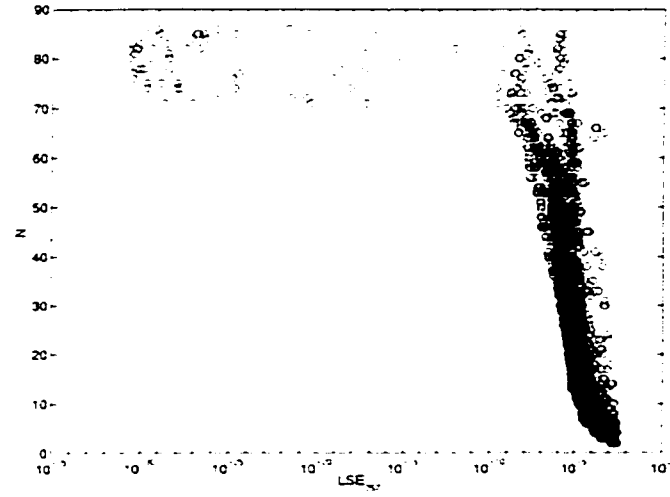

Figure 4.65 Variation of σ against N for the second order models of Λ_{13357} for $\sigma \leq 0.003$

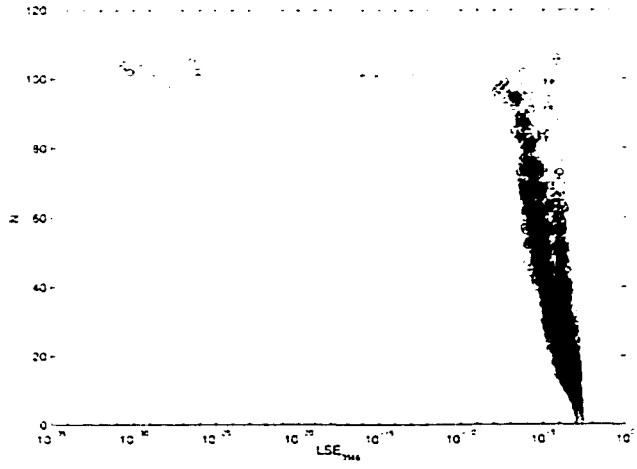

Figure 4.66 Variation of σ against N for the first order models of $\Lambda_{13356.6}$ for $\sigma \leq 0.0019$

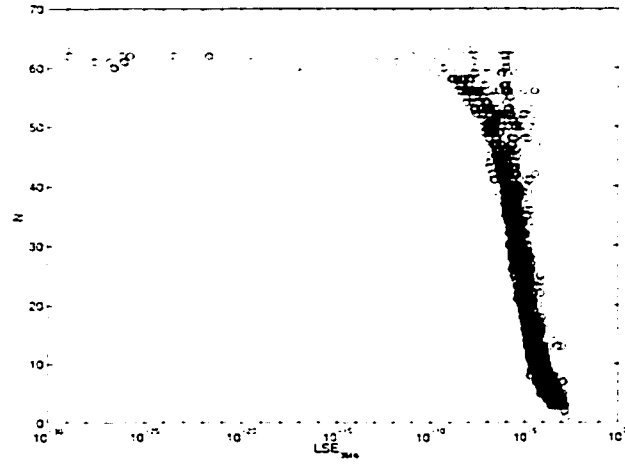

Figure 4.67 Variation of σ against N for the second order models of $\Lambda_{13356.6}$ for $\sigma \leq 0.0019$

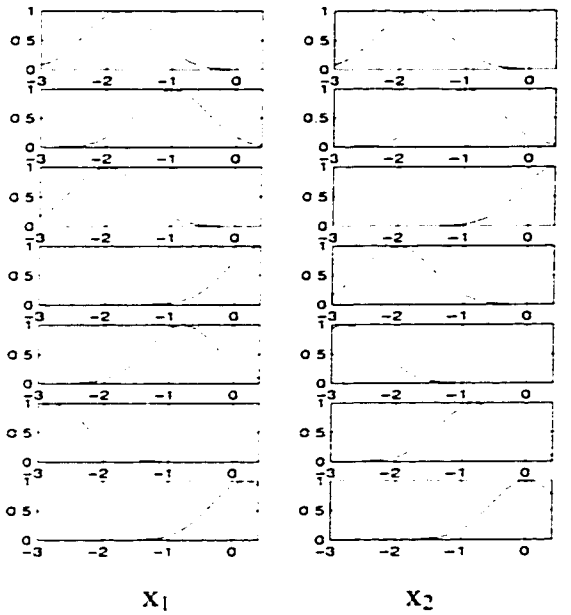

$$y^1 = 5.913e-03 - 6.491e-04x_1 - 6.940e-04x_2$$

$$y^2 = 9.958e-03 - 3.315e-04x_1 - 4.318e-04x_2$$

$$y^3 = 9.316e-03 + 2.737e-05x_1 + 1.725e-02x_2$$

$$y^4 = 9.485e-03 + 1.746e-02x_1 + 1.332e-04x_2$$

$$y^5 = 1.362e-02 + 6.086e-04x_1 + 1.086e-03x_2$$

$$y^6 = 1.369e-02 + 1.141e-03x_1 + 5.281e-04x_2$$

$$y^7 = 1.384e-02 + 4.300e-03x_1 + 4.090e-03x_2$$

Figure 4.68 A first order model for Λ_{13358} with r_a=0.44, η=2.0, $\bar{\varepsilon}$ =0.2, $\underline{\varepsilon}$ = 0.0, N=7 and σ=3.68e-5

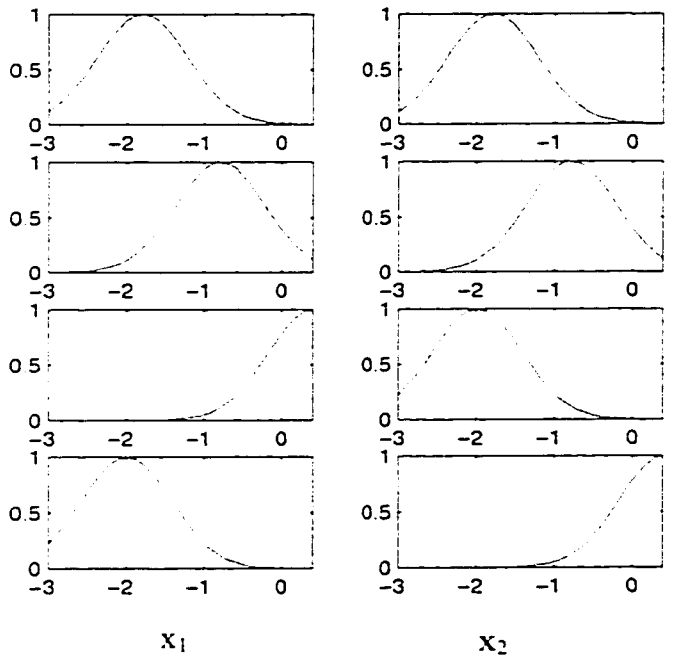

$$y^1 = 4.558e-03 - 1.832e-03x_1 - 1.832e-03x_2 - 3.557e-04x_1^2 - 3.557e-04x_2^2$$

$$y^2 = 1.288e-02 + 4.698e-03x_1 + 4.698e-03x_2 + 2.421e-03x_1^2 + 2.421e-03x_2^2$$

$$y^3 = 1.001e-02 + 1.058e-02x_1 + 8.709e-04x_2 + 1.384e-02x_1^2 + 2.280e-04x_2^2$$

$$y^4 = 1.001e-02 + 8.709e-04x_1 + 1.058e-02x_2 + 2.280e-04x_1^2 + 1.384e-02x_2^2$$

Figure 4.69 A second order model for Λ_{13358} with r_a=0.48, η=2.0, $\bar{\varepsilon}$ =0.2, $\underline{\varepsilon}$ = 0.0, N=4 and σ=2.26e-5

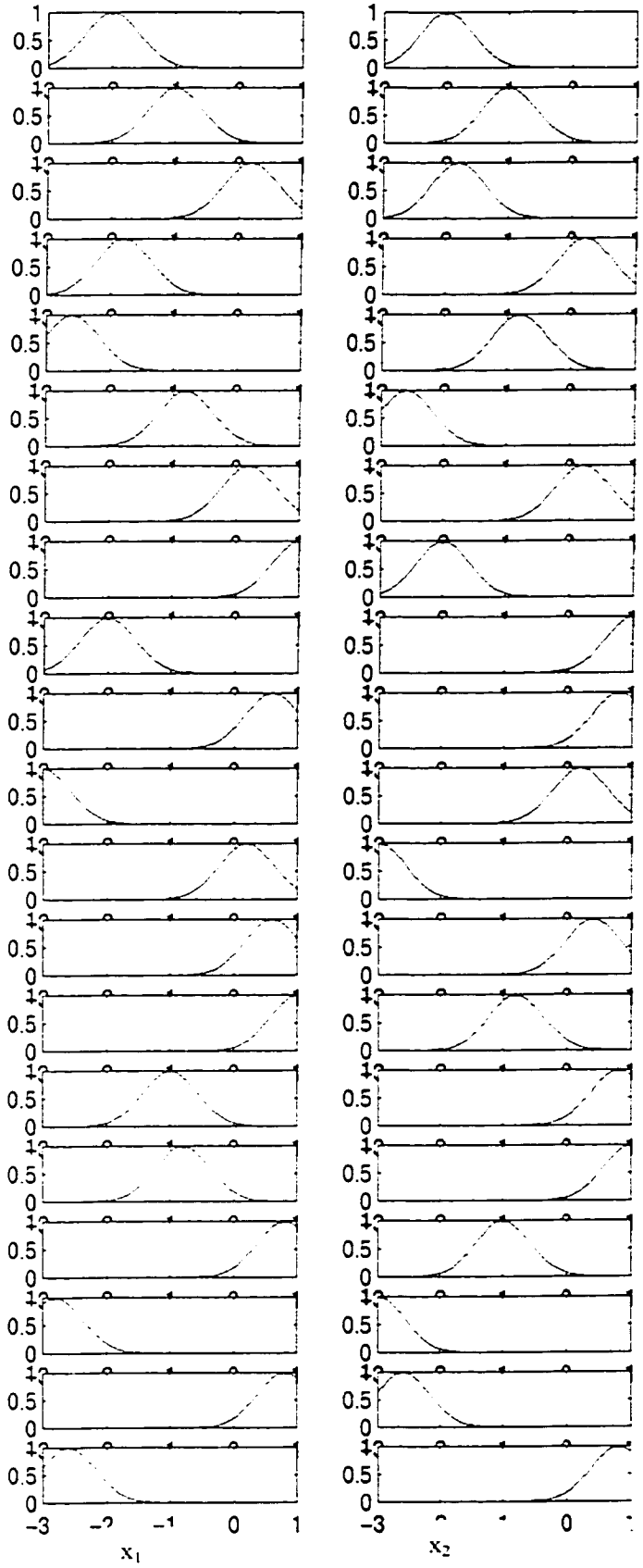

$$y^1 = 1.341e-02 - 3.176e-04x_1 - 3.528e-04x_2$$

$$y^2 = 6.297e-03 - 2.803e-03x_1 - 2.769e-03x_2$$

$$y^3 = 6.582e-03 - 8.788e-03x_1 + 2.713e-04x_2$$

$$y^4 = 6.636e-03 + 4.851e-04x_1 - 8.724e-03x_2$$

$$y^5 = 9.075e-03 - 5.643e-04x_1 - 2.880e-03x_2$$

$$y^6 = 8.879e-03 - 2.997e-03x_1 - 5.870e-04x_2$$

$$y^7 = 3.224e-03 - 1.306e-02x_1 - 6.248e-03x_2$$

$$y^8 = 4.163e-03 + 2.283e-02x_1 + 7.731e-03x_2$$

$$y^9 = 1.328e-03 + 6.390e-03x_1 + 2.261e-02x_2$$

$$y^{10} = -2.324e-03 + 1.247e-02x_1 + 2.101e-02x_2$$

$$y^{11} = 1.837e-02 + 3.099e-03x_1 - 6.084e-03x_2$$

$$y^{12} = 1.815e-02 - 5.959e-03x_1 + 2.990e-03x_2$$

$$y^{13} = 8.867e-03 + 1.071e-02x_1 + 1.039e-03x_2$$

$$y^{14} = -3.044e-02 + 6.393e-02x_1 + 1.631e-02x_2$$

$$y^{15} = 5.724e-03 - 1.734e-02x_1 - 1.092e-02x_2$$

$$y^{16} = -2.495e-02 + 2.179e-02x_1 + 6.178e-02x_2$$

$$y^{17} = 1.126e-02 - 1.252e-02x_1 - 1.197e-02x_2$$

$$y^{18} = 1.424e-02 - 2.040e-04x_1 - 1.362e-04x_2$$

$$y^{19} = 1.573e-02 + 2.459e-02x_1 + 8.089e-03x_2$$

$$y^{20} = 1.642e-02 + 8.279e-03x_1 + 2.439e-02x_2$$

Figure 4.70 A first order model for Λ_{13357} with r_a=0.30, η=2.0, $\bar{\varepsilon}$ =0.2, $\underline{\varepsilon}$ = 0.0, N=20 and σ=4.66e-5

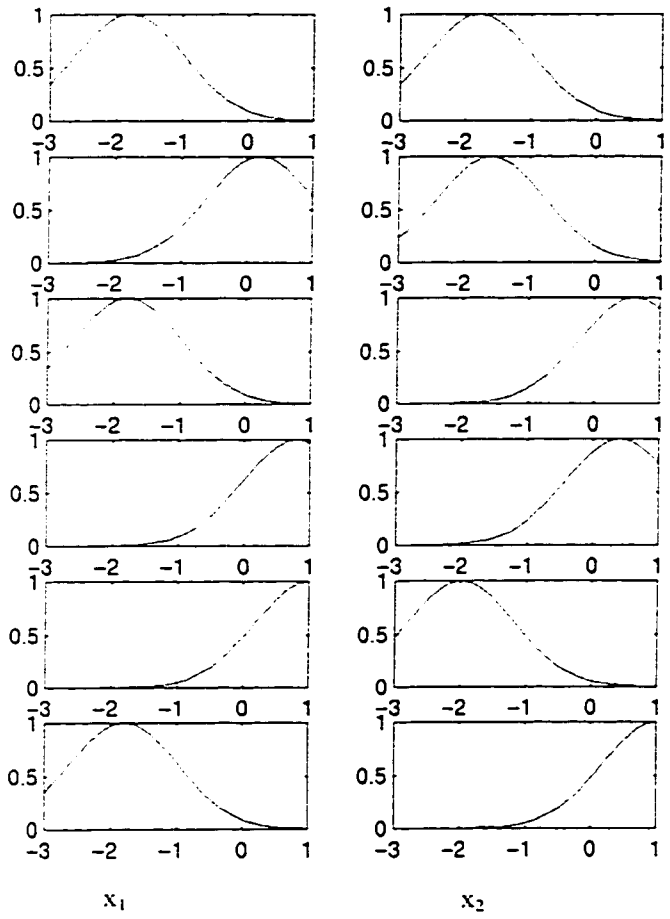

$$y^1 = -1.320e-03 - 8.904e-03x_1 - 3.550e-03x_2 - 1.518e-03x_1^2 - 8.478e-04x_2^2$$

$$y^2 = -1.301e-02 + 3.254e-03x_1 - 1.796e-02x_2 + 6.986e-03x_1^2 - 3.920e-03x_2^2$$

$$y^3 = 2.095e-02 + 1.474e-02x_1 + 7.758e-03x_2 + 3.404e-03x_1^2 - 1.157e-02x_2^2$$

$$y^4 = 6.011e-03 - 2.862e-03x_1 - 9.221e-04x_2 + 1.401e-02x_1^2 + 1.042e-02x_2^2$$

$$y^5 = 1.608e-03 - 2.927e-02x_1 + 1.377e-03x_2 + 3.528e-02x_1^2 + 1.097e-03x_2^2$$

$$y^6 = -1.759e-02 - 1.963e-02x_1 - 3.162e-02x_2 - 4.263e-03x_1^2 + 5.153e-02x_2^2$$

Figure 4.71 A second order model for Λ_{13357} with r_a=0.58, η=1.4, $\bar{\varepsilon}$ =0.2, $\underline{\varepsilon}$ = 0.0, N=6 and σ=4.74e-5

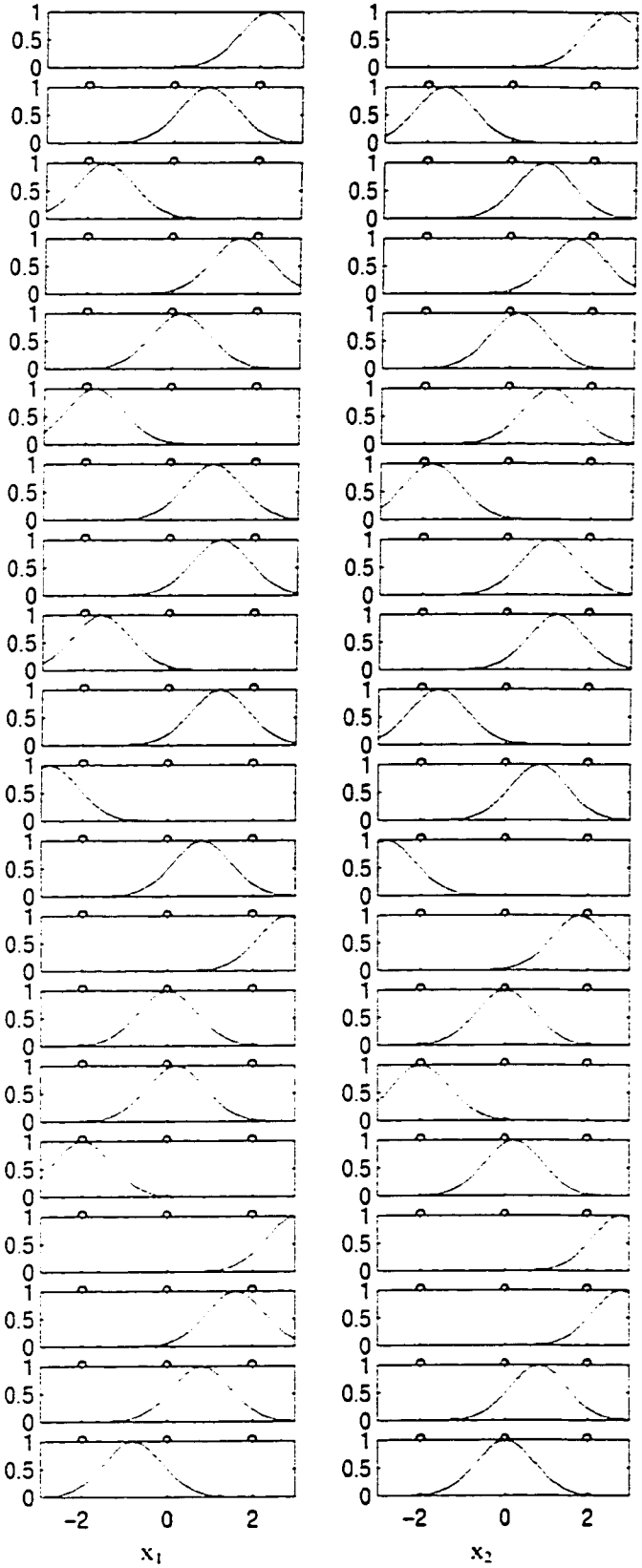

$$y^1 = -3.170e-02 + 8.493e-03x_1 + 9.892e-03x_2$$

$$y^2 = 2.996e-02 + 3.729e-03x_1 - 4.453e-03x_2$$

$$y^3 = 1.651e-01 + 4.759e-02x_1 - 2.900e-02x_2$$

$$y^4 = 6.538e-02 - 1.511e-02x_1 - 1.498e-02x_2$$

$$y^5 = 1.009e-02 + 2.093e-02x_1 + 2.555e-02x_2$$

$$y^6 = -1.824e-01 - 9.611e-02x_1 + 3.711e-02x_2$$

$$y^7 = -1.440e-01 - 2.913e-02x_1 - 9.819e-02x_2$$

$$y^8 = 2.880e-02 - 1.161e-02x_1 - 7.635e-03x_2$$

$$y^9 = -1.625e-02 + 2.797e-02x_1 + 6.796e-02x_2$$

$$y^{10} = 3.379e-02 + 1.062e-01x_1 + 7.158e-02x_2$$

$$y^{11} = -1.297e-01 - 3.234e-02x_1 + 2.074e-02x_2$$

$$y^{12} = -1.070e-01 + 2.446e-02x_1 - 2.483e-02x_2$$

$$y^{13} = 7.239e-02 - 1.129e-02x_1 - 1.412e-02x_2$$

$$y^{14} = -7.717e-03 - 5.007e-02x_1 - 5.348e-02x_2$$

$$y^{15} = 1.956e-02 - 5.502e-02x_1 - 1.612e-02x_2$$

$$y^{16} = 8.281e-03 - 2.271e-02x_1 - 6.156e-02x_2$$

$$y^{17} = 5.270e-02 - 4.045e-03x_1 - 9.139e-03x_2$$

$$y^{18} = 6.452e-02 - 1.298e-02x_1 - 9.020e-03x_2$$

$$y^{19} = 2.049e-03 + 1.142e-02x_1 + 1.097e-02x_2$$

$$y^{20} = 3.377e-02 + 2.444e-02x_1 - 2.812e-02x_2$$

Figure 4.72 A first order model for $\Lambda_{13356.6}$ with r_a=0.32, η=1.0, $\bar{\varepsilon}$ =0.2, $\underline{\varepsilon}$ = 0.0, N=20 and σ=6.03e-3

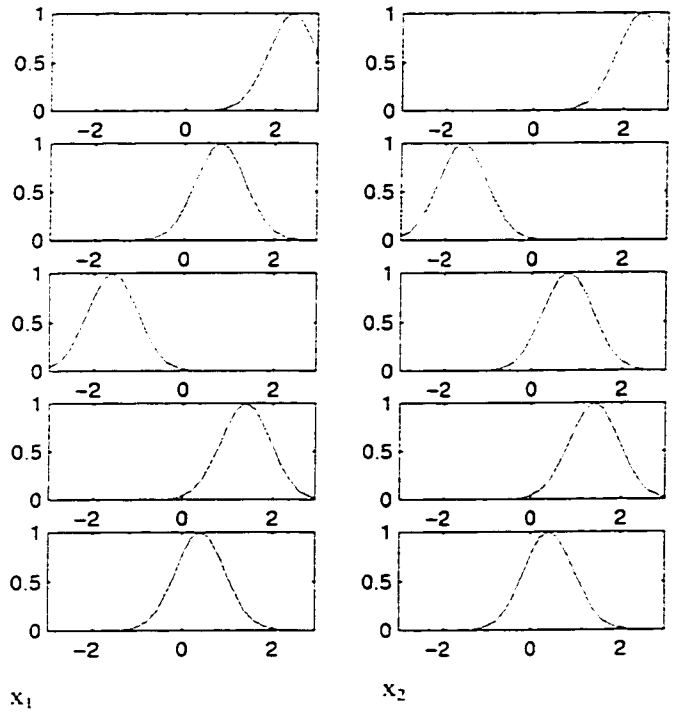

$$y^1 = 4.807e-02 - 1.481e-02x_1 - 1.481e-02x_2 + 2.890e-03x_1^2 + 2.890e-03x_2^2$$

$$y^2 = 1.244e-02 - 2.704e-02x_1 - 4.148e-03x_2 + 2.065e-02x_1^2 - 9.033e-04x_2^2$$

$$y^3 = 1.244e-02 - 4.148e-03x_1 - 2.704e-02x_2 - 9.033e-04x_1^2 + 2.065e-02x_2^2$$

$$y^4 = 3.565e-02 - 1.379e-02x_1 - 1.379e-02x_2 + 4.138e-03x_1^2 + 4.138e-03x_2^2$$

$$y^5 = 5.997e-03 - 4.350e-03x_1 - 4.350e-03x_2 + 7.360e-03x_1^2 + 7.360e-03x_2^2$$

Figure 4.73 A second order model for $\Lambda_{13356.6}$ with r_a=0.26, η=1.6, $\bar{\varepsilon}$ =0.6, $\underline{\varepsilon}$ = 0.4, N=5 and σ=6.67e-5

CHAPTER 5

APPLICATION OF BOUNDARY CONDITIONING TO THE SYNTHESIS OF MICROSYSTEMS

We have studied different fabrication methods of microsystems using XeF_2 etching in Chapter 2, theoretical modeling of boundary conditioning in Chapter 3 using equivalent springs and application of fuzzy system identification to boundary conditioning in Chapter 4. In this chapter, the application of boundary conditioning to the design synthesis of microsystems that were fabricated through XeF_2 etching and other dedicated MEMS process like MUMPs is demonstrated.

5.1 BOUNDARY CONDITIONING BY STRUCTURAL VARIATIONS

5.1.1 Stiffening of Microsystems

The addition of stiffeners is the common way of modifying the elastic property of the system which can be extended to microsystems also. In order to demonstrate the stiffening of microstructures, structures of different geometry were designed through Mitel 1.5 μm process and were post released using XeF_2 bulk etching. Plate structures of circular geometry are shown in Figures 5.1a and b, square type diaphragm are given in Figures 5.1c and d and beam type structures are shown in Figure 5.1.d. The structures shown in Figure 5.1 are made of Metal1, COX, IMO and PASS layers while the stiffeners are made out of Metal2 layer. The thickness of these layers are given in Table 2.1.

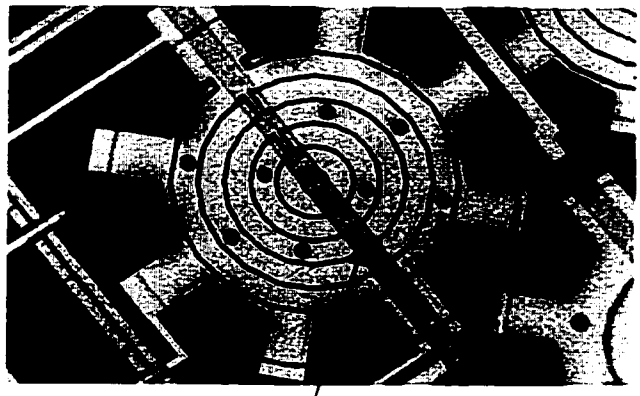

a) A circular diaphragm of Metal1 + COX + IMO + PASS with Metal2 stiffeners. Diaphragm diameter is 650μm.

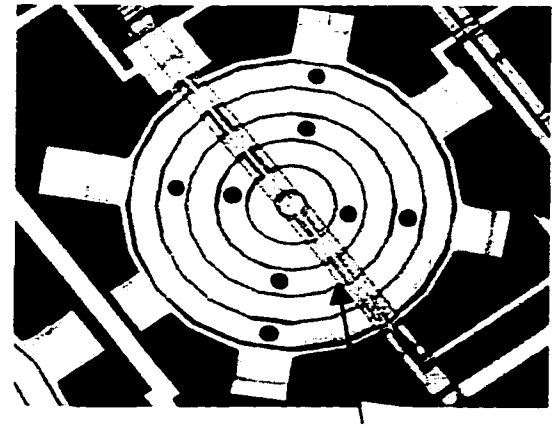

b) A circular diaphragm of Metal1 + COX + IMO + PASS with Metal2 stiffeners. Diaphragm diameter is 650μm.

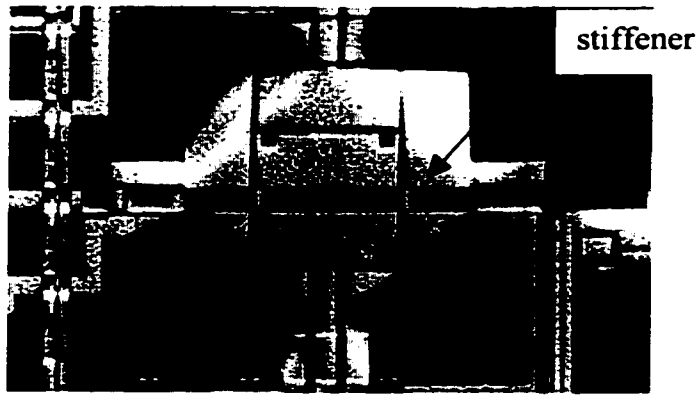

c) A square diaphragm of Metal1 + COX + IMO + PASS with Metal2 stiffeners. Diaphragm side is 600μm.

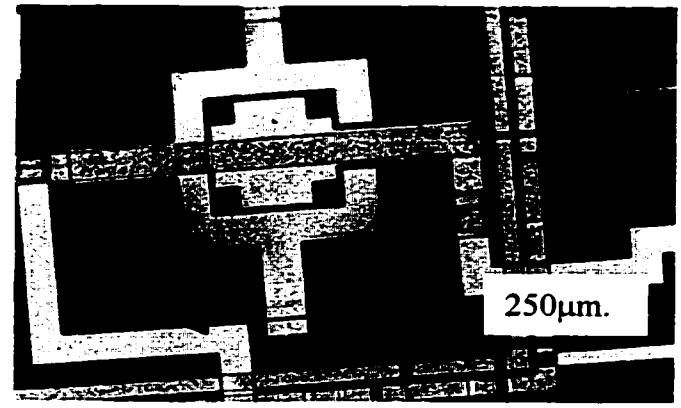

d) A square diaphragm of Metal1 + COX + IMO + PASS with Metal2 stiffeners. Diaphragm side is 250 μm.

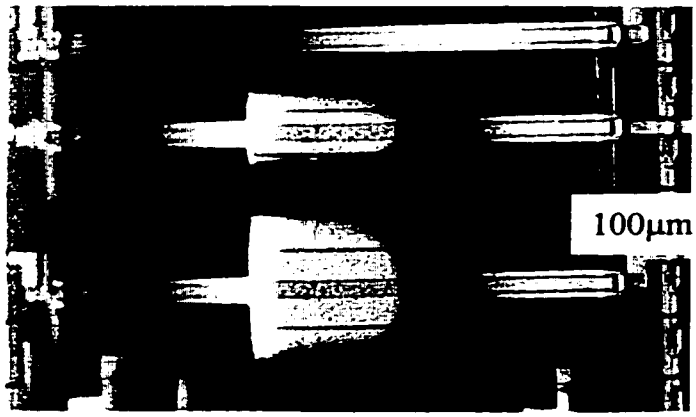

e) Beam structures of Metal1 + COX + IMO + PASS with Metal2 stiffeners. Beam width is 100 μm.

Figure 5.1: Microdiaphragms suitable for sensing pressure, noise level etc., fabricated through the Mitel 1.5 mm process combined with isotropic bulk post-processing. Microdiaphragms are stiffened with Metal2 stiffeners.

The elastic property of microsystem can be modified by changing the geometry or the number of stiffeners. The boundary conditioning by such structural modification can be predicted by combining the analytical formulations in Sections 3.1 and 3.2 as follows:

Consider the structure shown in Figure 5.1c-e represented by a scheme as shown in Figure 5.2. As in the analysis in Section 3.4.1, the plate structure is divided into N number of rectangular segments (i.e. k = 1, ... , N) in a similar way to the Figure 3.27. Each k^{th} segment can have stiffeners in a random fashion with NSX_k stiffeners in x direction and NSY_k stiffeners in y direction as shown in Figure 3.2.

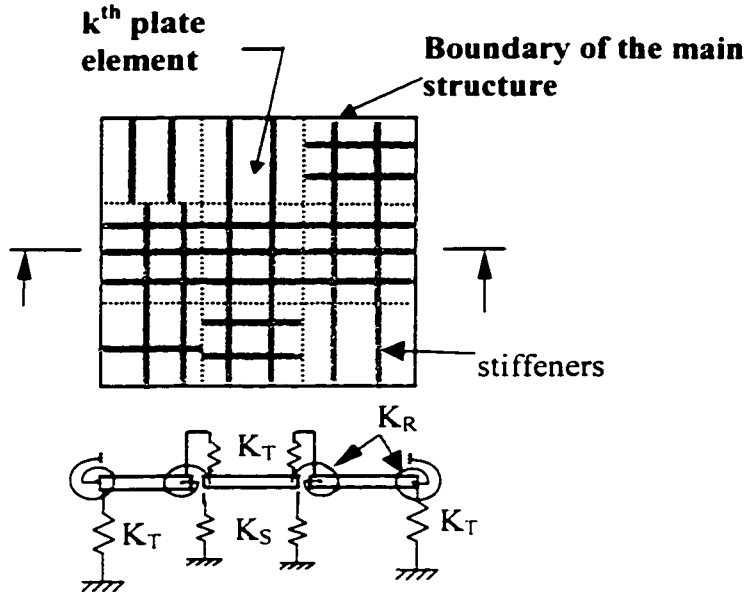

Figure 5.2: Scheme of a microstructure with stiffeners at random positions represented by joining many rectangular segments with artificial springs

The flexural deflection equation for k^{th} segment is defined as per Equation (3.25) as

$$W_k(x,y) = \sum_m \sum_n A_{mn,k}\phi_m(x)\varphi_n(y)$$

Combining the analysis of the Sections 3.4.1 and 3.1, the maximum total strain energy U_{max} and the maximum kinetic energy T_{max} of the structure can be obtained as,

$$U_{max} = \sum_{k=1}^{N} U_{max,k} + \sum_{k=1}^{N}\sum_{s=1}^{4} U_{T,k,s} + \sum_{k=1}^{N}\sum_{s=1}^{4} U_{R,k,s} + \sum_{k=1}^{N}\sum_{s=1}^{4} U_{S,k,s} + \sum_{k=1}^{N} U_{SX,k} + \sum_{k=1}^{N} U_{SY,k} \tag{5.1}$$

and

$$\begin{aligned} T_{max} = & \sum_{k=1}^{N} \frac{1}{2}\rho_k h_k a_k b_k \omega^2 \int_0^1\int_0^1 W_k^2(x,y)dxdy + \\ & \sum_{k=1}^{N} \frac{1}{2}\rho_k b_k \omega^2 \sum_{j=1}^{NSX_k} e_{k,j} f_{k,j} \int_0^1 W_k{}^2(x_j, y)\,dy + \\ & \sum_{k=1}^{N} \frac{1}{2}\rho_k a_k \omega^2 \sum_{i=1}^{NSY_k} e_{k,i} f_{k,i} \int_0^1 W_k{}^2(x, y_i)\,dx \end{aligned} \tag{5.2}$$

where the strain energy due to stiffeners in y direction for the k^{th} element is

$$U_{SY,k} = \frac{E}{2a_k{}^3} \sum_{i=1}^{NSY_k} I_{k,i} \int_0^1 W_{xx,k}^2(x, y_i)\,dx$$

and the strain energy due to stiffeners in x direction for the k^{th} element is

$$U_{SX,k} = \frac{E}{2b_k{}^3} \sum_{j=1}^{NSX_k} I_{k,j} \int_0^1 W_{yy,k}^2(x_j, y\ )\,dy$$

The remaining terms are:

$U_{max,k}$ - strain energy of the k^{th} plate

$U_{T,k,s}$ - potential energy of s^{th} side translational spring of k^{th} plate

$U_{R.k.s}$ - potential energy of s[th] side rotational spring of k[th] plate and

$U_{S.k.s}$ - potential energy of s[th] side support spring of k[th] plate can be estimated as per the Equations 3.40.

The subscript 'k' of the stiffener geometry refers to the k[th] segment. It is assumed that stiffener properties remain the same for a plate segment.

Substitution of deflection Equation (3.25) in strain energy and kinetic energy Equations (5.1) and (5.2), and optimization of Rayleigh quotient with respect to the coefficients of $A_{ij,k}$ result in the following eigenvalue equation:

$$\sum_m \sum_n \left[C_{mnij,k} + C^I_{mnij,k} + C^S_{mnij,k} - \lambda \Pi_k \left(E^{00}_{mi} F^{00}_{nj} + J_k \right) \right] A_{mn,k} - \sum_m \sum_n D_{mnij,s} A_{mn,s} = 0 \tag{5.3}$$

$$\forall \cdot k = 1,2,\ldots,N$$

where

$$C_{mnij,k} = E^{22}_{mi} F^{00}_{nj} + \alpha_k^4 E^{00}_{mi} F^{22}_{nj} + \upsilon \alpha_k^2 \left(E^{02}_{mi} F^{20}_{nj} + E^{20}_{mi} F^{02}_{nj} \right) + 2 \cdot (1-\upsilon) \alpha_k^2 E^{11}_{mi} F^{11}_{nj}$$
$$+ \sum_{i=1}^{NSY_k} 4\left(1-\gamma^2\right) \frac{e_{k,i}}{b_k} \left[\left(\frac{f_{k,i}}{h_k} \right)^3 + 1.5 \left(\frac{f_{k,i}}{h_k} \right)^2 + 0.75 \left(\frac{f_{k,i}}{h_k} \right) \right] E^{22}_{mi} . \varphi_n(y_i) . \varphi_j(y_i)$$
$$+ \sum_{j=1}^{NSX_k} 4\left(1-\gamma^2\right) \frac{e_{k,j}}{a_k} \alpha_k^4 \left[\left(\frac{f_{k,j}}{h_k} \right)^3 + 1.5 \left(\frac{f_{k,j}}{h_k} \right)^2 + 0.75 \left(\frac{f_{k,j}}{h_k} \right) \right] F^{22}_{nj} . \phi_m(x_j) . \phi_i(x_j)$$

$$C^I_{mnij,k} = K^*_{T.k.1} \alpha_k E^{00}_{mi} \varphi_n(0) \varphi_j(0) + K^*_{T.k.2} \phi_m(1) \phi_i(1) F^{00}_{nj} + K^*_{T.k.3} \alpha_k E^{00}_{mi} \varphi_n(1) \varphi_j(1)$$
$$+ K^*_{T.k.4} \phi_m(0) \phi_i(0) F^{00}_{nj} + K^*_{R.k.1} \alpha_k^3 E^{00}_{mi} \varphi^1_n(0) \varphi^1_j(0) + K^*_{R.k.2} \phi^1_m(1) \phi^1_i(1) F^{00}_{nj}$$
$$+ K^*_{R.k.3} \alpha_k^3 E^{00}_{mi} \varphi^1_n(1) \varphi^1_j(1) + K^*_{R.k.4} \phi^1_m(0) \phi^1_i(0) F^{00}_{nj}$$

$$C^{S}_{mnij.k} = K^{\bullet}_{S.k.1}\alpha_k E^{00}_{mi}\varphi_n(0)\varphi_j(0) + K^{\bullet}_{S.k.2}\phi_m(1)\phi_i(1)F^{00}_{nj} + K^{\bullet}_{S.k.3}\alpha_k E^{00}_{mi}\varphi_n(1)\varphi_j(1)$$

$$+ K^{\bullet}_{S.k.4}\phi_m(0)\phi_i(0)F^{00}_{nj}$$

$$D_{mnij.s}A_{mn.s} = [K^{\bullet}_{T.k.1}\alpha_k E^{00}_{mi}\varphi_n(1)\varphi_j(0) + K^{\bullet}_{R.k.1}\alpha_k^2\alpha_{s1}E^{00}_{mi}\varphi^1_n(1)\varphi^1_j(0)]A_{mn.s1} +$$

$$[K^{\bullet}_{T.k.2}\phi_m(0)\phi_i(1)F^{00}_{nj} + K^{\bullet}_{R.k.2}\frac{\alpha_k}{\alpha_{s2}}\phi^1_m(0)\phi^1_i(1)F^{00}_{nj}]A_{mn.s2} +$$

$$[K^{\bullet}_{T.k.3}\alpha_k E^{00}_{mi}\varphi_n(0)\varphi_j(1) + K^{\bullet}_{R.k.3}\alpha_k^2\alpha_{s3}E^{00}_{mi}\varphi^1_n(0)\varphi^1_j(1)]A_{mn.s3} +$$

$$[K^{\bullet}_{T.k.4}\phi_m(1)\phi_i(0)F^{00}_{nj} + K^{\bullet}_{R.k.4}\frac{\alpha_k}{\alpha_{s4}}\phi^1_m(1)\phi^1_i(0)F^{00}_{nj}]A_{mn.s4}$$

$$J_k = \sum_{i=1}^{NSY_k}\frac{f_{k,i}}{h_k}\frac{e_{k,i}}{b_k}E^{00}_{mi}.\varphi_n(y_i).\varphi_j(y_i) + \sum_{j=1}^{NSX_k}\frac{f_{k,i}}{h_k}\frac{e_{k,i}}{a_k}F^{00}_{nj}\phi_m(x_j)\phi_i(x_j)$$

$$E^{rs}_{mi} = \int_0^1\left(\frac{d^r\phi_m}{dx^r}\right)\times\left(\frac{d^s\phi_i}{dx^s}\right)dx$$

$$F^{rs}_{nj} = \int_0^1\left(\frac{d^r\varphi_n}{dy^r}\right)\times\left(\frac{d^s\varphi_j}{dy^s}\right)dy$$

$$\alpha_k = a_k/b_k,$$

$$K^{\bullet}_{T.k.i} = \frac{K_{T.k.i}a_k^3}{D_k}, K^{\bullet}_{R.k.i} = \frac{K_{R.k.i}a_k}{D_k}, K^{\bullet}_{S.k.i} = \frac{K_{S.k.i}a_k^3}{D_k}, \Pi_k = \frac{\rho_{r.k}a^4_{r.k}}{E_{r.k}h^2_{r.k}}, \lambda = \frac{\rho_1 h_1 a_1^4\omega^2}{D_1},$$

$$E^{rs}_{mi} = \int_0^1\left(\frac{d^r\phi_m}{dx^r}\right)\left(\frac{d^s\phi_i}{dx^s}\right)\cdot dx, \quad F^{rs}_{nj} = \int_0^1\left(\frac{d^r\varphi_n}{dy^r}\right)\left(\frac{d^s\varphi_j}{dy^s}\right)\cdot dy, \quad \phi^1_i = \frac{d\phi_i}{dx}, \quad \varphi^1_j = \frac{d\varphi_j}{dy}$$

Subscript (r,k) refers to ratio of parameter of k^{th} segment to that of the first segment and subscripts (k,i) and (k,j) refer to the ith and jth stiffener of the k^{th} segment.

The Equation (5.3) represents the boundary conditioning of microsystems due to structural modification such as adding stiffeners. The solution of the Equation (5.3) will be useful in applying boundary conditioning to the design synthesis of microsystems through adding positive stiffeners. The effect of stiffening can be expected to be similar to that of the results shown in the Figures 3.8 and 3.9. The Equation 5.3 was not solved explicitly in this chapter for a microsystem as it has been solved in Chapter 3.

5.1.2 Corrugations in Microsystems

Another important way of changing the elastic property of the microsystems through structural modification is by adding corrugations at anywhere in the structure or at the support ends. The corrugations that introduce boundary conditioning can be fabricated and analyzed using the present methods of synthesis of microsystems. This section shows that it is also possible to fabricate corrugated structure through type-III integration in order to modify the elastic property of the microsystems.

In order to study how the corrugations affect the structural properties of the microstructures, structures with corrugations of different geometry were designed through Mitel 1.5 μm process and were post released using XeF_2 bulk etching. Plate structures of circular geometry with corrugated beam extensions fabricated out of Mitel 1.5 μm process and post-released by bulk etching are given in Figure 5.3. The structures shown in Figure 5.3 are made of Metal1, COX, IMO and PASS layers. The elastic property of microsystem can be modified by changing the geometry and the number of corrugations. The micromechanical structure with transverse corrugations is shown in

Figure 5.3a. These corrugations were fabricated by stacking different layers (especially Metal1 and Metal2) of Mitel 1.5 μm process in order to weaken the structure rotationally and obtain larger deflection. The laterally corrugated structure is shown in Figure 5.3b. This example proves that it is possible to fabricate structures with different stiffness distribution using the present methods of synthesis of microsystems.

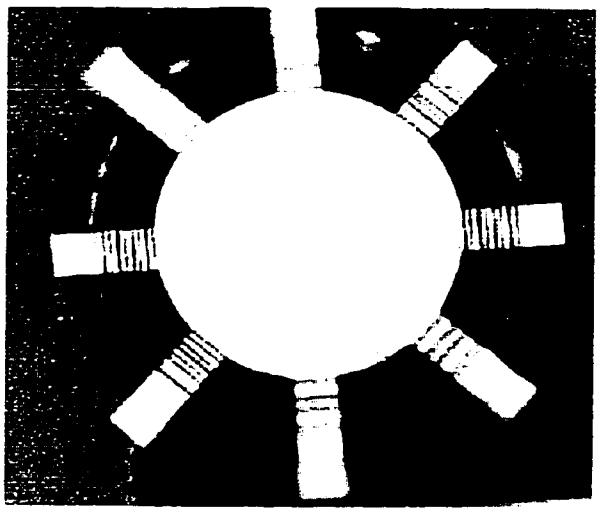

Figure 5.3a Transversely corrugated diaphragm of Metal1. Corrugations are obtained by stacking of different layers (Metal1 and 2) of the Mitel 1.5 μm process. Diameter of the diaphragm is 250μm

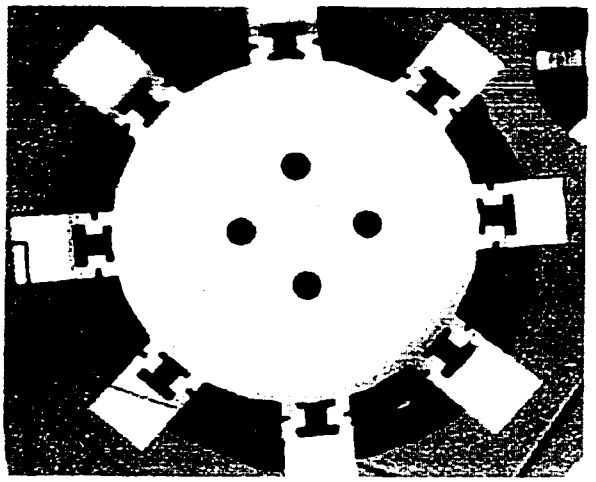

Figure 5.3b Laterally corrugated diaphragm of Metal1 obtained in the Mitel 1.5 μm process. Diameter of the diaphragm is 650 μm

Figure 5.3 Corrugated structures fabricated through the present synthesis of microsystems

These kinds of corrugations change the stiffness distribution locally which could be near the support in the structure as shown in Figure 5.3 or anywhere else in the structure. The corrugations near the ends change the elastic property and hence introduce rotational flexibility to the structure thus making the end conditions different from the classical clamped conditions. Corrugations present in the structure thus introduce both translational and rotational freedoms between the adjacent structural parts. As far as the

modeling of dynamic performance of such microsystems is concerned, the application of boundary conditioning is helpful as in the case of positive stiffening. In line with the analysis in Chapter 3 and Section 5.1.1 the change in stiffness can be modeled with the help of equivalent translational and rotational springs as shown in Figure 5.4. Results obtained with such models have already been presented in the previous chapters.

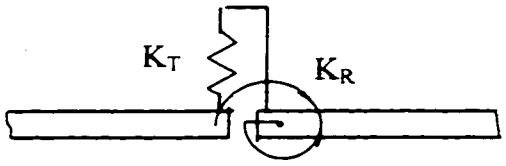

Figure 5.4: Scheme representing a corrugated joint with artificial springs

5.1.3 Different Support Conditions in Microsystems by Design

It is also possible to obtain the required stiffness characteristics of the structure by providing the required boundary conditions through structural design of the microsystems, for example, changing the end support conditions of the structure as schematically shown in Figure 5.5. The variable parameters affecting the structural stiffness properties could include the geometry of the main structure and number, position and geometry of the support beams. Fabrication of such structures is possible through the present synthesis (Mitel 1.5 μm) and also through other dedicated MEMS processes such as MUMPs. The prediction formulation explained in Section 5.1.1 can be extended to any such structures in order to find the dynamic behavior. The plate type micromechanical structures, with support conditions formed by structures of different

geometry, fabricated out of the Mitel 1.5 μm process are shown in Figure 5.6. Similar examples are shown in Figures 1.18, 1.22, 1.23, 1.25d, 1.28 and 2.26 to 2.30. These structures are fabricated out of COX, M1, M2, IMO and PASS layers and are suitable for the release using the proposed fabrication synthesis.

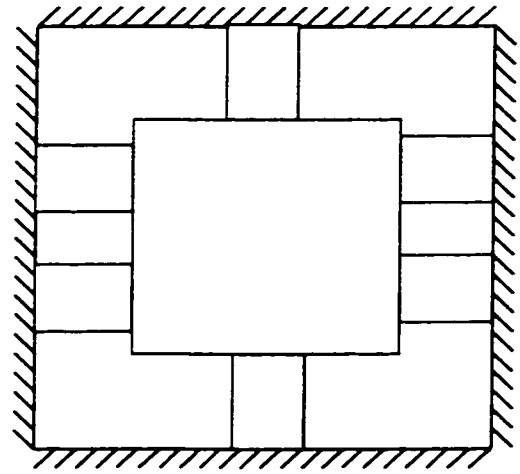

Figure 5.5 Scheme of a rectangular plate structure supported with six support beams

It is possible to fabricate the plate type structures with different support conditions through other dedicated process such as MUMPs [114]. This process has 7 layers in total: Si_3N_4 insulation layer, three polysilicon layers (Poly0, Poly1 and Poly2), two sacrificial PSG layers and a metal layer. Poly1 and Poly2 can be used as structural layers. The plate type structures fabricated out of Poly1 and Poly2 with different support conditions constituting different boundary conditions are shown in Figures 5.7 to 5.9. The vibration behavior of such structures can be predicted using the formulation in Section 5.1.1.

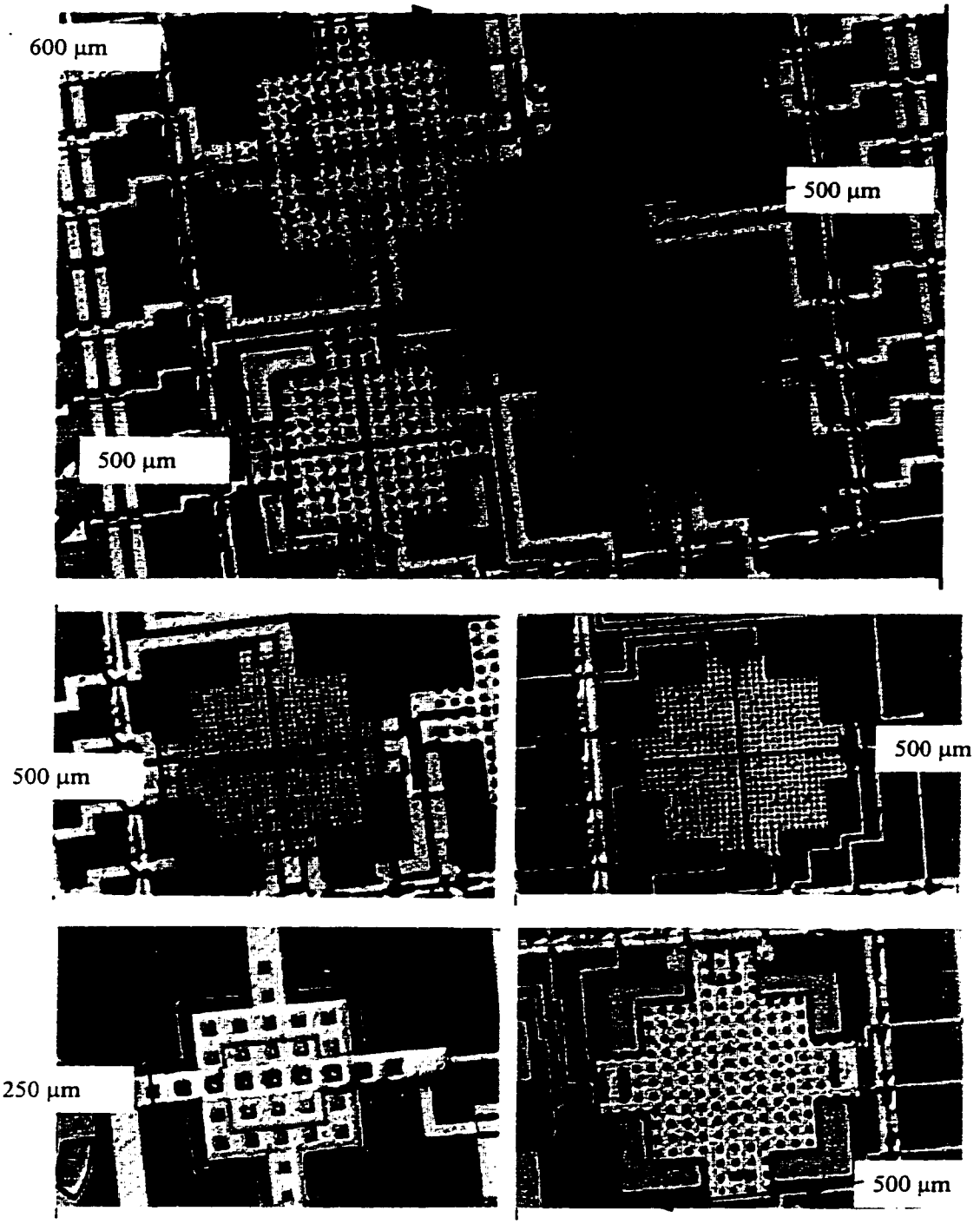

Figure 5.6 Photographs of plate structures with different support structures designed out of the Mitel 1.5µ m process suitable for the present fabrication synthesis. Structures are made out of M1, M2, COX, IMO and PASS layers.

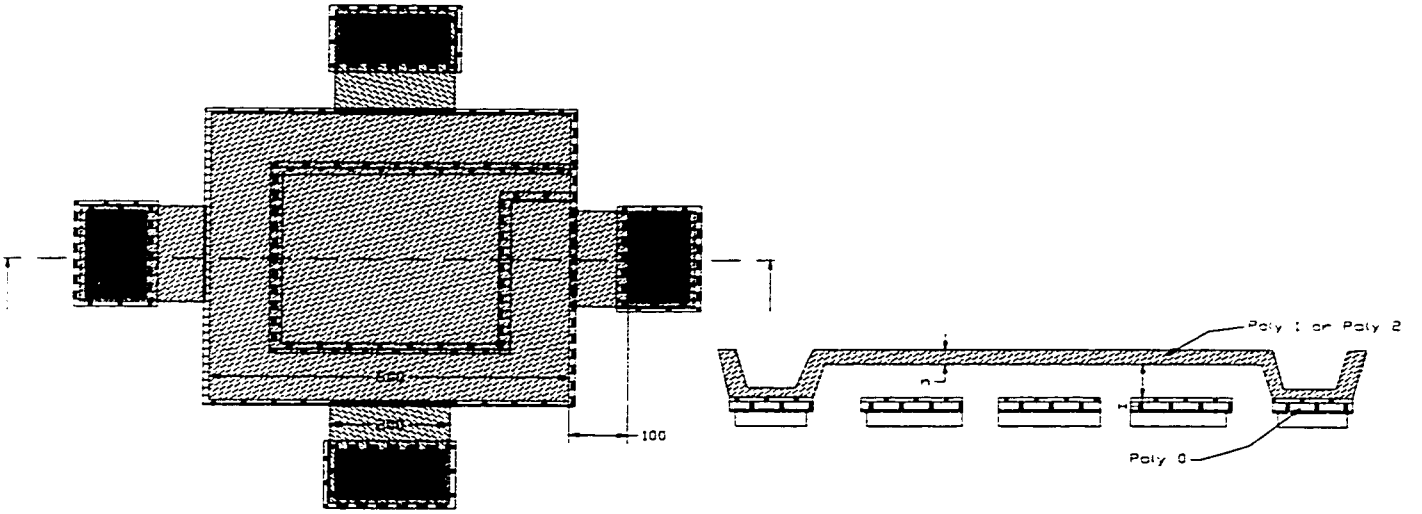

Diaphragm	Backplate	H	H
Poly 2 (SQ1)	Poly 0 + Poly 1	1.5021	0.7323
Poly 2 + metal (SQ5)	Poly 0 + Poly 1	1.5021	-

a) Schematic

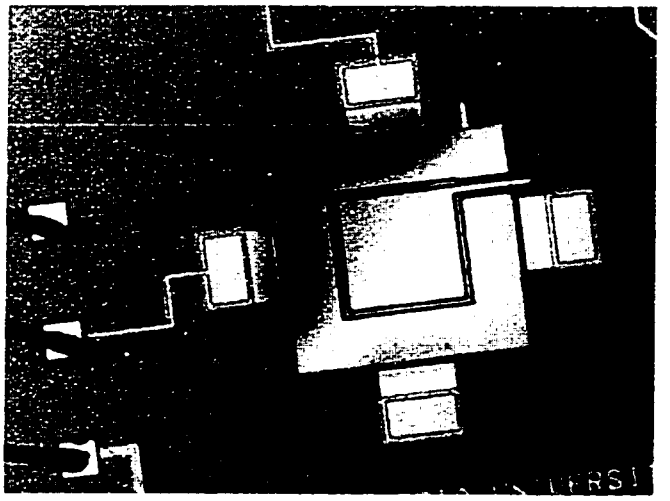

b) Photograph of Poly2 diaphragm of the design SQ1

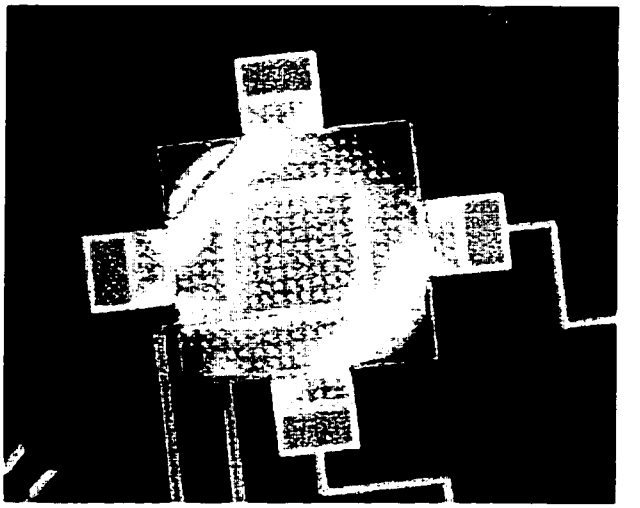

c) Photograph of Poly2+Metal diaphragm of the design SQ5

Figure 5.7 Plate type structure fabricated out of Poly2 with 4 support beams .

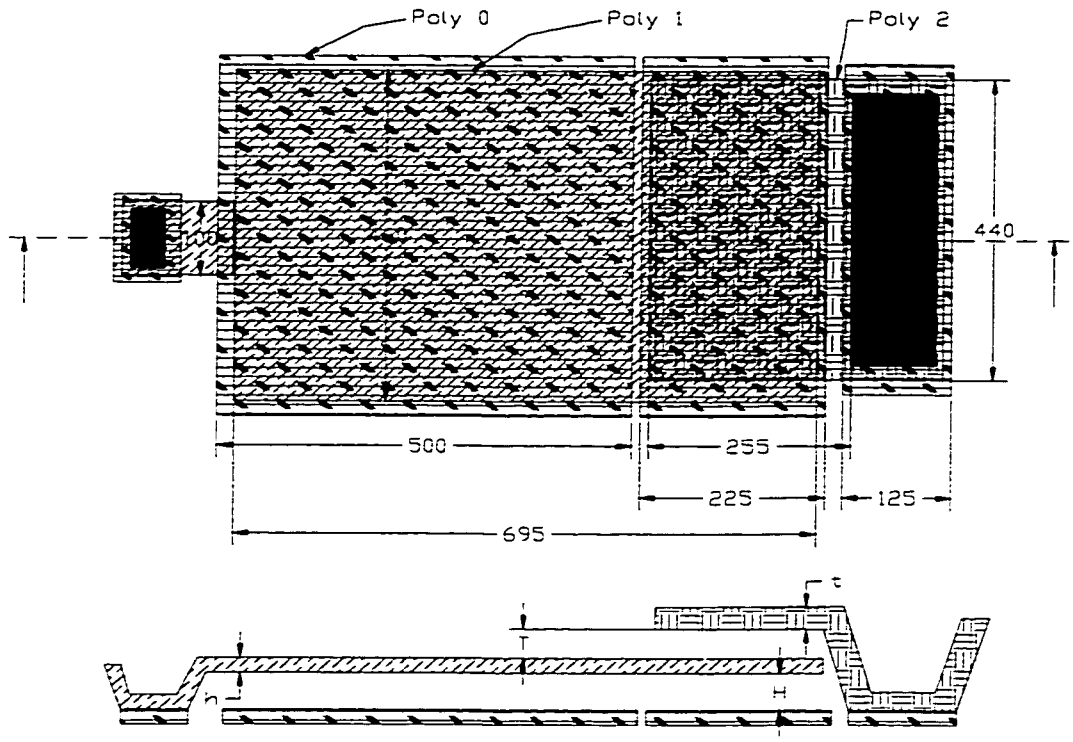

Design	Backplate	Diaphragm	Topplate	H	h	T	t
BC1	Poly 0	Poly 1	Poly 2	2.0731	2.0041	0.7323	1.5021

a) Schematic

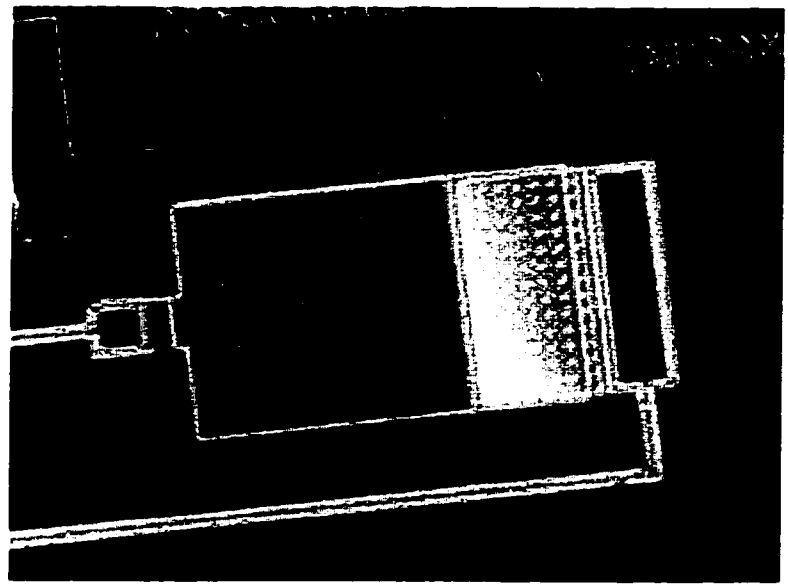

b) Photograph of a plate type structure with one support beam made out of poly1

Figure 5.8 Plate type structure fabricated out of Poly2 with one support beams .

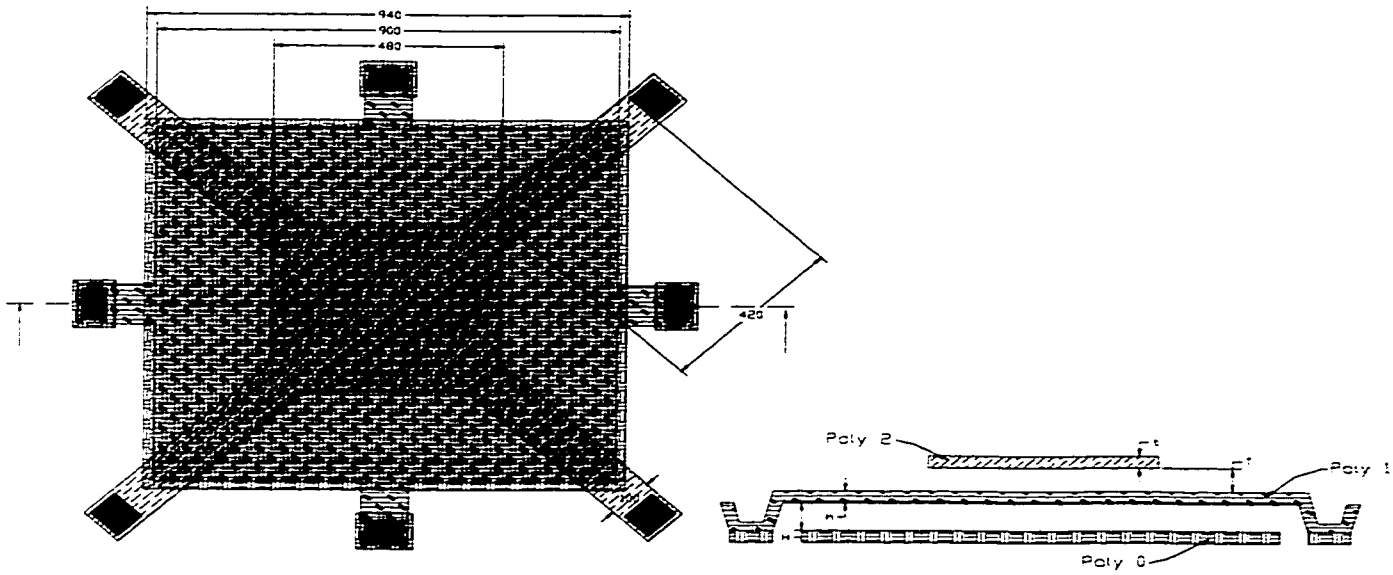

a) Schematic

Design	Backplate	Diaphragm	Topplate	H	h	T	t
SQ7	Poly 0	Poly 1	Poly 2	2.0731	2.004	0.7323	1.5021

b) SEM Micrograph of plate structures of Poly1 and Poly2 with support beams of different geometry

Figure 5.9 Plate type structures fabricated out of Poly1 and Poly2 with different support beams .

5.2 BOUNDARY CONDITIONING OF MICROSYSTEMS THROUGH FABRICATION METHODS

The fabrication of microsystems includes deposition techniques (LPCVD, PECVD, sputtering, PVD, etc.), thermal growth, bonding, etching etc. The limitations associated with fabrication techniques modify the elastic properties of the microsystems and hence influence the vibration behavior of the microsystems. The inherent limitations include non-classical end support conditions, residual stress in the structures due to thermal cycles involved in the process, etc.

Bulk micromachining and surface micromachining are the general etching fabrication methods available for the release of free standing structures of microsystems. The bulk micromachining could include isotropic or anisotropic etching. The anisotropic wet etching will result in the inclined support planes as shown in Figure 1.24. The isotropic bulk etching as part of the present fabrication synthesis results in under-etching as shown in Figure 2.25a while sacrificial etching forms stepped-up end condition as shown in Figure 2.25b. Thus the inherent limitations of the present fabrication synthesis using XeF_2 etching, which are stepped up conditions (Figures 1.25d, 2.26, 2.27, 5.1, 5.6) and under etching (Figures 2.14, 2.16b, 2.19, 2.26, 2.27, 2.28, 2.30) of silicon substrate, affect the dynamic behavior of the microstructures. The quantification of the influence of these limitations of the present fabrication synthesis in relation to dynamic behavior becomes very important part of the design synthesis of many microsystems such as pressure

sensors, inertial sensors, microresonators, etc. whose performance is strongly dependent upon the dynamic behavior of mechanical structures.

5.2.1 Prediction of the Influence of Support Conditions Resulting from Fabrication of Microsystems on their Dynamic Behavior

In order to demonstrate the application of boundary conditioning concept to the synthesis of microsystems, the influence of support conditions resulting from the fabrication of microsystems on their dynamic behavior is studied.

Performance of the free-standing structures released through surface micromachining is influenced by natural frequencies that are dependent upon the mass and stiffness properties of the structure. It is well known that the stiffness of the structure is strongly dependent on the fabrication process, geometric features and the boundary conditions of the structures. The formation of stepped-up ends introduce rotational elasticity and make the boundary conditions intermediate to the classical conditions such as clamped, pinned and free. Hence, the quantification of the influence of fabrication process on the dynamic behavior of the system, which will be very useful during the design process, is carried out using the concept of boundary conditioning.

5.2.1.1 Modeling of end conditions through rotational stiffness

The stepped-up boundary conditions shown schematically in Figure 5.10 is common for surface micromachining process such as XeF_2 etching of the polysilicon layers and MUMPs [114] (Multi-User MEMS Processes). To demonstrate the effect of different end conditions that are formed from surface micromachining process on dynamic behavior, a plate type microstructure (design SQ1) fabricated from polysilicon layers using the MUMPs process as shown in Figure 5.7b is considered. This kind of structure is common for pressure sensing applications. Similar structure was also made through the Mitel technology (shown in Figure 2.30). Prediction of vibration behavior of such structures is possible by the application of boundary conditioning technique.

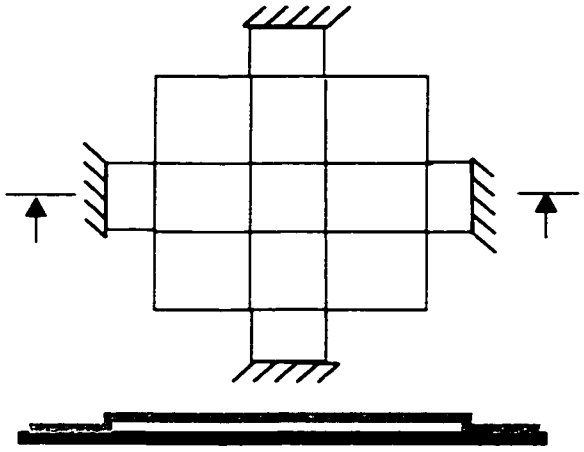

Figure 5.10 Structural scheme used for prediction of vibration behavior of SQ1 plate type structure shown in Figure 5.7a

As a general case, modeling of a plate element with boundaries supported by rotational and translational springs as shown schematically in Figure 3.16 is applied to microsystems in this section. The plate element is assumed to be supported at all the four edges with both translational and rotational springs with stiffness per unit length of K_T (N/m^2) and K_R (Nm/m), respectively. The mechanical microstructures can be

modeled by assembling many such plate elements with appropriate change in the boundary conditions of the elements. An arrangement of the connection between a plate element and the adjacent elements used for modeling is shown schematically in Figure 3.10*b*. Each segment is connected to adjacent segments through translational and rotational springs with stiffness per unit length of K_T and K_R, respectively. The fixed boundaries of the segments are represented by very high values of rotational and translational spring stiffnesses. For the present prediction, the structure shown in Figure 5.7b is modeled by assembling 13 number of boundary conditioned plate elements as schematically shown in Figure 5.10.

The elastic properties of the stepped-up boundaries shown in Figure 5.10 can be represented by both translational and rotational springs for pure bending as shown schematically in Figure 5.11. The boundary condition at the stepped-up ends of the beams is assumed to alter only the rotational stiffness. Hence, different stepped-up end conditions correspond to different values of rotational stiffness and a high value of translational stiffness.

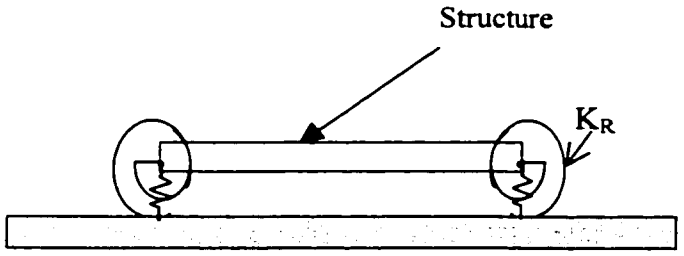

Figure 5.11: A scheme for representing stepped-up boundary conditions using translational and rotational springs

The geometrical dimensions and the material properties of the structure in Figure 5.7b used for the estimation of the first four natural frequencies are:

Side of the plate, a = 600 μm

Width of the beam, w = 200 μm

Length of the beam, l = 100 μm

Thickness of the plate, h = 1.5 μm

Modulus of rigidity, E = 170Gpa

Density, ρ =2300 kg/m^3

Poisson's ratio, ν = 0.42

The flexural deflection equation for kth segment is defined as per Equation (3.25) as

$$W_k(x,y) = \sum_m \sum_n A_{mn,k}\phi_m(x)\varphi_n(y)$$

where non-dimensional coordinates are used, $x = \frac{\xi_k}{a_k}$, $y = \frac{\eta_k}{b_k}$

ξ_κ and η_κ are coordinates of kth plate

a_k and b_k are dimensions of the kth plate with $\alpha_k = \frac{a_k}{b_k}$

$A_{mn,k}$ is the deflection coefficient of the kth plate

$\phi_m(x)$ and $\varphi_n(y)$ are the boundary characteristic orthogonal polynomials upto m = n = 6 generated using Gram-Schmidt process for each plate element so as to satisfy the free edge conditions on all boundaries of all segments.

The maximum total strain energy U_{max} and the maximum kinetic energy T_{max} of the microsystem are,

$$U_{\max} = \sum_{k=1}^{N} U_{\max,k} + \sum_{k=1}^{N}\sum_{s=1}^{4} U_{T,k,s} + \sum_{k=1}^{N}\sum_{s=1}^{4} U_{R,k,s} \tag{5.4}$$

and

$$T_{\max} = \sum_{k=1}^{N} \frac{1}{2}\rho_k h_k a_k b_k \omega^2 \int_0^1\int_0^1 W_k^2(x,y)dxdy \tag{5.5}$$

where

$U_{max,k}$ - strain energy of the k[th] plate element

$U_{T,k,s}$ - potential energy of s[th] side translational spring of k[th] plate element

$U_{R,k,s}$ - potential energy of s[th] side rotational spring of k[th] plate element and are estimated using the following equations:

$$U_{\max,k} = \frac{D_k a_k b_k}{2a_k^4}\int_0^1\int_0^1 \left[W_{xx,k}^2 + \alpha_k^4 W_{yy,k}^2 + 2\upsilon\alpha_k^2 W_{xx,k}W_{yy,k} + 2(1-\upsilon)\alpha_k^2 W_{xy,k}^2\right]dxdy$$

$$U_{T,k,s} = \frac{1}{2}K_{T,k,s}\int_0^{l_s}(\Delta W_s)^2 dl_s$$

$$U_{R,k,s} = \frac{1}{2}K_{R,k,s}\int_0^{l_s}(\Delta W_s^1)^2 dl_s$$

where

D_k - flexural rigidity of the k[th] plate

l_s - length of the side, s

ΔW_s - difference in deflection along the s[th] side of the k[th] plate

$\Delta W_s^{\ l}$ - difference in slope along the s^{th} side of the k^{th} plate element

$W_{k,s}$ - deflection of k^{th} plate element along side s

ρ_K - mass density of the k^{th} plate element

h_k - thickness of the k^{th} plate element

ω - natural frequency of entire structure

N - total number of plate elements = 13 and

subscripts x,y refer to differentiation with respect to respective coordinates.

$U_{\max,k}$ represents structural part while $U_{T,k,s}$ and $U_{R,k,s}$ represent environmental influence part of the combined microsystem.

Substitution of deflection Equation (3.25) in strain energy and kinetic energy Equations (5.4) and (5.5), and optimization of Rayleigh quotient with respect to $A_{ij,k}$ result in the following eigenvalue equation of the plate type microsystem

$$\sum_m \sum_n \left[C_{mnij,k} + C^I_{mnij,k} - \lambda \Pi_k E^{00}_{mi} F^{00}_{nj} \right] A_{mn,k} - \sum_m \sum_n D_{mnij,s} A_{mn,s} = 0 \qquad (5.6)$$

$$\forall \cdot k = 1,2,\ldots,N$$

where

$$C_{mnij,k} = E^{22}_{mi} F^{00}_{nj} + \alpha_k^4 E^{00}_{mi} F^{22}_{nj} + \upsilon \alpha_k^2 \left(E^{02}_{mi} F^{20}_{nj} + E^{20}_{mi} F^{02}_{nj} \right) + 2 \cdot (1-\upsilon) \alpha_k^2 E^{11}_{mi} F^{11}_{nj}$$

$$C^{I}_{mnij,k} = K^{\bullet}_{T,k,1}\alpha_k E^{00}_{mi}\varphi_n(0)\varphi_j(0) + K^{\bullet}_{T,k,2}\phi_m(1)\phi_i(1)F^{00}_{nj} + K^{\bullet}_{T,k,3}\alpha_k E^{00}_{mi}\varphi_n(1)\varphi_j(1)$$

$$+ K^{\bullet}_{T,k,4}\phi_m(0)\phi_i(0)F^{00}_{nj} + K^{\bullet}_{R,k,1}\alpha_k^3 E^{00}_{mi}\varphi^1_n(0)\varphi^1_j(0) + K^{\bullet}_{R,k,2}\phi^1_m(1)\phi^1_i(1)F^{00}_{nj}$$

$$+ K^{\bullet}_{R,k,3}\alpha_k^3 E^{00}_{mi}\varphi^1_n(1)\varphi^1_j(1) + K^{\bullet}_{R,k,4}\phi^1_m(0)\phi^1_i(0)F^{00}_{nj}$$

$$D_{mnij,s}A_{mn,s} = [K^{\bullet}_{T,k,1}\alpha_k E^{00}_{mi}\varphi_n(1)\varphi_j(0) + K^{\bullet}_{R,k,1}\alpha_k^2\alpha_{s1}E^{00}_{mi}\varphi^1_n(1)\varphi^1_j(0)]A_{mn,s1} +$$

$$[K^{\bullet}_{T,k,2}\phi_m(0)\phi_i(1)F^{00}_{nj} + K^{\bullet}_{R,k,2}\frac{\alpha_k}{\alpha_{s2}}\phi^1_m(0)\phi^1_i(1)F^{00}_{nj}]A_{mn,s2} +$$

$$[K^{\bullet}_{T,k,3}\alpha_k E^{00}_{mi}\varphi_n(0)\varphi_j(1) + K^{\bullet}_{R,k,3}\alpha_k^2\alpha_{s3}E^{00}_{mi}\varphi^1_n(0)\varphi^1_j(1)]A_{mn,s3} +$$

$$[K^{\bullet}_{T,k,4}\phi_m(1)\phi_i(0)F^{00}_{nj} + K^{\bullet}_{R,k,4}\frac{\alpha_k}{\alpha_{s4}}\phi^1_m(1)\phi^1_i(0)F^{00}_{nj}]A_{mn,s4}$$

and

$$K^{*}_{T,k,i} = \frac{K_{T,k,i}a_k^3}{D_k}, K^{\bullet}_{R,k,i} = \frac{K_{R,k,i}a_k}{D_k}, \quad \Pi_k = \frac{\rho_{r,k}a_{r,k}^4}{E_{r,k}h_{r,k}^2}, \quad \lambda = \frac{\rho_1 h_1 a_1^4\omega^2}{D_1},$$

$$E^{rs}_{mi} = \int_0^1 \left(\frac{d^r\phi_m}{dx^r}\right)\left(\frac{d^s\phi_i}{dx^s}\right)\cdot dx, \quad F^{rs}_{nj} = \int_0^1 \left(\frac{d^r\varphi_n}{dy^r}\right)\left(\frac{d^s\varphi_j}{dy^s}\right)\cdot dy, \quad \phi^1_i = \frac{d\phi_i}{dx}, \quad \varphi^1_j = \frac{d\varphi_j}{dy}$$

Subscript (r,k) refers to ratio of parameter of k^{th} segment to that of first plate segment.

The solution of Equation (5.4) yields both eigenvalues and mode shapes of the plate type microsystem. Plate segments that have an edge on the boundary of the main structure side 's' have, $A_{mn,s} = 0$. The required boundary conditions for any segment can be generated by suitable choice of the values of K_T and K_R.

The vibrational behavior of the microstructure such as mode shapes, natural frequencies and the vibrational response can be effected by modifying the stiffness values of artificial

springs which in turn represents the different boundary conditions that are inherent to the micromachining process.

The eigenvalue equation of this microsystem has been formulated and solved for eigenfrequencies for different values of $K^*_{R,a} = \frac{K_R * a}{D}$ at the four end supports of the beams. D = $\frac{Eh^3}{12(1-\gamma^2)}$ is the flexural rigidity of the plate. The predicted variation of four eigenfrequencies against different rotational stiffness is shown in Figure 5.12.

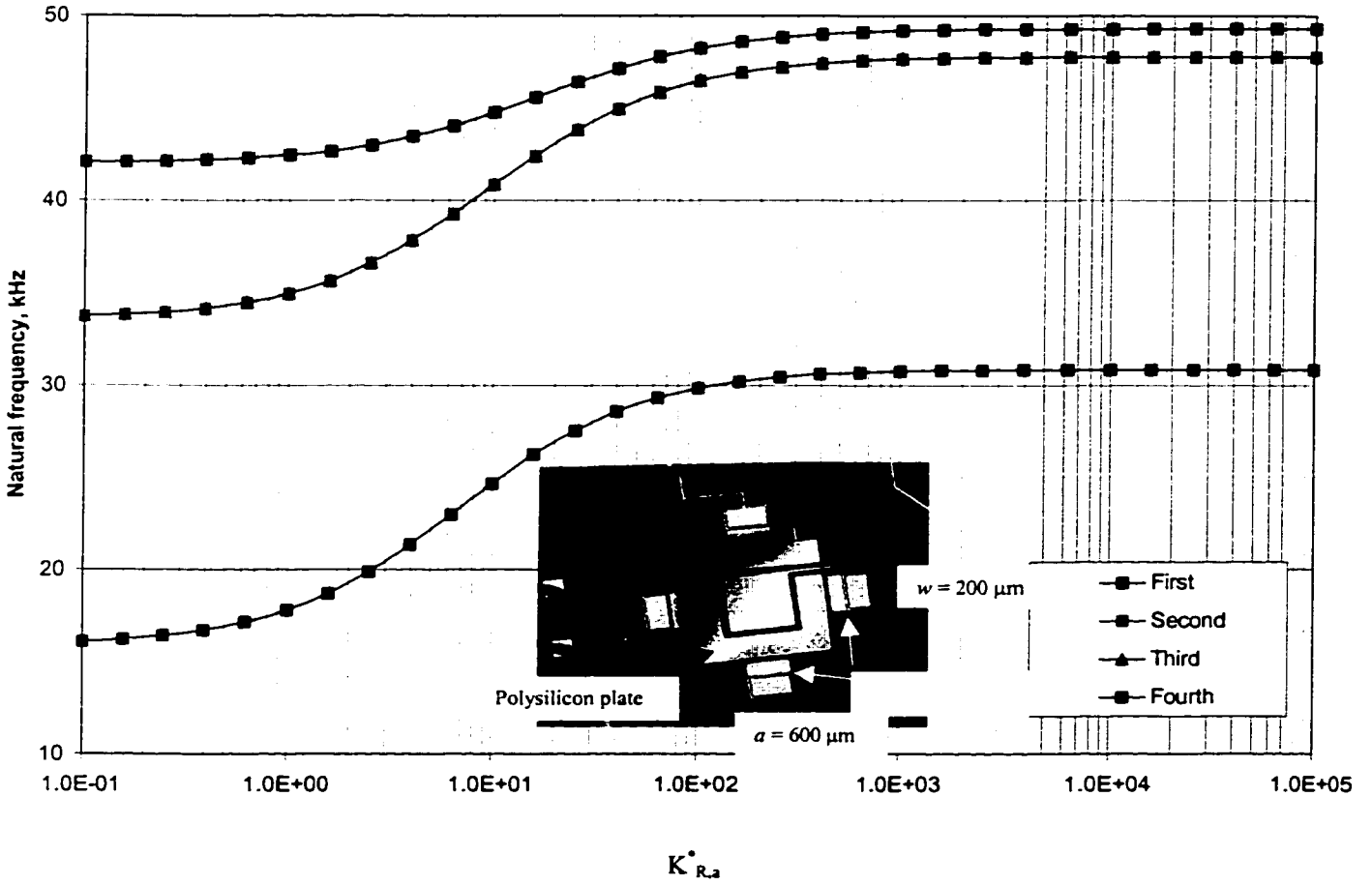

Figure 5.12: The predicted first four natural frequencies versus the boundary rotational stiffnesses for a plate type MEMS structure, design SQ1

This prediction will help in quantifying the boundary conditioning due to different end conditions obtained in MEMS fabrication process for plate type microsystems, if the natural frequncies of the microsystem is available through experiments or other approximate methods such as Finite Element Method.

5.2.1.2 Verification and quantification of boundary conditioning

In order to verify the present prediction the natural frequencies of the structure in Figure 5.7a are compared with those obtained by Finite Element methods using ANSYS (element: SHELL 63) for two different boundary conditions. One of the conditions corresponds to classical clamped condition that assumes no step at the boundaries. The predicted values of natural frequencies for no stepped-up condition given in Table 5.1 are in good agreement with the results of ANSYS. In reality, the structure is stepped-up by the height of 1.5μm which is the thickness of the sacrificial oxide layers. The first four mode shapes of this structure modeled through ANSYS is shown in Figure 5.13. The predicted first natural frequency using ANSYS for this stepped up structure is 30.589 kHz. The corresponding rotational stiffness, that quantifies the available stepped-up condition, can be estimated using the results shown in Figure 5.12 as $K^*_{R,a} = 398.11$. Thus, the boundary conditions from various micromachining process which will result in different rotational elasticity can be defined and quantified through rotational stiffnesses at the boundaries.

Table 5.1 Comparison of the first four natural frequencies of the design SQ1 (Figure 5.7a) for fully clamped boundary conditions i.e. with no step at the boundaries

	Natural Frequencies, kHz			
	First	Second	Third	Fourth
Present Prediction	30.844	47.788	47.788	49.303
ANSYS (SHELL 63)	30.869	48.719	48.934	50.591

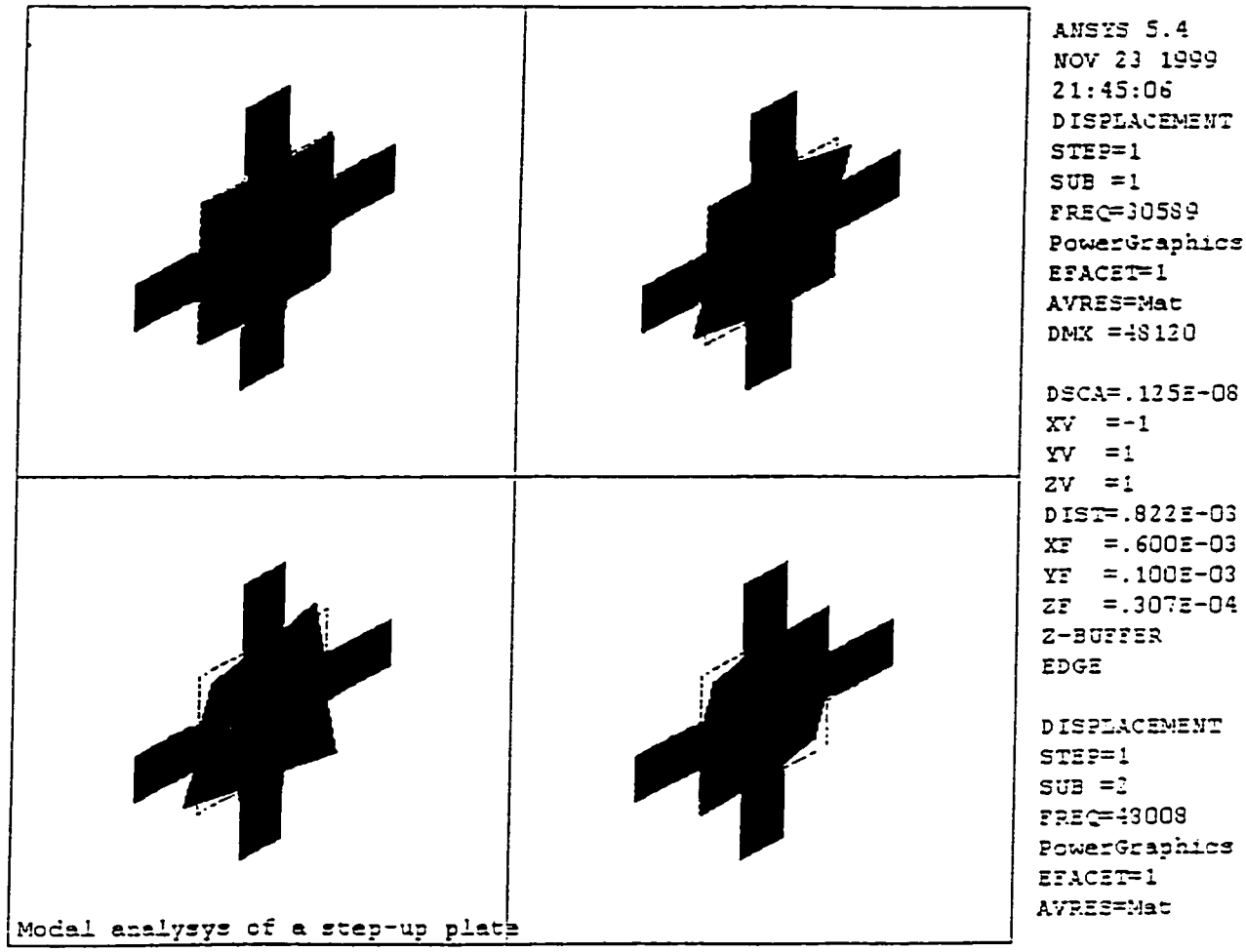

Figure 5.13 Four mode shapes of the design SQ1 predicted using ANSYS

In this demonstration of micro boundary conditioning, the rotational stiffness is the only boundary condition parameter considered in order to represent the influence of microfabrication methods on vibration behavior of the structure. In real situations, there could be many boundary condition parameters as seen in Chapter 4 available influencing the dynamic behavior of the structure.

5.3 BOUNDARY CONDITIONING OF MICROSYSTEMS THROUGH ENVIRONMENTAL INFLUENCE

We have studied so far the possible ways of influencing the dynamic behavior of microsystems by changing the system elastic properties through boundary conditioning with changes in the geometry and properties of the micromechanical structures, that could be by design or due to inherent limitations in the fabrication process itself. Apart from boundary conditioning through structural changes there are other phenomena that are present in the microsystems that affect the net elastic properties of the system. It has been seen in the Sections 1.2.5 and 1.4.3 that phenomena such as squeeze film effect, electrostatic field, Lorentz effect, fringe field, etc. affect the system stiffness. The boundary conditioning through the environmental influence is relevant only to the microsystems. The environmental phenomena influence the potential or strain energy distribution of the entire structure and hence the stiffness of the structure. This influence can be used to our advantage depending upon the performance requirement. If the change in potential energy of the structure due to the environmental phenomena can be quantified, the formulation of boundary conditioning can be extended to predict the

change in dynamic performance of the microsystems. In this section, the effect of electrostatic field on dynamic performance of microsystems is presented as an example to the boundary conditioning through environmental influence.

5.3.1 Prediction of the Influence of Electrostatic Field on Performance of Microsystems

Capacitive type microsystems find a variety of application such as in sensors for measuring pressure, noise level, frequency, acoustic intensity, resonance, acceleration, humidity. Similarly, capacitive type actuators based on electrostatic and fringe field effects find numerous applications. The capacitive type devices have two electrodes in common, as shown in Figure 1.7, which are separated by a very thin layer in the order of a few microns of dielectric medium. When bias voltage V is applied between the electrodes, electrostatic force will develop between the electrodes.

In such capacitive devices with significant polarization voltage, the diaphragm deflection is influenced by the electrostatic field. Previous investigations considered the electrostatic field only as external forces causing static and dynamic deflections in the diaphragm [187, 193, 194]. The effect of electrostatic field on the static deflection behavior was considered in [66] where it was found that the static deflection increased in the presence of electrostatic field. The static deflection of microphone diaphragm increases with electrostatic field which in turn enhances the field strength.

In micromachined capacitive devices the gap between the plates is of the order of micrometers and hence the electrostatic field strength is quite significant. When the electrostatic energy is comparable to the elastic strain energy in the system, it will have a significant influence on the dynamics of flexible plate. The change in energy due to the electrostatic field is given by [66]

$$\frac{-\partial U}{\partial w} = \frac{V^2}{2}\frac{\partial C}{\partial w} \tag{5.7}$$

where U is the energy stored, V is the voltage between the condenser plates and C is the capacitance .

In order to demonstrate the boundary conditioning by electrostatic field, a typical circular type condenser microphone is selected as shown schematically in Figure 5.14. Similar strucures (microphones) fabricated out of the Mitel 1.5 μm process and through the present fabrication synthesis are shown in Figures 1.18, 1.22. 1.23, 2.26, 2.30 , 5.1a, 5.1b and 5.3. Similar capacitive microphones fabricated out of MUMPs are shown in Figures 1.28, 5.7 to 5.9.

The simplified system model of the elastic system under electrostatic field is shown in Figure 5.15. K_b and F_b represent the influence of structural (geometry and property) part and K_e and F_e represent the influence of environmental part. The effect of electrostatic force in determining the static deflection limit and snap limit was explained in the Section 1.2.5.2 with the Figure 1.12. On consolidation, for a given bias voltage, the electrostatic

force pulls the structure through the deflection defined by $\overline{w}$. When the electrostatic force equals the restoring elastic force of the structure, the diaphragm reaches stable equilibrium position called static limit. If by some means the structure deflects further than the static limit, then the force and the stiffness requirements follow as shown in Figure 5.15. Further deflection after snap limit will cause the structure to get snapped to the backplate permanently. Hence, it becomes very important to predict the static limit, snap limit, snap voltage and dynamic behavior of the structure under the influence of electrostatic force for the design synthesis of microsystems. The concept of boundary conditioning is applied for predicting the electrostatic field influence as follows:

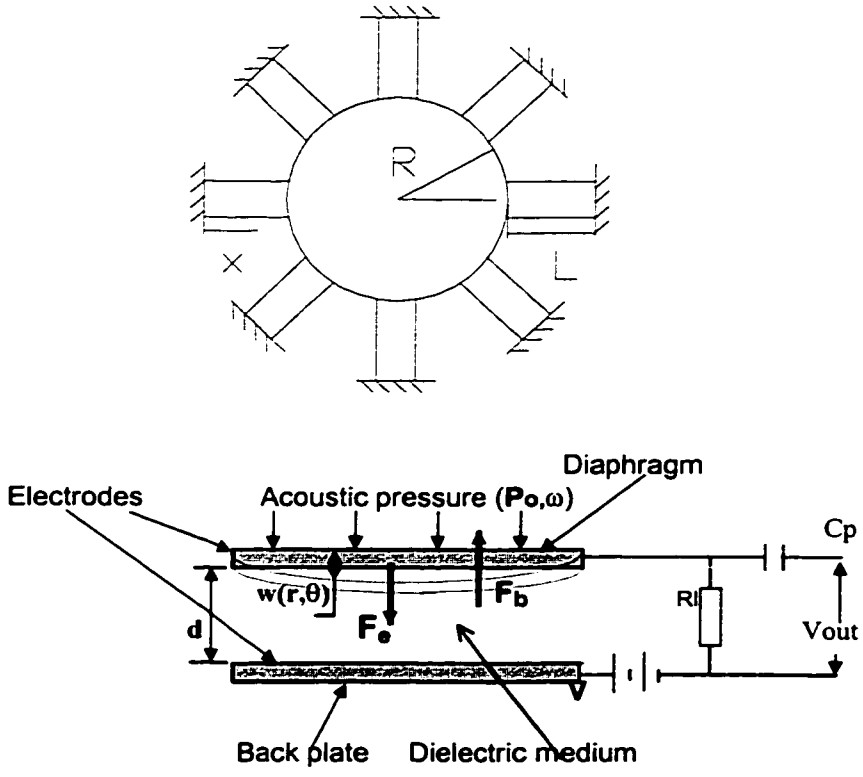

Figure 5.14 Schematic of a circular condenser microphone

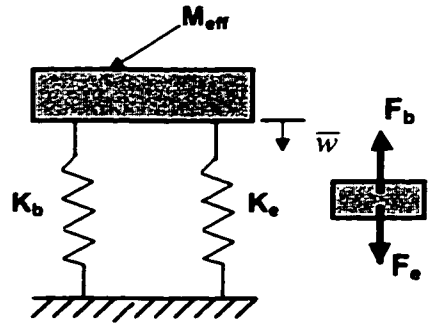

K_b - Equivalent Stiffness due to Bending of Diaphragm
K_e - Equivalent Stiffness representing Electrostatic Field
F_b - Equivalent force due to Bending of Diaphragm
F_e - Equivalent force representing Electrostatic Field

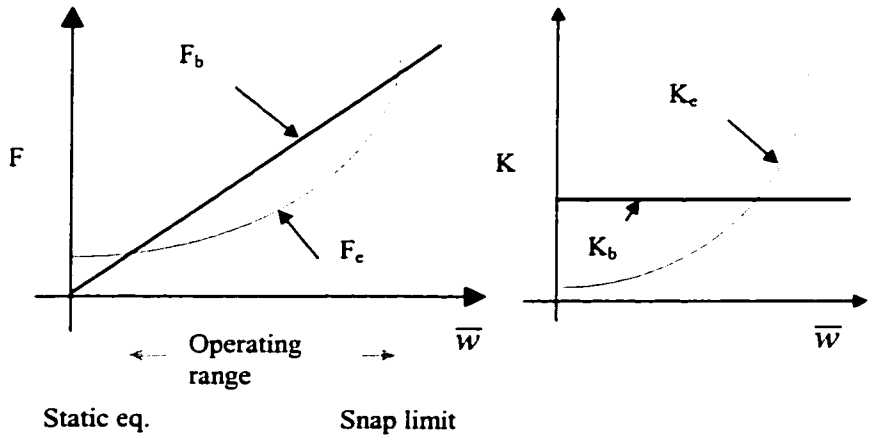

Figure 5.15 Simplified system model of a boundary conditioned elastic system under electrostatic field.

As the interest is to find only the fundamental natural frequency under electrostatic force, it is obtained using the Rayleigh method [180]. The deflections of the beam and the diaphragm are assumed, respectively, as

$$y(x) = (a_s + a_d)x^2 \tag{5.8}$$

$$w(r) = (a_s + a_d)(2 - r^2) \tag{5.9}$$

The geometrical Boundary Conditions are

$y(0) = y'(0) = 0$
$w'(0) = 0$
$w(1) = y(1)$
$w'(1) = -y'(1)$

where

$x = \xi/L$, $r = \eta/R$

a_s - static deflection coefficient and

a_d - dynamic deflection coefficient.

The deflection expressions y(x) and w (r) satisfy the geometrical boundary conditions as well as the continuity of deflection and slope at the beam and diaphragm junction.

5.3.1.1 Prediction of static limit, snap limit and snapping voltage

The lumped parameter modeling is used in this Section. The equations for static deflection are written after neglecting the dynamic part as

$$y(x) = a_s x^2 \tag{5.10}$$

$$w(r) = a_s(2 - r^2) \tag{5.11}$$

The maximum total elastic strain energy given as

$$U_{s\max} = U_{b\max} + U_{d\max} \tag{5.12}$$

where $U_{b\max}$ is the strain energy of the support beams and $U_{d\max}$ is the stain energy due to bending of diaphragm and are given by

$$\begin{aligned} U_{b\max} &= \frac{EI}{2L^3} N \int_0^1 (y''(x))^2 dx \\ &= \frac{2a_s{}^2 NEI}{L^3} \end{aligned} \tag{5.13}$$

$$\begin{aligned} U_{d\max} &= \frac{\pi D}{R^2} \int_0^1 \left[\left(w''(r) + \frac{w'(r)}{r} \right)^2 - 2(1-\upsilon) w''(r) \frac{w'(r)}{r} \right] r dr \\ &= \frac{4D\pi(1+\upsilon)a_s^2}{R^2} \end{aligned} \tag{5.14}$$

where EI is bending rigidity of beam, L is length of beam, N is number of beams, D is bending rigidity of plate diaphragm and R is radius of diaphragm. y' indicates differentiation with respect to x and w' indicates differentiation with respect to r. It is assumed that the deflections are axisymmetric.

Similarly, the maximum total electrostatic energy of the system, which represents the environmental influence on system elastic property, is given by

$$U_{e\max} = U_{ed\max} + U_{eb\max} \tag{5.15}$$

where $U_{ed\max}$ is the diaphragm part of electrostatic energy and $U_{eb\max}$ is support beams part of electrostatic energy and are given as

$$U_{ed\max} = -F\frac{Dd^3\pi}{R^2}\int_0^1 \left(\frac{w(r)}{(d-w(r))^2}\right) rdr \tag{5.16}$$

$$U_{eb\max} = -F\frac{Dd^3NLW}{2R^4}\int_0^1 \left(\frac{y\ (x)}{(d-y(x))^2}\right) dx \tag{5.17}$$

where

$$F = \frac{\varepsilon_0 R^4 V^2}{Dd^3} \tag{5.18}$$

ε_o - permittivity of the vacuum

d - effective distance between the electrodes

W - width of the beams and

V - supply voltage

It is possible to consider F as a parameter indicating the strength of the electrostatic field.

The total net strain energy of the microsystem is given by adding Equations (5.12) and (5.15) as

$$U_{\max} = U_{s\max} + U_{e\max} \tag{5.19}$$

For static equilibrium,

$$\partial U_{\max} = \frac{dU_{\max}}{da_s}\partial a_s = 0 \tag{5.20}$$

which results in the following condition:

$$\left[\frac{2NEI}{L^3} + \frac{4D\pi(1+\upsilon)}{R^2}\right]2a_s =$$

$$F\frac{Dd^3}{2R^4}\left[\int_0^1 2\pi R^2\left(\frac{2-r^2}{\left(d-w(a_s)\right)^2}\right)rdr + NLW\int_0^1\left(\frac{x^2}{\left(d-y(a_s)\right)^2}\right)dx\right] \tag{5.21}$$

The static deflection is obtained by minimizing the difference between elastic energy and electrostatic energy with respect to the static deflection coefficient a_s. The resulting Equation (5.21) is solved in an iterative fashion to obtain the static deflection. Hence, for the given field strength F and microsystem configuration, the static (x_{min}) and snap (x_{max}) limits as shown in Figure 1.12 can be estimated iteratively from the Equation (5.21). There exists a limiting value of F beyond which the diaphragm becomes unstable and snaps onto the back plate. The corresponding voltage called snapping voltage, for which $x_{min} = x_{max}$, can be estimated iteratively using the Equation (5.21)

5.3.1.2 Prediction of natural frequency under the influence of electrostatic field

The natural frequency of the microsystem is found out using lumped parameter model of the system based on energy principle as shown in Figure 5.15. The dynamic deflection equations with reference to the static limit are defined as

$$y(x) = a_d x^2 \tag{5.22}$$

$$w(r) = a_d (2 - r^2) \tag{5.23}$$

The maximum kinetic energy of the beams and the diaphragm are given, respectively, as

$$T_{b\max} = \frac{m\omega^2 LN}{2} \int \left[y^2(x)\right] dx \tag{5.24}$$

$$T_{d\max} = \pi \rho h \omega^2 R^2 \int_0^1 w^2(r) r dr \tag{5.25}$$

where m is the mass per unit length of beam and ρh is the mass per unit area of the diaphragm.

The maximum kinetic energy of the entire microsystem can be calculated by adding the Equations (5.24) and (5.25) as

$$T_{\max} = T_{b\max} + T_{d\max} \tag{5.26}$$

The net total strain energy is calculated using the Equations (5.12) to (5.19) by replacing the deflection equations with Equations (5.22) and (5.23). It must be noted from Equation (5.19) that $U_{e\max}$ decreases with increasing electrostatic energy producing a

weakening effect on the diaphragm stiffness. This is because the electrostatic field has a destabilizing effect on the diaphragm.

The natural frequency is calculated using the average properties of the system as follows:

The average deflection for the entire structure can be expressed as

$$\overline{w} = a\left[\frac{2R^2\pi\int_0^1\left(2-r^2\right)r.dr + NWL\int_0^1 x^2dx}{R^2\pi + NWL}\right] \tag{5.27}$$

Due to this average bending deflection, the equivalent reaction elastic force by the structure can be estimated from the strain energy Equation (5.12) as

$$F_b = \frac{dU_{s\max}}{d\overline{w}} = \frac{dU_{s\max}}{da}\frac{da}{d\overline{w}} \tag{5.28}$$

$$= \frac{\left[\frac{2NEI}{L^3} + \frac{4D\pi(1+\upsilon)}{R^2}\right]2a_s}{\left[\frac{2R^2\pi\int_0^1\left(2-r^2\right)r.dr + NWL\int_0^1 x^2dx}{R^2\pi + NWL}\right]} \tag{5.29}$$

Then the equivalent average spring constant for bending can be estimated from

$$K_b = \frac{dF_b}{d\overline{w}} = \frac{dF_b}{da}\frac{da}{d\overline{w}} \tag{5.30}$$

$$= \frac{\left[\frac{2NEI}{L^3} + \frac{4D\pi(1+\upsilon)}{R^2}\right]2}{\left[\frac{2R^2\pi\int_0^1 (2-r^2)r.dr + NWL\int_0^1 x^2 dx}{R^2\pi + NWL}\right]} \tag{5.31}$$

and using the Equation (5.28).

Similarly, the average force due to electrostatic field is estimated as

$$F_e = \frac{dU_{e\max}}{d\overline{w}} = \frac{dU_{e\max}}{da}\frac{da}{d\overline{w}} \tag{5.32}$$

$$= -\frac{F\frac{Dd^3}{2R^4}\left[\int_0^1 2\pi R^2\left(\frac{2-r^2}{\left(d-w(a_s)\right)^2}\right)rdr + NLW\int_0^1\left(\frac{x^2}{\left(d-y(a_s)\right)^2}\right)dx\right]}{\left[\frac{2R^2\pi\int_0^1 (2-r^2)r.dr + NWL\int_0^1 x^2 dx}{R^2\pi + NWL}\right]} \tag{5.33}$$

The equivalent spring constant for electrostatic force can be calculated from

$$K_e = \frac{dF_e}{d\overline{w}} = \frac{dF_e}{da}\frac{da}{d\overline{w}} \tag{5.34}$$

using the Equation (5.32).

The effective mass of the entire system is estimated from the kinetic energy defined by Equation (5.26) as follows:

$$M_{eq} = \frac{2T_{\max}}{\overline{w}^2 \omega^2} \tag{5.35}$$

$$= \frac{2\left[\frac{mLN}{2}\int\left[y^2(x)\right]dx + \pi\rho hR^2\int_0^1 w^2(r)rdr\right]}{\overline{w}^2} \tag{5.36}$$

Similarly, the equivalent stiffness is calculated by summing the bending stiffness (Equation (5.30)) and stiffness representing environmental electrostatic effect (Equation (5.34)) as

$$K_{eq} = K_b + K_e \tag{5.37}$$

The natural frequency of the complete microsystem under the influence of electrostatic effect can be estimated using the effective mass and stiffness values as

$$\omega^2 = \frac{K_{eq}}{M_{eq}} \tag{5.38}$$

The equivalent stiffness due to electrostatic force is strongly dependent upon the amplitude for a given bias voltage. For the calculation of natural frequency, the stiffnesses are estimated near the static equilibrium position. Thus, boundary conditioning of capacitive type microsystems is possible through the bias voltage between the electrodes.

5.3.2 Application to Proposed Fabrication Synthesis of Microsystems through the Mitel 1.5 μm process

The proposed fabrication synthesis of microsystems in the Chapter 2 includes fabrication of capacitive sensors by sacrificial post-processing of polysilicon2 as given in the Section 2.7 and Figure 2.20.

The boundary conditoning is demonstrated on a design with the following details as shown in Figure 5.1b. The diaphragm is made of a metal layer (Metlal2) sandwiched in between a oxide layer (IMO) and passivation layer (PASS). The geometrical details of the structure shown in Figure 5.16 is similar to the scheme in Figure 5.14 and are as follows.

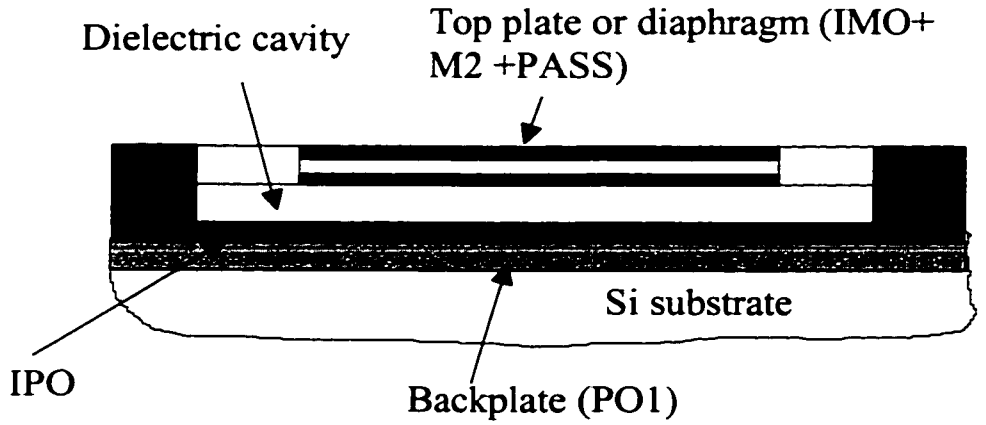

Figure 5.16 Scheme of the capacitive sensor used for prediction of the influence of electrostatic field

Radius of the diaphragm , R = 325 μm

Width of the support beams, W =125 μm

Length of the support beams, L = 50 μm

Thickness of the lower layer (IMO), h_L = 0.3 μm

Thickness of the structural layer M2, h_b = 0.8 μm

Thickness of the top layer, h_U = 1.0 μm

Thickness of the insulation layer (IPO) on the backplate (PO1), h_{Ub} = 0.048 μm

Modulus of elasticity of the lower layer (IMO), $E_L = 0.74 \times 10^{11}$ N/m^2

Modulus of elasticity of the structural layer M2, $E_b = 0.69 \times 10^{11}$ N/m^2

Modulus of elasticity of the top layer, $E_L = 0.74 \times 10^{11}$ N/m^2

Mass density of the lower layer (IMO), ρ_L = 2180 kg/m^3

Mass density of the structural layer M2, ρ_b = 2300 kg/m^3

Mass density of the top layer, ρ_U = 2180 kg/m^3

Thickness of the lower layer (IMO), h_L = 0.3 μm

Thickness of the structural layer M2, h_b = 0.8 μm

Thickness of the top layer, h_U = 1.0 μm

Thickness of the insulation layer (IPO) on the backplate (PO1), h_{Ub} = 0.048 μm

The initial dielectric gap, d_0 = 0.3 μm

Dielectric constant of the lower layer (IMO), ε_L = 3.8

Dielectric constant of the insulation layer (IPO) on the backplate (PO1), ε_{Ub} = 3.8

Dielectric constant of the air cavity, ε_{air} = 1 and

Permittivity of the free space, $\varepsilon_0 = 8.85 \times 10^{-12}$ F/m

The equivalent properties are calculated using the following equations:

Equivalent dielectric distance, $d_{eq} = d_0 + h_L/\varepsilon_L + h_{Ub}/\varepsilon_{Ub}$

Equivalent modulus of elasticity, $E_{eq} = \dfrac{E_L Vol_L + E_b Vol_b + E_U Vol_U}{Vol_L + Vol_b + Vol_U}$

Equivalent mass density, $\rho_{eq} = \dfrac{\rho_L Vol_L + \rho_b Vol_b + \rho_U Vol_U}{Vol_L + Vol_b + Vol_U}$

Equivalent thickness, $h_{eq} = h_U + h_b + h_L$

The prediction of static limit, snap limit and natural frequency were carried out for the above design and the results are given in Figures 5.16 to 5.20. The normal values were replaced with the equivalent values wherever possible for the prediction. The predicted variation of average electrostatic force F_e (Equation 5.32) and reaction force F_b (Equation 5.28) against deflection positions are given in Figure 5.17. When the field strength is increased the static limits and snap limits move closer. The increase in static equilibrium limit is noticed when field strength is increased. It can be seen that at very high field strengths, for example F=120, static and snap limits are the same and thus dictating the limit of the field strength that can be applied. The predicted variation of static limit and snap limit against field strength and bias voltage are shown in Figure 5.18. Bias voltage of around 11.5 volts at which static limit and snap limit is the snapping voltage as noticed in this figure. The diaphragm becomes totally unstable after the snapping voltage. The predicted variation of natural frequency as per the Equation 5.38 is shown in Figures 5.19 and 5.20 against field strength and bias voltage, respectively. Thus this study shows the possible prediction of environmental influence on the behavior of microsystems that are fabricated through the proposed fabrication synthesis with application of the concept of boundary conditioning.

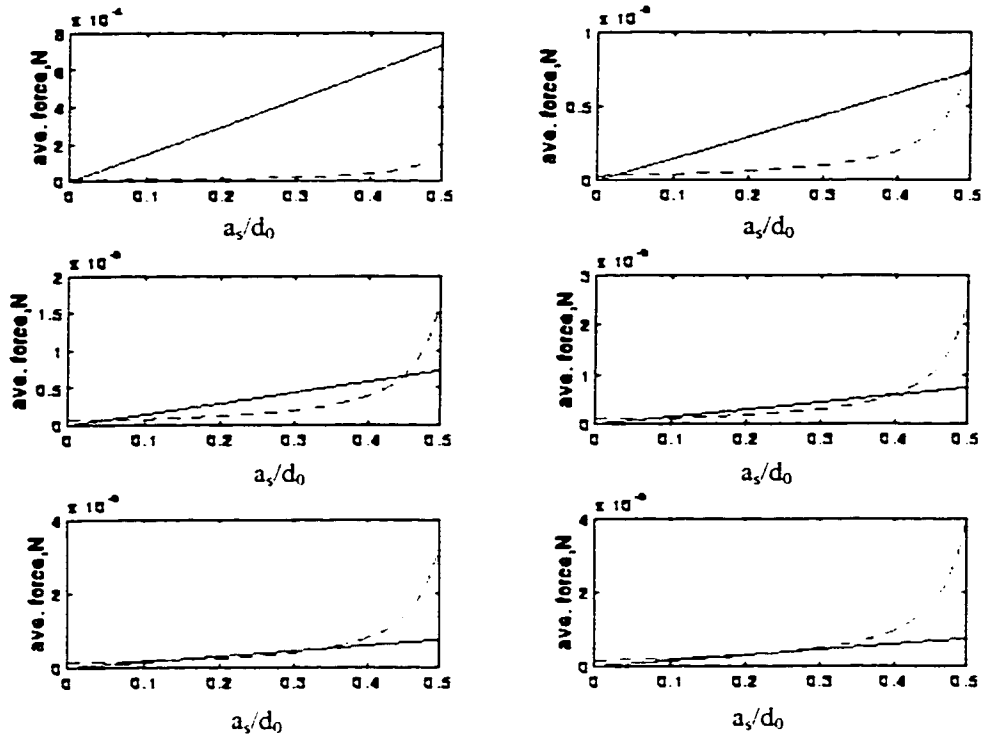

Figure 5.17 Predicted variation of average bending and electrostatic force for different field strengths for a condenser microphones fabricated through the Mitel 1.5mm process.

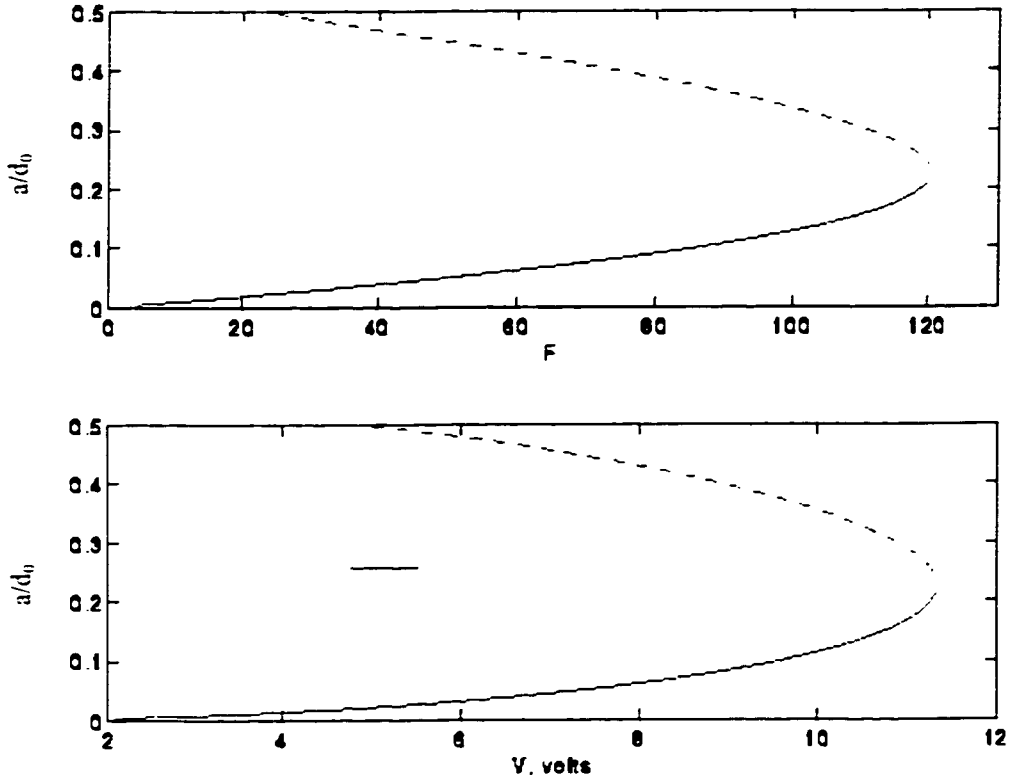

Static limit, x_{min}
Snap limit, x_{max}

Figure 5.18 Predicted variation of static limit and snap limit against electrostatic field strength and bias voltage

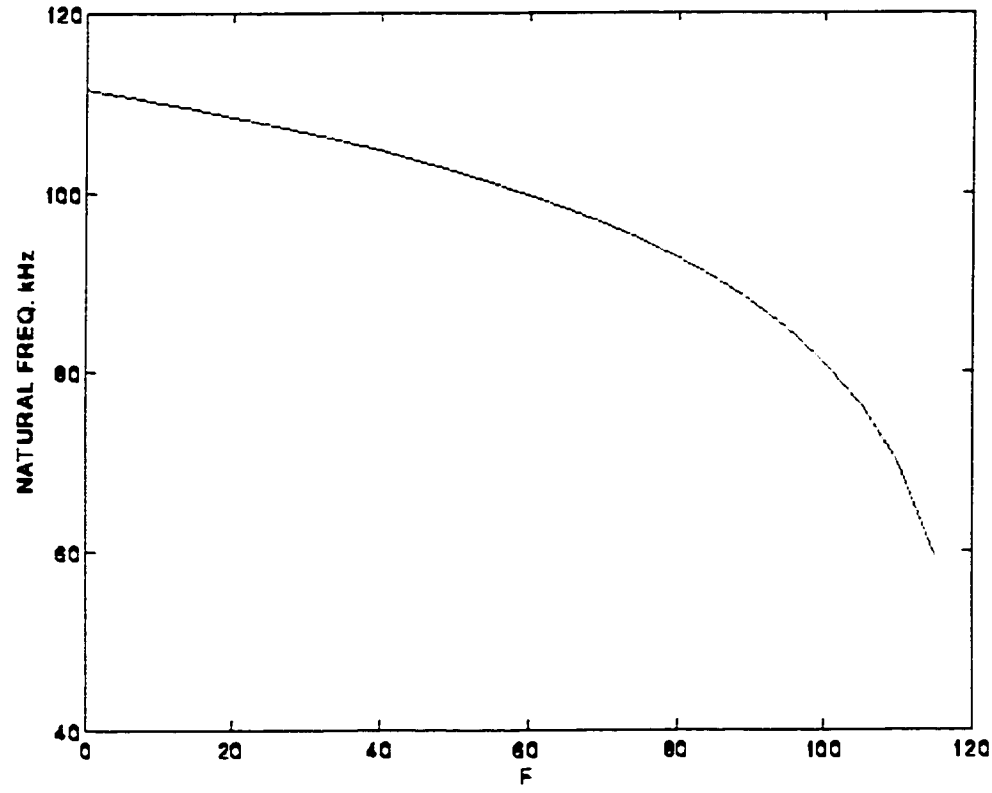

Figure 5.19 Predicted variation of natural frequency against field strength

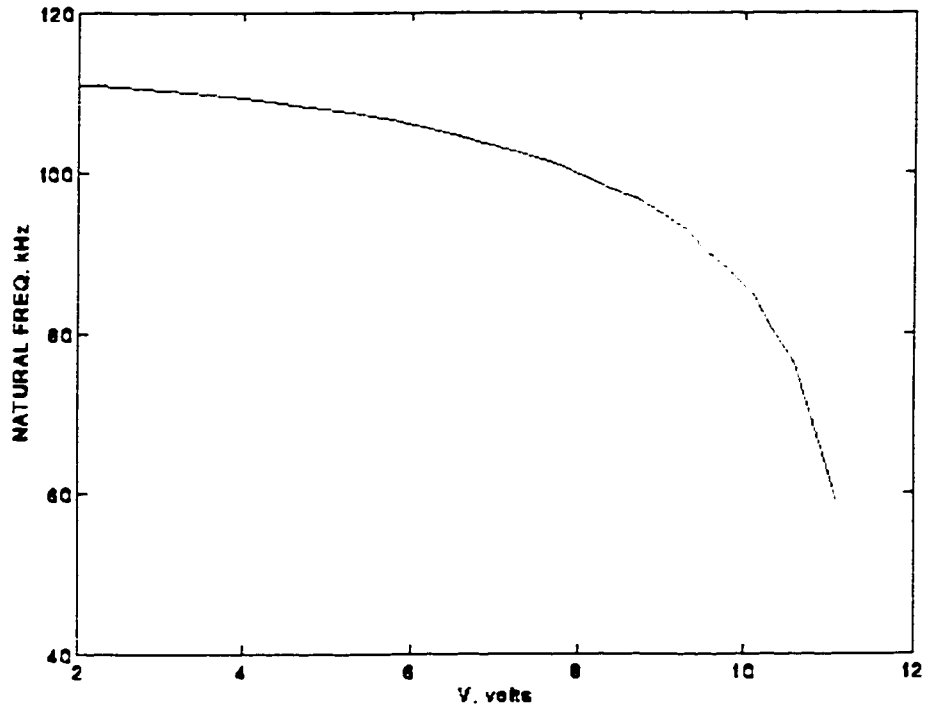

Figure 5.20 Predicted variation of natural frequency against bias voltage

5.3.3 Application to Microsystems Fabricated through MUMPs

In this section, boundary conditioning is applied to capacitive type microsystems fabricated through a dedicated process called MUMPs. The performance of the square type capacitive devices, shown in Figures 5.7 to 5.9, are also influenced by electrostatic field. The circular type capacitive sensors shown in Figures 5.21 and 5.22 are selected for the present demonstration of boundary conditioning. These devices were also subjected to residual stress that were inherent to the fabrication process apart from the electrostatic field. Thus, this section also presents the prediction of the effect of residual stress on the performance of microsystems as an extension to the boundary conditioning through fabrication process.

5.3.3.1 Prediction of the influence of residual stress on performance of microsystems

Consider the micromechanical structure subjected to residual stress σ_d. Residual stress is assumed to be distributed along the circumference. This residual stress changes the distribution of strain energy over the entire structure.

The vertical shear force due to the residual stress

$$\begin{aligned} R_v &= \sigma_d h \frac{d\phi}{dr} = \sigma_d h \frac{d^2 w(r)}{dr^2} \text{ for the diaphragm portion} \\ &= \sigma_d h \frac{d\phi}{dx} = \sigma_d h \frac{d^2 y(x)}{dx^2} \text{ for the support beam portion} \end{aligned} \tag{5.39}$$

The work done by residual stress on the microsystem over the circular diaphragm area

$$
\begin{aligned}
U_{\sigma d} &= -\oint R_v \cdot dA \cdot \partial w(r) \\
&= -\int_0^R R_v h \cdot \partial w(r) 2\pi r \cdot dr \\
&= -3\pi a \sigma_d h
\end{aligned}
\tag{5.40}
$$

Similarly the work done on the support beams area

$$
\begin{aligned}
U_{\sigma b} &= -N \oint R_v \cdot dA \cdot \delta y(x) \\
&= -NW \int_0^L R_v h \cdot \delta y(x) \cdot dx \\
&= -\frac{2NWh\sigma_d a}{3L}
\end{aligned}
\tag{5.41}
$$

where the deflection expressions are defined by the Equations (5.10) and (5.11) for the prediction of static and snap limits, and by the Equations 5.22 and 5.23 for the prediction of natural frequency.

Residual stress present in the structure alters the strain energy distribution of the system and hence the new strain energy is given by

$$
U_{s\max} = U_{d\max} + U_{b\max} + U_{\sigma d} + U_{\sigma b} \tag{5.42}
$$

For static equilibrium of the structure, the Equation (5.20)

$$
\partial U_{\max} = \frac{dU_{\max}}{da_s} \partial a_s = 0
$$

results in the following condition:

$$
\left[\frac{2NEI}{L^3} + \frac{4D\pi(1+\upsilon)}{R^2} - \frac{3\pi\sigma_d h}{2} - \frac{NWh\sigma_d}{3L} \right] 2a_s =
$$

$$F\frac{Dd^3}{2R^4}\left[\int_0^1 2\pi R^2\left(\frac{2-r^2}{\left(d-w(a_s)\right)^2}\right)rdr + NLW\int_0^1\left(\frac{x^2}{\left(d-y(a_s)\right)^2}\right)dx\right] \tag{5.43}$$

This equation presents the combined influence of residual stress inherent to fabrication process and electrostatic field on the static and snap limits of the device. The static and snap limits can be estimated iteratively for a given field strength F and residual stress σ_d.

With the revised strain energy formulation given by Equation (5.42), natural frequency can be found out with the following modifications:

The equivalent reaction elastic force by the structure under the bending and residual stress can be estimated from the strain energy Equation (5.42) as

$$F_b = \frac{dU_{s\max}}{d\overline{w}} = \frac{dU_{s\max}}{da}\frac{da}{d\overline{w}} \tag{5.44}$$

$$= \frac{\left[\frac{2NEI}{L^3} + \frac{4D\pi(1+\upsilon)}{R^2} - \frac{3\pi\sigma_d h}{2} - \frac{NWh\sigma_d}{3L}\right]2a_s}{\left[\frac{2R^2\pi\int_0^1\left(2-r^2\right)r.dr + NWL\int_0^1 x^2dx}{R^2\pi + NWL}\right]} \tag{5.45}$$

Then the equivalent average spring constant for bending can be estimated from

$$K_b = \frac{dF_b}{d\overline{w}} = \frac{dF_b}{da}\frac{da}{d\overline{w}} \tag{5.46}$$

Hence

$$K_b=\frac{\left[\frac{2NEI}{L^3}+\frac{4D\pi(1+\upsilon)}{R^2}-\frac{3\pi\sigma_d h}{2}-\frac{NWh\sigma_d}{3L}\right]2}{\left[\frac{2R^2\pi\int_0^1(2-r^2)r.dr+NWL\int_0^1 x^2dx}{R^2\pi+NWL}\right]} \tag{5.47}$$

By substituting the revised value of K_b from Equation (5.47) into the Equation (5.37), the new natural frequencies under the combined influence of electrostatic field and residual stress can be estimated using the Equation (5.38).

5.3.3.2 Combined influence of residual stress and electrostatic field on performance of devices CA and CB

The concept of boundary conditioning for determining the combined influence of electrostatic field (environmental) and residual stress (limitation of fabrication process) has been developed in the previous section. In order to validate the above formulation, it is applied on two capacitive devices namely CA and CB that are shown in Figure 5.21 and 5.22. These devices were fabricated through MUMPs process. The geometry and material properties used for the prediction are given in Table 5.2.

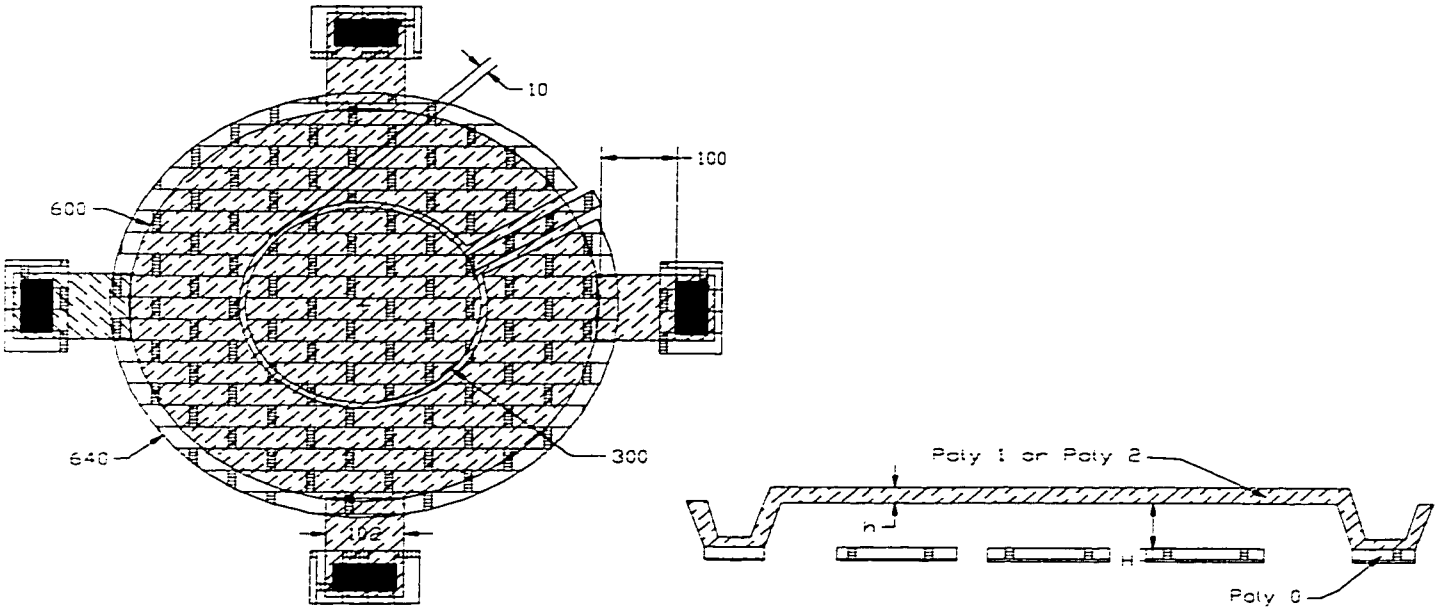

Diaphragm	Backplate	H	h
Poly 1	Poly 0	2.0731	2.0040
Poly 2	Poly 0	2.8054	1.5021

a) Schematic

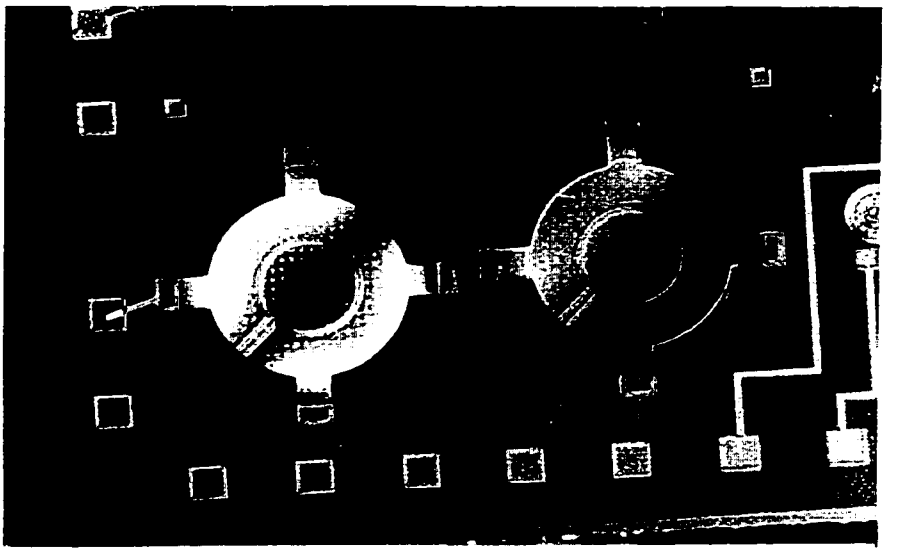

Figure 5.21 Photograph of the circular type capacitive devices fabricated through MUMPs (Designs CB and CA). Diameter of the diaphragm is 600μm.

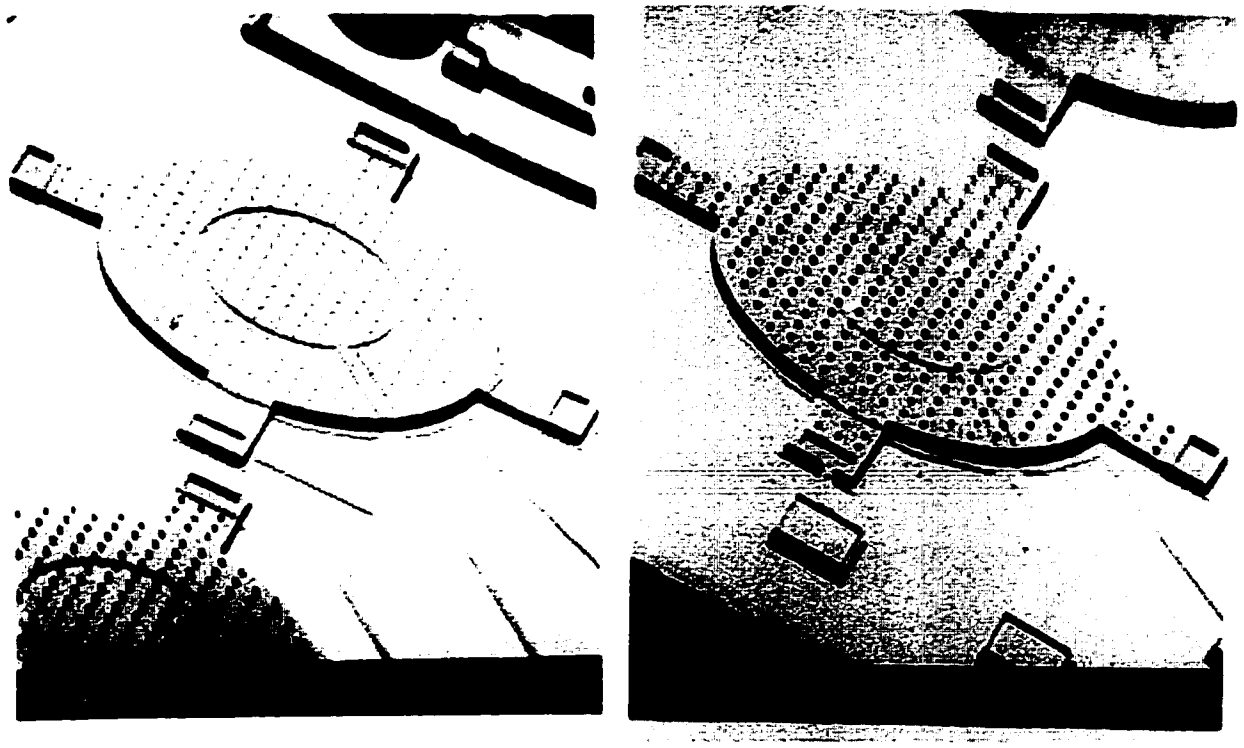

Figure 5.22 SEM micrograph of capacitive devices CA and CB fabricated through MUMPs. Diameter is 600μm.

Table 5.2 Structural and functional properties of sensors CA and CB

	CA	CB
Structural (diaphragm) layer	Poly1	Poly2
Radius of the diaphragm, R μm	300	300
Number of support beams, N	4	4
Width of support beams, W μm	102	102
Length of support beams, L μm	100	100
Thickness, h in A	20241	15162
Mass density, ρ kg/m^3	2300	2300
Modulus of elasticity, E GPa	170	170
Poisson's ratio	0.42	0.42
Dielectric gap, d_0 in A	22000	29869
Residual stress, σ_d, Mpa (compressive)	-28	-5

The predicted results under the combined influence of electrostatic field and residual stress, using the structural parametric values given in Table 5.2, are shown in Figures 5.23 to 5.26. The structural layer, Poly1, for the sensor CA has inherent compressive stress of 28 MPa while the Poly2 structural layer of the sensor CA has the inherent compressive residual stress of 5 MPa. Poly0 layer is the backplate for both sensors. The bias voltage V will be applied between the structure and the backplate.

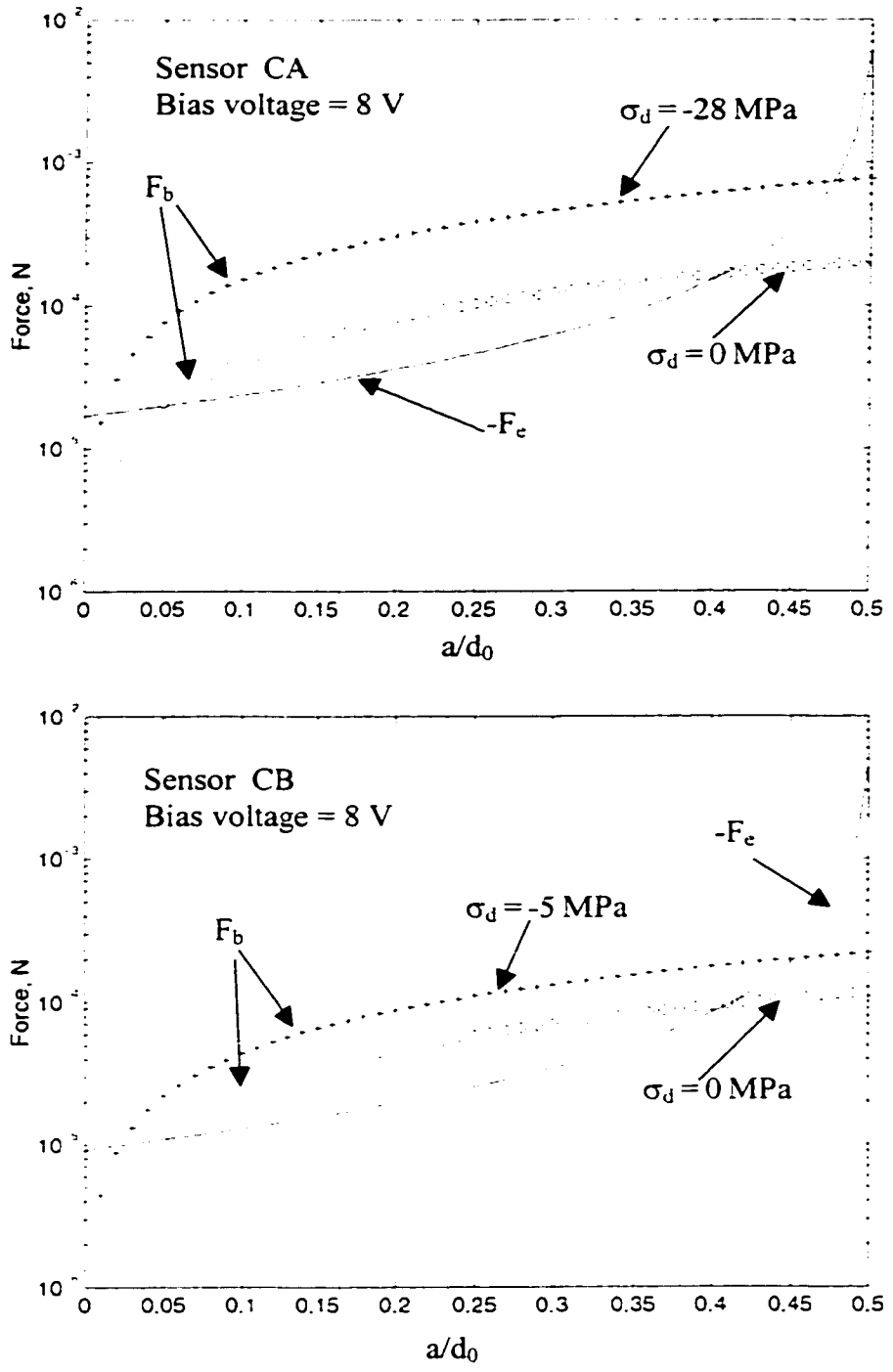

Figure 5.23 Predicted variation of average bending force and electrostatic force under the influence of residual stress at the bias voltage of 8V for two capacitive type devices fabricated through the MUMPs process.

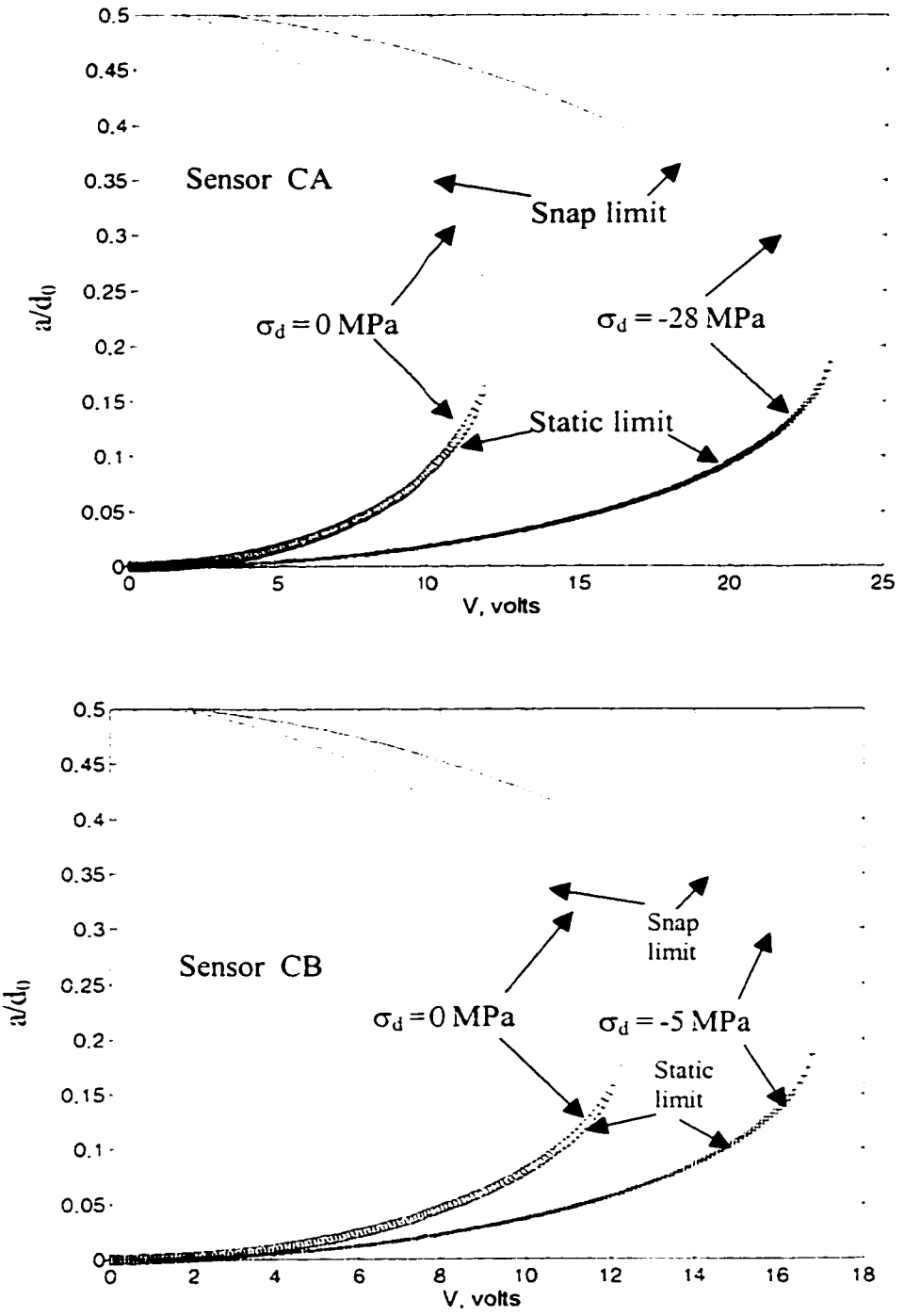

Figure 5.24 Predicted variation of static limit and snap limit under the influence of residual stress against bias voltage for two capacitive type devices fabricated through the MUMPs process.

Figure 5.23 shows the predicted variation of average reaction force F_b with and without the influence of residual stress along with electrostatic force F_e for a given bias voltage of 8V against deflection positions. The presence of residual stress increased the reaction force and resulted in a wider operating range (lower static limit and higher snap limit).

Static and snap limits were predicted against bias voltage as shown in Figure 5.24. It can be seen from the Table 5.3, that the presence of residual stress increased the snapping voltage from 12.1 to 23.3 for the sensor CA and from 12.3 to 16.8 volts for the sensor CB. Thus residual stress increased the operating voltage range. The snapping voltage given in Table 5.3 for the sensor CA was experimentally also found out. The comparison between the experimental and predicted values is good. The curling of structures could be the reason for the difference between the two values.

Table 5.3 Results of the snap study

		CA	**CB**
		Snap Voltage	
Experimental		26.7 - 27.3	----
Prediction with $\sigma_d = 0$ MPa		12.1	12.3
Prediction with	$\sigma_d = -28$ MPa	23.3	---
	$\sigma_d = -5$ MPa	---	16.8

In order to predict the influence of residual stress on dynamic behavior, equivalent stiffnesses such as K_b and K_e were calculated as shown in Figure 5.15. It can be seen that stiffness becomes deflection dependent and hence the natural frequencies were estimated

near the static equilibrium position. The predicted variation of natural frequency against bias voltage is given in Figure 5.25 for both sensors. It can be seen that residual stress increased the natural frequency and hence resulted in a wider dynamic operating range.

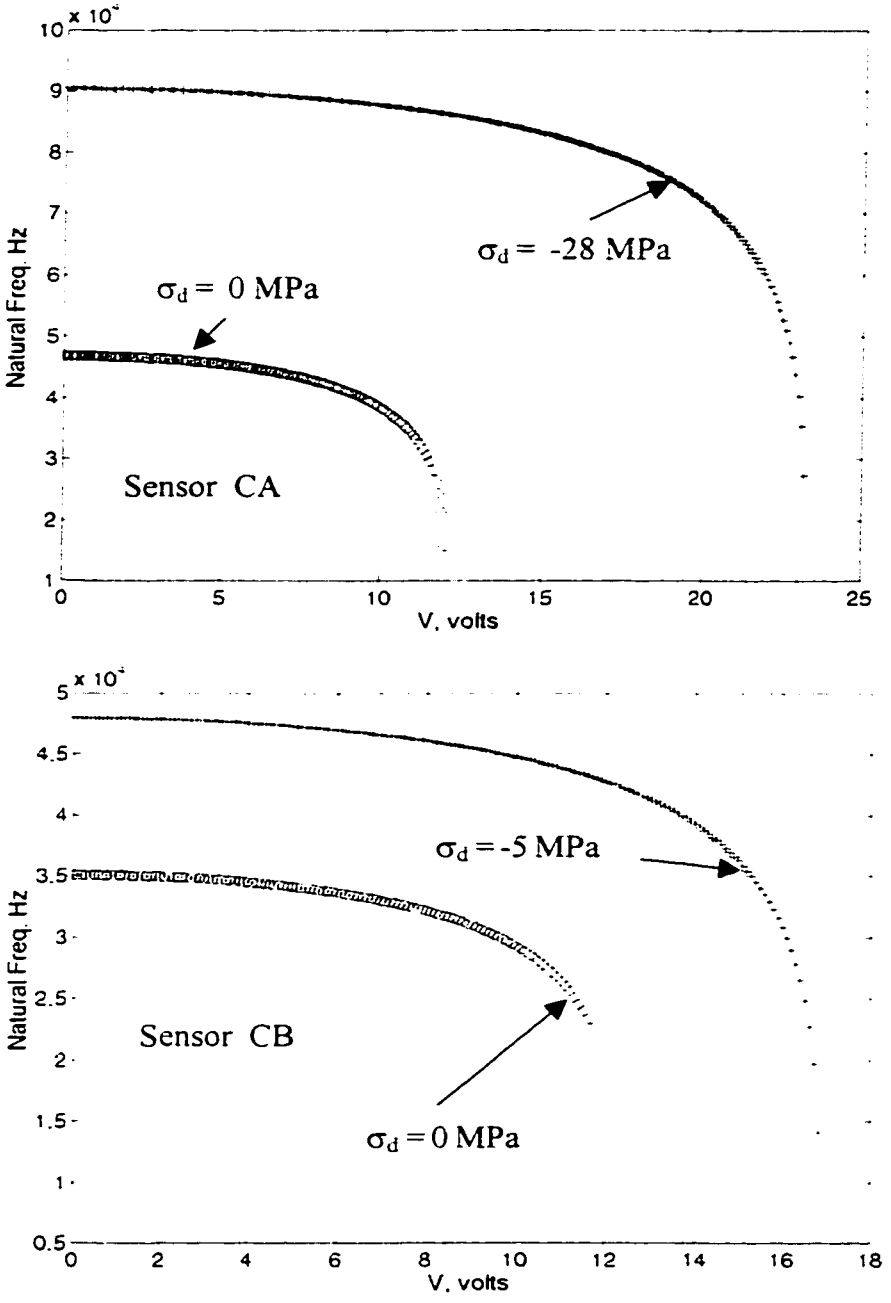

Figure 5.25 Predicted variation of natural frequency against bias voltage under the influence of residual stress for two capacitive type devices fabricated through the MUMPs process.

5.4 APPLICATION OF FUZZY SYSTEM IDENTIFICATION TO BOUNDARY CONDITIONING OF MICROSYSTEMS

The influence of geometrical variations, fabrication methods, fabrication process parameters and operational environment on boundary conditioning of microsystems has been studied so far in this chapter. Considering the nature of complications at the microlevel, it may not be possible to predict the dynamic behavior under the influence of many boundary conditioning parameters and it may be necessary to develop the system from *a priori* knowledge. It has been seen in Chapter 4 that fuzzy system identification suits such situations. Hence, fuzzy clustering technique is applied to microsytems in this section. For simplicity, SISO (single input and single output) modeling is considered just to demonstrate the application of fuzzy system identification to microsystems. The boundary conditioning of the MEMS plate type structure (design SQ1) due to stepped-up end condition, which was explained in Section 5.2.1, is considered for the present modeling. The input antecedent is the rotational stiffness $K_{R,a}^{\bullet}$ at the stepped-up ends and the consequent is the first natural frequency as shown in Figure 5.12.

The concept of boundary conditioning can be used in passive or active way for the manipulation of dynamic behavior of microsystems. In passive way, which is the direct design approach, the input boundary conditioning parameters are varied until the required performance is met. In active way, which is close to inverse design approach, the input parameters are selected for the given output. It would be advantageous if the same model of the system can be used for both active and passive manipulation of the system

behavior. In fuzzy system identification, passive manipulation is possible through Generalized Modus Ponens (GMP) inference mechanism as explained in Section 4.1.5. The GMP reasoning can be written as

Rule base:	x is $K_{R,a}^{\bullet} \Rightarrow$ y is $f_{n,l}$
New fact:	x is $K_{R,a}^{\bullet\bullet}$
New conclusion:	y is $f_{n,l}^{\bullet}$

The GMP reasoning is useful in predicting the new conclusion ($f_{n,l}^{\bullet}$) for a new input situation ($K_{R,a}^{\bullet\bullet}$) from the rule base or knowledge base depicting the system behavior. Hence, one can vary the fact $K_{R,a}^{\bullet\bullet}$ until the required performance, say, $f_{n,l}^{\bullet}$ is obtained. $K_{R,a}^{\bullet}$ and $f_{n,l}^{\bullet}$ represent fuzzy sets of rotational stiffness and natural frequency. The GMP reasoning will be useful for such direct design of microsystems using boundary conditioning.

For the case of inverse design, the reasoning of Generalized Modus Tollens can be used along with ,Mamdani reasoning (Min-Max) as shown below. The needed input can be obtained for the required output as given below:

Rule base:	x is $K_{R,a}^{\bullet} \Rightarrow$ y is $f_{n,l}$
New fact:	y is $f_{n,l}^{\bullet}$
New conclusion:	x is $K_{R,a}^{\bullet\bullet}$

Using GMT reasoning and the knowledge base, it is possible to predict the rotational stiffness required for a given natural frequency. The same fuzzy rule base obtained through system identification technique has to be used for both GMP and GMT reasoning. This is possible if and only if the relationship between input and output is continuous. Hence, the continuous variation of first natural frequency against rotational stiffness shown in Figure 5.12 is considered for system identification. The data used for system identification are shown in Figure 5.26. Fuzzy subtractive clustering with clustering parameters of $\bar{\varepsilon}$ =0.8, $\underline{\varepsilon}$=0.2, η=0.5 and r_a=0.05 has been applied to these data and the resulting rule base with $\sigma = 9.67666 \times 10^{-4}$ and N=21 is given in Figure 5.27. Mamdani type inference is applied for both GMP and GMT reasoning. The comparison between the model and predicted values shows a good agreement as seen from Figure 5.26. With the same rule base and min-max composition, the stiffness parameter has been estimated for the new frequency of 30589 Hz predicted from ANSYS for the stepped condition given in Section 5.2.1.2. A value of $K_{R,a}^{\bullet}$ = 401.9 that has been obtained using GMT reasoning is close to the model value of 398.11 which can be seen from Figure 5.12. Even though the fuzzy system identification has been applied to SISO system, it can be extended to MIMO sytems also.

The above example validates the use of fuzzy clustering with Mamdani inference mechanism for GMT reasoning. As the real microsystems are subjected to many parameters, the fuzzy system identification will be a suitable technique for the manipulation of boundary conditioning of microsystems.

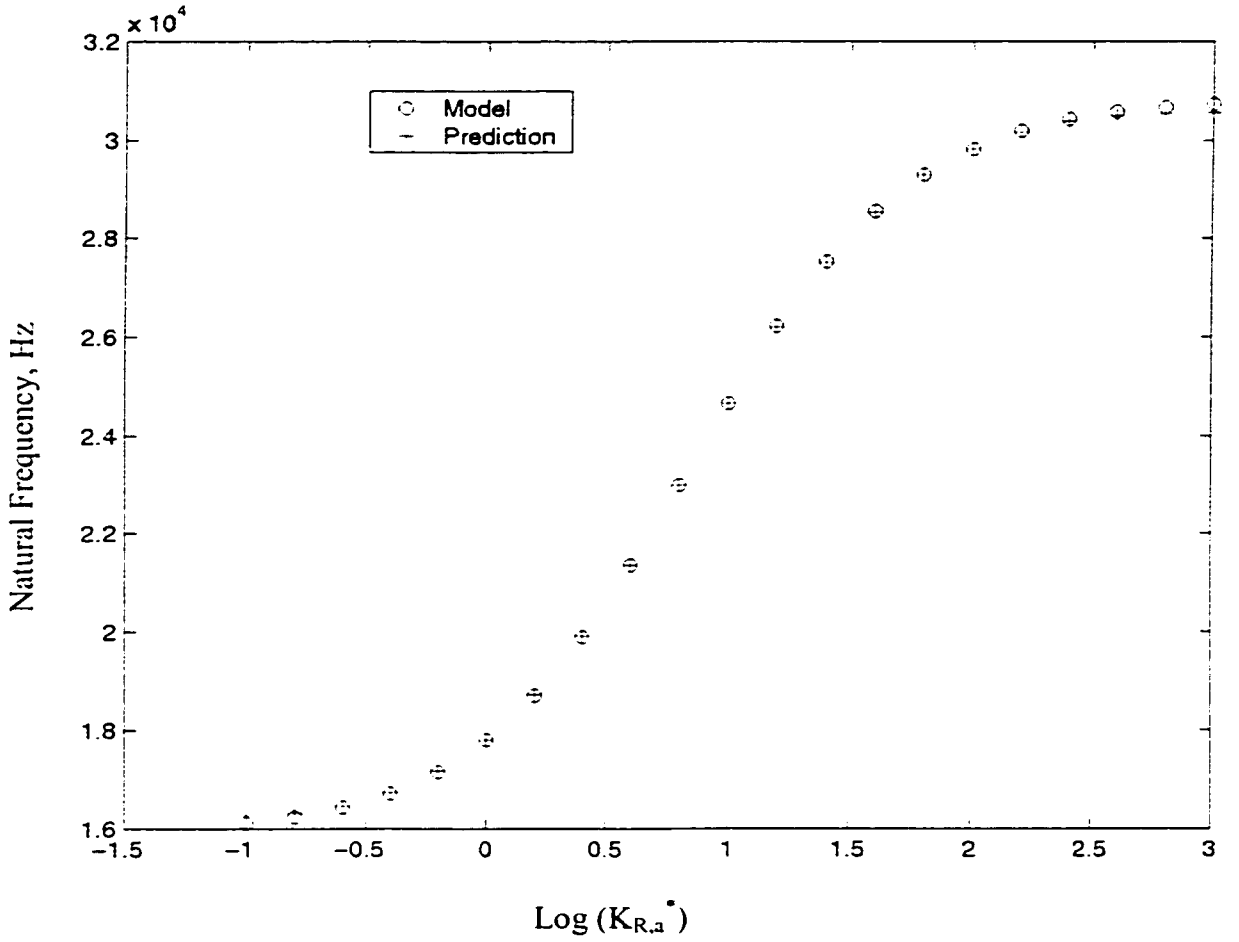

Figure5.26: The model and predicted values of the first natural frequency versus the boundary rotational stiffnesses for a plate type MEMS structure, design SQ1

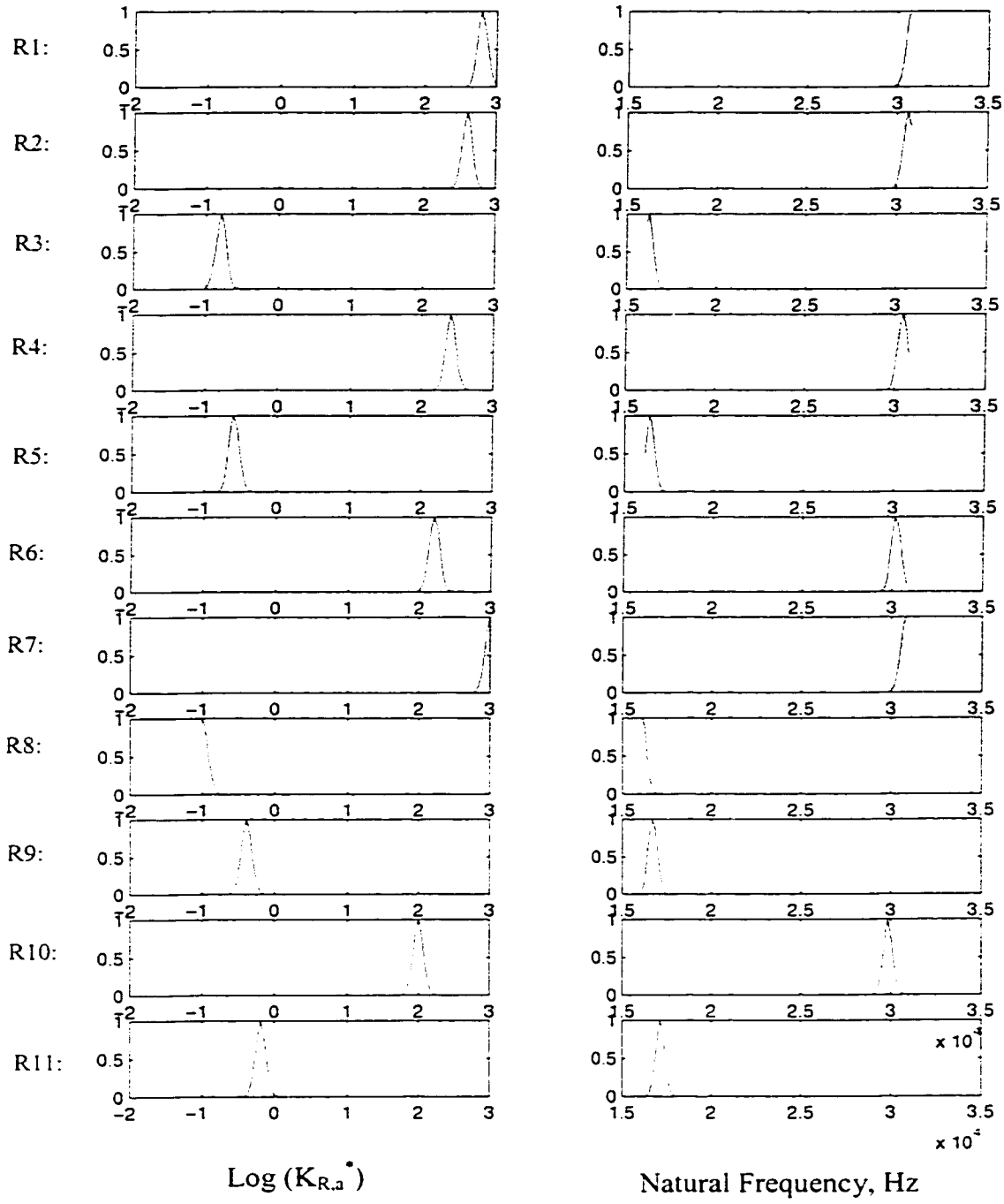

Figure 5.27: The first 11 rules of the fuzzy model of boundary conditioning due to stepped-up end conditions of a plate type MEMS design SQ1 for $\bar{\varepsilon}$ =0.8, $\underline{\varepsilon}$=0.2, η=0.5 and r_a=0.05

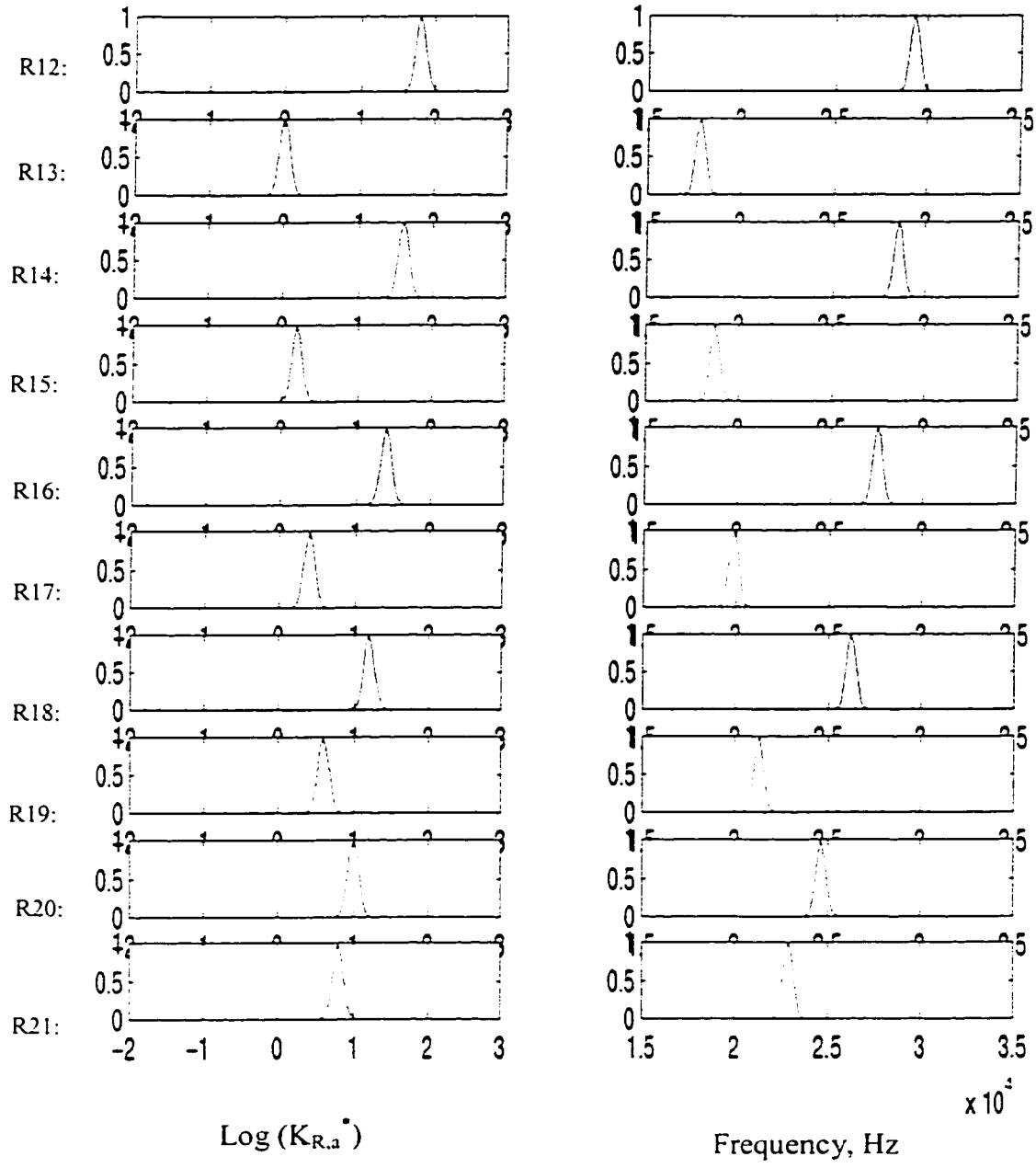

Figure 5.27 (contd.): The 12th to 21st rules of the fuzzy model of boundary conditioning due to stepped-up end conditions of a plate type MEMS design SQ1 for $\bar{\varepsilon}$ =0.8, $\underline{\varepsilon}$=0.2, η=0.5 and r_a=0.05

5.5 CONCLUSIONS

In this chapter the concept of boundary conditioning has been applied to various aspects of the synthesis of microsystems. Towards the design synthesis of microsystems, prediction formulation has been presented for boundary conditioning through structural changes such as geometry, stiffeners, corrugation etc. Towards fabrication synthesis of microsystems, MEMS engineers struggle to invent highly compatible fabrication processes so that in many occasions we have to accept some inherent limitations imposed by the micromachining process. In such cases, it is important to predict and manipulate the influence of process limitations such as non-classical support conditions, residual stress etc. on the system performance. Boundary conditioning concept has also been applied to predict the influence of support conditions that result from micromachining processes and residual stress. The present results have been compared with those obtained using ANSYS. The comparison showed good agreement. The environmental influence such as electrostatic field also affect the design synthesis of microsystems. Boundary conditioning has also been applied to predict the influence of environments on the system performance. Comparison with experimental study showed a good agreement. On consolidation the concept of boundary conditioning has been applied to different aspects of synthesis of microsystems such as fabrication synthesis and design synthesis. The fuzzy system identification along with comparison validated the application of fuzzy logic to boundary conditioning of microsystems.

CHAPTER 6

CONCLUSIONS AND EXTENSIONS

6.1 CONCLUSIONS

This thesis discusses the concept of boundary conditioning and uses it for the synthesis of micromechatronic systems using fuzzy logic. The three main sub areas of the thesis, i.e. synthesis of microsystems, boundary conditioning and fuzzy system identification are separately considered before combining them for the design synthesis of micromechatronic systems.

The success of MEMS in the future will depend upon the integration of higher level of microelectronics and larger number of micromechanical components on a single chip. This thesis proposes a fabrication synthesis for a possible integration of microelectronics and micromechanical components using an industrial CMOS process, namely the Mitel 1.5 μm process, along with XeF_2 gas phase etching, in order to take the full advantage of miniaturization, multiplicity and microelectronics. The etching was completely developed as part of the thesis project and described in Chapter 2.

The concept of boundary conditioning was developed in Chapter2 using plate type structures with edges supported on artificial springs which can be manipulated so as to be able to describe any general boundary conditions. The Rayleigh-Ritz method along with boundary characteristic orthogonal polynomials are used in the analysis.

The boundary conditioning concept has been introduced in this thesis as a unified technique in order to model, manipulate and quantify the influence of system and environmental conditions on dynamic behavior of the combined system. There are many boundary conditioning parameters such as geometry, process methods, environmental phenomena. Hence, a systemic approach has been used in this thesis in order to accommodate the influence of many boundary conditioning parameters. The systemic approach is so general that it can reproduce or identify the system using *a priori* knowledge which could be either from the theoretical understanding or from the intuitive knowledge of an expert or experimental evidence of the system behavior. Any such systemic inquiry is always approximate with limited certainty. The progress in inquiry is thus accompanied by an enhancment of certainty as the understanding of the system improves. The theory of fuzzy logic is a tool that can express qualitatively the approximation with a scope for further adaptation and hence this becomes right language for system identification technique.

There are several parameters which influence the final behavior of the microsystems. Fuzzy system identification was employed in order to capture the effects of many paramters and arrive at the successful synthesis. This is described in Chapter 4. Synthesis of boundary conditioning concept, fuzzy logic and system identification has been successfully applied to the synthesis of microsystems in Chapter 6. Thus, the present work expounded an exciting new interdisciplinary subspace of boundary conditioning, fuzzy system identification and synthesis of microsystems along with

analytical and experimental investigations. This new interdisciplinary subspace has a tremendous potential for further interesting inquiry. The thesis also outlined many areas through which the interdisciplinary subspace could be explored.

Conclusions were drawn on the individual aspects of the investigations already in the respective Chapters. The conclusions from a global point of view are:

Fabrication of MEMS devices and XeF_2 etching:

1. Integration of micromechanical and microelectronics components through an industrial CMOS process, namely, the Mitel 1.5 μm Double-Poly-Double-Metal process is possible through gas phase xenon difluoride isotropic pulse etching.
2. The post-release etch studies on the Mitel designs proved the possibility of fabricating many devices such as piezoresistive devices, capacitive devices, Lorentz devices.
3. The post-release XeF_2 etching resulted in stepped-up end condition for sacrificial type etching and under etched end conditions for bulk etching. These non-classical end conditions were observed in a more or less quantifiable fashion such that they can be incorporated in analysis using fuzzy logic for design synthesis.
4. The disadvantages such as stiction, attacking of metal pads associated with wet etching are avoided by resorting to XeF_2 etching.
5. Residual stresses and sharp corners associated with CMOS processing should be incorporated into the design synthesis

Boundary conditioning:

6. It is possible to model and quantify the influence of structural geometry and properties variation and operational environment in a unified way using boundary conditioning.
7. It is possible to manipulate eigenfrequencies as in the case of structural tuning or tuning of musical instruments. 8.
8. Localization of vibrational response and acoustic radiation is possible through modification of mode shapes through boundary conditioning. Control of vibrational response will become easier after localization.
9. Manipulation of arrangement of natural frequencies is possible through boundary conditioning.
10. The boundary conditioning parameters are numerous in complicated systems such as microsystems for which fuzzy logic approach is suitable.

Fuzzy system identification:

11. Automatic system identification is possible through fuzzy clustering technique.
12. Fuzzy system identification can be applied to complicated systems like boundary conditioning. This has been validated through the application to structural tuning.
13. Fuzzy clustering is suitable for both Mamdani and Sugeno reasoning.
14. Identification of higher order system is possible through higher order optimization proposed in this thesis.

Synthesis of microsystems:

Boundary conditioning in microsystems has several effects that are not common to macrosystems. Operational external environment such as electrostatic force, Lorentz force, special end conditions such as stepped-up and under-etched, corrugations, residual stresses affect the boundary conditioning of microsystems. In view of the above, the concept of boundary conditioning applied to synthesis of microsystems using fuzzy logic approach is a very significant contribution to the area of MEMS.

6.2 FUTURE STUDIES

A sense of completeness has been achieved in the investigations carried out so far which have helped in drawing the above meaningful conclusions. However, there are still some areas which could be explored to expand the scope of the concept of boundary conditioning in the synthesis of microsystem.

1. Experimental characterization of dynamic behavior of microsystems under the influence of electrostatic field, Lorentz force, squeeze film damping etc.
2. Integration of micromechanical structures with microelectronics circuits and development of a complete microdevice. Microelectronics needed for signal conditioning, signal processing have to be incorporated through the Mitel 1.5 μm process for the piezoresistive and capacitive devices that were released through XeF_2 gas phase etching.
3. Modeling the non-linear effects of boundary conditioning with electrostatic force, Lorentz force etc.

4. Quantification of residual stresses present in the microstructures.
5. Application of fuzzy system identification to a complete microsystem with many input boundary conditioning parameters and many output parameters
6. Effect of partial supports on the system behavior using boundary conditioning technique which could be applied to both macro and microsystems
7. Manipulation of acoustic radiation through boundary conditioning concept by modifying the mode shapes in order to achieve required radiation efficiency. This will be useful for both macro systems and microspeakers.
8. Incorporation of parameter optimization of fuzzy sets obtained through clustering technique, automatic generation of optimum rule base i.e. optimum generation of clustering parameters and automatic generation of unsymmetric fuzzy sets.
9. Application of boundary conditioning concept for adaptive control of system through controlling the parameters of the environment. This is possible by controlling the equivalent stiffness of the system, which could be implemented by using rheological liquids, semi-active vibration absorbers etc. in the case of macrosystems and by using bias voltage, Lorentz current etc. in the case of microsystems, as shown in the Figure 6.1.

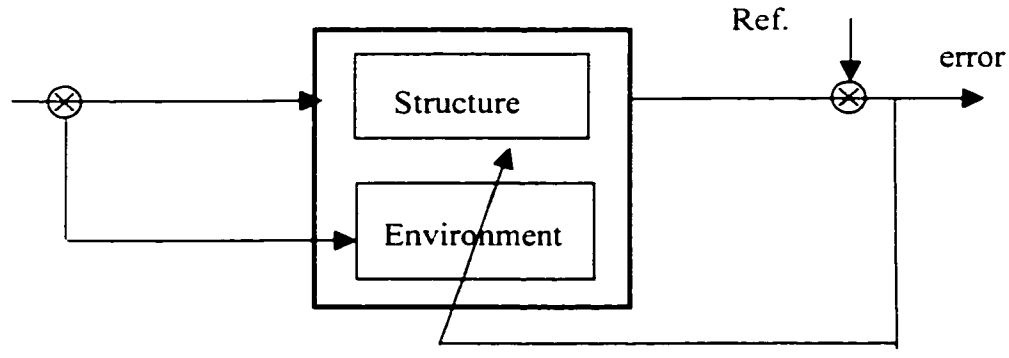

Figure 6.1: Control scheme using boundary conditioning of environment

REFERENCES

1. Achong, A., "The steel pan as a system of non-linear mode-localized oscillators, Part I: theory, simulations, experiments and bifurcation", Journal of Sound and Vibration, 197(4), 1996, pp. 471-487.

2. Achong, A. and Sinanan Singh, K.A., "The steel pan as a system of non-linear mode -localized oscillators, Part II: coupled sub - systems, simulations and experiments", Journal of Sound and Vibration, 1997, 203(4), pp. 547-561.

3. Adams, S.G., Bertsch, F.M., Shaw, K.A., Hartwell, P.G., MacDonald, N.C. and Moon, F.C., "Capacitance based tunable micromechanical resonators", Proc. of 8th Intl. conf. on solid-state sensors and actuators, TRANSDUCER'95, Stockholm, Sweden, June 25-29, 1995, pp. 438-441.

4. Adams, S.G., Bertsch, F.M., Shaw, K.A., and MacDonald, N.C., "Independent tuning of linear and nonlinear stiffness coefficients", Journal of Microelectomechanical systems, Vol. 7, No.2, June 1998, pp. 172-180.

5. Allen, H., Terry, S. and DeBruin, D., "Accelerometer system with self-testable features", Sensors and Actuators, Vol. 20, 1989, pp. 153-161.

6. An, S., Oh, Y.S., Lee, B.L, Park, K.Y., Kang, S.J., Choi, S.O., Go, Y. I. and Song, C.M., "Dual-Axis microgyroscope with closed-loop detection", Proc. 11th annual workshop on Micro Electro Mechanical Systems, MEMS 98, Heidelberg, Germany, Jan. 25-29, 1998, pp. 328 - 333.

7. Andrews, M., Turner, G., Harris, P. and Harris, I., "A wide range pressure sensor using the squeeze film effect", Proc. of 7th intl. Conf. on solid-state sensors and actuators, TRANSDUCER'93, Yokohama, Japan, June 7-10, 1993, pp. 214-216.

8. Arbel, A., "Controllability measures and actuators placement in oscillatory systems", International Journal of Control, 1981, Vol. 33, No. 3, pp. 565-574.

9. Baltes, H., Paul, O. and Brand, O., "Micromachined thermally based CMOS Microsensors", Proceedings of IEEE, Vol.86, No.8, August 1998, pp. 1660-1678.

10. Barth, P.W., Pourahmadi, F., Mayer, R., Poydock, J. and Petersen, K., "A monolithic silicon accelerometer with integral air damping and overrange protection", Tech. Dig. Solid State Sensors and Actuators wokshop, Hilton Head Island, June 1988, pp. 35-38.

11. Baumann, W.T., "An adaptive feedback approach to structural vibration suppression", Journal of Sound and Vibration, 205(1), 1997, pp 121-133.

12. Bergqvist, J.,"Finite-element modelling and characterization of a silicon condenser microphone with a highly perforated backplate", Sensors and Actuators A., 39, 1993, pp.191-200.

13. Bergqvist, J., Rudolf, F., "A new condenser microphone in silicon", Sensors and Actuators, A21-A23, 1990, pp.123-125.

14. Berry, A., Guyader, J. and Nicolas, J., "A general formulation for the sound radiation from rectangular baffled plates with arbitrary boundary conditions", Journal of Acoustical Society of America, 88(2), December 1990, pp.2792-2802.

15. Bezdek, J.C., "Cluster Validity with Fuzzy Sets." Journal of Cybernetics, Vol. 3, 1974, pp. 58-71.

16. Bezdek, J.C., Hathaway, R.J., Sabin, M.J., Tucker, W.T., "Convergence theory for fuzzy C-means: Counter examples and repairs." Fuzzy Models for Pattern Recognition, Bezdek , J.C. and Pal, S.K. (eds), IEEE Press, NY, 1992, pp.138-142.

17. Bhat, R.B., "Natural frequencies of rectangular plates using characteristic orthogonal polynomials in Rayleigh-Ritz Method", Journal of Sound and Vibration, 102(4), 1985, pp 493-499.

18. Bhat, R.B., "Plate defelections using orthogonal polynomials", Journal of Engineeing Mechanics, Trans. ASCE, Vol. 111, No. 11, 1985, pp. 1301-1309.

19. Bhat, R.B., "Vibration of rectangular plates using beam characteristic orthogonal polynomials in Rayleigh-Ritz Method", Proc. 3rd Intl. Modal Analysis Conf. Orlando, 1985.

20. Bhat, R.B., "Beam characteristics using orthogonal polynomials with fractional power increments", Journal of Sound and Vibration, Vol. 112, No.3, 1986, pp. 556-558.

21. Bhat, R.B., "Flexural vibration of polygonal plates using characteristic orthogonal polynomials in two variables", Journal of Sound Vibration, 114(1), 1987, pp.65-71.

22. Bhat, R.B., "Vibration of rectangular-plates on point and line supports using characteristics orthogonal polynomials in the Rayleigh-Ritz method", Journal of Sound and Vibration, Vol. 149, No. 1, 1991, pp. 170-172.

23. Bhat, R.B and Mundkur, G., "Plate Characteristic functions to study sound transmission loss through panels", Second International Congress on Recent Developments in Air and Structure-Borne Sound and Vibration, March 4-6, 1992, pp. 461-468.

24. Bhat, R.B., "Nature of stationarity of the natural frequencies at the natural-modes in the Rayleigh-Ritz method", Journal of Sound and Vibration, 1997, Vol. 203, No.2, pp. 251-263.

25. Bobbio, S.M., Lellam, M.D., Dudley, B.W., Goofwin-Johansson, S., Jones, S.K., Jacobson, J.D., Tranjan, F.M., Dubois, T.D., " Integrated Force Arrays", Proceedings of IEEE Conference on Micro Electro Mechanical Systems, February 1993, pp.149-154.

26. Borchers, I.U., Hackstein, H.J., Bartels, P., Grunewald, M. and Wenigwieser, C., "Summary of Dornier 328 interior noise control study", Inter-Noise 90, pp. 811-816.

27. Boser, B. and Howe, R.T., "Surface micromachined aceelerometers", IEEE J. Solid State Circuits, Vol. 31, Mar. 1996, pp. 366-375.

28. Brown, K.B., Allegretto, W., Vermeulen, F.E., Lawson, R.P.W. and Robinson, A.M., "Cantilever-in-cantilever micromachined pressure sensors fabricated in CMOS technology", Proc. IEEE Canadian Conf. on Electrical and Computer Engineering, Edmonton, Alberta, May 9-12, 1999, pp.1686-88.

29. Brugger, J., Blanc, N., Renaud, Ph., De Rooij, N.F., "Capacitive AFM microlever with combined integrated sensor/actuator functions", 7th Int. conf. On Solid State Sensors and Actuators, TRANSDUCERS '93, June 7-10, 1993, Japan, pp. 1044-1047.

30. Brunner, W.F.J. Batzer, T.H. "Practical vacuum techniques", Robert E. Kreiger Publishing Company, New York, 1974.

31. Bustillo, J.M., Howe, R.T., Muller, R.S., "Surface Micromachining for Microelectromechanical Systems", Proceedings of IEEE, Vol.86, No.8, August 1998, pp.1552-1573.

32. Chakraverty, S., Bhat, R.B. and Stiharu, I., "Recent research on vibration of structures using characteristic orthogonal polynomials in the Rayleigh-Ritz method", The Shock and Vibration Digest, May 1999, Vol. 31, No. 3, pp. 187-194.

33. Chan, I.W.T., Brown, K.B., Lawson, R.P.W., Robinson, A.M., Ma, Y. and Strembicke, D., "Gas phase pulse etching of silicon for MEMS with xenon difluoride", Proceedings of IEEE Canadian Conf. on Electrical and Computer Engineering, 1999, pp. 1637 - 1642.

34. Chang, I. F., Yeh, K.S.J., Lin, G., Chu, P.B., Kruglick, E.J.J.and Pister, K.S.J., "Gas phase silicon micro-machining with xenon diflouride", Microelectronic structures and microelectromecahnical devices for optical processing and multimedia applications, Proc. SPIE, 1995, pp. 117-128.

35. Chau, K., Lewis, S.R., Zhao, Y., Howe, R.T., Bart, S.F. and Marcheselli, R.G., "An integrated force balanced capacitive accelerometer for low-g applications", The 8th International Conference on Solid-State Sensors and Actuators, Transducers'95, June 1995. pp. 593-596.

36. Chen, J.Y., "CMOS the emerging VLSI technology", IEEE Circuits and Devices, 2, 1986, pp.16-31.

37. Chihara, T.S., "An introduction to orthogonal polynomials", Gordon and Beach Science publishers, London, 1978.

38. Chiu, S.L., "Fuzzy model identification based on cluster estimation." Journal of Intelligent and Fuzzy Systems, 2, 1994, pp.267-278.

39. Chiu, S.L., "Extracting fuzzy rules from data for function approximation" Fuzzy Information Engineering: A Guided Tour of Applications, Dubois, D., Prade, H., Yager, R.R. (eds), John Wiley & Sons, 1997.

40. Choi, J.J., Toda, R., Minami, K. and Esashi, M., "Silicon angular resonance gyroscope by deep ICPRIE and XeF2 etching", Proc. 11th annual workshop on Micro Electro Mechanical Systems, MEMS 98, Heidelberg, Germany, Jan. 25-29, 1998, pp. 322-327.

41. Chu, B., Patrick, Chen T. Jeffrey, Richard Yeh., Gisela Lin., Huang C.P. Jeff, Brett A. Warneke and Pister S.J. Kristofer, "Controlled Pulse etching with Xenon diflouride"., Transducers 1997, Ninth International conference on Solid State Sensors and Transducers, June 1997, pp. 1-4.

42. Chu, P.B., Nelson, P.R., Tachiki, M.L. and Pister, K.S.J., "Dynamics of polysilicon parallel electrostatic actuators", Proc. of 8th intl. Conf. on solid-state sensors and actuators, TRANSDUCER'95, Stockholm, Sweden, June 25-29, 1995, pp. 356-359.

43. Clark, R.L. and Fuller, C.R. "A model reference approach for implementing active structural acoustic control", Journal of Acoustic Society of America, 92(3), September 1992, pp. 1534-1544.

44. Clark, R.L. and Fuller, C.R. "Optimal placement of piezoelectric actuators and polyvinylidene fluoride error sensors in active structural acoustic control approaches", Journal of Acoustic Society of America, 92(3), September 1992, pp. 1521-1533.

45. Clark S.K. and Wise, K.W., "Pressure sensitivity in anisotropically etched thin-diaphragm presuure sensors", IEEE Transactions on Electron Devices, Vol. 26, No.12, December 1979, pp.1887-1896.

46. Cole, B.E., Higashi, R.E. and Wood, R.A.," Monolithic two-dimensional arrays of micromachined microsystems for infrared applications", Proc. of IEEE, MEMS 98, Vol. 86, No.8, August 1998, pp.1679-1686.

47. Coulon, Y. D, Smith, T., Hermann, J., Chevroulet, M. and Rudolf, F., "Design and test of a precision servo accelerometer with digital output", The 7th International Conference on Solid-State Sensors and Actuators, Transducers'93, June 1993, pp.832-835.

48. Demirli, K., Cheng, S.X., Muthukumaran, P., "Fuzzy modeling of job sequencing with subtractive clustering", Journal of Fuzzy Sets and Systems, (in review)

49. Demirli, K., "A unified and extended framework for operator selection in generalized Modus Ponens type fuzzy reasoning", Ph.D Thesis, University of Toronto, 1995.

50. Demirli, K., "An extended framework for operator selection in Generalized Modus Ponens", proc. IEEE Intl. Conf. On Systems, Man and Cybernetics, Vancouver, Canada, Oct. 22-25, 1995, pp. 357-363.

51. Demirli. K and Muthukumaran, P., "Higher order fuzzy system identification using subtractive clustering", Journal of Intelligent and Fuzzy Systems. (in print)

52. Dimitiadis, E. K.and Fuller, C.R. "Active control of sound transmission through elastic plates using piezoelectric actuators", AIAA Journal, 29, 11, November 1991, pp. 1773-1777.

53. Doelman, N. J., "Control strategies for active noise reduction", Proceedings of Inter-noise 90,1990, pp 1273-1276.

54. Dunn, J., "A Fuzzy Relative of the ISODATA process and its use in detecting compact, well-separated clusters", Journal of Cybernetics, 3, 1974, pp. 32-57.

55. Duval, P., "High vacuum production in the microelectronics industry ", Elsevier, 1988.

56. Eddy, D.S. and Sparks, D.R., "Application of MEMS technology in automotive sensors and actuators ", Proc. of IEEE, Vol. 86, No.8, August 1998, pp.1747-1755.

57. Emami, M.R., Turksen, I.B., Goldenberg, A.A. "Development of a systematic methodology of fuzzy logic modeling", IEEE Transactions on Fuzzy Systems 6(3), 1998, pp.346-361.

58. Emborg, U., "Applications of active noise control in Saab 340 and Saab 2000", Proceedings of Nordic Conference on Vehicle and Machinery Vibrations, Stockholm, Sweden, September 1994.

59. Esahi M., Sugiyama, S., Ikeda, K., Wang, Y. and Miyashita, H., "Vacuum-sealed silicon micromachined pressure sensors", Proceedings of IEEE, Vol.86, No.8, August 1998, pp.1627-1639.

60. Fan, L.S. and Crawforth, L., "Spring softening in MEMS microstructures", Proc. of 7th Intl. Conf. on solid-state sensors and actuators, TRANSDUCER'93, Yokohama, Japan, June 7-10, 1993, pp. 767-770.

61. Faucher, M., "Mitel 1.5 μm process review", MITEL Semiconductor, Feb., 1994.

62. Feynman, R.P., " There's plenty of room at the bottom", Journal Microelectromechanical Systems, Vol.1, No.1, March 1992, pp. 60-66.

63. Flamm, D.L, Ibbotson, D.E., Mucha, J.A. and Donnelly, V.M., "XeF2 and F-atom reactions with Si: their significance for plasma etching", Solid State Technology, April 1983, pp. 117-121.

64. Flotow, A.V. and et al., "Vibration and sound in aircraft cabin: a comparison of adaptive/passive and active controls", SAE Tech. Paper 971463,1997.

65. Fujita, H.,"Microactuators and micromachines " , Proc. of IEEE, August 1998, MEMS 98, Vol. 86, No.8, pp.1721-1732.

66. Fujita, H. and Ikoma, T., "Numerical determination of the electromechanical field for micro servosystems', Sensors and Actuators, A21-A23 1990, pp. 215-218.

67. Fuller, C. R. and Von Flotow, A.H., "Active control of sound and vibration", IEEE Control Systems, December 1995, pp. 9-19.

68. Fuller, C.R. and Jones, J.D., "Experiments on reduction of propeller induced interior noise by active control of cylinder vibration", Journal of Sound and Vibration, 1987(2), pp 389-395.

69. Gabriel, K., "Engineering microscopic machines", Scientific American, Sept. 1995.

70. Gibbs G.P., Fuller, C.R. and Paxton, S., "Piezoelectric actuator configuration optimization for active structural acoustic control in aircraft", SAE Technical paper 971461, 1997.

71. Gibelling, H.J. and Li, W.H., "Acoustic radiation from a rectangular plate reinforced by springs at arbitrary locations", Journal of Sound and Vibration, 220(1), 1999, pp. 117-133.

72. Gisela Lin., Kenneth P. Roos and Pister S.J Kristofer., "Standard CMOS piezoresistive sensor to quantify heart cell contractile forces"., IEEE Workshop on MEMS, February 11-15, 1996, pp. 150-155.

73. Gisela Lin.., Roy E Palmer., Kenneth P. Roos and Pister S.J Kristofer., "Single heart cell force measured in standard CMOS"., Transducers 1997, Ninth International conference , Solid State Sensors and Transducers., June 16-19, 1997, pp. 16-19.

74. Goodenough, F., "Airbags boom when IC accelerometer sees 50g", Electronic Design, 8 August 1991, pp. 45-56.

75. Guttierrez R.H. and Laura, P.A.A., " Transverse vibrations of stiffened rectangular plates elastically restrained against rotation along the edges with varying stiffeners length", Journal of Sound Vibration, 101, 1985, pp. 122-124.

76. Henrion, W., DiSanza, L., Terry, M.I.S. and Jerman, H., " Wide dynamic range direct digital accelerometer", Tech. Dig. Solid State Sensors and Actuators workshop, Hilton Head Island, Sc, June 1990, pp. 153-156.

77. Hin-Leung Chau, Wise, K.W., "Scaling limits in batch-fabricated silicon pressure Sensors", IEEE Transactions on Electron Devices, Vol.ED-34, No.4,1987, pp.850-858.

78. Hodges, C.H., "Confinement of vibration by structural irregularity", Journal of Sound and Vibration, 1982, 82(3), pp. 411-424.

79. Hoffman, E., Warneke, B., Weigold, J and Pister, K.S.J., "Structures with Piezorestitive sensors in standard CMOS", IEEE Transactions of Microelectromechanical systems, 1995, January 29 – February 2, 1995, pp. 288-293.

80. Hosticka, B. J., "CMOS Sensor Systems", Proc. of the 9th International Conference on Solid-State Sensors and Actuators, Transducers'97, June 16-19, 1997, pp.991-994.

81. Houle, F.A., "A reinvestigation of the etch products of silicon and XeF2: doping and pressure effects"., Journal of Applied Physics, Vol.60, No.9, November 1986, pp. 3018-3027.

82. Houle, F.A., "Dynamics of SiF4 desorption during etching of silicon by XeF2", Journal of Chemical Physics., Vol.87, No.3, August 1987, pp. 1866-1872.

83. Howe, R.T.,"Surface micromachining for microsensors and microactuators", Proceedings of IEEE Custom IC Conference-Microsensors, 1991, pp.117-121.

84. Hsu, P.C., Mastrangelo, C.H., Wise, K.D., "A high sensitivity polysilicon diaphragm condenser microphone", Proc. 11th annual workshop on Micro Electro Mechanical Systems, MEMS 98, Heidelberg, Germany, Jan. 25-29, 1998, pp.580-585.

85. Ibbotson, E. D., Daniel, F.L., John, M.A., and Donnelly, V.M., "Comparison of XeF2 and F-atom reactions with silicon and silicon-dioxide"., Applied Physics Letters, Vol.44, No.12, June 1984, pp. 1129-1131.

86. James, P.P. and Fahy, F.J., " A technique for the assessment of strength of coupling between SEA and subsystems: Experiments with coupled plates and two coupled rooms", Journal of Sound and Vibration, 1997, 203 (2), pp. 265 - 282.

87. Jang, J.S.R., Sun, C.T., Mizutani, E., "Least square methods for system identification", Neuro-Fuzzy and Soft computing, Prentice-Hall, NJ , 1997, Chap. 5.

88. Johnson, M.E., and Elliot, S.J., "Active control of sound radiatation using volume velocity cancellation", Journal of Acoustical Society of America, 98(4), October 1995, pp. 2174-2186.

89. Jornod, A., Rudolf, F., "High-precision capacitive absolute pressure sensor", Sensors and Actuators, Vol.17, 1989, pp. 415-421.

90. Kang, J.W., Guckel, H. and Ahn, Y., " Amplitude detecting micromechanical resonating beam magnetometer", Proc. 11th annual workshop on Micro Electro Mechanical Systems, MEMS 98, Heidelberg, Germany, Jan. 25-29, 1998, pp. 372-377.

91. Kloeck, B., Suzuki, S., Tuchitani, S., Miki, M., Matsumoto, M., Sato, K., Koide, A., and Sugisawa, Y., "Motion investigation of electrostatic servo-accelerometers by means of transparent ITO fixed electrodes", Proc. 6th Int. Conf. Solid-State Sensors and Actuators, Transducers '91, San Francisco, CA, USA, June 24-28, 1991, pp. 108-111.

92. Koers, P. and Doppenberg, Ed., "Some tracking capabilities of TNO 's aircraft ANC-systems", Inter-Noise 93, Belgium, August 24-25, 1983, pp. 89-94.

93. Kohl, M., Gottert, J., Mohr, J., "Verification of the micromechanical characteristics of electrostatic linear actuators", The 8th International Conference on Solid-State Sensors and Actuators, June 1995, pp.400-403.

94. Koshigoe, S., Teagle, A. and Godon, A., "A time domain study of active control of sound transmission due to acoustic pulse excitation", Journal of Acoustic Society of America, 97(1), January 1995, pp. 313-323.

95. Kovacs, G.T., Maluf, N.I., Petersen, K.E., "Bulk micromachining of silicon", Proceedings of the IEEE, Vol.86, No.8, August 1998, pp.1536-1549.

96. Kruglick, E.J.J., Warneke, B.A and Pister, K.S.J., "CMOS 3-AXIS accelerometers with integrated amplifier", IEEE Eleventh Annual Workshop, 1998, pp. 631-636.

97. Kuhnel, W. and Gisela, H., "A silicon condenser microphone with structured back plate and silicon nitride membrane", Sensors and Actuators A, 30, 1992, pp.251-258.

98. Lam, K.Y., Hung, K.C. and Chow, S.T., "Vibration of plates with cutouts by the modified Rayleigh-Ritz Method", Applied Acoustics, 0003-682X, 1989, pp. 49-60.

99. Laura, P.A.A. and Guttierrez, R.H., "A note on transverse vibrations of stiffened rectangular plates with edges elastically restrained against rotation ", Journal of Sound Vibration, 78, 1981, pp. 139-144.

100. Laura, P.A.A., Luisoni, L.E. and Filipich, C., "A note on the determination of the fundamental frequency of vibration of thin, rectangular plates with edges possessing different rotationally flexibility coefficients", Journal of Sound and Vibration, 55, 1977, pp. 327-333.

101. Legtenberg, R., Eldens J. and Elwenspoek, M., "Stiction of surface micromachined structures after rinsing and drying: Model and investigation of adhesion mechanism", Proceedings of Transducer 93, 1993, pp. 198-201.

102. Leissa, A.W., NASA SP160. Vibration of plates, 1969.

103. Leissa, A. W., "The free vibration of rectangular plates", Journal of Sound and Vibration, 31, 1973, pp.257-293.

104. Leng, P., "Process of silencing sound oscillations", U.S. Patent No.2, 043, 416, 1936.

105. Li, Z., Guigou, C., Fuller, C.R., and Burdisso, R.A., "Design of active structural acoustic control systems using a nonvolumetric eigenproperty assignment approach", Journal of Acoustical Society of America, 101(4), April 1997, pp. 2088-2096.

106. Ma, K.J., Yazdi, N. and Najafi, K., "A bulk-silicon capacitive microaccelerometer with built-in overrange and force feedback electrodes", Tech. Dig. Solid State Sensors and Actuators workshop, Hilton Head Island, SC, June 1994, pp. 160-163.

107. Ma, Y., Robinson, A.M, Lawson, P.W., Shen, B., Strembicke, D. and Allegretto, W., "Measuring the deflection of a micromachined cantilever - in - cantilever device using a piezoresistive sensor", Proc. IEEE Canadian Conf. on Electrical and Computer Engineering, Edmonton, Alberta, May 9-12, 1999, pp. 1632 - 1636.

108. Mamdani, E.H. and Assilian, S., "An experiment in linguistic synthesis with a fuzzy logic controller", International Journal of Man-Machine Studies, 7, 1975, pp.1-13.

109. Mason A., Yazdi N., Chavan A.V., Najafi K. and Wise K.D.,"A generic multielement microsystem for portable wireless applications", Proc. of IEEE, August 1998, Vol. 86, No.8, pp.1733-1746.

110. Mastrangelo, C.H., Burns, M.A. and Burke, D.T ., "Microfabricated devices for genetic diagnostics" , Proc. of IEEE, August 1998, Vol. 86, No.8, pp.1769-1787.

111. Mastrangelo, C.H. and Hsu, C.H., "Mechanical stability and adhesion of microstrcutures under capillary forces - Part I: Basic theory", Journal Microelectromechanical systems, 1993, Vol. 2, No.1, pp. 33-43.

112. Mastrangelo, C.H. and Hsu, C.H., "Mechanical stability and adhesion of microstrcutures under capillary forces - Part II: Experiments", Journal Microelectromechanical systems, 1993, Vol. 2, No.1, pp. 44-55.

113. Mc Neill,D. and Freiberger, P., "Fuzzy Logic", Simon & Schuster, 1993.

114. MCNC Center for Microelectronics Systems Technologies, Research Triangle Park, NC 27709 - 2889.

115. Mehner, J., Kurth, S., Billep, D., Kaufmann, C., Kehr, K. and Dotzel, W., "Simulation of gas damping in microstructures with nontrivial geometries", Proc. 11th annual workshop on Micro Electro Mechanical Systems, Heidelberg, Germany, Jan. 25-29, 1998, pp. 172-177.

116. Muller, R.S., and Lau, K.Y., "Surface-micromachined microoptical elements and systems" , Proc. of IEEE, August 1998, Vol. 86, No.8, pp. 1705-1720.

117. Muthukumaran, P. Bhat, R.B. and Stiharu, I., "Localization of structural vibration and acoustic radiation through boundary conditioning", Trans.CSME, Vol. 22, No. 4B, 1998, pp. 519-532.

118. Muthukumaran, P. Bhat, R.B. and Stiharu, I., "Boundary conditioning technique for structural tuning", Journal of Sound and Vibration, 220(5), 1999, pp.847-859.

119. Muthukumaran, P., Demirli, K. Bhat, R.B. and Stiharu, I.,. "Boundary conditioning technique for structural tuning using fuzzy logic approach", Intl. Journal of Computers and Structures, Jan. 2000, Vol. 74, Issue 5, pp. 547-557.

120. Muthukumaran. P. Bhat, R.B. and Stiharu, I., "Localization of structural vibration and acoustic radiation through boundary conditioning", CSME Forum, May 19-22 1998, Toronto, Ontario, 17-23.

121. Muthukumaran, P. Stiharu, I. and Bhat, R.B., "Study of boundary conditioned capacitive microsensors fabricated through MUMPS process", CWMEMS 99, Canadian Workshop on MEMS, August 13, 1999, Ottawa, Canada.

122. Muthukumaran, P. Stiharu, I. and Bhat, R.B., "Gas phase silicon micromachining of MEMS devices fabricated through an industrial CMOS process", Workshop on Smart Materials and Structures, September 13-14 1999, St. Hubert, Quebec, Canada., pp. 139-148.

123. Muthukumaran, P. Stiharu, I. and Bhat, R.B., "Gas phase xenon difluoride etching of microsystems fabricated through Mitel 1.5 mm CMOS Process", Canadian Journal of Electrical and Computer Engineering (In Print).

124. Nair, P.S. and Rao, M.S., "On vibration of plates with varying stiffener length", Journal of Sound and Vibration, 95, 1984, pp. 19-30.

125. Nguyen, C.T.C., Katehi, L.P.B. and Rebeiz, G.M.,"Micromachined devices for wireless communications", Proc. of IEEE, August 1998, Vol. 86, No.8, pp.1756-1768.

126. O' Hanlon, John, F., "A user's guide to vacuum technology", Second Edition, John-Wiley & Sons, 1989.

127. Olney, D., "Acceleration measurement using variable capacitance", Proc. Sensors Nüremberg '88, Germany, 1988, pp. 149--160.

128. Olson, H. F. and May, E.G., "Electronic sound absorbers", Journal Acoust. Soc. Am, Vol. 25, 1953, pp.1130-1136.

129. Packirisamy, M., Stiharu, I. and Bhat, R.B., "Vibration of micromachined condenser microphone plate diaphragms in electrostatic fields", CANCAM 97, 16th Canadian Cong. of Applied Mechanics, Quebec, Canada, June 1-6, 1997, pp. 87-88.

130. Parameswaran, M., Baltes, H.P., Ristic, Lj., Dhaded, A.C., Robinson A.M., "A new approach for the fabrication of micromechanical structures", Sensors and Actuators, 19,1989, pp.289-307.

131. Parameswaran, M., Baltes, H.P. and Robinson, A.M., "Polysilicon microbridge fabrication using standard CMOS technology", Digest of Technical paper, IEEE workshop on Solid-State Sensor and Actuators, June 6-9, 1999, pp. 148-150.

132. Park, K.Y., Lee, C.W., Jang, H.S., Oh, Y.S. and Ha, B.J., "Capacitive sensing type surface micromachined silicon accelerometer with a stiffness tuning capability", Proc. 11th annual workshop on Micro Electro Mechanical Systems, MEMS 98, Jan. 25-29, 1998, Heidelberg, Germany, pp. 637-641.

133. Park, Y.E. and Wise, K.D., "An MOS switched-capacitor readout amplifier For capacitive pressure sensors", Proceedings of Microsensors, 1991, pp.329-333.

134. Patel, J.,"A silicon micromachined subminiature condenser microphone: Analysis, Design, Fabrication and Testing", M.Asc. Thesis, Feb. 1995, Concordia University, Montreal.

135. Paul, O., Westberg, D., Hornung, M., Ziebart, V. and Baltes, H., " Sacrificial aluminum etching for CMOS microstructures", Proc. 10th annual workshop on Micro Electro Mechanical Systems, MEMS 97, Jan. 26-30, 1997, pp. 523-528.

136. Payne, R. and Dinswood, E., "Surface micromachined accelerometer: a technology update", SAE Int. Automotive Eng. Congress, Detroit, MI. USA, 1991, pp. 127-135.

137. Pedcycz, W., "Identification in fuzzy systems", IEEE Transactions on Systems, Man and Cybernetics, 14, 1984, pp. 361-366.

138. Pedersen, M., Olthuis, W. and Bergveld, P., "A polymer condenser microphone on silicon with on-chip CMOS amplifier", Proc. of the 9th International Conference on Solid-State Sensors and Actuators, Transducers'97, June 16-19, 1997, pp.445-446.

139. Peeters, E., Vergote, S., Puers, B. and Sansen, W., "A highly symmetrical capacitive micro-accelerometer with single degree of freedom response", Proc. 6th Int. Conf. Solid-State Sensors and Actuators, Transdueers '91, San Franeisco CA, USA. June 24-28, 1991, pp 97-100.

140. Peeters, E., Vergote, S., Puers, B. and Sansen, W., "A highly symmetrical capacitive microaccelerometer with single degree of freedom response", J. Micromech. Microeng., Vol.2, 1992, pp. 104-112.

141. Petersen, K.E., Shartel, A., and Raley, N.F., "Micromechanical accelerometer integrated with MOS detection circuitry", IEEE Transactions on Electron Devices, Vol.ED-29, No. 1, 1982, pp.23-27.

142. Pisano, A., "Microelectromechanical systems", DARPA MEMS Report, (Web material).

143. Pourahmadi, F, Christel, L and Petersen, K.,"Silicon accelerometer with new thermal self-test mechanism", Tech. Dig. Solid State Sensors and Actuators wokshop, Hilton Head Island, Sc, June 1988, pp. 122-125.

144. Rangsten, P., Smith, L., Rosengren, L. and Hok, B., "Electrostatically excited diaphragm driven as a loudspeaker", Proc. of 8th intl. Conf. on solid-state sensors and actuators, TRANSDUCER'95, Stockholm, Sweden, June 25-29, 1995, pp. 430-433.

145. Riethmuller, W., Benecke W., Schnakenberg U., Wagner B., "Development of commercial CMOS process-based technologies for the fabrication of smart accelerometers", Proc. Transducers'91, 1991, pp. 416-419.

146. Riethmuller, W., Benecke, W., Schnakenberg, U., Wagner B., "A smart accelerometer with on-chip electronics fabrocated by a commercial CMOS process", Sensors and Actuators, Vol. A-31, 1992, pp.121-124.

147. Ristic Lj., Gutteridge R., Kung J., Koury D., Dunn B. and Zunino H., "A capacitive type accelerometer with self-test feature based on a double-pinned polysilicon structure", The 7th International Conference on Solid-State Sensors and Actuators, Transducers'93, June 1993.pp.810-813.

148. Robert, L. C. and Fuller, R C., "Modal sensing of efficient acoustic radiators with polyvinylidene fluoride distributed sensors in active structural acoustic control approaches", Journal of Acoustical Society of America, 91(6), June1992, pp. 3321-3329.

149. Robert, L. Clark and Fuller, R Chris, "Optimal placement of piezoelectric actuators and polyvinylidine fluoride error sensors in active structural control approaches", Journal of Acoustical Society of America, 92(3), September 1992, pp. 1521-1533.

150. Rosengren, L., Soderkvist, J. and Smith, L., "Micromachined sensor structures with linear capacitive response", Sensors and Actuators A, 000(1992).pp.1-6.

151. Rossing, T.D, Hampton, D.S and Hansen,V.J, "Music from oil drums: the acoustics of the steel pan", Physics Today, March, 1996, pp 24-29.

152. Roylance, L.M. and Angell, J.B., "A batch-fabricated silicon accelerometer", IEEE Transactions on Electron Devices, Vol.ED-26, No. 12, December 1979, pp.1911-1917.

153. Rudolf, F., "A micromechanical capacitive accelerometer with a two-point inertial mass suspension", Sensors and Actuators, 1983, pp.191-198.

154. Rudolf, F., Jornod, A., and Bencze, P., "Silicon microaccelerometers", The 4th International Conference on Solid-State Sensors and Actuators, Transducers'87, June 1987, pp. 376-379.

155. Rudolf, F., Jornod, A. Bergqvist J. and Leuthold, H., "Precision accelerometers with μg resolution", Sensors and Actuators, A21 -A23, 1990, 297-302.

156. Scheeper, P.R., Van Der Donk A.G.H., Olthuis, W., Bergveld, P., "Fabrication of silicon condenser microphones using single wafer technology", Journal of Microelectromechanical Systems, Vol.1, No.3, September 1992, pp.147-154.

157. Schlaak, H., Arndt, F., Steckenborn, A., Gevatter, H., Kiesewetter L., and Grethen, H., "Micromechanical capacitive acceleration sensor with force compensation", in H. Reichl (ed.), Microsysterns, Springer, New York, 1990, pp. 617-622.

158. Schlichting, V., Pollak-Diener, G., Obermeier, E., Hammerschmidt, D., Schnatz, F.V., Hosticka, B.J., "Digital programmable pressure sensor with on-chip CMOS

signal processing and data storage", Proc. of 7th intl. Conf. on solid-state sensors and actuators, TRANSDUCER'93, Yokohama, Japan, June 7-10, 1993, pp.988-991.

159. Seidel, H. and Csepregi, L. "Design optimization for cantilever type accelerometers", Sensors and Actuators, 1984, vol.6, pp. 81-92.

160. Seidel, H., Fritsch, U., Gottinger, R. and Sehalk, J., " A piezoresistive silicon accelerometer with monolithically integrated CMOS circuitry", The 8th International Conference on Solid-State Sensors and Actuators, Transducers 95, June 1995, pp. 597-600

161. Seidel, H, Seidel, R. Kolbeck, R., Muck, G., Kupke, W. and Koniger, M., "Capacitive silicon accelerometer with highly symmetric design", Sensors Actuators, vol. A21/A23, 1990, pp.312-315.

162. Sherman, S.J., Tsang, W.K, Core, T.A., Payne, R.S, Quinn, D.E., Chau, K.H, Farash, J.A and Baum, S.K., "A low-cost monolithic accelerometer: product/technology update", IEEE electron devices meeting, (IEDM'92), Dec. 1992, pp. 160-161

163. Singhal, R.K. and Gorman, D.J., "Free vibration of partially clamped rectangular plates with and without rigid point supports", Journal of Sound and Vibration 203(2), 1997, pp.181-192.

164. Smith, M.J.S., Bowman, L. and Meindl, J.D., "Analysis, design, and performance of a capacitive pressure sensor IC", IEEE Transactions on Biomedical Engineering, Vol.BME-33, No.2, February 1986, pp.163-174.

165. Stiharu, I. and Bhat, R.B., "Vibration of micro Pplates in electrostatic fields using Rayleigh-Ritz method", Proc. of XVth Intl. Modal Analysis Conference, Orlando, Florida, 1997, Vol. 1, pp. 765-770.

166. Stiharu, I., Rakheja S. and Wang, L., "Humidity microsensor in CMOS Mitel15 technology", Proc. 1999 IEEE, Canadian Conf. on Electrical and Computer Engineering, 1999, pp. 1652-1657.

167. Strembicke, D., Robinson, A.M., Vermeulen, F.E., Seto, M. and Brown, K.B., "Humidity measurement using resonating CMOS microcantilever structures", Proc. IEEE Canadian Conf. on Electrical and Computer Engineering, Edmonton, Alberta, May 9-12, 1999, pp. 1656-1661.

168. Sugeno, M. and Kang, G.T., "Structure identification of fuzzy model," Fuzzy Sets and Systems, 28, 1988, pp.15-33.

169. Sugeno, M. and Yasukawa, T., "A fuzzy-logic-based approach to qualitative modeling," IEEE Transactions on Fuzzy Systems, 1(1), 1993, pp.7-31.

170. Sugeno, M. and Kang, G.T., "Fuzzy modeling and control of multilayer incinerator", Fuzzy Sets and Systems, 1986, 18, pp. 329-346.

171. Sugiyama, S., Shimaoka, K. and Tabata, O., "Surface micromachined micro-diaphragm pressure sensors", IEEE Proc., 1991. pp.188-191.

172. Sung, C.C. and Jan, C.T., "Active control of structurally radiated sound from plates", Journal of Acoustic Society of America, 102(1), July 1997, pp.370-381.

173. Suzuki, S., Tuchitani, S. Sato, K. Uneo, S. Yokota, Y. Sato, M. and Esashi, M., "Semiconductor capacitance-type accelerometer with PWM electrostatic servo technique", Sensors and Actuators, A21 -A23, 1990, pp. 316- 319.

174. Takagi, T. and Sugeno, M., "Derivation of fuzzy rules from human operators actions", Proc. of IFAC Symp. On Fuzzy Information, Marseille, 1983, pp. 55-60.

175. Takagi T, and Sugeno M., "Fuzzy identification of systems and its application to modeling and control," IEEE Transactions on Systems, Man and Cybernetics 15 (1): 1985, pp.116-132.

176. Takahagi, T., Nakai, M and Tamai, Y., "Near field sound radiation from simply supported rectangular plates", Journal of Sound and Vibration, 185(3), 1995, pp. 455-471.

177. Tea, N.H., Milanovic, V., Zincke, C.A., Suehle, J.S., Gaitan, M., Zaghloul, M.E. and Geist, J., "Hybrid postprocessing etching for CMOS - compatible MEMS", Journal of Microelectromechanical systems, Vol.6, No 4. 1997, pp. 363-372.

178. Terabe, H., Fukaya, Y., Sakurai, S., Tabata, O., Sugiyama, S. and Esahi, M., "Capacitive pressure sensor for low pressure measurements with high overpressure tolerance", Technical Digest of the 10th Sensor Symposium, 1991, pp.133-136.

179. Thielemann, C. and Hess, G., "Single-Chip Condenser Microphone", ACUSTICA-acta acustica, Vol.82, 1996, S 181.

180. Thomson, W.T., "Theory of Vibration with Applications', Prentice Hall, Third edition, 1988,

181. Tilmans, H.A.C., Baert, K., Verbist, A. and Puers, R., "CMOS foundry-based micromachining", IEEE Proc., 1996, pp.122-127.

182. Tong, R.M., "The construction and evaluation of fuzzy models," In Advances in Fuzzy Set Theory and Applications, Gupta MM, Ragade RK, Yager RR (eds), Amsterdam, 1979, pp.559-576.

183. Trojan, G.J, Kiszka, J.B, Gupta, M.M, and Nikiforuk, P.N., "Solution of multivariable fuzzy equation," Fuzzy Sets snd Systems , 22, 1987, pp. 271-279.

184. Turner, G.C., Andrews, M.K., "Frequency stabilisation of electrostatic oscillators", proc. of 8th intl. Conf. on solid-state sensors and actuators, TRANSDUCER'95, Stockholm, Sweden, June 25-29, 1995, pp.624-626.

185. Ulf Kronman, 'Steel Pan Tuning', Musikmuseet, Sweeden, July 1995 (WWW material).

186. Ura, N. and Esashi, M., "Differential capacitive accelerometer", Tech. Dig. 10th Sensor Symp., Japan, 1991, pp. 41-44.

187. Van der Donk, A.G.H., Scheeper, P.R., Olthuis, W. and Bergveld, P., "Modelling of silicon condenser microphones", Sensors and Actuators, 40, 1994, .pp.203-216.

188. Van Drieenhuizen, B.P., Maluf, N., Opris, I.E. and Kovacs, G., "Force balanced accelerometer with mg resolution fabricated using silicon fusion bonding and deep reactive ion etching", The 9th International Conference on Solid-State Sensors and Actuators, Transducers'97, June 1997, pp. 1229-1230.

189. Van Mullem, C.J., van Dam, F.W.A., Fluitman, J.H.J and Wallinga, H., " Towards a micromachined silicon integrated resonator", Proc. of 7th intl. Conf. on solid-state sensors and actuators, TRANSDUCER'93, Yokohama, Japan, June 7-10, 1993, pp. 787-790.

190. Vugts, M.J.M., Verschueren, G.L.J., Eurlings, M.F.A, Hermans, L.J and Beijerinck, H.C.W., "Si/XeF2 etching: temperature dependence", Journal of Vacuum Science and Technology A, Vol. 14, No.5, September-October 1996, pp. 2766-2774.

191. Wallace, C.E., "Radiation resistance of a rectangular panel", Journal of Acoustical Society of America, 51(3), 1972, pp. 946-952.

192. Wang, B.T., Fuller, C.R. and Dimitriadis, E.K. "Active control of noise transmission through rectangular plates using multiple piezoelectric point force actuators", Journal of Acoustic Society of America, 90(5), November 1991, pp. 2820-2830.

193. Warren, J.F., Brzezinski, A.M. and Hamilton, J.F., "Capacitance microphone static membrane deflections", Journal of Acoustical Society of America, Vol.52, No.3, (part 1, 1972), pp. 711-719.

194. Warren, J.E., Brzezinski, A.M., and Hamilton, J.F., "Capacitance microphone dynamic membrane deflections", Journal of Acoustical Society of America, Vol.54, No.5, 1973, pp. 1201-1213.

195. Warren, K., "Navigation grade silicon accelerometer with sacrificial etched SIMOX and BESOI structure", Tech. Dig. Solid State Sensors and Actuators workshop, Hilton Head Island, SC, June 1994, pp. 69-72.

196. Welham, C.J., Gardner, J.W. and Greenwood, J. "A laterally driven micromachined resonant pressure sensor", proc. of 8th intl. Conf. on solid-state sensors and actuators, TRANSDUCER'95, Stockholm, Sweden, June 25-29, 1995, pp.586-589.

197. Wendroff, B., "On orthogonal polynomials", American Mathematical Society, Vol. 12, 1961, pp. 554-555.

198. Winters, H.F. and Coburn, J. W., "The etching of silicon with XeF2 vapor"., Applied Physics Letters, Vol.34, No.1, January 1979, pp. 70-73.

199. Wu, J.R. and Liu, W.H., "Vibration of rectangular plates with edge constraints and intermediate stiffeners", Journal of Sound and Vibration , 123(1), (1988), pp. 103-113.

200. Yager, R.R. and Filev, D.P., "Generation of fuzzy rules by mountain clustering," Journal of Intelligent and Fuzzy Systems, 2, 1994, pp.209-219.

201. Yager, R.R. and Filev, D.P., "Essentials of fuzzy modeling and control", New York: Wiley, 1994.

202. Yazdi, N., Ayazi, F. and Najafi, K., "Micromachined inertial sensors", Proceedings of IEEE, Vol.86, August 1998, pp.1640-1659.

203. Yazdi, N. and Najafi, K., "An all silicon single wafer fabrication technology for precision microaccelerometers", The 9th International Conference on Solid-State Sensors and Actuators, Transducers'97, June 1997, pp. 1181-1184.

204. Yin T.S., David J.T and Daryoush A., "Influence of confined vibrations on sensor and actuator optimization", Society of Automotive Engineers, 971890, pp. 155-164.

205. Yoshida, M., Nomura, T., Mineta, T. and Esashi, M., "Capacitive accelerometers without fracture risk during fabrication process", Proc. 11th annual workshop on Micro Electro Mechanical Systems, MEMS 98, Jan. 25-29, 1998, Heidelberg, Germany, pp. 814-817.

206. Young, P.G. and Dickinson, S.M., "On the free flexural vibration of rectangular plates with straight or curved internal line supports", Journal of Sound and Vibration 162(1), 1993, pp.123-135.

207. Yu, B., Allegretto, W. and Robinson, A.M., "Dynamic response of a magnetically actuated micromachined cantilever with a permalloy electroplated film", Proc. IEEE Canadian Conf. on Electriacal and Coputer Engineering, Edmonton, Alberta, May 9-12, 1999, pp. 1643-1647.

208. Yuan, J. and Dickinson, S.M., "The flexural vibration of rectangular plate system approached by using artificial springs in the Rayleigh-Ritz", Journal of Sound and Vibration, 159(1), 1992, pp.39-55.

209. Yuan, J. and Dickinson, S.M, "On the use of artificial springs in the study of the free vibrations of systems comprised of straight and curved beams", Journal of Sound and Vibration, 153(2), 1992, pp 203-216.

210. Zadeh, L.A., "Fuzzy sets", Information and Control, 1965,8, pp. 338-353.

211. Zadeh L, "Outline of a new approach to the analysis of complex systems and decision process," IEEE Transactions on Systems, Man and Cybernetics 1. SMC-3, 1973, pp.28-44.

212. Zadeh, L.A., "A theory of approximate reasoning", Machine Intelligence, 1979, 9, pp.149-194.

213. Zahn, R., "Analysis of the acoustic response of circular electret condenser microphones", Journal of Acoustic Society of America, 69(4), April 1981, pp.1200-1203.

214. Zou, Q., Li, Z. and Liu, L., "Design and fabrication of silicon condenser microphone using corrugated diaphragm technique", Journal of Microelectromechanical Systems, Vol.5, No.3, September 1996, pp.197-203.

APPENDIX A

Table A.1: Input-Output Data For Objective Function Λ_{13358}

x_1	x_2	y
-0.3000E+01	-0.3000E+01	0.9415E-02
-0.3000E+01	-0.2800E+01	0.9415E-02
-0.3000E+01	-0.2600E+01	0.9415E-02
-0.3000E+01	-0.2400E+01	0.9427E-02
-0.3000E+01	-0.2200E+01	0.9376E-02
-0.3000E+01	-0.2000E+01	0.9355E-02
-0.3000E+01	-0.1800E+01	0.9345E-02
-0.3000E+01	-0.1600E+01	0.9331E-02
-0.3000E+01	-0.1400E+01	0.9264E-02
-0.3000E+01	-0.1200E+01	0.9175E-02
-0.3000E+01	-0.1000E+01	0.9047E-02
-0.3000E+01	-0.8000E+00	0.8904E-02
-0.3000E+01	-0.6000E+00	0.8741E-02
-0.3000E+01	-0.2000E+01	0.9355E-02
-0.3000E+01	-0.1000E+01	0.9047E-02
-0.3000E+01	0.0000E+00	0.9635E-02
-0.3000E+01	0.2000E+00	0.1171E-01
-0.3000E+01	0.4000E+00	0.1572E-01
-0.2800E+01	-0.3000E+01	0.9415E-02
-0.2800E+01	-0.2800E+01	0.9415E-02
-0.2800E+01	-0.2600E+01	0.9415E-02
-0.2800E+01	-0.2400E+01	0.9383E-02
-0.2800E+01	-0.2200E+01	0.9376E-02
-0.2800E+01	-0.2000E+01	0.9355E-02
-0.2800E+01	-0.1800E+01	0.9345E-02
-0.2800E+01	-0.1600E+01	0.9331E-02
-0.2800E+01	-0.1400E+01	0.9264E-02
-0.2800E+01	-0.1200E+01	0.9188E-02
-0.2800E+01	-0.1000E+01	0.9047E-02
-0.2800E+01	-0.8000E+00	0.8904E-02
-0.2800E+01	-0.6000E+00	0.8741E-02
-0.2800E+01	-0.2000E+01	0.9355E-02
-0.2800E+01	-0.1000E+01	0.9047E-02
-0.2800E+01	0.0000E+00	0.9635E-02
-0.2800E+01	0.2000E+00	0.1171E-01
-0.2800E+01	0.4000E+00	0.1572E-01
-0.2600E+01	-0.3000E+01	0.9415E-02
-0.2600E+01	-0.2800E+01	0.9415E-02
-0.2600E+01	-0.2600E+01	0.9427E-02
-0.2600E+01	-0.2400E+01	0.9383E-02
-0.2600E+01	-0.2200E+01	0.9388E-02
-0.2600E+01	-0.2000E+01	0.9367E-02
-0.2600E+01	-0.1800E+01	0.9335E-02
-0.2600E+01	-0.1600E+01	0.9298E-02
-0.2600E+01	-0.1400E+01	0.9264E-02
-0.2600E+01	-0.1200E+01	0.9188E-02
-0.2600E+01	-0.1000E+01	0.9047E-02
-0.2600E+01	-0.8000E+00	0.8904E-02
-0.2600E+01	-0.6000E+00	0.8755E-02
-0.2600E+01	-0.2000E+01	0.9367E-02
-0.2600E+01	-0.1000E+01	0.9047E-02
-0.2600E+01	0.0000E+00	0.9635E-02
-0.2600E+01	0.2000E+00	0.1174E-01
-0.2600E+01	0.4000E+00	0.1572E-01
-0.2400E+01	-0.3000E+01	0.9427E-02
-0.2400E+01	-0.2800E+01	0.9383E-02
-0.2400E+01	-0.2600E+01	0.9383E-02
-0.2400E+01	-0.2400E+01	0.9376E-02
-0.2400E+01	-0.2200E+01	0.9388E-02
-0.2400E+01	-0.2000E+01	0.9367E-02
-0.2400E+01	-0.1800E+01	0.9340E-02

x_1	x_2	y
-0.2400E+01	-0.1600E+01	0.9298E-02
-0.2400E+01	-0.1400E+01	0.9238E-02
-0.2400E+01	-0.1200E+01	0.9150E-02
-0.2400E+01	-0.1000E+01	0.9060E-02
-0.2400E+01	-0.8000E+00	0.8917E-02
-0.2400E+01	-0.6000E+00	0.8726E-02
-0.2400E+01	-0.2000E+01	0.9367E-02
-0.2400E+01	-0.1000E+01	0.9060E-02
-0.2400E+01	0.0000E+00	0.9650E-02
-0.2400E+01	0.2000E+00	0.1174E-01
-0.2400E+01	0.4000E+00	0.1574E-01
-0.2200E+01	-0.3000E+01	0.9376E-02
-0.2200E+01	-0.2800E+01	0.9376E-02
-0.2200E+01	-0.2600E+01	0.9388E-02
-0.2200E+01	-0.2400E+01	0.9386E-02
-0.2200E+01	-0.2200E+01	0.9367E-02
-0.2200E+01	-0.2000E+01	0.9345E-02
-0.2200E+01	-0.1800E+01	0.9307E-02
-0.2200E+01	-0.1600E+01	0.9300E-02
-0.2200E+01	-0.1400E+01	0.9228E-02
-0.2200E+01	-0.1200E+01	0.9162E-02
-0.2200E+01	-0.1000E+01	0.9028E-02
-0.2200E+01	-0.8000E+00	0.8874E-02
-0.2200E+01	-0.6000E+00	0.8726E-02
-0.2200E+01	-0.2000E+01	0.9345E-02
-0.2200E+01	-0.1000E+01	0.9028E-02
-0.2200E+01	0.0000E+00	0.9650E-02
-0.2200E+01	0.2000E+00	0.1174E-01
-0.2200E+01	0.4000E+00	0.1574E-01
-0.2000E+01	-0.3000E+01	0.9355E-02
-0.2000E+01	-0.2800E+01	0.9355E-02
-0.2000E+01	-0.2600E+01	0.9367E-02
-0.2000E+01	-0.2400E+01	0.9367E-02
-0.2000E+01	-0.2200E+01	0.9345E-02
-0.2000E+01	-0.2000E+01	0.9340E-02
-0.2000E+01	-0.1800E+01	0.9319E-02
-0.2000E+01	-0.1600E+01	0.9273E-02
-0.2000E+01	-0.1400E+01	0.9207E-02
-0.2000E+01	-0.1200E+01	0.9132E-02
-0.2000E+01	-0.1000E+01	0.9032E-02
-0.2000E+01	-0.8000E+00	0.8887E-02
-0.2000E+01	-0.6000E+00	0.8702E-02
-0.2000E+01	-0.2000E+01	0.9340E-02
-0.2000E+01	-0.1000E+01	0.9032E-02
-0.2000E+01	0.0000E+00	0.9648E-02
-0.2000E+01	0.2000E+00	0.1174E-01
-0.2000E+01	0.4000E+00	0.1577E-01
-0.1800E+01	-0.3000E+01	0.9345E-02
-0.1800E+01	-0.2800E+01	0.9345E-02
-0.1800E+01	-0.2600E+01	0.9335E-02
-0.1800E+01	-0.2400E+01	0.9340E-02
-0.1800E+01	-0.2200E+01	0.9307E-02
-0.1800E+01	-0.2000E+01	0.9319E-02
-0.1800E+01	-0.1800E+01	0.9300E-02
-0.1800E+01	-0.1600E+01	0.9264E-02
-0.1800E+01	-0.1400E+01	0.9199E-02
-0.1800E+01	-0.1200E+01	0.9125E-02
-0.1800E+01	-0.1000E+01	0.9021E-02
-0.1800E+01	-0.8000E+00	0.8844E-02
-0.1800E+01	-0.6000E+00	0.8701E-02
-0.1800E+01	-0.2000E+01	0.9319E-02
-0.1800E+01	-0.1000E+01	0.9021E-02

-0.1800E+01	0.0000E+00	0.9643E-02
-0.1800E+01	0.2000E+00	0.1175E-01
-0.1800E+01	0.4000E+00	0.1582E-01
-0.1600E+01	-0.3000E+01	0.9331E-02
-0.1600E+01	-0.2800E+01	0.9331E-02
-0.1600E+01	-0.2600E+01	0.9298E-02
-0.1600E+01	-0.2400E+01	0.9298E-02
-0.1600E+01	-0.2200E+01	0.9300E-02
-0.1600E+01	-0.2000E+01	0.9273E-02
-0.1600E+01	-0.1800E+01	0.9264E-02
-0.1600E+01	-0.1600E+01	0.9207E-02
-0.1600E+01	-0.1400E+01	0.9175E-02
-0.1600E+01	-0.1200E+01	0.9071E-02
-0.1600E+01	-0.1000E+01	0.8974E-02
-0.1600E+01	-0.8000E+00	0.8836E-02
-0.1600E+01	-0.6000E+00	0.8691E-02
-0.1600E+01	-0.2000E+01	0.9273E-02
-0.1600E+01	-0.1000E+01	0.8974E-02
-0.1600E+01	0.0000E+00	0.9636E-02
-0.1600E+01	0.2000E+00	0.1177E-01
-0.1600E+01	0.4000E+00	0.1582E-01
-0.1400E+01	-0.3000E+01	0.9264E-02
-0.1400E+01	-0.2800E+01	0.9264E-02
-0.1400E+01	-0.2600E+01	0.9264E-02
-0.1400E+01	-0.2400E+01	0.9238E-02
-0.1400E+01	-0.2200E+01	0.9228E-02
-0.1400E+01	-0.2000E+01	0.9207E-02
-0.1400E+01	-0.1800E+01	0.9199E-02
-0.1400E+01	-0.1600E+01	0.9175E-02
-0.1400E+01	-0.1400E+01	0.9125E-02
-0.1400E+01	-0.1200E+01	0.9043E-02
-0.1400E+01	-0.1000E+01	0.8910E-02
-0.1400E+01	-0.8000E+00	0.8782E-02
-0.1400E+01	-0.6000E+00	0.8645E-02
-0.1400E+01	-0.2000E+01	0.9207E-02
-0.1400E+01	-0.1000E+01	0.8910E-02
-0.1400E+01	0.0000E+00	0.9646E-02
-0.1400E+01	0.2000E+00	0.1179E-01
-0.1400E+01	0.4000E+00	0.1587E-01
-0.1200E+01	-0.3000E+01	0.9175E-02
-0.1200E+01	-0.2800E+01	0.9188E-02
-0.1200E+01	-0.2600E+01	0.9188E-02
-0.1200E+01	-0.2400E+01	0.9150E-02
-0.1200E+01	-0.2200E+01	0.9162E-02
-0.1200E+01	-0.2000E+01	0.9132E-02
-0.1200E+01	-0.1800E+01	0.9125E-02
-0.1200E+01	-0.1600E+01	0.9071E-02
-0.1200E+01	-0.1400E+01	0.9043E-02
-0.1200E+01	-0.1200E+01	0.8966E-02
-0.1200E+01	-0.1000E+01	0.8856E-02
-0.1200E+01	-0.8000E+00	0.8724E-02
-0.1200E+01	-0.6000E+00	0.8580E-02
-0.1200E+01	-0.2000E+01	0.9132E-02
-0.1200E+01	-0.1000E+01	0.8856E-02
-0.1200E+01	0.0000E+00	0.9650E-02
-0.1200E+01	0.2000E+00	0.1185E-01
-0.1200E+01	0.4000E+00	0.1592E-01
-0.1000E+01	-0.3000E+01	0.9047E-02
-0.1000E+01	-0.2800E+01	0.9047E-02
-0.1000E+01	-0.2600E+01	0.9047E-02
-0.1000E+01	-0.2400E+01	0.9060E-02
-0.1000E+01	-0.2200E+01	0.9028E-02
-0.1000E+01	-0.2000E+01	0.9032E-02
-0.1000E+01	-0.1800E+01	0.9021E-02
-0.1000E+01	-0.1600E+01	0.8974E-02
-0.1000E+01	-0.1400E+01	0.8910E-02
-0.1000E+01	-0.1200E+01	0.8856E-02

-0.1000E+01	-0.1000E+01	0.8757E-02
-0.1000E+01	-0.8000E+00	0.8634E-02
-0.1000E+01	-0.6000E+00	0.8520E-02
-0.1000E+01	-0.2000E+01	0.9032E-02
-0.1000E+01	-0.1000E+01	0.8757E-02
-0.1000E+01	0.0000E+00	0.9693E-02
-0.1000E+01	0.2000E+00	0.1192E-01
-0.8000E+00	-0.3000E+01	0.8904E-02
-0.8000E+00	-0.2800E+01	0.8904E-02
-0.8000E+00	-0.2600E+01	0.8904E-02
-0.8000E+00	-0.2400E+01	0.8917E-02
-0.8000E+00	-0.2200E+01	0.8874E-02
-0.8000E+00	-0.2000E+01	0.8887E-02
-0.8000E+00	-0.1800E+01	0.8844E-02
-0.8000E+00	-0.1600E+01	0.8836E-02
-0.8000E+00	-0.1400E+01	0.8782E-02
-0.8000E+00	-0.1200E+01	0.8724E-02
-0.8000E+00	-0.1000E+01	0.8634E-02
-0.8000E+00	-0.8000E+00	0.8524E-02
-0.8000E+00	-0.6000E+00	0.8419E-02
-0.8000E+00	-0.2000E+01	0.8887E-02
-0.8000E+00	-0.1000E+01	0.8634E-02
-0.8000E+00	0.0000E+00	0.9744E-02
-0.8000E+00	0.2000E+00	0.1205E-01
-0.6000E+00	-0.3000E+01	0.8741E-02
-0.6000E+00	-0.2800E+01	0.8741E-02
-0.6000E+00	-0.2600E+01	0.8755E-02
-0.6000E+00	-0.2400E+01	0.8726E-02
-0.6000E+00	-0.2200E+01	0.8726E-02
-0.6000E+00	-0.2000E+01	0.8702E-02
-0.6000E+00	-0.1800E+01	0.8701E-02
-0.6000E+00	-0.1600E+01	0.8691E-02
-0.6000E+00	-0.1400E+01	0.8645E-02
-0.6000E+00	-0.1200E+01	0.8580E-02
-0.6000E+00	-0.1000E+01	0.8520E-02
-0.6000E+00	-0.8000E+00	0.8419E-02
-0.6000E+00	-0.6000E+00	0.8333E-02
-0.6000E+00	-0.2000E+01	0.8702E-02
-0.6000E+00	-0.1000E+01	0.8520E-02
-0.6000E+00	0.0000E+00	0.9867E-02
-0.6000E+00	0.2000E+00	0.1229E-01
-0.2000E+01	-0.3000E+01	0.9355E-02
-0.2000E+01	-0.2800E+01	0.9355E-02
-0.2000E+01	-0.2600E+01	0.9367E-02
-0.2000E+01	-0.2400E+01	0.9367E-02
-0.2000E+01	-0.2200E+01	0.9345E-02
-0.2000E+01	-0.2000E+01	0.9340E-02
-0.2000E+01	-0.1800E+01	0.9319E-02
-0.2000E+01	-0.1600E+01	0.9273E-02
-0.2000E+01	-0.1400E+01	0.9207E-02
-0.2000E+01	-0.1200E+01	0.9132E-02
-0.2000E+01	-0.1000E+01	0.9032E-02
-0.2000E+01	-0.8000E+00	0.8887E-02
-0.2000E+01	-0.6000E+00	0.8702E-02
-0.2000E+01	-0.2000E+01	0.9340E-02
-0.2000E+01	-0.1000E+01	0.9032E-02
-0.2000E+01	0.0000E+00	0.9648E-02
-0.2000E+01	0.2000E+00	0.1174E-01
-0.2000E+01	0.4000E+00	0.1577E-01
-0.1000E+01	-0.3000E+01	0.9047E-02
-0.1000E+01	-0.2800E+01	0.9047E-02
-0.1000E+01	-0.2600E+01	0.9047E-02
-0.1000E+01	-0.2400E+01	0.9060E-02
-0.1000E+01	-0.2200E+01	0.9028E-02
-0.1000E+01	-0.2000E+01	0.9032E-02
-0.1000E+01	-0.1800E+01	0.9021E-02
-0.1000E+01	-0.1600E+01	0.8974E-02

-0.1000E+01	-0.1400E+01	0.8910E-02
-0.1000E+01	-0.1200E+01	0.8856E-02
-0.1000E+01	-0.1000E+01	0.8757E-02
-0.1000E+01	-0.8000E+00	0.8634E-02
-0.1000E+01	-0.6000E+00	0.8520E-02
-0.1000E+01	-0.2000E+01	0.9032E-02
-0.1000E+01	-0.1000E+01	0.8757E-02
-0.1000E+01	0.0000E+00	0.9693E-02
-0.1000E+01	0.2000E+00	0.1192E-01
0.0000E+00	-0.3000E+01	0.9635E-02
0.0000E+00	-0.2800E+01	0.9635E-02
0.0000E+00	-0.2600E+01	0.9635E-02
0.0000E+00	-0.2400E+01	0.9650E-02
0.0000E+00	-0.2200E+01	0.9650E-02
0.0000E+00	-0.2000E+01	0.9648E-02
0.0000E+00	-0.1800E+01	0.9643E-02
0.0000E+00	-0.1600E+01	0.9636E-02
0.0000E+00	-0.1400E+01	0.9646E-02
0.0000E+00	-0.1200E+01	0.9650E-02
0.0000E+00	-0.1000E+01	0.9693E-02
0.0000E+00	-0.8000E+00	0.9744E-02
0.0000E+00	-0.6000E+00	0.9867E-02
0.0000E+00	-0.2000E+01	0.9648E-02
0.0000E+00	-0.1000E+01	0.9693E-02
0.0000E+00	0.0000E+00	0.1194E-01
0.0000E+00	0.2000E+00	0.1473E-01
0.2000E+00	-0.3000E+01	0.1171E-01
0.2000E+00	-0.2800E+01	0.1171E-01

0.2000E+00	-0.2600E+01	0.1174E-01
0.2000E+00	-0.2400E+01	0.1174E-01
0.2000E+00	-0.2200E+01	0.1174E-01
0.2000E+00	-0.2000E+01	0.1174E-01
0.2000E+00	-0.1800E+01	0.1175E-01
0.2000E+00	-0.1600E+01	0.1177E-01
0.2000E+00	-0.1400E+01	0.1179E-01
0.2000E+00	-0.1200E+01	0.1185E-01
0.2000E+00	-0.1000E+01	0.1192E-01
0.2000E+00	-0.8000E+00	0.1205E-01
0.2000E+00	-0.6000E+00	0.1229E-01
0.2000E+00	-0.2000E+01	0.1174E-01
0.2000E+00	-0.1000E+01	0.1192E-01
0.2000E+00	0.0000E+00	0.1473E-01
0.4000E+00	-0.3000E+01	0.1572E-01
0.4000E+00	-0.2800E+01	0.1572E-01
0.4000E+00	-0.2600E+01	0.1572E-01
0.4000E+00	-0.2400E+01	0.1574E-01
0.4000E+00	-0.2200E+01	0.1574E-01
0.4000E+00	-0.2000E+01	0.1577E-01
0.4000E+00	-0.1800E+01	0.1582E-01
0.4000E+00	-0.1600E+01	0.1582E-01
0.4000E+00	-0.1400E+01	0.1587E-01
0.4000E+00	-0.1200E+01	0.1592E-01
0.4000E+00	-0.2000E+01	0.1577E-01

Table A.2: Input-Output Data For Objective Function Λ_{13357}

x_1	x_2	y
-0.3000E+01	-0.3000E+01	0.1523E-01
-0.3000E+01	-0.2800E+01	0.1523E-01
-0.3000E+01	-0.2600E+01	0.1523E-01
-0.3000E+01	-0.2400E+01	0.1520E-01
-0.3000E+01	-0.2200E+01	0.1515E-01
-0.3000E+01	-0.2000E+01	0.1509E-01
-0.3000E+01	-0.1800E+01	0.1501E-01
-0.3000E+01	-0.1600E+01	0.1488E-01
-0.3000E+01	-0.1400E+01	0.1467E-01
-0.3000E+01	-0.1200E+01	0.1436E-01
-0.3000E+01	-0.1000E+01	0.1382E-01
-0.3000E+01	-0.8000E+00	0.1305E-01
-0.3000E+01	-0.6000E+00	0.1193E-01
-0.3000E+01	-0.2000E+01	0.1509E-01
-0.3000E+01	-0.1000E+01	0.1382E-01
-0.3000E+01	0.0000E+00	0.6123E-02
-0.3000E+01	0.2000E+00	0.4302E-02
-0.3000E+01	0.4000E+00	0.3692E-02
-0.3000E+01	0.6000E+00	0.5063E-02
-0.3000E+01	0.8000E+00	0.8404E-02
-0.3000E+01	0.1000E+01	0.1309E-01
-0.2800E+01	-0.3000E+01	0.1523E-01
-0.2800E+01	-0.2800E+01	0.1523E-01
-0.2800E+01	-0.2600E+01	0.1523E-01
-0.2800E+01	-0.2400E+01	0.1516E-01
-0.2800E+01	-0.2200E+01	0.1515E-01
-0.2800E+01	-0.2000E+01	0.1509E-01
-0.2800E+01	-0.1800E+01	0.1501E-01
-0.2800E+01	-0.1600E+01	0.1488E-01
-0.2800E+01	-0.1400E+01	0.1467E-01
-0.2800E+01	-0.1200E+01	0.1433E-01
-0.2800E+01	-0.1000E+01	0.1382E-01
-0.2800E+01	-0.8000E+00	0.1305E-01
-0.2800E+01	-0.6000E+00	0.1193E-01
-0.2800E+01	-0.2000E+01	0.1509E-01
-0.2800E+01	-0.1000E+01	0.1382E-01
-0.2800E+01	0.0000E+00	0.6123E-02
-0.2800E+01	0.2000E+00	0.4302E-02
-0.2800E+01	0.4000E+00	0.3692E-02
-0.2800E+01	0.6000E+00	0.5058E-02
-0.2800E+01	0.8000E+00	0.8413E-02
-0.2800E+01	0.1000E+01	0.1309E-01
-0.2600E+01	-0.3000E+01	0.1523E-01
-0.2600E+01	-0.2800E+01	0.1523E-01
-0.2600E+01	-0.2600E+01	0.1520E-01
-0.2600E+01	-0.2400E+01	0.1516E-01
-0.2600E+01	-0.2200E+01	0.1513E-01
-0.2600E+01	-0.2000E+01	0.1507E-01
-0.2600E+01	-0.1800E+01	0.1500E-01
-0.2600E+01	-0.1600E+01	0.1485E-01
-0.2600E+01	-0.1400E+01	0.1467E-01
-0.2600E+01	-0.1200E+01	0.1433E-01
-0.2600E+01	-0.1000E+01	0.1382E-01
-0.2600E+01	-0.8000E+00	0.1305E-01
-0.2600E+01	-0.6000E+00	0.1191E-01
-0.2600E+01	-0.2000E+01	0.1507E-01
-0.2600E+01	-0.1000E+01	0.1382E-01
-0.2600E+01	0.0000E+00	0.6123E-02
-0.2600E+01	0.2000E+00	0.4292E-02
-0.2600E+01	0.4000E+00	0.3692E-02
-0.2600E+01	0.6000E+00	0.5058E-02
-0.2600E+01	0.8000E+00	0.8403E-02
-0.2600E+01	0.1000E+01	0.1309E-01
-0.2400E+01	-0.3000E+01	0.1520E-01
-0.2400E+01	-0.2800E+01	0.1516E-01
-0.2400E+01	-0.2600E+01	0.1516E-01
-0.2400E+01	-0.2400E+01	0.1515E-01
-0.2400E+01	-0.2200E+01	0.1513E-01
-0.2400E+01	-0.2000E+01	0.1507E-01
-0.2400E+01	-0.1800E+01	0.1497E-01
-0.2400E+01	-0.1600E+01	0.1485E-01
-0.2400E+01	-0.1400E+01	0.1460E-01
-0.2400E+01	-0.1200E+01	0.1429E-01
-0.2400E+01	-0.1000E+01	0.1380E-01
-0.2400E+01	-0.8000E+00	0.1303E-01
-0.2400E+01	-0.6000E+00	0.1188E-01
-0.2400E+01	-0.2000E+01	0.1507E-01
-0.2400E+01	-0.1000E+01	0.1380E-01
-0.2400E+01	0.0000E+00	0.6103E-02
-0.2400E+01	0.2000E+00	0.4292E-02
-0.2400E+01	0.4000E+00	0.3676E-02
-0.2400E+01	0.6000E+00	0.5058E-02
-0.2400E+01	0.8000E+00	0.8403E-02
-0.2400E+01	0.1000E+01	0.1308E-01
-0.2200E+01	-0.3000E+01	0.1515E-01
-0.2200E+01	-0.2800E+01	0.1515E-01
-0.2200E+01	-0.2600E+01	0.1513E-01
-0.2200E+01	-0.2400E+01	0.1513E-01
-0.2200E+01	-0.2200E+01	0.1507E-01
-0.2200E+01	-0.2000E+01	0.1501E-01
-0.2200E+01	-0.1800E+01	0.1493E-01
-0.2200E+01	-0.1600E+01	0.1481E-01
-0.2200E+01	-0.1400E+01	0.1459E-01
-0.2200E+01	-0.1200E+01	0.1427E-01
-0.2200E+01	-0.1000E+01	0.1376E-01
-0.2200E+01	-0.8000E+00	0.1298E-01
-0.2200E+01	-0.6000E+00	0.1188E-01
-0.2200E+01	-0.2000E+01	0.1501E-01
-0.2200E+01	-0.1000E+01	0.1376E-01
-0.2200E+01	0.0000E+00	0.6103E-02
-0.2200E+01	0.2000E+00	0.4292E-02
-0.2200E+01	0.4000E+00	0.3676E-02
-0.2200E+01	0.6000E+00	0.5060E-02
-0.2200E+01	0.8000E+00	0.8403E-02
-0.2200E+01	0.1000E+01	0.1308E-01
-0.2000E+01	-0.3000E+01	0.1509E-01
-0.2000E+01	-0.2800E+01	0.1509E-01
-0.2000E+01	-0.2600E+01	0.1507E-01
-0.2000E+01	-0.2400E+01	0.1507E-01
-0.2000E+01	-0.2200E+01	0.1501E-01
-0.2000E+01	-0.2000E+01	0.1497E-01
-0.2000E+01	-0.1800E+01	0.1491E-01
-0.2000E+01	-0.1600E+01	0.1475E-01
-0.2000E+01	-0.1400E+01	0.1454E-01
-0.2000E+01	-0.1200E+01	0.1420E-01
-0.2000E+01	-0.1000E+01	0.1373E-01
-0.2000E+01	-0.8000E+00	0.1296E-01
-0.2000E+01	-0.6000E+00	0.1182E-01
-0.2000E+01	-0.2000E+01	0.1497E-01
-0.2000E+01	-0.1000E+01	0.1373E-01
-0.2000E+01	0.0000E+00	0.6067E-02
-0.2000E+01	0.2000E+00	0.4261E-02
-0.2000E+01	0.4000E+00	0.3668E-02
-0.2000E+01	0.6000E+00	0.5053E-02
-0.2000E+01	0.8000E+00	0.8409E-02
-0.2000E+01	0.1000E+01	0.1310E-01
-0.1800E+01	-0.3000E+01	0.1501E-01
-0.1800E+01	-0.2800E+01	0.1501E-01

-0.1800E+01	-0.2600E+01	0.1500E-01
-0.1800E+01	-0.2400E+01	0.1497E-01
-0.1800E+01	-0.2200E+01	0.1493E-01
-0.1800E+01	-0.2000E+01	0.1491E-01
-0.1800E+01	-0.1800E+01	0.1481E-01
-0.1800E+01	-0.1600E+01	0.1467E-01
-0.1800E+01	-0.1400E+01	0.1445E-01
-0.1800E+01	-0.1200E+01	0.1412E-01
-0.1800E+01	-0.1000E+01	0.1365E-01
-0.1800E+01	-0.8000E+00	0.1284E-01
-0.1800E+01	-0.6000E+00	0.1175E-01
-0.1800E+01	-0.2000E+01	0.1491E-01
-0.1800E+01	-0.1000E+01	0.1365E-01
-0.1800E+01	0.0000E+00	0.6026E-02
-0.1800E+01	0.2000E+00	0.4234E-02
-0.1800E+01	0.4000E+00	0.3685E-02
-0.1800E+01	0.6000E+00	0.5044E-02
-0.1800E+01	0.8000E+00	0.8401E-02
-0.1800E+01	0.1000E+01	0.1310E-01
-0.1600E+01	-0.3000E+01	0.1488E-01
-0.1600E+01	-0.2800E+01	0.1488E-01
-0.1600E+01	-0.2600E+01	0.1485E-01
-0.1600E+01	-0.2400E+01	0.1485E-01
-0.1600E+01	-0.2200E+01	0.1481E-01
-0.1600E+01	-0.2000E+01	0.1475E-01
-0.1600E+01	-0.1800E+01	0.1467E-01
-0.1600E+01	-0.1600E+01	0.1454E-01
-0.1600E+01	-0.1400E+01	0.1436E-01
-0.1600E+01	-0.1200E+01	0.1399E-01
-0.1600E+01	-0.1000E+01	0.1353E-01
-0.1600E+01	-0.8000E+00	0.1276E-01
-0.1600E+01	-0.6000E+00	0.1166E-01
-0.1600E+01	-0.2000E+01	0.1475E-01
-0.1600E+01	-0.1000E+01	0.1353E-01
-0.1600E+01	0.0000E+00	0.5950E-02
-0.1600E+01	0.2000E+00	0.4194E-02
-0.1600E+01	0.4000E+00	0.3655E-02
-0.1600E+01	0.6000E+00	0.5038E-02
-0.1600E+01	0.8000E+00	0.8408E-02
-0.1600E+01	0.1000E+01	0.1310E-01
-0.1400E+01	-0.3000E+01	0.1467E-01
-0.1400E+01	-0.2800E+01	0.1467E-01
-0.1400E+01	-0.2600E+01	0.1467E-01
-0.1400E+01	-0.2400E+01	0.1460E-01
-0.1400E+01	-0.2200E+01	0.1459E-01
-0.1400E+01	-0.2000E+01	0.1454E-01
-0.1400E+01	-0.1800E+01	0.1445E-01
-0.1400E+01	-0.1600E+01	0.1436E-01
-0.1400E+01	-0.1400E+01	0.1412E-01
-0.1400E+01	-0.1200E+01	0.1382E-01
-0.1400E+01	-0.1000E+01	0.1331E-01
-0.1400E+01	-0.8000E+00	0.1256E-01
-0.1400E+01	-0.6000E+00	0.1147E-01
-0.1400E+01	-0.2000E+01	0.1454E-01
-0.1400E+01	-0.1000E+01	0.1331E-01
-0.1400E+01	0.0000E+00	0.5857E-02
-0.1400E+01	0.2000E+00	0.4108E-02
-0.1400E+01	0.4000E+00	0.3614E-02
-0.1400E+01	0.6000E+00	0.5025E-02
-0.1400E+01	0.8000E+00	0.8414E-02
-0.1400E+01	0.1000E+01	0.1312E-01
-0.1200E+01	-0.3000E+01	0.1436E-01
-0.1200E+01	-0.2800E+01	0.1433E-01
-0.1200E+01	-0.2600E+01	0.1433E-01
-0.1200E+01	-0.2400E+01	0.1429E-01
-0.1200E+01	-0.2200E+01	0.1427E-01
-0.1200E+01	-0.2000E+01	0.1420E-01

-0.1200E+01	-0.1800E+01	0.1412E-01
-0.1200E+01	-0.1600E+01	0.1399E-01
-0.1200E+01	-0.1400E+01	0.1382E-01
-0.1200E+01	-0.1200E+01	0.1352E-01
-0.1200E+01	-0.1000E+01	0.1300E-01
-0.1200E+01	-0.8000E+00	0.1228E-01
-0.1200E+01	-0.6000E+00	0.1122E-01
-0.1200E+01	-0.2000E+01	0.1420E-01
-0.1200E+01	-0.1000E+01	0.1300E-01
-0.1200E+01	0.0000E+00	0.5722E-02
-0.1200E+01	0.2000E+00	0.4036E-02
-0.1200E+01	0.4000E+00	0.3564E-02
-0.1200E+01	0.6000E+00	0.5003E-02
-0.1200E+01	0.8000E+00	0.8479E-02
-0.1200E+01	0.1000E+01	0.1314E-01
-0.1000E+01	-0.3000E+01	0.1382E-01
-0.1000E+01	-0.2800E+01	0.1382E-01
-0.1000E+01	-0.2600E+01	0.1382E-01
-0.1000E+01	-0.2400E+01	0.1380E-01
-0.1000E+01	-0.2200E+01	0.1376E-01
-0.1000E+01	-0.2000E+01	0.1373E-01
-0.1000E+01	-0.1800E+01	0.1365E-01
-0.1000E+01	-0.1600E+01	0.1353E-01
-0.1000E+01	-0.1400E+01	0.1331E-01
-0.1000E+01	-0.1200E+01	0.1300E-01
-0.1000E+01	-0.1000E+01	0.1257E-01
-0.1000E+01	-0.8000E+00	0.1186E-01
-0.1000E+01	-0.6000E+00	0.1084E-01
-0.1000E+01	-0.2000E+01	0.1373E-01
-0.1000E+01	-0.1000E+01	0.1257E-01
-0.1000E+01	0.0000E+00	0.5523E-02
-0.1000E+01	0.2000E+00	0.3900E-02
-0.1000E+01	0.4000E+00	0.3513E-02
-0.1000E+01	0.6000E+00	0.5026E-02
-0.1000E+01	0.8000E+00	0.8491E-02
-0.1000E+01	0.1000E+01	0.1318E-01
-0.8000E+00	-0.3000E+01	0.1305E-01
-0.8000E+00	-0.2800E+01	0.1305E-01
-0.8000E+00	-0.2600E+01	0.1305E-01
-0.8000E+00	-0.2400E+01	0.1303E-01
-0.8000E+00	-0.2200E+01	0.1298E-01
-0.8000E+00	-0.2000E+01	0.1296E-01
-0.8000E+00	-0.1800E+01	0.1284E-01
-0.8000E+00	-0.1600E+01	0.1276E-01
-0.8000E+00	-0.1400E+01	0.1256E-01
-0.8000E+00	-0.1200E+01	0.1228E-01
-0.8000E+00	-0.1000E+01	0.1186E-01
-0.8000E+00	-0.8000E+00	0.1120E-01
-0.8000E+00	-0.6000E+00	0.1023E-01
-0.8000E+00	-0.2000E+01	0.1296E-01
-0.8000E+00	-0.1000E+01	0.1186E-01
-0.8000E+00	0.0000E+00	0.5194E-02
-0.8000E+00	0.2000E+00	0.3703E-02
-0.8000E+00	0.4000E+00	0.3425E-02
-0.8000E+00	0.6000E+00	0.4999E-02
-0.8000E+00	0.8000E+00	0.8522E-02
-0.8000E+00	0.1000E+01	0.1323E-01
-0.6000E+00	-0.3000E+01	0.1193E-01
-0.6000E+00	-0.2800E+01	0.1193E-01
-0.6000E+00	-0.2600E+01	0.1191E-01
-0.6000E+00	-0.2400E+01	0.1188E-01
-0.6000E+00	-0.2200E+01	0.1188E-01
-0.6000E+00	-0.2000E+01	0.1182E-01
-0.6000E+00	-0.1800E+01	0.1175E-01
-0.6000E+00	-0.1600E+01	0.1166E-01
-0.6000E+00	-0.1400E+01	0.1147E-01
-0.6000E+00	-0.1200E+01	0.1122E-01

-0.6000E+00	-0.1000E+01	0.1084E-01
-0.6000E+00	-0.8000E+00	0.1023E-01
-0.6000E+00	-0.6000E+00	0.9349E-02
-0.6000E+00	-0.2000E+01	0.1182E-01
-0.6000E+00	-0.1000E+01	0.1084E-01
-0.6000E+00	0.0000E+00	0.4732E-02
-0.6000E+00	0.2000E+00	0.3407E-02
-0.6000E+00	0.4000E+00	0.3302E-02
-0.6000E+00	0.6000E+00	0.5029E-02
-0.6000E+00	0.8000E+00	0.8599E-02
-0.6000E+00	0.1000E+01	0.1334E-01
-0.2000E+01	-0.3000E+01	0.1509E-01
-0.2000E+01	-0.2800E+01	0.1509E-01
-0.2000E+01	-0.2600E+01	0.1507E-01
-0.2000E+01	-0.2400E+01	0.1507E-01
-0.2000E+01	-0.2200E+01	0.1501E-01
-0.2000E+01	-0.2000E+01	0.1497E-01
-0.2000E+01	-0.1800E+01	0.1491E-01
-0.2000E+01	-0.1600E+01	0.1475E-01
-0.2000E+01	-0.1400E+01	0.1454E-01
-0.2000E+01	-0.1200E+01	0.1420E-01
-0.2000E+01	-0.1000E+01	0.1373E-01
-0.2000E+01	-0.8000E+00	0.1296E-01
-0.2000E+01	-0.6000E+00	0.1182E-01
-0.2000E+01	-0.2000E+01	0.1497E-01
-0.2000E+01	-0.1000E+01	0.1373E-01
-0.2000E+01	0.0000E+00	0.6067E-02
-0.2000E+01	0.2000E+00	0.4261E-02
-0.2000E+01	0.4000E+00	0.3668E-02
-0.2000E+01	0.6000E+00	0.5053E-02
-0.2000E+01	0.8000E+00	0.8409E-02
-0.2000E+01	0.1000E+01	0.1310E-01
-0.1000E+01	-0.3000E+01	0.1382E-01
-0.1000E+01	-0.2800E+01	0.1382E-01
-0.1000E+01	-0.2600E+01	0.1382E-01
-0.1000E+01	-0.2400E+01	0.1380E-01
-0.1000E+01	-0.2200E+01	0.1376E-01
-0.1000E+01	-0.2000E+01	0.1373E-01
-0.1000E+01	-0.1800E+01	0.1365E-01
-0.1000E+01	-0.1600E+01	0.1353E-01
-0.1000E+01	-0.1400E+01	0.1331E-01
-0.1000E+01	-0.1200E+01	0.1300E-01
-0.1000E+01	-0.1000E+01	0.1257E-01
-0.1000E+01	-0.8000E+00	0.1186E-01
-0.1000E+01	-0.6000E+00	0.1084E-01
-0.1000E+01	-0.2000E+01	0.1373E-01
-0.1000E+01	-0.1000E+01	0.1257E-01
-0.1000E+01	0.0000E+00	0.5523E-02
-0.1000E+01	0.2000E+00	0.3900E-02
-0.1000E+01	0.4000E+00	0.3513E-02
-0.1000E+01	0.6000E+00	0.5026E-02
-0.1000E+01	0.8000E+00	0.8491E-02
-0.1000E+01	0.1000E+01	0.1318E-01
0.0000E+00	-0.3000E+01	0.6123E-02
0.0000E+00	-0.2800E+01	0.6123E-02
0.0000E+00	-0.2600E+01	0.6123E-02
0.0000E+00	-0.2400E+01	0.6103E-02
0.0000E+00	-0.2200E+01	0.6103E-02
0.0000E+00	-0.2000E+01	0.6067E-02
0.0000E+00	-0.1800E+01	0.6026E-02
0.0000E+00	-0.1600E+01	0.5950E-02
0.0000E+00	-0.1400E+01	0.5857E-02
0.0000E+00	-0.1200E+01	0.5722E-02
0.0000E+00	-0.1000E+01	0.5523E-02
0.0000E+00	-0.8000E+00	0.5194E-02
0.0000E+00	-0.6000E+00	0.4732E-02
0.0000E+00	-0.2000E+01	0.6067E-02

0.0000E+00	-0.1000E+01	0.5523E-02
0.0000E+00	0.0000E+00	0.2854E-02
0.0000E+00	0.2000E+00	0.2596E-02
0.0000E+00	0.4000E+00	0.3420E-02
0.0000E+00	0.6000E+00	0.5811E-02
0.0000E+00	0.8000E+00	0.9794E-02
0.0000E+00	0.1000E+01	0.1455E-01
0.2000E+00	-0.3000E+01	0.4302E-02
0.2000E+00	-0.2800E+01	0.4302E-02
0.2000E+00	-0.2600E+01	0.4292E-02
0.2000E+00	-0.2400E+01	0.4292E-02
0.2000E+00	-0.2200E+01	0.4292E-02
0.2000E+00	-0.2000E+01	0.4261E-02
0.2000E+00	-0.1800E+01	0.4234E-02
0.2000E+00	-0.1600E+01	0.4194E-02
0.2000E+00	-0.1400E+01	0.4108E-02
0.2000E+00	-0.1200E+01	0.4036E-02
0.2000E+00	-0.1000E+01	0.3900E-02
0.2000E+00	-0.8000E+00	0.3703E-02
0.2000E+00	-0.6000E+00	0.3407E-02
0.2000E+00	-0.2000E+01	0.4261E-02
0.2000E+00	-0.1000E+01	0.3900E-02
0.2000E+00	0.0000E+00	0.2596E-02
0.2000E+00	0.2000E+00	0.2895E-02
0.2000E+00	0.4000E+00	0.4135E-02
0.2000E+00	0.6000E+00	0.6778E-02
0.2000E+00	0.8000E+00	0.1080E-01
0.2000E+00	0.1000E+01	0.1545E-01
0.4000E+00	-0.3000E+01	0.3692E-02
0.4000E+00	-0.2800E+01	0.3692E-02
0.4000E+00	-0.2600E+01	0.3692E-02
0.4000E+00	-0.2400E+01	0.3676E-02
0.4000E+00	-0.2200E+01	0.3676E-02
0.4000E+00	-0.2000E+01	0.3668E-02
0.4000E+00	-0.1800E+01	0.3685E-02
0.4000E+00	-0.1600E+01	0.3655E-02
0.4000E+00	-0.1400E+01	0.3614E-02
0.4000E+00	-0.1200E+01	0.3564E-02
0.4000E+00	-0.1000E+01	0.3513E-02
0.4000E+00	-0.8000E+00	0.3425E-02
0.4000E+00	-0.6000E+00	0.3302E-02
0.4000E+00	-0.2000E+01	0.3668E-02
0.4000E+00	-0.1000E+01	0.3513E-02
0.4000E+00	0.0000E+00	0.3420E-02
0.4000E+00	0.2000E+00	0.4135E-02
0.4000E+00	0.4000E+00	0.5598E-02
0.4000E+00	0.6000E+00	0.8323E-02
0.4000E+00	0.8000E+00	0.1230E-01
0.6000E+00	-0.3000E+01	0.5063E-02
0.6000E+00	-0.2800E+01	0.5058E-02
0.6000E+00	-0.2600E+01	0.5058E-02
0.6000E+00	-0.2400E+01	0.5058E-02
0.6000E+00	-0.2200E+01	0.5060E-02
0.6000E+00	-0.2000E+01	0.5053E-02
0.6000E+00	-0.1800E+01	0.5044E-02
0.6000E+00	-0.1600E+01	0.5038E-02
0.6000E+00	-0.1400E+01	0.5025E-02
0.6000E+00	-0.1200E+01	0.5003E-02
0.6000E+00	-0.1000E+01	0.5026E-02
0.6000E+00	-0.8000E+00	0.4999E-02
0.6000E+00	-0.6000E+00	0.5029E-02
0.6000E+00	-0.2000E+01	0.5053E-02
0.6000E+00	-0.1000E+01	0.5026E-02
0.6000E+00	0.0000E+00	0.5811E-02
0.6000E+00	0.2000E+00	0.6778E-02
0.6000E+00	0.4000E+00	0.8323E-02
0.6000E+00	0.6000E+00	0.1050E-01

0.6000E+00	0.8000E+00	0.1399E-01
0.8000E+00	-0.3000E+01	0.8404E-02
0.8000E+00	-0.2800E+01	0.8413E-02
0.8000E+00	-0.2600E+01	0.8403E-02
0.8000E+00	-0.2400E+01	0.8403E-02
0.8000E+00	-0.2200E+01	0.8403E-02
0.8000E+00	-0.2000E+01	0.8409E-02
0.8000E+00	-0.1800E+01	0.8401E-02
0.8000E+00	-0.1600E+01	0.8408E-02
0.8000E+00	-0.1400E+01	0.8414E-02
0.8000E+00	-0.1200E+01	0.8479E-02
0.8000E+00	-0.1000E+01	0.8491E-02
0.8000E+00	-0.8000E+00	0.8522E-02
0.8000E+00	-0.6000E+00	0.8599E-02
0.8000E+00	-0.2000E+01	0.8409E-02
0.8000E+00	-0.1000E+01	0.8491E-02
0.8000E+00	0.0000E+00	0.9794E-02
0.8000E+00	0.2000E+00	0.1080E-01
0.8000E+00	0.4000E+00	0.1230E-01
0.8000E+00	0.6000E+00	0.1399E-01
0.8000E+00	0.8000E+00	0.1587E-01
0.1000E+01	-0.3000E+01	0.1309E-01
0.1000E+01	-0.2800E+01	0.1309E-01
0.1000E+01	-0.2600E+01	0.1309E-01
0.1000E+01	-0.2400E+01	0.1308E-01
0.1000E+01	-0.2200E+01	0.1308E-01
0.1000E+01	-0.2000E+01	0.1310E-01
0.1000E+01	-0.1800E+01	0.1310E-01
0.1000E+01	-0.1600E+01	0.1310E-01
0.1000E+01	-0.1400E+01	0.1312E-01
0.1000E+01	-0.1200E+01	0.1314E-01
0.1000E+01	-0.1000E+01	0.1318E-01
0.1000E+01	-0.8000E+00	0.1323E-01
0.1000E+01	-0.6000E+00	0.1334E-01
0.1000E+01	-0.2000E+01	0.1310E-01
0.1000E+01	-0.1000E+01	0.1318E-01
0.1000E+01	0.0000E+00	0.1455E-01
0.1000E+01	0.2000E+00	0.1545E-01

Table A.3: Input-Output Data For Objective Function Λ_{133566}

x_1	x_2	y
-0.3000E+01	0.2000E+00	0.1278E-01
-0.3000E+01	0.4000E+00	0.9473E-02
-0.3000E+01	0.6000E+00	0.7969E-02
-0.3000E+01	0.8000E+00	0.8576E-02
-0.3000E+01	0.1000E+01	0.1090E-01
-0.3000E+01	0.1200E+01	0.1402E-01
-0.2800E+01	0.2000E+00	0.1278E-01
-0.2800E+01	0.4000E+00	0.9473E-02
-0.2800E+01	0.6000E+00	0.7964E-02
-0.2800E+01	0.8000E+00	0.8567E-02
-0.2800E+01	0.1000E+01	0.1090E-01
-0.2800E+01	0.1200E+01	0.1402E-01
-0.2600E+01	0.2000E+00	0.1275E-01
-0.2600E+01	0.4000E+00	0.9473E-02
-0.2600E+01	0.6000E+00	0.7964E-02
-0.2600E+01	0.8000E+00	0.8557E-02
-0.2600E+01	0.1000E+01	0.1090E-01
-0.2600E+01	0.1200E+01	0.1402E-01
-0.2400E+01	0.2000E+00	0.1275E-01
-0.2400E+01	0.4000E+00	0.9438E-02
-0.2400E+01	0.6000E+00	0.7964E-02
-0.2400E+01	0.8000E+00	0.8557E-02
-0.2400E+01	0.1000E+01	0.1089E-01
-0.2400E+01	0.1200E+01	0.1402E-01
-0.2200E+01	0.2000E+00	0.1275E-01
-0.2200E+01	0.4000E+00	0.9438E-02
-0.2200E+01	0.6000E+00	0.7948E-02
-0.2200E+01	0.8000E+00	0.8557E-02
-0.2200E+01	0.1000E+01	0.1089E-01
-0.2200E+01	0.1200E+01	0.1400E-01
-0.2000E+01	0.2000E+00	0.1270E-01
-0.2000E+01	0.4000E+00	0.9411E-02
-0.2000E+01	0.6000E+00	0.7941E-02
-0.2000E+01	0.8000E+00	0.8546E-02
-0.2000E+01	0.1000E+01	0.1089E-01
-0.2000E+01	0.1200E+01	0.1400E-01
-0.1800E+01	0.2000E+00	0.1266E-01
-0.1800E+01	0.4000E+00	0.9410E-02
-0.1800E+01	0.6000E+00	0.7914E-02
-0.1800E+01	0.8000E+00	0.8538E-02
-0.1800E+01	0.1000E+01	0.1087E-01
-0.1800E+01	0.1200E+01	0.1401E-01
-0.1600E+01	0.2000E+00	0.1258E-01
-0.1600E+01	0.4000E+00	0.9360E-02
-0.1600E+01	0.6000E+00	0.7871E-02
-0.1600E+01	0.8000E+00	0.8510E-02
-0.1600E+01	0.1000E+01	0.1086E-01
-0.1600E+01	0.1200E+01	0.1399E-01
-0.1400E+01	0.2000E+00	0.1243E-01
-0.1400E+01	0.4000E+00	0.9263E-02
-0.1400E+01	0.6000E+00	0.7823E-02
-0.1400E+01	0.8000E+00	0.8482E-02
-0.1400E+01	0.1000E+01	0.1084E-01
-0.1400E+01	0.1200E+01	0.1397E-01
-0.1200E+01	0.2000E+00	0.1228E-01
-0.1200E+01	0.4000E+00	0.9155E-02
-0.1200E+01	0.6000E+00	0.7746E-02
-0.1200E+01	0.8000E+00	0.8494E-02
-0.1200E+01	0.1000E+01	0.1082E-01
-0.1200E+01	0.1200E+01	0.1395E-01
-0.1000E+01	0.0000E+00	0.1590E-01
-0.1000E+01	0.2000E+00	0.1203E-01

x_1	x_2	y
-0.1000E+01	0.4000E+00	0.8992E-02
-0.1000E+01	0.6000E+00	0.7660E-02
-0.1000E+01	0.8000E+00	0.8420E-02
-0.1000E+01	0.1000E+01	0.1078E-01
-0.1000E+01	0.1200E+01	0.1392E-01
-0.8000E+00	0.0000E+00	0.1535E-01
-0.8000E+00	0.2000E+00	0.1164E-01
-0.8000E+00	0.4000E+00	0.8715E-02
-0.8000E+00	0.6000E+00	0.7489E-02
-0.8000E+00	0.8000E+00	0.8330E-02
-0.8000E+00	0.1000E+01	0.1072E-01
-0.8000E+00	0.1200E+01	0.1389E-01
-0.6000E+00	0.0000E+00	0.1454E-01
-0.6000E+00	0.2000E+00	0.1103E-01
-0.6000E+00	0.4000E+00	0.8330E-02
-0.6000E+00	0.6000E+00	0.7285E-02
-0.6000E+00	0.8000E+00	0.8200E-02
-0.6000E+00	0.1000E+01	0.1066E-01
-0.6000E+00	0.1200E+01	0.1384E-01
-0.2000E+01	0.2000E+00	0.1270E-01
-0.2000E+01	0.4000E+00	0.9411E-02
-0.2000E+01	0.6000E+00	0.7941E-02
-0.2000E+01	0.8000E+00	0.8546E-02
-0.2000E+01	0.1000E+01	0.1089E-01
-0.2000E+01	0.1200E+01	0.1400E-01
-0.1000E+01	0.0000E+00	0.1590E-01
-0.1000E+01	0.2000E+00	0.1203E-01
-0.1000E+01	0.4000E+00	0.8992E-02
-0.1000E+01	0.6000E+00	0.7660E-02
-0.1000E+01	0.8000E+00	0.8420E-02
-0.1000E+01	0.1000E+01	0.1078E-01
-0.1000E+01	0.1200E+01	0.1392E-01
0.0000E+00	-0.1000E+01	0.1590E-01
0.0000E+00	-0.8000E+00	0.1535E-01
0.0000E+00	-0.6000E+00	0.1454E-01
0.0000E+00	-0.1000E+01	0.1590E-01
0.0000E+00	0.0000E+00	0.1036E-01
0.0000E+00	0.2000E+00	0.8321E-02
0.0000E+00	0.4000E+00	0.6818E-02
0.0000E+00	0.6000E+00	0.6663E-02
0.0000E+00	0.8000E+00	0.8187E-02
0.0000E+00	0.1000E+01	0.1083E-01
0.0000E+00	0.1200E+01	0.1390E-01
0.2000E+00	-0.3000E+01	0.1278E-01
0.2000E+00	-0.2800E+01	0.1278E-01
0.2000E+00	-0.2600E+01	0.1275E-01
0.2000E+00	-0.2400E+01	0.1275E-01
0.2000E+00	-0.2200E+01	0.1275E-01
0.2000E+00	-0.2000E+01	0.1270E-01
0.2000E+00	-0.1800E+01	0.1266E-01
0.2000E+00	-0.1600E+01	0.1258E-01
0.2000E+00	-0.1400E+01	0.1243E-01
0.2000E+00	-0.1200E+01	0.1228E-01
0.2000E+00	-0.1000E+01	0.1203E-01
0.2000E+00	-0.8000E+00	0.1164E-01
0.2000E+00	-0.6000E+00	0.1103E-01
0.2000E+00	-0.2000E+01	0.1270E-01
0.2000E+00	-0.1000E+01	0.1203E-01
0.2000E+00	0.0000E+00	0.8321E-02
0.2000E+00	0.2000E+00	0.7437E-02
0.2000E+00	0.4000E+00	0.6643E-02
0.2000E+00	0.6000E+00	0.6897E-02

x_1	x_2	y
0.2000E+00	0.8000E+00	0.8570E-02
0.2000E+00	0.1000E+01	0.1120E-01
0.2000E+00	0.1200E+01	0.1420E-01
0.4000E+00	-0.3000E+01	0.9473E-02
0.4000E+00	-0.2800E+01	0.9473E-02
0.4000E+00	-0.2600E+01	0.9473E-02
0.4000E+00	-0.2400E+01	0.9438E-02
0.4000E+00	-0.2200E+01	0.9438E-02
0.4000E+00	-0.2000E+01	0.9411E-02
0.4000E+00	-0.1800E+01	0.9410E-02
0.4000E+00	-0.1600E+01	0.9360E-02
0.4000E+00	-0.1400E+01	0.9263E-02
0.4000E+00	-0.1200E+01	0.9155E-02
0.4000E+00	-0.1000E+01	0.8992E-02
0.4000E+00	-0.8000E+00	0.8715E-02
0.4000E+00	-0.6000E+00	0.8330E-02
0.4000E+00	-0.2000E+01	0.9411E-02
0.4000E+00	-0.1000E+01	0.8992E-02
0.4000E+00	0.0000E+00	0.6818E-02
0.4000E+00	0.2000E+00	0.6643E-02
0.4000E+00	0.4000E+00	0.6997E-02
0.4000E+00	0.6000E+00	0.7667E-02
0.4000E+00	0.8000E+00	0.9445E-02
0.4000E+00	0.1000E+01	0.1195E-01
0.4000E+00	0.1200E+01	0.1460E-01
0.6000E+00	-0.3000E+01	0.7969E-02
0.6000E+00	-0.2800E+01	0.7964E-02
0.6000E+00	-0.2600E+01	0.7964E-02
0.6000E+00	-0.2400E+01	0.7964E-02
0.6000E+00	-0.2200E+01	0.7948E-02
0.6000E+00	-0.2000E+01	0.7941E-02
0.6000E+00	-0.1800E+01	0.7914E-02
0.6000E+00	-0.1600E+01	0.7871E-02
0.6000E+00	-0.1400E+01	0.7823E-02
0.6000E+00	-0.1200E+01	0.7746E-02
0.6000E+00	-0.1000E+01	0.7660E-02
0.6000E+00	-0.8000E+00	0.7489E-02
0.6000E+00	-0.6000E+00	0.7285E-02
0.6000E+00	-0.2000E+01	0.7941E-02
0.6000E+00	-0.1000E+01	0.7660E-02
0.6000E+00	0.0000E+00	0.6663E-02
0.6000E+00	0.2000E+00	0.6897E-02
0.6000E+00	0.4000E+00	0.7667E-02
0.6000E+00	0.6000E+00	0.9026E-02
0.6000E+00	0.8000E+00	0.1066E-01
0.6000E+00	0.1000E+01	0.1284E-01
0.6000E+00	0.1200E+01	0.1515E-01
0.8000E+00	-0.3000E+01	0.8576E-02
0.8000E+00	-0.2800E+01	0.8567E-02
0.8000E+00	-0.2600E+01	0.8557E-02
0.8000E+00	-0.2400E+01	0.8557E-02
0.8000E+00	-0.2200E+01	0.8557E-02
0.8000E+00	-0.2000E+01	0.8546E-02
0.8000E+00	-0.1800E+01	0.8538E-02
0.8000E+00	-0.1600E+01	0.8510E-02
0.8000E+00	-0.1400E+01	0.8482E-02
0.8000E+00	-0.1200E+01	0.8494E-02
0.8000E+00	-0.1000E+01	0.8420E-02
0.8000E+00	-0.8000E+00	0.8330E-02
0.8000E+00	-0.6000E+00	0.8200E-02
0.8000E+00	-0.2000E+01	0.8546E-02
0.8000E+00	-0.1000E+01	0.8420E-02
0.8000E+00	0.0000E+00	0.8187E-02
0.8000E+00	0.2000E+00	0.8570E-02
0.8000E+00	0.4000E+00	0.9445E-02
0.8000E+00	0.6000E+00	0.1066E-01
0.8000E+00	0.8000E+00	0.1213E-01
0.8000E+00	0.1000E+01	0.1377E-01

x_1	x_2	y
0.8000E+00	0.1200E+01	0.1551E-01
0.1000E+01	-0.3000E+01	0.1090E-01
0.1000E+01	-0.2800E+01	0.1090E-01
0.1000E+01	-0.2600E+01	0.1090E-01
0.1000E+01	-0.2400E+01	0.1089E-01
0.1000E+01	-0.2200E+01	0.1089E-01
0.1000E+01	-0.2000E+01	0.1089E-01
0.1000E+01	-0.1800E+01	0.1087E-01
0.1000E+01	-0.1600E+01	0.1086E-01
0.1000E+01	-0.1400E+01	0.1084E-01
0.1000E+01	-0.1200E+01	0.1082E-01
0.1000E+01	-0.1000E+01	0.1078E-01
0.1000E+01	-0.8000E+00	0.1072E-01
0.1000E+01	-0.6000E+00	0.1066E-01
0.1000E+01	-0.2000E+01	0.1089E-01
0.1000E+01	-0.1000E+01	0.1078E-01
0.1000E+01	0.0000E+00	0.1083E-01
0.1000E+01	0.2000E+00	0.1120E-01
0.1000E+01	0.4000E+00	0.1195E-01
0.1000E+01	0.6000E+00	0.1284E-01
0.1000E+01	0.8000E+00	0.1377E-01
0.1000E+01	0.1000E+01	0.1448E-01
0.1000E+01	0.1200E+01	0.1550E-01
0.1200E+01	-0.3000E+01	0.1402E-01
0.1200E+01	-0.2800E+01	0.1402E-01
0.1200E+01	-0.2600E+01	0.1402E-01
0.1200E+01	-0.2400E+01	0.1402E-01
0.1200E+01	-0.2200E+01	0.1400E-01
0.1200E+01	-0.2000E+01	0.1400E-01
0.1200E+01	-0.1800E+01	0.1401E-01
0.1200E+01	-0.1600E+01	0.1399E-01
0.1200E+01	-0.1400E+01	0.1397E-01
0.1200E+01	-0.1200E+01	0.1395E-01
0.1200E+01	-0.1000E+01	0.1392E-01
0.1200E+01	-0.8000E+00	0.1389E-01
0.1200E+01	-0.6000E+00	0.1384E-01
0.1200E+01	-0.2000E+01	0.1400E-01
0.1200E+01	-0.1000E+01	0.1392E-01
0.1200E+01	0.0000E+00	0.1390E-01
0.1200E+01	0.2000E+00	0.1420E-01
0.1200E+01	0.4000E+00	0.1460E-01
0.1200E+01	0.6000E+00	0.1515E-01
0.1200E+01	0.8000E+00	0.1551E-01
0.1200E+01	0.1000E+01	0.1550E-01
0.1200E+01	0.1200E+01	0.1532E-01
0.1200E+01	0.1400E+01	0.1567E-01
0.1400E+01	0.1200E+01	0.1567E-01
0.1400E+01	0.1400E+01	0.1491E-01
0.1400E+01	0.1600E+01	0.1485E-01
0.1400E+01	0.1800E+01	0.1485E-01
0.1400E+01	0.2000E+01	0.1491E-01
0.1400E+01	0.2200E+01	0.1496E-01
0.1400E+01	0.2400E+01	0.1502E-01
0.1400E+01	0.2600E+01	0.1504E-01
0.1400E+01	0.2800E+01	0.1503E-01
0.1400E+01	0.3000E+01	0.1507E-01
0.1600E+01	0.1400E+01	0.1485E-01
0.1600E+01	0.1600E+01	0.1397E-01
0.1600E+01	0.1800E+01	0.1376E-01
0.1600E+01	0.2000E+01	0.1366E-01
0.1600E+01	0.2200E+01	0.1359E-01
0.1600E+01	0.2400E+01	0.1355E-01
0.1600E+01	0.2600E+01	0.1358E-01
0.1600E+01	0.2800E+01	0.1356E-01
0.1600E+01	0.3000E+01	0.1357E-01
0.1800E+01	0.1400E+01	0.1485E-01
0.1800E+01	0.1600E+01	0.1376E-01
0.1800E+01	0.1800E+01	0.1305E-01

x_1	x_2	y
0.1800E+01	0.2000E+01	0.1277E-01
0.1800E+01	0.2200E+01	0.1266E-01
0.1800E+01	0.2400E+01	0.1260E-01
0.1800E+01	0.2600E+01	0.1251E-01
0.1800E+01	0.2800E+01	0.1249E-01
0.1800E+01	0.3000E+01	0.1248E-01
0.2000E+01	0.1400E+01	0.1491E-01
0.2000E+01	0.1600E+01	0.1366E-01
0.2000E+01	0.1800E+01	0.1277E-01
0.2000E+01	0.2000E+01	0.1225E-01
0.2000E+01	0.2200E+01	0.1202E-01
0.2000E+01	0.2400E+01	0.1195E-01
0.2000E+01	0.2600E+01	0.1187E-01
0.2000E+01	0.2800E+01	0.1184E-01
0.2000E+01	0.3000E+01	0.1176E-01
0.2200E+01	0.1400E+01	0.1496E-01
0.2200E+01	0.1600E+01	0.1359E-01
0.2200E+01	0.1800E+01	0.1266E-01
0.2200E+01	0.2000E+01	0.1202E-01
0.2200E+01	0.2200E+01	0.1169E-01
0.2200E+01	0.2400E+01	0.1157E-01
0.2200E+01	0.2600E+01	0.1146E-01
0.2200E+01	0.2800E+01	0.1142E-01
0.2200E+01	0.3000E+01	0.1137E-01
0.2400E+01	0.1400E+01	0.1502E-01
0.2400E+01	0.1600E+01	0.1355E-01
0.2400E+01	0.1800E+01	0.1260E-01
0.2400E+01	0.2000E+01	0.1195E-01
0.2400E+01	0.2200E+01	0.1157E-01
0.2400E+01	0.2400E+01	0.1129E-01
0.2400E+01	0.2600E+01	0.1122E-01
0.2400E+01	0.2800E+01	0.1114E-01
0.2400E+01	0.3000E+01	0.1111E-01
0.2600E+01	0.1400E+01	0.1504E-01
0.2600E+01	0.1600E+01	0.1358E-01
0.2600E+01	0.1800E+01	0.1251E-01
0.2600E+01	0.2000E+01	0.1187E-01
0.2600E+01	0.2200E+01	0.1146E-01
0.2600E+01	0.2400E+01	0.1122E-01
0.2600E+01	0.2600E+01	0.1107E-01
0.2600E+01	0.2800E+01	0.1100E-01
0.2600E+01	0.3000E+01	0.1094E-01
0.2800E+01	0.1400E+01	0.1503E-01
0.2800E+01	0.1600E+01	0.1356E-01
0.2800E+01	0.1800E+01	0.1249E-01
0.2800E+01	0.2000E+01	0.1184E-01
0.2800E+01	0.2200E+01	0.1142E-01
0.2800E+01	0.2400E+01	0.1114E-01
0.2800E+01	0.2600E+01	0.1100E-01
0.2800E+01	0.2800E+01	0.1088E-01
0.2800E+01	0.3000E+01	0.1085E-01
0.3000E-01	0.1400E+01	0.1507E-01
0.3000E+01	0.1600E+01	0.1357E-01
0.3000E+01	0.1800E+01	0.1248E-01
0.3000E+01	0.2000E+01	0.1176E-01
0.3000E+01	0.2200E+01	0.1137E-01
0.3000E+01	0.2400E+01	0.1111E-01
0.3000E+01	0.2600E+01	0.1094E-01
0.3000E+01	0.2800E+01	0.1085E-01
0.3000E+01	0.3000E+01	0.1079E-01